



PHD

## Developing a Theranostic Device for the Treatment of Staphylococcus aureus Infections

Gwynne, Lauren

*Award date:*  
2021

*Awarding institution:*  
University of Bath

[Link to publication](#)

### Alternative formats

If you require this document in an alternative format, please contact:  
[openaccess@bath.ac.uk](mailto:openaccess@bath.ac.uk)

#### General rights

Copyright and moral rights for the publications made accessible in the public portal are retained by the authors and/or other copyright owners and it is a condition of accessing publications that users recognise and abide by the legal requirements associated with these rights.

- Users may download and print one copy of any publication from the public portal for the purpose of private study or research.
- You may not further distribute the material or use it for any profit-making activity or commercial gain
- You may freely distribute the URL identifying the publication in the public portal ?

#### Take down policy

If you believe that this document breaches copyright please contact us providing details, and we will remove access to the work immediately and investigate your claim.

**Developing a Theranostic  
Device for the Treatment of  
*Staphylococcus aureus*  
Infections**

Lauren Gwynne

A thesis submitted for the degree of Doctor of  
Philosophy

University of Bath

Department of Chemistry

January 2021



# Abstract

Chronic wounds are a global health problem, affecting approximately 1 – 2% of the general population in developed countries. Chronic wounds are also an economic burden, with the NHS in the UK spending approximately £4.5 – 5.1 billion per annum, after adjusting for comorbidities. Chronic wounds also have a negative effect on the patient's quality of life and can lead to a range of psychological consequences such as depression, anxiety and embarrassment, all of which can lead to social isolation, further perpetuating psychological illness.

Current methods to detect wound infection are lacking. Sampling techniques are often imprecise and cause pain to the patient. Additionally, standard microbiological techniques are time consuming, have to be performed by a trained specialist, and are often only able to identify bacteria that can be routinely grown in a laboratory.

Owing to these aforementioned issues, there is a growing need to create novel 'smart' systems that can detect or treat pathogenic bacteria accurately and rapidly, without the need of invasive, painful sampling techniques, and time consuming microbiological analysis.

This thesis outlines the development of a novel theranostic wound dressing capable of detecting and treating *S. aureus* infections. Bacteriophage K and ciprofloxacin were encapsulated within a pH-responsive polymer matrix, and upon a rise in pH were released from the system to treat the *S. aureus* infection. Concurrently, a novel colorimetric and fluorescent probe was designed to detect *S. aureus*, to notify the patient or health care practitioner to the presence of an infection. Both components of this theranostic system were tested against *S. aureus* species using a variety of microbiological techniques, including suspension assays, biofilm models, and *ex vivo* porcine skin assays.

# Acknowledgements

Words cannot express how truly thankful I am for everyone who has supported me over the last four years. Without all of you, this would not have been possible. So from the bottom of my heart, thank you.

Thank you to all members of the Jenkins group, both past and present, for their guidance and support during my time at Bath. Thet, Rachel, Liam, Hollie and Scarlet, thank you for your advice on all things scientific as well as constant moral support over the last four years. Most of all, I would like to thank Toby for his unwavering confidence in my ability to carry out this PhD, offering guidance and support when I needed it the most. I will always look fondly on all our trips and Hirschegg will always have a special place in my heart.

A big thank you to all members of the Cardiff group, Leo, Maru, Rebecca, Joanna, Issy, Helene, Greg, Melissa, Andy, and Kate for your support and friendship over the last four years. Mike, you are fabulous. You are an exceptional person, in both your scientific expertise and kind heart. Thank you for taking me under your wing; you made life in Cardiff so enjoyable and fun. A special thanks must go to Jean-Yves, for being such a supportive supervisor and helping me get through a particularly difficult time in my life.

Beth – what can I say. Thank you for your positive outlook, cooking the best paella known to man (sorry, George), and just generally making sure I didn't have a nervous breakdown. I'm so glad I've made a friend like you, even if it means I get annual flashbacks of the Christmas party...

A big thank you also goes to Jordan and Adam, without these two in my life, my PhD would have not been a success. Thank you both for your friendship over the last four years. Jordan, thank you for all your constant support - whenever I was having a bad day, I knew I could always count on you to be miserable with me. Ad, thank you. While you are one of the most stressful people I know, I am so glad we are friends, and I look forward too many more chaotic years of knowing you (don't worry, you will always be a 10).

George, where do I start. 8 long years of friendship – I have no idea how you have managed to put up with me for so long! Friends for life now pal. I cannot express how lucky I am to have you as a friend and the acknowledgement here does not do justice. You are the kind, helpful, supportive, honest, annoyingly talented, and only a tiny bit annoying. While it will be weird not working together anymore, I look forward to seeing where your career takes you, while (probably) complaining about mine.

I also have to say a big thank you to Laura, my lab partner in crime. Thank you for also being an evening person, working alongside me into the small hours while singing along to all things Disney. You are such an amazing friend – you are kind, sincere, supportive and most importantly, empathetic and non-judgemental. Thank you for being there for me, through every high and every low, offering support, advice, and most importantly, friendship. In you, I have made a friend for life.

A big massive thanks must also go to my family, most importantly my mum. She has constantly said that she deserves a PhD for putting up with me during mine, and I couldn't agree more. A special thank you also goes out to Lee; it couldn't have been easy putting up with me while I have been writing this thesis! I hope now we can enjoy a more stress-free life. I look forward to seeing where the next chapter of our lives takes us!

# Dissemination of Research

## Conference Participation

Poster Presentation at ACCIS, Kathmandu, Nepal, 2019

Oral Presentation at Bolland Symposium, University of Bath, United Kingdom, 2019

Oral Presentation at BioNano Summer School, Hirscheegg, Austria, 2017, 2018, 2019

Oral Presentation at VBST, Hirscheegg, Austria (2019) and Attendorn, Germany, 2017

Oral Presentation at ECCMID, Amsterdam, Netherlands, 2019

Poster Presentation at the 5<sup>th</sup> World Congress on Targeting Infectious Diseases, Florence, Italy, 2018

Oral Presentation at CITER, Cardiff, United Kingdom, 2018

Delegate at Wounds UK Conference, Birmingham, United Kingdom, 2017

## Awards

Awarded the President Fund Grant (2019)

Awarded £800 by the Society for Applied Microbiology for travel to ECCMID to present an oral presentation.

## Publications

**Investigating the phage-antibiotic synergy of bacteriophage K and conventional antibiotics.** L Gwynne, L.Wallace, GT Williams, BL Patenall, AC Sedgwick, JY Maillard and ATA Jenkins (*under development*)

**Development of a pH responsive wound dressing for the treatment of *S. aureus*.** L Gwynne, L.Wallace, GT Williams, BL Patenall, AC Sedgwick, JY Maillard and ATA Jenkins (*under development*)

**The evaluation of ester functionalised TCF-based fluorescent probes for the detection of bacterial species.** L Gwynne, GT Williams, K-C Yan, JE Gardiner, KLF Hilton, BL Patenall, JR Hiscock, JY Maillard, X-P He, TD James, AC Sedgwick and ATA Jenkins. Israel Journal of Chemistry, 61, 234–238

**TCF-ALP: A fluorescent probe for the selective detection of gram-positive bacteria and application in “Smart” wound dressings.** L Gwynne, GT Williams, K-C Yan, JE Gardiner, BL Patenall, X-P He, JY Maillard, TD James, AC Sedgwick and ATA Jenkins. Biomaterials Science (epub available)

**Enhanced colorimetric differentiation between *Staphylococcus aureus* and *Pseudomonas aeruginosa* using a shape-encoded sensor hydrogel.** Z Jia, L Gwynne, AC Sedgwick, M Müller, GT Williams, ATA Jenkins, TD James and H Schönherr. ACS Applied Bio Materials, 3(7) 4398–4407

**Protein encapsulation: A Nanocarrier approach to the fluorescence imaging of an enzyme-based biomarker.** Z Jia .HH Han, AC Sedgwick, GT Williams, L Gwynne, JT Brewster, SD Bull, ATA Jenkins, XP He, H Schönherr, JL Sessler and TD James. 2020. Frontiers in Chemistry, 8, 389

**Boronate ester cross-linked PVA hydrogels for the capture and H<sub>2</sub>O<sub>2</sub>-mediated release of active fluorophores.** GT Williams, AC Sedgwick, S Sen, L Gwynne, JD Gardiner, JT Brewster, J Hiscock, TD James, ATA Jenkins and JL Sessler. 2020. Chemical Communications, 56, 5516–5519

**Long wavelength TCF-based fluorescence probe for the detection of Alkaline Phosphatase in live cells.** L Gwynne, AC Sedgwick, JE Gardiner, GT Williams, G Kim, JY Maillard, ATA Jenkins, SD Bull, JL Sessler, J Yoon and TD James. 2019. Frontiers in Chemistry, 7, 255

**Challenges and opportunities of pH in Chronic Wounds.** LA Wallace, L Gwynne and ATA Jenkins. 2019. Therapeutic Delivery. 10(11), 719–735

**Reaction-based indicator displacement assay (RIA) for the development of a triggered release system capable of biofilm inhibition.** BL Patenall, GT Williams, L Gwynne, LJ Stephens, EV Lampard, HJ Hathaway, NT Thet, AE Young, MJ Sutton, RD Short, SD Bull, TD James, AC Sedgwick and ATA Jenkins. 2019. Chemical Communications. 55(100), 15129–15132

**Surface coatings with covalently attached caspofungin are effective in eliminating fungal pathogens.** BR Coad, SJ Lamont-Friedrich, L Gwynne, M Jasieniak, SS Griesser, A Traven, AY Peleg and HJ Griesser. 2015. Journal of Materials Chemistry B. 3(43), 8469–8476



# Table of Contents

<b>Abstract.....</b>	<b>i</b>
<b>Acknowledgments .....</b>	<b>ii</b>
<b>Dissemination of Work .....</b>	<b>iv</b>
<b>Table of Contents.....</b>	<b>vi</b>
<b>Abbreviations.....</b>	<b>xvii</b>
<b>List of Tables .....</b>	<b>xx</b>
<b>List of Figures .....</b>	<b>xxii</b>
<b>Chapter 1: Introduction .....</b>	<b>1</b>
<b>1.1. Clinical Problem .....</b>	<b>1</b>
<b>1.2. Wounds and Wound Healing .....</b>	<b>2</b>
1.2.1. Types of Wound.....	2
1.2.2. Wound Healing and the Wound Healing Cascade.....	3
1.2.2.1. Haemostasis .....	4
1.2.2.2. Inflammation.....	5
1.2.2.3. Proliferation .....	5
1.2.2.4. Remodelling .....	6
1.2.3. Delayed Wound Healing .....	7
<b>1.3. Wounds Infection .....</b>	<b>7</b>
1.3.1. Microbiology of Chronic Wounds.....	8
1.3.2. Biofilm Formation .....	9
<b>1.4. Staphylococcus aureus .....</b>	<b>11</b>
1.4.1. Virulence Factors and Regulators .....	12
1.4.1.1. Regulators.....	12
1.4.1.2. Virulence Factors .....	13
1.4.1.2.1. Toxins.....	14
1.4.1.2.2. Enzymes .....	15
1.4.2. Biofilms.....	15

1.4.3.	Methicillin-resistant <i>Staphylococcus aureus</i> .....	16
<b>1.5.</b>	<b>Bacteriophage .....</b>	<b>17</b>
1.5.1.	Discovery and Historical Use .....	17
1.5.2.	Bacteriophage Taxonomy .....	18
1.5.3.	Bacteriophage Life Cycle .....	20
1.5.3.1.	Adsorption .....	21
1.5.3.2.	Lytic Lifecycle .....	21
1.5.3.3.	Lysogenic Lifecycle .....	22
1.5.4.	Transduction .....	23
1.5.5.	Bacterial Resistance to Bacteriophage .....	23
1.5.6.	Bacteriophage Therapy .....	24
1.5.6.1.	Advantages .....	25
1.5.6.2.	Disadvantages .....	25
<b>1.6.</b>	<b>Wound Dressings .....</b>	<b>26</b>
1.6.1.	Characteristics of an Ideal Wound Dressing .....	27
1.6.2.	Traditional Wound Dressings .....	27
1.6.3.	Modern Wound Dressings .....	27
1.6.3.1.	Semi-permeable Dressings .....	28
1.6.3.2.	Hydrogels .....	28
1.6.3.3.	Hydrocolloids .....	28
1.6.4.	Medicated Dressings .....	28
<b>1.7.</b>	<b>Overall Aims and Objectives .....</b>	<b>29</b>
<b>1.8.</b>	<b>References .....</b>	<b>30</b>
<b>Chapter 2: General Materials and Methods .....</b>		<b>47</b>
<b>2.1.</b>	<b>Materials .....</b>	<b>47</b>
<b>2.2.</b>	<b>Methods .....</b>	<b>48</b>
2.2.1.	Bacteria .....	48
2.2.1.1.	Bacterial Strains .....	48
2.2.1.2.	Principles of Bacterial Growth .....	48
2.2.1.3.	Bacterial Culture Conditions .....	49
2.2.1.4.	Bacterial Enumeration .....	49
2.2.1.5.	Minimum Inhibitory Concentration .....	49

2.2.2.	<i>In vitro</i> Biofilm Models .....	50
2.2.2.1.	96-Microtiter Biofilm Models .....	50
2.2.2.1.1.	Minimum Biofilm Inhibitory Concentration .....	50
2.2.2.1.2.	Minimum Biofilm Eradication Concentration .....	50
2.2.2.1.3.	Crystal Violet Assay .....	51
2.2.2.2.	Colony Biofilm Model .....	51
2.2.3.	Bacteriophage .....	52
2.2.3.1.	Principles of Bacteriophage Growth .....	52
2.2.3.2.	Bacteriophage Propagation .....	52
2.2.3.2.1.	Soft Overlay Method .....	52
2.2.3.2.2.	Liquid Lysate .....	53
2.2.3.3.	Bacteriophage Enumeration .....	53
2.2.3.4.	Increasing Bacteriophage Titre .....	54
2.2.4.	Data Analysis and Statistics .....	54
<b>2.3.</b>	<b>References .....</b>	<b>55</b>
<b>Chapter 3: Evaluation of Phage-Antibiotic Synergy.....</b>		<b>56</b>
<b>3.1.</b>	<b>Overview of Chapter .....</b>	<b>56</b>
<b>3.2.</b>	<b>Introduction .....</b>	<b>56</b>
3.2.1.	Phage-Antibiotic Synergy .....	56
3.2.2.	Phage-Antibiotic Synergy Studies .....	57
3.2.2.1.	Planktonic Studies .....	57
3.2.2.2.	Biofilm Models .....	58
3.2.2.3.	<i>In vivo</i> Models .....	59
3.2.3.	Mechanism of Action .....	61
3.2.4.	Objectives .....	63
<b>3.3.</b>	<b>Methods .....</b>	<b>64</b>
3.3.1.	Bacterial and Bacteriophage Methods .....	64
3.3.2.	Bacteriophage Efficacy .....	64
3.3.2.1.	Spot Tests .....	64
3.3.2.2.	Detecting Temperate (Lysogenic) Phage .....	65
3.3.2.3.	Multiplicity of Infection (MOI) .....	65
3.3.3.	Minimum Inhibitory Concentration .....	66

3.3.4.	Evaluating Phage-Antibiotic Synergy in Planktonic Suspensions .....	66
3.3.4.1.	Phage-Antibiotic Synergy Assay .....	66
3.3.4.2.	Bacterial Cell Count Assay .....	66
3.3.4.3.	One Step Growth Curve .....	66
3.3.4.4.	Scanning Electron Microscopy .....	67
3.3.5.	Phage-Antibiotic Synergy Activity in Biofilms .....	67
3.3.5.1.	Minimum Biofilm Inhibition Concentration .....	67
3.3.5.2.	Biofilm Inhibition Phage-Antibiotic Synergy Assay .....	67
3.3.5.3.	Minimum Biofilm Eradication Concentration .....	68
3.3.5.4.	Biofilm Eradication Phage-Antibiotic Synergy Assay .....	68
<b>3.4.</b>	<b>Results and Discussion .....</b>	<b>69</b>
3.4.1.	Single-Therapy Efficacy .....	69
3.4.1.1.	Bacterial Sensitivity to Bacteriophage K .....	69
3.4.1.2.	Detection of Temperate Bacteriophage .....	70
3.4.1.3.	Multiplicity of Infection .....	71
3.4.1.4.	Antibiotic Susceptibility .....	72
3.4.2.	Determination of Phage-Antibiotic Synergy .....	74
3.4.2.1.	Bacteriophage K Survival in the Presence of Antibiotics .....	74
3.4.2.2.	Phage-Antibiotic Synergy Assay .....	75
3.4.2.3.	Bacterial Cell Counts .....	79
3.4.2.3.1.	Mixed Model Analysis .....	81
3.4.2.4.	Bacteriophage Cell Counts .....	82
3.4.2.5.	One Step Growth Curves .....	84
3.4.2.6.	Scanning Electron Microscopy (SEM) Images .....	86
3.4.3.	The Efficacy of PAS Within Bacterial Biofilms .....	88
3.4.3.1.	Minimum Biofilm Inhibitory Concentrations .....	88
3.4.3.2.	Biofilm Prevention .....	90
3.4.3.3.	Biofilm Eradication .....	94
<b>3.5.</b>	<b>Conclusions and Future Work .....</b>	<b>97</b>
<b>3.6.</b>	<b>References .....</b>	<b>98</b>

## **Chapter 4: Antimicrobial-loaded poly(lactic acid)-poly(ethylene glycol) Films for the Treatment of *S. aureus* Infections ..... 107**

### **4.1. Overview of Chapter ..... 107**

### **4.2. Introduction ..... 107**

#### 4.2.1. Polymers ..... 107

##### 4.2.1.1. Polymer Weight ..... 108

##### 4.2.1.2. Linear, Branched, and Crosslinked Polymers ..... 109

##### 4.2.1.3. Copolymer Arrangements ..... 110

##### 4.2.1.4. Polymer Classification ..... 110

##### 4.2.1.5. Configuration and Conformation ..... 111

##### 4.2.1.6. Polymer Synthesis ..... 112

#### 4.2.2. Poly(lactic acid) ..... 113

##### 4.2.2.1. Poly(lactic acid) Drug Delivery Systems ..... 114

#### 4.2.3. Aims of Study ..... 115

### **4.3. Methods ..... 116**

#### 4.3.1. Bacterial and Bacteriophage Methods ..... 116

#### 4.3.2. Development of PLA-PEG System ..... 116

##### 4.3.2.1. Creating the Polymer Blend ..... 116

##### 4.3.2.2. Encapsulation Efficacy ..... 116

##### 4.3.2.3. Swelling and Weight Loss ..... 116

#### 4.3.3. Bacteriophage Survival ..... 117

##### 4.3.3.1. pH ..... 117

##### 4.3.3.2. Dichloromethane and PEG 400 ..... 117

##### 4.3.3.3. Temperature ..... 117

#### 4.3.4. Scanning Electron Microscopy ..... 117

#### 4.3.5. *In vitro* Release Studies ..... 117

#### 4.3.6. Stability ..... 118

#### 4.3.7. Microbiological Testing ..... 118

##### 4.3.7.1. Suspension Assays ..... 118

##### 4.3.7.2. Colony Biofilm Wound Model ..... 119

##### 4.3.7.3. *Ex vivo* Porcine Skin Models ..... 119

###### 4.3.7.3.1. Sterilisation ..... 119

###### 4.3.7.3.2. Optimisation ..... 119

4.3.7.3.3. Microbiological Assay .....	119
<b>4.4. Results and Discussion .....</b>	<b>121</b>
4.4.1. PLA-PEG (PPEG) Films .....	121
4.4.1.1. Pore Size .....	122
4.4.1.2. Weight Loss and Water Sorption .....	123
4.4.2. Bacteriophage-loaded Films .....	123
4.4.2.1. Bacteriophage Survival .....	123
4.4.2.2. Encapsulation Efficacy and <i>In vitro</i> Release .....	125
4.4.2.3. Stability .....	127
4.4.2.4. Suspension Assays .....	128
4.4.2.5. Colony Biofilm Wound Model .....	130
4.4.2.6. <i>Ex vivo</i> Porcine Skin Models .....	132
4.4.3. Ciprofloxacin-loaded Films .....	135
4.4.3.1. Encapsulation Efficacy and <i>In vitro</i> Release .....	136
4.4.3.2. Stability .....	138
4.4.3.3. Suspension Assays .....	139
4.4.3.4. Colony Biofilm Wound Model .....	140
4.4.3.5. <i>Ex vivo</i> Porcine Skin Models .....	141
4.4.4. Combination-loaded Films .....	143
4.4.4.1. Stability .....	143
4.4.4.2. Suspension Assays .....	143
4.4.4.3. Colony Biofilm Wound Model .....	146
4.4.4.4. <i>Ex vivo</i> Porcine Skin Models .....	147
<b>4.5. Conclusions and Future Work .....</b>	<b>149</b>
<b>4.6. References .....</b>	<b>151</b>
<b>Chapter 5: Triggered Release of Bacteriophage K and Ciprofloxacin</b>	
<b>From a pH-responsive System .....</b>	<b>157</b>
<b>5.1. Overview of Chapter.....</b>	<b>157</b>
<b>5.2. Introduction.....</b>	<b>158</b>
5.2.1. pH .....	158
5.2.1.1. Acid and Bases .....	158
5.2.1.2. Buffer Solutions .....	159

5.2.2.	Wound pH .....	160
5.2.2.1.	Wound Healing and pH .....	161
5.2.2.2.	Microbial Biofilms and pH .....	161
5.2.2.3.	Antimicrobials and pH .....	162
5.2.3.	Triggered Release Systems .....	162
5.2.3.1.	Response Systems Based on Temperature .....	163
5.2.3.2.	Response Systems Based on Enzymes and Toxins .....	163
5.2.3.3.	Response Systems Based on pH .....	164
5.2.4.	Aims of Study .....	165
<b>5.3.</b>	<b>Methods .....</b>	<b>166</b>
5.3.1.	Bacterial and Bacteriophage Methods .....	166
5.3.2.	Evaluation of Biofilm pH .....	166
5.3.3.	Development of a pH-responsive System .....	166
5.3.4.	Bacteriophage Survival .....	166
5.3.4.1.	pH .....	166
5.3.4.2.	Organic Solvents .....	166
5.3.5.	<i>In vitro</i> Release Profiles .....	167
5.3.6.	Stability of pH-responsive System .....	167
5.3.7.	Colony Biofilm Wound Model .....	167
<b>5.4.</b>	<b>Results and Discussion .....</b>	<b>168</b>
5.4.1.	pH Change in <i>S. aureus</i> Biofilms .....	168
5.4.2.	EUDRAGIT®-coated Films .....	169
5.4.3.	Bacteriophage-loaded Films .....	170
5.4.3.1.	Bacteriophage Survival .....	170
5.4.3.2.	<i>In vitro</i> Release .....	171
5.4.3.3.	Stability .....	173
5.4.3.4.	Colony Biofilm Wound Models .....	174
5.4.4.	Ciprofloxacin-loaded Films .....	176
5.4.4.1.	Thickness of pH-responsive Layer .....	176
5.4.4.2.	<i>In vitro</i> Release .....	177
5.4.4.3.	Stability .....	178
5.4.4.4.	Colony Biofilm Wound Models .....	179
5.4.5.	Combination-loaded Films .....	181

5.4.5.1.	Stability .....	181
5.4.5.2.	Colony Biofilm Wound Models .....	182
<b>5.5.</b>	<b>Conclusions and Future Work .....</b>	<b>186</b>
<b>5.6.</b>	<b>References .....</b>	<b>188</b>
<b>Chapter 6: TCF-based Fluorescent Probe for the Detection of Alkaline Phosphatase .....</b>		<b>195</b>
<b>6.1.</b>	<b>Overview of Chapter.....</b>	<b>195</b>
<b>6.2.</b>	<b>Introduction.....</b>	<b>196</b>
6.2.1.	Fluorescence .....	196
6.2.1.1.	Basis of Fluorescence .....	196
6.2.1.2.	Design of Fluorescent Probes .....	198
6.2.1.3.	Fluorescence Mechanisms .....	199
6.2.1.3.1.	Photoinduced Electron Transfer .....	199
6.2.1.3.2.	Förster Resonance Energy Transfer .....	200
6.2.1.3.3.	Excited-state Intramolecular Proton Transfer .....	201
6.2.1.3.4.	Internal Charge Transfer .....	201
6.2.1.3.4.1.	TCF-based Fluorescent Probes .....	202
6.2.2.	Enzymes .....	202
6.2.2.1.	Enzyme Kinetics .....	204
6.2.2.2.	Clinical Diagnostic Applications of Enzymes .....	207
6.2.2.3.	Alkaline Phosphatase .....	207
6.2.3.	Aims of Study.....	208
<b>6.3.</b>	<b>Methods .....</b>	<b>209</b>
6.3.1.	Synthesis of TCF-ALP .....	209
6.3.1.1.	2-(3-Cyano-4,5,5-trimethylfuran-2(5H)-ylidene .....	209
6.3.1.2.	(E)-2-(3-Cyano-4-(4-hydroxystyryl)-5,5-dimethylfuran-2(5H)-ylidene)malonitrile ....	210
6.3.1.3.	(E)-4-(2-(4-Cyano-5-(dicyanomethylene)-2,2-dimethyl-2,5-dihydrofuran-3-yl)vinyl)phenyl diethyl phosphate .....	210
6.3.1.4.	(E)-4-(2-(4-Cyano-5-(dicyanomethylene)-2,2-dimethyl-2,5-dihydrofuran-3-yl)vinyl)phenyl phosphate .....	210
6.3.2.	Mass Spectrometry .....	210
6.3.3.	UV-Vis Spectroscopy of TCF-ALP .....	211
6.3.4.	Fluorescence of TCF-ALP Over Time .....	211



6.3.5.	Limit of Detection .....	211
6.3.6.	Inhibition Assay .....	211
6.3.7.	Enzyme Kinetics Assay .....	212
6.3.8.	Selectivity of TCF-ALP .....	212
6.3.9.	Cell Culture .....	212
6.3.10.	Confocal Microscopy Imaging .....	212
6.3.11.	Cytotoxicity Tests .....	213
<b>6.4.</b>	<b>Results and Discussion .....</b>	<b>214</b>
6.4.1.	pH Optima .....	214
6.4.2.	Conformation of ALP-mediated Hydrolysis .....	215
6.4.3.	UV-Vis Spectroscopy .....	216
6.4.4.	Fluorescence Assays .....	217
6.4.4.1.	Time Drive .....	217
6.4.4.2.	Limit of Detection .....	217
6.4.5.	Inhibition of TCF-ALP .....	219
6.4.6.	Selectivity of TCF-ALP .....	221
6.4.7.	Enzyme Kinetics .....	224
6.4.8.	Cell-based Assays .....	226
<b>6.5.</b>	<b>Conclusions and Future Work .....</b>	<b>229</b>
<b>6.6.</b>	<b>Appendix .....</b>	<b>230</b>
<b>6.7.</b>	<b>References .....</b>	<b>239</b>
<b>Chapter 7: Using TCF-ALP for the Detection of <i>Staphylococcus aureus</i></b>		
<b>..... 249</b>		
<b>7.1.</b>	<b>Overview of Chapter .....</b>	<b>249</b>
<b>7.2.</b>	<b>Introduction .....</b>	<b>249</b>
7.2.1.	Detecting Pathogenic Bacteria .....	249
7.2.2.	Use of Fluorescent and Colorimetric Probes for the Detection of Pathogenic Bacteria .....	250
7.2.2.1.	Glycosidases .....	251
7.2.2.1.1.	β-D-Glucuronidase .....	251
7.2.2.1.2.	β-D-Galactosidase .....	253
7.2.2.1.3.	β-D-Glucosidase .....	255
7.2.2.1.4.	α-Amylase and α-Glucosidase.....	256

7.2.2.2.	Esterases and Lipases .....	257
7.2.2.3.	Aminopeptidases .....	258
7.2.2.4.	Antibiotic-resistance Enzymes .....	261
7.2.3.	Alkaline Phosphatase .....	262
7.2.3.1.	Pho Regulatory System .....	263
7.2.3.2.	Alkaline Phosphatase Expression .....	263
7.2.3.2.1.	<i>Staphylococcus aureus</i> Alkaline Phosphatase .....	264
7.2.3.3.	Use of Alkaline Phosphatase in Literature .....	264
7.2.4.	Aims and Objectives .....	265
<b>7.3.</b>	<b>Methods .....</b>	<b>266</b>
7.3.1.	Synthesis of TCF-ALP .....	266
7.3.2.	Preparation of TCF-ALP Based PVA Hydrogels .....	266
7.3.3.	Bacterial Growth Conditions .....	266
7.3.4.	Bacterial Enumeration .....	266
7.3.5.	Effect of Broth on Alkaline Phosphatase Production .....	266
7.3.6.	Detecting Alkaline Phosphatase in Planktonic Bacteria .....	267
7.3.7.	Detecting Alkaline Phosphatase in 96-well Plate Biofilm Models .....	267
7.3.7.1.	Alkaline Phosphatase Activity of Biofilms .....	267
7.3.7.2.	Inhibition of Alkaline Phosphatase Activity .....	268
7.3.7.2.1.	Preparation of Sodium Orthovanadate .....	268
7.3.7.2.2.	Minimum Inhibitory Concentration .....	268
7.3.7.2.3.	Minimum Biofilm Inhibitory Concentration .....	268
7.3.7.2.4.	Inhibition of Alkaline Phosphatase Activity .....	268
7.3.8.	Colony Biofilm Wound Model .....	268
7.3.9.	<i>Ex vivo</i> Porcine Skin Model .....	269
7.3.9.1.	Sterilisation .....	269
7.3.9.2.	Alkaline Phosphatase Activity .....	269
<b>7.4.</b>	<b>Results and Discussion .....</b>	<b>270</b>
7.4.1.	UV-Vis of TCF-ALP .....	270
7.4.2.	Optimisation of Assay .....	271
7.4.2.1.	Role of Bacterial Growth Media on Alkaline Phosphatase Production .....	271
7.4.2.2.	Washing Steps .....	273
7.4.2.3.	Incubation Temperatures .....	273

7.4.3.	Time-dependent Alkaline Phosphatase Detection .....	275
7.4.4.	Relationship Between Alkaline Phosphatase Production and Bacterial Concentration .....	275
7.4.5.	Selectivity of TCF-ALP .....	279
7.4.6.	Alkaline Phosphatase Production in Established Biofilms .....	283
7.4.6.1.	96-well Microtiter Plate Biofilm Model .....	284
7.4.6.2.	Colony Biofilm Model .....	286
7.4.7.	<i>Ex vivo</i> Porcine Skin Assay .....	290
7.4.8.	TCF-ALP Based Hydrogels .....	292
7.4.8.1.	Detecting planktonic <i>Staphylococcus aureus</i> .....	294
7.4.8.2.	Colony Biofilm Wound Model .....	296
7.4.8.3.	<i>Ex vivo</i> Porcine Skin Assay .....	298
<b>7.5.</b>	<b>Conclusions and Future Work .....</b>	<b>300</b>
<b>7.6.</b>	<b>Appendix .....</b>	<b>301</b>
<b>7.7.</b>	<b>References .....</b>	<b>305</b>
<b>Chapter 8:</b>	<b>Overall Conclusions and Future Work.....</b>	<b>322</b>

# Abbreviations

Abbreviation	Full Name
ACP	Acid Phosphatase
agr	Accessory Gene Regulator
AIP	Autoinducing Peptide
ALP	Alkaline Phosphatase
AMP	2-Amino-2-Methyl-1-Propanol
a-PPEG	Antibiotic-Loaded PLA-PEG Film
AWF	Artificial Wound Fluid
BAVS	Bacterial and Archaeal Viruses Subcommittee
bFF	Basic Fibroblast Factor
BHI	Brain Heart Infusion
CA-MRSA	Community-Associated MRSA
CAUTI	Catheter-Associated Urinary Tract Infection
CC30	Clonal Complex 30
CDC	Centers For Disease Control and Prevention
CFU	Colony Forming Units
CI	Confidence Interval
CSLI	Clinical Standard Laboratory Institute
CV	Crystal Violet
CWA	Cell-Wall Anchored
dH <sub>2</sub> O	Deionised water
<i>E. coli</i>	<i>Escherichia coli</i>
eDNA	Extracellular DNA
EPS	Extracellular Polymeric Substance
ESIPT	Excited State Intramolecular Proton Transfer
EUCAST	European Committee on Antimicrobial Susceptibility Testing
FESEM	Field Emission Scanning Electron Microscope
FGF	Fibroblast Growth Factor
FRET	Forster Resonance Energy Transfer
GUD	B-D-Glucuronidase
HA-MRSA	Healthcare-Associated MRSA
HDMS	Hexamethyldisilazane
HGT	Horizontal Gene Transfer
HIF	Hypoxia-Inducible Factor
HMDS	Hexamethyldisilazane
HOMO	Highest Occupied Molecular Orbital
IC	Internal Conversion
ICT	Internal Charge Transfer
ICTV	International Committee on The Taxonomy Of Viruses
IL-1	Interleukin-1

---

ISC	Intersystem Crossing
<i>K. pneumoniae</i>	<i>Klebsiella pneumonia</i>
LOD	Limit of Detection
LUMO	Lowest Unoccupied Molecular Orbital
MBEC	Minimum Biofilm Eradication Concentration
MBIC	Minimum Biofilm Inhibitory Concentration
MDR	Multi-drug Resistant
MIC	Minimum Inhibitory Concentration
MMPs	Metalloproteinases
MOA	Mechanism of Action
MOI	Multiplicity of Infection
MRSA	Methicillin-resistant <i>Staphylococcus aureus</i>
MSCRAMMs	Microbial Surface Components Recognising Adhesive Matrix Molecules
MUG	4-Methylumbelliferyl-B-D-Glucuronide
MW	Molecular Weight
NIR	Near Infra-red
OD <sub>600</sub>	Optical Density of 600 nm
<i>P. aeruginosa</i>	<i>Pseudomonas aeruginosa</i>
<i>P. mirabilis</i>	<i>Proteus mirabilis</i>
PAS	Phage-Antibiotic Synergy
PDGF	Platelet-Derived Growth Factor
PEG	Poly(ethylene glycol)
PET	Photoinduced Electron Transfer
PFU/mL	Plaque Forming Units per Millilitre
Phage	Bacteriophage
Pi	Inorganic Phosphate
PLA	Poly(lactic acid)
PNIPAM	Poly(N-Isopropylacrylamide)
PoC	Point of Care
PPEG	PLA-PEG Polymer Blend
PSMs	Phenol-Soluble Modulins
PVL	Panton-Valentine Leukocidin
RFI	Relative Fluorescence Intensity
ROP	Ring-opening Polymerisation
<i>S. aureus</i>	<i>Staphylococcus aureus</i>
<i>S. epidermidis</i>	<i>Staphylococcus epidermidis</i>
SC	Stratum Corneum
SEM	Scanning Electron Microscope
SSSS	Staphylococcal Scalded Skin Syndrome
TCSs	Two-Component Systems
T <sub>g</sub>	Glass transition temperature
TGF-β	Transforming Growth Factor-Beta
TNFα	Tumour Necrosis Alpha
TSA	Tryptic Soy Agar

---

---

TSB	Tryptic Soy Broth
TSBg	Tryptic Soy Broth with 1% w/v Glucose
TSST-1	Toxic Shock Syndrome Toxin-1
VBNC	Viable, But Nonculturable
VEGF	Vascular Endothelial Growth Factor
vWF	von Willebrand Factor
$\beta$ -gal	B-Galactosidase
$\mu$ PAD	Paper-Based Device

---

# List of Tables

<b>Table 1.1:</b> Local and systemic factors that may impede wound healing. ....	7
<b>Table 1.2:</b> Major virulence regulatory systems of <i>S. aureus</i> .....	12
<b>Table 1.3:</b> Classification of phage families (non-exhaustive list).....	19
<b>Table 1.4:</b> Virulence factors encoded by genes acquired via prophage integration .....	22
<b>Table 2.1:</b> List of reagents and materials .....	47
<b>Table 3.1:</b> Examples of PAS in planktonic bacteria.....	57
<b>Table 3.2:</b> Examples of PAS in bacterial biofilms .....	60
<b>Table 3.3:</b> Examples of PAS in <i>in vivo</i> assays .....	61
<b>Table 3.4:</b> Scoring system for assessment of bacteriophage activity .....	65
<b>Table 3.5:</b> Efficacy of bacteriophage K against <i>S. aureus</i> at a MOI of 0.1. ....	70
<b>Table 3.6:</b> Minimum Inhibitory Concentrations of the antibiotics used in this study ....	74
<b>Table 3.7:</b> Calculated co-efficients for the mixed model analysis .....	82
<b>Table 3.8:</b> Latent period and burst size of bacteriophage K in <i>S. aureus</i> H560 .....	84
<b>Table 3.9:</b> Latent period and burst size of bacteriophage K in <i>S. aureus</i> MRSA252 .....	85
<b>Table 3.10:</b> Latent period and burst size of bacteriophage K in <i>S. aureus</i> MSSA101 .....	85
<b>Table 3.11:</b> Minimum Biofilm Inhibitory Concentrations of antibiotics .....	89
<b>Table 4.1:</b> Commonly used synthetic polymers and their applications .....	108
<b>Table 4.2:</b> Kinetic model and corresponding R <sup>2</sup> value for the release of bacteriophage K from a pH-responsive system .....	127
<b>Table 4.3:</b> Comparison of human and porcine skin.....	132
<b>Table 4.4:</b> Kinetic model and corresponding R <sup>2</sup> value for the release of ciprofloxacin from a pH-responsive system .....	138

<b>Table 5.1:</b> Kinetic model and corresponding $R^2$ value for the release of bacteriophage K from a pH-responsive system .....	173
<b>Table 5.2:</b> Kinetic model and corresponding $R^2$ value for the release of ciprofloxacin from a pH-responsive system .....	178
<b>Table 5.3:</b> Calculated co-efficients for the mixed model analysis .....	184
<b>Table 6.1:</b> Enzymes commonly used in the clinical diagnosis of disease .....	207
<b>Table 6.2:</b> HRMS of <b>TCF-ALP</b> before and 1 h after incubation with ALP .....	216
<b>Table 6.2:</b> HRMS of <b>TCF-ALP</b> before and 1 h after incubation with ALP .....	216
<b>Table 6.3:</b> Fluorescent probes and their corresponding Limit of Detection .....	219
<b>Table 7.1:</b> Table outlining Limits of Detection for fluorescent and colorimetric probes for the detection of bacterial enzymes. ....	278



# List of Figures

<b>Figure 1.1:</b> Skin anatomy viewed in a cross-section. ....	2
<b>Figure 1.2:</b> Overview of the distinct, but overlapping, phases of wound healing. ....	4
<b>Figure 1.3:</b> Wound infection continuum. ....	8
<b>Figure 1.4:</b> Formation of a biofilm. ....	10
<b>Figure 1.5:</b> SEM image of <i>S. aureus</i> MRSA252 .....	11
<b>Figure 1.6:</b> Selected <i>S. aureus</i> virulence factors .....	14
<b>Figure 1.7:</b> <i>Staphylococcal</i> biofilm cycle .....	16
<b>Figure 1.8:</b> Bacteriophage structure and lifecycles. ....	20
<b>Figure 2.1:</b> Typical growth curve of a closed-system bacterial culture .....	48
<b>Figure 2.2:</b> Schematic of the Colony Biofilm Model .....	52
<b>Figure 2.3:</b> Schematic of the plaque counting (PFU/mL) .....	53
<b>Figure 3.1:</b> Visual representation of the spot test assay.....	64
<b>Figure 3.2:</b> An example of a soft-overlay plate to detect lysogenic phage .....	71
<b>Figure 3.3:</b> OD <sub>600</sub> measurements to investigate the MOI of bacteriophage K .....	72
<b>Figure 3.4:</b> Log PFU/mL of bacteriophage K in the presence of antibiotics .....	75
<b>Figure 3.5:</b> OD <sub>600</sub> measurements for <i>S. aureus</i> H560 upon the addition of differing concentrations of bacteriophage and/or antibiotic as a single therapy/combination .....	76
<b>Figure 3.6:</b> OD <sub>600</sub> measurements for <i>S. aureus</i> MRSA252 upon the addition of differing concentrations of bacteriophage and/or antibiotic as a single therapy/combination .....	77
<b>Figure 3.7:</b> OD <sub>600</sub> measurements for <i>S. aureus</i> MSSA101 upon the addition of differing concentrations of bacteriophage and/or antibiotic as a single therapy/combination .....	79
<b>Figure 3.8:</b> Log CFU/mL of A) <i>S. aureus</i> H560, B) <i>S. aureus</i> MRSA252 and C) <i>S. aureus</i> MSSA101 in the presence of 1/2 MIC antibiotics and 10 <sup>3</sup> PFU/mL of bacteriophage K .....	81

<b>Figure 3.9:</b> Log PFU/mL of A) <i>S. aureus</i> H560, B) <i>S. aureus</i> MRSA252 and C) <i>S. aureus</i> MSSA101 in the presence of 1/2 MIC antibiotics and 10 <sup>3</sup> PFU/mL of bacteriophage K .....	83
<b>Figure 3.10:</b> SEM images of untreated <i>S. aureus</i> H560, MRSA252 and MSSA101 compared with their counterparts incubated for 18 h with 1/2 MIC of antibiotics .....	87
<b>Figure 3.11:</b> Minimum Biofilm Inhibitory Concentration of bacteriophage K .....	89
<b>Figure 3.12:</b> Determination of the ability of bacteriophage and/or antibiotics to inhibit biofilm formation of <i>S. aureus</i> H560 as a single therapy or in combination .....	91
<b>Figure 3.13:</b> Determination of the ability of bacteriophage and/or antibiotics to inhibit biofilm formation of <i>S. aureus</i> MRSA252 as a single therapy or in combination .....	92
<b>Figure 3.14:</b> Determination of the ability of bacteriophage and/or antibiotics to inhibit biofilm formation of <i>S. aureus</i> MSSA101 as a single therapy or in combination .....	93
<b>Figure 3.15:</b> Minimum Biofilm Eradication Concentration of bacteriophage K .....	94
<b>Figure 3.16:</b> Minimum Biofilm Inhibitory Concentration of antibiotics .....	95
<b>Figure 3.17:</b> Determination of the ability of antibiotics and 10 <sup>8</sup> PFU/mL phage K to eradicate <i>S. aureus</i> MRSA252 biofilms K as a monotherapy or in combination .....	96
<b>Figure 4.1:</b> Structures of lactic acid, lactide, and poly(lactic acid) .....	113
<b>Figure 4.2:</b> Structure of poly(ethylene glycol) .....	114
<b>Figure 4.3:</b> SEM of the top layer of the PLA-PEG polymer blend .....	122
<b>Figure 4.4:</b> Weight loss and water sorption of the PPEG film .....	123
<b>Figure 4.5:</b> Phage K survival in DCM and PEG 400 .....	124
<b>Figure 4.6:</b> Phage K survival at varying temperatures .....	125
<b>Figure 4.7:</b> <i>In vitro</i> release of bacteriophage K from the PPEG film .....	126
<b>Figure 4.8:</b> Phage K survival in the PPEG films .....	128
<b>Figure 4.9:</b> Log CFU/mL of <i>S. aureus</i> after incubation with bacteriophage-loaded PPEG films .....	129
<b>Figure 4.10:</b> Log PFU/mL of bacteriophage K after release from PPEG film .....	129

<b>Figure 4.11:</b> Log CFU/membrane of <i>S. aureus</i> biofilms after incubation with bacteriophage-loaded PPEG films .....	131
<b>Figure 4.12:</b> Log CFU/mL counts of the initial <i>S. aureus</i> H560 suspension, and the <i>S. aureus</i> H560 suspension after recovery from porcine skin .....	133
<b>Figure 4.13:</b> Log CFU/mL of <i>S. aureus</i> on porcine skin after incubation with bacteriophage-loaded PPEG films .....	134
<b>Figure 4.14:</b> Log PFU/mL counts of phage K after 24 h incubation of phage K-PPEG films with <i>S. aureus</i> .....	135
<b>Figure 4.15:</b> UV-Vis spectra and calibration curve of ciprofloxacin .....	136
<b>Figure 4.16:</b> <i>In vitro</i> release of ciprofloxacin from the PPEG film .....	137
<b>Figure 4.17:</b> Ciprofloxacin stability in the PPEG films .....	138
<b>Figure 4.18:</b> Log CFU/mL of <i>S. aureus</i> after incubation with ciprofloxacin-loaded PPEG films .....	139
<b>Figure 4.19:</b> Log CFU/membrane of <i>S. aureus</i> biofilms after incubation with ciprofloxacin-loaded PPEG films .....	141
<b>Figure 4.20:</b> Log CFU/mL of <i>S. aureus</i> on porcine skin after incubation with bacteriophage-loaded PPEG films .....	142
<b>Figure 4.21:</b> Concentration of phage K (displayed as Log PFU/mL) and ciprofloxacin after 5 days incubation at room temperature within the PPEG film .....	143
<b>Figure 4.22:</b> Log CFU/mL of <i>S. aureus</i> after incubation with combination-loaded PPEG films .....	145
<b>Figure 4.23:</b> Log PFU/mL counts of phage K after 24 h incubation of combination-loaded PPEG films with <i>S. aureus</i> .....	146
<b>Figure 4.24:</b> Log CFU/membrane of <i>S. aureus</i> biofilms after incubation with combination-loaded PPEG films .....	147
<b>Figure 4.25:</b> Log CFU/mL of <i>S. aureus</i> on porcine skin after incubation with combination-loaded PPEG films .....	148

<b>Figure 5.1:</b> Schematic of a novel pH-responsive wound dressing for the treatment of chronic wounds. ....	157
<b>Figure 5.2:</b> pH values associated with developing <i>S. aureus</i> biofilms. ....	168
<b>Figure 5.3:</b> Chemical structure of EUDRAGIT® FS 30 D .....	170
<b>Figure 5.4:</b> Phage K survival in the presence of acetone and increasing pH. ....	171
<b>Figure 5.5:</b> <i>In vitro</i> release of bacteriophage K from the pH-responsive films .....	172
<b>Figure 5.6:</b> Log PFU/mL of bacteriophage K released from the pH-responsive system upon incubation in PBS, pH 6.50 .....	173
<b>Figure 5.7:</b> Log CFU/membrane counts of <i>S. aureus</i> biofilms upon incubation with bacteriophage-loaded pH-responsive systems .....	175
<b>Figure 5.8:</b> Log PFU/membrane counts of phage K released from the pH-responsive film after incubation with <i>S. aureus</i> biofilms.....	176
<b>Figure 5.9:</b> Concentration of ciprofloxacin released from pH-responsive systems with increasing EUDRAGIT® layers .....	177
<b>Figure 5.10:</b> <i>In vitro</i> release of ciprofloxacin from the pH-responsive films, pH 8.00 .	177
<b>Figure 5.11:</b> Release of ciprofloxacin from the pH-responsive films, pH 6.50 .....	179
<b>Figure 5.12:</b> Log CFU/membrane counts of <i>S. aureus</i> biofilms upon incubation with bacteriophage-loaded pH-responsive systems .....	180
<b>Figure 5.13:</b> Release of bacteriophage K from the pH-responsive films, pH 6.50 .....	181
<b>Figure 5.14:</b> Release of ciprofloxacin from the pH-responsive films, pH 6.50 .....	182
<b>Figure 5.15:</b> Log CFU/membrane counts of <i>S. aureus</i> biofilms upon incubation with combination-loaded pH-responsive systems .....	183
<b>Figure 5.16:</b> Log PFU/membrane counts of phage K released from the pH-responsive film after incubation with <i>S. aureus</i> biofilms.....	184
<b>Figure 6.1:</b> Schematic of a Jablonski diagram .....	196

<b>Figure 6.2:</b> Diagram depicting the excitation and emission spectra of a fluorescent molecule, and the corresponding stokes shift. ....	197
<b>Figure 6.3:</b> Photoinduced electron transfer (PET) quenching by a donor (D). ....	199
<b>Figure 6.4:</b> Energy diagram for FRET .....	200
<b>Figure 6.5:</b> Schematic representation of the ESIPT process .....	201
<b>Figure 6.6:</b> Energy diagram correlating ICT with solvation, in polar solvents. ....	202
<b>Figure 6.7:</b> Energy diagram depicting a catalysed and un-catalysed reaction .....	203
<b>Figure 6.8:</b> Schematic of enzyme-substrate binding .....	204
<b>Figure 6.9:</b> Relative fluorescence intensity of <b>TCF-ALP</b> (10 $\mu$ M) at pH 3 – 10 .....	215
<b>Figure 6.10:</b> $^{31}\text{P}$ NMR monitoring of <b>TCF-ALP</b> in the presence of ALP .....	215
<b>Figure 6.11:</b> UV-Vis spectra of <b>TCF-ALP</b> (10 $\mu$ M) with and without ALP .....	216
<b>Figure 6.12:</b> Time drive of <b>TCF-ALP</b> (10 $\mu$ M) with the addition of ALP .....	217
<b>Figure 6.13:</b> Fluorescence spectra of <b>TCF-ALP</b> (10 $\mu$ M) produced via the addition of ALP (0 – 0.2 U/mL) .....	218
<b>Figure 6.14:</b> Relative fluorescence intensity versus ALP concentration .....	218
<b>Figure 6.15:</b> : Fluorescence intensity of <b>TCF-ALP</b> (10 $\mu$ M) in the presence of 0.8 U/mL of ALP pre-treated for 30 minutes with $\text{Na}_3\text{VO}_4$ (0.0 – 2000 $\mu$ M).....	220
<b>Figure 6.16:</b> Inhibition study of <b>TCF-ALP</b> (10 $\mu$ M) in the presence of different concentrations of $\text{Na}_3\text{VO}_4$ . ....	220
<b>Figure 6.17:</b> Selectivity assay at each enzyme's optimal pH .....	222
<b>Figure 6.18:</b> Selectivity of ALP and ACP at pH 7.1 .....	222
<b>Figure 6.19:</b> Selectivity of ALP and ACP at pH 5.0.....	223
<b>Figure 6.20:</b> Selectivity of ALP and ACP at pH 9.2 .....	223
<b>Figure 6.21:</b> Time-dependent fluorescence intensity seen for increasing concentrations of <b>TCF-ALP</b> (0 – 20 $\mu$ M) in the presence of 0.2 U/mL of ALP, pH 9.2.....	224

<b>Figure 6.22:</b> Time-dependent fluorescence intensity seen for increasing concentrations of TCF-ALP (0 – 20 $\mu$ M) in the presence of 0.2 U/mL of ALP, pH 7.1. ....	225
<b>Figure 6.23:</b> Time-dependent fluorescence intensity seen for increasing concentrations of TCF-ALP (0 – 20 $\mu$ M) in the presence of 0.2 U/mL of ACP, pH 7.1.....	225
<b>Figure 6.24:</b> MTT cytotoxicity assay for TCF-ALP .....	226
<b>Figure 6.25:</b> Images of HeLa cells treated with TCF-ALP .....	227
<b>Figure 6.26:</b> Images of C2C12 cells treated with TCF-ALP .....	228
<b>Figure 7.1:</b> Chemical structure of 4-methylumbelliferyl- $\beta$ -D-glucuronide (MUG) and 6-chloro-4-methylumbelliferyl- $\beta$ -D-glucuronide (CMUG). ....	252
<b>Figure 7.2:</b> Chemical structure of 5-bromo-4-choro- $\beta$ -D-glucuronic acid (X- $\beta$ -gluc) and schematic of the paper-based device using this probe .....	253
<b>Figure 7.3:</b> Chemical structure of 4-MU and its derivatives .....	255
<b>Figure 7.4:</b> Chemical structures of DDAO-AME 1 and DDAO-AME 2 .....	257
<b>Figure 7.5:</b> Chemical structures of probes, 5 and 6 .....	258
<b>Figure 7.6:</b> Chemical structures of probes, 7 and 8 .....	259
<b>Figure 7.7:</b> Chemical structure of CDC-599 .....	261
<b>Figure 7.8:</b> Chemical structure of CB-1, CPC-1, and 1b .....	262
<b>Figure 7.9:</b> UV-Vis spectra of TCF-ALP (10 $\mu$ M) after 24 h incubation at 32 $^{\circ}$ C with <i>S. aureus</i> NCTC 10788 .....	270
<b>Figure 7.10:</b> ALP activity of <i>S. aureus</i> NCTC 10788 ( $10^8$ CFU/mL) grown in Mueller Hinton, LB or TSB after 1 h .....	271
<b>Figure 7.11:</b> ALP activity of <i>S. aureus</i> NCTC 10788 ( $10^8$ CFU/mL) grown in Mueller Hinton, LB or TSB after 24 h .....	272
<b>Figure 7.12:</b> Log CFU/mL of <i>S. aureus</i> NCTC 10788 after increasing wash cycles .....	273
<b>Figure 7.13:</b> Change in fluorescence ( $I/I_0$ ) of TCF-ALP (10 $\mu$ M) after 1 h and 24 h incubation with <i>S. aureus</i> NCTC 10788 upon various incubation temperatures.....	274

<b>Figure 7.14:</b> Fluorescence spectra of <b>TCF-ALP</b> (10 $\mu$ M) recorded over 24 h upon addition of <i>S. aureus</i> NCTC 10788 .....	275
<b>Figure 7.15:</b> Limit of detection of <b>TCF-ALP</b> after 1 h .....	276
<b>Figure 7.16:</b> Limit of detection of <b>TCF-ALP</b> after 24 h .....	277
<b>Figure 7.17:</b> Selectivity bar chart of <b>TCF-ALP</b> (10 $\mu$ M) after 24 h incubation with various bacterial strains .....	280
<b>Figure 7.18:</b> Selectivity bar chart of <b>TCF-ALP</b> (10 $\mu$ M) after 1 h incubation with various <i>S. aureus</i> strains .....	281
<b>Figure 7.19:</b> Selectivity bar chart of <b>TCF-ALP</b> (10 $\mu$ M) after 24 h incubation with various <i>S. aureus</i> strains .....	282
<b>Figure 7.20:</b> Fluorescence spectra of <b>TCF-ALP</b> (10 $\mu$ M) after 1 h incubation with a 96-well plate biofilm of <i>S. aureus</i> NCTC 10788 .....	284
<b>Figure 7.21:</b> Fluorescence spectra of <b>TCF-ALP</b> (10 $\mu$ M) after 24 h incubation with a 96-well plate biofilm of <i>S. aureus</i> NCTC 10788 .....	285
<b>Figure 7.22:</b> Fluorescence intensity of <b>TCF-ALP</b> upon increasing inhibitor concentrations after 1 h incubation .....	286
<b>Figure 7.23:</b> Fluorescence intensity of <b>TCF-ALP</b> upon increasing inhibitor concentrations after 24 h incubation .....	286
<b>Figure 7.24:</b> Fluorescence spectra of <b>TCF-ALP</b> (10 $\mu$ M) after 1 h incubation with biofilms of <i>S. aureus</i> NCTC 10788 .....	287
<b>Figure 7.25:</b> Fluorescence spectra of <b>TCF-ALP</b> (10 $\mu$ M) after 24 h incubation with biofilms of <i>S. aureus</i> NCTC 10788 .....	288
<b>Figure 7.26:</b> Images of biofilms of <i>S. aureus</i> NCTC 10788 after 0, 1, and 24 h incubation with 10 $\mu$ M <b>TCF-ALP</b> .....	288
<b>Figure 7.27:</b> Fluorescence spectra of <b>TCF-ALP</b> (10 $\mu$ M) after 1 h incubation with biofilms of <i>E. coli</i> NSM59 and <i>P. aeruginosa</i> PAO1 .....	289
<b>Figure 7.28:</b> Fluorescence spectra of <b>TCF-ALP</b> (10 $\mu$ M) after 1 h incubation with biofilms of <i>E. coli</i> NSM59 and <i>P. aeruginosa</i> PAO1 .....	289

<b>Figure 7.29:</b> Images of biofilms of <i>E. coli</i> NSM59 and <i>P. aeruginosa</i> PAO1 after 0, 1, and 24 h incubation with 10 $\mu$ M <b>TCF-ALP</b> .....	290
<b>Figure 7.30:</b> Fluorescence spectra of <b>TCF-ALP</b> (10 $\mu$ M) after 24 h incubation with <i>S. aureus</i> NCTC 10788 inoculated porcine skin .....	291
<b>Figure 7.31:</b> Images of <b>TCF-ALP</b> after 24 h incubation with <i>S. aureus</i> NCTC 10788 on porcine skin.....	291
<b>Figure 7.32:</b> 10% w/v PVA hydrogel loaded with 100 $\mu$ M of <b>TCF-ALP</b> in PBS, pH = 7.4 .....	294
<b>Figure 7.33:</b> Images taken of 10% w/v PVA hydrogels loaded with 100 $\mu$ M <b>TCF-ALP</b> at 0 – 8 h and 24 h incubation with <i>S. aureus</i> NCTC 10788 planktonic culture .....	295
<b>Figure 7.34:</b> Fluorescence spectra of <b>TCF-ALP</b> (100 $\mu$ M) in a 10% w/v PVA hydrogel after 24 h incubation at 32 $^{\circ}$ C with planktonic cultures of <i>S. aureus</i> NCTC 10788 .....	296
<b>Figure 7.35:</b> Images taken of 10% w/v PVA hydrogels loaded with 100 $\mu$ M <b>TCF-ALP</b> at 0 – 8 h and 24 h incubation with <i>S. aureus</i> NCTC 10788 biofilms .....	297
<b>Figure 7.36:</b> Fluorescence spectra of <b>TCF-ALP</b> (100 $\mu$ M) in a 10% w/v PVA hydrogel after 24 h incubation at 32 $^{\circ}$ C with <i>S. aureus</i> NCTC 10788 biofilms.....	298
<b>Figure 7.37:</b> Images taken of 10% w/v PVA hydrogels loaded with 100 $\mu$ M <b>TCF-ALP</b> after 24 h incubation with <i>S. aureus</i> NCTC 10788 on porcine skin .....	299
<b>Figure 7.38:</b> Fluorescence spectra of <b>TCF-ALP</b> (100 $\mu$ M) in a 10% w/v PVA hydrogel after 24 h incubation at 32 $^{\circ}$ C with <i>S. aureus</i> NCTC 10788 on porcine skin .....	299





# Chapter 1: Introduction

## 1.1. Clinical Problem

Chronic wounds are a global health problem, often affecting patients older than 60 years of age.<sup>1</sup> In developed countries, chronic wounds are prevalent in 1 – 2% of the general population,<sup>2</sup> and the NHS spends approximately £4.5 – 5.1 billion per annum on wound care, after adjusting for co-morbidities.<sup>3</sup> In addition to physical consequences, chronic wounds have a negative effect on the patient's quality of life and can lead to a range of psychological issues such as depression, anxiety and embarrassment, all of which can lead to social isolation, further perpetuating psychological illness. Renner *et al* reported that at least 30% of patients with chronic wounds have symptoms of depression and anxiety;<sup>4</sup> therefore, it is imperative that new management techniques are implemented to help diagnose, manage, and treat chronic wounds to improve patient's lives and reduce the economic burden placed on healthcare settings.

For successful management of chronic wounds, it is important to detect the presence of any bacterial pathogens within the wound that may be impeding healing. Methods to obtain bacteriological samples include swabbing, needle aspiration, and wound biopsy; the most common technique is wound swabbing, although this may not result in an accurate depiction of the bacterial topology within the wound environment as it mainly detects surface colonising bacteria.<sup>5</sup> Additionally, these techniques are often invasive and painful; hence, most clinicians often rely on other clinical indications (e.g., pain, erythema, and oedema) to diagnose wound infections before resorting to microbiological assessment.<sup>6,7</sup>

Regardless of the sampling technique used, clinical assessment of infection is performed via standardised microbiological tests that have inherent limitations including the time-consuming protocols and the need for trained specialists. Additionally, it has been stated that traditional culturing methodology only identifies 1% of the bacteria within chronic wounds,<sup>8–10</sup> resulting in the patient receiving inaccurate antibiotic therapy, perpetuating antibiotic resistance and ensuing the non-healing nature of the wound.

Owing to the issues in wound sampling and the need for rapid determination of the causative pathogenic bacteria, there is a growing need to create novel 'smart' systems that can accurately and rapidly detect or treat pathogenic bacteria within wounds, without the need of invasive, painful sampling techniques and time consuming microbiological analysis.

## 1.2. Wounds and Wound Healing

The skin is the largest organ in the body, acting as a first line of defence against pathogenic microbial infections.<sup>11,12</sup> Skin is composed of two layers, the epidermis and dermis. The epidermis is avascular and is composed of keratinized, stratified squamous epithelium; while the dermis is composed of two layers of connective tissue containing blood and lymph vessels, nerves, hair follicles and sweat glands. The skin is connected to the underlying fibrous tissue of the bones and muscles via the hypodermis (Figure 1.1).

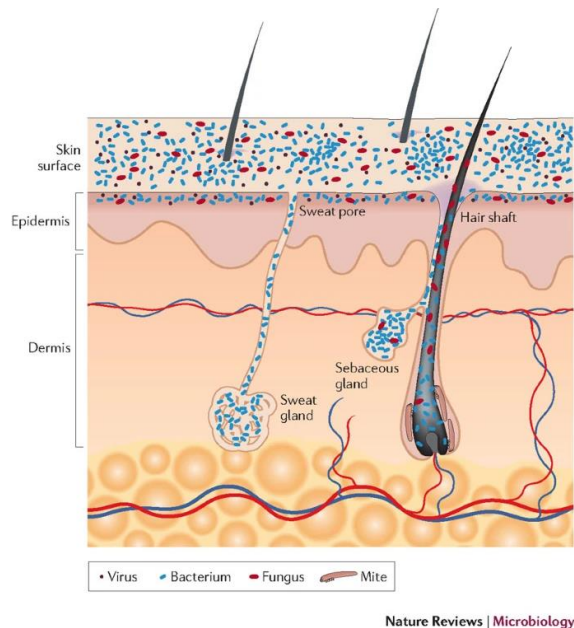


**Figure 1.1:** Skin anatomy viewed in a cross-section. Reprinted from Grice et al with permission. Copyright © 2011, Nature Publishing Group

### 1.2.1. Types of Wound

According to the Wound Healing Society, a wound is the “*disruption of normal anatomic structure and function*”.<sup>13</sup> Wounds can be classified as either acute or chronic depending on the nature of the repair process.<sup>14</sup> Acute wounds are typically caused by cuts or surgical incisions that complete the wound healing process in a timely and expected manner and result in sustained restoration of anatomic and functional integrity.<sup>13</sup> Conversely, chronic wounds are wounds that fail to heal within the expected time frame due to repeated damage to the tissue or underlying co-morbidities that interfere with the wound healing process.<sup>15,16</sup> Chronic wounds are also defined as wounds that have proceeded through the healing process without sustained anatomical and functional integrity.<sup>13</sup> Examples include venous ulcers, diabetic foot ulcers, and pressure ulcers.<sup>17</sup>

## 1.2.2. Wound Healing and the Wound Healing Cascade

Wound healing starts immediately after injury and involves the removal of damaged tissue and restoration of the skin integrity.<sup>18</sup> Healing is defined by the Wound Healing Society as a “*complex and dynamic process that results in the restoration of anatomic continuity and function*”.<sup>13</sup>

The different types of wound healing (primary, secondary, or tertiary intention) are categorised based on the anticipated nature of the repair process.<sup>14</sup> Wound healing by primary intention involves the approximation of wound edges by sutures, clips, or skin adhesion. Primary intention is often seen for injuries where minimal epithelialization and new tissue are needed to repair the skin defect, resulting in slight scarring.<sup>19,20</sup>

Secondary intention occurs when the wound edges cannot be approximated, and as such, the wound is left open to heal via the production of connective tissue, following the steps of the wound healing cascade. Secondary intention is often witnessed for patients with underlying co-morbidities, or in patients with post-surgical wound dehiscence. Secondary intention wounds are often slow to heal and prone to complications (e.g., infections), further delaying the wound healing process.<sup>18</sup> Additionally, this intention can be associated with substantial scarring.<sup>19,21</sup>

Finally, wound healing via tertiary intention is where the wound is left open until any contaminants, non-viable tissue, or infection is removed; after this, the wound edges are approximated, and healing continues via primary intention.<sup>18</sup> This intention is also known as “delayed primary intention” in literature.<sup>14</sup>

The physiologic process of wound healing is complex, consisting of a cascade of sequential yet overlapping physiological processes.<sup>14</sup> For the purposes of this chapter, the general stages of wound healing described by Schultz are used (haemostasis, inflammation, proliferation, and remodelling; Figure 1.2).<sup>16</sup> Haemostasis occurs immediately after injury and is usually complete within hours, inflammation begins shortly after haemostasis and lasts for up to 72 h after injury<sup>12</sup> – although wounds can remain in this phase for several days after injury. Proliferation generally occurs 1 – 3 weeks after injury, and remodelling occurs 3 weeks after injury, but could take up to one year to be completed.<sup>15,20</sup>

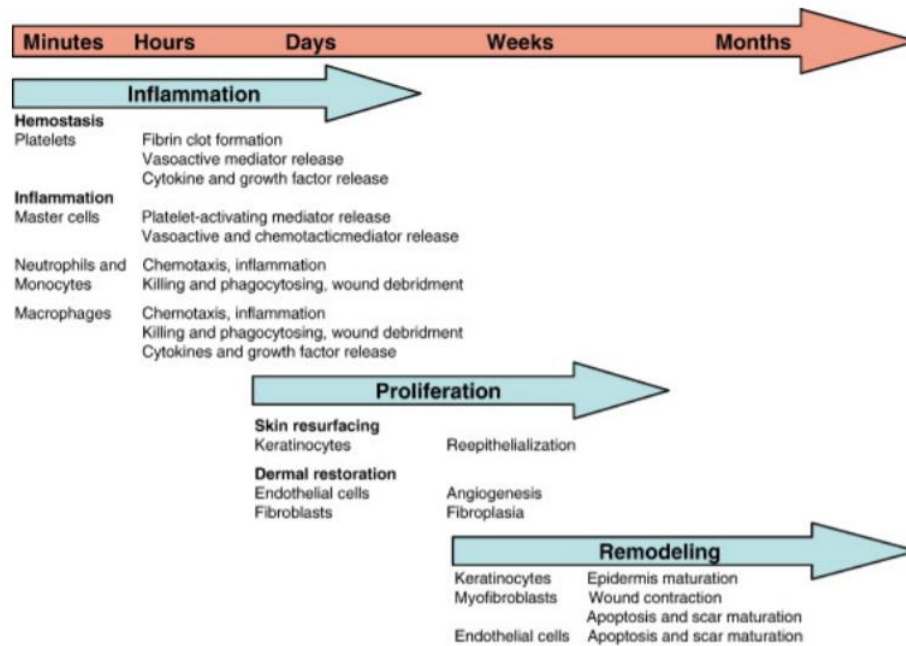


**Figure 1.2:** Overview of the distinct, but overlapping, phases of wound healing.

### 1.2.2.1. Haemostasis

Immediately after injury, vasoconstriction occurs to prevent further blood loss. This arises when clotting factors are released by the injured skin cells, activating the clotting cascade.<sup>22,23</sup> Additionally, platelets adhere to the wall of the injured blood vessels and to the exposed collagen within the extracellular matrix, triggering the release of cytokines (signalling molecules that are secreted by certain cells of the immune system that mediate and regulate immunity, inflammation, and haematopoiesis), growth factors, and pro-inflammatory mediators. This, in turn, results in platelet aggregation, activating the intrinsic and extrinsic coagulation pathways that lead to fibrin clot formation, which seals the exposed blood vessels, preventing further blood loss<sup>24</sup> and creates a temporary seal over the wound to prevent microbial infection.<sup>14</sup> Additionally, the fibrin clot acts as a scaffold, supporting the influx of fibroblasts and keratinocytes into the wound bed.<sup>25</sup>

Platelet activation results in the release of potent cytokines that initiate the wound healing cascade. The specific mechanisms mediated by these cytokines include the activation of the inflammatory response and proliferation of new cells (epithelialization) and blood vessels (angiogenesis) at the injury site.<sup>14</sup> For example, platelet-derived growth factor (PDGF) initiates the chemotaxis of neutrophils, macrophages, smooth muscle cells, and fibroblasts. Furthermore, transforming growth factor-beta (TGF- $\beta$ ) attracts macrophages to the wound area and stimulates them to produce additional cytokines, such as fibroblast growth factor (FGF), PDGF, tumour necrosis alpha (TNF $\alpha$ ) and interleukin-1 (IL-1).<sup>18</sup>

### **1.2.2.2. Inflammation**

The inflammatory response is triggered by tissue injury and the activation of the coagulation cascade, increasing the local vasodilation and capillary permeability, which subsequently allows for the migration of monocytes into the wound bed.<sup>18</sup>

Within minutes, neutrophils accumulate within the wound bed to remove any microorganisms present via phagocytosis.<sup>12,14,15</sup> Neutrophils also contribute to wound healing by activating local fibroblasts and epithelial cells.<sup>26</sup> After 2 – 3 days, neutrophils leave the wound bed via apoptosis, unless the wound becomes infected; in which case, neutrophil infiltration continues until the infection is controlled.<sup>15,23</sup>

In the absence of infection, monocytes differentiate into macrophages, which are arguably the most important cell within the wound healing process as any inhibition of macrophage function results in a delay in wound healing.<sup>18,27</sup> Macrophages remove non-viable cells, bacteria-filled neutrophils, damaged extracellular matrix, debris, and any bacteria from the wound site; they also release PDGF and TGF- $\beta$  to further attract fibroblasts and smooth muscle cells into the wound site.<sup>18</sup>

The responsibility of the inflammatory phase is to control the bleeding and removal of any contaminants. If the wound is following the normal wound healing process, this phase should take approximately three days to complete; however, if the wound bed is contaminated, or becomes infected, then the inflammation phase will be prolonged.<sup>18</sup>

### **1.2.2.3. Proliferation**

Generally, there is an overlap between the inflammation phase and the proliferation phase,<sup>18</sup> with the latter focusing on re-epithelization, restoration of the vascular integrity to the region, and repair of the structural integrity of the tissue defect by creating new connective tissue (granulation).<sup>27,28</sup>

During the proliferative phase, the wound is hypoxic, and the partial pressure of oxygen decreases to about 10 mm Hg.<sup>14</sup> This hypoxic environment induces the release of hypoxia-inducible factor (HIF), which regulates the expression of vascular endothelial growth factor (VEGF). VEGF, in combination with basic fibroblast factor (bFF), and TGF- $\beta$  activate neovascularization or angiogenesis along the wound edges.<sup>12,18</sup> Simultaneously, the endothelial cells produce enzymes that breakdown the adjacent extracellular matrix to create tissue defects, which allow the capillary vessels to infiltrate the tissue to form a network to restore vascularity. As a consequence, this process of angiogenesis is

interdependent on the production of new extracellular matrix, which acts as a scaffold to support the newly formed blood vessels.<sup>18</sup>

Re-epithelization of a wound occurs when stimulated keratinocytes proliferate and migrate across the wound bed,<sup>19</sup> prior to upward migration and differentiation, which occurs until the epidermis regains its normal thickness and stratification.<sup>18</sup> Keratinocytes can only migrate over a moist, vascular wound surface,<sup>29</sup> if the wound surface is not moist, keratinocytes secrete proteolytic enzymes that enable it to burrow into the wound bed to find the necessary moisture for migration.<sup>15,30</sup> When the skin is completely covered with epidermal cells, the wound is considered closed; it has been shown that the chance of developing hypertrophic scar tissue is greatly reduced by early wound closure.<sup>19</sup>

The final mechanism of the proliferation phase is the formation of granulation tissue.<sup>14</sup> The fibrin clot created in the haemostasis phase is replaced by fibronectin, hyaluronic acid, and other extracellular matrix components, which promote cell migration and proliferation. Fibroblasts are the main cell responsible for the formation of granulation tissue as they attach to the provisional fibrin matrix and begin collagen production. These fibroblasts responsible for the granulation tissue have been activated into wound fibroblasts that have decreased proliferative activity and increased collagen production behaviour. Initially, the type of collagen is 'type 3', with limited tensile strength. Over time, collagen matures to 'type 1 collagen' that is normally found in dermal tissue.<sup>18</sup>

It is important to mention that contraction can occur in open wounds, which is beneficial to the wound healing process as the less granulation tissue required, the quicker the healing time.<sup>31</sup> While it is currently unknown how contraction works, three theories have been proposed: modified fibroblasts are responsible for generating contractile forces that pull the wound edges together,<sup>32</sup> wound fibroblasts act collectively to contract the connective tissue matrix,<sup>33</sup> and newly formed collagen fibres produce a pulling force on the surrounding tissues.<sup>34</sup>

#### **1.2.2.4. Remodelling**

The final stage of wound healing is remodelling, where the granulation tissue matures into connective and scar tissue.<sup>14</sup> The remodelling phase can last for up to one year, during which fibroblasts regulate the process of wound matrix breakdown by metalloproteinases (MMPs). This process slowly increases the strength of the wound; however, scar tissue is only 80% as strong as unwounded tissue. Occasionally, an imbalance in matrix degradation and synthesis are disrupted, resulting in abnormal scar formation (e.g. keloid or hypertrophic scarring).<sup>18</sup>

### 1.2.3. Delayed Wound Healing

There are several factors that may impede wound healing;<sup>35</sup> they are briefly outlined in Table 1.1. In terms of microbial infections, the prolonged time spent within the inflammation phase leads to continued regulation of inflammatory cytokines, which in turn result in the increased production of proteases, reactive oxygen species, and MMPs that degrade collagen, leading to delayed wound healing.<sup>36</sup>

**Table 1.1:** Local and systemic factors that may impede wound healing. Adapted from Grey *et al*<sup>35</sup>

<b>Local factors</b>	<b>Systemic factors</b>
Inadequate blood supply	Age and immobility
Increased skin tension	Obesity
Poor surgical apposition	Smoking
Wound dehiscence	Malnutrition
Poor venous drainage	Illness
Infection	Immunosuppressant drugs, corticosteroids, anticoagulants

### 1.3. Wound Infection

Upon a breach of the epidermal layer, the subcutaneous tissue is exposed, resulting in a moist and warm environment containing devitalised tissue that is favourable for microbial colonisation and proliferation. Typical signs of infection include heat, pain, oedema, erythema, purulence, and loss of function within the wound area. Indications for chronic wounds also include friable granulation tissue, wound breakdown, pain, and odour.<sup>11,37</sup>

All wounds are colonised with bacteria from either endogenous or exogenous sources,<sup>37,38</sup> and the development of an infection follows the “wound infection continuum” (Figure 1.3). This continuum consists of five stages of wound infection, ranging from contamination through to a systemic infection.<sup>7</sup> However, there is no consensus as to when the wound shifts from colonised to infected – a phenomenon previously called “critical colonisation”<sup>7,17</sup> Cutting *et al* suggested that the critical colonisation of bacteria is where the wound has become compromised by bacteria, resulting in delayed wound healing without any clinical symptoms associated with infection.<sup>39</sup>



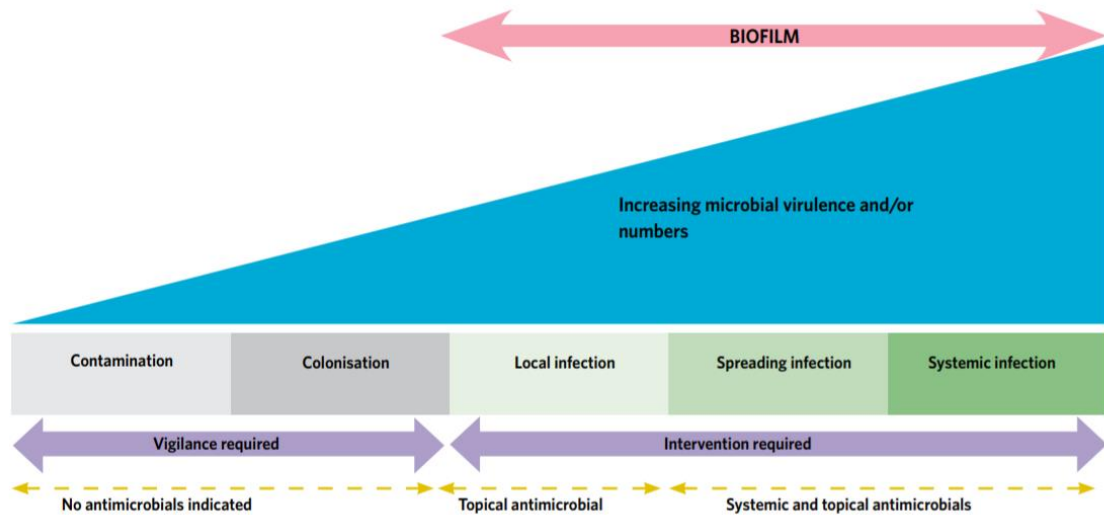


**Figure 1.3:** Wound infection continuum. Reproduced from Wounds International with permission.<sup>40</sup>  
 Copyright © 2016, Wounds International

Clinically, the definition of a wound infection, or a strong propensity to develop an infection, occurs when concentration of cultivable bacteria from a tissue biopsy or a swab exceeds  $10^5$  colony forming units per gram (CFU/g).<sup>5,41</sup> At this concentration, the host’s immune system is no longer able to control the proliferation of the bacterial species,<sup>42,43</sup> resulting in a local infection, delayed wound healing, and the need for clinical intervention (e.g., antimicrobial treatment, debridement).<sup>38</sup> This has been shown in literature, where wounds with  $>10^6$  CFU/g tissue, between  $10^5 - 10^6$  CFU/g tissue, and no microbial bioburden, healed at a rate of 0.05 cm, 0.15 cm, and 0.2 cm per week, respectively.<sup>44</sup>

However, this guideline fails to consider the polymicrobial nature of the wound and the potential for synergistic interactions between microbes, which could result in clinically infected wounds at lower bacterial concentrations.<sup>5</sup> Therefore, a system such as the “critical infection threshold” may be more apt as it encompasses multiple markers of infection that cannot be explained by the bacterial concentration alone.

### 1.3.1. Microbiology of Chronic Wounds

Traditional culturing methods to detect pathogenic bacteria in chronic wounds only identify approximately 1% of the pathogens present at the wound site,<sup>8</sup> due to the bacteria within the wound existing as a viable, but nonculturable (VBNC) state, often in response to environmental triggers such as antimicrobial exposure, low pH and nutrient availability, and hypoxia.<sup>45,46</sup> The VBNC state is challenging as it may lead to an underestimate of the

bacterial bioburden within the wound, owing to the VBNC bacteria being unable to be cultured on conventional agar plates.<sup>47</sup>

The bacterial species present within chronic wounds changes over time; however, *Staphylococcus aureus* and coagulase-negative staphylococci are among the most frequently isolated bacterial species within chronic wounds.<sup>7</sup> Hannson *et al* showed that *S. aureus* was present in 88% of venous leg ulcers that had no clinical signs of infection, closely followed by *Enterococcus faecalis* (74%), *Enterobacter cloacae* (29%), and *Peptococcus magnus* (29%).<sup>48</sup> This observation was further supported by Gjødsbøl *et al* who found that *S. aureus* was the most frequently identified bacteria within chronic venous leg ulcers<sup>49</sup> and by Frank *et al*, who found that 25% of chronic wounds were isolated with *Staphylococcus* spp.<sup>50</sup>

Anaerobic bacteria are often overlooked in conventional microbiological assessments of chronic wounds; however, chronic wounds have a statistically higher proportion of anaerobes compared to acute wounds (2.0 species vs 1.1 species, respectively; p=0.05). Common anaerobes within chronic wounds include *Prevotella* spp., *Peptostreptococcus* spp., and *Porphyromonas*.<sup>51,52</sup>

### **1.3.2. Biofilm Formation**

Bacteria can exist in a planktonic state or as sessile cells within a bacterial community, called a biofilm. Biofilms are defined as a complex three-dimensional community of microorganisms surrounded by an extracellular polymeric substance (EPS). The EPS consists of polysaccharides, proteins, glycoproteins, lipids, metal ions, and extracellular DNA (eDNA);<sup>38,53,54</sup> the composition of the EPS determines the biofilm architecture.<sup>38</sup>

Biofilms are reported in approximately 60 – 80% of chronic wounds<sup>55–57</sup> and are thought to cause the wounds to remain in the inflammatory phase of wound healing – resulting in the non-healing nature that is characteristic of these types of wounds. Conversely, biofilms are associated with only 6% of acute wounds.<sup>55</sup>

The development of a biofilm occurs through five discrete, well-regulated processes (Figure 1.4); however, the exact mechanisms of biofilm formation can differ between bacterial species. Generally speaking, the formation of a biofilm starts with microbial attachment to an abiotic or biotic surface, leading to the cell proliferation and the formation of microcolonies within the EPS and finally towards maturation and dissemination of the microbial cells.<sup>38</sup>

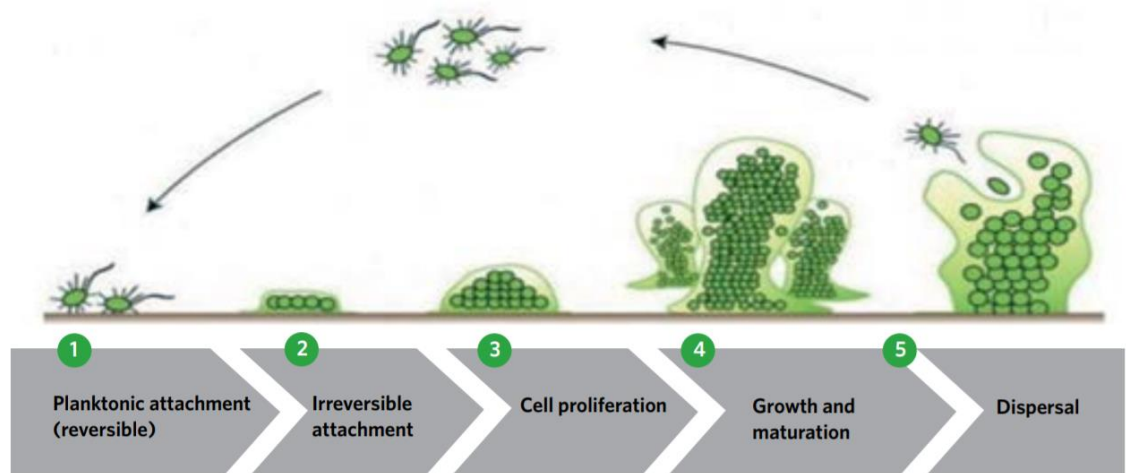


**Figure 1.4:** Formation of a biofilm. Reproduced from Wounds International with permission.<sup>40</sup> Copyright © 2016, Wounds International

Attachment of microbial cells onto a surface, or to each other at a surface interface (i.e., air-water), is facilitated through weak interactions between the surface and attachment appendages on the microbial cell surface and adhesion molecules.<sup>38,58,59</sup>

After attachment, the biofilm grows via the proliferation of cells or recruitment of new cells to the biofilm. Upon development of the biofilm, the EPS is produced to provide structure and integrity to the biofilm.<sup>60</sup>

The development of a biofilm is structurally and metabolically heterogenous and is constantly changing.<sup>38</sup> Upon increasing bacterial concentration, bacteria produce quorum sensing molecules that accumulate in the environment that aid in microbial communication to help co-ordinate the development of the biofilm through processes such as enzyme production, toxin production, and managing microbial growth rates.<sup>5,38</sup> A developing biofilm is composed of approximately 10 – 20% bacterial cells and 80 – 90% EPS.<sup>54</sup> If the biofilm is polymicrobial in nature, the individual microbial species can share defence advantages, such as molecules that aid in antimicrobial resistance or protection from phagocytosis.<sup>61–63</sup>

The three-dimensional structure develops as the biofilm becomes more complex; the structure is dependent on the bacteria present, but is often depicted as that of a mushroom (Stage 4, Figure 1.4).<sup>64–66</sup> Water channels are formed to delivery nutrients and remove waste to adjoining microcolonies.<sup>38</sup>

To colonise new surfaces, microbial cells are removed from the biofilm via shedding, detachment or shearing. These released cells retain the characteristics of the parent biofilm before reforming on a new surface.<sup>38</sup>

A mature biofilm can develop resistance to the host's immune cells (e.g., neutrophils and macrophages) and conventional antimicrobials, making the infection harder to treat and further delaying the wound healing process.<sup>38</sup> The increased resistance is due to a multitude of factors, including the limited diffusion of the antimicrobials through the dense and negatively charged EPS, induced expression of efflux pumps, and secretion of molecules and enzymes that bind or inactivate antimicrobial agents. Additionally, some bacteria within a biofilm are metabolically inactive, further preventing the effectiveness of antimicrobials.<sup>62,67-73</sup>

## 1.4. *Staphylococcus aureus*

*S. aureus* is a gram-positive bacterium, whose name derives from its tendency to grow in grape-like clusters of golden colonies (Figure 1.5).<sup>74,75</sup> Unlike other *Staphylococci* spp. (e.g., *Staphylococcus epidermidis*), *S. aureus* is able to produce the pigment, carotenoid, and the enzyme, coagulase.<sup>74</sup> The presence of the latter has been used extensively in microbiological assays to distinguish *S. aureus* from other *Staphylococci* spp. (who are frequently referred to as coagulase negative *Staphylococci*).<sup>76</sup> While the growth of *S. aureus* is optimum in aerobic conditions at incubation temperatures between 35 – 40 °C,<sup>75</sup> *S. aureus* is a facultative anaerobe; therefore, it is capable of growing in anaerobic conditions.<sup>74</sup>

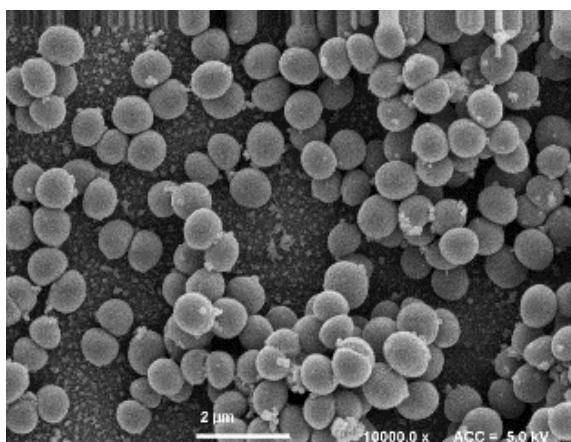


**Figure 1.5:** Scanning Electron Microscopy (SEM) image of planktonic *S. aureus* MRSA252

*S. aureus* is an opportunistic pathogen, first identified in purulent fluid from a leg abscess by Ogston in the 1880s.<sup>77</sup> *S. aureus* primarily colonises the upper respiratory tract, such as the throat and the anterior nares, but it has also been shown to be present on the scalp and hands.<sup>75</sup> It has been reported that up to 30% of individuals have anterior nares colonised with *S. aureus*,<sup>74,77,78</sup> although some reports have stated that it could be as high as 50%, as the frequency of asymptomatic carriage varies from one study to another. Researchers have noted two distinct patterns of colonisation: intermittent and persistent *S. aureus* carriage.<sup>75</sup>

### 1.4.1. Virulence Factors and Regulators

Upon breach of the skin barrier, *S. aureus* has the capability to produce a wide range of diseases, such as skin and soft tissue infection, toxic shock syndrome, necrotizing pneumonia, bacteraemia, and endocarditis<sup>74,77,79</sup> The capability of *S. aureus* to cause such a myriad of disease is associated with the ability of *S. aureus* to produce numerous virulence factors that aid in invasion and dissemination of the pathogen (Section 1.4.2).<sup>74,76</sup>

#### 1.4.1.1. Regulators

The genes that encode and regulate the virulence factors of *S. aureus* are highly regulated and integrate host and environmental-derived cues in a co-ordinated manner, occurring in tandem with bacterial growth and controlled by a quorum sensing mechanism.<sup>80,81</sup> Two-component systems (TCSs) detect the environmental changes via an external signal that activates the histidine kinase, leading to its autophosphorylation and subsequent phosphorylation of the response regulator. Upon phosphorylation, the response regulator binds to a specific DNA sequence, resulting in the alteration of the target gene expression.<sup>81</sup> Major virulence regulatory systems of *S. aureus* are shown in Table 1.2.

**Table 1.2:** Major virulence regulatory systems of *S. aureus*. Adopted from Jenul *et al.*<sup>81</sup>

Receptor System	Role
<i>agr</i>	Cell-to-cell communication (quorum sensing) with AIP as a signal; leads to expression of exotoxins and enzymes
SaeRS	Induces exoprotein production
SrrAB	Repression of <i>agr</i> and TSST-1
ArlRS	Expression and repression of <i>agr</i> and autolysis
SarA	Cytoplasmic regulator of toxins and extracellular proteases
Rot	Cytoplasmic regulator of toxins and extracellular proteases
MgrA	Cytoplasmic regulator; induction of efflux pumps and capsule expression; repression of surface proteins
SigB	Stationary phase sigma factor, inhibits <i>agr</i> activity

The regulation of these virulence factors are largely controlled by the accessory gene regulator (*agr*),<sup>76</sup> first described in 1986 as a regulator of haemolysins, toxic shock syndrome toxin-1 (TSST-1), staphylokinase, and protein A.<sup>82</sup> *agr* is a quorum-sensing two-component system that senses a signal (an autoinducing peptide [AIP]), which accumulates in the extracellular environment with increasing bacterial concentration. Upon reaching a critical density of bacteria, the *agr* system is activated to adapt to the changing conditions and regulates virulence.<sup>82-84</sup>

The *agr* system consists of two transcription units RNAII and RNAIII, driven by the promoters P<sub>2</sub> and P<sub>3</sub>, respectively.<sup>85,86</sup> RNAII contains four cistrons *agrA*, *agrB*, *agrC*, and *agrD*, that encode the AgrBCDA structural proteins. Together the AgrB and AgrD constitute the quorum-sensing system; AIP is encoded by *agrD*, which subsequently gets modified and secreted by AgrB, to drive the transcription of both P<sub>2</sub> and P<sub>3</sub> promoters.<sup>87</sup> AgrC, acts as a histidine kinase and the AgrA acts as response regulator in a two-component system that senses the AIP present in the environment.<sup>80,85</sup>

RNAIII is the effector module of the *agr* system, which upon the post-exponential growth phase of *S. aureus* activates the transcription of exoproteins, while repressing the expression of surface-associated virulence factors.<sup>80,88</sup> This pattern of gene expression, where surface proteins involved in adhesion and defence against the host's immune system (e.g., protein A, coagulase, fibronectin) are synthesised prior to the production of secreted proteins (e.g., haemolysins, cytotoxins, proteases, etc.) portray a strategy whereby *S. aureus* first establishes itself on the host before subsequent attack.<sup>80</sup>

*S. aureus* virulence factors can also be regulated by the staphylococcal accessory regulator (SarA), which was shown to be necessary for transcription of *agr* RNAII and RNAIII.<sup>89</sup> However, SarA can act in an *agr*-independent manner, down regulating several proteases, and activating  $\alpha$ -haemolysin, TSST-1, and staphylococcal enterotoxin B expression.<sup>90</sup>

#### **1.4.1.2. Virulence Factors**

*S. aureus* expresses an abundance of virulence factors including surface proteins, toxins, superantigens and enzymes (Figure 1.6).<sup>77</sup>

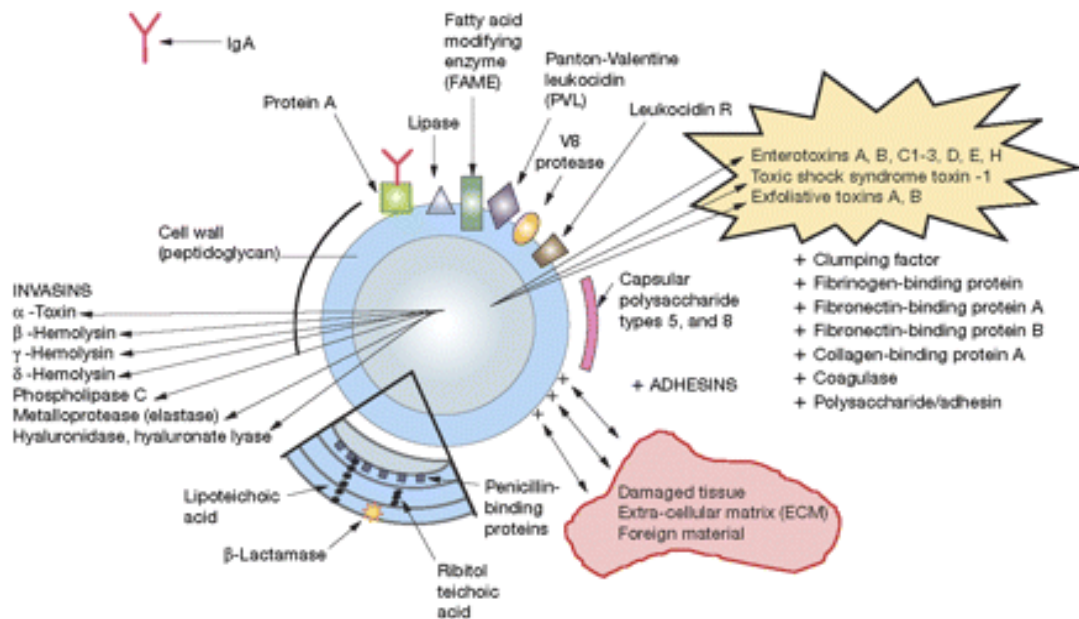


**Figure 1.6:** Selected *Staphylococcus aureus* virulence factors. Reproduced from Daum *et al* with permission.<sup>91</sup> Copyright © 2011, Oxford University Press

#### 1.4.1.2.1. Toxins

Enterotoxins are typically secreted superantigens, which trigger T cell activation and proliferation without the need for antigen processing by allowing non-specific interaction of the class II major histocompatibility complex MHC II with T cell receptors. *S. aureus* has been shown to produce approximately 20 different enterotoxin and enterotoxin-like toxins. One example is TSST-1, which causes TSS by stimulating the release of interleukins (IL-1 and IL-2), TNF- $\alpha$ , and other cytokines.<sup>92</sup>

Cytotoxic toxins cause pore formation in the membrane, leading to the efflux of vital molecules and metabolites; most lyse red (haemolysin) and/or white (leukotoxin) blood cells.<sup>92</sup> Alpha-toxin is probably the best known toxin of *S. aureus*;<sup>93</sup> it is lytic to red blood cells and a series of leukocytes, but not neutrophils.<sup>94</sup> Alpha-toxin also causes apoptosis in human monocytes, T and B cells.<sup>95</sup> Alpha-toxin is the model  $\beta$ -barrel pore-forming membrane-damaging cytotoxin, it creates a pore within the membrane, resulting in leakage of cellular contents and ultimately cell lysis.<sup>76</sup> It is essential for infections that disrupt epithelial barriers such as pneumonia,<sup>96</sup> keratoconjunctivitis and infections of the skin.<sup>76</sup>

*S. aureus* also produces a number of bi-component toxins that are structurally similar to alpha-toxin: Pantone-Valentine Leukocidin (PVL), leukocidins, and gamma-toxin.<sup>92</sup> PVL has been shown to aid in *S. aureus* pathogenicity by lysing polymorphonuclear leukocytes, ultimately destroying lung tissue, prolonging the infection, and helping with the dissemination of the infection to adjacent tissues.<sup>97</sup>

Delta-toxin is a member of the secreted phenol-soluble modulins (PSMs) that are produced by most *S. aureus* strains.<sup>98,99</sup> PSMs have multiple functions in *Staphylococcal* pathogenesis, including biofilm formation (Section 1.4.3).<sup>99</sup>

Exfoliating toxins A and B (ETA and ETB) are commonly associated with skin damage.<sup>100</sup> Approximately, 5% of *S. aureus* strains produce exfoliative toxins,<sup>101</sup> which cleave the desmosomal cadherins of the superficial skin layers, leading to staphylococcal scalded skin syndrome (SSSS).<sup>92,102</sup>

#### **1.4.1.2.2. Enzymes**

Most of the enzymes secreted by *S. aureus* degrade host molecules or interfere with the host's metabolic or signalling cascades. Enzymes include: non-specific proteases, aureolysin and endopeptidases, staphopain A and B, and collagenase. *S. aureus* also produce lipases, nucleases and phosphatases, although their function in pathogenesis is poorly understood.<sup>92</sup>

Staphylokinase degrades the fibrin clots by activating plasminogen to plasmin, diminishing the ability of the fibrin clot to keep the infection localised helping to facilitate greater bacterial penetration through the skin.<sup>103</sup>

*S. aureus* is able to produce two coagulases, staphylocoagulase and von Willebrand factor (vWF), which convert fibrinogen to fibrin, resulting in fibrin clots on the surface of *S. aureus* cells inhibiting phagocytosis.<sup>92,104</sup> Additionally, the production of coagulases have been associated with enterotoxin production.<sup>97</sup>

### **1.4.2. Biofilms**

*S. aureus* is frequently associated with infections of indwelling medical devices such as central venous catheters and prosthetic joints because of its ability to form biofilms.<sup>105,106</sup> *S. aureus* biofilms are mediated by the *agr* system, as this system regulates the production of proteases and PSMs, which are the main contributors of biofilm maturation and assembly.<sup>107-109</sup>

*S. aureus* initially attaches to biotic or abiotic surfaces using surface adhesions,<sup>110,111</sup> wall teichoic acids,<sup>112,113</sup> cell-wall anchored (CWA) proteins, eDNA production,<sup>114</sup> and changes in cell surface hydrophobicity (Figure 1.7).<sup>115</sup> The best characterised system is the microbial surface components recognising adhesive matrix molecules (MSCRAMMs), which are CWA-proteins that promote biofilm formation by facilitating the initial attachment to the host matrix components.<sup>116</sup>



The attached bacteria then proliferate. During this stage, *S. aureus* starts to produce EPS, and dependent in the EPS composition, polysaccharide-dependent biofilms, or biofilms consisting of proteinaceous matrix are formed;<sup>117,118</sup> the latter is usually found for MRSA isolates. Independent of EPS composition, *S. aureus* cells are held together within the EPS matrix by adhesive factors to build microcolonies, which develop into an established biofilm. Concurrently, biofilm development can be mediated by the polysaccharide intracellular adhesin (PIA) molecule – a matrix of poly-N-acetylglucosamine that surrounds and connects bacteria within the biofilm.<sup>116</sup>

Staphylococcal biofilms do not grow uniformly; remodelling of the biofilm occurs via nucleases and phenol soluble modulins (PSMs), which help to create a mature biofilm with its distinctive three-dimensional tower-like structures interspaced with water channels.<sup>116</sup>

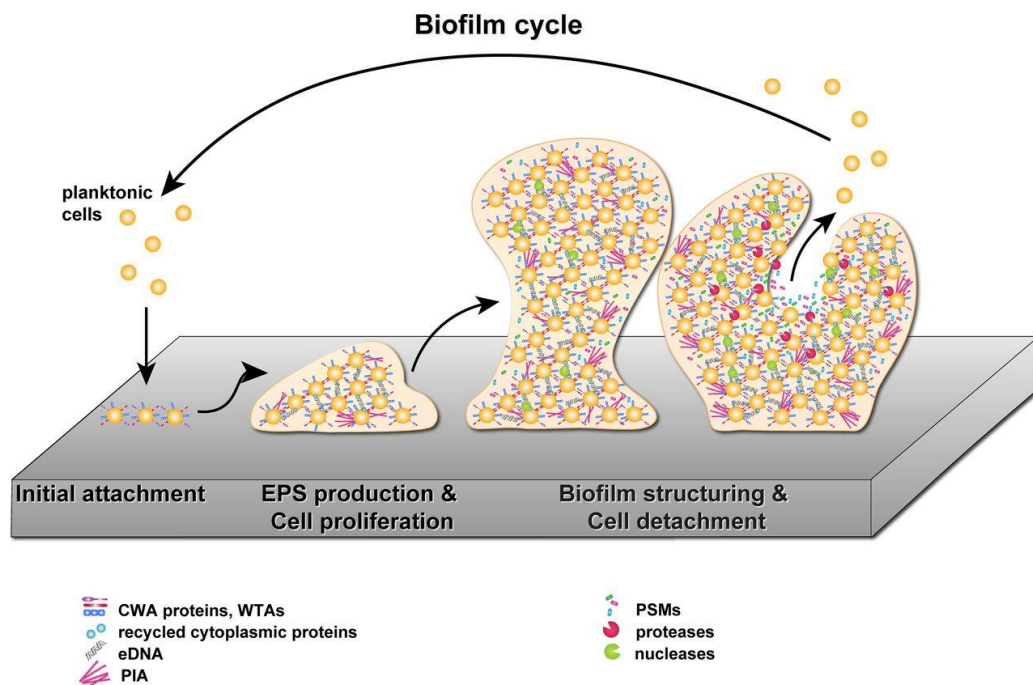


**Figure 1.7:** *Staphylococcal* biofilm cycle. Adapted from Schicher with permission.<sup>116</sup> Copyright © 2020, American Society for Microbiology

### 1.4.3. Methicillin-resistant *Staphylococcus aureus*

Methicillin-resistant *Staphylococcus aureus* (MRSA) was observed within one year of the first clinical use of methicillin; however, genomic analysis suggests that the resistance to methicillin predates the first clinical use of  $\beta$ -lactams.<sup>77</sup>

Methicillin resistance is mediated by the *mecA* gene, which is acquired via horizontal gene transfer (HGT) of a mobile genetic element called the *Staphylococcal* cassette chromosome *mec* (SCC*mec*).<sup>119</sup> *mecA* encodes for an alternative penicillin-binding protein 2a (PBP2a)

that is responsible for crosslinking peptidoglycan within the bacterial cell wall. PBP2a has a low affinity towards  $\beta$ -lactams, subsequently resulting in resistance to this class of antibiotics.<sup>80,120</sup>

Since the 1990s, MRSA has spread rapidly within the hospital environment and the community, often occurring in waves, with the serial emergence of predominant strains.<sup>77</sup> Recent examples of emergent MRSA strains include the healthcare-associated MRSA (HA-MRSA) clonal complex 30 (CC30) isolated in North America and Europe, community-associated MRSA (CA-MRSA) USA300 in North America, and MRSA ST93 isolated in Australia.<sup>121–124</sup> It has been estimated that MRSA is responsible for 171 200 healthcare-related infections in Europe annually, corresponding to an extra 5400 deaths; the 30-day mortality of MRSA is double that observed when compared to its methicillin-sensitive counterparts.<sup>97</sup>

## 1.5. Bacteriophage

Bacteriophages (phages) are viruses that infect and kill bacteria. Phage have been isolated in a variety of different environments; one such environment is Norwegian fjord water,<sup>125</sup> where it was discovered that the concentration of phage was approximately  $10^7$  Plaque Forming Units per millilitre (PFU/mL), with roughly 5 – 10 phage per bacterium. On the basis of this study, it was assumed that phage are the most ubiquitous organisms on earth. Today, it is thought that there are approximately  $10^{30-31}$  phage present in the world<sup>126–128</sup> capable of infecting more than 140 different bacterial genera;<sup>129,130</sup> however, the true number of phage is probably higher, with the only factor limiting their incidence is the presence of microbial hosts.<sup>126</sup>

### 1.5.1. Discovery and Historical Use

While Abedon *et al* identified at least 30 actual or presumptive “bacteriophage” references, some of which date back to 1895,<sup>131</sup> the beginning of bacteriophage research is generally thought to have originated from the paper written by Frederick W Twort in 1915.<sup>132</sup> Twort was growing viruses and found that they formed zones of clearance upon incubation with micrococcus bacteria. He concluded that the viruses must be multiplying while simultaneously killing the bacteria. Independently, Felix d’Hérelle observed this phenomenon in 1917 when investigating severe haemorrhagic dysentery among French troops stationed in Maisons-Laffite.<sup>133</sup> d’Hérelle described a microbe that was antagonistic to bacteria, but needed living cells to replicate, suggesting that cell lysis was involved in the

multiplication process. He termed this microbe ‘bacteriophage’ – implying to “eat” or “devour” bacteria.<sup>125,134</sup>

As such, both scientists are credited with the discovery of bacteriophage. However, d’Hérelle conducted further research, discovering that phage had steps of infection that included multiplication, release, and reinfection steps.<sup>125</sup> d’Hérelle primarily focused on the therapeutic use of bacteriophage, isolating phage from stool samples of patients suffering from diarrhoea to successfully treat bacterial dysentery.<sup>133</sup>

While the idea of phage therapy seemed promising, little was known about phage themselves, so unsurprisingly phage therapy led to variable success. This, in combination with poor documentation of the studies, resulted in controversy surrounding phage therapy.<sup>135</sup> The advent of conventional antibiotics in the 1950’s further diminished phage research, with the West favouring conventional antibiotics for the treatment of bacterial infections due to a greater understanding of their mechanism of action and more reproducible studies. However, phage therapy continued in the East, with the Eliava Institute in Tbilisi, Georgia considered to be the pioneer in phage therapy, where research continues to this day.<sup>136</sup>




















### **1.5.2. Bacteriophage Taxonomy**

Currently, bacteriophage classification is the responsibility of the Bacterial and Archaeal Viruses subcommittee (BAVS) within the International Committee on the Taxonomy of Viruses (ICTV). The ICTV published their first report in 1971, where classification was based on numerous bacteriophage properties, including: genetic information (single stranded (ss)/double stranded (ds) DNA/RNA), sequence similarity, morphology, and host range.<sup>134,137</sup> Since then, the number of bacteriophages discovered, and successfully sequenced, has dramatically increased, owing to the improvement of nucleotide sequencing techniques. Currently, there are over 400 phage genome sequences deposited into the GenBank database.<sup>138</sup>

There is a remarkable diversity in phage, for instance over 500 different phage have been identified for a single bacterial species *Mycobacterium smegmatis*.<sup>139</sup> Owing to the varying morphologies and size of phage, there are issues in classification. In 2015 it was suggested that there were 14 subfamilies, 204 genera and 873 species. However, this is constantly being updated as new bacteriophage are being sequenced; in 2017 two new families, eight sub-families, 34 genera and 91 species were proposed. The most recent literature from BAVS have proposed the creation of a new order (*Tublavirales*), 10 families, 22 sub-families, 424 new genera and 964 new species.<sup>140</sup> An overview of the families regarding

bacteriophage classification are outlined in Table 1.3. However, it is important to note that this list is not exhaustive, with re-classification/creation of new orders and families constantly ongoing due to the increasing amount of sequenced phage present in the literature.

**Table 1.3:** Classification of phage families (non-exhaustive list). L = linear, C = circular, NC = nucleocapsid, and S = supercoiled

Shape	Family	Nucleic Acid	Characteristics	Member
	<i>Myoviridae</i>	dsDNA (L)	No envelope, contractile tail	T4
	<i>Siphoviridae</i>	dsDNA (L)	No envelope, non-contractile long tail	$\lambda$
	<i>Podoviridae</i>	dsDNA (L)	No envelope, non-contractile short tail	T7
	<i>Microviridae</i>	ssDNA (C)	Knoblike capsomers	$\phi$ X174
	<i>Corticoviridae</i>	dsDNA (C)	No envelope, complex capsid	PM2
	<i>Tectiviridae</i>	dsDNA (L)	Double capsid, pseudo-tail	PRD1
	STIV	dsDNA (C)	Turret-shaped protrusions	STIV
	<i>Leviviridae</i>	ssRNA (L)	No envelope	MS2
	<i>Cryoviridae</i>	dsRNA (C)	Segmented, lipidic envelope	$\phi$ 6
	<i>Inoviridae</i>	ssDNA (C)	No envelope, filaments or rods	Fd
	<i>Lipothrixviridae</i>	dsDNA (L)	Envelope, lipids	TTV1
	<i>Rudiviridae</i>	dsDNA (L)	Stiff rods	SIRV-1
	<i>Plasmaviridae</i>	dsDNA (C)	Lipidic envelope, no capsid	MVL2
	Salterprovirus	dsDNA (L, S)	Lemon shaped, envelope	His1
	<i>Fuselloviridae</i>	dsDNA (C, S)	Lemon-shaped, envelope	SSV1
	<i>Guttaviridae</i>	dsDNA (C, S)	Droplet shaped	SNDV
	<i>Ampullaviridae</i>	dsDNA (L)	Bottle-shaped, helical NC	ABV
	<i>Bicaudaviridae</i>	dsDNA (C)	Two-tailed development, NC	ATV
	<i>Globuloviridae</i>	dsDNA (L)	Envelope, spherical, NC	PSV

While the classification system is complex, almost all (96%) of the currently classified bacteriophage belong to the *Caudovirals* and *Tublavirales* orders.<sup>140,141</sup> That is, they are tailed and predominately contain dsDNA encapsulated in a icosahedral protein shell, known as a capsid.<sup>125,134,137</sup> The size of these phage can vary, but are often between 24 – 200 nm,<sup>142</sup> with T4 phages being one of the largest (approx. 200 nm in length and 80-100 nm in width).<sup>134</sup>

### 1.5.3. Bacteriophage Life Cycle

Bacteriophage have four characterised life cycles: lytic, lysogenic, pseudo-lysogenic, and chronic infection, with the former two being the most prevalent (Figure 1.8). Virulent phage exclusively follow the lytic cycle, while temperate phage follow the lysogenic cycle until a stressor event occurs, causing the prophage to become induced and switch to the lytic life cycle of growth.<sup>143</sup> Both virulent and temperate bacteriophage can undergo the pseudo-lysogeny life cycle, and although the current cause of this life cycle is unknown, it is thought to be related to starvation stress of the bacterial host. While in the bacterial cell, the genetic material remains inactive in the form of a circular episome, and the development cycle is halted until environmental conditions improve.<sup>126</sup> Chronic infection occurs predominately with filamentous phage, where they continuously release their progeny from bacteria without lysing the bacterial cell or causing bacterial cell death.<sup>125,144</sup>

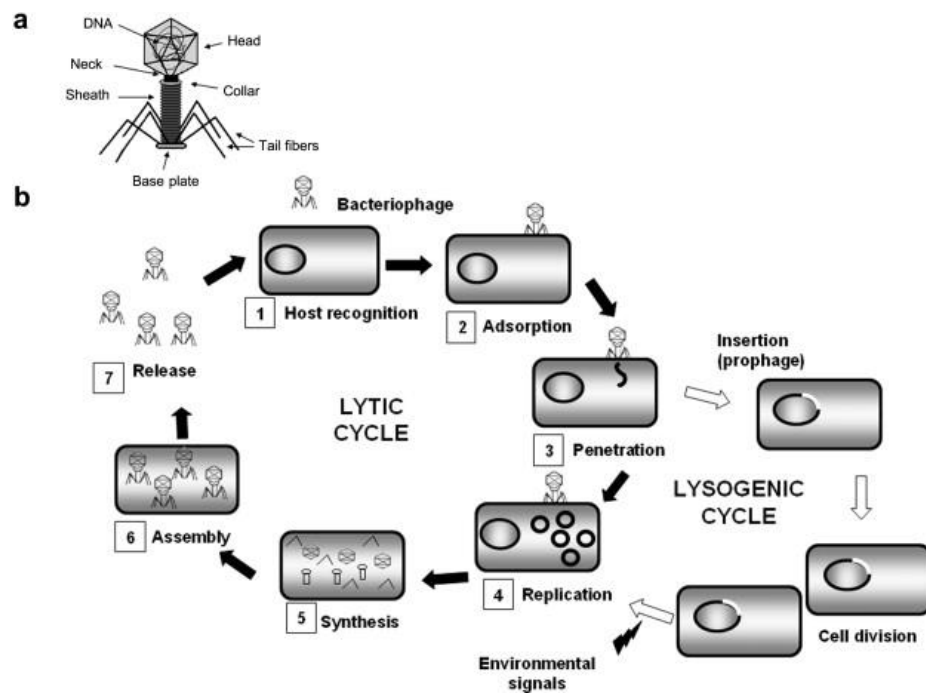


**Figure 1.8:** **A)** Structure of a typical tailed bacteriophage, and **B)** the steps during the bacteriophage lytic and lysogenic life cycles. Reproduced from Garcia *et al* with permission.<sup>145</sup> Copyright Elsevier® 2010.

### **1.5.3.1. Adsorption**

Regardless of the life cycle, phage infection begins when the virion attaches to its host cell, in a process known as adsorption.<sup>146</sup> For adsorption to occur, the phage must first recognise receptors on the target's bacterial cell wall. For gram-negative bacteria, the receptors can be the transmembrane proteins, porins, selective transport proteins (e.g. LamB for phage  $\lambda$ ), proteases and lipopolysaccharides (LPS). Gram-positive bacteria tend to have teichoic acids, lipoteichoic acids and the polysaccharide cell wall for their receptors for phage adsorption.<sup>143</sup>

Bacteriophage adsorption is initiated by random collisions between phage and their bacterial host, usually governed by diffusion, dispersion, or Brownian motion.<sup>147</sup> Phage reversibly bind to the bacterium upon contact until successful recognition of the receptor, leading to irreversible phage adhesion.<sup>126</sup> This step triggers conformational rearrangements within the phage that allow for the insertion of genetic material into the host, and/or the release enzymes to help with the penetration of the bacterial cell envelope depending on the type of bacteriophage.<sup>126,134,148</sup>

The aftermath of the infection depends on the host and the circumstances of infection: either the phage survive and undergoes its respective lifestyle, the phage dies and/or doesn't produce progeny (often due to resistance mechanisms), or both the phage and bacterium die due to abortive infection systems.<sup>146</sup>

### **1.5.3.2. Lytic Lifecycle**

Bacteriophage that undergo the lytic lifecycle are termed lytic or virulent phage; these phage produce daughter progeny at the expense of the bacterial host.<sup>146</sup> After adsorption, phage DNA is translocated into the bacterial cytoplasm and the host metabolism is re-directed to the development of viral progeny, owing to the expression of phage-encoded genes.<sup>134,149</sup> Newly transcribed proteins are assembled to form viral particles.<sup>146</sup> The formation of these phage particles will differ depending on the phage/host; however, the viral particles are essentially composed of nucleic acids and a protein capsid.

Upon a threshold number of virion particles, specific lysis proteins are released to help the phage particles lyse the bacterial cell. These include: holins (form pores within the plasma membrane), endolysins (cell wall peptidoglycan hydrolases), and spanins (destabilisation of the gram-negative bacterial outer membrane).<sup>150,151</sup> These lysis proteins are responsible for the destruction of the bacterial host wall, and subsequent release of the phage progeny to the extracellular matrix, allowing for re-infection.<sup>146,152</sup>

### 1.5.3.3. Lysogenic Lifecycle

Phage which undergo the lysogenic lifecycle are termed temperate phage. They have a stable relationship with their host, remaining as a prophage (where the genetic material of the phage is integrated within the host's chromosome); this is termed lysogenic state,<sup>126</sup> where the infections are not productive (i.e. no structural virions are produced) but rather replicate vertically in tandem with host replication. Therefore, daughter cells of the host inherit at least one copy of phage DNA. Prophages can also exist extra-chromosomally as a stable low copy plasmid, e.g. Phage P1.<sup>125,146</sup>

In the lysogenic state, the expression of lytic genes is inhibited by repressors. However, external factors can trigger the bacterial hosts' SOS regulatory circuit.<sup>125</sup> This can result in the temperate phage becoming 'induced', leading to a conversion of temperate phage to the lytic life cycle.<sup>126</sup>

One potential issue with temperate phage is that they can affect the pathogenicity of the host bacterium. Lysogenic phage can carry non-essential genes that are not required for the lytic or lysogenic lifecycle, but upon incorporation of the prophage can lead to a change in phenotype of the infected bacterium in a process termed 'lysogenic conversion'.<sup>125,153,154</sup> Lysogenic conversion is present in many bacterial species, and the "extra" genes are likely maintained as they allow for a selective advantage to the host or to the phage, contributing to improved bacterial fitness.<sup>125,155</sup> Lysogenic conversion has been shown to help spread virulence factors such as adhesions, toxins, enzymes and other proteins required for successful bacterial infection. Temperate phages have also been shown to influence biofilm development and dispersal.<sup>156</sup> Additionally, active lysogeny can also occur where the phage genome affects bacterial toxin production via expression regulation, rather than expression of virulence factors.<sup>157</sup> Interestingly, lysogenic conversion can still occur if the prophage becomes non-viable. Some examples where virulence factors have been induced by prophages are shown in Table 1.4

**Table 1.4:** Virulence factors encoded by genes acquired via prophage integration. Adapted from Olszak *et al.*<sup>126</sup>

Gene Name	Phage	Encoded Feature	Host
<i>stx</i>	933, H19B	Shiga toxin	E. coli O157:H7
<i>ctxAB</i>	CTX $\phi$	Cholera toxin	Vibrio cholerae
<i>entA, sak</i>	$\phi$ 13	Enterotoxin A, Staphylokinase	Staphylococcus aureus

#### 1.5.4. Transduction

Transduction is the process where foreign DNA is introduced into a bacterial cell by phage or a viral vector; often, this contributes to the pathogenicity of the bacterial host.<sup>125</sup>

Transduction can be further split into specialised and general transduction. Specialised transduction is typical of temperate phage and arises when the prophage is incorrectly excised with an adjacent part of the host genome.<sup>126</sup> Owing to this, specialised transduction involves the transfer of bacterial genes that would not normally be associated with the phage genome.<sup>125</sup> After infection of a new host cell, site-specific recombination or homologous recombination results in the integration of the packaged DNA into the host genome.<sup>158</sup>

General transduction was first identified by Zinder and Lederberg in 1952 for *Salmonella* phage P22. It is the accidental packaging of random bacterial DNA fragments into the virion particles. While the resultant virion can still adsorb to bacterial cells and is able to transfer the packaged bacterial DNA to a subsequent bacterium, it can no longer produce phage progeny. Therefore, generalised transduction does not result in serial DNA transfer. However, it can transfer large amounts of DNA, and both lytic and lysogenic phage are capable of generalised transduction.<sup>125,159</sup>

#### 1.5.5. Bacterial Resistance to Bacteriophage

While the reported frequency of resistance *in vivo* is low,<sup>160,161</sup> bacteria can develop resistance to bacteriophage through multiple mechanisms of resistance.<sup>162,163</sup> These mechanisms, and how phage can overcome them, are listed below:

- **Adsorption blocking.** Perhaps the main method of resistance is the ability of bacteria to prevent phage adsorption through modification, masking, or removal of receptors.<sup>126,164,165</sup> Synthesis of exopolysaccharide (EPS) or masking proteins (e.g. protein A of *S. aureus*) are other strategies bacteria employ to prevent phage adsorption. However, phage have adapted to recognise these modified receptors and have been shown to produce polysaccharide lyase or polysaccharide hydrolase enzymes that degrade the EPS.<sup>134</sup>
- **DNA injection blocking.** Temperate and lytic phage can prevent further infection by other phage (termed superinfection) through the expression of superinfection exclusion (SIE) proteins. SIE proteins are anchored to the cell wall or associated with other membrane components, and act by preventing DNA from reacting the cytoplasm of the host.<sup>166,167</sup>



- **Restriction modification (R/M) of foreign DNA.** Most bacteria possess R/M systems which utilise restriction endonucleases to digest foreign DNA that is not methylated at the appropriate sites.<sup>126</sup> Phage can inactivate R/M systems by methylation of phage DNA (e.g. phage T4, which contain hydroxymethylcytosine instead of cytosine, is protected from R/M systems) or by reducing the frequency of restriction sites by mutation.<sup>149</sup>
- **Clustered regulatory interspaced short palindromic repeats (CRISPR)-Cas systems.** CRISPR-Cas systems often work in tandem with R/M systems and allow bacteria to recognise and degrade foreign DNA entering the cell.<sup>168</sup> CRISPR-Cas systems have been detected in approximately 40% of bacteria. Phage can overcome CRISPR-Cas systems by promoting mutations in the protospacer-adjacent motifs or preventing the formation of CRISPR-Cas systems.<sup>126,169</sup>
- **Abortive infections.** An abortive infection is an ‘altruistic’ cell death system activated by phage infection, whereby the bacterial cell dies to prevent phage multiplication. This programmed cell death of a low number of bacterial cells enables the larger population to survive.<sup>126,170</sup> Currently, there are over 20 abortive infection systems known, including toxin-antitoxin systems, which control bacterial cell death via protein-protein, protein-RNA or RNA-RNA interactions. Phage can overcome abortive infection through the production of bacterial-like antitoxins.<sup>126</sup>

### 1.5.6. Bacteriophage Therapy

Bacteriophage therapy is facing a revival due to the development of antibiotic resistance and the dwindling production of novel antibiotics from pharmaceutical industries. Typically, phage therapy involves the use of lytic phage as they result in bacterial cell death and do not possess the disadvantages associated with temperate phage.<sup>137</sup>

Prior to use, phage (as a monotherapy or in a phage mixture, known as a phage cocktail) must undergo strict testing to deem its suitability for phage therapy. This includes fully characterising the phage by determining its structure, host-range, receptor on the bacterial cell, stability, etc. Moreover, genetic sequencing should be undertaken to ensure the phage is lytic and does not possess toxic/resistant genes. Additionally, the phage suspension should be adequately purified to remove any harmful endotoxins, meet regulatory guidelines, and should have undergone several *in vitro* and *in vivo* efficacy studies.<sup>137,171</sup>

### **1.5.6.1. Advantages**

There are several advantages to bacteriophage therapy. Firstly, bacteriophage have a limited host range, acting as a narrow spectrum antibiotic, which reduces the chances of developing dysbacteriosis (an imbalance in gut microflora) and secondary infections. Conversely, conventional antibiotics can act on the hosts' normal microflora, potentially leading to secondary infections.<sup>143</sup> Phage are able to infect both gram-positive and negative bacteria, as well as remaining effective against multi-drug resistant (MDR) bacteria due to their different mechanism of action (MOA) compared to conventional antibiotics.<sup>172</sup> Additionally, some phage have been shown to be effective in eliminating bacterial biofilms,<sup>173</sup> and because of the wide distribution of phages upon systemic administration, phage are able to pass the blood-brain barrier and target central nervous system infections.<sup>174–176</sup> Owing to their self-replicating nature, phage may require less frequent administration, and to the best of the authors knowledge, phage been shown to be safe for human use.<sup>143,177</sup> Bruttin and Brussow showed that no adverse effects were identified from participants who received an oral suspension of T4 phage.<sup>178</sup> Other studies have reported minor side effects, primarily due to the release of endotoxins upon the lysis of the bacteria; however, this is a common phenomenon witnessed with conventional bactericidal antibiotics.<sup>143</sup>

Phage are ubiquitous and easy to isolate, providing an easier route to antibiotic therapy than the synthesis of novel conventional antibiotics. Additionally, if bacteria become resistant to the therapeutic phage, there are a plethora of phage that could be used instead.<sup>143</sup>

### **1.5.6.2. Disadvantages**

However, phage therapy is not without its disadvantages. Technical hurdles include the inherent specificity of the phage, resulting in the need to identify the precise etiological microorganism causing the infection before bacteriophage can be used successfully. While this can be overcome by the use of phage cocktails to expand the host range of the phage to target multiple strains of a bacterial species, there are no clear standardised methods, or official guidelines on the preparation of phage cocktails.<sup>179,180</sup>

One disadvantage of bacteriophage therapy has been mentioned earlier – bacteriophage resistance. However, this disadvantage of phage-resistant bacteria can be overcome by using other, susceptible phage that have a similar host range, again showing the promise of phage cocktails, or modified bacteriophage, as a therapy. Additionally, there may be a fitness cost associated with the development of phage resistance which could make the bacterium susceptible to conventional antibiotics.<sup>143</sup>

Phage need to undergo genetic sequencing before being accepted as a viable therapy; however, there are many genes whose function is currently unknown.<sup>181</sup> While phages are easy to isolate, purification is a convoluted process. If the phage lysate is not sufficiently pure, the endotoxins could lead to a potentially life-threatening inflammatory cascade resulting in multiple organ failure.<sup>182</sup> However, Merabishivii *et al* created a phage stock of clinical trial grade purity through the use of a commercially available endotoxin removal kit.<sup>179</sup> Additionally, the majority of lysate used in research are small in volume, hence there may be additional issues in the scale-up of phage preparations and the long-term stability of such suspensions.<sup>143</sup>

Non-technical disadvantages include the regulatory status of phage therapy and the public perception of using viruses to treat bacterial infections.<sup>143</sup> Phage therapy is not presently recognised as a medicinal product, with current European pharmaceutical regulations, definitions, and standards not adequately adapted to suit phage therapy; nor is there an approval process in place for the multiple phage cocktails needed to combat MDR bacterial infections.<sup>183</sup> Regulation of phage therapy has largely been avoided due to the unreliable and inconsistent results of early phage therapy trials. While today it is accepted that this was due to poor understanding of the phage biology, further reproducible clinical trials need to be conducted before regulatory approval can be granted. Furthermore, phages are antigenic, eliciting a response from the immune system. Some studies have suggested that serum antibodies have inactivated several different phages,<sup>171,184</sup> and others have reported that the phage are rapidly cleared by the immune system.<sup>177,184</sup>

## **1.6. Wound Dressings**

Wound dressings date back to 2500 – 1600 BC, where linen strips soaked in oil or grease covered in plasters were used to seal wounds.<sup>185</sup> Previously, it was believed that wounds healed more quickly if kept dry and uncovered. However, there was a shift in wound dressing design in the mid-20<sup>th</sup> century towards occlusive dressings, designed to protect and provide a moist environment to the wound. These new dressings resulted in faster re-epithelialisation, collagen synthesis, angiogenesis promotion and a reduction in wound bed pH, leading to a decrease in wound infection.<sup>186</sup> Following this, further dressings were designed that provided moisture and absorbed fluids (e.g., polyurethane foams and hydrocolloids) and by the mid 1990's, synthetic polymers had been employed to further develop and improve wound dressings (e.g., hydrogels, hydrocolloids, and silver/collagen containing dressings).<sup>185</sup>

### **1.6.1. Characteristics of an Ideal Wound Dressing**

Usually, a dressing is selected based on the type, depth, and location of the wound.<sup>185,187</sup>

While this list is not exhaustive, a successful dressing must be able to:<sup>185</sup>

- Provide or maintain a moist wound environment
- Promote epidermal migration, angiogenesis and connective tissue synthesis
- Allow gas exchange between the wound and the environment
- Maintain appropriate temperature and humidity to the wound to improve blood flow
- Provide protection against pathogenic microbials
- Be non-adherent and easy to remove with limited pain to the patient
- Be sterile, non-toxic, and non-allergic.

While there are currently over 3000 types of wound dressings available for all aspects of wound care, there is not one product that is superior for the treatment of chronic wounds.

### **1.6.2. Traditional Wound Dressings**

Traditional wound dressings include gauze, lint, plasters, bandages, and cotton wool; they are used as primary or secondary wound dressings to protect the wound from microbial contaminants.<sup>188</sup> These dressings are not very cost-effective as they require frequent changing to protect from maceration of healthy tissues.<sup>185</sup> Additionally, once these dressings become moist due to wound drainage, they tend to become adherent to the wound bed, causing pain to the patient on removal. Traditional dressings were used for clean and dry wounds with mild exudate levels, or used as secondary dressings, but nowadays they are being replaced with modern dressings that promote faster wound healing.<sup>188</sup>

### **1.6.3. Modern Wound Dressings**

Modern wound dressings are often based on synthetic polymers and can be classified as passive (non-occlusive), interactive (semi-occlusive/occlusive), or medicated (releasing a drug from the wound dressing to promote wound healing).<sup>185</sup>

### **1.6.3.1. Semi-permeable Dressings**

Semi-permeable film dressings are generally composed of poly(urethane) which permits the transmission of water vapour, oxygen, and carbon dioxide from the wound, while providing autolytic debridement of eschar.<sup>189</sup> These dressings are recommended for re-epithelializing wounds that superficial with low exudate; common examples include Oposite™ and Biooclusive™.<sup>190</sup>

Semi-permeable foam dressings are also available and are typically used for lower leg ulcers and wounds with moderate-to-high exudate.<sup>191</sup> Typical examples include Lyofoam™ and Alleyn™.<sup>185</sup>

### **1.6.3.2. Hydrogels**

Hydrogels are hydrophilic polymer networks with a high water content, often created using polymers such as poly(vinyl alcohol), poly(methacrylate), and poly(vinyl pyrrolidone).<sup>185,192,193</sup> The high water content promotes granulation and facilitates autolytic debridement of necrotic tissue within the wound bed. Hydrogels are often used for burns, surgical wounds, and pressure ulcers.<sup>187</sup> Typical examples include Nu-gel™ and Aquaform™.<sup>185</sup> A more detailed review of hydrogels can be found in Chapter 7.

### **1.6.3.3. Hydrocolloids**

Hydrocolloid dressings are one of the most frequently used wound dressings, composed of a mixture of colloidal materials (carboxymethylcellulose, gelatin, and pectin)<sup>194</sup> and elastomers and alginates<sup>187</sup> within two layers – an inner colloidal layer and an outer, water-impermeable layer. Hydrocolloids are used on light-to-moderate exuding wounds, such as pressure sores and minor burn wounds, as they are permeable to water vapour, aid in debridement, absorb wound exudate, and protect against microbial contamination.<sup>195,196</sup> Hydrocolloid dressings are also recommended for paediatric patients as they do not cause pain on removal.<sup>196</sup> However, they are not appropriate for deeper wounds, or wounds that are heavily contaminated.<sup>197</sup> Examples include Granuflex™, Tegaserb™, and DuoDerm®.<sup>185</sup>

### **1.6.4. Medicated dressings**

Medicated dressings are wound dressings that contain a drug which aids in the wound healing process (e.g., antimicrobials, growth factors, and enzymes), often used to overcome issues associated with topical agents.<sup>194</sup>

Antimicrobial-loaded wound dressings have been reported for use in the treatment of diabetic foot ulcers and surgical and accidental wounds.<sup>188,198</sup> The most reported medicated dressings are those that incorporate silver, with silver-loaded dressings available as hydrocolloids, silicone gels, and poly(urethane) foam films.<sup>185,194</sup> Antiseptics, such as povidone-iodine have also been used in the development of medicated wound dressings,<sup>199</sup> although prolonged use of iodine has been known to result in staining and skin irritation.<sup>185</sup> Recently, dialkylcarbamoyl chloride coated dressings have been used to combat wound infections by irreversibly binding to bacteria at the wound surface via hydrophobic interactions, removing the bacteria from the wound site upon dressing change.<sup>200</sup> Antibiotic-loaded wound dressings have also been investigated, with gentamicin, norfloxacin, and minocycline loaded chitosan films currently under investigation.<sup>188</sup>

## 1.7. Overall Aims and Objectives

The overall aim of this research was to develop novel systems that could detect and subsequently treat *S. aureus* infections, which could be ultimately combined to create a theranostic device.

This thesis will focus on the relationship between phage and antibacterials, investigating the role of phage-antibiotic synergy and the efficacy of such combinations against clinically relevant *S. aureus* isolates. From here, phage K, ciprofloxacin, or a combination of both, would be encapsulated within a poly(lactic acid)-poly(ethylene glycol) polymer blend and assessed for release kinetics and microbiological efficacy. Attention will then turn to the development of a pH responsive system via use of a pH-responsive polymer coating.

Concurrently, the design and synthesis of a novel fluorescent probe for the detection of *S. aureus* will be employed. Upon created of the probe, focus will turn to the optimisation of the probe to detect *S. aureus* in planktonic, biofilm, and *ex vivo* models.

## 1.8. References

1. Mustoe T. Understanding chronic wounds: a unifying hypothesis on their pathogenesis and implications for therapy. *Am J Surg*. 2004;187(5):S65–70.
2. Gottrup F. A specialized wound-healing center concept: importance of a multidisciplinary department structure and surgical treatment facilities in the treatment of chronic wounds. *Am J Surg*. 2004;187(5):S38–43.
3. Guest JF, Ayoub N, McIlwraith T, Uchegbu I, Gerrish A, Weidlich D, et al. Health economic burden that wounds impose on the National Health Service in the UK. *BMJ Open*. 2015;5(12).
4. Renner R, Erfurt-Berge C. Depression and quality of life in patients with chronic wounds: ways to measure their influence and their effect on daily life. *Chronic Wound Care Manag Res*. 2017;4:143.
5. Phillips P, Sampson E, Yang Q, Antonelli P, Progulsk-Fox A, Schultz G. Bacterial biofilms in wounds: chronic wounds. *Wound Heal South Africa*. 2008;1(2):10–2.
6. Haalboom M, Blokhuis-Arkes MHE, Beuk RJ, Meerwaldt R, Klont R, Schijffelen MJ, et al. Culture results from wound biopsy versus wound swab: does it matter for the assessment of wound infection? *Clin Microbiol Infect*. 2019;25(5):629-e7.
7. Siddiqui AR, Bernstein JM. Chronic wound infection: facts and controversies. *Clin Dermatol*. 2010;28(5):519–26.
8. Wu Y-K, Cheng N-C, Cheng C-M. Biofilms in chronic wounds: pathogenesis and diagnosis. *Trends Biotechnol*. 2019;37(5):505–17.
9. Váradi L, Luo JL, Hibbs DE, Perry JD, Anderson RJ, Orenga S, et al. Methods for the detection and identification of pathogenic bacteria: past, present, and future. *Chem Soc Rev*. 2017;46(16):4818–32.
10. Habimana J de D, Ji J, Sun X. Minireview: trends in optical-based biosensors for point-of-care bacterial pathogen detection for food safety and clinical diagnostics. *Anal Lett*. 2018;51(18):2933–66.
11. Velnar T, Bailey T, Smrkolj V. The wound healing process: an overview of the cellular and molecular mechanisms. *J Int Med Res*. 2009;37(5):1528–42.

12. Martin P. Wound healing--aiming for perfect skin regeneration. *Science* (80- ). 1997;276(5309):75–81.
13. Lazarus GS, Cooper DM, Knighton DR, Margolis DJ, Percoraro RE, Rodeheaver G, et al. Definitions and guidelines for assessment of wounds and evaluation of healing. *Wound repair Regen.* 1994;2(3):165–70.
14. Strodbeck F. Physiology of wound healing. *Newborn infant Nurs Rev.* 2001;1(1):43–52.
15. Waldrop J, Doughty D. Wound healing physiology. In: *Acute and chronic wounds: Nursing management.* Mosby; 2000. p. 17–39.
16. Schultz GS. Molecular regulation of wound healing. *Acute chronic wounds Nurs Manag 2nd Ed St Louis, MO Mosby.* 1999;413–29.
17. Alves PJ, Barreto RT, Barrois BM, Gryson LG, Meaume S, Monstrey SJ. Update on the role of antiseptics in the management of chronic wounds with critical colonisation and/or biofilm. *Int Wound J.* 2020;
18. Beldon P. Basic science of wound healing. *Surg.* 2010;28(9):409–12.
19. Iocono J. The biology of healing. *Wounds; Biol Manag.* 1998;
20. Russell L. Understanding physiology of wound healing and how dressings help. *Br J Nurs.* 2000;9(1):10–21.
21. Parks WC. Matrix metalloproteinases in repair. *Wound Repair Regen.* 1999;7(6):423–32.
22. Cooper DM. Wound healing: new understandings. In: *Nurse Practitioner Forum.* 1999. p. 74–86.
23. Mast BA. The skin. *Wound Heal.* 1992;344–55.
24. Verhamme P, Hoylaerts MF. Hemostasis and inflammation: two of a kind? *Thromb J.* 2009;7(1):15.
25. Clark RAF. Wound repair. In: *The molecular and cellular biology of wound repair.* Springer; 1988. p. 3–50.
26. Hübner G, Brauchle M, Smola H, Madlener M, Fässler R, Werner S. Differential



- regulation of pro-inflammatory cytokines during wound healing in normal and glucocorticoid-treated mice. *Cytokine*. 1996;8(7):548–56.
27. George Broughton II, Janis JE, Attinger CE. Wound healing: an overview. *Plast Reconstr Surg*. 2006;117(7S):1e-S.
  28. Diegelman RF, Evans MC. Wound healing: An overview of acute, fibrotic and delayed. *Front Biosci*. 2004;9–283.
  29. Winter GD. Formation of the scab and the rate of epithelization of superficial wounds in the skin of the young domestic pig. *Nature*. 1962;193(4812):293–4.
  30. Kerstein MD. The scientific basis of healing. *Adv Skin Wound Care*. 1997;10(3):30–6.
  31. Calvin M. Cutaneous wound repair. *Wounds*. 1998;10:12–32.
  32. Berry DP, Harding KG, Stanton MR, Jasani B, Ehrlich HP. Human wound contraction: collagen organization, fibroblasts, and myofibroblasts. *Plast Reconstr Surg*. 1998;102(1):124–31.
  33. Rudolph R. Location of the force of wound contraction. *Surg Gynecol Obstet*. 1979;148(4):547–51.
  34. Kuhn MA, Smith PD, Hill DP, Ko F, Meltzer DD, Vande Berg JS, et al. In vitro fibroblast populated collagen lattices are not good models of in vivo clinical wound healing. *Wound Repair Regen*. 2000;8(4):270–6.
  35. Grey JE, Enoch S, Harding KG. Wound assessment. *Bmj*. 2006;332(7536):285–8.
  36. Guo S al, DiPietro LA. Factors affecting wound healing. *J Dent Res*. 2010;89(3):219–29.
  37. Bowler PG, Duerden BI, Armstrong DG. Wound microbiology and associated approaches to wound management. *Clin Microbiol Rev*. 2001;14(2):244–69.
  38. Percival SL, McCarty SM, Lipsky B. Biofilms and wounds: an overview of the evidence. *Adv wound care*. 2015;4(7):373–81.
  39. Cutting KF. Wound healing, bacteria and topical therapies. *EWMA J*. 2003;3(1):17–9.

40. Swanson T, Angel D, Sussman G, Cooper R, Haesler E, Ousey K, et al. Wound infection in clinical practice: principles of best practice. 2016;
41. Bowler PG. The bacterial growth guideline: reassessing its clinical relevance in wound healing. *Ostomy Wound Manage.* 2003;49(1):44.
42. Percival SL. Importance of biofilm formation in surgical infection. *Br J Surg.* 2017;104(2):e85–94.
43. Kingsley A. A proactive approach to wound infection. *Nurs Stand (through 2013).* 2001;15(30):50.
44. Browne AC, Vearncombe M, Sibbald RG. High bacterial load in asymptomatic diabetic patients with neurotrophic ulcers retards wound healing after application of Dermagraft. *Ostomy Wound Manage.* 2001;47(10):44.
45. Flemming H-C, Wingender J, Szewzyk U, Steinberg P, Rice SA, Kjelleberg S. Biofilms: an emergent form of bacterial life. *Nat Rev Microbiol.* 2016;14(9):563.
46. Pinto G. Refactoring multicore applications towards energy efficiency. In: *Proceedings of the 2013 companion publication for conference on Systems, programming, & applications: software for humanity.* 2013. p. 61–4.
47. Li L, Mendis N, Trigui H, Oliver JD, Faucher SP. The importance of the viable but non-culturable state in human bacterial pathogens. *Front Microbiol.* 2014;5:258.
48. Hansson C, Hoborn J, Möller A, Swanbeck G. The microbial flora in venous leg ulcers without clinical signs of infection. Repeated culture using a validated standardised microbiological technique. *Acta Derm Venereol.* 1995;75(1):24.
49. Gjødsbøl K, Christensen JJ, Karlsmark T, Jørgensen B, Klein BM, Krogfelt KA. Multiple bacterial species reside in chronic wounds: a longitudinal study. *Int Wound J.* 2006;3(3):225–31.
50. Frank DN, Wysocki A, Specht-Glick DD, Rooney A, Feldman RA, St. Amand AL, et al. Microbial diversity in chronic open wounds. *Wound repair Regen.* 2009;17(2):163–72.
51. Howell-Jones RS, Wilson MJ, Hill KE, Howard AJ, Price PE, Thomas DW. A review of the microbiology, antibiotic usage and resistance in chronic skin wounds. *J Antimicrob Chemother.* 2005;55(2):143–9.

52. Bowler PG, Davies BJ. The microbiology of infected and noninfected leg ulcers. *Int J Dermatol.* 1999;38(8):573–8.
53. Donlan RM. Biofilms: microbial life on surfaces. *Emerg Infect Dis.* 2002;8(9):881.
54. Flemming H-C, Wingender J. The biofilm matrix. *Nat Rev Microbiol.* 2010;8(9):623–33.
55. James GA, Swogger E, Wolcott R, Pulcini E deLancey, Secor P, Sestrich J, et al. Biofilms in chronic wounds. *Wound Repair Regen.* 2008;16(1):37–44.
56. Malone M, Bjarnsholt T, McBain AJ, James GA, Stoodley P, Leaper D, et al. The prevalence of biofilms in chronic wounds: a systematic review and meta-analysis of published data. *J Wound Care.* 2017;26(1):20–5.
57. Khatoun Z, McTiernan CD, Suuronen EJ, Mah T-F, Alarcon EI. Bacterial biofilm formation on implantable devices and approaches to its treatment and prevention. *Heliyon.* 2018;4(12):e01067.
58. Costerton W, Veeh R, Shirtliff M, Pasmore M, Post C, Ehrlich G. The application of biofilm science to the study and control of chronic bacterial infections. *J Clin Invest.* 2003;112(10):1466–77.
59. Denkhaus E, Meisen S, Telgheder U, Wingender J. Chemical and physical methods for characterisation of biofilms. *Microchim Acta.* 2007;158(1–2):1–27.
60. Floyd KA, Eberly AR, Hadjifrangiskou M. Adhesion of bacteria to surfaces and biofilm formation on medical devices. In: *Biofilms and implantable medical devices.* Elsevier; 2017. p. 47–95.
61. Davis E. Don't deny the chance to heal. In: *2nd joint Meeting of the Wound healing Society and the European Tissue Repair Society Boston.* 1996.
62. Nikolaev YA, Plakunov VK. Biofilm—"City of microbes" or an analogue of multicellular organisms? *Microbiology.* 2007;76(2):125–38.
63. Xavier JB, Foster KR. Cooperation and conflict in microbial biofilms. *Proc Natl Acad Sci.* 2007;104(3):876–81.
64. Wolcott RD, Rumbaugh KP, James G, Schultz G, Phillips P, Yang Q, et al. Biofilm maturity studies indicate sharp debridement opens a time-dependent therapeutic

- window. *J Wound Care*. 2010;19(8):320–8.
65. Watters C, DeLeon K, Trivedi U, Griswold JA, Lyte M, Hampel KJ, et al. *Pseudomonas aeruginosa* biofilms perturb wound resolution and antibiotic tolerance in diabetic mice. *Med Microbiol Immunol*. 2013;202(2):131–41.
  66. Zhao G, Usui ML, Underwood RA, Singh PK, James GA, Stewart PS, et al. Time course study of delayed wound healing in a biofilm-challenged diabetic mouse model. *Wound Repair Regen*. 2012;20(3):342–52.
  67. Davies DG, Parsek MR, Pearson JP, Iglewski BH, Costerton JW, Greenberg EP. The involvement of cell-to-cell signals in the development of a bacterial biofilm. *Science* (80- ). 1998;280(5361):295–8.
  68. Brooun A, Liu S, Lewis K. A dose-response study of antibiotic resistance in *Pseudomonas aeruginosa* biofilms. *Antimicrob Agents Chemother*. 2000;44(3):640–6.
  69. Haagensen JAJ, Klausen M, Ernst RK, Miller SI, Folkesson A, Tolker-Nielsen T, et al. Differentiation and distribution of colistin-and sodium dodecyl sulfate-tolerant cells in *Pseudomonas aeruginosa* biofilms. *J Bacteriol*. 2007;189(1):28–37.
  70. Harrison JJ, Ceri H, Turner RJ. Multimetal resistance and tolerance in microbial biofilms. *Nat Rev Microbiol*. 2007;5(12):928–38.
  71. Lewis K. Persister cells, dormancy and infectious disease. *Nat Rev Microbiol*. 2007;5(1):48–56.
  72. Chen X, Stewart PS. Role of electrostatic interactions in cohesion of bacterial biofilms. *Appl Microbiol Biotechnol*. 2002;59(6):718–20.
  73. Koseoglu H, Aslan G, Esen N, Sen BH, Coban H. Ultrastructural stages of biofilm development of *Escherichia coli* on urethral catheters and effects of antibiotics on biofilm formation. *Urology*. 2006;68(5):942–6.
  74. Brenner S, Miller JH. Brenner's encyclopedia of genetics. Elsevier Science; 2014. 553–555 p.
  75. Martin E, Lina G, Dumitrescu O. STAPHYLOCOCCUS| *Staphylococcus aureus*. *Encycl Food Microbiol*. 2014;501–7.

76. Foster TJ, Geoghegan JA. Chapter 37 - *Staphylococcus aureus*. In: Tang Y-W, Sussman M, Liu D, Poxton I, Schwartzman JBT-MMM (Second E, editors. Boston: Academic Press; 2015. p. 655–74.
77. Turner NA, Sharma-Kuinkel BK, Maskarinec SA, Eichenberger EM, Shah PP, Carugati M, et al. Methicillin-resistant *Staphylococcus aureus*: an overview of basic and clinical research. *Nat Rev Microbiol*. 2019;17(4):203–18.
78. Wertheim HFL, Melles DC, Vos MC, van Leeuwen W, van Belkum A, Verbrugh HA, et al. The role of nasal carriage in *Staphylococcus aureus* infections. *Lancet Infect Dis*. 2005;5(12):751–62.
79. Tong SYC, Davis JS, Eichenberger E, Holland TL, Fowler VG. *Staphylococcus aureus* infections: epidemiology, pathophysiology, clinical manifestations, and management. *Clin Microbiol Rev*. 2015;28(3):603–61.
80. Plata K, Rosato AE, Wegrzyn G. *Staphylococcus aureus* as an infectious agent: overview of biochemistry and molecular genetics of its pathogenicity. *Acta Biochim Pol*. 2009;56(4).
81. Jenul C, Horswill AR. Regulation of *Staphylococcus aureus* virulence. *Gram-Positive Pathog*. 2019;669–86.
82. Recsei P, Kreiswirth B, O'reilly M, Schlievert PM, Gruss A, Novick RP. Regulation of exoprotein gene expression in *Staphylococcus aureus* by agr. *Mol Gen Genet MGG*. 1986;202(1):58–61.
83. Thoendel M, Kavanaugh JS, Flack CE, Horswill AR. Peptide signaling in the staphylococci. *Chem Rev*. 2011;111(1):117–51.
84. Dunman P áM, Murphy E, Haney S, Palacios D, Tucker-Kellogg G, Wu S, et al. Transcription Profiling-Based Identification of *Staphylococcus aureus* Genes Regulated by the agr and/or sarA Loci. *J Bacteriol*. 2001;183(24):7341–53.
85. Pragman AA, Schlievert PM. Virulence regulation in *Staphylococcus aureus*: the need for in vivo analysis of virulence factor regulation. *FEMS Immunol Med Microbiol*. 2004;42(2):147–54.
86. Janson L, Arvidson S. The role of the delta-lysin gene (hld) in the regulation of virulence genes by the accessory gene regulator (agr) in *Staphylococcus aureus*. *EMBO J*. 1990;9(5):1391–9.

87. Novick RP. Autoinduction and signal transduction in the regulation of staphylococcal virulence. *Mol Microbiol.* 2003;48(6):1429–49.
88. Novick RP. Pathogenicity factors and their regulation. *Gram-positive Pathog.* 1999;392–407.
89. Heinrichs JH, Bayer MG, Cheung AL. Characterization of the sar locus and its interaction with agr in *Staphylococcus aureus*. *J Bacteriol.* 1996;178(2):418–23.
90. Chan PF, Foster SJ. Role of SarA in virulence determinant production and environmental signal transduction in *Staphylococcus aureus*. *J Bacteriol.* 1998;180(23):6232–41.
91. Daum RS, Spellberg B. Progress toward a *Staphylococcus aureus* vaccine. *Clin Infect Dis.* 2012;54(4):560–7.
92. Otto M. *Staphylococcus aureus* toxins. *Curr Opin Microbiol.* 2014;17:32–7.
93. Berube BJ, Wardenburg JB. *Staphylococcus aureus*  $\alpha$ -toxin: nearly a century of intrigue. *Toxins (Basel).* 2013;5(6):1140–66.
94. Valeva A, Walev I, Pinkernell M, Walker B, Bayley H, Palmer M, et al. Transmembrane  $\beta$ -barrel of staphylococcal  $\alpha$ -toxin forms in sensitive but not in resistant cells. *Proc Natl Acad Sci.* 1997;94(21):11607–11.
95. Nygaard TK, Pallister KB, DuMont AL, DeWald M, Watkins RL, Pallister EQ, et al. Alpha-toxin induces programmed cell death of human T cells, B cells, and monocytes during USA300 infection. *PLoS One.* 2012;7(5):e36532.
96. Inoshima N, Wang Y, Wardenburg JB. Genetic requirement for ADAM10 in severe *Staphylococcus aureus* skin infection. *J Invest Dermatol.* 2012;132(5):1513.
97. Leung YL. *Staphylococcus aureus*. In: Wexler PBT-E of T (Third E, editor. Oxford: Academic Press; 2014. p. 379–80.
98. Li M, Diep BA, Villaruz AE, Braughton KR, Jiang X, DeLeo FR, et al. Evolution of virulence in epidemic community-associated methicillin-resistant *Staphylococcus aureus*. *Proc Natl Acad Sci.* 2009;106(14):5883–8.
99. Wang R, Braughton KR, Kretschmer D, Bach T-HL, Queck SY, Li M, et al. Identification of novel cytolytic peptides as key virulence determinants for

- community-associated MRSA. *Nat Med*. 2007;13(12):1510–4.
100. Lee CY, Schmidt JJ, Johnson-Winegar AD, Spero L, Iandolo JJ. Sequence determination and comparison of the exfoliative toxin A and toxin B genes from *Staphylococcus aureus*. *J Bacteriol*. 1987;169(9):3904–9.
  101. Mariutti RB, Tartaglia NR, Seyffert N, de Paula Castro TL, Arni RK, Azevedo VA, et al. Exfoliative toxins of *Staphylococcus aureus*. *Rise Virulence Antibiot Resist Staphylococcus aureus InTech*. 2017;127–43.
  102. Bukowski M, Wladyka B, Dubin G. Exfoliative toxins of *Staphylococcus aureus*. *Toxins (Basel)*. 2010;2(5):1148–65.
  103. Kwiecinski J, Jacobsson G, Karlsson M, Zhu X, Wang W, Bremell T, et al. Staphylokinase promotes the establishment of *Staphylococcus aureus* skin infections while decreasing disease severity. *J Infect Dis*. 2013;208(6):990–9.
  104. Thomer L, Schneewind O, Missiakas D. Multiple ligands of von Willebrand factor-binding protein (vWbp) promote *Staphylococcus aureus* clot formation in human plasma. *J Biol Chem*. 2013;288(39):28283–92.
  105. O’Gara JP, Humphreys H. *Staphylococcus epidermidis* biofilms: importance and implications. *J Med Microbiol*. 2001;50(7):582–7.
  106. Zimmerli W, Trampuz A, Ochsner PE. Prosthetic-joint infections. *N Engl J Med*. 2004;351(16):1645–54.
  107. Lister JL, Horswill AR. *Staphylococcus aureus* biofilms: recent developments in biofilm dispersal. *Front Cell Infect Microbiol*. 2014; 4: 178. 2014.
  108. Peschel A, Otto M. Phenol-soluble modulins and staphylococcal infection. *Nat Rev Microbiol*. 2013;11(10):667–73.
  109. Le KY, Villaruz AE, Zheng Y, He L, Fisher EL, Nguyen TH, et al. Role of phenol-soluble modulins in *Staphylococcus epidermidis* biofilm formation and infection of indwelling medical devices. *J Mol Biol*. 2019;431(16):3015–27.
  110. Foster TJ, Geoghegan JA, Ganesh VK, Höök M. Adhesion, invasion and evasion: the many functions of the surface proteins of *Staphylococcus aureus*. *Nat Rev Microbiol*. 2014;12(1):49–62.

111. Foster TJ. The MSCRAMM family of cell-wall-anchored surface proteins of gram-positive cocci. *Trends Microbiol.* 2019;27(11):927–41.
112. Gross M, Cramton SE, Götz F, Peschel A. Key role of teichoic acid net charge in *Staphylococcus aureus* colonization of artificial surfaces. *Infect Immun.* 2001;69(5):3423–6.
113. Holland LM, Conlon B, O’Gara JP. Mutation of tagO reveals an essential role for wall teichoic acids in *Staphylococcus epidermidis* biofilm development. *Microbiology.* 2011;157(2):408–18.
114. Qin Z, Ou Y, Yang L, Zhu Y, Tolker-Nielsen T, Molin S, et al. Role of autolysin-mediated DNA release in biofilm formation of *Staphylococcus epidermidis*. *Microbiology.* 2007;153(7):2083–92.
115. Otto M. Physical stress and bacterial colonization. *FEMS Microbiol Rev.* 2014;38(6):1250–70.
116. Schilcher K, Horswill AR. Staphylococcal biofilm development: structure, regulation, and treatment strategies. *Microbiol Mol Biol Rev.* 2020;84(3).
117. O’Gara JP. *ica* and beyond: biofilm mechanisms and regulation in *Staphylococcus epidermidis* and *Staphylococcus aureus*. *FEMS Microbiol Lett.* 2007;270(2):179–88.
118. Speziale P, Pietrocola G, Foster TJ, Geoghegan JA. Protein-based biofilm matrices in *Staphylococci*. *Front Cell Infect Microbiol.* 2014;4:171.
119. Katayama Y, Ito T, Hiramatsu K. A new class of genetic element, staphylococcus cassette chromosome *mec*, encodes methicillin resistance in *Staphylococcus aureus*. *Antimicrob Agents Chemother.* 2000;44(6):1549–55.
120. Hartman BJ, Tomasz A. Low-affinity penicillin-binding protein associated with beta-lactam resistance in *Staphylococcus aureus*. *J Bacteriol.* 1984;158(2):513–6.
121. Kennedy AD, Otto M, Braughton KR, Whitney AR, Chen L, Mathema B, et al. Epidemic community-associated methicillin-resistant *Staphylococcus aureus*: recent clonal expansion and diversification. *Proc Natl Acad Sci.* 2008;105(4):1327–32.
122. McAdam PR, Templeton KE, Edwards GF, Holden MTG, Feil EJ, Aanensen DM, et al. Molecular tracing of the emergence, adaptation, and transmission of hospital-associated methicillin-resistant *Staphylococcus aureus*. *Proc Natl Acad Sci.*



2012;109(23):9107–12.

123. David MZ, Daum RS, Bayer AS, Chambers HF, Fowler Jr VG, Miller LG, et al. Staphylococcus aureus bacteremia at 5 US academic medical centers, 2008–2011: significant geographic variation in community-onset infections. *Clin Infect Dis*. 2014;59(6):798–807.
124. Casey JA, Curriero FC, Cosgrove SE, Nachman KE, Schwartz BS. High-density livestock operations, crop field application of manure, and risk of community-associated methicillin-resistant Staphylococcus aureus infection in Pennsylvania. *JAMA Intern Med*. 2013;173(21):1980–90.
125. Waldor MK, Friedman DI, Adhya SL. Phages: their role in bacterial pathogenesis and biotechnology. ASM press; 2005.
126. Olszak T, Latka A, Roszniowski B, Valvano MA, Drulis-Kawa Z. Phage life cycles behind bacterial biodiversity. *Curr Med Chem*. 2017;24(36):3987–4001.
127. Hendrix RW, Hatfull GF, Ford ME, Smith MCM, Burns RN. Evolutionary relationships among diverse bacteriophages and prophages: all the world's a phage. In: *Horizontal Gene Transfer*. Elsevier; 2002. p. 133–VI.
128. Abedon ST, Kuhl SJ, Blasdel BG, Kutter EM. Phage treatment of human infections. *Bacteriophage*. 2011;1(2):66–85.
129. Bergh Ø, Børsheim KY, Bratbak G, Heldal M. High abundance of viruses found in aquatic environments. *Nature*. 1989;340(6233):467–8.
130. Whitman WB, Coleman DC, Wiebe WJ. Prokaryotes: the unseen majority. *Proc Natl Acad Sci*. 1998;95(12):6578–83.
131. Abedon ST, Thomas-Abedon C, Thomas A, Mazure H. Bacteriophage prehistory: is or is not Hankin, 1896, a phage reference? *Bacteriophage*. 2011;1(3):174–8.
132. Twort FW. An investigation on the nature of ultra-microscopic viruses. *Lancet*. 1915;186(4814):1241–3.
133. d'Herelle MF. Sur un microbe invisible antagoniste des bacilles dysentériques. *Acta Kravsi*. 1961;
134. Sharma S, Chatterjee S, Datta S, Prasad R, Dubey D, Prasad RK, et al. Bacteriophages

- and its applications: an overview. *Folia Microbiol (Praha)*. 2017;62(1):17–55.
135. Lin DM, Koskella B, Lin HC. Phage therapy: An alternative to antibiotics in the age of multi-drug resistance. *World J Gastrointest Pharmacol Ther*. 2017;8(3):162.
  136. Sulakvelidze A. *Bacteriophages: biology and applications*. CRC Press; 2005.
  137. O’Flaherty S, Ross RP, Coffey A. Bacteriophage and their lysins for elimination of infectious bacteria. *FEMS Microbiol Rev*. 2009;33(4):801–19.
  138. Breitbart M, Rohwer F. Here a virus, there a virus, everywhere the same virus? *Trends Microbiol*. 2005;13(6):278–84.
  139. Hatfull GF. Mycobacteriophages: windows into tuberculosis. *PLoS Pathog*. 2014;10(3):e1003953.
  140. Adriaenssens EM, Sullivan MB, Knezevic P, van Zyl LJ, Sarkar BL, Dutilh BE, et al. Taxonomy of prokaryotic viruses: 2018-2019 update from the ICTV Bacterial and Archaeal Viruses Subcommittee. *Arch Virol*. 2020;1–8.
  141. Ackermann HW. Bacteriophage taxonomy. *Microbiol Aust*. 2011;32(2):90–4.
  142. Mayer G. Bacteriophage [Internet]. [cited 2020 Jan 2]. Available from: <http://www.microbiologybook.org/mayer/phage.htm>
  143. Rastogi V, Verma N, Mishra AK, Nath G, Gaur PK, Verma A. An overview on bacteriophages: A natural nanostructured antibacterial agent. *Curr Drug Deliv*. 2018;15(1):3–20.
  144. Gill JJ, Hyman P. Phage choice, isolation, and preparation for phage therapy. *Curr Pharm Biotechnol*. 2010;11(1):2–14.
  145. García Suárez MP, Rodríguez L, Rodríguez González A, Martínez Fernández B. Food biopreservation: Promising strategies using bacteriocins, bacteriophages and endolysins. 2010;
  146. Nicastro J. Overview of Bacteriophage Lifecycles and Applications. In: *Bacteriophage Applications-Historical Perspective and Future Potential*. Springer; 2016. p. 1–8.
  147. Bertozzi Silva J, Storms Z, Sauvageau D. Host receptors for bacteriophage adsorption. *FEMS Microbiol Lett*. 2016;363(4).

148. Molineux IJ, Panja D. Popping the cork: mechanisms of phage genome ejection. *Nat Rev Microbiol.* 2013;11(3):194–204.
149. Samson JE, Magadán AH, Sabri M, Moineau S. Revenge of the phages: defeating bacterial defences. *Nat Rev Microbiol.* 2013;11(10):675–87.
150. Weinbauer MG. Ecology of prokaryotic viruses. *FEMS Microbiol Rev.* 2004;28(2):127–81.
151. Young R. Phage lysis: three steps, three choices, one outcome. *J Microbiol.* 2014;52(3):243–58.
152. Catalao MJ, Gil F, Moniz-Pereira J, Sao-Jose C, Pimentel M. Diversity in bacterial lysis systems: bacteriophages show the way. *FEMS Microbiol Rev.* 2013;37(4):554–71.
153. Brüßow H, Canchaya C, Hardt W-D. Phages and the evolution of bacterial pathogens: from genomic rearrangements to lysogenic conversion. *Microbiol Mol Biol Rev.* 2004;68(3):560–602.
154. Keen EC. Paradigms of pathogenesis: targeting the mobile genetic elements of disease. *Front Cell Infect Microbiol* 2012; 2: 1-3. 2012.
155. Chaturongakul S, Ounjai P. Phage–host interplay: examples from tailed phages and Gram-negative bacterial pathogens. *Front Microbiol.* 2014;5:442.
156. Fortier L-C, Sekulovic O. Importance of prophages to evolution and virulence of bacterial pathogens. *Virulence.* 2013;4(5):354–65.
157. Feiner R, Argov T, Rabinovich L, Sigal N, Borovok I, Herskovits AA. A new perspective on lysogeny: prophages as active regulatory switches of bacteria. *Nat Rev Microbiol.* 2015;13(10):641–50.
158. Kropinski AMB, Clokie MRJ. *Bacteriophages: methods and protocols.* Humana; 2008.
159. Neuhard J. *Escherichia coli* and *Salmonella typhimurium*. *Cell Mol Biol.* 1987;445–67.
160. Kutter E, De Vos D, Gvasalia G, Alavidze Z, Gogokhia L, Kuhl S, et al. Phage therapy in clinical practice: treatment of human infections. *Curr Pharm Biotechnol.*

2010;11(1):69–86.

161. Drulis-Kawa Z, Majkowska-Skrobek G, Maciejewska B, Delattre A-S, Lavigne R. Learning from bacteriophages-advantages and limitations of phage and phage-encoded protein applications. *Curr Protein Pept Sci.* 2012;13(8):699–722.
162. Oechslin F, Piccardi P, Mancini S, Gabard J, Moreillon P, Entenza JM, et al. Synergistic interaction between phage therapy and antibiotics clears *Pseudomonas aeruginosa* infection in endocarditis and reduces virulence. *J Infect Dis.* 2017;215(5):703–12.
163. Ajuebor J, Buttner C, Arroyo-Moreno S, Chanishvili N, Gabriel EM, O'Mahony J, et al. Comparison of *Staphylococcus* phage K with close phage relatives commonly employed in phage therapeutics. *Antibiotics.* 2018;7(2):37.
164. Riede I, Eschbach M-L. Evidence that TraT interacts with OmpA of *Escherichia coli*. *FEBS Lett.* 1986;205(2):241–5.
165. Liu M, Deora R, Doulatov SR, Gingery M, Eiserling FA, Preston A, et al. Reverse transcriptase-mediated tropism switching in *Bordetella* bacteriophage. *Science (80-)*. 2002;295(5562):2091–4.
166. Turner PE, Duffy S. Evolutionary ecology of multiple phage adsorption and infection. *Bacteriophage Ecol Popul growth, Evol impact Bact viruses.* 2008;195–216.
167. Hofer B, Ruge M, Dreiseikelmann B. The superinfection exclusion gene (*sieA*) of bacteriophage P22: identification and overexpression of the gene and localization of the gene product. *J Bacteriol.* 1995;177(11):3080–6.
168. Van Der Oost J, Westra ER, Jackson RN, Wiedenheft B. Unravelling the structural and mechanistic basis of CRISPR–Cas systems. *Nat Rev Microbiol.* 2014;12(7):479–92.
169. Kelly D, McAuliffe O, O'Mahony J, Coffey A. Development of a broad-host-range phage cocktail for biocontrol. *Bioeng Bugs.* 2011;2(1):31–7.
170. Dy RL, Przybilski R, Semeijn K, Salmond GPC, Fineran PC. A widespread bacteriophage abortive infection system functions through a Type IV toxin–antitoxin mechanism. *Nucleic Acids Res.* 2014;42(7):4590–605.
171. Weber-Dąbrowska B, Jończyk-Matysiak E, Żaczek M, Łobocka M, Łusiak-

- Szelachowska M, Górski A. Bacteriophage procurement for therapeutic purposes. *Front Microbiol.* 2016;7:1177.
172. Hanlon GW. Bacteriophages: an appraisal of their role in the treatment of bacterial infections. *Int J Antimicrob Agents.* 2007;30(2):118–28.
173. Azeredo J, Sutherland IW. The use of phages for the removal of infectious biofilms. *Curr Pharm Biotechnol.* 2008;9(4):261–6.
174. Gorski A, Miedzybrodzki R, Borysowski J, Weber-Dabrowska B, Lobočka M, Fortuna W, et al. Bacteriophage therapy for the treatment of infections. *Curr Opin Investig drugs (London, Engl 2000).* 2009;10(8):766–74.
175. Alisky J, Iczkowski K, Rapoport A, Troitsky N. Bacteriophages show promise as antimicrobial agents. *J Infect.* 1998;36(1):5–15.
176. Pouillot F, Chomton M, Blois H, Courroux C, Noelig J, Bidet P, et al. Efficacy of bacteriophage therapy in experimental sepsis and meningitis caused by a clone O25b:H4-ST131 *Escherichia coli* strain producing CTX-M-15. *Antimicrob Agents Chemother.* 2012;56(7):3568–75.
177. Wittebole X, De Roock S, Opal SM. A historical overview of bacteriophage therapy as an alternative to antibiotics for the treatment of bacterial pathogens. *Virulence.* 2014;5(1):226–35.
178. Bruttin A, Brüßow H. Human volunteers receiving *Escherichia coli* phage T4 orally: a safety test of phage therapy. *Antimicrob Agents Chemother.* 2005;49(7):2874–8.
179. Merabishvili M, Pirnay JP, Verbeken G, Chanishvili N, Tediashvili M, Lashkhi N, et al. Quality-controlled small-scale production of a well-defined bacteriophage cocktail for use in human clinical trials. *PLoS One.* 2009;4(3).
180. Pirnay J-P, De Vos D, Verbeken G, Merabishvili M, Chanishvili N, Vaneechoutte M, et al. The phage therapy paradigm: pret-a-porter or sur-mesure? *Pharm Res.* 2011;28(4):934–7.
181. Ackermann H-W, Kropinski AM. Curated list of prokaryote viruses with fully sequenced genomes. *Res Microbiol.* 2007;158(7):555–66.
182. Goodridge LD. Designing phage therapeutics. *Curr Pharm Biotechnol.* 2010;11(1):15–27.

183. Międzybrodzki R, Borysowski J, Weber-Dąbrowska B, Fortuna W, Letkiewicz S, Szufnarowski K, et al. Clinical aspects of phage therapy. In: *Advances in virus research*. Elsevier; 2012. p. 73–121.
184. Donlan RM. Preventing biofilms of clinically relevant organisms using bacteriophage. *Trends Microbiol*. 2009;17(2):66–72.
185. Dhivya S, Padma VV, Santhini E. Wound dressings—a review. *BioMedicine*. 2015;5(4).
186. Sarabahi S. Recent advances in topical wound care. *Indian J Plast Surg Off Publ Assoc Plast Surg India*. 2012;45(2):379.
187. Rezvani Ghomi E, Khalili S, Nouri Khorasani S, Esmaeely Neisiany R, Ramakrishna S. Wound dressings: Current advances and future directions. *J Appl Polym Sci*. 2019;136(27):47738.
188. Boateng JS, Matthews KH, Stevens HNE, Eccleston GM. Wound healing dressings and drug delivery systems: a review. *J Pharm Sci*. 2008;97(8):2892–923.
189. Moshakis V, Fordyce MJ, Griffiths JD, McKinna JA. Tegadern versus gauze dressing in breast surgery. *Br J Clin Pract*. 1984;38(4):149.
190. Thomas S, Loveless P, Hay NP. Comparative review of the properties of six semipermeable film dressings. *Pharm J*. 1988;240:785–7.
191. Ramos-e-Silva M, de Castro MCR. New dressings, including tissue-engineered living skin. *Clin Dermatol*. 2002;20(6):715–23.
192. Kamoun EA, Kenawy E-RS, Chen X. A review on polymeric hydrogel membranes for wound dressing applications: PVA-based hydrogel dressings. *J Adv Res*. 2017;8(3):217–33.
193. Fan L, Yang H, Yang J, Peng M, Hu J. Preparation and characterization of chitosan/gelatin/PVA hydrogel for wound dressings. *Carbohydr Polym*. 2016;146:427–34.
194. Borda LJ, Macquhae FE, Kirsner RS. Wound dressings: a comprehensive review. *Curr Dermatol Rep*. 2016;5(4):287–97.
195. Thomas S. A comparative study of twelve hydrocolloid dressings. *Surgical Material*

- Testing Laboratory technical notes. *World Wide Wounds*. 1997;
196. Thomas S. Hydrocolloids. *J Wound Care*. 1992;1(2):27–30.
  197. Vowden K, Vowden P. Wound dressings: principles and practice. *Surg*. 2017;35(9):489–94.
  198. Phaechamud T, Issarayungyuen P, Pichayakorn W. Gentamicin sulfate-loaded porous natural rubber films for wound dressing. *Int J Biol Macromol*. 2016;85:634–44.
  199. Meaume S, Vallet D, Nguyen Morere M, Teot L. Evaluation of a silver-releasing hydroalginate dressing in chronic wounds with signs of local infection. *J Wound Care*. 2005;14(9):411–9.
  200. Totty JP, Bua N, Smith GE, Harwood AE, Carradice D, Wallace T, et al. Dialkylcarbamoyl chloride (DACC)-coated dressings in the management and prevention of wound infection: a systematic review. *J Wound Care*. 2017;26(3):107–14.

# Chapter 2: General Materials and Methods

## 2.1. Materials

**Table 2.1:** List of reagents and materials

<b>Material</b>	<b>Supplier</b>
Acetone	Sigma-Aldrich
Acid phosphatase	Sigma-Aldrich
Alkaline phosphatase	Sigma-Aldrich
Amikacin hydrate	Sigma-Aldrich
Amoxicillin	Sigma-Aldrich
Bacteriological agar	Sigma-Aldrich
Bovine Serum albumin	Sigma-Aldrich
Brain Heart Infusion agar	Sigma-Aldrich
Chloroform	Sigma-Aldrich
Ciprofloxacin hydrochloride hydrate	Fischer Scientific
Crystal violet	Sigma-Aldrich
D-(+)-glucose	Sigma-Aldrich
Dichloromethane	Sigma-Aldrich
Ethanol	Sigma-Aldrich
Eudragit® FS 30 D	Evonik Industries
Fetal bovine serum	Sigma-Aldrich
Glycerol	Sigma-Aldrich
Luria Broth Base (Miller's LB Broth Base)	Fischer Scientific
Mannitol salt agar	Sigma-Aldrich
Mueller Hinton agar	Sigma-Aldrich
Mueller Hinton broth	Sigma-Aldrich
pH probe large surface flat tip, HDPE junction 662-1769	VWR International
Phosphate buffered saline	Sigma-Aldrich
Poly(ethylene glycol) 400	Sigma-Aldrich
Poly(vinyl alcohol) MW 146000 – 186000, 99+% hydrolysed	Sigma-Aldrich
Polylactic acid $M_w \sim 60\ 000$	Sigma-Aldrich
Polystyrene tissue culture microplates (12-well)	Sigma-Aldrich
Polystyrene tissue culture microplates (96-well)	Sigma-Aldrich
Porcine liver esterase	Sigma-Aldrich
Protease from <i>Streptomyces griseus</i>	Sigma-Aldrich
Proteinase K	Sigma-Aldrich
Sodium chloride, BioXtra $\geq 99.5$ (AT)	Sigma-Aldrich
Sodium hydroxide, BioXtra $\geq 98$ (acidmetric)	Sigma-Aldrich
Spin-X® UF Concentrator Corning®	Sigma-Aldrich



Tris-HCl	Fischer Scientific
Trypsin	Sigma-Aldrich
Tryptic Soy agar	Sigma-Aldrich
Tryptic Soy broth	Sigma-Aldrich
Vancomycin hydrate from <i>Streptomyces orientalis</i>	Sigma-Aldrich
Whatman® Nucleopore™ Track-Etched Membranes (diameter 25 mm, pore size 0.2 µm, polycarbonate)	Sigma-Aldrich

## 2.2. Methods

### 2.2.1. Bacteria

#### 2.2.1.1. Bacterial Strains

All bacterial strains used in this thesis were obtained from Professor Toby Jenkins, University of Bath, UK or Professor Jean-Yves Maillard, Cardiff University, UK. Bacterial cultures were stored at  $-80\text{ }^{\circ}\text{C}$  in phosphate buffer solution (PBS) containing 20 % (v/v) glycerol. Working stocks were cultured from frozen by streaking onto a TSA plate and incubating at  $37\text{ }^{\circ}\text{C}$  for 24 h. Plates were subsequently stored at  $4\text{ }^{\circ}\text{C}$  for up to a month for further use.

#### 2.2.1.2. Principles of Bacterial Growth

Bacteria proliferate through an asexual process called binary fission, and their growth curve is depicted in Figure 2.1.

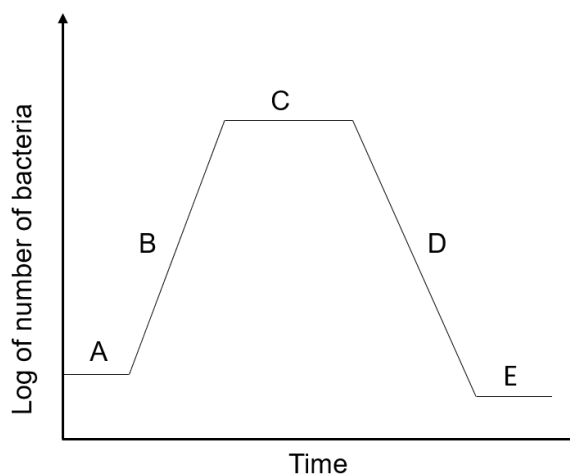


**Figure 2.1:** Typical growth curve of a closed-system bacterial culture. **A)** Lag phase, **B)** Logarithmic phase, **C)** Stationary phase, **D)** Death phase and **E)** Long-term stationary phase

The first stage of bacterial growth is the lag phase, where the bacteria are maturing and synthesising RNA, enzymes, and other molecules. Although bacterial cells are not yet able to divide, they are not dormant. The length of this period is dependent on the bacterial species and the length of time the cells have undergone starved conditions before entering this stage. Next, is the logarithmic (or exponential) phase, characterised by the exponential growth of bacteria. The slope of this line is dependent upon both the organism and the growth conditions. However, as the medium becomes depleted, bacterial cells enter the stationary phase of growth. This arises when the rate of growth is equal to the rate of death, resulting in a plateau with no net increase in cell density. Upon the depletion of all nutrients and/or the formation of inhibitory waste products, the bacteria enter the death phase. This is where the number of viable bacterial cells decrease exponentially until about 90-99% of the population die.

### **2.2.1.3. Bacterial Culture Conditions**

Bacterial overnights were routinely prepared using colonies obtained from the respective bacterial strain's tryptic soy agar (TSA) plate. Colonies were grown in tryptic soy broth (TSB) and incubated at 37 °C with 150 rpm shaking for 18 h. After incubation, cultures were centrifuged at 4000 g for 10 min and re-suspended in PBS. Cultures were standardised to an optical density (OD) at 600 nm of 0.2 (c. 10<sup>7</sup> CFU/mL) before use, unless otherwise stated.

### **2.2.1.4. Bacterial Enumeration**

Estimation of the total viable count of bacterial cultures were calculated using the drop count method, as outlined by Miles and Misra.<sup>1</sup> The initial bacterial suspension underwent a series of 10-fold dilutions in PBS, and subsequently three 10 µL spots of each dilution were pipetted onto the surface of a TSA plate. The spots were allowed to dry for 20 min at room temperature before incubation at 37 °C for 18 h. The number of Colony Forming Units per mL (CFU/mL) was calculated as follows:

$$\text{CFU/mL} = \frac{\text{Average number of colonies}}{d \cdot V} \quad (1)$$

Where d = dilution factor and V = volume of inoculum.

### **2.2.1.5. Minimum Inhibitory Concentration**

The Minimum Inhibitory Concentration (MIC) of an antimicrobial was conducted according to the Clinical and Laboratory Standards Institute (CLSI) guidelines.<sup>2</sup> Briefly,

stock solutions of antimicrobials were prepared at twice the starting concentration in sterile deionised water (dH<sub>2</sub>O). Then, 100 µL of the chosen antimicrobial was added to a 96 well plate and serially diluted two-fold in TSB (unless otherwise stated). An overnight culture of bacteria, previously adjusted to an OD<sub>600</sub> of 0.2 underwent a 10-fold dilution in fresh TSB to attain a concentration of 10<sup>6</sup> CFU/mL, before 100 µL of the suspension was added to all relevant wells in the 96 well plate. A negative (bacteria only) and positive (broth only) control was carried out in tandem. The plate was incubated for 18 h at 37 °C and the MIC was determined as the concentration of antibiotic that resulted in no detectable bacterial growth, assessed by measuring the OD<sub>600</sub> using a SPECTROstar® Omega microplate reader (BMG LabTech, UK). Three independent biological replicates per biological species were performed.

## **2.2.2. *In vitro* Biofilm Models**

### **2.2.2.1. 96-Microtiter Biofilm Models**

#### **2.2.2.1.1. Minimum Biofilm Inhibitory Concentration**

Biofilm formation was conducted in a 96-well polystyrene microtiter plate. First, the chosen antimicrobial was prepared at twice the starting concentration in TSB containing 1% (w/v) D-(+)-glucose (TSBg). Then, 100 µL of the chosen antimicrobial was added to the 96 well plate and serially diluted two-fold in 1% TSBg (unless otherwise stated). Next, overnight cultures of bacteria were sub-cultured into fresh 1% TSBg to attain a concentration of 10<sup>6</sup> CFU/mL, before 100 µL was added into relevant wells in the plate and statically incubated at 37 °C for 18 h. Following incubation, plates were washed three times with sterile dH<sub>2</sub>O to remove planktonic bacteria and evaluated for biofilm formation via Crystal Violet (CV) assay (Section 2.2.2.1.3). The Minimum Biofilm Inhibitory Concentration (MBIC) was the concentration that resulted in no detectable biofilm growth compared to the control. Negative and positive controls were carried out in tandem, and three independent biological replicates per biological species were performed.

#### **2.2.2.1.2. Minimum Biofilm Eradication Concentration**

Overnight cultures of bacteria were sub-cultured into fresh 1% TSBg to attain a concentration of 10<sup>6</sup> CFU/mL. Next, 200 µL of the adjusted bacterial suspension was added into the relevant wells within the 96-well microtiter plate, and statically incubated at 37 °C for 24 h. Following incubation, plates were washed three times with sterile dH<sub>2</sub>O and left to air dry for 5 min. Concurrently, stock solutions of antimicrobials were prepared at twice the starting concentration in 1% TSBg (unless otherwise stated), and 100 µL was serially diluted

in equal volume of 1% TSBg across the microtiter plate. Finally, 100  $\mu$ L of 1% TSBg was added to relevant wells to achieve a final volume of 200  $\mu$ L per well. The plate was further incubated at 37 °C for 18 h, before being washed three times with sterile dH<sub>2</sub>O to remove planktonic bacteria and evaluated for biofilm formation by the CV assay (Section 2.2.2.1.3). The Minimum Biofilm Eradication Concentration (MBEC) was the concentration that resulted in no detectable biofilm growth, compared to the control after incubation with the antimicrobials. Negative and positive controls were carried out in tandem, and three independent biological replicates per biological species were performed.

#### **2.2.2.1.3. Crystal Violet Assay**

Biofilms of the bacterial isolates were prepared as outlined in Section 2.2.2.1.1 and 2.2.2.1.2. After washing three times in sterile dH<sub>2</sub>O, the microtiter plate was left to dry for 20 min at room temperature. Next, 220  $\mu$ L of 0.1% CV was added to all relevant wells, and the microtiter plate was incubated at room temperature for 30 min. After incubation, the stain was removed, and the plate was washed three times with sterile dH<sub>2</sub>O before being left to dry for at least 3 h at room temperature. To quantify the biofilm biomass, 220  $\mu$ L of 33 % acetic acid was added to the CV-stained biofilms for 15 min at room temperature, after which 100  $\mu$ L was transferred to a new microtiter plate and the optical density at 590 nm (OD<sub>590</sub>) was measured using a SPECTROstar® Omega microplate reader (BMG LabTech, UK).

#### **2.2.2.2. Colony Biofilm Model**

The colony biofilm model was prepared as outlined in Thet *et al* with some modifications (Figure 2.2.).<sup>3</sup> Polycarbonate membranes (19 mm) were UV sterilised for 10 min on Brain Heart Infusion (BHI) agar before addition of 30  $\mu$ L of Artificial Wound Fluid (AWF; 50% fetal bovine serum in 50% peptone water [0.9% sodium chloride in 0.1% peptone]). The AWF was left to dry at room temperature. After, 50  $\mu$ L of a sub-cultured bacterial isolate (10<sup>6</sup> CFU/mL) was placed onto the membrane and left to dry at room temperature. Inoculated plates were then incubated for 24 h at 32 °C or 37 °C depending on experimental procedure. After incubation, the membranes were placed into 10 mL of PBS and the biofilms were stripped by sonication (44 KHz) for 15 min twice, with a 60 s interval of vortexing between sonication cycles. Viable cells were quantified as outlined in Section 2.2.1.4

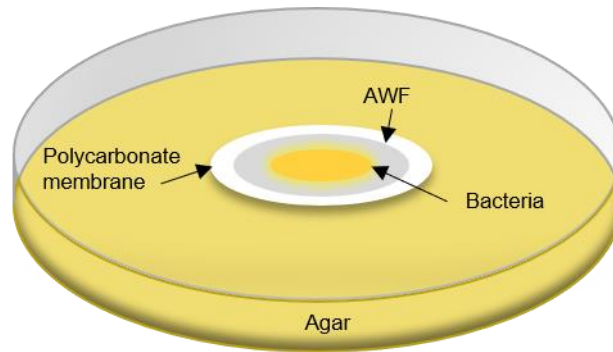


**Figure 2.2:** Schematic of the Colony Biofilm Model. AWF = Artificial Wound Fluid.

## **2.2.3. Bacteriophage**

Bacteriophage K used in this project was provided by American Type Culture Collection (ATCC; Manassas, Virginia, United States).

### **2.2.3.1. Principles of Bacteriophage Growth**

Immediately following phage incubation with bacteria, phage enter the latent period, whereby there is no release of virions. After the latent period, the host cells are rapidly lysed, releasing the phage into the extracellular environment. This is known as the rise period, and the term “burst size” is used in relation to the number of phage released from a single infected bacterium.<sup>4</sup>

### **2.2.3.2. Bacteriophage Propagation**

#### **2.2.3.2.1. Soft Overlay Method**

Propagation of bacteriophage using the soft agar overlay method used molten top agar (65% strength TSA) stored at 60 °C until required. Briefly, 100 µL of phage lysate and 100 µL of an overnight culture of host *S. aureus* H560 (c. 10<sup>9</sup> CFU/mL) were added to 5 mL of cooling molten agar and vortexed. The mixture was then poured onto TSA plates and spread to ensure uniform coverage. After overnight incubation at 37 °C, 5 mL of PBS was added to plates that displayed confluent lysis and left for 20 min. Using a sterile L-shaped spreader, the solution and top agar were collected from the plate and centrifuged at 4000 g for 15 min to remove agar and cell debris. The supernatant was subsequently filter-sterilised using 0.22 µm filters (Millipore, Cork, Ireland), enumerated, and stored at 4 °C until further use.

### 2.2.3.2.2. Liquid Lysate

Briefly, 1 mL of standardised *S. aureus* H560 suspension (c.10<sup>6</sup> CFU/mL) was added to 19 mL of TSB and incubated at 37 °C with 150 rpm shaking for 3 h to achieve early-exponential phase bacteria. After this, 100 µL of phage lysate was added at a multiplicity of infection (MOI) of approximately 0.1 (c. 10<sup>6</sup> PFU/mL), and the suspension was incubated for a further 18 h at 37 °C. Following incubation, the suspension was centrifuged (4000 g, 15 min) to remove cell debris, filter sterilised (0.22 µM filter), enumerated, and stored at 4 °C until further use.

### 2.2.3.3. Bacteriophage Enumeration

Total viable count for bacteriophage suspensions were performed using an adapted drop counting method (Figure 2.3). For this, 100 µL of an overnight culture of host strain *S. aureus* H560 (c. 10<sup>9</sup> CFU/mL) was added to 5 mL of TSA molten top agar, vortexed, poured onto TSA plates and left to air dry at room temperature for 15 min. Meanwhile, the initial bacteriophage suspension underwent a series of 10-fold dilutions in PBS buffer, before three 10 µL of selected dilutions were pipetted onto the surface of the agar plates and allowed to dry for 15 min at room temperature. The plates were subsequently incubated at 37 °C for 18 h. Following incubation, plaques (clearings in the bacterial lawn) were counted and the plaque forming units per millilitre (PFU/mL) was calculated as follows:

$$\text{PFU/mL} = \frac{\text{Number of plaques}}{d \cdot V} \quad (2)$$

Where d = dilution factor, and V = volume of inoculum.

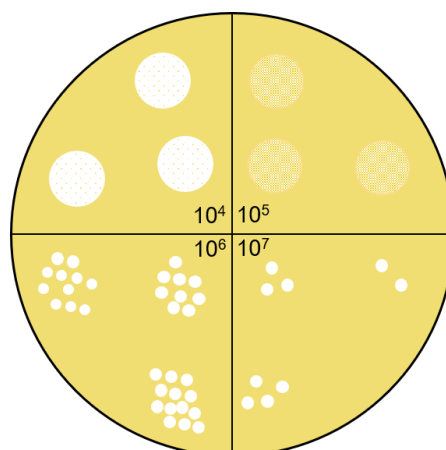


**Figure 2.3:** Schematic of plaque counting (PFU/mL) for bacteriophage enumeration.

#### **2.2.3.4. Increasing Bacteriophage Titre**

In instances where a high bacteriophage titre was needed, bacteriophage lysate solutions were concentrated using Spin-X® UF Concentrator Corning® centrifuge tubes (Sigma-Aldrich, Poole, UK) Briefly, 20 mL of phage lysate were added into the Spin-X® UF Concentrator Corning® centrifuge tubes and centrifuged until concentrated to a volume of 1 mL. Once concentrated, the lysate was filter sterilised (0.22 µm filter) and enumerated as outlined in Section 2.2.3.3

#### **2.2.4. Data Analysis and Statistics**

All data analysis and statistical modelling was performed using GraphPad Prism, version 7.0. All experiments undertaken in this thesis were carried out in triplicate using three biological replicates and displayed as the mean ± standard deviation (SD), unless otherwise stated.

## 2.3. References

1. Miles AA, Misra SS, Irwin JO. The estimation of the bactericidal power of the blood. *J Hyg (Lond)*. 1938;38(6):732–49.
2. Weinstein MP. Performance standards for antimicrobial susceptibility testing. Clinical and Laboratory Standards Institute; 2019.
3. Thet NT, Alves DR, Bean JE, Booth S, Nzakizwanayo J, Young AER, et al. Prototype development of the intelligent hydrogel wound dressing and its efficacy in the detection of model pathogenic wound biofilms. *ACS Appl Mater Interfaces*. 2016;8(24):14909–19.
4. Neelesh T. Growth Curve of Bacteriophage [Internet]. [cited 2020 Jan 2]. Available from: <https://www.biologydiscussion.com/viruses/growth-curve-of-bacteriophage/47107>



# Chapter 3: Evaluation of Phage-Antibiotic Synergy

## 3.1. Overview of Chapter

The research presented in this chapter investigated the antibiotic efficacy of phage K and antibiotics against isolates of *S. aureus*, both individually and as a combination therapy. Herein, this chapter aims to discover whether interactions between phage and antibiotics were synergistic, and if so, why this was occurring.

## 3.2. Introduction

### 3.2.1. Phage-Antibiotic Synergy

One potential treatment strategy in clinical environments is to combine phage with antibiotics.<sup>1</sup> It is thought that the efficacy of specific phage and antibiotic combinations may be better than that of the individual therapies at targeting and eliminating pathogenic bacteria at an infection site. As such, there has been an increasing interest in phage-antibiotic combinations, with current research looking promising.<sup>2-4</sup>

The positive interaction between phage and antibiotics was first reported by Comeau *et al* in 2007, who termed this interaction “phage-antibiotic synergy” (PAS).<sup>4</sup> PAS was originally used to describe the phenomenon where sub-lethal concentrations of antibiotics increase the host bacterium’s production of virulent phage.<sup>4-6</sup> Nowadays, it is frequently used to describe interactions between phage and antibiotics that result in a significant decrease in bacterial concentration.<sup>5,7</sup> However, the term “synergy” is not well defined in the literature regarding PAS; hence, often encompasses “true synergy”, where the outcome of the combined treatment is greater than both of the monotherapies acting independently, and “facilitation/additive,” where the combined treatment is better than the best monotherapy, but is no better than both the monotherapies acting independently.<sup>7</sup>

One of the main advantages of phage-antibiotic combinations is that they could increase the therapeutic efficacy of antibiotics *in vivo*; therefore, antibiotics that have lost all clinical utility could potentially be used in phage-antibiotic combinations, resulting in improved patient outcomes.

### 3.2.2. Phage-Antibiotic Synergy Studies

Previous studies have investigated the role of PAS in several phage-antibiotic combinations (See below). Currently, several phage-antibiotic combinations have been shown to be effective in targeting bacterial species including: *P. aeruginosa* (*P. aeruginosa*),<sup>7-10</sup> *S. aureus*,<sup>11,12</sup> *Escherichia coli* (*E. coli*),<sup>4,5</sup> *Burkholderia cepacia* (*B. cepacia*),<sup>13</sup> *Pseudomonas fluorescens* (*P. fluorescens*),<sup>14</sup> *Klebsiella pneumoniae* (*K. pneumoniae*),<sup>2</sup> and *Acinetobacter baumannii* (*A. baumannii*).<sup>15</sup> Research into PAS has utilised planktonic bacterial suspensions, biofilm models, and *in vivo* testing to determine the clinical utility of phage-antibiotic combinations. However, there is no consensus as to what experimental procedure must be performed to confirm synergy between therapies, and as such many studies cannot be compared. This introduction will briefly highlight a selection of studies within in this field, outlining the many ways in which PAS has been defined.

#### 3.2.2.1. Planktonic Studies

Originally, PAS was identified by increasing plaque size and phage concentration, assayed by incubating phage on soft-agar impregnated with varying concentrations of antibiotics. The phenomenon of PAS was thought to be attributed to antibiotics increasing the burst size or reducing the latent period of the phage lifecycle.<sup>5</sup> Ryan *et al* found that increasing sub-lethal concentrations of cefotaxime led to increased T4 plaque sizes and concurrent increase in phage concentration.<sup>5</sup> This finding was confirmed by Jansen *et al*, who observed an increase in *A. baumannii* phage burst sizes upon combination with meropenem; hypothesising that the increased phage propagation was due to a cellular stress response.<sup>15</sup> Alternatively, in a study conducted by Knezevic and co-workers, they termed “synergy” as phage-antibiotic concentrations that decreased bacterial concentration (CFU/mL) by >2 log, compared to the most potent single therapy.<sup>16</sup> A summary of studies using planktonic bacterial suspensions is shown in Table 3.1.

**Table 3.1:** Examples of PAS in planktonic bacteria. Adapted from Malik *et al*<sup>17</sup> and Morrisette *et al*.<sup>18</sup>

Bacteria	Phage + Antibiotic	Outcome	Reference
<b>Plaque assays</b>			
<i>E. coli</i>	Phage $\Phi$ MFP + aztreonam, cefixime, cefotaxime, ceftazidime, ceftriaxone	Increase in plaque size and < 7-fold increase in phage population	Comeau 2007 <sup>4</sup>
<i>E. coli</i>	Phage RB32, RB33, T3, T4, T7 + cefotaxime	Increase in plaque size	Comeau 2007 <sup>4</sup>
<i>E. coli</i>	Phage T4 + cefotaxime	Approx. 9.6 fold increase in plaque size	Ryan 2012 <sup>5</sup>

**Table 3.1 (cont).**: Examples of PAS in planktonic bacteria. Adapted from Malik *et al*<sup>17</sup> and Morrisette *et al*.<sup>18</sup>

<b>Bacteria</b>	<b>Phage + Antibiotic</b>	<b>Outcome</b>	<b>Reference</b>
<b>Bacterial cell viability</b>			
<i>P. aeruginosa</i>	Phage LUZ7 + streptomycin	Up to a 6 log decrease in bacterial viability after 24 h	Torres-Barcelo 2014 <sup>19</sup>
<i>B. cepacia</i>	Phage KS12 and KS14 + ciprofloxacin, levofloxacin, ceftazidime, tetracycline, minocycline, and meropenem	Decrease in bacterial cell density	Kamal and Dennis 2015 <sup>13</sup>
<i>P. aeruginosa</i>	Phage Pf3 and Pfl + Carbenicillin, gentamicin, tetracycline, chloramphenicol	Decline in bacterial viability after 60 min, with a 3 log reduction after 6 h	Hagens 2006 <sup>20</sup>
<i>P. aeruginosa</i>	Phage Sigma-1 + ceftriaxone	2.56 log reduction in bacterial count	Knezevic 2013 <sup>16</sup>
<i>P. aeruginosa</i>	Phage KP22 + ceftazidime and piperacillin	Decrease in bacterial turbidity	Uchiyama 2018 <sup>21</sup>
<i>E. coli</i>	Phage ECA2 + ciprofloxacin	4 log reduction compared to the best monotherapy	Valério 2017 <sup>22</sup>
<i>S. aureus</i>	Phage SA5 + gentamicin	Lower cell densities compared to individual monotherapies	Kirby 2012 <sup>11</sup>
<i>A. baumannii</i>	Phage vB_AbaM-KARL-1 + ciprofloxacin, colistin, meropenem.	Decrease in bacterial turbidity	Jansen 2018 <sup>15</sup>

### 3.2.2.2. Biofilm Models

PAS has been shown to be effective in killing bacterial biofilms<sup>5</sup> including, *S. aureus*<sup>23</sup> and *P. aeruginosa*<sup>24</sup> due to the phage and antibiotic working synergistically to modify the biofilm structure, increasing susceptibility.<sup>25,26</sup> Ryan *et al* found that there was a marked decrease in antibiotic MBEC upon on the addition of T4 phage, which was enhanced with higher phage concentrations,<sup>5</sup> and Chan *et al* found that phage-resistant *P. aeruginosa* biofilms were more susceptible to the antibiotics tested compared with non-resistant strains.<sup>9</sup>

The presence of PAS in biofilms has also been attributed to phage-antibiotic combinations reducing the frequency of plasmid-borne resistance by targeting the plasmid-bearing cells.<sup>27</sup> Experiments conducted by Verma *et al*, found that there was a statistically significant decrease in the resistant variant population ( $p < 0.0001$ ) in *K. pneumoniae* biofilms treated with a phage-antibiotic (ciprofloxacin) combination compared to either antibiotic or phage treatment alone.<sup>28</sup> PAS is thought to help eradicate bacterial biofilms as phage produce

enzymes that breakdown the EPS, leading to better penetration of antibiotics into the bacterial biofilm. Additionally, if phage eliminate the bacteria at the exterior of the biofilm, the interior bacterial cells have increased metabolic activity due to the increased oxygenation and nutrient exposure, and therefore become more susceptible to both phage and antibiotics.<sup>7,29,30</sup> A summary of studies using biofilm models is shown in Table 3.2.

### 3.2.2.3. *In vivo* Models

Recently, several studies have used animal models to investigate PAS *in vivo* (Table 3.3). Kamal *et al* found that some antibiotics induce increased phage production of several Bcc phage in *Galleria mellonella* larvae.<sup>13</sup> Owing to this, there was increased survival of *Galleria mellonella* larvae 48 h post-infection when treated with the phage-antibiotic combination (88% survival) compared to phage K12 (33% survival) or meropenem (20% survival) alone.<sup>13</sup> Additionally, Blasco *et al* showed that infected *Galleria mellonella* were more likely to survive when treated with a combination of a phage and antibiotic, compared to treatment with the individual components.<sup>31</sup>

Murine models have also been used to investigate PAS; local administration of phage MR-10, combined with the oral administration of the antibiotic linezolid was used to treat acute hindpaw MRSA infections in 48 diabetic mice.<sup>12</sup> Additionally, Oechslin *et al* explored the efficacy of an anti-*Pseudomonas* phage cocktail (PP1131; 12 phage) in combination with ciprofloxacin for the treatment of *P. aeruginosa* endocarditis in a rat model.<sup>3</sup> The results showed enhanced killing with the combination therapy (residual bacterial titre of <2 log CFU/g), compared to the monotherapy groups (residual bacterial titres of >6 log CFU/g; p<0.0001). Interestingly, no phage-resistant bacterial isolates were isolated after 24 h incubation with the combination therapy.<sup>3</sup> Another study investigated phage-antibiotic combinations for the treatment of implant-related biofilm MRSA and *P. aeruginosa* osteomyelitis in rat models.<sup>32</sup> Antibiotics were administered intraperitoneally once daily for 14 days, while phage were administered directly into the medullary canal once daily for 3 days. Combination therapy was more effective than individual phage and antibiotics, resulting in a 6.2- and 3.4- fold lower bacterial cell count, respectively.<sup>32</sup>

Research has shifted to focus on the efficacy of phage-antibiotic concentrations in treating complex multi-drug resistant (MDR) bacterial infections in humans,<sup>33-35</sup> with Chan *et al* showing the utility of PAS in treating a patient with a *P. aeruginosa* infected wound (phage OMKO1 and ceftazidime).<sup>8</sup>

**Table 3.2:** Examples of PAS in bacterial biofilms. Adapted from Malik *et al.*<sup>17</sup> and Morrisette *et al.*<sup>18</sup>

<b>Bacteria</b>	<b>Phage + Antibiotic</b>	<b>Outcome</b>	<b>Results</b>
<i>K. pneumoniae</i>	Phage + amoxicillin	Statistically significant ( $p < 0.01$ ) reduction in bacterial count	Bedi 2009 <sup>2</sup>
<i>E. coli</i>	T4 + cefotaxime	Significant reduction in bacterial count	Ryan 2012 <sup>5</sup>
<i>E. coli</i>	T4 + tobramycin	99% and 39% reduction in antibiotic and phage-resistant bacterial cell count, respectively.	Coulter 2014 <sup>36</sup>
<i>P. aeruginosa</i>	PB-1 phage + tobramycin	2 log reduction and 60% reduction in antibiotic and phage-resistant bacterial cell count, respectively.	Coulter 2014 <sup>36</sup>
<i>P. aeruginosa</i>	Phage NP1 and NP3 + ceftazidime, ciprofloxacin, tobramycin	Greater than 2 log reduction observed when antibiotics were combined with both phages compared to the best monotherapy	Chaudhry 2017 <sup>7</sup>
<i>P. aeruginosa</i>	Phage KP22 + ceftazidime, piperacillin	Synergistic effects observed when 10 <sup>6</sup> and 10 <sup>4</sup> PFU/mL of phage KP22 was incubated with 10 nm/mL of piperacillin and 5 ng/mL ceftazidime	Uchiyama 2018 <sup>21</sup>
<i>K. pneumoniae</i>	Phage KPO1K2 + ciprofloxacin	No statistical difference between biofilm log reduction between the combination treatment and phage-treated biofilms; however, statistically significant reduction in resistant variant population	Verma 2009 <sup>28</sup>
<i>K. pneumoniae</i>	“B5055-specific bacteriophages” + amoxicillin	Using 8-day old biofilms, a significant reduction in bacterial biofilm biomass was observed after incubation with the combination therapy ( $p < 0.01$ versus control)	Bedi 2009 <sup>2</sup>
<i>Klebsiella pneumoniae</i>	Phage KPO1K2 + ciprofloxacin	Phage-antibiotic combinations resulted in slightly increased biofilm eradication compared to phage-only in mature biofilms	Verma 2010 <sup>25</sup>
<i>S. aureus</i>	Phage SAP-26 + azithromycin, rifampicin, vancomycin	Approximately 5 log reduction of 24 h biofilms of <i>S. aureus</i> when treated with combination compared to the control	Rahman 2011 <sup>26</sup>
<i>S. aureus</i>	Phage PYO + ciprofloxacin, tetracycline	The addition of phage to low concentrations of antibiotics (2xMIC) lead to improved efficacy	Dickey 2019 <sup>37</sup>

**Table 3.3** Examples of PAS in *in vivo* assays. Adapted from Morrisette *et al.*<sup>18</sup>

<b>Bacteria</b>	<b>Phage + Antibiotic</b>	<b>Outcome</b>	<b>Results</b>
<b>Animal models</b>			
<i>P. aeruginosa</i>	Phage Pfl + gentamicin	Greatest survival when treated with 10 <sup>10</sup> PFU/mL phage and 0.8 mg/kg body weight gentamicin	Hagens 2006 <sup>20</sup>
<i>P. aeruginosa</i>	vB_PasP pAT14 + imipenem/cilastatin, amikacin	Reduced bacterial density when phage-antibiotic combination used compared to the control	Yilmaz 2013 <sup>32</sup>
<i>P. aeruginosa</i>	PP131 cocktail + ciprofloxacin	Phage-antibiotic combination highly synergistic, successfully treating 64% of rats	Oechslin 2017 <sup>3</sup>
<i>S. aureus</i>	Phage MR-10 + linezolid	The combination therapy was more successful in arresting the entire infection process (bacterial load, lesion score, histopathological analysis etc.)	Chhibber 2013 <sup>12</sup>
<i>S. aureus</i>	Phage Sb-1 + teicoplanin	Reduced bacterial density and lack of biofilm observed when phage-antibiotic combination used compared to the control	Yilmaz 2013 <sup>32</sup>
<i>Enterococcus faecalis</i>	Phages EFDG1 and EFLK1 + ampicillin	Combined bacteriophage-antibiotic therapy leads to the most significant decrease in bacterial titre	Gelman 2018 <sup>38</sup>
<b>Clinical experience</b>			
<i>P. aeruginosa</i>	Phage OMKO1 + ceftazidime, ciprofloxacin	Following a single application of the combination therapy, the infection resolved with no signs of recurrence	Chan 2018 <sup>8</sup>
<i>A. baumannii</i>	dIV cocktail + minocycline	Patient demonstrated continued clinical improvement	Schooley 2017 <sup>33</sup>

### 3.2.3. Mechanism of Action

The mechanism behind PAS is somewhat disputed; it has been suggested that PAS is a result of sub-lethal antibiotic concentrations altering the morphology and biosynthetic capacity of bacterial cells, which in turn can lead to increased phage propagation. Comeau *et al* suggested that this change in bacterial morphology can enhance phage infection, increasing the rate of phage maturation and cell lysis. Sub-lethal concentrations of  $\beta$ -lactam and fluoroquinolone antibiotics can induce morphological changes to bacterial cell walls, as they inhibit cell wall synthesis and cell division, ultimately resulting in bacterial cell

filamentation.<sup>4</sup> Other studies have suggested that this phenomenon could increase phage production as they have increased accessibility to the receptors,<sup>13</sup> increased precursors available for phage propagation,<sup>4,18</sup> and easier cell lysis, potentially contributing to increased burst sizes.<sup>39</sup>

Furthermore, Kim *et al* suggested that sub-inhibitory concentrations of antibiotics act as a “stress-inducer”, resulting in a delay in bacterial lysis, leading to increased phage production.<sup>39</sup> They also identified synergistic interactions between phage and other SOS-response inducing compounds (e.g., hydrogen peroxide [H<sub>2</sub>O<sub>2</sub>]) and suggested that PAS is dependent on either bacterial filamentation and/or SOS response; both do not need to be present for PAS to occur.<sup>39</sup>

Other researchers have suggested that PAS is beneficial from a genetic perspective, as it was thought that targeting bacteria with two different antibiotic agents, with different mechanisms of actions, may suppress the emergence of phage and/or antibiotic resistance during treatment.<sup>6,28</sup> Allen *et al* found that there was minimal cross-resistance between phage and antibiotics compared to two different types of antibiotics, or two different types of phage.<sup>40</sup> Further studies have confirmed that there is little cross-resistance between phage and antibiotics, as simultaneous multiple mutations are required for bacterial resistance.<sup>14</sup> This was termed “evolutionary synergy” by Chan and co-workers,<sup>9</sup> with studies suggesting that resistant mutants arising from the combined therapy are less virulent than those resistant to either the phage or antibiotic.<sup>14,28</sup>

Owing to their different mechanisms of action, phage-antibiotic combinations can be used to target MDR bacterial pathogens, as they can still be killed by phage.<sup>13,28</sup> Alternatively, phage-resistant bacterial isolates remain susceptible to antibiotics.<sup>28</sup> From an evolutionary point of view, this has been called the “see-saw effect”<sup>18</sup> – where phage impose a selection pressure on the bacteria, resulting in the emergence of phage-resistant isolates; this ultimately leads to the bacteria re-gaining their sensitivity to antibiotics, to lower the fitness cost for the bacteria.<sup>9</sup>

While there doesn't seem to be a specific type of phage or class of antibiotic that universally results in PAS,<sup>17,18</sup> it seems that it is dependent on the combination of phage, antibiotic, and bacterial strain under investigation.<sup>13</sup> Multiple studies have found that synergy was both strain-dependent and dependent on the specific antibiotic used,<sup>39,41</sup> with Kamal *et al* showing that there was a change in efficacy when different phage were used in combination with the same antibiotic against the same *B. cepacia* strain.<sup>13</sup>

An important thing to note is that not all phage-antibiotic combinations result in positive interactions. In fact, there have been several studies that have shown no interaction, or antagonism, between the phage and antibiotics;<sup>4,18,42,43</sup> one study showed that the combination of phage and antibiotics resulted in an increase in antibiotic resistance within *P. fluorescens*.<sup>43</sup> Therefore, there is a need for further study into PAS to understand the mechanism behind phage-antibiotic interactions, and how they can be applied in a clinical setting.

### **3.2.4. Objectives**

- To determine if the combination of sub-inhibitory phage K and antibiotic concentrations (ciprofloxacin, vancomycin, amikacin, and amoxicillin) result in positive PAS interactions against three *S. aureus* strains.
- To determine the efficacy of several planktonic-based bacterial assays in detecting PAS, and therefore if the assays can be compared to one another.
- To determine if phage-antibiotic combinations can be used to prevent and eliminate biofilm formation of three *S. aureus* species.
- To investigate the mechanism behind PAS by evaluating the morphology of bacterial cells after sub-inhibitory concentrations of antibiotics and the role of the antibiotics on the phage's lifecycle.



## 3.3. Methods

### 3.3.1. Bacterial and Bacteriophage Methods

All methods relating to growth conditions of *S. aureus* isolates and propagation of phage K were outlined in Chapter 2, Section 2.2.1.3 and Section 2.2.3.2, unless otherwise stated. Enumeration of bacterial and phage cell density were performed as outlined in Chapter 2, Section 2.2.1.4 and Section 2.2.3.3.

### 3.3.2. Bacteriophage Efficacy

#### 3.3.2.1. Spot Tests

This protocol was adapted from Merabishvili *et al.*,<sup>44</sup> whereby 10  $\mu\text{L}$  of a standardised *S. aureus* suspension (approx.  $10^7$  CFU/mL) was streaked over the surface of a 100 x100 mm TSA plate previously divided into 5 x 5 grid and air-dried at room temperature ( $\sim 25$  °C) for 20 min. Subsequently, 10  $\mu\text{L}$  of a phage suspension adjusted to a MOI of 0.1 in PBS was spotted onto each intersection and left to air-dry at room temperature for 1 h. PBS buffer was used as a negative control. Inoculated plates were incubated at 37 °C for 24 h, after which phage activity was assessed visually (Figure 3.1). Spots at the intersections were given a score based on plaque formation ranging from '0' (no plaques) to '+5' (confluent lysis) as described in Table 3.4, resulting in a score out of 25. This was repeated for four biological replicates to give a final score out of 100.

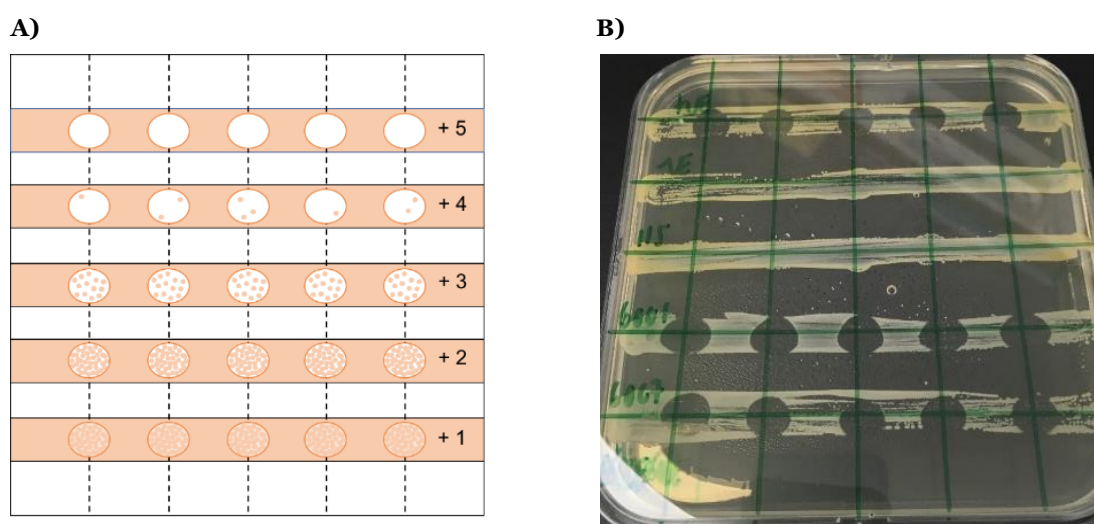


**Figure 3.1:** **A)** Schematic of plate showing plaque scores ranging from '+1' to '+5'. **B)** An example of a plate after 24 h incubation at 37 °C. The top row shows the positive control (host strain *S. aureus* H560 and phage K), while the second row is the negative control (*S. aureus* H560 and PBS).

**Table 3.4:** Scoring system for assessment of bacteriophage activity.<sup>44</sup>

Observation	Score
Confluent lysis – bacterial streak completely broken; no bacterial colonies present at spotted intersection	+5
Overgrowth – bacterial streak completely broken, presence of singular bacterial colonies on spot	+4
Semi-confluent lysis – bacterial streak incompletely broken.	+3
Multiple small phage plaques	+2
Bacterial streak just affected i.e. little observable disruption to bacterial growth	+1
Negative result – no lysis present	0

### 3.3.2.2. Detecting Temperate (Lysogenic) Phage

*S. aureus* strains used in this Chapter were assessed for the presence of temperate phage using previously published procedures.<sup>45</sup> Briefly, 100 µL of a bacterial culture (Chapter 2, Section 2.2.1.3) was mixed with 5 mL of molten top agar (65% strength TSA) and poured onto TSA plates. Once the top agar solidified, 10 µL of bacterial strains under investigation were spotted onto the plate and allowed to dry for 10 min at room temperature. The effect of antibiotics on the induction of temperate phage was also investigated. *S. aureus* strains were pre-incubated with ½ MIC concentrations of antibiotics for 24 h before being added to 5 mL molten top agar and poured onto TSA plates. The plates were then incubated overnight at 37 °C and subsequently analysed for the presence of lysis zones.

### 3.3.2.3. Multiplicity of Infection

Standardised isolates of *S. aureus* H560, MRSA252, and MSSA101 (Chapter 2, Section 2.2.1.3) were diluted 10-fold in fresh TSB to attain bacterial concentrations of approximately 10<sup>6</sup> CFU/mL, and 180 µL of each isolate was added to the relevant wells of a 96-well plate. Concurrently, a dilution series of phage K was performed to achieve concentrations of 10<sup>9</sup>-10<sup>1</sup> PFU/mL, with 20 µL of each concentration added to selected wells (to achieve MOIs of 0.00001 – 100). Negative and positive controls were carried out in tandem. The turbidity of the suspensions was monitored using a SPECTROstar® Omega UV-Vis spectrometer (BMG LabTech, UK) at an OD of 600 nm (OD<sub>600</sub>) for 17 h at 37 °C. Readings were taken every 4 min after a 2 s linear shake cycle.

### 3.3.3. Minimum Inhibitory Concentration

The MIC of antibiotics against *S. aureus* H560, MRSA252, and MSSA101 were determined using methodology outlined in Chapter 2, Section 2.2.1.5. The antibiotics used in this study were ciprofloxacin-HCl, vancomycin, amoxicillin, and amikacin. All stocks were prepared in sterile deionised water (dH<sub>2</sub>O).

### 3.3.4. Evaluating Phage-Antibiotic Synergy in Planktonic Suspensions

#### 3.3.4.1. Phage-Antibiotic Synergy Assay

Stock solutions of antimicrobials were prepared at two times the MIC concentration, with 100  $\mu$ L of each antibiotic serially diluted in the wells of a 96 microtiter plate to attain antibiotic concentrations of MIC,  $\frac{1}{2}$  MIC, and  $\frac{1}{4}$  MIC. Following this, phage K solutions were prepared in TSB ( $10^5 - 10^2$  PFU/mL) and 20  $\mu$ L added to all relevant wells. Finally, 80  $\mu$ L of sub-cultured *S. aureus* isolates (Chapter 2, Section 2.2.1.3) were added to the wells and the plate was incubated at 37 °C for 18 h. **After incubation, the OD<sub>600</sub> of each condition was measured and normalised against the blank control. For statistical analysis, each combination therapy was compared to the best-acting single therapeutic agent.**

#### 3.3.4.2. Bacterial Cell Count Assay

Bacterial isolates were grown and standardised as outlined in Chapter 2, Section 2.2.1.3, and subsequently diluted 10-fold in TSB to attain a bacterial concentration of  $10^6$  CFU/mL. Next, antibiotics and phage K were added to the bacterial suspension to achieve a final concentration of  $\frac{1}{2}$  MIC and  $10^3$  PFU/mL, respectively. The isolates were subsequently incubated at 37 °C for 18 h.  $\frac{1}{2}$  MIC antibiotic and  $10^3$  PFU/mL phage-only controls, broth and bacteria-only controls were carried out in tandem. After incubation, isolates were enumerated for bacterial and phage concentration (Chapter 2, Section 2.2.1.4 and 2.2.3.3, respectively), and compared to that of the bacteria-only control. **For statistical analysis, each combination therapy was compared to the best-acting single therapeutic agent.**

#### 3.3.4.3. One Step Growth Curve

Bacterial cultures (Chapter 2, Section 2.2.1.3) were re-suspended in 10 mL TSB to attain concentrations of  $10^6$  CFU/mL, before subsequent addition of  $\frac{1}{2}$  MIC of the chosen antimicrobials. The cultures were incubated at 37 °C until mid-exponential growth (OD  $\sim$ 2),

at which time they were harvested by centrifugation (4 000 g, 10 min, 4 °C) and re-suspended in 5 mL TSB. To this, 5 µL of phage K was added to obtain a MOI of 0.001 and allowed to adsorb for 5 min at room temperature. Subsequently, the solutions were centrifuged (4 000 g, 10 min, 4 °C), and re-suspended in 10 mL TSB. A sample was taken every 5 min for 1 h at 37 °C under constant shaking (150 rpm), and enumerated as outlined previously (Chapter 2, Section 2.2.3.3).

#### **3.3.4.4. Scanning Electron Microscopy**

Bacterial cultures with and without the presence of ½ MIC antibiotics were grown on Melinex® films in 2 mL TSB for 18 h at 37°C with minimal (70 rpm) agitation. After incubation, samples were fixed with 2.5% glutaraldehyde in 0.1 M sodium cacodylate buffer, post-fixed in aqueous 1% osmium tetroxide, dehydrated in an increasing acetone series (50 – 100%), and chemically dried in hexamethyldisilazane (HMDS). Samples were stored under vacuum overnight to ensure complete dehydration, and subsequently sputter-coated with 20 nm of chromium (Edwards S150B, 60 s) to reduce charging effects and thermal damage. Images were obtained using a Field Emission Scanning Electron Microscope (FESEM) (JEOL JSM6301F) operating at 5 kV.

#### **3.3.5. Phage-Antibiotic Synergy Activity in Biofilms**

##### **3.3.5.1. Minimum Biofilm Inhibition Concentration**

The MBIC of antibiotics against *S. aureus* H560, MRSA252, and MSSA101 was determined using the methodology outlined in Chapter 2, Section 2.2.2.1.1. The antibiotics used in this study were ciprofloxacin-HCl, vancomycin, amoxicillin, and amikacin. All stocks were prepared in sterile dH<sub>2</sub>O.

To determine the MBIC for phage K, 180 µL of the sub-cultured bacterial suspension in 1% TSBg (c. 10<sup>6</sup> CFU/mL) was added to the wells of a 96 well plate. This was followed by 20 µL of different concentrations of phage K (10<sup>9</sup> PFU/mL – 10<sup>1</sup> PFU/mL), before the plate was incubated statically at 37 °C for 24 h. The plates were then assessed for biofilm formation as outlined in **Chapter 2, Section 2.2.1.3**. A bacteria and broth only control was carried out in tandem; experiments were performed in triplicate with three separate bacterial and phage suspensions.

##### **3.3.5.2. Biofilm Inhibition Phage-Antibiotic Synergy Assay**

The assay was conducted as outlined in Chapter 3, Section 3.3.4.1 with some modifications. In brief, stock solutions of antimicrobials were prepared at twice the MBIC in 1% TSBg, and

further serially diluted using 1% TSBg in the wells of a 96 microtiter plate to attain MBIC, 1/2 MBIC, and 1/4 MBIC antibiotic concentrations. Concurrently, phage K concentrations were prepared in 1% TSB (10<sup>5</sup> – 10<sup>1</sup> PFU/mL), with 20  $\mu$ L of each concentration added to all relevant wells. Finally, 80  $\mu$ L of a sub-cultured *S. aureus* isolate (**Chapter 2, Section 2.2.1.3**) was added to the wells, and the plate was incubated at 37 °C for 18 h. After incubation, the biofilm inhibition was assessed via CV as outlined in Chapter 2, Section 2.2.2.1.3.

### **3.3.5.3. Minimum Biofilm Eradication Concentration**

The MBEC of antibiotics against *S. aureus* H560, MRSA252, and MSSA101 was determined using methodology outlined in Chapter 2, Section 2.2.2.1.2. The antibiotics used in this study were ciprofloxacin-HCl, vancomycin, amoxicillin, and amikacin. All stocks were prepared in sterile dH<sub>2</sub>O.

For phage K MBEC determination, the procedure was modified. Once the plates were washed three times to remove planktonic bacteria, 180  $\mu$ L 1% TSBg was added to the wells, followed by 20  $\mu$ L of different dilutions of phage K (10<sup>11</sup> PFU/mL – 10<sup>5</sup> PFU/mL). The plate was then statically incubated at 37 °C for a further 18 h. After incubation, the plates were washed three times with sterile dH<sub>2</sub>O and assessed for biofilm formation as outlined in Chapter 2, Section 2.2.2.1.3. A bacteria and broth only control was carried out in tandem; experiments were performed in triplicate with three separate bacterial and phage suspensions.

### **3.3.5.4. Biofilm Eradication Phage-Antibiotic Synergy Assay**

Overnight cultures of bacteria were sub-cultured into fresh 1% TSBg to attain a concentration of 10<sup>6</sup> CFU/mL. Next, 200  $\mu$ L of the adjusted bacterial suspension was added into the relevant wells within the 96-well microtiter plate, and statically incubated at 37 °C for 24 h. After incubation the biofilms were washed three times with sterile dH<sub>2</sub>O to remove planktonic bacteria. Concurrently, stock solutions of antimicrobials were in 1% TSBg (concentration dependent on the assay) and 100  $\mu$ L of each antibiotic was added to the relevant wells in the microtiter plate. Subsequently, 20  $\mu$ L of phage K (concentration dependent on the assay) and 80  $\mu$ L of 1% TSBg were added to obtain a final volume of 200  $\mu$ L. The microtiter plate was incubated at 37 °C for 24 h. Antibiotic and phage-only controls were carried out in tandem to broth and bacteria only controls. After incubation, biofilm eradication was assessed via CV (Chapter 2, Section 2.2.2.1.3.)

## 3.4. Results and Discussion

### 3.4.1. Single-Therapy Efficacy

#### 3.4.1.1. Bacterial Sensitivity to Bacteriophage K

Lytic phage that display broad-spectrum activity against a range of clinically relevant bacterial species are the most likely phage to be successful as a mass-market therapeutic. In this instance, phage K was used as it has previously had its genome sequenced,<sup>46,47</sup> was reported to have a broad host range,<sup>48-50</sup> and had little effect on the expression of numerous cytokines (IL-6, IL-8, and RANTES) and surface markers.<sup>50</sup>

Phage K is thought to have been isolated over 90 years ago;<sup>51,52</sup> it is also identical to phage Au2 isolated by Burnet and Lush,<sup>53</sup> and the polyvalent phage 812.<sup>54</sup> Phage K has recently been designated to the genus of *Kayvirus*, of subfamily *Twortvirinae* in the *Herelleviridae* family. Members of the *Herelleviridae* family possess a head-tail morphology with contractile tails and icosahedral heads; their genomes are linear dsDNA of 125 – 170 kilobases (kb) with long terminal repeats of various lengths.<sup>55</sup> The subfamily *Twortvirinae* generally infect *Staphylococcus* and *Lactobacillus* strains,<sup>56</sup> with the genus *Kayvirus* specifically infecting *Staphylococcus* spp., mainly *S. aureus*.<sup>57</sup> Phage K is the type species in this genus.<sup>57</sup> It has a regular icosahedral head, approximately 66 – 77 nm in diameter, with a contractile tail approximately 225 – 191 nm in length (non-contracted) and 14 – 16 nm width, dependent on the staining technique used.<sup>58</sup>

Phage K is a lytic,<sup>47</sup> polyvalent phage that utilises N-acetylglucosamine in the cell wall teichoic acid for phage adsorption.<sup>59</sup> As such, it possesses a broad host range,<sup>47</sup> inhibiting *S. aureus* and coagulase-negative *Staphylococci*.<sup>51,60</sup> Literature states that phage K is active against 47 – 84% of *S. aureus* strains<sup>48-50</sup> and can be modified to expand its host range after serial passage through phage-resistant cultures.<sup>60</sup> Therefore, phage K ( $10^6$  PFU/mL) was tested for its efficacy against 30 *S. aureus* strains standardised to a known concentration ( $10^7$  CFU/mL) and given an overall score out of 100. Bacterial strains with a score between 0-20 displayed little to no phage susceptibility (termed “resistant”), between 21 – 60 displayed moderate susceptibility to phage (termed “intermediate”), and scores between 61 – 100 showed good susceptibility to phage K (termed “susceptible”).

From the results shown in Table 3.5, 46.7% of strains were susceptible, 20.0% were intermediate, and 33.3% were resistant to phage K activity. These results confirmed the broad-spectrum nature of phage K previously reported.<sup>48-50</sup> However, there were more

“resistant” strains compared to literature; this result could be due to numerous factors, one of which could be the relatively small (n = 30) sample size, which could be improved upon by increasing the number of *S. aureus* isolates tested.

Additionally, this study used a MOI of 0.1 (10 bacterial cells to one phage cell), while other reports used higher MOIs. The lower MOI was used to reduce the presence of “lysis-from-without”, which occurs when high-multiplicity virion adsorption results in lysis without viral production; hence, higher MOIs could overestimate phage infectivity.

**Table 3.5:** Efficacy of phage K against *S. aureus* isolates at a Multiplicity of Infection (MOI) of 0.1. Plates were incubated at 37 °C for 18 h prior to being assessed visually (n = 4). Bacterial strains with a score between 0-20 displayed little to no bacteriophage susceptibility (termed “resistant”), between 21 – 60 displayed moderate susceptibility to phage (termed “intermediate”), and scores between 61 – 100 showed good susceptibility to phage K (termed “susceptible”).

<i>S. aureus</i> strain	Score / 100	<i>S. aureus</i> strain	Score / 100
6125	84	NCTC 10788	50
6009	83	6138	48
6022	80	MSSA101	41
6124	80	MRSA252	39
6019	79	6027	29
6097	79	6020	8
6007	78	6107	5
6132	75	6133	5
99518	73	6004	3
6114	69	MRSA17	1
6001	65	6021	0
H560	65	6032	0
6129	63	6115	0
6135	61	6128	0
6008	50	USA300	0

### 3.4.1.2. Detection of Temperate Bacteriophage

*S. aureus* H560, MRSA252, and MSSA101 were chosen for all future experiments. *S. aureus* H560 was selected as it was used to propagate phage K, and *S. aureus* MRSA252 and MSSA101 were selected as they had similar susceptibility to phage K. While it is unclear if *S. aureus* H560 and MSSA101 have any prophage within their genome, *S. aureus* MRSA252 has two known prophages,  $\Phi$ Sa2 and  $\Phi$ Sa3.<sup>61,62</sup>

Due to this, mixed host overlays (Section 3.3.2.2) were employed to ensure that any temperate phage present within the *S. aureus* isolates' genome would not affect the outcome of the experiments. No lysis areas were observed for any of the *S. aureus* strains

used, suggesting that without any external influence on the bacterial cells, temperate phage cannot be detected using the assay (Figure 3.2).

However, prophages can be induced by environmental stressors, such as mitomycin C and antibiotics.<sup>63,64</sup> Therefore, it was important to ensure that the antibiotics used in this study did not induce temperate phage. All antibiotics tested (ciprofloxacin, vancomycin, amikacin, and amoxicillin) failed to induce temperate phage, with no visible plaques present on their corresponding bacterial lawns. Therefore, it can be concluded that any plaques formed in future studies would be due to the presence of phage K only.

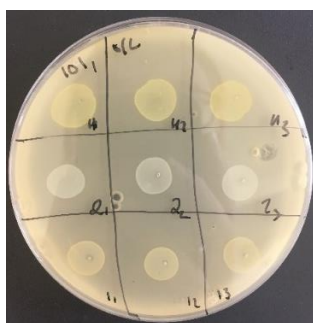


**Figure 3.2:** An example of a soft-overlay plate showing no visible lysis of *S. aureus* H560, MRSA252 and MSSA101 (top to bottom respectively) on an overlay of *S. aureus* MSSA101.

### 3.4.1.3. Multiplicity of Infection

The MOI is a ratio of the number of viruses to the number of host cells. As phage adsorption is a chance event, the MOI is displayed as an average, encompassing cases where multiple phage adsorb onto a single host cell, and instances where host cells remain uninfected.<sup>65</sup> Importantly, the calculated MOI may not correlate to  $MOI_{actual}$  due to anti-phage mechanisms outlined in Chapter 1. However,  $MOI_{actual}$  is difficult to determine experimentally, therefore, all MOI values quoted in this study are representative of initial MOI concentrations.

Figure 3.3 shows a reduction in OD for all three bacterial strains tested upon incubation with increasing phage concentrations (0 –  $10^7$  PFU/mL) after 18 h incubation at 37 °C. Bacterial growth was completely inhibited with  $10^4$  PFU/mL phage K for all bacterial strains, corresponding to a MOI of 0.01. This was not surprising as all three strains displayed similar activity in the spot test (Table 3.5). Additionally, there was no evidence of bacterial re-growth, indicating that there was no development of phage-resistant strains during this experiment.



Interestingly, there was no difference in trend observed when the samples were continuously agitated at 150 rpm, compared to when they were statically incubated. While there are increased OD<sub>600</sub> values observed for shaking incubation compared to static, OD<sub>600</sub> isn't linear to cell concentrations at high absorbance values – hence it is possible to assume similar growth was observed for both conditions.

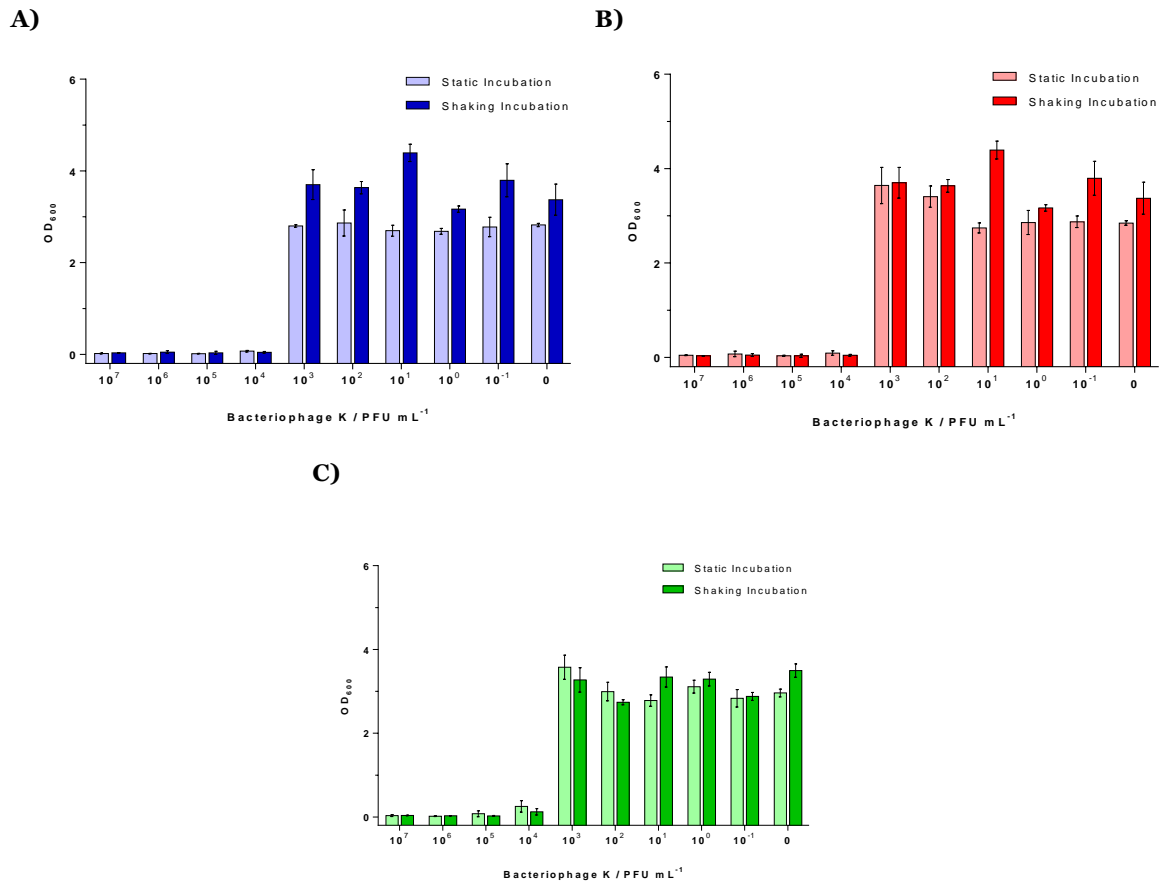


**Figure 3.3:** OD<sub>600</sub> measurements for A) *S. aureus* H560, B) *S. aureus* MRSA252 and C) *S. aureus* MSSA101 upon incubation with varying phage K concentration (10<sup>1</sup> – 10<sup>7</sup> PFU/mL). Measurements taken after 18 h incubation at 37 °C, error bars indicate standard deviation (n = 3).

#### 3.4.1.4. Antibiotic Susceptibility

The antibiotics used in this study were ciprofloxacin-HCl, vancomycin, amikacin, and amoxicillin. Ciprofloxacin is a fluoroquinolone, therefore works by inhibiting DNA topoisomerase and DNA gyrase, preventing DNA replication.<sup>66</sup> While predominately used for gram-negative bacterial species (e.g., *E. coli*,<sup>66</sup> *Salmonella* spp.,<sup>66</sup> and *P. aeruginosa*<sup>67</sup>), it has also shown efficacy against some gram-positive bacteria.<sup>67</sup> Vancomycin is a tricyclic glycopeptide antibiotic originally produced by *Streptococcus orientalis*.<sup>68,69</sup> It works by binding to the C-terminal D-alanyl-D-alanine moieties of the N-acetylmuramic acid

(NAM)/N-acetylglycosamine (NAG) peptides, which in turn inhibits glucosyltransferase, preventing the synthesis and polymerisation of NAM and NAG within the peptidoglycan layer of the cell wall. Owing to this, the cell wall becomes weakened and ultimately results in the leakage of intracellular components and subsequent bacterial cell death.<sup>68</sup> Amikacin is an aminoglycoside and therefore works by binding to the A-site on the 16S ribosomal RNA of the 30S ribosome;<sup>70</sup> this in turn inhibits protein synthesis by causing premature protein termination and incorporation of incorrect amino acids, causing bacterial cell death.<sup>71</sup> Amikacin is potent towards both gram-positive and gram-negative bacteria,<sup>71</sup> typically displaying bactericidal efficacy and prolonged post-antibiotic effect.<sup>72</sup> Finally, the  $\beta$ -lactam amoxicillin targets and kills bacteria by binding, and subsequently inhibiting, penicillin binding proteins (PBPs); thus, preventing the crosslinking of peptidoglycan and ultimately leading to cell death.<sup>73,74</sup>

To undertake PAS assays, the antibiotic concentration needs to be sub-inhibitory, therefore it is important to first establish the antibiotic's respective MIC. The MIC is the lowest concentration of antibiotic that inhibits the visible growth of a bacterial culture after 18 h incubation at 37 °C. The MIC values in this study were determined using the broth micro-dilution method as outlined in the European Committee on Antimicrobial Susceptibility Testing (EUCAST) guidelines.<sup>75</sup>

A phenomenon called the inoculum effect can cause an 8-fold increase in MIC owing to higher-than-recommended bacterial concentrations and is commonly seen for  $\beta$ -lactam antibiotics.<sup>76</sup> To prevent this phenomenon from occurring, the assay used approximately  $5 \times 10^5$  CFU/mL of each bacterial strain.

The MIC concentrations for the antibiotics are shown in Table 3.6. According to the EUCAST breakpoints, *S. aureus* H560 and MSSA 101 were susceptible to amikacin, had intermediate susceptibility towards ciprofloxacin, and were resistant to vancomycin. *S. aureus* MRSA252 was resistant to all antibiotics tested. Amoxicillin breakpoints are not outlined by EUCAST, who instead recommend testing the bacterial species against benzylpenicillin and cefoxitin. *S. aureus* that are susceptible to both antibiotics can be said to be susceptible to all penicillins, whereas the strains that are only susceptible to cefoxitin are susceptible only to  $\beta$ -lactam/ $\beta$ -lactamase inhibitor combinations. However, as *S. aureus* MRSA252 has such a high MIC against amoxicillin (500  $\mu$ g/mL), one can assume that the bacterial strain would be resistant to amoxicillin.

**Table 3.6:** Minimum Inhibitory Concentrations of the antibiotics used in this study

	Minimum Inhibitory Concentration ( $\mu\text{g/mL}$ )		
	<i>S. aureus</i>	<i>S. aureus</i>	<i>S. aureus</i>
	H560	MRSA252	MSSA101
<b>Ciprofloxacin</b>	0.50	62.50	0.50
<b>Vancomycin</b>	4.00	4.00	4.00
<b>Amoxicillin</b>	8.00	500	4.00
<b>Amikacin</b>	4.00	32.0	2.00

### 3.4.2. Determination of Phage-Antibiotic Synergy

#### 3.4.2.1. Bacteriophage K Survival in the Presence of Antibiotics

One, perhaps obvious, but overlooked, parameter in determining PAS is the survival of phage in the presence of antibiotics. It is often assumed that phage will remain stable when in solution with other antimicrobials – however, this is not always the case. For instance, replication of T4-like phage could be suppressed in the presence of fluoroquinolones due to the T4-like phage encoding for DNA topoisomerases.<sup>15</sup> This antagonistic nature can also be found when certain phage are combined with protein and DNA synthesis inhibitors.<sup>77</sup>

Suspensions of phage K were incubated with 1 mg/mL of ciprofloxacin, vancomycin, amikacin, or amoxicillin for up to 24 h at 37 °C prior to enumeration. Phage viability remained stable when incubated with amoxicillin and vancomycin (Figure 3.4). While the reduction in phage viability after 24 h incubation with vancomycin was statistically significant, it only corresponded to a 0.2 log reduction that could be explained by other factors such as pipetting error.

Conversely, when phage K was incubated with amikacin there was a slight decrease in phage concentration after 1 h (t-test,  $p < 0.05$ ; 0.27 log reduction), and a further decrease after 24 h incubation (t-test,  $p < 0.001$ ; 1.88 log reduction). With ciprofloxacin, there was a significant decrease in phage concentration after 1 h (t-test,  $p < 0.05$ ; 0.49 log reduction), and a further substantial decrease after 24 h incubation (t-test,  $p < 0.001$ ; 4 log reduction). Both of these antibiotics target bacterial functions involved in cell transcription and translation, which can also be present in the phage genome.<sup>78</sup> Due to this, phage viability may be reduced in the presence of these antibiotics (in these experiments, this phenomenon was observed during incubation with bacteria where phage needed to successfully replicate to produce plaques).

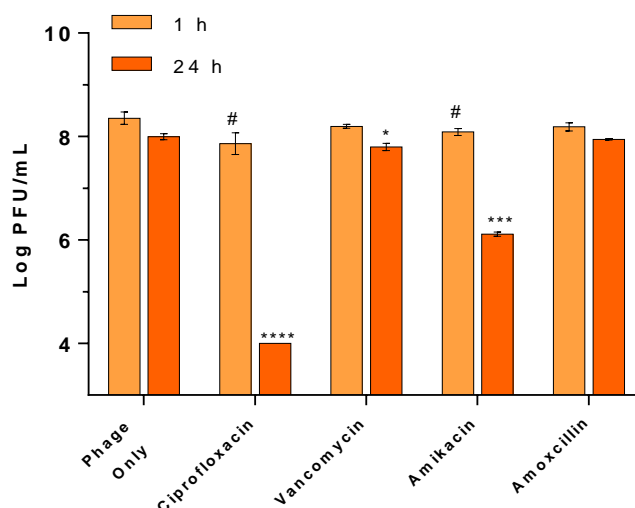


**Figure 3.4:** Log PFU/mL of phage K in the presence of 1 mg/mL of ciprofloxacin, vancomycin, amikacin and amoxicillin. Phage counts were taken after 1 h or 24 h incubation at 37 °C. Error bars indicate standard deviation (n = 3). Statistical analysis was conducted using a Student's t-test, with each variable compared to their respective 'Phage only' control. #  $p < 0.05$  compared to phage only control at 1 h, \*  $p < 0.05$ , \*\*\*  $p < 0.001$ , \*\*\*\*  $p < 0.0001$  compared to phage only control at 24 h.

### 3.4.2.2. Phage-Antibiotic Synergy Assay

Antibiotic concentrations at  $\frac{1}{2}$  and  $\frac{1}{4}$  their MIC were combined with varying concentrations of phage K ( $10^1$  -  $10^4$  PFU/mL) to evaluate their ability to reduce the OD of *S. aureus* isolates. Statistical analysis was conducted by comparing the OD<sub>600</sub> of the combination therapy against the individual treatment that had the lowest OD<sub>600</sub> value, i.e., the more potent component of the combination.

For *S. aureus* H560, ciprofloxacin, amikacin, and amoxicillin all showed positive (i.e., synergistic or additive) interactions with phage K (Figure 3.5). A significant reduction in OD<sub>600</sub> was found when  $\frac{1}{2}$  MIC ciprofloxacin was combined with sub-inhibitory concentrations of phage K (t-test,  $p < 0.01$ ) and when  $\frac{1}{4}$  MIC ciprofloxacin was combined with  $10^3$  PFU/mL (t-test,  $p < 0.0001$ ). When phage K was combined with amikacin, a significant reduction in OD<sub>600</sub> was seen for the  $\frac{1}{2}$  MIC amikacin and  $10^3$  PFU/mL phage K (t-test,  $p < 0.001$ ) and  $10^2$  PFU/mL phage K (t-test,  $p < 0.05$ ) combinations. A significant decrease in OD<sub>600</sub> was also witnessed when  $\frac{1}{4}$  MIC amikacin was combined with  $10^3$  PFU/mL phage K (t-test,  $p < 0.0001$ ). These positive interactions were somewhat surprising, considering that phage K viability is diminished in the presence of these antibiotics. However, the concentration of antibiotic used for the viability assay was much higher, hence any inhibitory effects may be negligible at these lower concentrations.

When 1/2 MIC of amoxicillin was combined with phage K, a significant reduction in OD<sub>600</sub> was observed for phage K concentrations of 10<sup>3</sup> PFU/mL (t-test, p<0.0001) and 10<sup>2</sup> and 10<sup>1</sup> PFU/mL (t-test, p<0.01). A statistical decrease in OD<sub>600</sub> was also witnessed when 1/4 MIC amoxicillin was combined with 10<sup>3</sup> PFU/mL phage K (t-test, p<0.0001). Conversely, no significant reduction in OD<sub>600</sub> was found for all phage and vancomycin combinations tested. In fact, the presence of 1/4 MIC vancomycin with 10<sup>1</sup> and 10<sup>2</sup> PFU/mL phage K increased the optical density of the isolates – although this does not mean that the combination increased bacterial cell concentration, as bacterial concentration is not linearly correlated to OD at these high OD values.

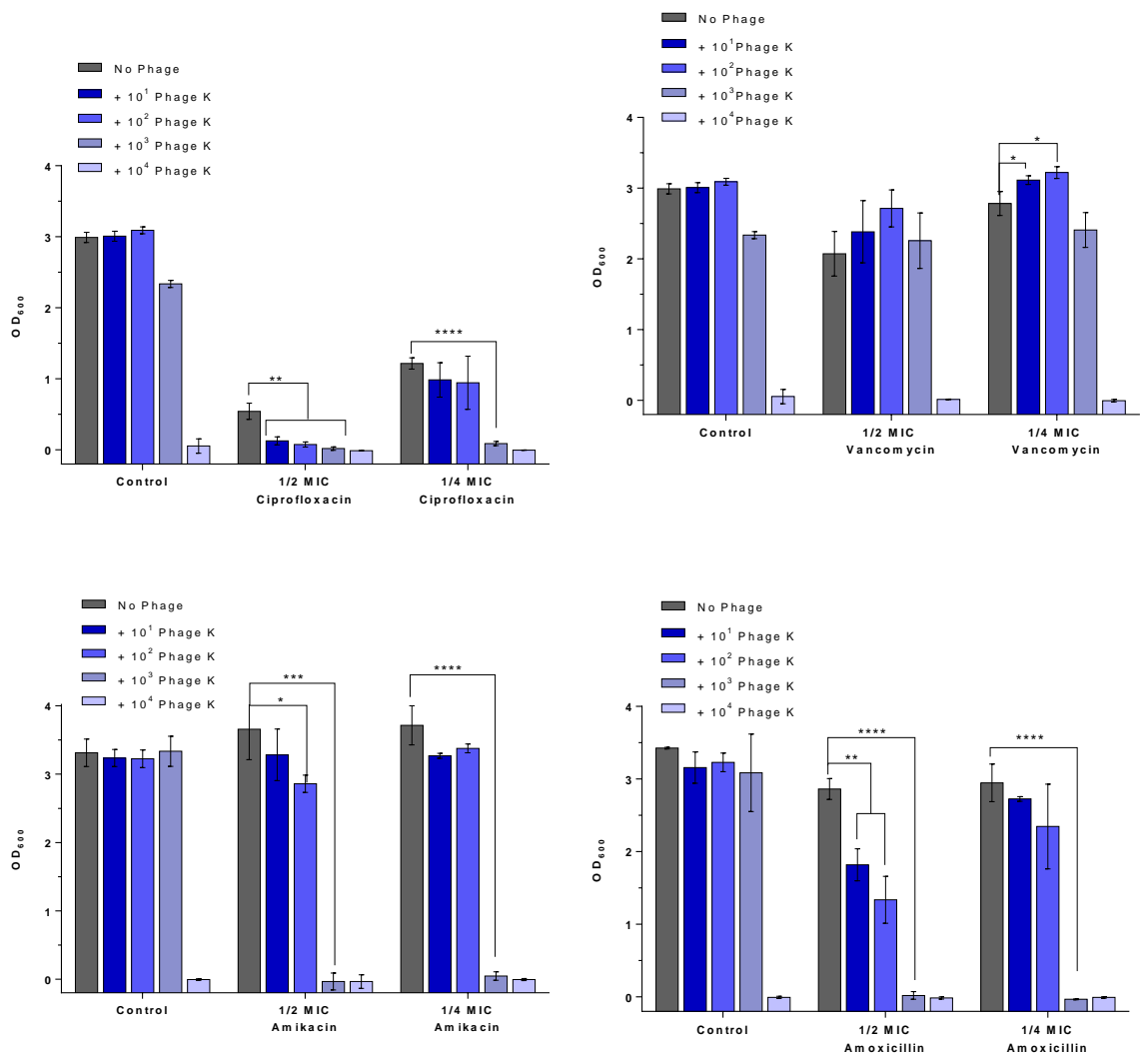


**Figure 3.5:** OD<sub>600</sub> measurements for *S. aureus* H560 upon the addition of differing concentrations of phage and/or antibiotic as a single therapy or in combination. OD<sub>600</sub> measured after 18 h incubation at 37 °C. n = 3 and error bars indicate standard deviation. Statistical analysis was conducted using a Student's t-test, with each variable compared to the control which displayed the lowest OD<sub>600</sub> value. \* p < 0.05, \*\*\* p < 0.001, \*\*\*\* p < 0.0001

For *S. aureus* MRSA252, favourable interactions were observed when 1/2 MIC ciprofloxacin was combined with  $10^3$  or  $10^2$  PFU/mL phage K (t-test,  $p < 0.0001$ ) (Figure 3.6). However, the use of 1/4 MIC ciprofloxacin with  $10^1$  and  $10^2$  PFU/mL phage K statistically increased the  $OD_{600}$  of *S. aureus* MRSA252. When 1/2 MIC amikacin or amoxicillin were combined with  $10^3$  phage K, there was a significant reduction in  $OD_{600}$  (t-test,  $p < 0.01$  and  $p < 0.001$  for amikacin and amoxicillin, respectively). When 1/4 MIC amikacin or 1/4 MIC amoxicillin were combined with  $10^3$  PFU/mL of phage K, a significant reduction in  $OD_{600}$  was observed (t-test,  $p < 0.01$  and  $p < 0.001$  for amikacin and amoxicillin, respectively). Additionally, the combinations of 1/4 MIC amoxicillin or amikacin and  $10^2$  PFU/mL phage K resulted in a favourable interactions (t-test,  $p < 0.05$  and  $p < 0.01$ , respectively).

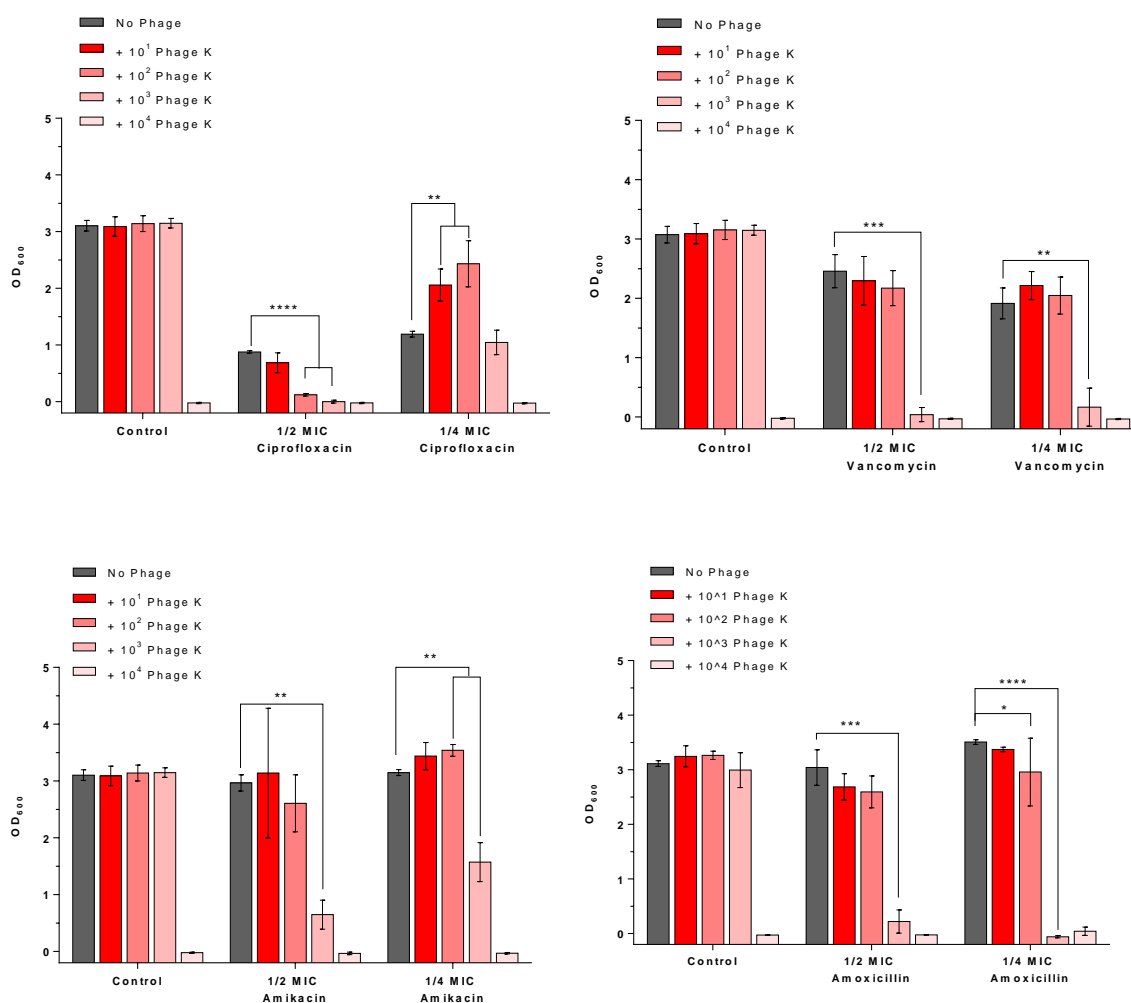


**Figure 3.6:**  $OD_{600}$  measurements for *S. aureus* MRSA252 upon the addition of differing concentrations of phage and/or antibiotic as a single therapy or in combination.  $OD_{600}$  measured after 18 h incubation at 37 °C.  $n = 3$  and error bars indicate standard deviation. Statistical analysis was conducted using a Student's t-test, with each variable compared to the control which displayed the lowest  $OD_{600}$  value. \*  $p < 0.05$ , \*\*\*  $p < 0.001$ , \*\*\*\*  $p < 0.0001$

*S. aureus* MRSA252 was the only strain tested where  $\frac{1}{2}$  and  $\frac{1}{4}$  MIC of vancomycin displayed a positive interaction with  $10^3$  PFU/mL phage K (t-test  $p < 0.001$  and  $p < 0.01$ , respectively). Although the reason for this is, as yet, unclear, it demonstrates the strain-specific nature of PAS interactions.

Next, the efficacy of the combinations were tested against *S. aureus* MSSA101 (Figure 3.7). When  $\frac{1}{2}$  or  $\frac{1}{4}$  MIC of ciprofloxacin was combined with phage K ( $10^3 - 10^1$  PFU/mL), all combinations reduced the  $OD_{600}$  of *S. aureus* MSSA101 suspensions in a statistically significant manner in comparison to the corresponding controls. When  $\frac{1}{2}$  MIC of amikacin or amoxicillin were combined with  $10^3$  PFU/mL of phage K, a significant reduction in  $OD_{600}$  of *S. aureus* MSSA101 was observed (t-test,  $p < 0.01$ ). This result was also observed when  $10^3$  PFU/mL of phage K was combined with  $\frac{1}{4}$  MIC amikacin (t-test,  $p < 0.05$ ) and amoxicillin (t-test,  $p < 0.01$ ). Finally, when phage K and vancomycin were used in combination, there was no significant reduction in  $OD_{600}$  for all combinations tested. In fact, the presence of  $10^3$  and  $10^2$  PFU/mL phage K with  $\frac{1}{2}$  MIC vancomycin increased the optical density of the isolates, showing a similar trend to that of *S. aureus* H560.

Overall, the most effective combinations for the treatment of all three *S. aureus* species were  $\frac{1}{2}$  MIC antibiotic and  $10^3$  PFU/mL of phage K. This observation implies that the concentrations of antibiotic/phage need to be close to their MIC values, and that lower concentrations would not provide a therapeutic benefit. Furthermore, ciprofloxacin in combination with phage K seemed to consistently provide the best results across all three *S. aureus* strains tested. However, as ciprofloxacin seemed to have an inhibitory effect towards phage K in the absence of bacteria, further experiments are needed to examine this phenomenon.

Other literature sources have used similar OD assays to determine PAS.<sup>79,80</sup> Jansen *et al*, used end-OD measurements to show that there was significant inhibition of *A. baumannii* upon incubating with phage KARL-1 and meropenem. However, this PAS phenomenon was not observed for all combinations tested, with minimal increases in efficacy witnessed when KARL-1 was incubated with ciprofloxacin or colistin.<sup>15</sup> These studies further corroborate the results found in this study, suggesting that PAS is not only dependent on the phage and antibiotic concentrations used, but also the specific bacterial isolate under investigation.

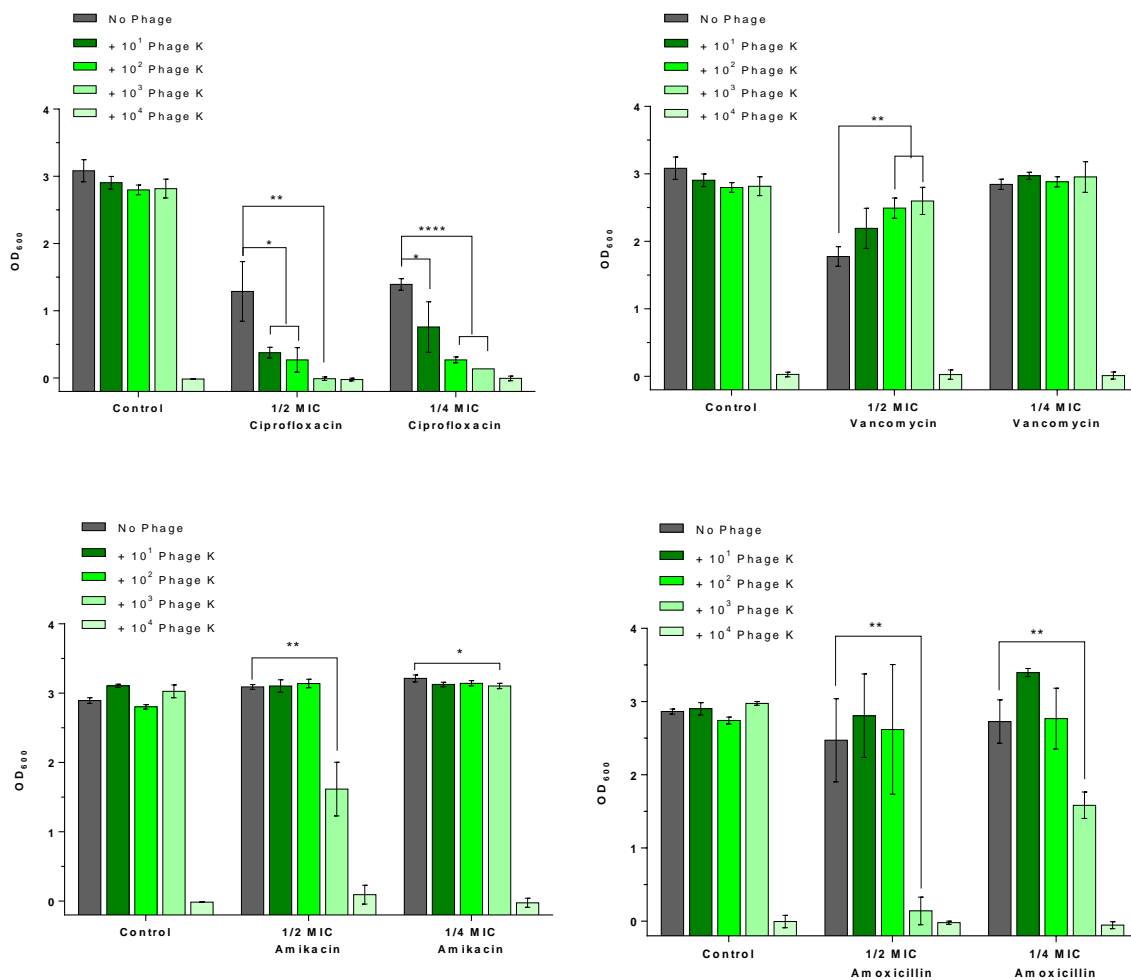


**Figure 3.7** OD<sub>600</sub> measurements for *S. aureus* MSSA101 upon the addition of differing concentrations of phage and/or antibiotic as a single therapy or in combination. OD<sub>600</sub> measured after 18 h incubation at 37 °C. n = 3 and error bars indicate standard deviation. Statistical analysis was conducted using a Student's t-test, with each variable compared to the control which displayed the lowest OD<sub>600</sub> value. \*  $p < 0.05$ , \*\*\*  $p < 0.001$ , \*\*\*\*  $p < 0.0001$

### 3.4.2.3. Bacterial Cell Counts

One disadvantage with the PAS assay is that OD<sub>600</sub> values are not proportional to bacterial cell concentrations at high OD values, with linearity usually seen for a limited CFU/mL range (approx. 10<sup>6</sup> – 10<sup>8</sup> CFU/mL). Therefore, results that show significant reductions in OD<sub>600</sub> values might not correspond to significant decreases in bacterial concentration. Owing to this, other assays have been developed that determine PAS by calculating the concentration of bacterial isolates after incubation with phage-antibiotic combinations, or the individual monotherapies.<sup>28,31,79</sup> Consequently, 10<sup>6</sup> CFU/mL of *S. aureus* H560, MRSA252, and MSSA101 were incubated with 1/2 MIC antibiotic, 10<sup>3</sup> PFU/mL phage K, or a combination of both. After 18 h incubation at 37 °C, the bacterial suspensions were



collected and enumerated. Statistical significance was determined by comparing the dual therapy to the most potent monotherapy.

For *S. aureus* H560, all combination therapies produced statistically significant reductions in Log CFU/mL when compared to their most potent monotherapy counterparts (Figure 3.8A). When combined with  $10^3$  PFU/mL of phage K,  $\frac{1}{2}$  MIC ciprofloxacin, amoxicillin, and amikacin resulted in average log reductions of 5.14, 2.17, and 1.65, respectively. While the combination of  $\frac{1}{2}$  MIC vancomycin and  $10^3$  phage K resulted in a statistically significant reduction, it only corresponded to a 0.25 log reduction, which is not clinically significant.

For the treatment of *S. aureus* MRSA252,  $\frac{1}{2}$  MIC amikacin was the most effective antibiotic in combination with  $10^3$  PFU/mL phage K (log reduction of 3.95; **Figure 3.8B**). The combination utilising  $\frac{1}{2}$  MIC ciprofloxacin also resulted in a statistically significant log reduction of 2.62. Conversely, amoxicillin failed to produce a statistically significant reduction in bacterial concentration when combined with  $10^3$  PFU/mL phage K.

Perhaps the most interesting observation is that the combination of  $\frac{1}{2}$  MIC vancomycin and  $10^3$  PFU/mL phage K failed to reduce *S. aureus* MRSA252 concentration. This discrepancy between this assay and the PAS OD<sub>600</sub> assay could be due to a variety of reasons. Firstly, it could be due to the inherent variation between bacterial isolates. Secondly, it could be due to the disparity between methodologies, with differences in working volumes, and extra dilution steps required in bacterial enumeration. However, further work would be needed to understand this discrepancy.

All antibiotics, except vancomycin, significantly reduced *S. aureus* MSSA101 bacterial concentration in the presence of  $10^3$  PFU/mL phage K, compared to their respective control (Figure 3.8C). The most effective combination was  $\frac{1}{2}$  MIC amoxicillin and  $10^3$  phage K (log reduction of 3.00). Similar efficacies were observed when  $\frac{1}{2}$  MIC ciprofloxacin or amikacin was combined with  $10^3$  PFU/mL phage K (log reductions of 2.17 and 2.15, respectively).  $\frac{1}{2}$  MIC vancomycin and  $10^3$  PFU/mL phage K was not effective in reducing *S. aureus* MSSA101 cell count (log reduction of 0.12).

Overall, the best PAS combination in reducing bacterial cell concentration across all three bacterial species tested was  $\frac{1}{2}$  MIC ciprofloxacin and  $10^3$  PFU/mL of phage K, with an average log reduction of 3.31 across all three strains tested. The second-best combination was phage K and amikacin, with an average log reduction of 2.29. The bacterial cell counts further supported the results found in the OD assay (Figures 3.5 – 3.7), the differences in therapeutic efficacy of the same combinations against different *S. aureus* strains shows that

PAS combinations are inherently strain-specific, and not a ‘one-combination-suits-all’ therapy.

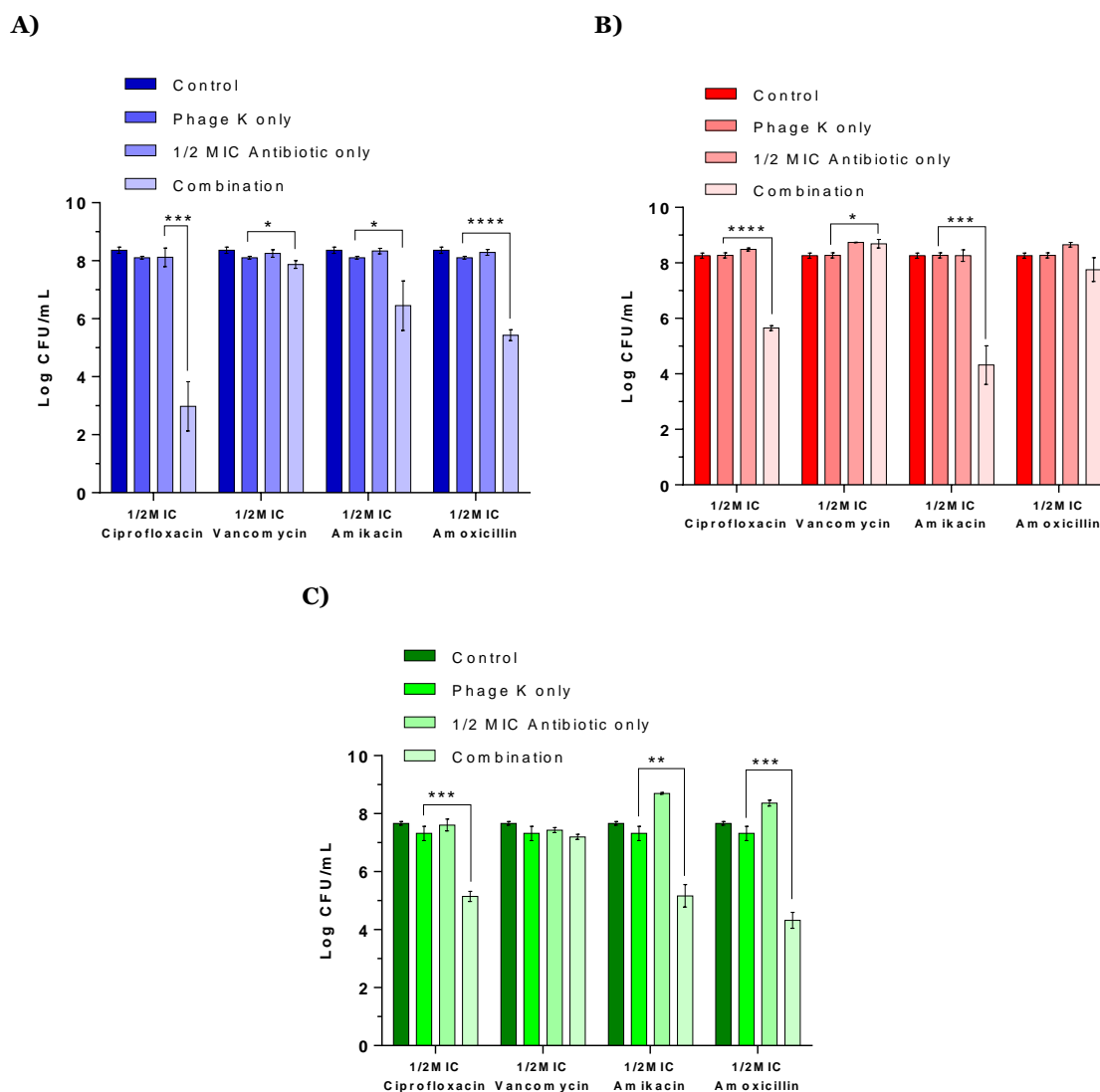


**Figure 3.8:** Log CFU/mL of A) *S. aureus* H560, B) *S. aureus* MRSA252 and C) *S. aureus* MSSA101 in the presence of 1/2 MIC antibiotics and 10<sup>3</sup> PFU/mL of phage K. Cultures were incubated statically for 18 h at 37 °C. n = 3 and error bars indicate standard deviation. Statistical analysis was conducted using a Student’s t-test, with each variable compared to the control which displayed the lowest OD<sub>600</sub> value. \*  $p < 0.05$ , \*\*\*  $p < 0.001$ , \*\*\*\*  $p < 0.0001$

### 3.4.2.3.1. Mixed-Model Analysis

Mixed-model analysis can be performed on the Log CFU/mL bacterial counts to determine the nature of the interaction between the antibiotic and phage when used in combination. These interactions can be defined as synergistic, additive, or antagonistic, as described by Kumaran *et al.*<sup>23</sup> The equation used to determine this interaction is shown below (Equation 1):

$$COEF_{int} = \log_{10}(AB^R) - (\log_{10}(A^R) + \log_{10}(B^R)) \quad (1)$$

COEF<sub>int</sub> is the coefficient of the interaction, AB<sup>R</sup> is the reduction in bacterial counts followed by the combined treatment (AB), A<sup>R</sup> is the reduction on bacterial counts due to treatment A and B<sup>R</sup> is the reduction in bacterial counts due to treatment B.

If the coefficient value is > 0, the interaction was synergistic - where the combination of therapies led to a greater reduction in bacterial cell concentration than the sum of the individual therapies. An interaction was additive if the value = 0, signifying that the therapeutic benefit of the combination therapy was equal to the sum of the individual counterparts. Finally, if the value was < 0, the interaction was termed antagonistic - where the bacterial cell reduction was lower than the sum of the individual therapies. The calculated coefficients for this assay are shown in Table 3.7.

When ½ MIC ciprofloxacin or amikacin was combined with 10<sup>3</sup> PFU/mL phage K, a synergistic interaction was observed for all bacterial species tested. ½ MIC amoxicillin provided synergistic interactions with 10<sup>3</sup> PFU/mL phage K when tested against *S. aureus* H560 and *S. aureus* MSSA101, and an additive interaction when tested against *S. aureus* MRSA252. Finally, ½ MIC vancomycin provided an additive interaction with phage K for all three bacterial species tested. These results further highlight the differences in the efficacy of the antibiotic and phage combinations when tested against different *S. aureus* isolates. Therefore, detailed microbiological analysis will be needed before PAS combinations can be used as a therapeutic technique for the treatment of bacterial infections.

**Table 3.7:** Calculated co-efficients of interaction for *S. aureus* H650, MRSA252 and MSSA101 for the combined use of selected antimicrobials (1/2 MIC) and phage K (10<sup>3</sup> PFU/mL). Values > 0 are considered synergistic, = 0 are additive/no interaction and < 0 are antagonistic interactions.

	<i>S. aureus</i> H560	<i>S. aureus</i> MRSA252	<i>S. aureus</i> MSSA101
<b>Ciprofloxacin</b>	4.88	2.84	2.12
<b>Vancomycin</b>	0.12	0.05	-0.11
<b>Amikacin</b>	1.63	3.95	3.19
<b>Amoxicillin</b>	2.60	0.90	3.69

#### 3.4.2.4. Bacteriophage Cell Counts

Reports in literature have suggested that the presence of sub-lethal doses of antibiotics increases the phage concentration;<sup>13</sup> therefore the number of plaques formed in the presence of ½ MIC of antibiotics were also investigated.

When  $10^3$  PFU/mL phage K was combined with  $\frac{1}{2}$  MIC ciprofloxacin, amikacin, or amoxicillin, a significant increase in phage K concentration was observed for all bacterial strains tested compared to the control (phage only; Figure 3.9). What is most surprising is that the PAS combination with  $\frac{1}{2}$  MIC amoxicillin displayed the greatest increase in phage K production, but not the largest decrease in bacterial concentration. Therefore, increased phage K production may not translate to improved therapeutic efficacy of the PAS combinations.

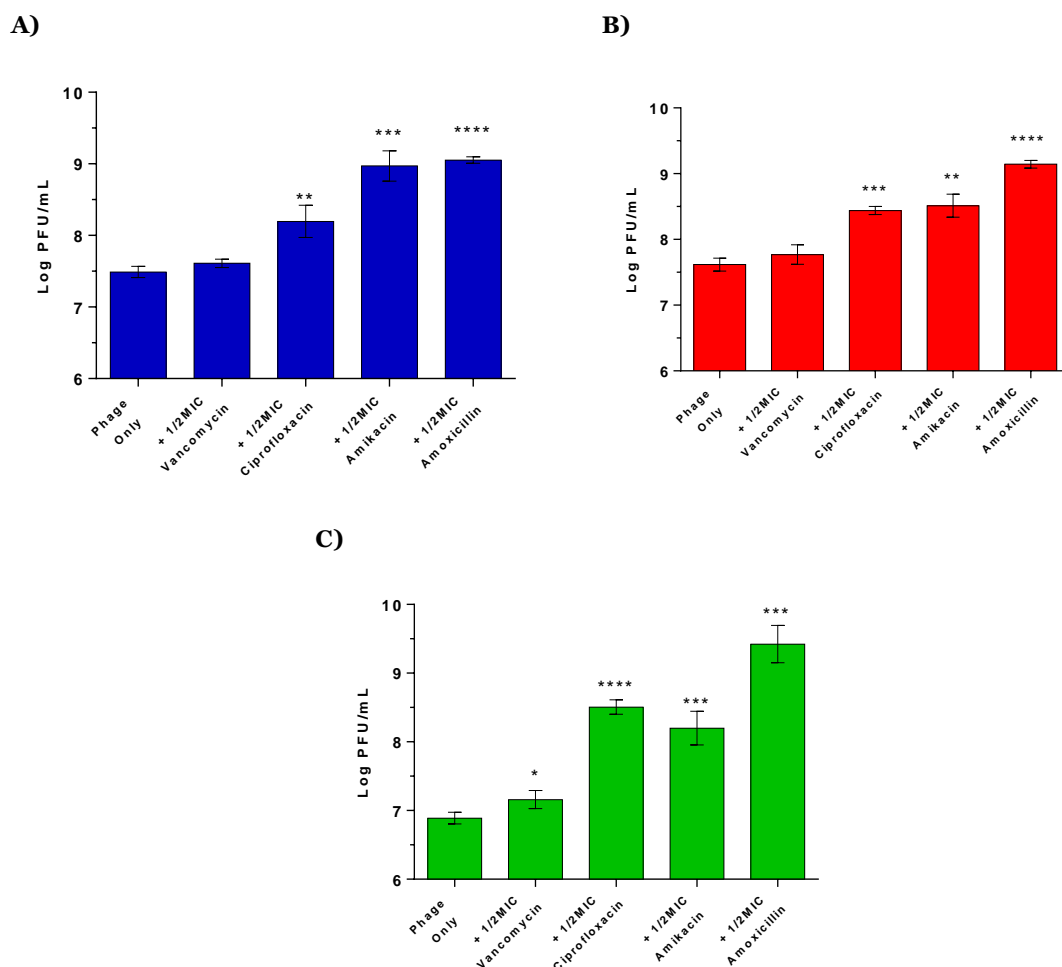


**Figure 3.9:** Log PFU/mL of A) *S. aureus* H560, B) *S. aureus* MRSA252 and C) *S. aureus* MSSA101 in the presence of  $\frac{1}{2}$  MIC antibiotics and  $10^3$  PFU/mL of phage K. Log PFU/mL was calculated after 18 h static incubation at 37 °C. n = 3 and error bars indicate standard deviation. Statistical analysis was conducted using a Student's t-test, with each variable compared to the phage-only control. \*  $p < 0.05$ , \*\*\*  $p < 0.001$ , \*\*\*\*  $p < 0.0001$

$\frac{1}{2}$  MIC vancomycin did not result in any statistical difference in the production of phage K when incubated with *S. aureus* H560 and MRSA252. For *S. aureus* H560, this result is not surprising, as this PAS combination failed to display enhanced therapeutic efficacy compared to its monotherapy counterparts. For *S. aureus* MRSA252, this result reflects the results observed for the bacterial cell counts (Figure 3.8) but is contradictory towards the OD<sub>600</sub>-based assay (Figure 3.6). As previously mentioned, further work would be needed to

examine this phenomenon. While  $\frac{1}{2}$  MIC vancomycin resulted in a statistically significant increase in the phage K concentration with *S. aureus* MSSA101, it only represented an increase of 0.27 Log PFU/mL, which could be due to experimental inaccuracies such as pipetting error.

It has been suggested that an increase in phage production is due to the filamentation of bacterial cells,<sup>4,81</sup> with several studies highlighting the increase of phage concentration in the presence of sub-inhibitory antibiotic concentrations.<sup>4,13,81</sup> Interestingly, this study found that the antibiotic which resulted in the most phage K production (amoxicillin) was not the most effective antibiotic in combination with phage K in reducing bacterial cell counts (Figure 3.8). Therefore, an increase in phage K production might not translate to increased efficacy in reducing bacterial cell density and as such, studies that only focus on phage concentration may not give a true indication of that combinations' clinical efficacy.

### 3.4.2.5. One Step Growth Curves

One-step growth curves were performed to determine the effect of sub-inhibitory concentrations of antibiotics on the life cycle of phage K. It has been hypothesised that sub-inhibitory concentrations of antibiotics result in a change in latent periods of the phage growth cycle and a larger burst size of phage K. Therefore, this phenomenon should result in the increased efficacy of phage K, and thus the therapeutic benefit of the combination therapy.<sup>82</sup>

In the system established, the latent period and burst size of phage K in *S. aureus* H560 without any co-incubation with antibiotics were 30 min and  $39.70 \pm 3.17$  PFU, respectively (Table 3.8). When co-incubated with  $\frac{1}{2}$  MIC ciprofloxacin, the latent period and burst size were 25 min and  $44.05 \pm 7.53$  PFU. When phage K was co-incubated with  $\frac{1}{2}$  MIC vancomycin, the latent period and burst size were fairly consistent with results obtained with the phage K only control, displaying a latent period of 30 min and a burst size of  $43.26 \pm 14.61$  PFU. Interestingly, upon incubation with  $\frac{1}{2}$  MIC amikacin, the latent period reduced in time to 25 min, but an increase in burst size was also witnessed ( $52.62 \pm 8.08$  PFU).

**Table 3.8:** Latent period (min) and burst size (PFU) of phage K in *S. aureus* H560. n = 3  $\pm$  standard deviation

	Latent period / min	Burst size / PFU
Phage K	30	$39.70 \pm 3.17$
$\frac{1}{2}$ MIC ciprofloxacin	25	$44.05 \pm 7.53$
$\frac{1}{2}$ MIC vancomycin	30	$43.26 \pm 14.61$
$\frac{1}{2}$ MIC amikacin	25	$52.62 \pm 8.08$

For *S. aureus* MRSA252, the latent period and burst size of phage K without co-incubation with antibiotics was 35 min and  $45.61 \pm 11.77$  PFU, respectively (Table 3.9); similar results were observed when phage K was incubated with  $\frac{1}{2}$  MIC amikacin. When phage K was incubated with  $\frac{1}{2}$  MIC ciprofloxacin, the latent period was reduced to 30 min, and an increase in burst size was witnessed ( $62.05 \pm 0.82$  PFU). While there was no reduction in latent period, when phage K was incubated with  $\frac{1}{2}$  MIC vancomycin, a large increase in the burst size was observed.

**Table 3.9:** Latent period (min) and burst size (PFU) of phage K in *S. aureus* MRSA252. n = 3  $\pm$  standard deviation

	Latent period / min	Burst size / PFU
Phage K	35	$45.61 \pm 11.77$
$\frac{1}{2}$ MIC ciprofloxacin	30	$62.05 \pm 0.82$
$\frac{1}{2}$ MIC vancomycin	35	$75.64 \pm 5.46$
$\frac{1}{2}$ MIC amikacin	35	$34.25 \pm 8.36$

For *S. aureus* MSSA101, the latent period and burst size of phage K without co-incubation with antibiotics was 25 min and  $74.72 \pm 5.87$  PFU, respectively (Table 3.10). When phage K was incubated with  $\frac{1}{2}$  MIC ciprofloxacin, the latent period increased to 40 min, and a decrease in burst size was witnessed ( $62.05 \pm 0.82$  PFU). For both  $\frac{1}{2}$  MIC amikacin and amoxicillin, the latent period increased (40 and 30 min, respectively), correlating to burst sizes of  $57.92 \pm 21.63$  PFU and  $30.87 \pm 29.36$  PFU, respectively. Interestingly, vancomycin resulted in a reduced latent period (25 min) and increased burst size ( $100.95 \pm 22.67$  PFU)

**Table 3.10:** Latent period (min) and burst size (PFU) of phage K in *S. aureus* MSSA101. n = 3  $\pm$  standard deviation

	Latent period / min	Burst size / PFU
Phage K	25	$74.72 \pm 5.87$
$\frac{1}{2}$ MIC ciprofloxacin	40	$62.05 \pm 0.82$
$\frac{1}{2}$ MIC vancomycin	25	$100.95 \pm 22.67$
$\frac{1}{2}$ MIC amikacin	40	$57.92 \pm 21.63$
$\frac{1}{2}$ MIC amoxicillin	30	$30.87 \pm 29.36$

Our results implied that that there is no consensus between phage lifecycle and the efficacy of the antibiotic combinations in reducing bacterial cell density. This finding is also observed in literature, where Kamal *et al* found that the addition of cefotaxime increased the burst size of T4 phage and reduced the latent period from 24 minutes to 18 minutes, ultimately reducing the time to lysis.<sup>13</sup> The authors correlated this to bacterial cell filamentation<sup>13</sup> and thus will be examined in Section 3.4.2.6. However, other authors have noted that the latent period of T4 phage increased by 5 minutes in combination with

cefotaxime, which they then attributed to the increased burst size (by 2.5-fold).<sup>39</sup> Therefore, further investigations need to be undertaken to determine the relationship between phage lifecycle and the efficacy of phage-antibiotic combinations.

#### **3.4.2.6. Scanning Electron Microscopy (SEM) Images**

To further understand the phenomenon of PAS, SEM images were obtained of *S. aureus* H560, MRSA252 and MSSA101 after 18 h incubation at 37 °C with ½ MIC antibiotic on Melinex® films in 2 mL TSB.

As shown in Figure 3.10, *S. aureus* H560, MRSA252, and MSSA101 are uniform cocci, approximately 2 µm in diameter. On exposure to ½ MIC ciprofloxacin, *S. aureus* H560 and MSSA101 were visibly stressed, with the bacterial cells much larger in diameter than that of the controls (7.4 µm and 9.6 µm for *S. aureus* H560 and MSSA101, respectively), and had very uneven cell walls. This was also observed in *S. aureus* MRSA252, which displayed ‘bloated’ cells approximately 9.2 µm in diameter, as well as long filamentous cells 18.8 µm in diameter.

Upon incubation with ½ MIC vancomycin, both *S. aureus* H560 and MSSA101 bacterial cells were similar in size and morphology to that of the controls. This is not surprising as vancomycin failed to elicit an effective therapeutic response when combined with phage K. Conversely, *S. aureus* MRSA252 cells were larger and uneven in appearance compared to the controls (9.3 µm versus 2.4 µm, respectively), suggesting an alteration to the cell structure of the bacterial isolate, which may explain why there was a “synergistic” activity witnessed in the OD<sub>600</sub> assay.

½ MIC amikacin had a marked increase in cell size for *S. aureus* H560 (12.6 µm), and a modest increase in cell diameter for *S. aureus* MRSA252 and MSSA101 (5.0 µm and 4.4 µm, respectively). All cell-wall morphologies looked deformed on inspection.

Finally, ½ MIC amoxicillin also increased the cell size of *S. aureus* H560, MRSA252, and MSSAA101 to 13.5 µm, 16.4 µm, and 7.0 µm, respectively. Once again, the bacterial cells looked distressed with uneven cell shape and pitted cell walls. This was found in literature, where subinhibitory concentrations of penicillin inhibited lysis of the bacterial cell wall without inhibiting cell division; this resulted in clusters of staphylococci unable to separate, therefore presented as an abnormally large cell.<sup>83</sup>

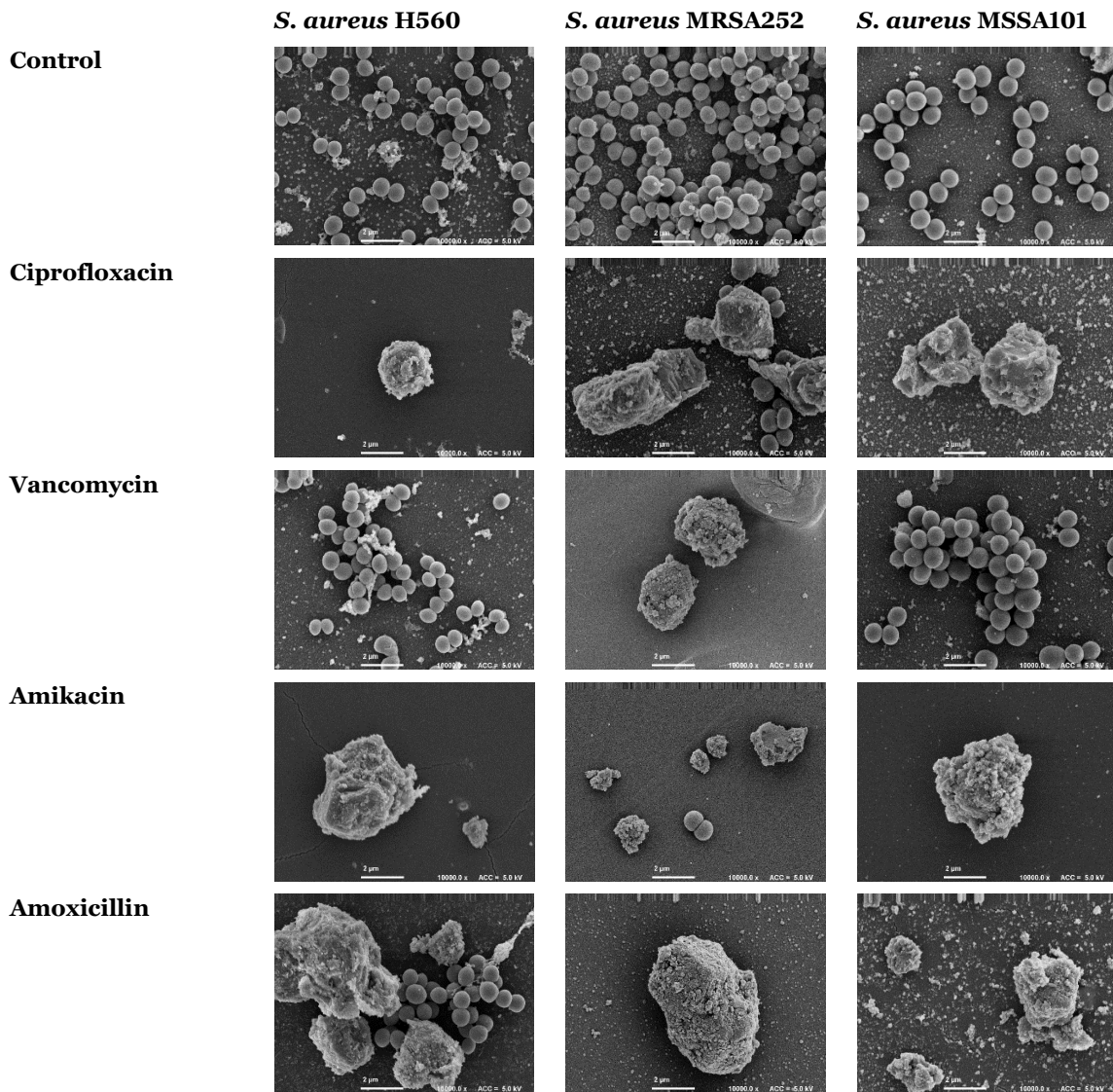


**Figure 3.10:** SEM images of untreated *S. aureus* H560, MRSA252 and MSSA101 compared with their counterparts incubated for 18 h with  $\frac{1}{2}$  MIC of ciprofloxacin, vancomycin, amikacin and amoxicillin.

All bacterial cells that elicited a positive “synergistic response” when treated with  $\frac{1}{2}$  MIC and phage K combinations were distressed in appearance and meaningfully larger. In literature, the increase in phage production with sub-lethal concentrations of antibiotics is attributed to the change in bacterial cell morphology;<sup>4,39,81</sup> this has been observed when sub-inhibitory concentrations of antibiotics such as  $\beta$ -lactams,<sup>83</sup> fluoroquinolones,<sup>84</sup> and aminoglycosides<sup>79</sup> have been used. Cell filamentation is thought to help with phage production as it escalates the production of essential precursors for phage and helps ease the cell for lysis.<sup>4</sup> However, like all other PAS-related assays, PAS has been observed without any changes to phage morphology. Kamal *et al* found that when sub-inhibitory concentrations of tetracycline were used in combination with phage KARL-1 against *B. cepacia*, no filamentation was observed although the combination exhibited PAS.



Therefore, while changes in cell morphology may help facilitate PAS, it is not a requirement.<sup>13</sup>

### **3.4.3. The Efficacy of PAS Within Bacterial Biofilms**

Much of the early work on the PAS phenomenon has focused on planktonic bacteria, with only a recent shift towards investigating PAS in bacterial biofilms. As biofilms are commonly found within chronic wounds,<sup>85,86</sup> it is imperative to determine whether PAS combinations would be successful in these conditions.

#### **3.4.3.1. Minimum Biofilm Inhibitory Concentrations**

The first PAS test to be conducted was to examine the efficacy of the sub-inhibitory concentration of antibiotic and phage K to *prevent* biofilm formation. To find the correct PAS concentration for each of the components, preliminary experiments were conducted to determine the MBIC, which was the concentration of the agent that resulted in no biofilm growth, as determined by the CV assay.

The MBIC concentrations for phage K are shown in Figure 3.11. A phage K concentration of  $10^4$  PFU/mL was needed to prevent biofilm formation for *S. aureus* H560, MRSA252, and MSSA101. This concentration was equivalent to a MOI of 0.01, which was the same concentration required for the complete inhibition of the bacteria's planktonic counterparts.

The MBIC concentrations for the antibiotics are shown in **Table 3.11**. For *S. aureus* H560, the MBICs of ciprofloxacin and amoxicillin were identical to their MIC counterparts (0.5 and 8.0  $\mu\text{g}/\text{mL}$ , respectively). Conversely, the MBICs of vancomycin and amikacin doubled to 8.0  $\mu\text{g}/\text{mL}$ . For *S. aureus* MRSA252, MBICs were identical to the MICs for all antibiotics tested. Finally, for *S. aureus* MSSA101, the MBICs of ciprofloxacin and vancomycin remained the same as their MIC values (0.5 and 4.0  $\mu\text{g}/\text{mL}$ , respectively). However, MBICs of amoxicillin and amikacin increased to 8.0 and 4.0  $\mu\text{g}/\text{mL}$ , respectively.

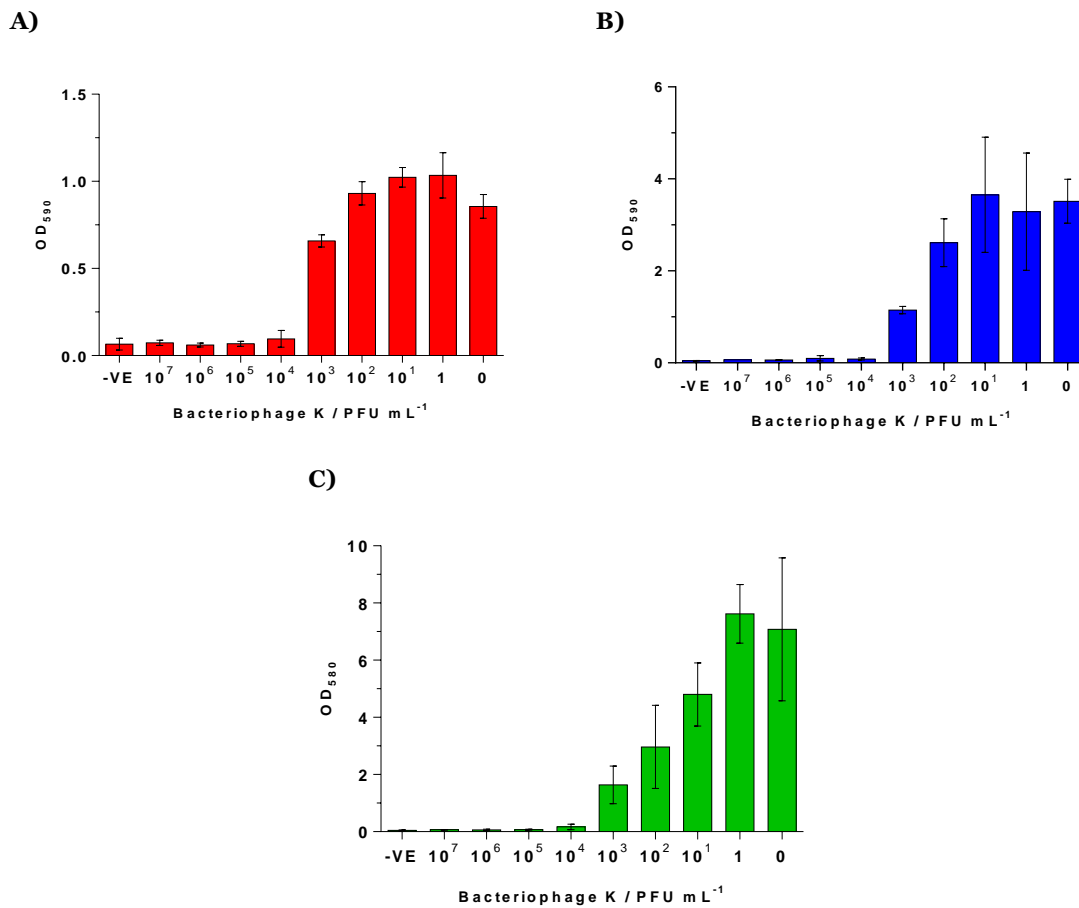


**Figure 3.11:** Determination of the ability of phage K to disrupt biofilm formation of **A)** *S. aureus* MRSA252, **B)** *S. aureus* H560 and **C)** *S. aureus* MSSA101. Reduction in biofilm biomass was quantified using crystal violet biofilm staining by measuring the absorbance at 590 nm. Bacteria were treated with differing concentrations of phage K over 18 h at 37 °C. Error bars show standard deviation (n = 3).

**Table 3.11:** Minimum Biofilm Inhibitory Concentration (MBIC) of the antibiotics used in this assay

	Minimum Biofilm Inhibitory Concentration (µg/mL)		
	<i>S. aureus</i> H560	<i>S. aureus</i> MRSA252	<i>S. aureus</i> MSSA101
<b>Ciprofloxacin</b>	0.50	62.50	0.50
<b>Vancomycin</b>	8.00	4.00	4.00
<b>Amoxicillin</b>	8.00	500.00	8.00
<b>Amikacin</b>	8.00	32.00	4.00

### 3.4.3.2. Biofilm Prevention

Similar to the planktonic assays, antibiotic concentrations at  $\frac{1}{2}$  and  $\frac{1}{4}$  MIC were used in combination with varying concentrations of phage K ( $10^1 - 10^3$  PFU/mL) and added to suspensions of *S. aureus* ( $10^6$  CFU/mL) before subsequent incubation at 37 °C for 18 h. The ability of the combinations in preventing biofilm formation was assessed using CV. Statistical analysis was conducted by comparing the combination in question to the control that had the lowest OD<sub>590</sub> value. 1 x MIC concentrations of antibiotics and  $10^4$  PFU/mL phage K were used as controls to ensure correct PAS concentrations were being used.

For *S. aureus* H560, all antibiotics showed a positive interaction with phage K, resulting in statistically significant decreases in OD<sub>590</sub> compared to the appropriate control (**Figure 3.12**). When  $\frac{1}{2}$  MIC ciprofloxacin was used in combination with phage K ( $10^3$  and  $10^2$  PFU/mL), it resulted in a significant reduction in OD<sub>590</sub>, corresponding to a decrease in biofilm biomass (t-test,  $p < 0.01$  and  $p < 0.0001$ , respectively). A statistically significant decrease in biofilm biomass was also observed when all phage concentrations were combined with  $\frac{1}{4}$  MIC ciprofloxacin.

Surprisingly, when  $\frac{1}{2}$  MIC vancomycin was investigated, it produced a statistically significant reduction in OD<sub>590</sub> (t-test,  $p < 0.01$ ) with all phage K concentrations. This result implies that while phage K and  $\frac{1}{2}$  MIC vancomycin combinations might not be able to kill *S. aureus* H560, they are capable of preventing the cells from forming a biofilm. However, this effect is concentration-dependent, as no increase in efficacy was observed when  $\frac{1}{4}$  MIC vancomycin was used in the combination.

A significant reduction in bacterial biomass was observed when  $\frac{1}{2}$  MIC amikacin was combined with  $10^2$  PFU/mL (t-test,  $p < 0.001$ ) and  $10^1$  PFU/mL (t-test,  $p < 0.01$ ) phage K, and when  $\frac{1}{4}$  MIC amikacin was combined with  $10^1$  PFU/mL phage K (t-test,  $p < 0.01$ ). These results were similar to that observed with the planktonic PAS assay.

The combinations of phage K and amoxicillin were the least effective. A significant reduction was only observed when  $\frac{1}{2}$  MIC amoxicillin was combined with  $10^2$  PFU/mL phage K (t-test,  $p < 0.05$ ). These results suggest that phage K-amoxicillin combinations are less effective when treating biofilms.

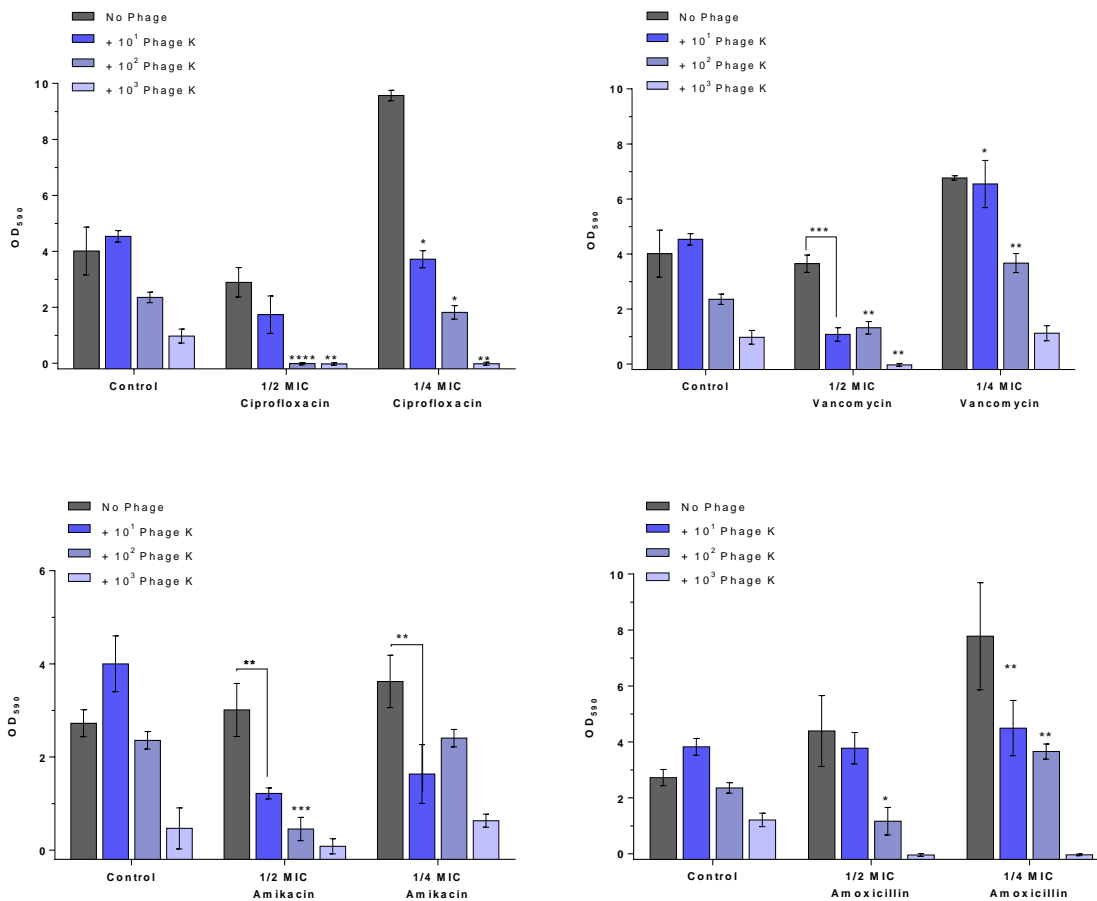


**Figure 3.12:** Determination of the ability of phage K and/or antibiotics to inhibit biofilm formation of *S. aureus* H560 as a single therapy or in combination. Reduction in biofilm biomass was quantified using crystal violet by measuring the absorbance at 590 nm. Bacteria were incubated for 18 h at 37 °C prior to staining. Error bars show standard deviation (n = 3). Statistical analysis was conducted using a Student's t-test, with each variable compared to the control which displayed the lowest OD<sub>590</sub> value. \*  $p < 0.05$ , \*\*\*  $p < 0.001$ , \*\*\*\*  $p < 0.0001$

The same phage-antibiotic combinations were tested on *S. aureus* MRSA252 (Figure 3.13). Favourable interactions were observed when 1/2 MIC ciprofloxacin was combined with 10<sup>3</sup> and 10<sup>2</sup> PFU/mL of phage K (t-test,  $p < 0.05$  and  $p < 0.001$ , respectively). Statistically significant decreases in bacterial biomass were also observed when 1/4 MIC ciprofloxacin was combined with 10<sup>3</sup> and 10<sup>2</sup> PFU/mL of phage K (t-test,  $p < 0.05$  for both). For vancomycin, the only combination that resulted in a significant reduction in biofilm biomass was 1/2 MIC vancomycin and 10<sup>3</sup> PFU/mL of phage K (t-test,  $p < 0.05$ ).

Amikacin was successful in decreasing bacterial biomass when combined with varying concentrations of phage K. Statistically relevant combinations included: 1/2 MIC amikacin with 10<sup>3</sup> and 10<sup>2</sup> PFU/mL of phage K ( $p < 0.05$  for both), and 1/4 MIC amikacin with 10<sup>3</sup> and 10<sup>2</sup> PFU/mL of phage K ( $p < 0.0001$  and  $p < 0.01$ , respectively). A significant reduction in

bacterial biomass was also observed when 1/2 MIC amoxicillin was combined with 10<sup>2</sup> PFU/mL phage K (t-test,  $p < 0.05$ ), and when 1/4 MIC amoxicillin was combined with 10<sup>3</sup> PFU/mL phage K (t-test,  $p < 0.0001$ ).

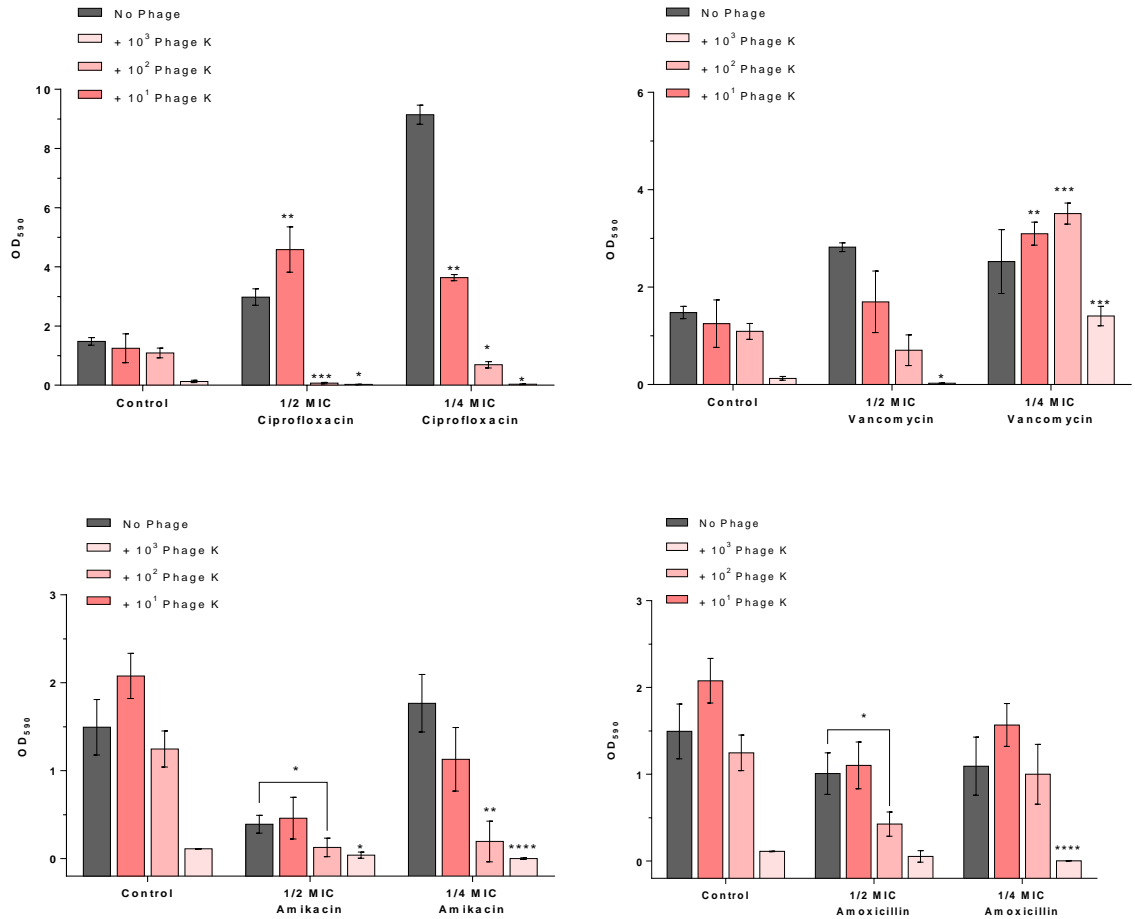


**Figure 3.13:** Determination of the ability of phage K and/or antibiotics to inhibit biofilm formation of *S. aureus* MRSA252 as a single therapy or in combination. Reduction in biofilm biomass was quantified using crystal violet by measuring the absorbance at 590 nm. Bacteria were incubated for 18 h at 37 °C prior to staining. Error bars show standard deviation (n = 3). Statistical analysis was conducted using a Student’s t-test, with each variable compared to the control which displayed the lowest OD<sub>590</sub> value. \*  $p < 0.05$ , \*\*\*  $p < 0.001$ , \*\*\*\*  $p < 0.0001$

Finally, the efficacy of the phage-antibiotic combinations were tested against *S. aureus* MSSA101 (Figure 3.14). All combinations tested were effective when combined with 1/2 MIC or 1/4 MIC ciprofloxacin, consistent with results obtained in the planktonic assay. When 1/2 MIC vancomycin was in combination with 10<sup>2</sup> PFU/mL phage K, it resulted in a statistically significant reduction in OD<sub>590</sub> (t-test,  $p < 0.01$ ), implying that while this combination was not able to kill planktonic *S. aureus* MSSA101, it was capable of preventing biofilm formation. For the majority of phage K-amikacin concentrations tested, a significant reduction in bacterial biomass was observed; these results were better than those obtained for the planktonic assay. When 10<sup>3</sup> PFU/mL phage K was combined with 1/2 or 1/4 MIC

amoxicillin, it resulted in statistically significant reductions in biofilm biomass (t-test,  $p < 0.001$  for both), with efficacy similar to that observed when using planktonic *S. aureus* MSSA101.

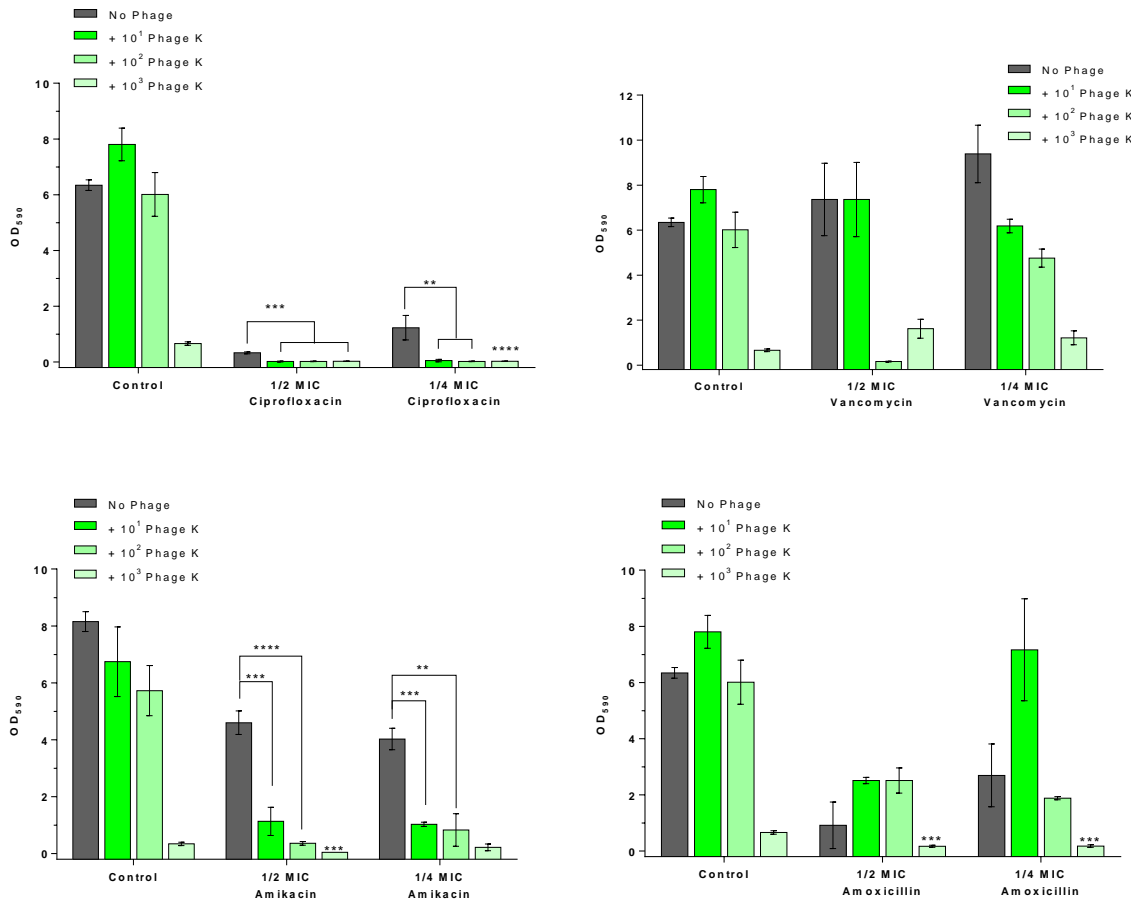


**Figure 3.14:** Determination of the ability of phage K and/or antibiotics to inhibit biofilm formation of *S. aureus* MSSA101 as a single therapy or in combination. Reduction in biofilm biomass was quantified using crystal violet by measuring the absorbance at 590 nm. Bacteria were incubated for 18 h at 37 °C prior to staining. Error bars show standard deviation (n = 3). Statistical analysis was conducted using a Student's t-test, with each variable compared to the control which displayed the lowest OD<sub>590</sub> value. \*  $p < 0.05$ , \*\*\*  $p < 0.001$ , \*\*\*\*  $p < 0.0001$

Overall, there is evidence to suggest that phage K-antibiotic combinations are capable of preventing *S. aureus* biofilms. Similar to the planktonic assays, variations in efficacy were observed between *S. aureus* isolates. Interestingly, the combination of phage K (10<sup>3</sup> or 10<sup>2</sup> PFU/mL) and 1/2 MIC vancomycin was able to prevent biofilm formation of all *S. aureus* isolates tested – even though it was unable to reduce bacterial cell density of *S. aureus* H560 and MSSA101 in planktonic assays. These results suggest that instances of PAS using planktonic bacteria may not be representative of the effects witnessed in biofilm models; therefore, for conclusive PAS determination both planktonic and biofilm assays should be carried out.

### 3.4.3.3. Biofilm Eradication

Some phage are capable of targeting bacteria within a biofilm.<sup>87–91</sup> Biofilm eradication is inherently harder to treat via phage therapy as the presence of the EPS shields the phage binding sites on the bacterial cell wall. Additionally, biofilms have a heterogeneous microenvironment of bacterial populations, some of which exhibit reduced metabolic activity or dormancy, preventing phage multiplication.<sup>89</sup>

To the best of the authors knowledge, phage K does not possess depolymerases to help with biofilm eradication; however, the function of many phage genes are unknown.<sup>46,47</sup> As such, phage K has been exploited in the treatment of several *S. aureus* and *S. epidermidis* biofilms.<sup>92–94</sup> Owing to this, the MBEC of phage K was evaluated for all three *S. aureus* strains. However, the highest concentration of phage K ( $10^9$  PFU/mL) was only capable of eradicating biofilms of *S. aureus* MRSA252 (Figure 3.15) and did not affect *S. aureus* H560 or MSSA101 (not shown); this was thought to be due to the fact that *S. aureus* MRSA252 displayed the weakest biofilm of the three isolates (as it had the lowest bacterial biomass measured by CV).

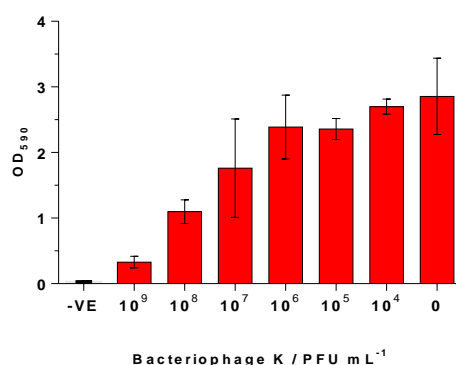


**Figure 3.15:** Determination of the ability of phage K to eradicate *S. aureus* MRSA252 biofilms. Reduction in biofilm biomass was quantified using crystal violet biofilm staining by measuring the absorbance at 590 nm. Bacteria were treated with differing concentrations of phage K over 18 h at 37 °C. Error bars show standard deviation (n = 3).

As MBEC concentrations of phage K were only obtained for *S. aureus* MRSA252, this bacterial strain was used to find the MBEC concentrations of the antibiotics used in this assay (Figure 3.16). Amoxicillin was not used as the MBEC was above the solubility of the drug. All MBEC values obtained were much higher than their MIC/MBIC counterparts, with both ciprofloxacin and vancomycin showing an 8- and 7.75-fold increase in concentration, respectively. *S. aureus* MRSA252 biofilms had the greatest tolerance to amikacin, with a 78-fold increase in antibiotic concentration needed to eradicate the biofilm; this result is not surprising as it is well known that biofilm formation confers increased resistance to

antibiotics. For example, it is known that ciprofloxacin has limited activity against biofilms as it is only effective in areas adjacent to the air-biofilm interface and not the interior of the biofilm. This is thought to be due to the interior of the biofilm having bacterial cells with reduced metabolic activity, most likely due to lack of oxygen.<sup>95</sup>

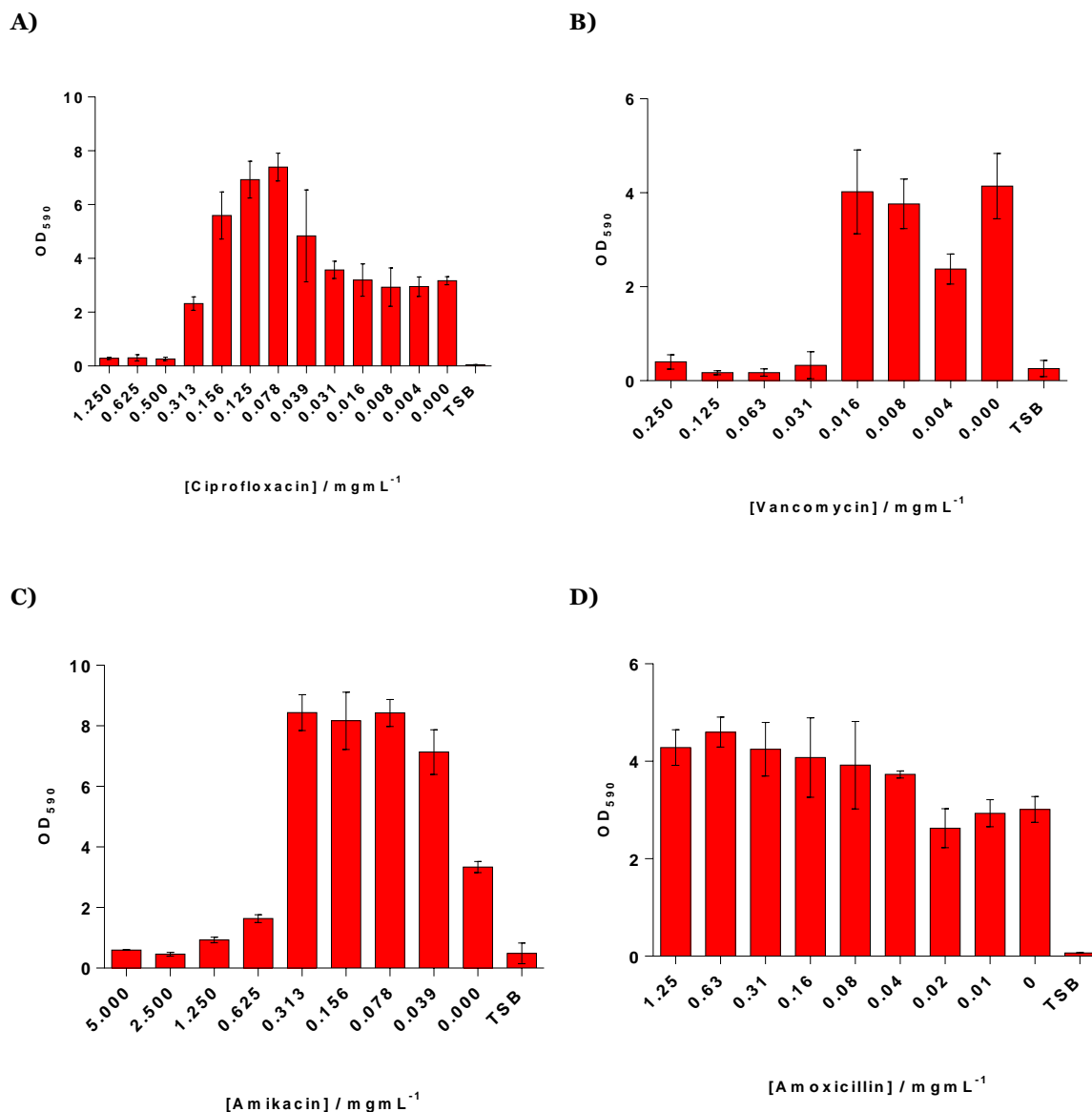


**Figure 3.16:** Determination of the ability of phage K to eradicate *S. aureus* MRSA252 biofilms. Reduction in biofilm biomass was quantified using crystal violet biofilm staining by measuring the absorbance at 590 nm. Bacteria were treated with differing concentrations of phage K over 18 h at 37 °C. Error bars show standard deviation (n = 3).

To determine if phage K-antibiotic combinations could eliminate established biofilms, *S. aureus* MRSA252 biofilms were grown in 96-well microtiter plates for 24 h, before subsequent incubation for an additional 24 h with combinations of 10<sup>8</sup> PFU/mL phage K and antibiotics at their ½ MBEC concentrations (Figure 3.17).



The results show that there was a decrease in biofilm biomass when phage K and 1/2 MBEC ciprofloxacin or phage K and 1/2 MBEC vancomycin were used in combination, compared to the antibiotics only (Figure 3.17).

These results suggest that phage K can be used in combination with ciprofloxacin or vancomycin to help eliminate *S. aureus* MRSA252 biofilms. While other authors have reported PAS when using phage-antibiotic combinations to treat both early and established biofilms,<sup>7,28,77,79</sup> the mechanism has not been elucidated, and as such further experiments would need to be undertaken to explain this phenomenon.

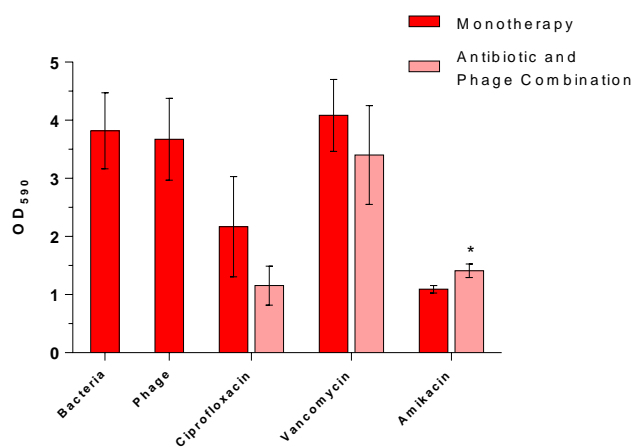


**Figure 3.17:** Determination of the ability of 1/2 MBEC antibiotics and 10<sup>8</sup> PFU/mL phage K as monotherapies and in combination to eradicate *S. aureus* MRSA252 biofilms. Reduction in biofilm biomass was quantified using crystal violet biofilm staining by measuring the absorbance at 590 nm. Bacteria were treated with differing concentrations of phage K over 18 h at 37 °C. Error bars show standard deviation (n = 3). Statistical analysis was conducted using a Student’s t-test, with each variable compared to the control which displayed the lowest OD<sub>590</sub> value. \*,  $p < 0.05$ .

### 3.5. Conclusion and Future Work

Overall, this study shows that sub-inhibitory concentrations of phage K and antibiotics can act in a synergistic manner to eliminate both planktonic and biofilm *S. aureus* isolates. However, the efficacy of phage-antibiotic combinations depends on the phage, antibiotic and bacterial strain under investigation, with not all combinations displaying a similar effect across all three *S. aureus* isolates used in this assay. Additionally, these results found that planktonic bacterial cell reduction (both OD and CFU/mL measurements) could be due to the distressed morphology of the bacterial cells in the presence of antibiotics, although the mechanisms behind this are not yet fully elucidated. The presence of antibiotics did alter phage K's life cycle, and result in increased burst sizes; however, increased burst sizes, and by extension increased phage concentration, did not necessarily result in the best phage-antibiotic combinations to reduce bacterial cell density, and therefore these assays should be used in tandem with bacterial cell reduction assays (e.g. OD measurements or time-kill assays).

The results presented in this chapter show that sub-inhibitory concentrations of phage K and antibiotics can be used in combination to prevent biofilm formation of *S. aureus* H560, MRSA252, and MSSA101. Unfortunately, to examine the ability of phage-antibiotic concentrations in eradicating biofilms, only *S. aureus* MRSA252 could be used owing to the phage titre not being high enough for complete biofilm eradication of *S. aureus* H560 and MSSA101. While the results looked promising, with reductions in biofilm biomass observed, further experiments will need to be conducted to determine whether this positive interaction is found for other *S. aureus* isolates.

Further work must be undertaken to establish the mechanism of action of PAS. This could be achieved by repeating this study with different phage and/or different antibiotics and testing them against a library of *S. aureus* isolates. Additionally, further experiments should be undertaken to establish the bacteria's fitness upon exposure to phage-antibiotic combinations to determine if "evolutionary synergy" is witnessed, whereby bacterial strains become more susceptible to antibiotics as they develop resistance to phage, and vice versa.

Additionally, research has shown that sequential administration of phage and antibiotics promoted an enhanced PAS efficacy,<sup>18</sup> therefore future experiments should be undertaken with phage K and antibiotic combinations used in this study to see if it increases the efficacy of combinations such as phage K and 1/2 MIC vancomycin, which were previously facilitative/agnostic.

### 3.6. References

1. Tagliaferri TL, Jansen M, Horz H-P. Fighting pathogenic bacteria on two fronts: Phages and antibiotics as combined strategy. *Front Cell Infect Microbiol.* 2019;9:22.
2. Bedi MS, Verma V, Chhibber S. Amoxicillin and specific bacteriophage can be used together for eradication of biofilm of *Klebsiella pneumoniae* B5055. *World J Microbiol Biotechnol.* 2009;25(7):1145.
3. Oechslin F, Piccardi P, Mancini S, Gabard J, Moreillon P, Entenza JM, et al. Synergistic interaction between phage therapy and antibiotics clears *Pseudomonas aeruginosa* infection in endocarditis and reduces virulence. *J Infect Dis.* 2017;215(5):703–12.
4. Comeau AM, Tétart F, Trojet SN, Prere M-F, Krisch HM. Phage-antibiotic synergy (PAS):  $\beta$ -lactam and quinolone antibiotics stimulate virulent phage growth. *PLoS One.* 2007;2(8):e799.
5. Ryan EM, Alkawareek MY, Donnelly RF, Gilmore BF. Synergistic phage-antibiotic combinations for the control of *Escherichia coli* biofilms in vitro. *FEMS Immunol Med Microbiol.* 2012;65(2):395–8.
6. Torres-Barceló C, Hochberg ME. Evolutionary rationale for phages as complements of antibiotics. *Trends Microbiol.* 2016;24(4):249–56.
7. Chaudhry WN, Concepcion-Acevedo J, Park T, Andleeb S, Bull JJ, Levin BR. Synergy and order effects of antibiotics and phages in killing *Pseudomonas aeruginosa* biofilms. *PLoS One.* 2017;12(1):e0168615.
8. Chan BK, Turner PE, Kim S, Mojibian HR, Eleftheriades JA, Narayan D. Phage treatment of an aortic graft infected with *Pseudomonas aeruginosa*. *Evol Med public Heal.* 2018;2018(1):60–6.
9. Chan BK, Siström M, Wertz JE, Kortright KE, Narayan D, Turner PE. Phage selection restores antibiotic sensitivity in MDR *Pseudomonas aeruginosa*. *Sci Rep.* 2016;6:26717.
10. Lin Y, Chang RYK, Britton WJ, Morales S, Kutter E, Chan H-K. Synergy of nebulized phage PEV20 and ciprofloxacin combination against *Pseudomonas aeruginosa*. *Int J Pharm.* 2018;551(1–2):158–65.

11. Kirby AE. Synergistic action of gentamicin and bacteriophage in a continuous culture population of *Staphylococcus aureus*. *PLoS One*. 2012;7(11):e51017.
12. Chhibber S, Kaur T, Kaur S. Co-therapy using lytic bacteriophage and linezolid: effective treatment in eliminating methicillin resistant *Staphylococcus aureus* (MRSA) from diabetic foot infections. *PLoS One*. 2013;8(2):e56022.
13. Kamal F, Dennis JJ. *Burkholderia cepacia* complex phage-antibiotic synergy (PAS): antibiotics stimulate lytic phage activity. *Appl Environ Microbiol*. 2015;81(3):1132–8.
14. Zhang Q, Buckling A. Phages limit the evolution of bacterial antibiotic resistance in experimental microcosms. *Evol Appl*. 2012;5(6):575–82.
15. Jansen M, Wahida A, Latz S, Krüttgen A, Häfner H, Buhl EM, et al. Enhanced antibacterial effect of the novel T4-like bacteriophage KARL-1 in combination with antibiotics against multi-drug resistant *Acinetobacter baumannii*. *Sci Rep*. 2018;8(1):1–12.
16. Knezevic P, Curcin S, Aleksic V, Petrusic M, Vlaski L. Phage-antibiotic synergism: a possible approach to combatting *Pseudomonas aeruginosa*. *Res Microbiol*. 2013;164(1):55–60.
17. Malik S, Sidhu PK, Rana JS, Nehra K. Managing urinary tract infections through phage therapy: a novel approach. *Folia Microbiol (Praha)*. 2020;65(2):217–31.
18. Morrisette T, Kebriaei R, Lev KL, Morales S, Rybak MJ. Bacteriophage Therapeutics: A Primer for Clinicians on Phage-Antibiotic Combinations. *Pharmacother J Hum Pharmacol Drug Ther*. 2020;40(2):153–68.
19. Torres-Barceló C, Arias-Sánchez FI, Vasse M, Ramsayer J, Kaltz O, Hochberg ME. A window of opportunity to control the bacterial pathogen *Pseudomonas aeruginosa* combining antibiotics and phages. *PLoS One*. 2014;9(9):e106628.
20. Hagens S, Habel A, Bläsi U. Augmentation of the antimicrobial efficacy of antibiotics by filamentous phage. *Microb Drug Resist*. 2006;12(3):164–8.
21. Uchiyama J, Shigehisa R, Nasukawa T, Mizukami K, Takemura-Uchiyama I, Ujihara T, et al. Piperacillin and ceftazidime produce the strongest synergistic phage–antibiotic effect in *Pseudomonas aeruginosa*. *Arch Virol*. 2018;163(7):1941–8.

22. Valério N, Oliveira C, Jesus V, Branco T, Pereira C, Moreirinha C, et al. Effects of single and combined use of bacteriophages and antibiotics to inactivate *Escherichia coli*. *Virus Res.* 2017;240:8–17.
23. Kumaran D, Taha M, Yi Q, Ramirez-Arcos S, Diallo J-S, Carli A, et al. Does treatment order matter? Investigating the ability of bacteriophage to augment antibiotic activity against *Staphylococcus aureus* biofilms. *Front Microbiol.* 2018;9:127.
24. Danis-Wlodarczyk K, Vandenheuvel D, Jang H Bin, Briers Y, Olszak T, Arabski M, et al. A proposed integrated approach for the preclinical evaluation of phage therapy in *Pseudomonas* infections. *Sci Rep.* 2016;6:28115.
25. Verma V, Harjai K, Chhibber S. Structural changes induced by a lytic bacteriophage make ciprofloxacin effective against older biofilm of *Klebsiella pneumoniae*. *Biofouling.* 2010;26(6):729–37.
26. Rahman M, Kim S, Kim SM, Seol SY, Kim J. Characterization of induced *Staphylococcus aureus* bacteriophage SAP-26 and its anti-biofilm activity with rifampicin. *Biofouling.* 2011;27(10):1087–93.
27. Jalasvuori M, Friman V-P, Nieminen A, Bamford JKH, Buckling A. Bacteriophage selection against a plasmid-encoded sex apparatus leads to the loss of antibiotic-resistance plasmids. *Biol Lett.* 2011;7(6):902–5.
28. Verma V, Harjai K, Chhibber S. Restricting ciprofloxacin-induced resistant variant formation in biofilm of *Klebsiella pneumoniae* B5055 by complementary bacteriophage treatment. *J Antimicrob Chemother.* 2009;64(6):1212–8.
29. Harper DR, Parracho H, Walker J, Sharp R, Hughes G, Werthén M, et al. Bacteriophages and biofilms. *Antibiotics* 3: 270–284. 2014.
30. Abedon ST. Ecology of anti-biofilm agents I: antibiotics versus bacteriophages. *Pharmaceuticals.* 2015;8(3):525–58.
31. Blasco L, Ambroa A, Lopez M, Fernandez-Garcia L, Bleriot I, Trastoy R, et al. Combined use of the Ab105-2 $\phi$  $\Delta$ CI lytic mutant phage and different antibiotics in clinical isolates of multi-resistant *Acinetobacter baumannii*. *Microorganisms.* 2019;7(11):556.
32. Yilmaz C, Colak M, Yilmaz BC, Ersoz G, Kutateladze M, Gozlugol M. Bacteriophage therapy in implant-related infections: an experimental study. *JBJS.* 2013;95(2):117–

- 25.
33. Schooley RT, Biswas B, Gill JJ, Hernandez-Morales A, Lancaster J, Lessor L, et al. Development and use of personalized bacteriophage-based therapeutic cocktails to treat a patient with a disseminated resistant *Acinetobacter baumannii* infection. *Antimicrob Agents Chemother.* 2017;61(10).
  34. Khawaldeh A, Morales S, Dillon B, Alavidze Z, Ginn AN, Thomas L, et al. Bacteriophage therapy for refractory *Pseudomonas aeruginosa* urinary tract infection. *J Med Microbiol.* 2011;60(11):1697–700.
  35. Nir-Paz R, Gelman D, Khouri A, Sisson BM, Fackler J, Alkalay-Oren S, et al. Successful treatment of antibiotic-resistant, poly-microbial bone infection with bacteriophages and antibiotics combination. *Clin Infect Dis.* 2019;69(11):2015–8.
  36. Coulter LB, McLean RJC, Rohde RE, Aron GM. Effect of bacteriophage infection in combination with tobramycin on the emergence of resistance in *Escherichia coli* and *Pseudomonas aeruginosa* biofilms. *Viruses.* 2014;6(10):3778–86.
  37. Dickey J, Perrot V. Adjunct phage treatment enhances the effectiveness of low antibiotic concentration against *Staphylococcus aureus* biofilms in vitro. *PLoS One.* 2019;14(1):e0209390.
  38. Gelman D, Beyth S, Lerer V, Adler K, Poradosu-Cohen R, Copenhagen-Glazer S, et al. Combined bacteriophages and antibiotics as an efficient therapy against VRE *Enterococcus faecalis* in a mouse model. *Res Microbiol.* 2018;169(9):531–9.
  39. Kim M, Jo Y, Hwang YJ, Hong HW, Hong SS, Park K, et al. Phage-antibiotic synergy via delayed lysis. *Appl Environ Microbiol.* 2018;84(22).
  40. Allen RC, Pfrunder-Cardozo KR, Meinel D, Egli A, Hall AR. Associations among antibiotic and phage resistance phenotypes in natural and clinical *Escherichia coli* isolates. *MBio.* 2017;8(5).
  41. Segall AM, Roach DR, Strathdee SA. Stronger together? Perspectives on phage-antibiotic synergy in clinical applications of phage therapy. *Curr Opin Microbiol.* 2019;51:46–50.
  42. Torres-Barceló C, Gurney J, Gougat-Barberá C, Vasse M, Hochberg ME. Transient negative effects of antibiotics on phages do not jeopardise the advantages of combination therapies. *FEMS Microbiol Ecol.* 2018;94(8):fyi107.

43. Cairns J, Becks L, Jalasvuori M, Hiltunen T. Sublethal streptomycin concentrations and lytic bacteriophage together promote resistance evolution. *Philos Trans R Soc B Biol Sci.* 2017;372(1712):20160040.
44. Merabishvili M, Pirnay JP, Verbeken G, Chanishvili N, Tediashvili M, Lashkhi N, et al. Quality-controlled small-scale production of a well-defined bacteriophage cocktail for use in human clinical trials. *PLoS One.* 2009;4(3).
45. Milho, C., Andrade, M., Vilas Boas, D., Alves, D., Sillankorva S. Antimicrobial assessment of phage therapy using porcine model of biofilm infection. *Int J Pharm.* 2019;557:112–23.
46. O’Flaherty S, Coffey A, Edwards R, Meaney W, Fitzgerald GF, Ross RP. Genome of staphylococcal phage K: a new lineage of Myoviridae infecting gram-positive bacteria with a low G+ C content. *J Bacteriol.* 2004;186(9):2862–71.
47. Gill JJ. Revised genome sequence of *Staphylococcus aureus* bacteriophage K. *Genome Announc.* 2014;2(1).
48. Kelly D, McAuliffe O, O’Mahony J, Coffey A. Development of a broad-host-range phage cocktail for biocontrol. *Bioeng Bugs.* 2011;2(1):31–7.
49. Hsieh S-E, Lo H-H, Chen S-T, Lee M-C, Tseng Y-H. Wide host range and strong lytic activity of *Staphylococcus aureus* lytic phage Stau2. *Appl Environ Microbiol.* 2011;77(3):756–61.
50. Freyberger HR, He Y, Roth AL, Nikolich MP, Filippov AA. Effects of *Staphylococcus aureus* bacteriophage K on expression of cytokines and activation markers by human dendritic cells in vitro. *Viruses.* 2018;10(11):617.
51. Rountree PM. The serological differentiation of staphylococcal bacteriophages. *Microbiology.* 1949;3(2):164–73.
52. Krueger AP. A method for the quantitative determination of bacteriophage. *J Gen Physiol.* 1930;13(5):557.
53. Burnet FM, Lush D. The staphylococcal bacteriophages. *J Pathol Bacteriol.* 1935;40(3):455–69.
54. Pantůček R, Rosypalová A, Doškař J, Kailarová J, Růžičková V, Borecká P, et al. The polyvalent staphylococcal phage  $\phi$ 812: its host-range mutants and related phages.

Virology. 1998;246(2):241–52.

55. ICTV. Herelleviridae [Internet]. [cited 2020 Nov 4]. Available from: [https://talk.ictvonline.org/ictv-reports/ictv\\_online\\_report/dsdna-viruses/w/herelleviridae](https://talk.ictvonline.org/ictv-reports/ictv_online_report/dsdna-viruses/w/herelleviridae)
56. ICTV. Twortvirinae [Internet]. [cited 2020 Nov 4]. Available from: [https://talk.ictvonline.org/ictv-reports/ictv\\_online\\_report/dsdna-viruses/w/herelleviridae/1279/subfamily-twortvirinae](https://talk.ictvonline.org/ictv-reports/ictv_online_report/dsdna-viruses/w/herelleviridae/1279/subfamily-twortvirinae)
57. ICTV. Kayvirus [Internet]. [cited 2020 Nov 4]. Available from: [https://talk.ictvonline.org/ictv-reports/ictv\\_online\\_report/dsdna-viruses/w/herelleviridae/1280/genus-kayvirus](https://talk.ictvonline.org/ictv-reports/ictv_online_report/dsdna-viruses/w/herelleviridae/1280/genus-kayvirus)
58. Rees PJ, Fry BA. The morphology of staphylococcal bacteriophage K and DNA metabolism in infected *Staphylococcus aureus*. *J Gen Virol*. 1981;53(2):293–307.
59. Chatterjee AN. Use of bacteriophage-resistant mutants to study the nature of the bacteriophage receptor site of *Staphylococcus aureus*. *J Bacteriol*. 1969;98(2):519–27.
60. O’Flaherty S, Ross RP, Meaney W, Fitzgerald GF, Elbreki MF, Coffey A. Potential of the polyvalent anti-*Staphylococcus* bacteriophage K for control of antibiotic-resistant staphylococci from hospitals. *Appl Environ Microbiol*. 2005;71(4):1836–42.
61. McCarthy AJ, Witney AA, Lindsay JA. *Staphylococcus aureus* temperate bacteriophage: carriage and horizontal gene transfer is lineage associated. *Front Cell Infect Microbiol*. 2012;2:6.
62. Cervera-Alamar M, Guzmán-Markevitch K, Žiemytė M, Ortí L, Bernabé-Quispe P, Pineda-Lucena A, et al. Mobilisation Mechanism of Pathogenicity Islands by Endogenous Phages in *Staphylococcus aureus* clinical strains. *Sci Rep*. 2018;8(1):1–13.
63. Goerke C, Köller J, Wolz C. Ciprofloxacin and trimethoprim cause phage induction and virulence modulation in *Staphylococcus aureus*. *Antimicrob Agents Chemother*. 2006;50(1):171–7.
64. Matsushiro A, Sato K, Miyamoto H, Yamamura T, Honda T. Induction of Prophages of Enterohemorrhagic *Escherichia coli* O157: H7 with Norfloxacin. *J Bacteriol*. 1999;181(7):2257–60.



65. Sinha S, Grewal RK, Roy S. Modeling Bacteria–Phage Interactions and Its Implications for Phage Therapy. In: *Advances in applied microbiology*. Elsevier; 2018. p. 103–41.
66. Campoli-Richards DM, Monk JP, Price A, Benfield P, Todd PA, Ward A. Ciprofloxacin. *Drugs*. 1988;35(4):373–447.
67. LeBel M. Ciprofloxacin: chemistry, mechanism of action, resistance, antimicrobial spectrum, pharmacokinetics, clinical trials, and adverse reactions. *Pharmacother J Hum Pharmacol Drug Ther*. 1988;8(1):3–30.
68. Gupta A, Biyani M, Khaira A. Vancomycin nephrotoxicity: myths and facts. *Neth J Med*. 2011;69(9):379–83.
69. Dehority W. Use of vancomycin in pediatrics. *Pediatr Infect Dis J*. 2010;29(5):462–4.
70. Kotra LP, Haddad J, Mobashery S. Aminoglycosides: perspectives on mechanisms of action and resistance and strategies to counter resistance. *Antimicrob Agents Chemother*. 2000;44(12):3249–56.
71. Krause KM, Serio AW, Kane TR, Connolly LE. Aminoglycosides: an overview. *Cold Spring Harb Perspect Med*. 2016;6(6):a027029.
72. Zhanel GG, Hoban DJ, Harding GKM. The postantibiotic effect: a review of in vitro and in vivo data. *DICP*. 1991;25(2):153–63.
73. Weber DJ, Tolkoff-Rubin NE, Rubin RH. Amoxicillin and potassium clavulanate: An antibiotic combination mechanism of action, pharmacokinetics, antimicrobial spectrum, clinical efficacy and adverse effects. *Pharmacother J Hum Pharmacol Drug Ther*. 1984;4(3):122–33.
74. Dowling A, O’Dwyer J, Adley C. Antibiotics: mode of action and mechanisms of resistance. *Formatex Res Cent Badajoz, Spain*. 2017;536–45.
75. European Committee on Antimicrobial Susceptibility Testing. MIC determination of non-fastidious and fastidious organisms [Internet]. [cited 2020 Nov 4]. Available from: [https://www.eucast.org/ast\\_of\\_bacteria/mic\\_determination/?no\\_cache=1](https://www.eucast.org/ast_of_bacteria/mic_determination/?no_cache=1)
76. Wiegand I, Hilpert K, Hancock REW. Agar and broth dilution methods to determine the minimal inhibitory concentration (MIC) of antimicrobial substances. *Nat Protoc*.

2008;3(2):163.

77. Akturk E, Oliveira H, Santos SB, Costa S, Kuyumcu S, Melo LDR, et al. Synergistic action of phage and antibiotics: parameters to enhance the killing efficacy against mono and dual-species biofilms. *Antibiotics*. 2019;8(3):103.
78. Roucourt B, Lavigne R. The role of interactions between phage and bacterial proteins within the infected cell: a diverse and puzzling interactome. *Environ Microbiol*. 2009;11(11):2789–805.
79. Shlezinger M, Copenhagen-Glazer S, Gelman D, Beyth N, Hazan R. Eradication of vancomycin-resistant enterococci by combining phage and vancomycin. *Viruses*. 2019;11(10):954.
80. Moradpour Z, Yousefi N, Sadeghi D, Ghasemian A. Synergistic bactericidal activity of a naturally isolated phage and ampicillin against urinary tract infecting *Escherichia coli* O157. *Iran J Basic Med Sci*. 2020;23(2):257.
81. Santos SB, Carvalho CM, Sillankorva S, Nicolau A, Ferreira EC, Azeredo J. The use of antibiotics to improve phage detection and enumeration by the double-layer agar technique. *BMC Microbiol*. 2009;9(1):148.
82. Abedon ST, Herschler TD, Stopar D. Bacteriophage latent-period evolution as a response to resource availability. *Appl Environ Microbiol*. 2001;67(9):4233–41.
83. Lorian V. Some effects of subinhibitory concentrations of penicillin on the structure and division of staphylococci. *Antimicrob Agents Chemother*. 1975;7(6):864–70.
84. Diver JM, Wise R. Morphological and biochemical changes in *Escherichia coli* after exposure to ciprofloxacin. *J Antimicrob Chemother*. 1986;18(Supplement\_D):31–41.
85. Malone M, Bjarnsholt T, McBain AJ, James GA, Stoodley P, Leaper D, et al. The prevalence of biofilms in chronic wounds: a systematic review and meta-analysis of published data. *J Wound Care*. 2017;26(1):20–5.
86. Khatoon Z, McTiernan CD, Suuronen EJ, Mah T-F, Alarcon EI. Bacterial biofilm formation on implantable devices and approaches to its treatment and prevention. *Heliyon*. 2018;4(12):e01067.
87. Hansen MF, Svenningsen S Lo, Røder HL, Middelboe M, Burmølle M. Big Impact of the Tiny: bacteriophage–bacteria Interactions in Biofilms. *Trends Microbiol*.

2019;27(9):739–52.

88. Donlan RM. Preventing biofilms of clinically relevant organisms using bacteriophage. *Trends Microbiol.* 2009;17(2):66–72.
89. Hanlon GW. Bacteriophages: an appraisal of their role in the treatment of bacterial infections. *Int J Antimicrob Agents.* 2007;30(2):118–28.
90. Ryan EM, Gorman SP, Donnelly RF, Gilmore BF. Recent advances in bacteriophage therapy: how delivery routes, formulation, concentration and timing influence the success of phage therapy. *J Pharm Pharmacol.* 2011;63(10):1253–64.
91. Harper DR, Parracho HMRT, Walker J, Sharp R, Hughes G, Werthén M, et al. Bacteriophages and biofilms. *Antibiotics.* 2014;3(3):270–84.
92. Kelly D, McAuliffe O, Ross RP, Coffey A. Prevention of *Staphylococcus aureus* biofilm formation and reduction in established biofilm density using a combination of phage K and modified derivatives. *Lett Appl Microbiol.* 2012;54(4):286–91.
93. Sutherland IW, Hughes KA, Skillman LC, Tait K. The interaction of phage and biofilms. *FEMS Microbiol Lett.* 2004;232(1):1–6.
94. Cerca N, Oliveira R, Azeredo J. Susceptibility of *Staphylococcus epidermidis* planktonic cells and biofilms to the lytic action of staphylococcus bacteriophage K. *Lett Appl Microbiol.* 2007;45(3):313–7.
95. Walters MC, Roe F, Bugnicourt A, Franklin MJ, Stewart PS. Contributions of antibiotic penetration, oxygen limitation, and low metabolic activity to tolerance of *Pseudomonas aeruginosa* biofilms to ciprofloxacin and tobramycin. *Antimicrob Agents Chemother.* 2003;47(1):317–23.

# **Chapter 4: Antimicrobial-loaded Poly(lactic acid)-poly(ethylene glycol) Films for the Treatment of *S. aureus* Infections**

## **4.1. Overview of Chapter**

This proof-of-concept study aimed to demonstrate the utility of antimicrobial-loaded poly(lactic acid)-polyethylene glycol (PLA-PEG; PPEG) films as antimicrobial wound dressings for the treatment of *S. aureus* infections.

Herein, this chapter will discuss the physical properties of the PPEG films and the effect this has on the release of phage K and ciprofloxacin from these films. Additionally, this chapter investigated the efficacy of the antimicrobial-loaded PPEG films against three strains of *S. aureus* using a variety of microbiological assays (suspension assays, colony biofilm models, and *ex vivo* models). Finally, experiments were conducted to determine if the phage-antibiotic synergy between phage K and ciprofloxacin observed in Chapter 3 could be observed when the antimicrobials were combined into the PPEG film.

## **4.2. Introduction**

### **4.2.1. Polymers**

The name ‘polymer’ is derived from two terms, ‘poly’ meaning many, and ‘mer’ meaning unit,<sup>1</sup> as polymers are macromolecules formed via the chemical bonding of repeating units of smaller molecules (termed monomers).<sup>2</sup> Polymers are used in numerous industries; however, this chapter is going to focus on the use of polymers for biomedical applications. Table 4.1 highlights some common examples of synthetic polymers used in the biomedical field.<sup>1</sup>

**Table 4.1:** Commonly used synthetic polymers and their applications. Adapted from Hill et al.<sup>1</sup>

Polymer	Application
Poly(methylmethacrylate)	Hard contact lenses, interocular lenses, bone cements, denture base
UHMWPE (ultra-high molecular weight polyethylene)	Bearing surfaces in artificial joints
Polyethylene terephthalate	Artificial arteries
Polyurethanes	Catheters
Polyhydroxyethylmethacrylate	Soft contact lenses, wound dressings, drug release, matrices
Polypropylene	Sutures, heart valves, finger joints
Silicones	Breast implants, facial modifications
Poly(glycolide)	Biodegradable sutures

#### 4.2.1.1. Polymer Weight

With the exception of biological polymers, whose molecular weight (MW) is strongly controlled, polymerisation results in a distribution of chain lengths, and consequently, a distribution of molar mass.<sup>1</sup> Polymer MW can be calculated by either the number average molecular weight ( $M_n$ ), or the weight average molecular weight ( $M_w$ ).

$M_n$  counts as the total number of molecules in a unit mass of polymer, irrespective of shape or size; it can be determined by techniques that count molecules via the following equation:<sup>1</sup>

$$M_n = \frac{\sum N_i M_i}{\sum N_i} \quad (1)$$

Where  $M_i$  is the molecular weight of a chain,  $N_i$  is the number of chains of that molecular weight, and  $i$  is the number of polymer molecules.<sup>3</sup>  $M_n$  is used for the determination of boiling point elevation, freezing point depression, vapour pressure depression, and osmotic pressure changes.<sup>4</sup>

The weight average molar mass is the mass of the individual chains that contribute to the overall molecular weight of the polymer; it is calculated using the following equation:

$$M_w = \frac{\sum_i N_i M_i^2}{\sum_i N_i M_i} \quad (2)$$

Where  $M_i$  is the molecular weight of a chain,  $N_i$  is the number of chains of that molecular weight, and  $i$  is the number of polymer molecules.  $M_w$  is typically measured by light scattering experiments.<sup>5</sup>

The number of monomers within the polymer can vary greatly; however, the average number of monomers per polymer chain can be determined by calculating the degree of

polymerisation.<sup>2</sup> The degree of polymerisation can be defined in terms of either number average or weight average:

$$N = \frac{M_w}{M_{mer}} \text{ or } = \frac{M_n}{M_{mer}} \quad (3)$$

Where  $M_{mer}$  is the molecular weight of the monomer unit.

Additionally, the ratio of  $M_w/M_n$  can be used to calculate the polydispersity index (PDI; Equation 3). PDI is used as a measure of broadness of molecular weight distribution, the smaller the PDI the narrower the molecular weight.<sup>4</sup>

$$PD = \frac{M_w}{M_n} \quad (4)$$

For monodisperse polymers, where all chains are the same length, the PDI is 1; biological examples of this include DNA and enzyme structure. Additionally, some synthetic polymers (such as polystyrene used for the calibration curve) have a PDI of 1.02 – 1.10.<sup>4</sup>

#### **4.2.1.2. Linear, Branched, and Crosslinked Polymers**

In linear polymers, the repeating units are joined together in a chain-like arrangement and are often more rigid compared to branched and cross-linked polymers. Typically, they arise when the monomer contains a single end group; some examples include, polyethylene, polystyrene, and polyamides.<sup>4</sup>

Branched polymers have side chains, which often are composed of the same monomer within the main polymer chain. Side chains typically arise from side reactions during polymerisation, and monomers with two or more end groups are more likely to support this branching. Often, branched polymers have a lower density due to the reduced packing efficiency. One of the most common examples of a branched polymer is the low-density poly(ethylene), often used for plastic bags, containers, and textiles, etc.<sup>4</sup>

Finally, crosslinked polymers arise when polymer chains covalently bond to one another to form a large three-dimensional network; this often changes the properties of the polymer.<sup>2</sup> Chemical crosslinks are generally permanent and once they arise, the polymer becomes thermoset in nature<sup>4</sup> Crosslinked polymers are usually characterised by their degree of crosslink<sup>6</sup> and common examples include epoxies, rubber, and various adhesives.<sup>4</sup>

#### **4.2.1.3. Copolymer Arrangements**

The simplest polymer is a homopolymer, which consists of repeating units of only one monomer. Copolymers are composed using monomers that differ from one another and can exist various sequences:<sup>1,2,4</sup>

- Random – this is where the two monomers (A and B) do not follow any specific order e.g., ABABBABAAABABA.
- Alternating – occurs when the two monomers (A and B) are arranged in an alternating fashion, e.g., ABABABABABABAB.
- Block – in a block copolymer, each monomer (A or B) is grouped together and can be thought of as two homopolymers joined together, e.g., AAAAAAABBBBBBBB. Copolymers are often used as adhesives, surfactants, membranes, foams, and cosmetics.

#### **4.2.1.4. Polymer Classification**

There are numerous ways in which polymers are classified – but generally speaking, they are usually classified according to their structure. Firstly, they are differentiated between inorganic and organic, dependent on if the polymer backbone contains carbon atoms. Then, the polymers are further classified according to the specific identity or order of the atoms within the polymer backbone, as well as their occurrence.<sup>2</sup>

Inorganic polymers have a polymer backbone that contains atoms other than carbon; these include poly(siloxanes), poly(silazanes), poly(sulphides), etc. Conversely, organic polymers are more common and are generally divided into either natural or synthetic. Natural polymers include starch, cellulose, and glycogen, while synthetic polymers include poly(styrene), poly(propylene), poly(glycolic acid), and poly(lactic acid). Semi-synthetic polymers have also been synthesised, which are generally functionalised natural polymers, e.g., methylcellulose and cellulose acetate.<sup>2</sup>

Additionally, crosslinked polymers can form a three dimensional hydrophilic network that swells in the presence of water, termed a hydrogel. They can exist as homopolymers or copolymers and are generally biocompatible due to their large water content. Hydrogels can be tailored to produce a wide range of swelling characteristics, dependent on the application, as the swelling ratio alters the properties of the polymer (diffusion rates, surface properties, refractive indexes, mechanical characteristics, etc).<sup>2</sup>

#### 4.2.1.5. Configuration and Conformation

The configuration of a polymer is determined by its chemical structure, while the conformation of a polymer relates to its three dimensional structure. Many polymers are composed of monomers that contain chiral centres, which is where a carbon atom has four different groups attached to them. Owing to this, the monomer can exist in two optical isomers, left handed (L) and right handed (D).<sup>1</sup>

A polymer containing monomers with chiral centres can have different conformations upon polymerisation. Tacticity refers to the ordering of the polymer, describing the stereochemistry of the pendant groups on the polymer backbone. If the chiral centres are linked randomly, the polymer is termed atactic; if the chiral centres are linked with the substituents in an alternating fashion, the polymer is termed syndiotactic; and if the chiral centres are linked together with the substituents in the same relative positions, the polymer is termed isotactic. Generally, polymers are atactic; however, steric constraints of the monomers and/or specialised reaction conditions can result in isotactic and syndiotactic polymers.<sup>1,7</sup>

Tacticity influences the thermal and mechanical properties of the polymer, including the glass transition temperature ( $T_g$ ), melting temperature, and solubility.<sup>1</sup> Atactic polymers are generally amorphous, resulting in polymers which are less brittle than their crystalline counterparts, exhibiting glass-like properties below their  $T_g$  and elastomeric properties above the  $T_g$ .<sup>1,7</sup>

Crystallinity is favoured by ordered/stereoregular chains; however, no polymer is 100% crystalline, often containing both amorphous and crystalline regions. The degree of crystallinity influences the mechanical properties (e.g. Young's modulus, toughness, and strength) in addition to gas permeability and water uptake of the polymer. The crystallinity of a homopolymer can be reduced via copolymerisation with a small amount of a second monomer, while conversely, crystallinity can be increased by holding a polymer above its  $T_g$ , but below its  $T_m$  to provide more time for crystallisation to occur.<sup>1</sup>

$T_g$  is calculated for amorphous, or amorphous sections of a polymer and describes the temperature at which there is a characteristic change in the physical properties of a polymer. At temperatures below the  $T_g$ , the physical property of the polymer changes to that of a 'glassy' or brittle and crystalline state; however, above the  $T_g$ , the polymer exists in its 'rubbery' state, with soft and flexible physical characteristics owing to the long-range sequential motion of the polymer chains.<sup>8,9</sup>



#### 4.2.1.6. Polymer Synthesis

Polymerisation is a process where the monomer subunits are covalently bonded together to produce the macromolecular polymers.<sup>7</sup> Typically, polymer synthesis can be divided into addition, condensation, and ring-opening polymerisation, although other types exist (e.g., chain transfer and plasma polymerisation).<sup>4</sup>

Addition polymerisation is where the polymer grows exclusively by reactions between the monomer(s) and the reactive site(s) on the polymer chain; monomers are added once at a time via a chain reaction. Polymers created using addition polymerisation are generally produced using unsaturated monomers containing C-C double bonds and all the monomers are consumed without the formation of byproducts. Common examples of polymers synthesised through addition polymerisation include poly(ethylene), poly(vinyl chloride), and poly(styrene).<sup>1,4</sup>

In addition polymerisation, the reaction occurs via three distinct steps: chain initiation, chain propagation, and chain termination.<sup>5</sup> Chain initiation occurs via the use of an initiator to a reactive site. This could be a radical (free radical polymerisation), cation (cationic polymerisation), anion (anionic polymerisation), and organometallic complexes (coordination polymerisation). Next, in chain propagation, the monomers attach to the molecular chain, propagating the chain length. Finally, the chain growth is terminated through the neutralisation of the reactive centre.<sup>4</sup>

Condensation polymerisation, or step-growth polymerisation, is where two monomers are reacted together, and molecule is eliminated – often water. The reaction progresses in a step-wise manner and monomers, dimers, trimers, oligomers, etc., are able to be utilised to create a larger molecule.<sup>6</sup> Often, condensation polymerisation combines two different components, with at least two reactive sites, in an alternating fashion. Examples include polyamides and polyesters, proteins, and polysaccharides.<sup>1,4</sup>

Ring-opening polymerisation (ROP) is used in industry as it yields higher molecular weight polymers in a relatively short space of time. ROP utilises cyclic monomers and a catalyst/initiator to expedite the ring-opening process. The polymers produced by ROP are often linear, with a narrow molecular weight range, which is typically hard to achieve via condensation polymerisation. An example of a polymer produced via ROP is poly(lactic acid).<sup>4</sup>

## 4.2.2. Poly(lactic acid)

Poly(lactic acid) (PLA) is a hydrophobic polyester, first discovered in the 1700's by Scheele.<sup>10,11</sup> PLA is composed of monomers of lactic acid, produced via fermentation of starch from plants (e.g. corn, sugarcane, potatoes, and beets)<sup>12</sup> and can be synthesised by direct polycondensation of lactic acid, or ring-opening polymerisation of the lactide dimer using a suitable catalyst (Figure 4.1).<sup>13</sup>

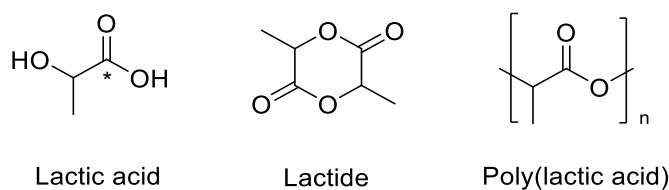


**Figure 4.1:** Structures of lactic acid, lactide and poly(lactic acid)

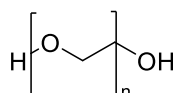
Lactic acid is a hydroxyl acid that exists as two optical isomers (L and D) due to the presence of a chiral carbon.<sup>13</sup> Therefore, PLA can exist in three optical forms: PLDA, PLLA, and PDLA;<sup>14</sup> for biological applications, the L isomer is preferred as the D isomer can be harmful to human metabolism and can result in decalcification and acidosis.<sup>13</sup>

The properties of PLA, such as the rate of degradation, are dependent on the optical form of the monomer and the resultant polymer's crystallinity.<sup>15</sup> Polymerisation using the optical isomers of lactide (L or D) result in a polymer chain that is approximately 40% crystalline, whereas polymerisation using a racemic mixture (DL) of lactic acid results in an amorphous polymer with low mechanical strength. As the polymer tends from crystalline to amorphous, the melting and glass transition temperatures decrease, resulting in an alteration of physical characteristics such as density, heat capacity, and rheological properties.<sup>15,16</sup>

Drug delivery systems often use PLA due to its biodegradability, biocompatibility, low levels of immunogenicity and toxicity, ease of modification (either by copolymerisation or functionalisation),<sup>17,18</sup> and thermal processability<sup>10,15,19</sup>

PLA was originally used for the repair of mandibular fractures in dogs.<sup>20</sup> Since then, PLA has been used in a variety of applications in orthopaedics,<sup>21,22</sup> cardiac surgery,<sup>23,24</sup> dentistry,<sup>25,26</sup> plastic surgery,<sup>27,28</sup> and oncology.<sup>29,30</sup> For a more comprehensive review, please see Tyler *et al.*<sup>10</sup> PLA has also been used for wound dressings and will be discussed in Section 4.2.2.1.

PLA is often used in combination with poly(ethylene glycol) (PEG) to increase the hydrophilicity, toughness, and flexibility of the PLA polymer.<sup>10,12</sup> Additionally, the incorporation of PEG in PLA-PEG blends enhance the degradation rate and drug release of the resultant films.<sup>31</sup> PEG is derived from the polymerisation of ethylene glycol (Figure 4.2), and dependent on the molecular mass of the polymer, can have a linear or branched structure. As PEG is hydrophilic, every PEG unit is tightly associated with two or three water molecules, preventing any incorporated drugs from enzymatic degradation, rapid renal clearance, and interactions with cell surface proteins.<sup>32,33</sup>



Poly(ethylene glycol)

**Figure 4.2:** Structure of poly(ethylene glycol)

#### 4.2.2.1. Poly(lactic acid) Drug Delivery Systems

Drug delivery systems have been used in recent years to combat issues associated with traditional pharmaceuticals (poor solubility, non-specific targeting, high dosage, etc.) by protecting the drug from the physiological environment, increasing the bioavailability or solubility of the drug, or controlling the release of a drug from a suitable matrix.<sup>13,19</sup> This section will focus on the use of PLA or delivery systems utilising conventional antibiotics and/or phage therapy, with a particular focus on wound dressings.

There have been several reports of PLA-based drug delivery systems as potential candidates for wound dressings.<sup>19,34</sup> Toncheva *et al* created PLA and PLA-PEG membranes containing a variety of antimicrobials, both as single and monotherapies. When PLA films containing diclofenac sodium and benzalkonium chloride were incubated with *S. aureus*, there were clear zones of lysis of  $33.0 \pm 13.0$  mm and  $27.0 \pm 13.0$  mm, respectively.<sup>35</sup> Additionally, PLA membranes containing a combination of diclofenac sodium and lidocaine hydrochloride or diclofenac sodium, lidocaine hydrochloride and benzalkonium chloride resulted in zones of inhibition of  $30.0 \pm 1.1$  mm and  $19.0 \pm 1.1$  mm, respectively, when treated with *S. aureus*.<sup>36</sup> Furthermore, Han *et al* created electrospun PLA nanofibers containing nanoparticles composed of tetracycline hydrochloride blended with Fe<sub>3</sub>O<sub>4</sub>-COOH. This system displayed antimicrobial activity against *S. aureus* and *E. coli*, with zones of inhibitions of  $25.8 \pm 1.4$  mm and  $23.6 \pm 1.6$  mm, respectively.<sup>37</sup> While Nazari *et al* showed that electrospun PLA-PEG nanofibers containing cefixime had a good release profile in the presence of graphene oxide, further studies must be undertaken to determine the antimicrobial efficacy of the film.<sup>38</sup>

PLA films have also been used to release anti-oxidant molecules to aid in wound healing.<sup>39,40</sup> For example, Perumal *et al* created electrospun nanofibers using a blend of PLA and hyperbranched polyglycerol for the release of curcumin for wound healing applications. Their results found that the nanofibers had high hydrophilicity, swelling and drug uptake, which in turn led to better cell viability, adhesion, and proliferation.<sup>41</sup>

There is currently limited literature on phage encapsulation within PLA films. Jamaledin *et al* described the synthesis of microparticles of poly(lactic-co-glycolic acid) to encapsulate phage, whereby the phage could be used as an antigen delivery system. Their preliminary results suggested that phage was stable within the microspheres and retained its immunogenic properties.<sup>42</sup> Additionally, Radford *et al* developed two phage based xanthan coatings on PLA films that significantly inhibited *Salmonella typhimurium* and *Listeria monocytogenes* growth.<sup>43</sup> While the latter study was investigating the use of phage-based systems for prolonging the life of food, there is no reason to suggest that this film could not be utilised in a clinical setting.

### **4.2.3. Aims of Study**

This study aimed to create a proof-of-concept wound dressing demonstrating the utility of a PLA-PEG film containing antimicrobials as an antimicrobial wound dressing capable of eliminating *S. aureus* infections. Experiments included:

- Optimisation of the weight ratio of PEG:PLA. Following on from this, *in vitro* release kinetics and stability of the films containing phage K/ciprofloxacin, or a combination of the two, will be determined.
- Microbiological analysis of PPEG films containing phage K, ciprofloxacin, or a combination of the two, against three clinically relevant *S. aureus* species (*S. aureus* H560, MRSA252, and MSSA101). Microbiological assays included:
  - Planktonic suspension assays
  - Colony biofilm wound models
  - *Ex vivo* porcine skin models

## 4.3. Methods

### 4.3.1. Bacterial and Bacteriophage Methods

All methods relating to growth conditions of *S. aureus* isolates and propagation of phage K were followed as outlined in Chapter 2, Section 2.2.1.3 and 2.2.3.2, unless otherwise stated. Enumeration of bacterial and phage cell density were performed as outlined in Chapter 2, Section 2.2.1.4 and 2.2.3.3.

### 4.3.2. Development of the PLA-PEG System

#### 4.3.2.1. Creating the Polymer Blend

Antibiotic-loaded porous films (a-PPEG) were prepared by the solvent casting method.<sup>19</sup> Twenty microliters of ciprofloxacin (30 mg/mL), phage K (c.  $1 \times 10^{11}$  PFU/mL) or a combination of both, were dispersed into 88.8  $\mu$ L of PEG 400 and mixed into 10% w/w PLA in dichloromethane (DCM) homogeneously at room temperature. The weight ratio of PEG:PLA was 2:1. The mixtures were then poured into 10 mm diameter scintillation vials for casting, before being placed at -20 °C for 24 h and dried at room temperature for 4 h. Antibiotic-free porous films (PPEG) were also prepared as controls.

##### 4.3.2.1.1. Encapsulation Efficacy

a-PPEG films were placed in 2 mL PBS (pH 7.4) and incubated for 24 h at room temperature. After incubation, the concentration of antimicrobial released from a-PPEG was calculated. For phage K, this was undertaken by determining the PFU/mL and for ciprofloxacin this was measured using UV-Vis, with the concentration of ciprofloxacin determined by use of a calibration curve. Encapsulation efficacy was calculated as follows:

$$EE (\%) = \left( \frac{\text{Concentration of antimicrobial released}}{\text{Total concentration of antimicrobial}} \right) \times 100 \quad (5)$$

##### 4.3.2.2. Swelling and Weight Loss

A known weight ( $W_0$ ) of the porous matrix was subjected to degradation measurements in phosphate buffer solution (PBS, pH 7.4). The measurements were undertaken at room temperature for 24 h, 48 h, 1, 2 and 3 weeks. At each time point, the film was collected and blotted with filter paper to remove excess surface water and weighted ( $W_1$ ), allowed to dry to a constant weight at 60 °C and re-weighed ( $W_2$ ). Water sorption (%WS) and weight loss

(%WL) were calculated using the following equations. The measurements were performed in triplicate using three separate films.

$$WS (\%) = \left( \frac{W_1 - W_2}{W_2} \right) \times 100 \quad (6)$$

$$WL (\%) = \left( \frac{W_0 - W_2}{W_0} \right) \times 100 \quad (7)$$

### **4.3.3. Bacteriophage Survival**

#### **4.3.3.1. pH**

To determine if pH had an effect on phage titre, TSB was adjusted with 1 M NaOH/HCl to achieve a pH range between 2 – 10 and filter sterilised with a 0.22  $\mu$ M filter before use. Stock phage lysates ( $10^9$  PFU/mL) were diluted 10-fold into the pH-adjusted TSB and incubated for 1 h at room temperature. After incubation, viable phage concentration at each pH was determined as outlined in Chapter 2, Section 2.2.3.3.

#### **4.3.3.2. Dichloromethane and PEG 400**

In brief, differing concentrations of dichloromethane and PEG 400 (0 – 90% v/v) in PBS were prepared. Subsequently phage lysate was added to achieve a final phage concentration of  $10^8$  PFU/mL and incubated for 1 h at room temperature. After incubation, viable phage concentration was determined as outlined in Chapter 2, Section 2.2.3.3.

#### **4.3.3.3. Temperature**

Known concentrations of phage K in PBS ( $10^8$  PFU/mL) were incubated at various temperatures (-20, 4, 25, 32, 37, 60 °C) for 1 h. After incubation, viable phage concentration was determined as outlined in Chapter 2, Section 2.2.3.3.

### **4.3.4. Scanning Electron Microscopy**

The porous structure of the PPEG films were assessed by SEM. Films were stored under vacuum overnight to ensure complete dehydration before sputter-coating with chromium (Edwards S150B, 60 s) to reduce charging effects and thermal damage, prior to images being obtained using a scanning electron microscope (JEOL SEM6480LV) operated at 10 kV.

### **4.3.5. *In vitro* Release Studies**

*In vitro* phage release studies were performed at room temperature, where phage loaded-PPEG films were placed into 2 mL buffer (PBS; pH 7.4). At pre-determined time intervals,

the buffer was withdrawn and replaced with equal volume of fresh solution. The removed buffer was assessed for phage concentration by enumeration (Chapter 2, Section 2.2.3.3) and the % cumulative release of phage was calculated and plotted against time.

*In vitro* ciprofloxacin release studies were carried out as outlined above, with slight modifications. To assess ciprofloxacin concentration at each time point, the absorbance of the removed buffer was monitored using a UV-Vis spectrophotometer (Shimadzu UV-1800) and transformed into ciprofloxacin concentration by use of a calibration curve. The cumulative release of ciprofloxacin from films was calculated and plotted as a function of time.

All *in vitro* release studies were carried out using three independent films and 100% cumulative release referred to the amount of therapeutic released from the uncoated PPEG after 24 h in the buffer solution (PBS, pH 7.4).

#### **4.3.6. Stability**

The stability of the films at 25 °C was also investigated. Briefly, a-PPEG films were created and placed in a 12-well microtiter plate for up to five days. At pre-determined time intervals, the a-PPEG films were submerged in 2 mL of PBS (pH 7.4.) for 24 h prior to phage enumeration and/or determination of ciprofloxacin concentration using methods outlined in Section 4.3.5.

#### **4.3.7. Microbiological Testing**

##### **4.3.7.1. Suspension Assays**

Overnight cultures of three *Staphylococcus* spp., *S. aureus* H560, *S. aureus* MRSA252 and *S. aureus* MSSA101 were prepared as outlined in Chapter 2, Section 2.2.1.3. After dilution to an optical density of 0.2 (c. 10<sup>8</sup> CFU/mL) in PBS, the cultures were further diluted 10-fold into fresh TSB medium. After inoculation, antimicrobial free and antimicrobial loaded PPEG films, along with the relevant controls (phage K, ciprofloxacin, or a combination of both) were added to the relevant cultures. The bacteria were allowed to grow at 32 °C with 150 rpm shaking for 24 h. After incubation, the bacterial and phage (if required) concentrations were determined as outlined in Chapter 2, Section 2.2.1.4 and Section 2.2.3.3.

#### **4.3.7.2. Colony Biofilm Wound Model**

The colony biofilms were prepared as outlined in Chapter 2, Section 2.2.2.2. After inoculation of the polycarbonate membrane with AWF and bacterial culture (c 10<sup>6</sup> CFU/mL), the membrane was left to dry at room temperature for approximately 15 minutes. Once dry, a-PPEG films were placed on top of the inoculated membranes and incubated at 32 °C for 24 h. After incubation, the biofilms were stripped and enumerated as outlined in Chapter 2, Section 2.2.1.4

#### **4.3.7.3. Ex vivo Porcine Skin Models**

##### **4.3.7.3.1. Sterilisation**

Porcine skin was washed to remove dirt and contamination and shaved to remove hair. After, the skin was cut into 2 x 2 cm squares and stored at -20 °C. When needed, skin was thawed overnight at 4 °C, before sonication for 15 min (44 KHz) in sterile dH<sub>2</sub>O; this was repeated three times. After, the skin was soaked for 15 min in 70% ethanol (EtOH) and underwent a further two rounds of 15 min sonication (44 KHz) in sterile dH<sub>2</sub>O. Finally, the skin was UV-sterilised for 10 min prior to use.

##### **4.3.7.3.2. Optimisation**

Sterilised porcine skin was placed into 10 mL PBS and sonicated for 15 min (44 KHz). Next, 100 µL was spread onto TSA plates in duplicate, and subsequently incubated for 24 h at 32 °C. Porcine skin was considered sufficiently free of bacteria if < 20 colonies were present.

To assess for bacterial recovery, sterilised skin was placed onto bacteriological agar and 10 µL of optically-adjusted *S. aureus* (c. 10<sup>8</sup> CFU/mL; Chapter 2, Section 2.2.1.3) was spotted onto the skin and left to dry at room temperature for 20 min. Once dry, the skin was removed from the agar, and placed into 10 mL of PBS. Then, the skin underwent a 15 min cycle of sonication (44 KHz), before being enumerated (Chapter 2, Section 2.2.1.4) and compared to the CFU/mL of the stock bacterial suspension. To circumvent any microbial contamination, mannitol salt agar was used in tandem with TSA for enumeration of *S. aureus* colonies.

##### **4.3.7.3.3. Microbiological Assay**

Sterilised skin was placed onto bacteriological agar and 10 µL of optically-adjusted *S. aureus* (c. 10<sup>8</sup> CFU/mL; Chapter 2, Section 2.2.1.3) was spotted onto the skin and left to dry at room temperature for 20 min. Once dry, 10 µL of the antimicrobial (phage K and/or ciprofloxacin) was spotted onto the skin and left to dry for a further 20 min at room temperature. The skin



was then placed into a sterile container and incubated at 32 °C for 24 h. After incubation, the skin was removed from the agar, placed into 10 mL of PBS, and sonicated (44 KHz) for 15 minutes prior to enumeration (Chapter 2, Section 2.2.1.4). A sterilisation control (porcine skin without the addition of *S. aureus*) and a bacteria-only control (*S. aureus* and PBS) were carried out in tandem. In cases where phage were used, PFU/mL was also determined as outlined in (Chapter 2, Section 2.2.3.3). The assay was repeated in triplicate, and to circumvent any microbial contamination, mannitol salt agar was used in tandem with TSA for enumeration of *S. aureus* colonies.

## 4.4. Results and Discussion

### 4.4.1. PLA-PEG (PPEG) Films

The PPEG film was created via polymer blending of PLA and PEG. Polymer blending can be used to overcome the inherent disadvantages of PLA (poor toughness, low degradation rate, high hydrophobicity)<sup>44–46</sup> by blending it with another polymer (such as PEG) to create a system with a more favourable morphology and physical characteristics.<sup>12,15</sup>

Polymer blends can<sup>47</sup> be prepared by either solvent blending or melt blending. Solvent blending is where the polymers are dissolved in a co-solvent and processed to form the end material before evaporation of the solvent; this method is useful for polymer films and porous materials.<sup>12,48</sup> Melt blending is achieved through the use of a melt extruder and the melt-blended polymers can be cast into films via compression.<sup>12</sup>

Polymer blends is dictated by the Gibbs-free energy equation (Equation 8):

$$dG_M = dH_M - TdS_M \quad (8)$$

Where  $dG_M$ ,  $dH_M$ , and  $dS_M$  are energy, enthalpy, and entropy of mixing, respectively.  $dG$  must be  $< 0$  for two or more polymers to be miscible.

Upon removal of either temperature or solvent during blend formation, phase separation occurs,<sup>49</sup> and the extent of this separation dictates the morphology of the resulting blend. Work conducted by Phaechamud *et al* investigated the formation of the PLA-PEG polymer blends and found that PLA-PEG in DCM changed from solution into a porous film via a two-step process (liquid-liquid phase separations and solidification). Liquid-liquid phase separation was thought to occur due to the increase in Gibbs free energy of the system upon addition of a non-solvent (PEG 400), causing some solvent evaporation and the formation of a polymer concentration gradient. The liquid-liquid phase separation led to an interpenetrating network structure of polymer-rich and polymer-poor phases and continued until the two phases were combined in a stable condition with the lowest free energy prior to solidification; the porous structure of the PLA matrix was created once the solvent evaporated and the polymer blend was dry.<sup>50</sup>

#### 4.4.1.1. Pore Size

Porosity is advantageous for wound dressings as it can help to reduce the wound contact area, avoiding adherence when the wound is dried. Generally, the smaller the pore size and porosity, the less painful the dressing change is. However, the optimum pore size and porosity depends on the wound type and application of the dressing as it affect other properties of the dressing, including the water vapour transmission rate, oxygen transmission rate, and drug release (if loaded with an antimicrobial).<sup>19,51</sup>

The formation of the PLA-PEG (PPEG) films created in this study was based on previous work conducted by Chitrattha *et al.*<sup>19</sup> The initial weight ratio of PEG:PLA used was 1.5:1; however, this led to minimal release of phage from the polymer (data not shown). This was attributed to the lack of flexibility within the polymer; hence, the weight ratio of PEG:PLA was increased to 2:1.<sup>19</sup>

The PPEG film was highly porous in nature, similar to other reports in literature (Figure 4.3).<sup>19</sup> Nevertheless, the pore size observed in this study was heterogenous in nature, primarily due to rate of DCM evaporation from the films. The porosity of the film could be altered using different temperatures/humidities during the solvent evaporation stage. However, as phage were successfully released from this film (further details below) it was deemed sufficient for this proof-of-concept design. Future experiments could be conducted to further improve this dressing for optimal porosity leading to maximum phage release.

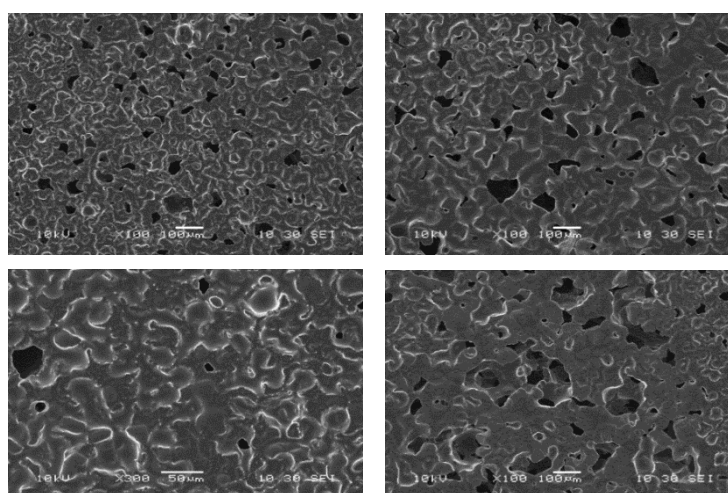


**Figure 4.3:** SEM of the top layer of the PPEG film

#### 4.4.1.2. Weight Loss and Water Sorption

The % weight loss (%WL) and % water sorption (%WS) of the PPEG films are shown in Figure 4.4. After 24 h, the weight loss of the polymer was ~58% and a corresponding water sorption of ~240% was observed. After this time, the %WL and %WS remained relatively stable, with values of ~60% and ~250%, respectively. Once again, these results are similar to those observed in literature, and substantially higher than PLA only.<sup>19</sup> These results indicate the importance of PEG within this PPEG blend, increasing the hydrophilic nature of the film, while promoting degradation, and therefore release of any encapsulated materials.

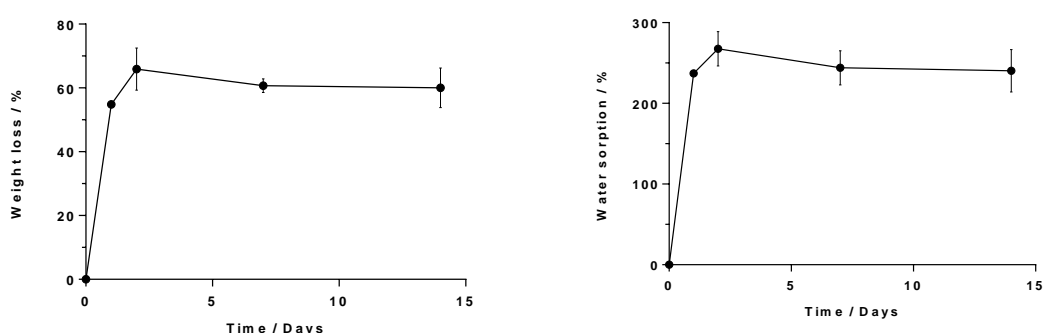


**Figure 4.4:** *In vitro* degradation profiles of **A)** %WL and **B)** %WS of the PPEG film. n = 3, error bars indicate standard deviation

#### 4.4.2. Bacteriophage-loaded Films

##### 4.4.2.1. Bacteriophage Survival

As phage are proteinaceous, they are susceptible to degradation by stimuli such as organic solvents and extreme temperatures. As the creation of the PPEG films required the use of DCM, PEG 400, and temperatures ranging from -20 and 60 °C, it was imperative to determine phage viability under these conditions (Figure 4.5).

Upon incubation with varying concentrations of DCM (% v/v) in PBS, the phage K concentration remained comparable to the control (phage K in PBS). This agrees with other literature sources, who have shown that phage remain viable upon incubation with high concentrations of organic solvent such as DCM and chloroform (CHCl<sub>3</sub>).<sup>52</sup> Although, this depends on the type of phage used, as there have been instances where phage have degraded in the presence of organic solvents. For example, Jurczak-Kurek *et al.* found that their isolated phage degraded upon exposure to acetone and 50% (v/v) DMSO, while they were resistant to degradation from chloroform.<sup>53</sup>

Next, the viability of phage K was investigated in the presence of PEG 400. As PEG 8000 is commonly used for phage precipitation to achieve higher titres, and there have been examples where PEG has been used as a delivery material of phage, it was assumed that there would be minimal effect on phage K viability.<sup>54</sup> Surprisingly, Figure 4.5 shows a significant decrease in phage titre upon PEG 400 concentrations of 80% v/v (t-test,  $p < 0.05$ ) and 90% v/v (t-test,  $p < 0.01$ ), compared to the control. However, this decrease in phage concentration was not clinically significant, as it only corresponded to a log reduction of 0.49 and 0.73, respectively. Therefore, the decrease in concentration would not drastically impact the viability of phage K within the PPEG film, hence, was used in this proof-of-concept study.

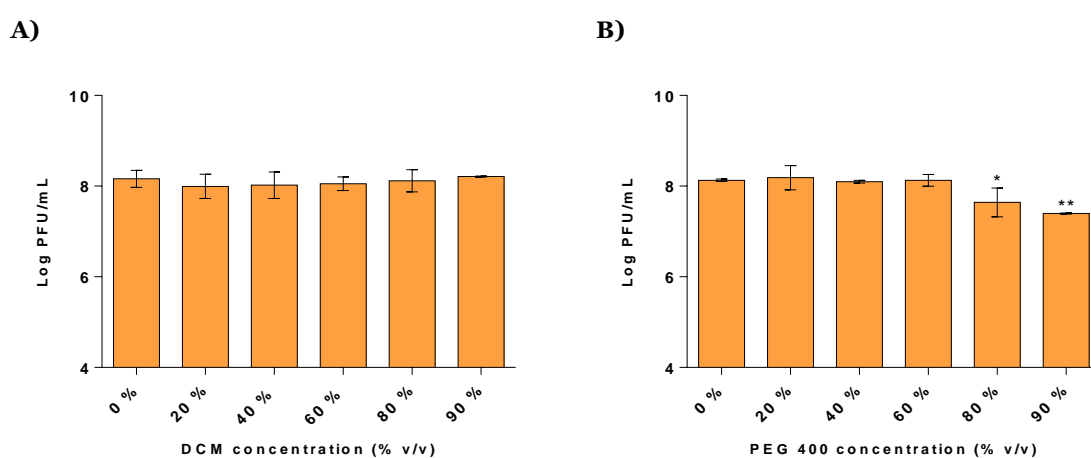


**Figure 4.5:** Phage K survival in the presence of increasing concentrations of **A)** DCM, and **B)** PEG 400.  $n = 3$ , error bars indicate standard deviation. Statistical analysis conducted using a One-way ANOVA. \*  $p < 0.05$ , \*\*  $p < 0.01$

The original methodology stated that the films had to be stored at  $-20\text{ }^{\circ}\text{C}$  for 24 h prior to drying at  $60\text{ }^{\circ}\text{C}$  for a further 24 h.<sup>19</sup> Phage viability is strongly dependent on temperature, with many studies showing decreased phage viability at higher temperatures.

To assess this, phage K was incubated in PBS at varying temperatures between  $-20\text{ }^{\circ}\text{C}$  to  $60\text{ }^{\circ}\text{C}$  for 1 h before enumeration to determine phage survival. As shown in Figure 4.6, incubation at  $60\text{ }^{\circ}\text{C}$  for 1 h significantly reduced phage concentration by 5.5 log compared to the control (incubation at  $4\text{ }^{\circ}\text{C}$ ). As this is a large reduction in phage K viability, the methodology was changed so that the phage K-loaded PPEG films were dried at room temperature for 4 h prior to use. Additionally, these results showed that phage K has good survival at clinically significant temperatures. For example, phage K concentration remained stable when incubated at  $32\text{ }^{\circ}\text{C}$ , which is the temperature of healthy skin. This is a promising result as it indicates that phage K would be a viable topical antimicrobial capable of eliminating *S. aureus* at the wound bed.

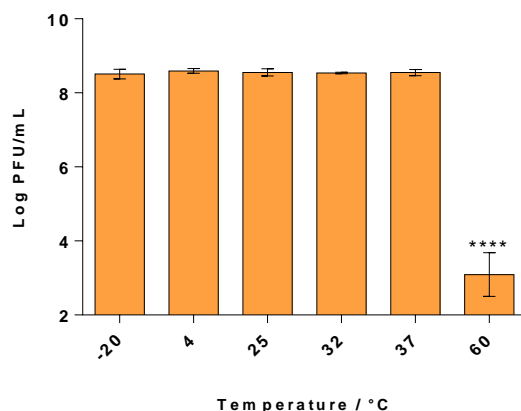


**Figure 4.6:** Phage K survival after 1 h incubation in PBS at varying temperatures. n = 3, error bars indicate standard deviation. Statistical analysis conducted using a One-way ANOVA. \*\*\*\* p<0.0001

#### 4.4.2.2. Encapsulation Efficacy and *In vitro* Release

Phage K was successfully encapsulated within the PPEG film, so the next step was to quantify the encapsulation efficacy and *in vitro* release of phage K from this film. The encapsulation efficacy was determined using Equation 5 and found to be  $1.71 \pm 1.08\%$  (assuming 100% of phage K is released after 24 h). While this value initially seems disappointing, it corresponds to a 2-log reduction in viable phage K after incorporation into the PPEG film. Using the results shown above, it is possible to assume that 1-log reduction arose due to external environmental impacts on the phage survival, predominately incubation with PEG 400. The other 1-log reduction could be attributed to the formation of the film at -20 °C; the semi-crystalline nature of the PPEG film could affect the protein structure of phage K, ultimately reducing viability as its structure is intrinsically linked to its survival. Additionally, error could be due to the methodology used to determine encapsulation efficacy. The method used in this study assumes that all viable phage would be released from the PPEG film after 24 h incubation, when in fact, there could be viable phage still trapped within the film unable to diffuse out. Therefore, the ‘true’ encapsulation efficacy could be higher than what was obtained experimentally in this study; however, these phage would have minimal clinical effect as they would not be able to target the pathogenic bacteria. The encapsulation efficacy could be improved by introducing sugars into the preparation, e.g., maltose and sucrose to prevent phage denaturation upon formation of the film as they ‘coat’ the phage to protect their protein structure.

Next, the *in vitro* release of phage K was determined, with 100% incubation defined as the phage concentration after 24 h incubation in PBS (pH 7.4; Figure 4.7). There was a rapid release of phage K from the PPEG polymer, with almost a 4 log PFU/mL release of phage K into the PBS upon contact with the buffer. After 2 h incubation with PBS, approximately

80% of phage K were released ( $3.86 \times 10^7$  CFU/mL), rising to 90% release after 6 h incubation with PBS ( $4.20 \times 10^7$  CFU/mL).

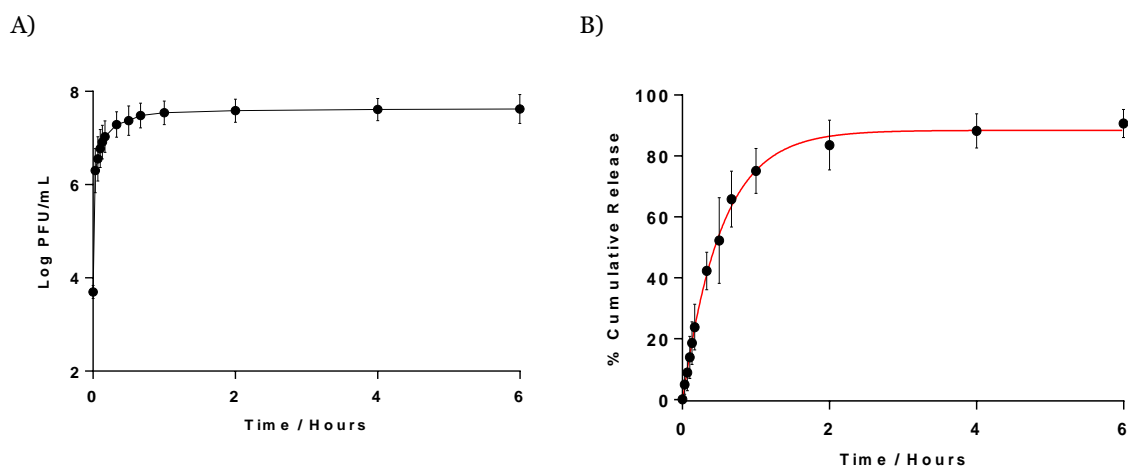


**Figure 4.7:** **A)** Log PFU/mL and **B)** % Cumulative release *in vitro* release profiles of phage K from PPEG films in PBS (pH 7.4, 25 °C). n = 3, error bars indicate standard deviation

Next, mathematical models were used to evaluate the release kinetics of the PPEG system for phage K release. According to Table 4.2, the release profile observed in Figure 4.7 most closely resembled that of the Higuchi model of drug release. Higuchi developed this method based on the release of a drug from a thin ointment film (planar systems), therefore there are several assumptions including:<sup>55</sup>

- The matrix contains an initial drug concentration much higher than the solubility of the drug
- The diffusion is unidirectional
- The thickness of the matrix is much larger than the size of the drug molecules
- The swelling or dissociation of the matrix is negligible
- The diffusivity of the drug is constant
- The perfect sink conditions are attained in the release environment.

As the initial rate of reaction happened relatively quickly, with the majority of phage released after 2 h, it was hypothesised that the swelling of the PPEG film at this time point would be negligible. However, further experiments would have to be conducted to confirm this hypothesis.

Higuchi's model for drug release can be described using the following equation:

$$f_1 = Q = \sqrt{\frac{D\varepsilon}{\tau}(2C - \varepsilon C_s)C_s t} \quad (9)$$

Where Q is the amount of drug release on time  $t$  by area unit,  $\varepsilon$  is the porosity of matrix,  $\tau$  is the capillary tortuosity factor, C is the initial amount of drug contained in the dosage form,  $C_s$  is the solubility of the active agent in the matrix medium, and D is the diffusion coefficient in the matrix medium.

Hence, the amount of drug released is proportional to the square root of time:

$$f_1 = Q = K_H \sqrt{t} \quad (10)$$

Where  $K_H$  is the release constant of Higuchi

This result was consistent with previous reports in literature and suggests that the release of phage K was governed by simple diffusion upon penetration of the solvent into the polymer matrix.<sup>19,50,56</sup>

**Table 4.2:** Kinetic model and corresponding R<sup>2</sup> value for the release of phage K from the PPEG system (PBS, pH 7.4).

Kinetic Model	R <sup>2</sup> value
Zero order	0.8692
First order	0.8971
Higuchi	0.9184
Korsmeyer-Peppas	0.8850
Hixson-Crowell	0.9052

#### 4.4.2.3. Stability

The stability of the phage K-loaded film at 25 °C was measured over 5 days in PBS (pH 7.4); room temperature was chosen for consistency. The results of this stability assay found that there was no significant decrease in phage K concentration at day 5 compared to day 0; therefore, phage K were stable within the PPEG polymer matrix (Figure 4.8). In fact, there was a statistically significant increase in phage K concentration (t-test,  $p < 0.05$ ), but this only corresponded to a 0.50 log increase in PFU/mL count, which could be attributed to discrepancies in loading concentration, as well as human error within the assay. This result was promising, as it suggests that phage K-PPEG films remain stable for long periods of time, making it a suitable candidate for a wound dressing as it could be created en masse.



However, further experiments would need to be undertaken over a longer time period to confirm the long-term stability of phage K within the PPEG matrix. Additionally, future experiments could investigate the effect of storing the PPEG-loaded films at different storage temperatures to see if this has a positive/negative effect on the viability of phage K.

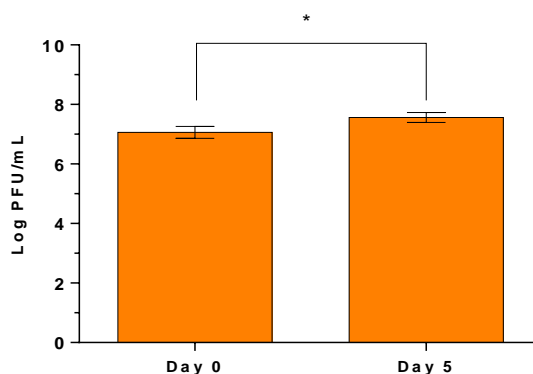


**Figure 4.8:** Phage K survival after 5 days incubation at room temperature within the PPEG film. n = 3, error bars indicate standard deviation. Statistical analysis conducted using a t-test. \* p<0.05

#### 4.4.2.4. Suspension Assays

With these promising results in hand, attention shifted towards testing the antimicrobial efficacy of phage K-PPEG films against planktonic suspensions of *S. aureus* H560, MRSA252, and MSSA101 (initial starting concentration of  $10^6$  CFU/mL; MOI of 0.1). The results displayed in Figure 4.9, show that for *S. aureus* H560, MRSA252, and MSSA101 there was a >6-log reduction in viable count when the bacterial suspensions were incubated with phage K-PPEG films compared to the control, often reaching the limit of detection of the assay. These results were comparable to when phage K was used in a suspension as the control, indicating that there is no loss in efficacy of the phage K entrapped within the PPEG film when targeting planktonic bacteria. The PPEG film without any phage K did not result in any statistical reduction in bacterial density for *S. aureus* MRSA252 and MSSA101. For *S. aureus* H560, there was a statistically significant decrease in bacterial concentration (One-way ANOVA, p<0.01). However, this corresponded to a 0.14 log reduction in bacterial count, which was not clinically relevant.

When assessing the log reductions in Figure 4.9, it is possible to conclude that the system behaves as an antimicrobial as the log reduction is  $\geq 3$ , meeting the requirement set out by the European standard prEN 16756 for antimicrobial testing of wound dressings.<sup>57</sup>

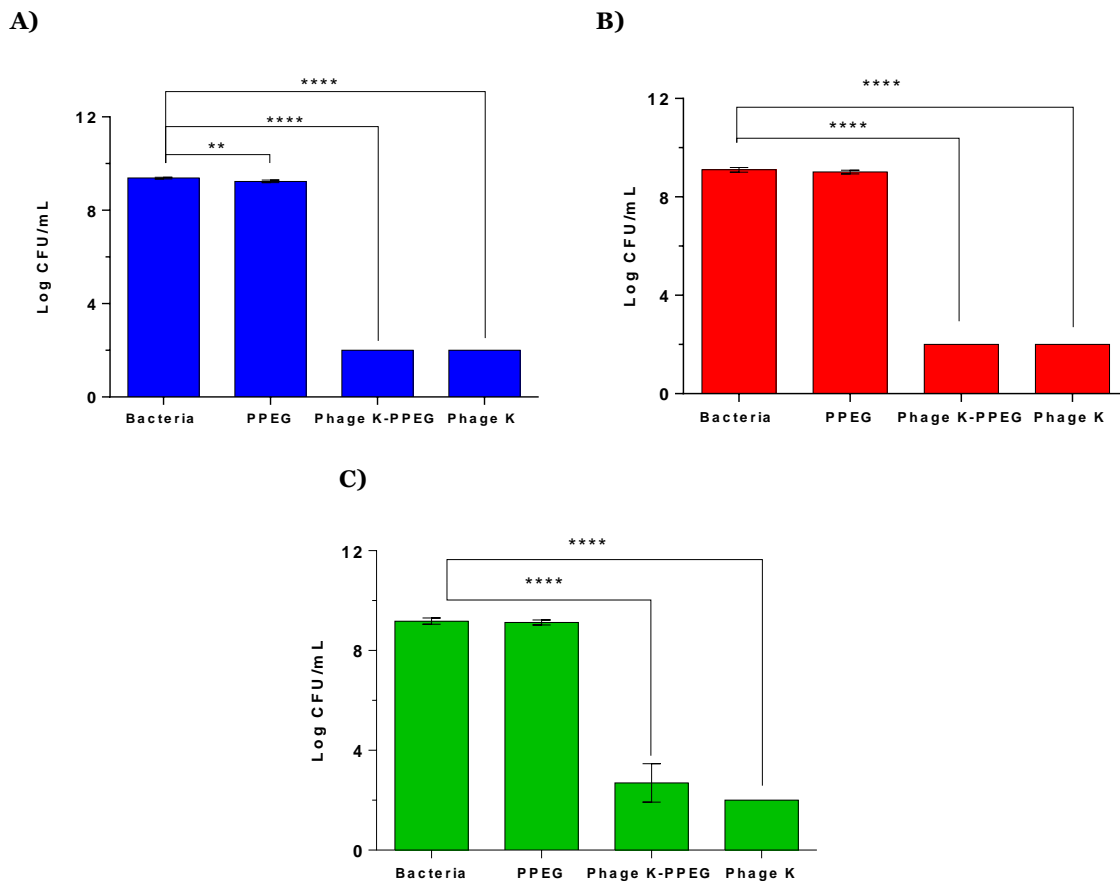


**Figure 4.9:** Log CFU/mL counts of **A)** *S. aureus* H560, **B)** *S. aureus* MRSA252, and **C)** *S. aureus* MSSA101 upon incubation with PPEG films, phage K-PPEG films, and suspensions of phage K (c.  $10^7$  CFU/mL) for 24 h at 32°C. n = 3, error bars indicate standard deviation. Statistical analysis conducted using a One-way ANOVA

Phage K were successfully released from the PPEG film and able to infect and multiply (Figure 4.10).

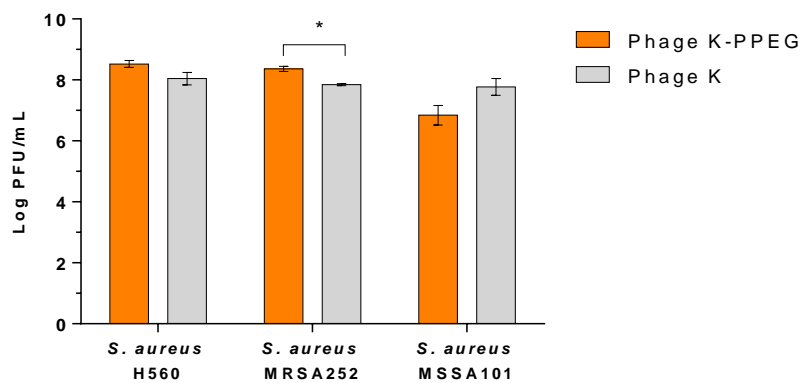


**Figure 4.10:** Log PFU/mL of phage K released from the pH-responsive films and the phage K control after incubation with *S. aureus* H560, MRSA252, and MSSA101 for 24 h at 32°C. n = 3, error bars indicate standard deviation. Statistical analysis conducted using multiple t-tests. \*p<0.05

The concentration of phage K was similar to that observed for the control, with the exception of when the phage K-PPEG film was incubated with *S. aureus* MRSA252, as the phage K concentration was greater than the control (t-test,  $p < 0.05$ ), most likely due to the variation in loading and environmental variation within the assay.

#### **4.4.2.5. Colony Biofilm Wound Model**

As the majority of bacteria within wounds exist within biofilms,<sup>58–60</sup> it was important to determine if the phage K-PPEG film was capable of preventing biofilm formation through the use of a modified colony biofilm model. This model is a static system where colonies are grown over agar; it mimics biofilm development at the air-solid interface, with nutrient enrichment occurring from below and gaseous exchange occurring at the top of biofilm – as observed in wounds. Additionally, this model maintains the basic biofilm characteristics such as a structured environment and chemical gradients. This model is advantageous as is reproducible and amenable to high-throughput screening.<sup>61</sup>

In this study, the colony biofilm model involved adding AWF onto 19 mm polycarbonate membranes, before subsequent inoculation with 50  $\mu$ L of bacterial suspension. Once dry, the films were then placed on top of the membranes and incubated at 32 °C for 24 h; the incubation temperature of 32 °C was used to mimic healthy skin surface temperature.

The results displayed in Figure 4.11 show that for *S. aureus* H560 there was a statistically significant decrease in biofilm concentration after incubation with phage K-PPEG films compared to the biofilm-only control (3.44 log reduction; One-way ANOVA,  $p < 0.0001$ ). This was a remarkable result as this log reduction is greater than the recommended  $>3$  log reduction in the prEN 16756 standard, demonstrating the clinical utility of the phage K-PPEG films. Additionally, there was no significant decrease in bacterial viability when *S. aureus* H560 was treated with the un-loaded PPEG films, indicating that any therapeutic benefit of these films was a result of the encapsulated phage K, and not the polymer itself.

A similar effect was observed, albeit to a lesser extent, when *S. aureus* MRSA252 was incubated with phage K-PPEG films, exhibiting a 3.13 log reduction in cell density (One-way ANOVA,  $p < 0.001$ ). While this effect was slightly lower than what was observed from the phage K control, it was still greater than the 3 log reduction recommended in prEN 16756 standard. Once again, there was no statistically significant decrease in bacterial concentration when *S. aureus* MRSA252 was incubated with the PPEG control; therefore, the therapeutic efficacy of the phage K-PPEG film was solely due to the encapsulated phage K.

For *S. aureus* MSSA101, there was a 2.79 log reduction of bacterial viability upon incubation with phage K-PPEG films. Unlike the previous bacterial strains, this did not meet the threshold of the 3-log reduction recommended by the prEN 16756 standard. However, the reduction in bacterial cell density was still significant when compared to the biofilm-only control (One-way ANOVA,  $p < 0.001$ ). Like the previous bacterial strains tested, the log reduction of *S. aureus* MSSA101 was lower compared to the phage K-only control and the PPEG film without phage K encapsulation did not statistically significantly reduce the biofilm density of *S. aureus* MSSA101; therefore, the therapeutic activity was due to the encapsulated phage K.

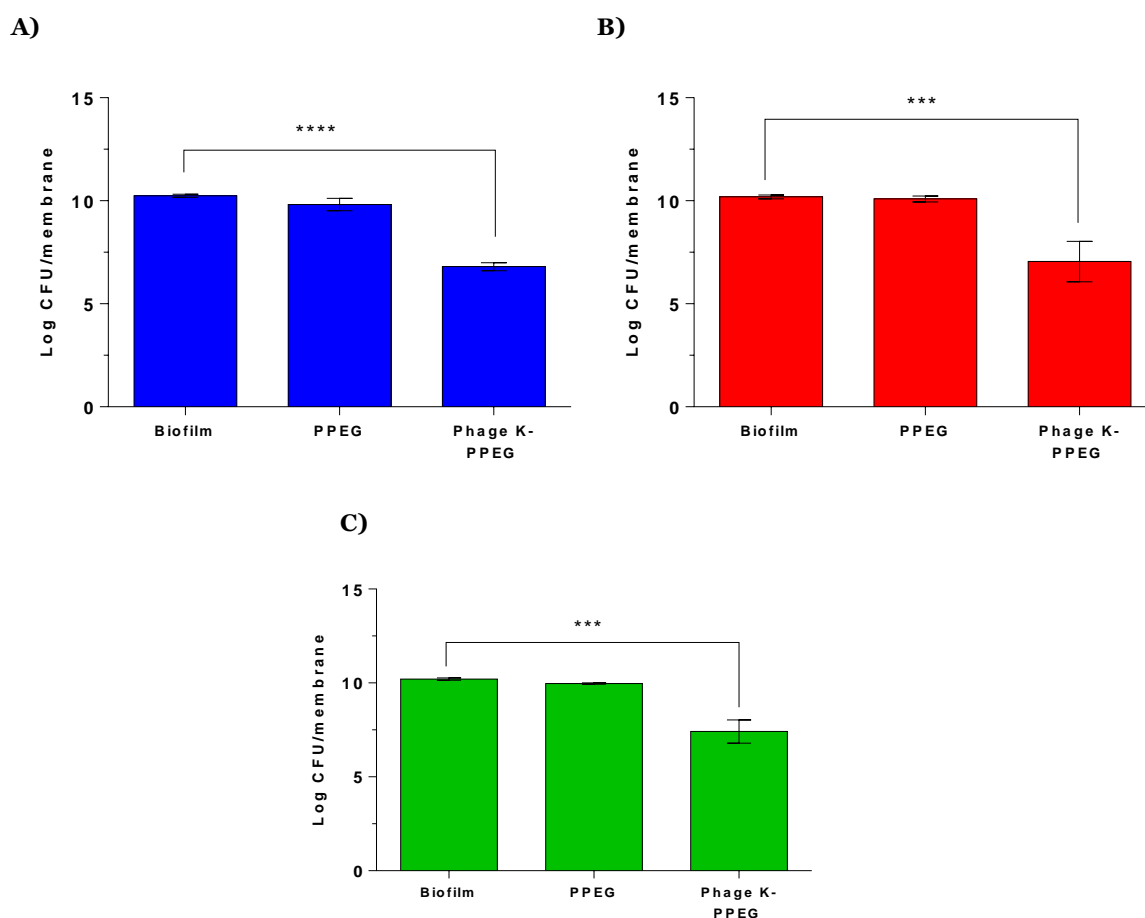


**Figure 4.11:** Log CFU/membrane counts of **A)** *S. aureus* H560, **B)** *S. aureus* MRSA252, and **C)** *S. aureus* MSSA101 biofilms upon incubation with PPEG films, phage K-PPEG films, and suspensions of phage K (c.  $10^7$  CFU/mL) for 24 h at 32°C.  $n = 3$ , error bars indicate standard deviation. Statistical analysis conducted using a One-way ANOVA. \* $p < 0.05$ , \*\* $p < 0.01$ , \*\*\* $p < 0.001$ , \*\*\*\* $p < 0.0001$

#### 4.4.2.6. *Ex vivo* Porcine Skin Models

*Ex vivo* studies are advantageous over *in vitro* assays as the latter cannot always be correlated with results obtained in real-life situations.<sup>62,63</sup> *Ex vivo* studies refer to experiments using tissues and performed under conditions mimicking real-world environments, overcoming some of the limitations associated with *in vitro* testing, while allowing for controlled experiments to be undertaken in an ethically responsible way.<sup>63,64</sup>

Porcine skin has been used as a model for human skin,<sup>65</sup> especially in the fields of wound healing<sup>66,67</sup> and burns.<sup>66</sup> Several studies have assessed the capability of porcine skin as an *ex vivo* model.<sup>66</sup> Porcine skin is histologically similar to that of human skin,<sup>68</sup> with the *stratum corneum* (SC) thickness (20 – 26  $\mu\text{m}$ ) and complete epidermis (30 – 140  $\mu\text{m}$ ) comparable to that of humans.<sup>66</sup> Additionally, the average hair-follicle density in porcine ear skin is 20/cm<sup>2</sup> compared to 14 – 32/cm<sup>2</sup> in human forehead skin,<sup>68</sup> and the blood supply in the dermis of pigs is similar to that of humans.<sup>66</sup> Porcine skin has been shown to produce reproducible results in a large number of studies. Other similarities are highlighted in Table 4.3.

**Table 4.3:** Comparison of human and porcine skin, adapted from Summerfield et al<sup>66</sup>

	<b>Human</b>	<b>Pig</b>
<b>Skin attachment</b>	Firmly attached	Firmly attached
<b>Hair coat</b>	Sparse	Sparse
<b>Epidermis</b>	Thick	Thick
<b>Dermis</b>	Thick	Thick
<b>Panniculus carnosus</b>	Absent	Absent
<b>Healing mechanism</b>	Re-epithelization	Re-epithelization

Using the skin as a substrate for bacterial proliferation would produce a biofilm that more closely resembles that of a biofilm found within wounds. Yang *et al* outlined that bacterial biofilms should remain on the “wound bed” and not penetrate through to the bottom of the explants.<sup>67</sup>

The *ex vivo* porcine skin experiments conducted in this study utilised bacteriological agar to provide moisture to the porcine skin, preventing the skin from drying out. Bacteriological agar was used over the traditional Franz cell experiments due to the quantity of samples that required assessment and the limited amount of Franz cells in the laboratory. In this model we placed the 2 x 2 cm sterilised porcine skin onto bacteriological agar before inoculation with *S. aureus* bacterial strains. Once dry, the films were placed on top of the porcine skin and incubated at 32 °C for 24 h. After incubation, these samples were placed into 5 mL of PBS and sonicated before enumeration.

To determine the effect of the recovery of *S. aureus* bacterial density, optimisation experiments were performed. Porcine skin inoculated with *S. aureus* H560 was immediately vortexed and enumerated, and subsequently compared to the bacterial concentration of the initial *S. aureus* suspension (Figure 4.12).

There was no statistical difference in bacterial concentration of the recovered *S. aureus* H560 suspension compared to the initial *S. aureus* H560 suspension. This result highlights that the recovery method used in this *ex vivo* testing has negligible influence on bacterial cell density; therefore, any reduction in concentration witnessed in the subsequent experiments would be due to the films themselves, and not the methodology.

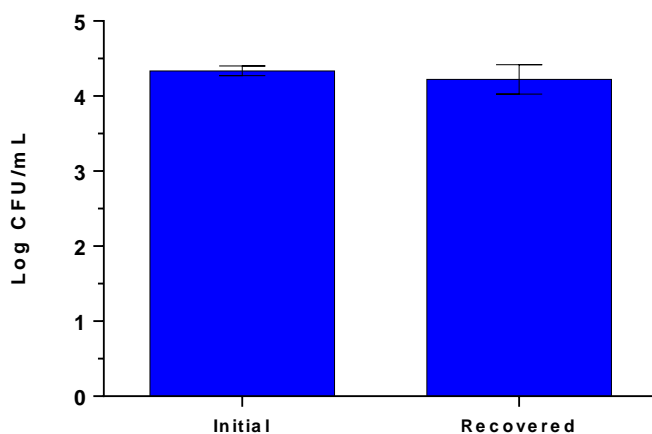


**Figure 4.12:** Log CFU/mL counts of the initial *S. aureus* H560 suspension, and the *S. aureus* H560 suspension after recovery from porcine skin.  $n = 3$ , error bars indicate standard deviation. Statistical analysis conducted using a t-test, no significance found

When *S. aureus* H560 inoculated on porcine skin was incubated with PPEG, there was a slight reduction in bacterial density (0.83 log reduction, Figure 4.13). This decrease in bacterial viability could be due to reduced oxygen transmission through the film required for optimal *S. aureus* survival as they are aerobic; however, further experiments must be conducted before any hypothesis can be made. When *S. aureus* H560 was incubated with phage K-PPEG there was no significant reduction in bacterial density compared to incubation with PPEG only; therefore, any reduction in bacterial concentration was due to the film and phage K had no extra therapeutic benefit.

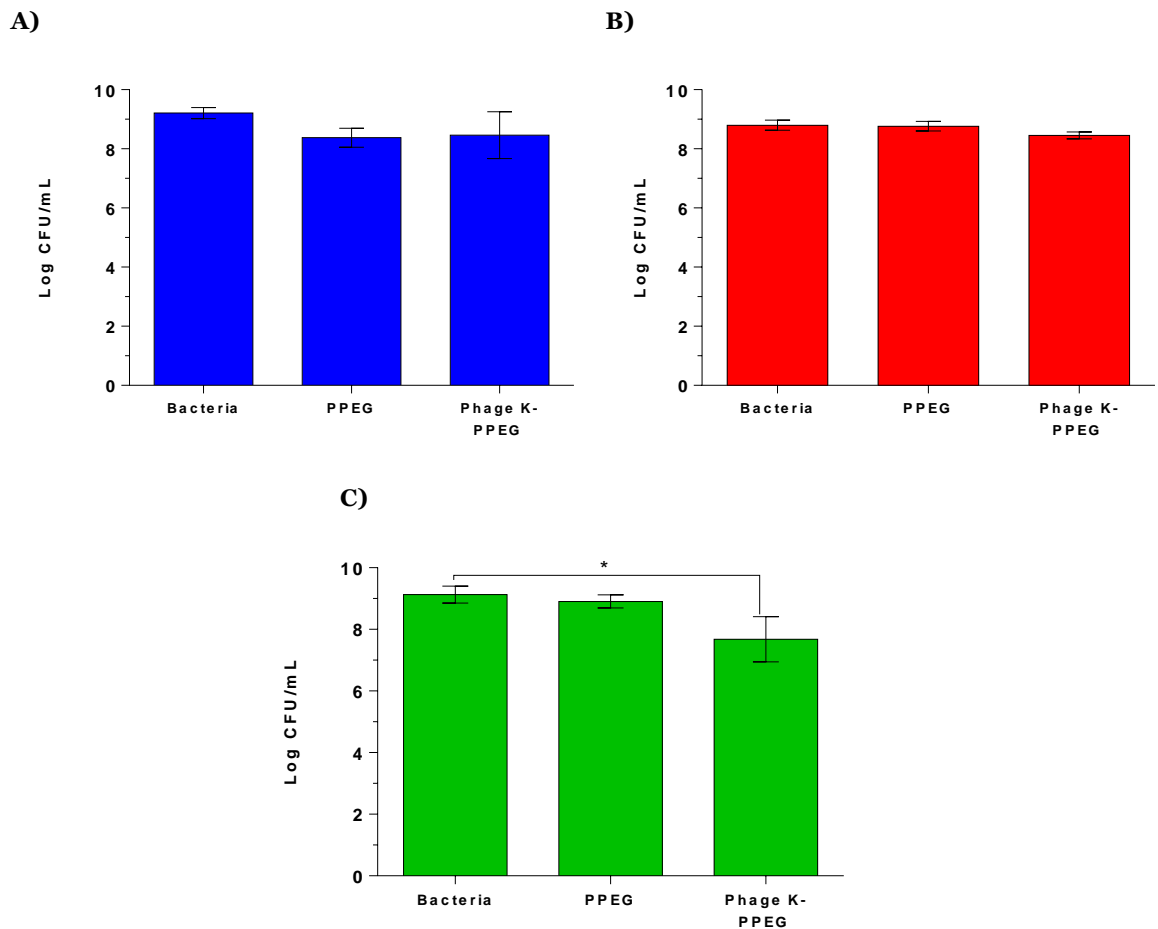


**Figure 4.13:** Log CFU/mL counts of **A)** *S. aureus* H560, **B)** *S. aureus* MRSA252, and **C)** *S. aureus* MSSA101 on porcine skin incubated with PPEG films and phage K-PPEG films for 24 h at 32°C. n = 3, error bars indicate standard deviation. Statistical analysis conducted using a One-way ANOVA. \*p<0.05, \*\*p<0.01, \*\*\*p<0.001, \*\*\*\*p<0.0001

A similar observation was witnessed for *S. aureus* MRSA252, with no significant reduction in bacterial cell density witnessed when *S. aureus* MRSA252 was incubated with PPEG and phage K-PPEG (log reductions of 0.04 and 0.34, respectively, compared to the bacteria-only control). This experiment highlights how important it is to conduct *ex vivo* experiments, as phage K-PPEG films demonstrated good activity against planktonic and biofilm models of *S. aureus* MRSA252. However, based on these *ex vivo* results, the ability of phage K-PPEG films to eliminate *S. aureus* MRSA252 infections real-world setting might be low, reducing its clinical utility.

Interestingly, phage K-PPEG films were able to statistically significantly reduce the bacterial concentration of *S. aureus* MSSA101 on porcine skin (1.08 log reduction vs bacteria-only control). This was due to the phage K, as the PPEG film did not statistically significantly reduce the bacterial concentration (0.22 log reduction vs bacteria-only control). This result was surprising, as previously, phage K-PPEG films were less effective in treating *S. aureus*

MSSA101 biofilms compared to the other two *S. aureus* strains under investigation. Again, this further supports the need for *ex vivo* testing, as results obtained *in vitro* may not correlate to real-life efficacy.

Another interesting result witnessed was that of the phage K titres after *S. aureus* incubation with phage K-PPEG films (Figure 4.14). While phage K-PPEG films did not reduce *S. aureus* H560 and MRSA252 bacterial concentrations, phage K were successfully released and able to replicate to achieve concentrations of 7.63 and 9.00 Log PFU/mL, respectively. Conversely, phage K-PPEG films were capable of reducing *S. aureus* MSSA101 cell density; however, there was a lower phage K concentration observed of 6.57 Log PFU/mL. Further experiments will need to be undertaken to determine why this effect was observed.

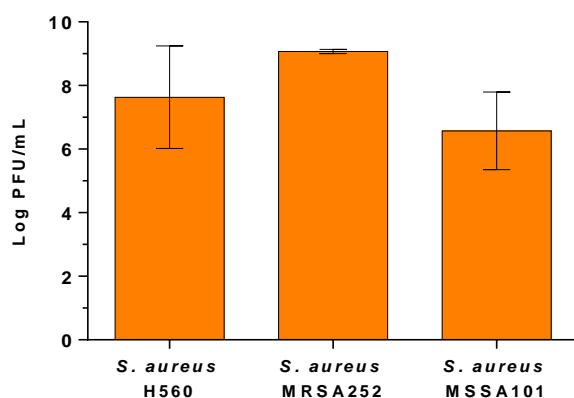


**Figure 4.14:** Log PFU/mL counts of phage K after 24 h incubation of phage K-PPEG films on *S. aureus* H560, MRSA252, and MSSA101 at 32°C. n = 3, error bars indicate standard deviation. Statistical analysis conducted using a One-way ANOVA. \*p<0.05, \*\*p<0.01, \*\*\*p<0.001, \*\*\*\*p<0.0001

### 4.4.3. Ciprofloxacin-loaded Films

While the results of the phage K-PPEG films were promising, their utility in clinical environments was questionable due to poor *ex vivo* results. In order to improve the efficacy of the films, our attention turned to incorporating conventional antimicrobials into the film, in the hope of creating a system that utilises the phage-antibiotic synergy witnessed in the previous chapter (Chapter 3). Owing to this, ciprofloxacin was chosen as it displayed the best PAS across all three *S. aureus* isolates tested. However, before combining the antimicrobials in the PPEG film, experiments were conducted to determine the efficacy of ciprofloxacin-loaded PPEG films in inhibiting the growth of the *S. aureus* strains studied, which will be discussed further in this section.



#### 4.4.3.1. Encapsulation and *in vitro* Release

It is possible to determine the concentration of ciprofloxacin using a UV-Vis spectrophotometer, due to its absorbance characteristic peak at ~270 nm. Owing to this a calibration curve was created using varying concentrations of ciprofloxacin (0 – 40 µg/mL; Figure 4.15).

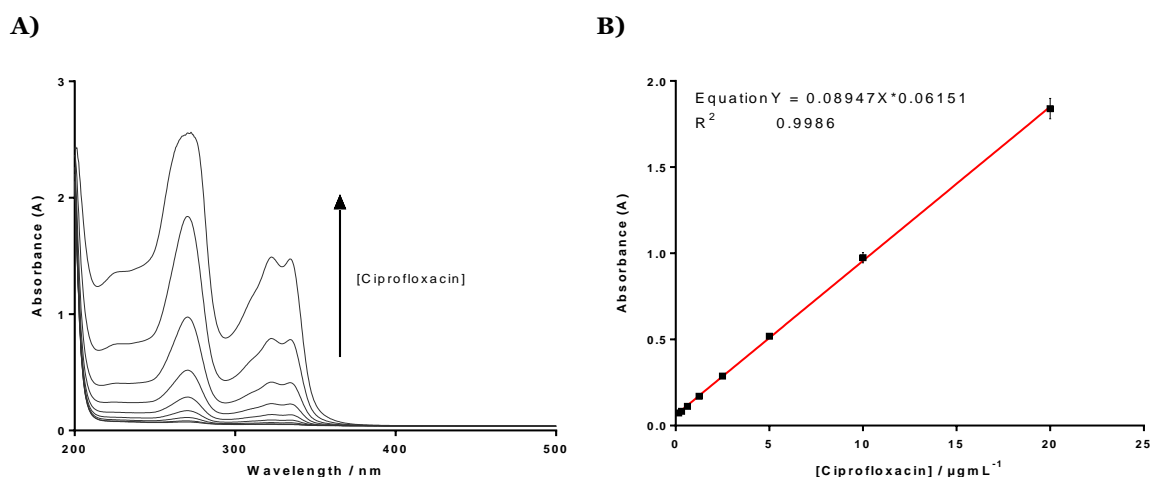


**Figure 4.15:** A) UV-Vis spectra and B) corresponding calibration curve of increasing concentrations of ciprofloxacin-HCl (0 – 40 µg/mL) in PBS (pH 7.4) at 25 °C. n = 3, error bars indicate standard deviation.  $Y = 0.08947x + 0.06151$ ,  $R^2 0.9986$

*In vitro* release kinetics was determined for ciprofloxacin release from PPEG films at 25 °C. As shown in Figure 4.16, there was a rapid release of ciprofloxacin from the PPEG films, with over 80% of ciprofloxacin released after 1 h, rising to 98% released after 6 h incubation in PBS (pH 7.4).

After 24 h incubation in PBS, ciprofloxacin-PPEG films released  $411.67 \pm 21.62$  µg/mL of ciprofloxacin. As the loading concentration was 824.18 µg/mL, this corresponded to an encapsulation efficacy of  $49.95 \pm 2.62\%$  (assuming 100% of ciprofloxacin is released after 24 h). Again, while this encapsulation efficacy is quite low, it is still above the MIC for all three bacterial isolates tested (Chapter 3). Therefore, this encapsulation efficacy was deemed sufficient for this proof-of-concept study.

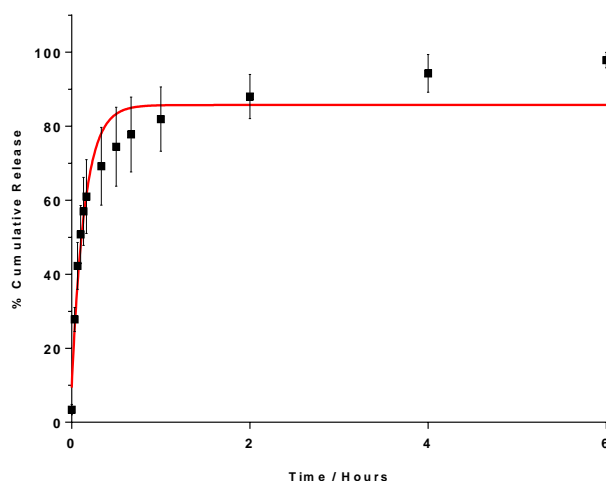


**Figure 4.16:** % Cumulative release *in vitro* release profile of ciprofloxacin from PPEG films in PBS (pH 7.4, 25 °C). n = 3, error bars indicate standard deviation

Mathematical models were used to evaluate the release kinetics of ciprofloxacin release from the PPEG system. According to Table 4.3, the release profile observed in Figure 4.16 most closely resembled that of the Higuchi model of drug release, as seen for the phage K release in Figure 4.7. This was in agreement with results observed in literature, with Chitrattha *et al* for metronidazole and gentamicin release from PPEG films.<sup>19</sup> However, this system does not fit all of Higuchi’s assumptions, as the ciprofloxacin concentration loaded into the film was not higher than the solubility of the drug; it was in fact, the maximum soluble concentration (30 µg/mL). Owing to this, it might not be possible to use this release model for this system, and therefore, the drug release may be modelled using zero-order kinetics.

The zero order model outlines the process of constant drug release from a drug delivery system and can be modelled using the following equation:

$$C_0 - C_t = K_0 t \quad (11)$$

Where  $C_t$  is the amount of drug released at time  $t$ ,  $C_0$  is the initial concentration of the drug  $t=0$ ,  $K_0$  is the zero-order rate constant.

Both the Higuchi and zero order methods are diffusion controlled; hence, it can be suggested that the release of ciprofloxacin was governed by simple diffusion upon penetration of the solvent into the polymer matrix.<sup>19</sup> To further confirm the release profile, this experiment should be repeated, with focus placed on the early time points, perhaps measuring every 30 seconds for the first 10 minutes to get a more accurate insight into the rapid release of ciprofloxacin from this matrix.

**Table 4.3** Kinetic model and corresponding R<sup>2</sup> value for the release of ciprofloxacin from PPEG system (PBS pH 7.4)

Kinetic Model	R <sup>2</sup> value
Zero order	0.8975
First order	0.8543
Higuchi	0.9170
Korsmeyer-Peppas	0.8307
Hixson-Crowell	0.8466

#### 4.4.3.2. Stability

The stability of the ciprofloxacin-loaded film at 25 °C was measured over 5 days in PBS (pH 7.4). The results of this stability assay found that there was a significant decrease in ciprofloxacin concentration at day 5 compared to day 0 (t-test,  $p < 0.0001$ ); Figure 4.17). This result was surprising as phage K had previously shown to be stable and ciprofloxacin in combination with phage K was stable of the course of 5 days (Chapter 4, Section 4.4.2.3). While the reduction in ciprofloxacin concentration was significant, the concentration was higher than the MIC for all bacterial isolates under investigation, so, in theory, should still display antibacterial activity towards the bacterial isolates. However, this experiment should be repeated as it doesn't follow the trend observed for the other two systems discussed in this chapter and could have been a result of loading-error upon fabrication of the ciprofloxacin-loaded films.

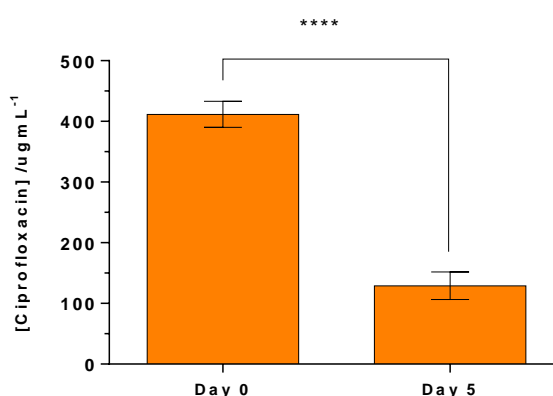


**Figure 4.17:** Concentration of ciprofloxacin after 5 days incubation at room temperature within the PPEG film. n = 3, error bars indicate standard deviation. Statistical analysis conducted using a t-test. \*\*\*\*  $p < 0.05$

#### 4.4.3.3. Suspension Assays

Firstly, planktonic suspensions of *S. aureus* isolates were treated with ciprofloxacin-loaded PPEG films and the results obtained compared to the bacteria-only and ciprofloxacin-only controls. As 10 mL of *S. aureus* suspensions were used, it is important to note that ciprofloxacin concentration was diluted 10-fold in broth, hence the final concentration of ciprofloxacin released from the PPEG films was 41.17 $\mu$ g/mL; the concentration of ciprofloxacin in the control was 30  $\mu$ g/mL (Figure 4.18).

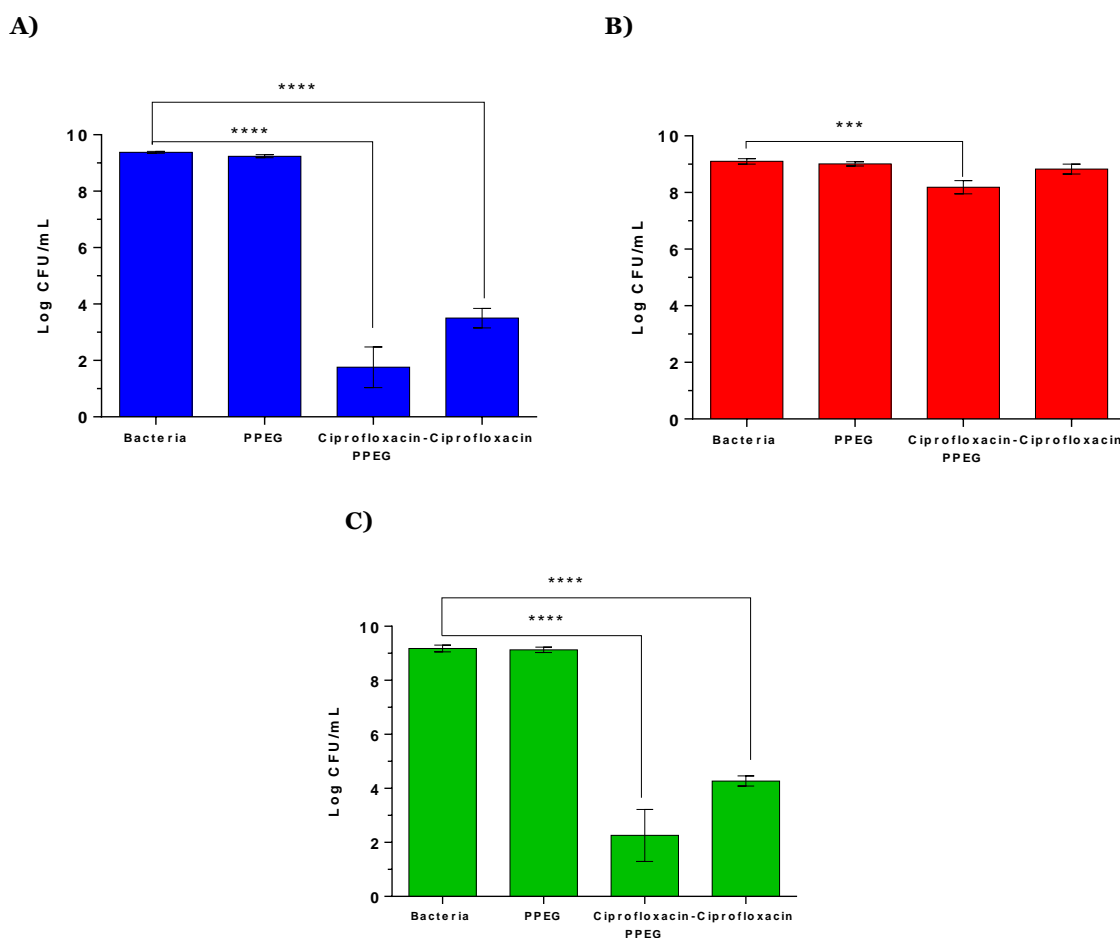


**Figure 4.18:** Log CFU/mL counts of **A)** *S. aureus* H560, **B)** *S. aureus* MRSA252, and **C)** *S. aureus* MSSA101 upon incubation with PPEG films, ciprofloxacin-PPEG films, and ciprofloxacin control for 24 h at 32°C. n = 3, error bars indicate standard deviation. Statistical analysis conducted using a One-way ANOVA, \*p<0.05, \*\*p<0.01, \*\*\*p<0.001, \*\*\*\*p<0.0001

The ciprofloxacin-PPEG films were successful in treating *S. aureus* H560 (7.62 log reduction compared to bacteria-only control; One-way ANOVA, p<0.0001; Figure 4.18A), resulting in a greater log reduction compared to the ciprofloxacin-only control (5.88 log reduction compared to the bacteria-only control; One-way ANOVA, p<0.0001) due to the higher amount of ciprofloxacin released from the PPEG films. There was no statistically

significant decrease in bacterial concentration with the un-loaded PPEG films; hence, the reduction in cell density was solely due to the release of ciprofloxacin from the films. This phenomenon was also observed for *S. aureus* MSSA101, with log reductions of 0.05, 6.92 (One-way ANOVA,  $p < 0.0001$ ), and 4.90 (One-way ANOVA,  $p < 0.0001$ ) compared to the bacteria control for PPEG, ciprofloxacin-PPEG, and ciprofloxacin, respectively (Figure 4.18C).

For *S. aureus* MRSA252 there was minimal reduction of bacterial cell density when *S. aureus* MRSA252 was incubated with ciprofloxacin-PPEG (0.91 log reduction compared to bacteria-only control; One-way ANOVA,  $p < 0.001$ ; Figure 4.18B ). This was due to the ciprofloxacin concentration released being lower than the MIC value for *S. aureus* MRSA252 (62.50  $\mu\text{g}/\text{mL}$ ; Chapter 3).

#### **4.4.3.4. Colony Biofilm Wound Model**

Next, the efficacy of ciprofloxacin-PPEG films was investigated using *in vitro* wound biofilm models (Figure 4.19). The ciprofloxacin-PPEG films resulted in a 3.82 log reduction compared to the biofilm control (One-way ANOVA,  $p < 0.0001$ ), higher than the 3-log reduction recommended by the prEN 16756 standard. As before, there was minimal reduction in biofilm density for the PPEG film compared to the biofilm, suggesting that any reduction in cell density was due to the therapeutic and not the film itself.

Like the suspension assays, there was minimal reduction in *S. aureus* MRSA252 biofilms upon incubation with ciprofloxacin-loaded PPEG films (0.84 log reduction compared to the biofilm control; One-way ANOVA,  $p < 0.01$ ). While this result is surprising, as the MBIC determined in Chapter 3 was 62.50  $\mu\text{g}/\text{mL}$ , and the concentration of ciprofloxacin in the PPEG film and the control was 411.67  $\mu\text{g}/\text{mL}$  and 400  $\mu\text{g}/\text{mL}$ , respectively, it could be due to using the colony biofilm model, rather than the 96-well plates that were used to determine the MBIC values. As the biofilm under investigation within this study is based on the colony biofilm model, the biofilm produced could be more robust, and hence more tolerant, to antimicrobials compared to biofilms produced in a 96-well plate. However, further experiments should be performed to support this.

For *S. aureus* MSSA101, there was a 3.49 log reduction compared to the biofilm control (One-way ANOVA,  $p < 0.0001$ ), which was higher than the 3-log reduction recommended by the prEN 16756 standard. Like *S. aureus* H560 and MRSA252, there was minimal reduction in bacterial cell density when *S. aureus* MSSA101 was incubated with the PPEG film, indicating that any reduction in cell count was due to the ciprofloxacin released from the film.

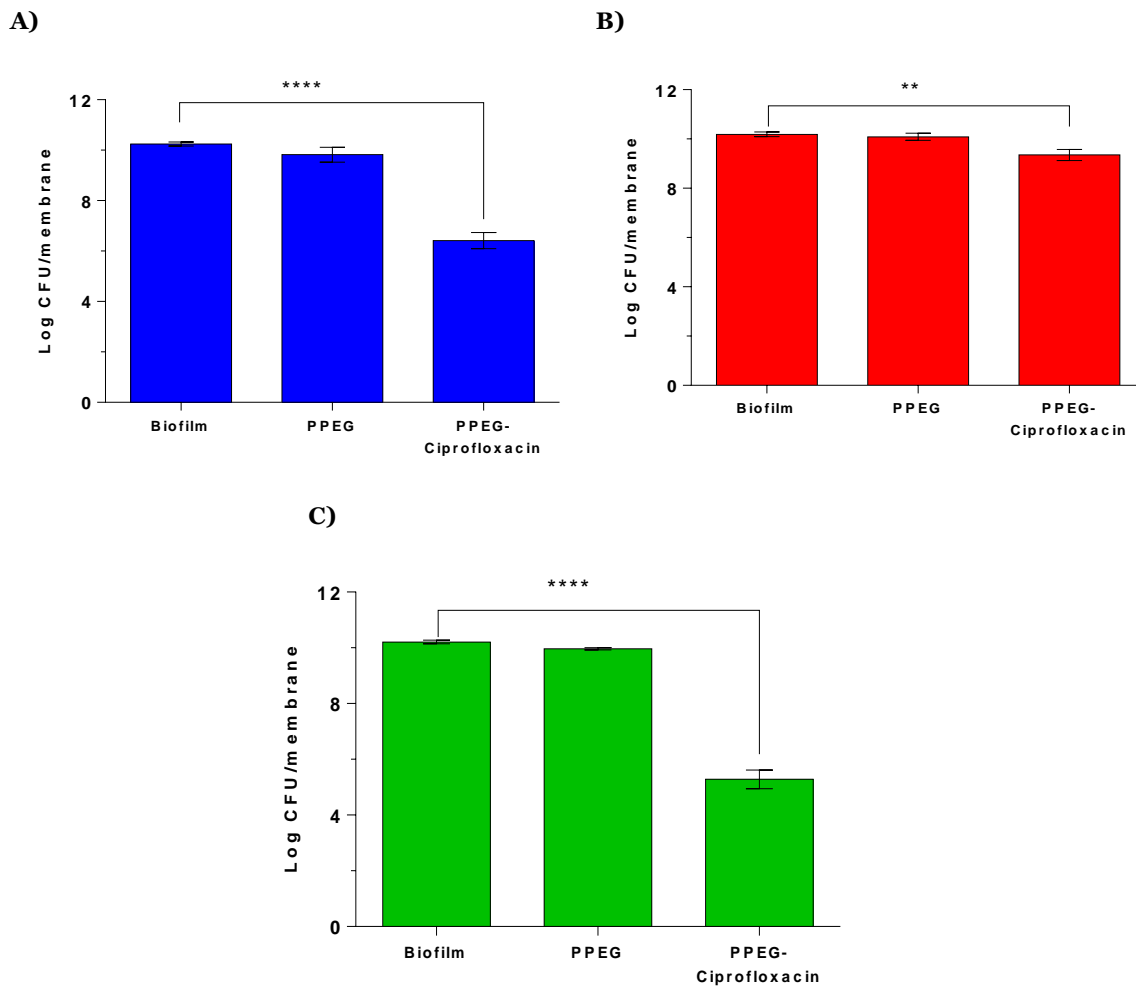


**Figure 4.19:** Log CFU/membrane counts of **A)** *S. aureus* H560, **B)** *S. aureus* MRSA252, and **C)** *S. aureus* MSSA101 biofilms upon incubation with PPEG films, and ciprofloxacin-PPEG films for 24 h at 32°C. n = 3, error bars indicate standard deviation. Statistical analysis conducted using a One-way ANOVA. \*p<0.05, \*\*p<0.01, \*\*\*p<0.001, \*\*\*\*p<0.0001

#### 4.4.3.5. *Ex vivo* Porcine Skin Models

Finally, *ex vivo* porcine skin studies were conducted (Figure 4.20). For *S. aureus* H560, there was a slight decrease in bacterial cell concentration observed when *S. aureus* H560 was incubated with PPEG films (0.83 log reduction compared to biofilm control), further increasing to 3.77 log reduction compared to the biofilm control when incubated with ciprofloxacin-PPEG films (One-way ANOVA, p<0.01). This was exciting, as it showed clinical significance in a real-world setting as outlined by the prEN 16756 standard.

For *S. aureus* MRSA252, there was minimal change in bacterial cell density when *S. aureus* MRSA252 was incubated with PPEG and ciprofloxacin-PPEG films compared to the bacteria-only control (0.04 and 0.05 log reduction, respectively). This result is not surprising, as all previous experiments using ciprofloxacin-loaded films for the treatment

of *S. aureus* MRSA252 planktonic and biofilm bacteria did not display any meaningful reduction in bacterial cell count.

Finally, for *S. aureus* MSSA101, there was a minimal reduction in bacterial cell density upon incubation with the PPEG film (0.22 log reduction compared to the bacteria-only control) and a 1.4 log reduction compared to the bacteria-only control when incubated with ciprofloxacin-PPEG films (One-way ANOVA,  $p < 0.001$ ). While these results do not reach the 3 log reduction 'gold standard' as outlined in the prEN 16756 standard, it is still a promising result as it shows the clinical utility of this PPEG film in the treatment of *S. aureus* infections.

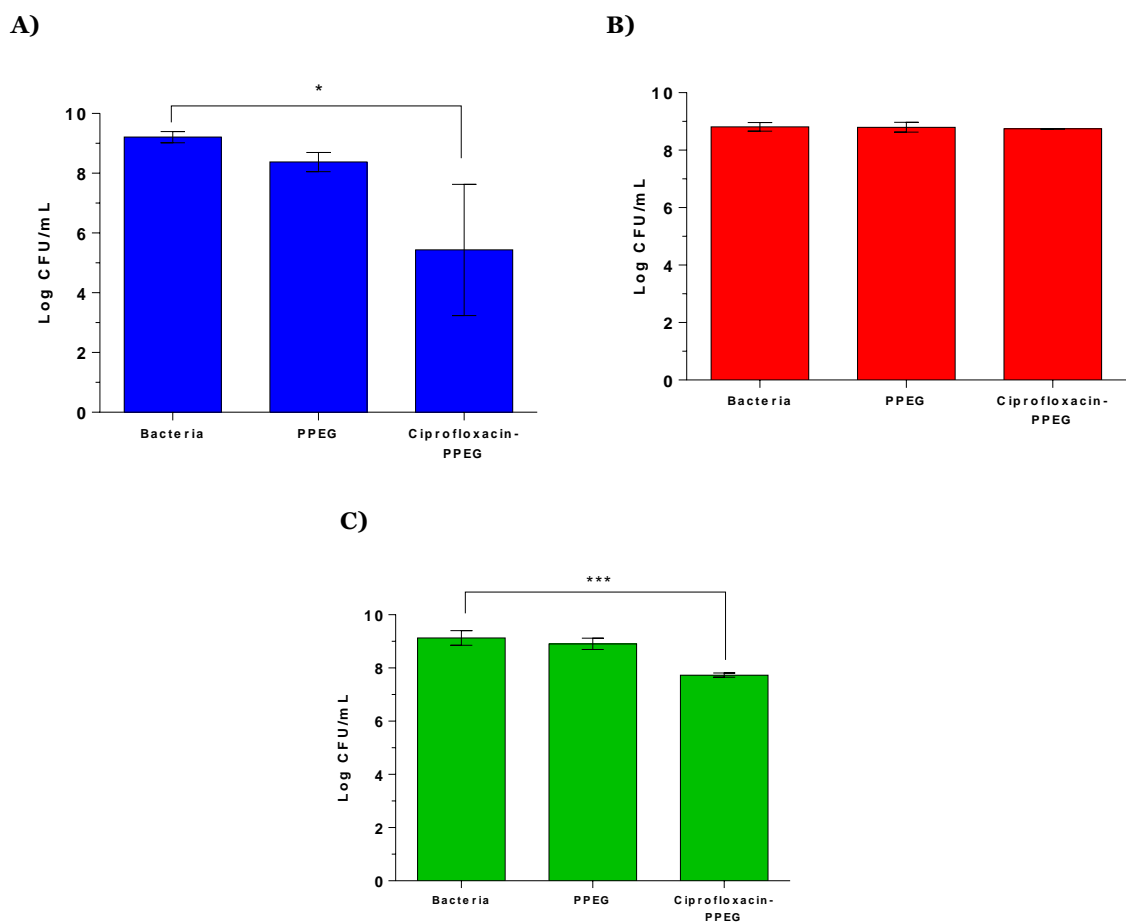


**Figure 4.20:** Log CFU/mL counts of **A)** *S. aureus* H560, **B)** *S. aureus* MRSA252, and **C)** *S. aureus* MSSA101 on porcine skin incubated with PPEG films and ciprofloxacin-PPEG films for 24 h at 32°C. n = 3, error bars indicate standard deviation. Statistical analysis conducted using a One-way ANOVA. \* $p < 0.05$ , \*\* $p < 0.01$ , \*\*\* $p < 0.001$ , \*\*\*\* $p < 0.0001$

## 4.4.4. Combination-loaded Films

### 4.4.4.1. Stability

Phage K was stable in the PPEG film containing a combination of ciprofloxacin and phage K for up to 5 days, with no statistically significant decrease in phage K concentration observed compared to day 0 (Figure 4.21). However, there was a statistically significant reduction in ciprofloxacin concentration after 5 days incubation at 25 °C compared to the day 0 control (t-test,  $p < 0.05$ ), but this only responded to a loss of 8.23  $\mu\text{g}/\text{mL}$ , which was not deemed clinically significant.

Overall, this result shows that phage K was stable in the presence of ciprofloxacin, which was an effect that was not observed in Chapter 3. Therefore, it can be suggested that the PPEG film offers some protection of the phage from the inhibitory effects of ciprofloxacin, increasing its long-term viability.

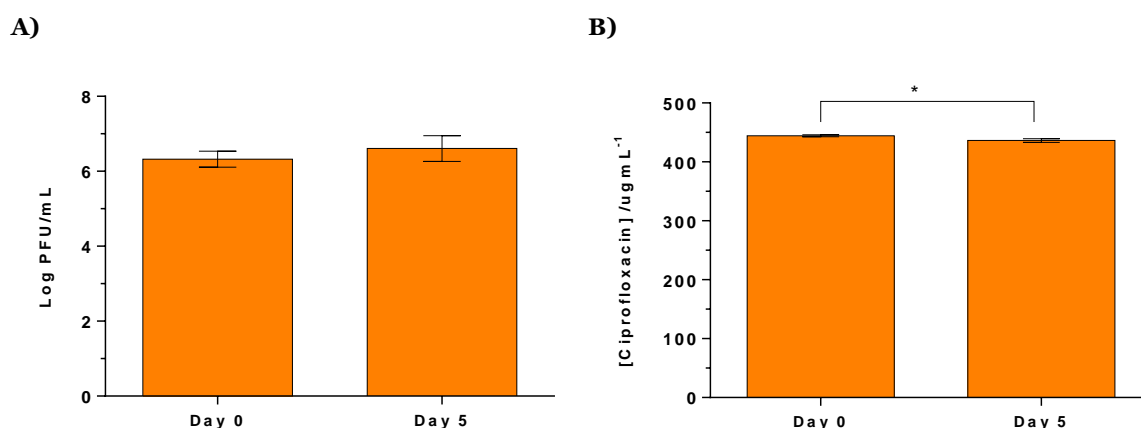


**Figure 4.21:** Concentration of **A)** phage K (displayed as Log PFU/mL) and **B)** ciprofloxacin after 5 days incubation at room temperature within the PPEG film.  $n = 3$ , error bars indicate standard deviation. Statistical analysis conducted using a t-test. \*\*\*\*  $p < 0.05$

### 4.4.4.2. Suspension Assay

The combination of ciprofloxacin and phage K within PPEG films was evaluated (Figure 4.22). For these experiments, the maximum concentration of phage K and ciprofloxacin were used ( $10^9$  PFU/mL and 824.18  $\mu\text{g}/\text{mL}$ , respectively), rather than PAS combinations used in Chapter 3, so the results could be compared with the monotherapy results obtained in the earlier sections.

For all bacterial strains tested, there was minimal reduction in bacterial density when the bacterial isolates were incubated with the PPEG films compared to the bacterial control (log reductions of 0.14, 0.09, and 0.05 for *S. aureus* H560, MRSA252, and MSSA101,



respectively). Therefore, any reduction in bacterial concentration was due to the combination therapy of phage K and ciprofloxacin.

For *S. aureus* H560, there was a statistically significant decrease in bacterial concentration when incubated with PPEG films loaded with phage K and ciprofloxacin (5.88 log reduction compared to bacteria-only control; One-way ANOVA,  $p < 0.0001$ ), which was comparable to the combination therapy control (5.29 log reduction compared to bacteria control; One-way ANOVA,  $p < 0.0001$ ).

For *S. aureus* MRSA252, there was a statistically significant decrease in bacterial concentration when incubated with PPEG films loaded with phage K and ciprofloxacin (3.41 log reduction compared to the bacterial control; One-way ANOVA,  $p < 0.0001$ ). However, this was less effective than using the combination of phage K and ciprofloxacin in a suspension, as the control resulted in a 5.26 log reduction compared to the bacteria-only control (One-way ANOVA,  $p < 0.0001$ ).

Finally, for *S. aureus* MSSA101, there was a statistically significant decrease in bacterial concentration when incubated with PPEG films loaded with phage K and ciprofloxacin (5.05 log reduction compared to bacteria-only control; One-way ANOVA,  $p < 0.0001$ ), which was 1-log lower than the combination therapy control (6.66 log reduction compared to bacteria control; One-way ANOVA,  $p < 0.0001$ ).

These results were interesting, as the monotherapies (bar ciprofloxacin for *S. aureus* MRSA252) achieved log reductions of  $\sim 7$  compared to the control, which was far higher than what was observed when phage K and ciprofloxacin were used in combination. One reason for this antagonistic interaction could be due to the higher concentrations of phage and ciprofloxacin used. PAS has been shown to be more effective when applied sequentially (e.g. phage first then the antimicrobial) as this gives the phage time to adsorb and replicate within the host bacterium. However, if high concentrations of antimicrobials are used in tandem, and have a quicker mechanism of action compared to phage, then they can eliminate the bacteria before the phage have chance to infect them, resulting in a non-productive phage infection. However, it is worth noting that the combination met the threshold of the 3-log reduction recommended by the prEN 16756 standard for all bacterial isolates tested.

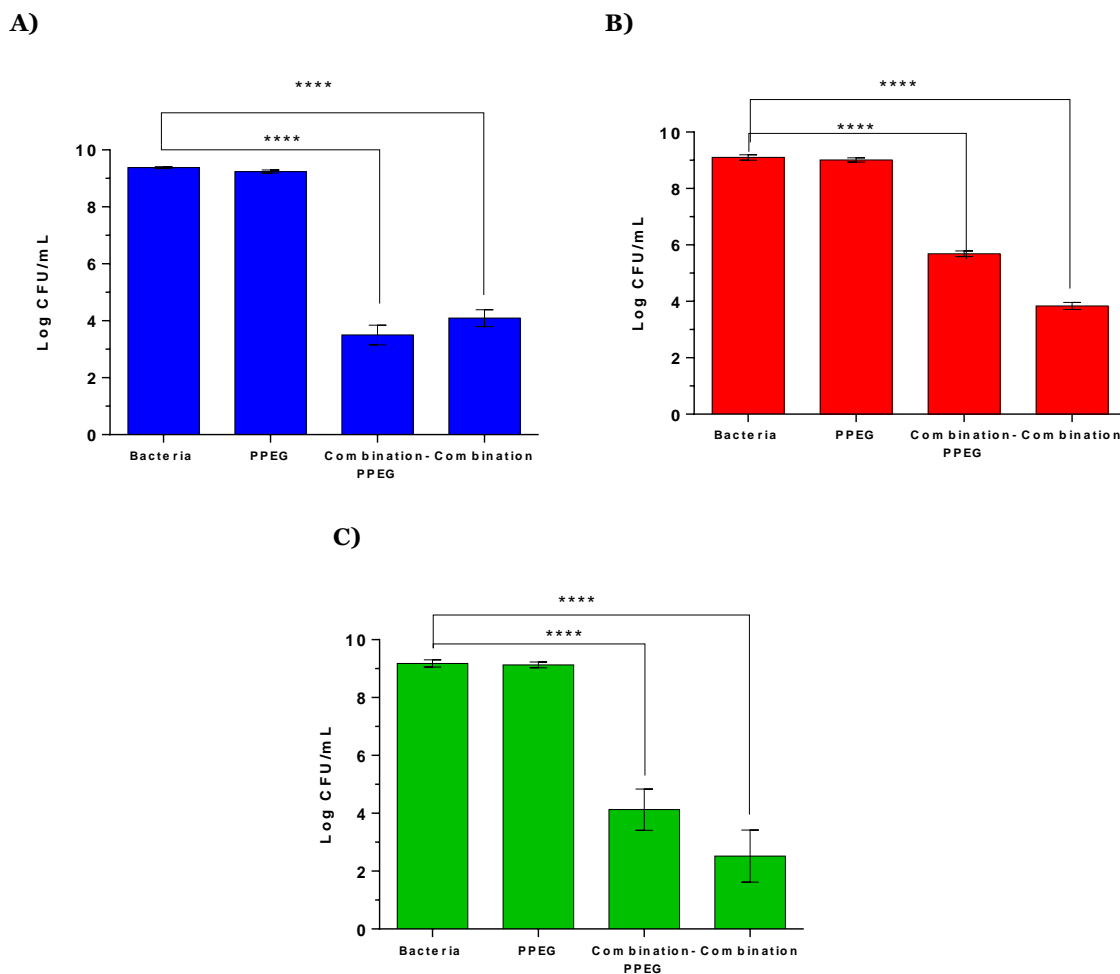


**Figure 4.22:** Log CFU/mL counts of **A)** *S. aureus* H560, **B)** *S. aureus* MRSA252, and **C)** *S. aureus* MSSA101 upon incubation with PPEG films, phage K and ciprofloxacin-PPEG films, and suspensions of phage K and ciprofloxacin ( $10^7$  CFU/mL and  $30 \mu\text{g/mL}$ , respectively) for 24 h at  $32^\circ\text{C}$ .  $n = 3$ , error bars indicate standard deviation. Statistical analysis conducted using a One-way ANOVA.

The corresponding phage concentrations are shown in Figure 4.23. Overall, for *S. aureus* H560 and MSSA101, the phage K concentrations were lower than what was observed for the monotherapy phage K-PPEG films. This could be due to ciprofloxacin being released faster than phage K, leading to a non-productive phage infection. For both these bacterial species, the phage K concentrations were similar to the control. While the concentration of phage K was statistically significantly higher in the combination-PPEG group compared to the control (t-test,  $p < 0.05$ ) for *S. aureus* H560, this was most likely due to the variation in loading and environmental variation within the assay and the release kinetics from the system.

For *S. aureus* MRSA252, the phage K concentrations were similar to that observed for the monotherapy PPEGs. This was probably due to ciprofloxacin being less effective towards this bacterial strain, resulting in more time for phage K to launch a successful infection of *S. aureus* MRSA252 cells. Similarly to *S. aureus* H560, the concentration of phage K was

statistically significantly higher in the combination control group compared to the combination-PPEG film (t-test,  $p < 0.05$ ); this was most likely due to the variation in the methodology of this assay.

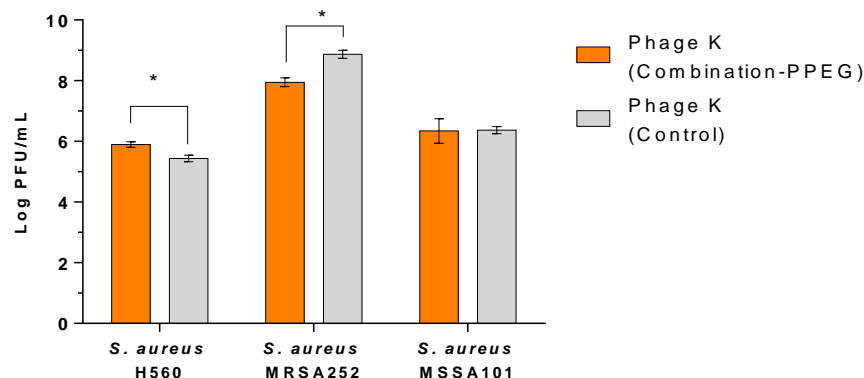


**Figure 4.23:** Log PFU/mL of phage K released from the pH-responsive films and the phage K control after incubation with *S. aureus* H560, MRSA252, and MSSA101 for 24 h at 32°C.  $n = 3$ , error bars indicate standard deviation. Statistical analysis conducted using multiple t-tests.  $*p < 0.05$

#### 4.4.4.3. Colony Biofilm Wound Model

Next, the efficacy of phage K and ciprofloxacin-loaded films was assessed using a colony biofilm model of *S. aureus* isolates (Figure 4.24).

PPEG films loaded with phage K and ciprofloxacin were most effective against *S. aureus* H560, achieving a log reduction of 5.95 compared to the biofilm control (One-way ANOVA,  $p < 0.0001$ ). However, it is important to note that in this experiment, the PPEG film resulted in a 1.19 log reduction compared to the biofilm control (One-way ANOVA,  $p < 0.05$ ), hence had slightly inhibitory effects towards *S. aureus* H560.

For *S. aureus* MRSA252, there was a slight reduction in biofilm count upon incubation with the PPEG film (0.91 log reduction compared to biofilm control; One-way ANOVA,  $p < 0.05$ ). This was further increased when the PPEG film contained the combination of phage K and ciprofloxacin, with the log reduction rising to 2.22 compared to the biofilm control (One-way ANOVA,  $p < 0.001$ ).

For *S. aureus* MSSA101, there was negligible difference in bacterial concentration upon incubation with the PPEG films (0.37 log reduction compared to the biofilm control). However, upon *S. aureus* MSSA101 incubation with the combination of phage K and ciprofloxacin, a log reduction of 3.23 was observed compared to the biofilm control (One-way ANOVA,  $p < 0.001$ ).

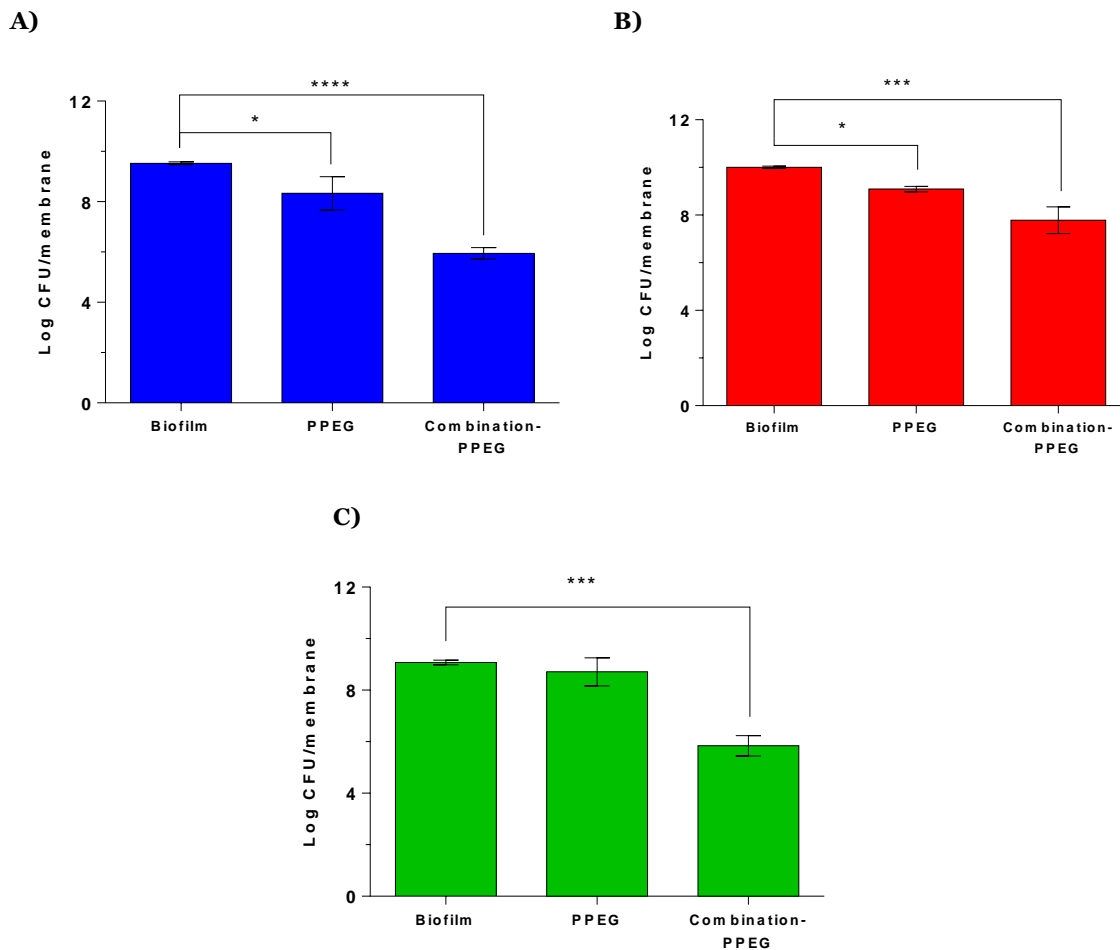


**Figure 4.24:** Log CFU/membrane counts of **A)** *S. aureus* H560, **B)** *S. aureus* MRSA252, and **C)** *S. aureus* MSSA101 biofilms upon incubation with PPEG films, phage K and ciprofloxacin-PPEG films for 24 h at 32°C. n = 3, error bars indicate standard deviation. Statistical analysis conducted using a One-way ANOVA. \*p<0.05, \*\*p<0.01, \*\*\*p<0.001, \*\*\*\*p<0.0001

The combination therapy released from the PPEG film led to a greater than 3 log reduction in bacterial density for *S. aureus* H560 and MSSA101, therefore met the threshold recommended by the prEN 16756 standard.

#### 4.4.4.4. *Ex vivo* Porcine Skin Model

Finally, the PPEG films containing phage K and ciprofloxacin were tested against *S. aureus* isolates inoculated on porcine skin (Figure 4.25). For *S. aureus* H560, there was a 0.83 and 4.44 (One-way ANOVA, p<0.001) log reduction in bacterial concentration compared to the bacterial control for the PPEG and combination-PPEG films, respectively. For *S. aureus* MRSA252, there was a 0.04 and 1.91 (One-way ANOVA, p<0.001) log reduction in bacterial concentration compared to the bacterial control for the PPEG and combination-PPEG films, respectively. For *S. aureus* MSSA101, there was a 0.22 and 3.98 (One-way ANOVA, p<0.001) log reduction in bacterial concentration compared to the bacterial control for the

PPEG and combination-PPEG films, respectively. It is worth noting, that for *S. aureus* H560 and MSSA101, the combination therapy released from the PPEG film led to a greater than 3 log reduction in bacterial density; therefore met the threshold recommended by the prEN 16756 standard.

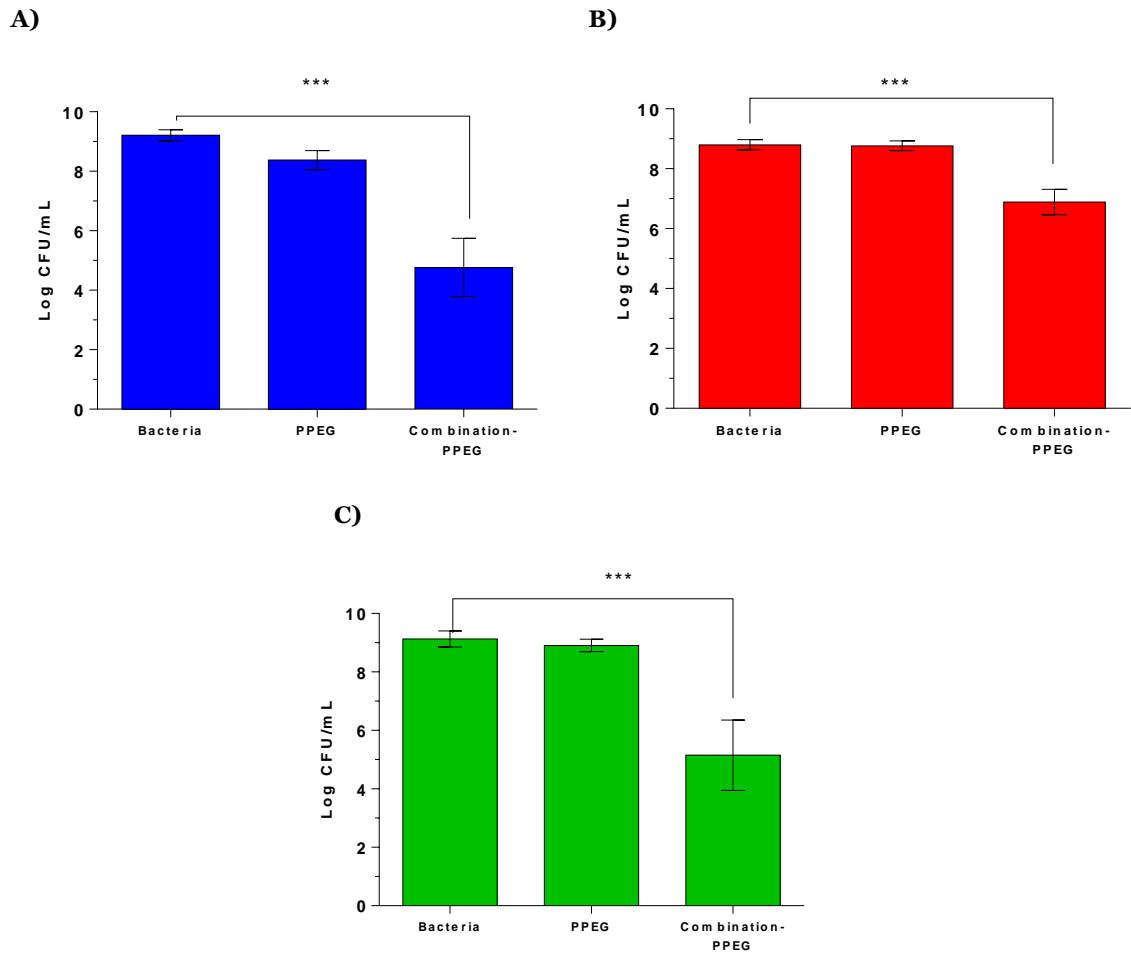


**Figure 4.25:** Log CFU/mL counts of **A)** *S. aureus* H560, **B)** *S. aureus* MRSA252, and **C)** *S. aureus* MSSA101 on porcine skin incubated with PPEG films and phage K and ciprofloxacin-PPEG films for 24 h at 32°C. n = 3, error bars indicate standard deviation. Statistical analysis conducted using a One-way ANOVA. \*p<0.05, \*\*p<0.01, \*\*\*p<0.001, \*\*\*\*p<0.0001

## 4.5. Conclusions and Future Work

This proof-of-concept study demonstrated the utility of PLA-PEG (PPEG) films as antimicrobial wound dressings for the treatment of *S. aureus* infections.

Experiments showed that both phage K and ciprofloxacin were released from the PPEG matrix in a diffusion based manner, owing to the fast rate of release and/or the large pore size of the film in comparison to the size of the antimicrobials. Phage K was shown to be stable within the film for over 5 days at room temperature, demonstrating its utility as a wound dressing as it could have a long shelf-life. Additionally, phage K viability remained when incubated with ciprofloxacin, which was not observed when the two antibiotics were incubated together in solution in Chapter 3, suggesting that the PPEG film offers phage K some protection against the inhibitory effects of ciprofloxacin. Conversely, reductions in ciprofloxacin concentration were observed, and owing to this, further experiments would need to be investigated to determine if this was due to antimicrobial loading within this study, or due to passive diffusion of the ciprofloxacin out of the PPEG matrix.

PPEG films containing phage K or ciprofloxacin demonstrated good efficacy in planktonic and biofilm suspensions, often meeting the 'gold standard' of a 3-log reduction compared to their corresponding bacterial control. However, their clinical utility was questionable, with poor results obtained using the *ex vivo* porcine skin model. To overcome this, PPEG films were made which combined phage K and ciprofloxacin in the hope of increasing the efficacy of the antimicrobial film. While the PPEG films containing phage K and ciprofloxacin displayed statistically significant reductions in bacterial density of *S. aureus* H560, MRSA252 and MSSA101 in planktonic and biofilm assays, they were lower than what was observed for the monotherapies. This agonistic effect was attributed to the concentrations of ciprofloxacin and phage K used and their conflicting mechanism of actions. However, surprisingly, the combination was more successful in eliminating *S. aureus* infections on porcine skin, demonstrating superior clinical efficacy compared to the monotherapies.

This chapter only described a proof-of-concept system, therefore, there remain many experiments that could be conducted to optimise the system. Firstly, experiments could be conducted to investigate the role of pore size in release kinetics. Secondly, to improve phage K encapsulation, the role of adding in sugars to the phage solution to protect the protein structure should be investigated. Experiments should also be conducted to further investigate the weight ratio of PEG:PLA, to see if further increasing the PEG component results in better release profiles of phage K and ciprofloxacin. Additionally, the

concentrations of phage K and ciprofloxacin should be investigated when used in combination to see if it is possible to get an additive or synergistic interaction between the two antimicrobials.

Furthermore, there was a clear difference in *in vitro* and *ex vivo* results for all antimicrobials tested, whether that be enhanced or reduced efficacy in *ex vivo* testing compared to *in vitro*. Therefore, it is important that further tests are conducted to evaluate the clinical utility of the antimicrobial-loaded PPEG films. In addition to those previously mentioned this could involve using more robust biofilm models, repeating the current *ex vivo* porcine skin methodology to gain better power for the statistical analysis, or use *in vivo* mouse models, which will also investigate the immune response to this system.

Overall, these results show that antimicrobials can be incorporated within PLA-PEG films, whether that be phage or conventional antibiotics, and are capable of reducing *S. aureus* density. While further work must be carried out to optimise these films, this Chapter has demonstrated their utility as an antibiotic wound dressing. Furthermore, this system can be optimised to contain different antimicrobials to treat a variety of different microbial infections, it is not limited to *S. aureus* infections or phage K and ciprofloxacin as antimicrobials.

## 4.6. References

1. Hill RG. 4 - Polymers. In: Hench LL, Jones Artificial Organs and Tissue Engineering JRBT-B, editors. Woodhead Publishing Series in Biomaterials. Woodhead Publishing; 2005. p. 37–47.
2. Gad SE. Polymers. In: Wexler PBT-E of T (Third E, editor. Oxford: Academic Press; 2014. p. 1045–50.
3. Chanda M. Introduction to polymer science and chemistry: a problem-solving approach. CRC Press; 2013.
4. Shrivastava A. 2 - Polymerization. In: Shrivastava ABT-I to PE, editor. Plastics Design Library. William Andrew Publishing; 2018. p. 17–48.
5. McKeen LW. Permeability properties of plastics and elastomers. William Andrew; 2016.
6. Ebeuele RO. Polymer science and technology. CRC press; 2000.
7. Darvell BW. Chapter 3 - Polymers. In: Darvell BWBT-MS for D (Tenth E, editor. Woodhead Publishing Series in Biomaterials. Woodhead Publishing; 2018. p. 70–91.
8. Ebnesajjad S. Introduction to Plastics. In: Baur E, Ruhrberg K, Woishnis WBT-CR of CT, editors. Plastics Design Library. William Andrew Publishing; 2016. p. xiii–xxv.
9. Campo EA. 3 - Thermal Properties of Polymeric Materials. In: Campo EABT-S of PM, editor. Plastics Design Library. Norwich, NY: William Andrew Publishing; 2008. p. 103–40.
10. Tyler B, Gullotti D, Mangraviti A, Utsuki T, Brem H. Polylactic acid (PLA) controlled delivery carriers for biomedical applications. *Adv Drug Deliv Rev.* 2016;107:163–75.
11. Sheikh Z, Najeeb S, Khurshid Z, Verma V, Rashid H, Glogauer M. Biodegradable materials for bone repair and tissue engineering applications. *Materials (Basel).* 2015;8(9):5744–94.
12. Saini P, Arora M, Kumar MNVR. Poly (lactic acid) blends in biomedical applications. *Adv Drug Deliv Rev.* 2016;107:47–59.
13. Ruiz-Ruiz F, Mancera-Andrade EI, Parra-Saldivar R, Keshavarz T, Iqbal H. Drug



- delivery and cosmeceutical applications of poly-lactic acid based novel constructs-A review. *Curr Drug Metab.* 2017;18(10):914–25.
14. Griffith LG. Polymeric biomaterials. *Acta Mater.* 2000;48(1):263–77.
  15. Singhvi MS, Zinjarde SS, Gokhale D V. Polylactic acid: synthesis and biomedical applications. *J Appl Microbiol.* 2019;127(6):1612–26.
  16. Auras R, Harte B, Selke S. An overview of polylactides as packaging materials. *Macromol Biosci.* 2004;4(9):835–64.
  17. Anderson JM, Shive MS. Biodegradation and biocompatibility of PLA and PLGA microspheres. *Adv Drug Deliv Rev.* 2012;64:72–82.
  18. Reed AM, Gilding DK. Biodegradable polymers for use in surgery—poly (glycolic)/poly (lactic acid) homo and copolymers: 2. In vitro degradation. *Polymer (Guildf).* 1981;22(4):494–8.
  19. Chitrattha S, Phaechamud T. Porous poly (DL-lactic acid) matrix film with antimicrobial activities for wound dressing application. *Mater Sci Eng C.* 2016;58:1122–30.
  20. Tan L, Yu X, Wan P, Yang K. Biodegradable materials for bone repairs: a review. *J Mater Sci Technol.* 2013;29(6):503–13.
  21. Baek J, Chen X, Sovani S, Jin S, Grogan SP, D’Lima DD. Meniscus tissue engineering using a novel combination of electrospun scaffolds and human meniscus cells embedded within an extracellular matrix hydrogel. *J Orthop Res.* 2015;33(4):572–83.
  22. Senatov FS, Niaza K V, Zadorozhnyy MY, Maksimkin A V, Kaloshkin SD, Estrin YZ. Mechanical properties and shape memory effect of 3D-printed PLA-based porous scaffolds. *J Mech Behav Biomed Mater.* 2016;57:139–48.
  23. Le Roux BT, Shama DM. Resection of tumors of the chest wall. *Curr Probl Surg.* 1983;20(6):345–86.
  24. Meredith IT, Verheye S, Dubois CL, Dens J, Fajadet J, Carrié D, et al. Primary endpoint results of the EVOLVE trial: a randomized evaluation of a novel bioabsorbable polymer-coated, everolimus-eluting coronary stent. *J Am Coll Cardiol.* 2012;59(15):1362–70.

25. Soliman MM, Zaki AA, El Gazaerly HM, Al Shemmrani A, Sorour AEL. Clinical and radiographic evaluation of copolymerized Polylactic/polyglycolic acids as a bone filler in combination with a cellular dermal matrix graft around immediate implants. *Int J Health Sci (Qassim)*. 2014;8(4):381.
26. Kao C-T, Lin C-C, Chen Y-W, Yeh C-H, Fang H-Y, Shie M-Y. Poly (dopamine) coating of 3D printed poly (lactic acid) scaffolds for bone tissue engineering. *Mater Sci Eng C*. 2015;56:165–73.
27. Wang W, Fang K, Wang X, Li M, Wu Y, Chen F, et al. Antigen-specific killer polylactic-co-glycolic acid (PLGA) microspheres can prolong alloskin graft survival in a murine model. *Immunol Invest*. 2015;44(4):385–99.
28. Hillary CJ, Roman S, Bullock AJ, Green NH, Chapple CR, MacNeil S. Developing repair materials for stress urinary incontinence to withstand dynamic distension. *PLoS One*. 2016;11(3):e0149971.
29. Strohbahn G, Coman D, Han L, Ragheb RRT, Fahmy TM, Huttner AJ, et al. Imaging the delivery of brain-penetrating PLGA nanoparticles in the brain using magnetic resonance. *J Neurooncol*. 2015;121(3):441–9.
30. Pandey SK, Ghosh S, Maiti P, Haldar C. Therapeutic efficacy and toxicity of tamoxifen loaded PLA nanoparticles for breast cancer. *Int J Biol Macromol*. 2015;72:309–19.
31. Cai Q, Bei J, Wang S. In vitro study on the drug release behavior from Polylactide-based blend matrices. *Polym Adv Technol*. 2002;13(7):534–40.
32. Pandey SP, Shukla T, Dhote VK, Mishra DK, Maheshwari R, Tekade RK. Use of polymers in controlled release of active agents. In: *Basic Fundamentals of Drug Delivery*. Elsevier; 2019. p. 113–72.
33. D'souza AA, Shegokar R. Polyethylene glycol (PEG): a versatile polymer for pharmaceutical applications. *Expert Opin Drug Deliv*. 2016;13(9):1257–75.
34. De Braekt MMHI, Van Alphen FAM, Kuijpers-Jagtman AM, Maltha JC. Wound healing and wound contraction after palatal surgery and implantation of poly-(L-lactic) acid membranes in beagle dogs. *J oral Maxillofac Surg*. 1992;50(4):359–64.
35. Toncheva A, Mincheva R, Kancheva M, Manolova N, Rashkov I, Dubois P, et al. Antibacterial PLA/PEG electrospun fibers: comparative study between grafting and blending PEG. *Eur Polym J*. 2016;75:223–33.

36. Mogoşanu GD, Grumezescu AM. Natural and synthetic polymers for wounds and burns dressing. *Int J Pharm.* 2014;463(2):127–36.
37. Han C, Cai N, Chan V, Liu M, Feng X, Yu F. Enhanced drug delivery, mechanical properties and antimicrobial activities in poly (lactic acid) nanofiber with mesoporous Fe<sub>3</sub>O<sub>4</sub>-COOH nanoparticles. *Colloids Surfaces A Physicochem Eng Asp.* 2018;559:104–14.
38. Nazari T, Moghaddam AB, Davoodi Z. Optimized polylactic acid/polyethylene glycol (PLA/PEG) electrospun fibrous scaffold for drug delivery: effect of graphene oxide on the cefixime release mechanism. *Mater Res Express.* 2019;6(11):115351.
39. Kontogiannopoulos KN, Assimopoulou AN, Tsivintzelis I, Panayiotou C, Papageorgiou VP. Electrospun fiber mats containing shikonin and derivatives with potential biomedical applications. *Int J Pharm.* 2011;409(1–2):216–28.
40. Locilento DA, Mercante LA, Andre RS, Mattoso LHC, Luna GLF, Brassolatti P, et al. Biocompatible and biodegradable electrospun nanofibrous membranes loaded with grape seed extract for wound dressing application. *J Nanomater.* 2019;2019.
41. Perumal G, Pappuru S, Chakraborty D, Nandkumar AM, Chand DK, Doble M. Synthesis and characterization of curcumin loaded PLA–Hyperbranched polyglycerol electrospun blend for wound dressing applications. *Mater Sci Eng C.* 2017;76:1196–204.
42. Jamaledin R, Sartorius R, Di Natale C, Vecchione R, De Berardinis P, Netti PA. Recombinant Filamentous Bacteriophages Encapsulated in Biodegradable Polymeric Microparticles for Stimulation of Innate and Adaptive Immune Responses. *Microorganisms.* 2020;8(5):650.
43. Radford D, Guild B, Strange P, Ahmed R, Lim L-T, Balamurugan S. Characterization of antimicrobial properties of Salmonella phage Felix O1 and Listeria phage A511 embedded in xanthan coatings on Poly (lactic acid) films. *Food Microbiol.* 2017;66:117–28.
44. Garlotta D. A literature review of poly (lactic acid). *J Polym Environ.* 2001;9(2):63–84.
45. Nampoothiri KM, Nair NR, John RP. An overview of the recent developments in polylactide (PLA) research. *Bioresour Technol.* 2010;101(22):8493–501.

46. Rasal RM, Janorkar A V, Hirt DE. Poly (lactic acid) modifications. *Prog Polym Sci.* 2010;35(3):338–56.
47. Lu Z, Wu J, Liu W, Zhang G, Wang P. A ratiometric fluorescent probe for quantification of alkaline phosphatase in living cells. *RSC Adv.* 2016;6(38):32046–51.
48. Wu PX, Zhang LC. *Polymer Blending.* Chinese Light Ind Publ Beijing. 1998;267.
49. Van de Witte P, Dijkstra PJ, Van den Berg JWA, Feijen J. Phase separation processes in polymer solutions in relation to membrane formation. *J Memb Sci.* 1996;117(1–2):1–31.
50. Phaechamud T, Chitrattha S. Pore formation mechanism of porous poly(dl-lactic acid) matrix membrane. *Mater Sci Eng C.* 2016;61:744–52.
51. Heit YI, Dastouri P, Helm DL, Pietramaggiore G, Younan G, Erba P, et al. Foam pore size is a critical interface parameter of suction-based wound healing devices. *Plast Reconstr Surg.* 2012;129(3):589–97.
52. Malik DJ, Sokolov IJ, Vinner GK, Mancuso F, Cinquerrui S, Vladislavljevic GT, et al. Formulation, stabilisation and encapsulation of bacteriophage for phage therapy. Vol. 249, *Advances in Colloid and Interface Science.* 2017. p. 100–33.
53. Jurczak-Kurek A, Gąsior T, Nejman-Faleńczyk B, Bloch S, Dydecka A, Topka G, et al. Biodiversity of bacteriophages: morphological and biological properties of a large group of phages isolated from urban sewage. *Sci Rep.* 2016;6(1):1–17.
54. Loh B, Gondil VS, Manohar P, Khan FM, Yang H, Leptihn S. Encapsulation and Delivery of Therapeutic Phages. *Appl Environ Microbiol.* 2020;
55. Siepmann J, Peppas NA. Higuchi equation: Derivation, applications, use and misuse. *Int J Pharm.* 2011;418(1):6–12.
56. Hu Y, Zou S, Chen W, Tong Z, Wang C. Mineralization and drug release of hydroxyapatite/poly (l-lactic acid) nanocomposite scaffolds prepared by Pickering emulsion templating. *Colloids Surfaces B Biointerfaces.* 2014;122:559–65.
57. British Standards Institution. PREN 16756 [Internet]. 2014 [cited 2021 Feb 8]. p. 35. Available from: [https://global.ihs.com/doc\\_detail.cfm?document\\_name=PREN16756&item\\_s\\_key=00624702](https://global.ihs.com/doc_detail.cfm?document_name=PREN16756&item_s_key=00624702)

58. James GA, Swogger E, Wolcott R, Pulcini E deLancey, Secor P, Sestrich J, et al. Biofilms in chronic wounds. *Wound Repair Regen.* 2008;16(1):37–44.
59. Malone M, Bjarnsholt T, McBain AJ, James GA, Stoodley P, Leaper D, et al. The prevalence of biofilms in chronic wounds: a systematic review and meta-analysis of published data. *J Wound Care.* 2017;26(1):20–5.
60. Khatoon Z, McTiernan CD, Suuronen EJ, Mah T-F, Alarcon EI. Bacterial biofilm formation on implantable devices and approaches to its treatment and prevention. *Heliyon.* 2018;4(12):e01067.
61. Lebeaux D, Chauhan A, Rendueles O, Beloin C. From in vitro to in vivo models of bacterial biofilm-related infections. *Pathogens.* 2013;2(2):288–356.
62. Moleiro AF, Conceicao G, Leite-Moreira AF, Rocha-Sousa A. A critical analysis of the available in vitro and ex vivo methods to study retinal angiogenesis. *J Ophthalmol.* 2017;2017.
63. Kapila R, Kapila S, Vij R. Efficacy of Milk-Derived Bioactive Peptides on Health by Cellular and Animal Models. In: *Nutrients in Dairy and their Implications on Health and Disease.* Elsevier; 2017. p. 303–11.
64. Wang X, So K-F, Xu X-M. Advances and challenges for neural regeneration research. In: *Neural regeneration.* Elsevier; 2015. p. 3–17.
65. Lademann J, Richter H, Meinke M, Sterry W, Patzelt A. Which skin model is the most appropriate for the investigation of topically applied substances into the hair follicles? *Skin Pharmacol Physiol.* 2010;23(1):47–52.
66. Summerfield A, Meurens F, Ricklin ME. The immunology of the porcine skin and its value as a model for human skin. *Mol Immunol.* 2015;66(1):14–21.
67. Yang Q, Phillips PL, Sampson EM, Progulske-Fox A, Jin S, Antonelli P, et al. Development of a novel ex vivo porcine skin explant model for the assessment of mature bacterial biofilms. *Wound Repair Regen.* 2013;21(5):704–14.
68. Abd E, Yousef SA, Pastore MN, Telaprolu K, Mohammed YH, Namjoshi S, et al. Skin models for the testing of transdermal drugs. *Clin Pharmacol Adv Appl.* 2016;8:163.

# Chapter 5: Triggered Release of Bacteriophage K and Ciprofloxacin from a pH-Responsive System

## 5.1. Overview of Chapter

This chapter describes the creation of a novel, pH-responsive wound dressing to treat *S. aureus* infections. The PLA-PEG (PPEG) film created and analysed in Chapter 4 was capped with a pH-responsive polymer, EUDRAGIT® FS 30 D – a co-polymer of methyl acrylate, methyl methacrylate and methacrylic acid. Upon an increase in pH above pH 7.0, the polymer swells, releasing phage K and/or ciprofloxacin that were encapsulated within the PPEG reservoir (Figure 5.1).

This chapter assessed the stability and release profiles of phage K and/or ciprofloxacin upon incubation of the pH-responsive system in buffer solutions of pH 6.5 and pH 8.0, respectively. Further experiments investigated the relationship between pH and *S. aureus* biofilm formation and evaluated the release of the therapeutic from the pH-responsive system upon incubation with developing *S. aureus* biofilms.

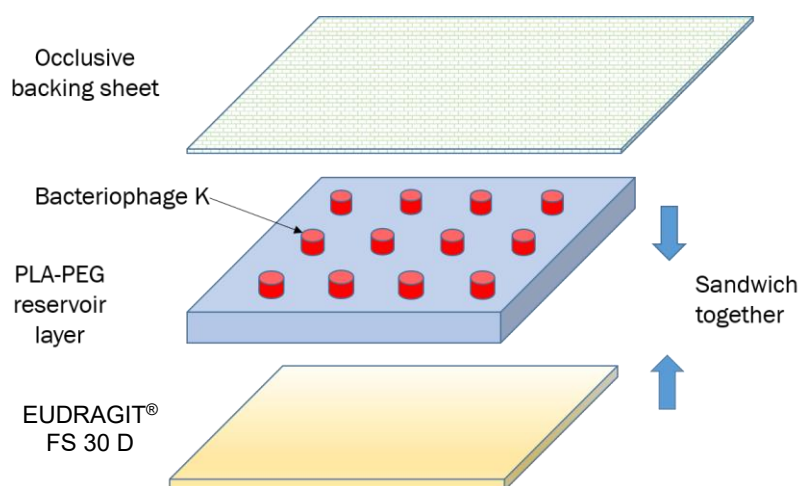


**Figure 5.1:** Schematic of a novel pH-responsive wound dressing for the treatment of chronic wounds. Upon an increase in pH above pH 7, the pH-responsive polymer becomes soluble and swells, resulting in the release of the therapeutic (phage K and/or ciprofloxacin) to treat *S. aureus* infections

## 5.2. Introduction

### 5.2.1. pH

pH is an inverse logarithmic measure of the thermodynamic activity of hydrogen ions ( $a_{[H^+]}$ ) in solution. For solutions containing a low concentration of  $H^+$ , the activity of hydrogen ions can be correlated to the concentration of hydrogen ions (Equation 1):<sup>1</sup>

$$pH = -\log_{10} a_{[H^+]} \approx -\log_{10} [H^+] \quad (1)$$

Typically, the logarithmic pH scale ranges from 0 – 14, although negative pH values have been recorded; solutions with a pH <7 are acidic ( $[H^+] > [OH^-]$ ), solutions with a pH ~7 are neutral ( $[H^+] = [OH^-]$ ), and solutions >7 are alkaline ( $[H^+] < [OH^-]$ ).<sup>1</sup>

#### 5.2.1.1. Acid and Bases

Acids and bases have free hydrogen and hydroxyl ions, respectively. A Brønsted-Lowry acid is defined as a proton donor, while a Brønsted-Lowry base is a proton acceptor. In an acid-base reaction, there is a transfer of a proton amongst the conjugate acid-base pairs.

The strength of the Brønsted-Lowry acid is dependent on the acid's ability to donate a proton and dissociate into ions (protons  $[H^+]$  and anions  $[A^-]$ ). A strong acid can fully dissociate and donate a proton, whereas a weak acid has a lower tendency to donate a proton and is thus only partially ionised in aqueous solution. The strength of the acid in solution can be calculated by determining the acid dissociation constant ( $K_a$ ), which is the dissociated reaction of the acid expressed as mol dm<sup>-3</sup>:

$$K_a = \frac{[H^+]_{(aq)}[A^-]_{(aq)}}{[HA]_{(aq)}} \quad (2)$$

The larger the value of  $K_a$ , the further the equilibrium lies to the right, the stronger the acid as it results in a higher dissociation of the acid.  $K_a$  can be expressed in terms of  $pK_a$ ; the lower the  $pK_a$  value, the stronger the acid (Equation 3).

$$pK_a = -\log_{10} K_a \quad (3)$$

As previously mentioned, a Brønsted-Lowry base is a proton acceptor; a strong base is fully ionised in aqueous solutions whereas a weak base has a lower tendency to accept a proton and is only partially ionised in aqueous solutions. Similarly to Brønsted-Lowry acids, a base

dissociation constant ( $K_b$ ) can be calculated to determine the strength of the base (Equation 4). The larger the value of  $K_b$ , the stronger the base.  $K_b$  can also be expressed in terms of  $pK_b$ , with stronger bases having a higher  $pK_b$  value (Equation 5). However, usually, the strength of the base is referred to in terms of the  $K_a$  of the conjugate acid.

$$K_b = \frac{[BH^+]_{(aq)}[OH^-]_{(aq)}}{[B]_{(aq)}} \quad (4)$$

$$pK_b = -\log_{10} K_b \quad (5)$$

### 5.2.1.2. Buffer Solutions

Buffer solutions are solutions that can resist changes in pH. The Henderson-Hasselbalch equation is often used to show that the pH of the buffer solution is dependent on the value of  $K_a$  and the ratio of the [conjugate base] to [acid]. Generally, the equilibrium established in a weak acid is:



Making  $[H^+]$  the subject of the acid dissociation constant (Equation 6) results in:

$$[H^+] = \frac{K_a[HA]}{[A^-]} \quad (7)$$

Substituting into the equation for pH (Equation 5) gives,

$$pH = -\log_{10} \left( \frac{K_a[HA]}{[A^-]} \right) \quad (8)$$

$$pH = -\log_{10} K_a - \log_{10} \left( \frac{[HA]}{[A^-]} \right) \quad (9)$$

Substituting in  $pK_a$  gives,

$$pH = pK_a - \log_{10} \left( \frac{[HA]}{[A^-]} \right) \quad (10)$$

Which can be re-written as:

$$pH = pK_a - \log_{10} \left( \frac{[A^-]}{[HA]} \right) \quad (11)$$



### 5.2.2. Wound pH

Healthy skin was found to be acidic by E. Heuss in 1892<sup>2</sup> and was confirmed through further studies aided by the invention of the planar glass electrode in 1955.<sup>3</sup> It is more appropriate to refer to skin pH as ‘apparent skin pH’ as the *stratum corneum* is not an aqueous solution; the hydrogen ions measured when evaluating skin pH are actually released by components of the *stratum corneum* (e.g., lipids and secretions from sebaceous and sweat glands).<sup>4,5</sup>

Various values for skin pH have been reported in literature; however, they generally vary between pH 4.0 and 6.0.<sup>6–8</sup> This discrepancy in pH values can be attributed to the lack of a standardised protocol for pH determination, anatomical location of the skin under investigation, and even the sex of the patient, with some studies showing that female skin is more acidic compared to male skin;<sup>9</sup> however, this is disputed in other studies.<sup>10–12</sup> Interestingly, there seems to be no difference in skin pH observed between different ethnic groups,<sup>13–15</sup> but apparent skin pH varies with age, with neonates and the elderly often having an elevated skin pH.<sup>12,16,17</sup> Fluhr *et al* categorised skin pH according to anatomical location and found that regions with a higher density of sebaceous glands had slightly elevated pH values (pH 5.8 – 6.6),<sup>17</sup> thought to be due to the high humidity within these areas decreasing the production of urocanic acid.<sup>10,17</sup>

Increases in skin pH arise due to a variety of reasons; skin disorders such as eczema, atopic dermatitis, and irritant contact dermatitis can result in the disruption of the skin barrier function, consequently leading to higher pH values compared to healthy skin.<sup>17,18</sup> Additionally, the use of cleansers, detergents and cosmetics can alter the apparent pH of the skin, often causing a transient increase in pH.<sup>6</sup>

The acidic mantle of the skin is essential in regulating the normal flora of the skin, preventing infection by pathogenic bacteria<sup>8</sup> through the production of bacteriocins, toxic metabolites, depletion of essential nutrients, induction of a low reduction-oxidation potential, inhibition of translocation, and induction of the host to enhance antibody and cytokine production and stimulation of phagocytosis.<sup>19</sup> The commensal flora of the skin are able to survive in these acidic conditions, while the growth of pathogenic bacteria is restricted. For example, *Propionibacterium*, a commensal bacterium, grows well between pH 6.0 – 6.5; however, pathogenic bacteria such as *S. aureus* have an optimum pH of 7.5 and slow proliferation between pH 5.0 – 6.0.<sup>20</sup>

### 5.2.2.1. Wound Healing and pH

Any injury to the skin leads to a localised loss of the *stratum corneum*, bleeding, and exposure of internal tissue and interstitial fluid, all of which result in an elevated pH of the skin (between pH 7.0 – 8.0). In a non-infected acute wound, as the wound heals the pH decreases due to various factors including hypoxia and increased production of lactic acid<sup>8</sup> as the *stratum corneum* is repaired, restoring the acidic mantle of the skin.<sup>7</sup> Conversely, non-healing chronic wounds have been shown to be more alkaline compared to acute wounds, with pH values between 7.2 – 8.9,<sup>21</sup> and even as high as 9.3.<sup>22</sup> These wounds do not transverse to an acidic pH, with alkalinity observed for a long period of time, often months.<sup>22</sup> Roberts *et al* found that the mean apparent pH of venous leg ulcers was significantly lower in the healing group compared to the non-healing group<sup>23</sup> and Leveen *et al* found that the non-healing nature of surface wounds was correlated with alkaline pH.<sup>24</sup>

The elevated pH of chronic wounds alters the biochemical reactions and cellular processes involved in wound healing,<sup>8,25</sup> affecting oxygen release, angiogenesis, protease activity, bacterial toxicity, and antimicrobial activity.<sup>21,22</sup> For a more detailed review, please see Wallace *et al.*<sup>22</sup>

### 5.2.2.2. Microbial Biofilms and pH

The elevated pH within chronic wounds creates an optimum environment for colonisation by pathogenic bacteria.<sup>8,25</sup> It is generally accepted that pathogenic bacteria require a pH of >6.0 for successful proliferation, with lower pH values inhibiting the proliferation of such bacteria. Additionally, it has been found that the colonisation of pathogenic bacteria can cause the wound to become more alkaline in nature, thus perpetuating proliferation.<sup>25</sup>

One of the most frequently cited studies involving pH in wound care is that by Tsukada *et al*,<sup>26</sup> who found that pressure injuries tend towards an acidic pH as the wound progresses towards healing. As such, one of the current theories to combat chronic wound infections is to restore the skin to an acidic pH.<sup>22,27–29</sup> An interventional clinical study found that cleansing with acidic mineral water caused a greater decrease in bacterial load compared to cleansing with water with a neutral pH.<sup>30</sup> Additionally Strohal *et al* found that topical acidification of chronic wounds led to decreased microbial bioburden and decreased wound size; however, they did not use any controls and hence cannot be used to evaluate the effectiveness of acidification of chronic wounds.<sup>31</sup> Modulation of wound pH from alkaline (pH 9.0) to an acidic pH by daily application of 1% acetic acid was investigated by Agrawal *et al* and resulted in a decrease in pathogenic microorganisms and improved wound healing outcomes.<sup>32</sup> While these results show that an acidic environment results in greater infection

control, increased oxygenation, and reduction of the toxicity of bacterial by-products,<sup>22</sup> one of the drawbacks of this method is the longevity of the acidic solution. For instance, the moist wound dressings that contained 1% acetic acid remained acidic for only one hour, after which the pH rises to neutrality or above.<sup>24</sup> In a clinical environment, a wound dressing can remain *in situ* on the wound for up to seven days; hence, acidification would need to be consistent throughout this time period. Therefore, there is a growing need to develop materials that can sense the pH of a wound environment, and release antimicrobials to treat the infection only when needed; this prevents the unnecessary use of antimicrobials when the wound is healing in a normal fashion (tending to acidic pH) and clinical intervention is not needed.

### **5.2.2.3. Antimicrobials and pH**

pH has been shown to affect the activity of antiseptics<sup>8</sup> and the bactericidal activity of antimicrobial agents.<sup>33</sup> For example, hypochlorite requires twice as long to kill microorganisms at pH 8.0 compared to pH 6.0.<sup>34</sup> pH has also been shown to affect the antimicrobial activity of silver, with a lower pH resulting in enhanced activity of silver (ionic silver) in wound dressings.<sup>35,36</sup> Aminoglycoside antibiotics are also affected by pH, with gentamicin demonstrating a 90-fold increase in efficacy at pH 7.8 compared to pH 5.5.<sup>25</sup> As chronic wounds almost certainly contain a biofilm requiring clinical intervention,<sup>37-39</sup> the effect of pH must be considered when choosing the appropriate antimicrobial therapy.

### **5.2.3. Triggered Release Systems**

The ideal antimicrobial wound dressing should release its therapeutic load in response to an active infection at a high enough local concentration for a set duration in order to eliminate the pathogenic bacteria present at the infection site.<sup>40</sup>

To achieve this, many environmentally-responsive polymers (or ‘smart’ polymers) have been developed that release their therapeutic payload in response to an external stimulus. Often, the stimuli are physical (e.g., temperature, ultrasound, light, magnetic and electrical fields) or chemical (e.g., pH, redox potential, ionic strength, and chemical agents) in nature. Physical stimuli often induce a response by modulating the energy level of the polymer/solvent system, while chemical stimuli act by altering the molecular interactions between the polymer and solvent, or between polymer chains.<sup>40</sup>

### 5.2.3.1. Response Systems Based on Temperature

The most widely reported trigger is temperature, owing to its applicability in drug delivery applications.<sup>40–42</sup> One of the most reported thermo-responsive polymers is poly(N-isopropylacrylamide) (PNIPAM), which undergoes a reversible, entropically driven phase transition at a lower critical solution temperature (LCST) of approximately 32 °C that leads to the expulsion of water and a change in polymer volume.<sup>43</sup> Below the LCST, PNIPAM exists as a hydrophilic coil as water molecules are arranged in an ordered state in the local environment of the polymer chain.<sup>44,45</sup> Above the LCST, there is a change in the hydrophilic/hydrophobic balance of the polymer chain and polymer-polymer hydrophobic interactions dominate.<sup>44,46</sup> Consequently, the polymer chains collapse, and the water molecules are expelled from the bulk, resulting in PNIPAM existing as a hydrophobic globule.<sup>44</sup>

Hathaway *et al* created a thermo-responsive wound dressing utilising PNIPAM copolymerised with allylamine (PNIPAM-*co*-ALA) for the selective release of phage K. PNIPAM was chosen as temperatures above the LCST were associated with a bacterial skin infection. The results found that upon incubation at temperatures above the LCST (37 °C), phage K-incorporated PNIPAM-*co*-ALA nanospheres successfully lysed *S. aureus* ST288, while at temperatures below the LCST (25 °C) bacterial growth was unaffected.<sup>47</sup> The researchers further investigated the release of a combination of a truncated phage endolysin, CHAP<sub>K</sub>, and lysostaphin, from PNIPAM nanoparticles, and found similar results to their previous study; above the LCST temperature, bacterial inhibition was observed, whereas at temperatures below the LCST, the bacterial growth was unaffected.<sup>48</sup>

### 5.2.3.2. Response Systems Based on Enzymes and Toxins

Enzyme-responsive drug delivery systems release their therapeutic payload upon enzymatic degradation of the ‘smart’ polymer.<sup>49,50</sup> Particular focus has been placed on proteases as triggers due to their over-expression in infectious diseases and cancer.<sup>42</sup> Additionally, trypsin and hyaluronidase have been used to selectively deliver anticancer agents inside cancer cells.<sup>51</sup> Bean *et al* also utilised hyaluronidase as a trigger to selectively release phage K from a dual-layer system by degrading the hyaluronic acid ‘capping’ layer.<sup>52</sup>

Thet *et al* developed biosensors for the detection of *S. aureus* and *P. aeruginosa*. Briefly, carboxyfluorescein was entrapped within vesicles that degraded in response to toxin/enzyme production by the pathogenic bacteria, resulting in a fluorescence “turn-on” response. The selectivity of the system was due to the modification of the vesicles; by altering the composition of lipids and fatty acids within the membrane, the vesicles were

sensitised to either toxin production by *S. aureus* (delta toxin), enzyme production by *P. aeruginosa* (phospholipase), or both.<sup>53</sup> Laabei *et al* went on to use the *S. aureus*-targeting phospholipid vesicles to develop a new method to determine *agr* activity,<sup>54</sup> while Thet *et al*, went on to further develop the sensor and recently published preliminary results from a pilot clinical study. The probe is now named SPaCE in accordance with the sensor being able to detect *S. aureus*, *P. aeruginosa*, *Candida albicans/auris*, and *Enterococcus faecalis*, and was found to have a sensitivity of 57% and specificity of 71%.<sup>55</sup>

Enzymes have been used extensively for the selective ‘turn on’ for fluorescent and colorimetric probes. For a more detailed review, please see Chapter 7.

### **5.2.3.3. Response Systems Based on pH**

pH has been used as a trigger for ‘smart’ drug delivery systems due to the variation of pH within the body, for instance, the stomach has a high acidic pH of approximately pH 2.0, whereas the small intestine has an alkaline pH of approximately 6.2 – 7.5. Additionally, it has been proven that diseased or inflamed tissue have a different pH profile compared to normal tissue,<sup>56</sup> for example tumours have been reported to produce acidic conditions in the extracellular milieu (pH ~ 6.5).<sup>57</sup>

Several researchers have created polymers that are responsive towards changes in the pH of the extracellular environment.<sup>40,58,59</sup> Researchers have created pH-responsive hydrogels containing poly(methacrylic acid) grafted with PEG for oral protein delivery; the polymer hydrogel was capable of encapsulating, protecting and mediating the release of insulin,<sup>60</sup> calcitonin,<sup>61</sup> and interferon beta.<sup>62</sup> Additionally, Milo *et al* has successfully utilised pH to treat *Proteus mirabilis* (*P. mirabilis*) infections for the treatment of catheter-associated urinary tract infections (CAUTIs). *P. mirabilis* secretes urease, which in turn increases the urinary pH, leading to the formation of struvite and apatite crystals that become lodged in the biofilm and result in the blockage of urine flow through the catheter.<sup>63</sup> The researchers developed a dual-layered system where a hydrogel layer containing phage was capped with a trigger layer of the pH-responsive poly(methyl methacrylate-co-methacrylic acid) (EUDRAGIT® S 100). Upon the increase in pH by *P. mirabilis*, phage was released from the technology and the time to catheter blockage doubled (13 h vs 26 h). Conversely, the coatings were stable in the absence of infection and in the presence of urease-negative bacteria.<sup>63</sup> Milo *et al* went on to create an infection-detection system using this system, swapping out phage for the fluorescent carboxyfluorescein, and showed its effectiveness as a coating on the catheter<sup>64</sup> and as a lozenge placed within the catheter drainage bag.<sup>65</sup>

Recently, Rasool *et al* have created chitosan/poly(N-vinyl-2-pyrrolidone)-based, pH-sensitive hydrogels that exhibited increased swelling with increasing pH, resulting in the controlled release of silver sulfadiazine.<sup>66</sup> Wallace *et al* have also developed pH-responsive wound dressings utilising EUDRAGIT® FS 30 D for the treatment of *P. aeruginosa* biofilms within chronic wounds. The wound dressing successfully resulted in a statistically significant decrease in *P. aeruginosa* biofilm density after 24 h incubation at 32 °C compared to the untreated control [manuscripts under preparation].

#### **5.2.4. Aims of Study**

This study aimed to create a proof-of-concept wound dressing to demonstrate the utility of an antimicrobial-loaded, pH-responsive system for the treatment of *S. aureus* infections within non-healing wounds where clinical intervention is needed. Experiments included:

- Investigation of the relationship between pH and *S. aureus* biofilm formation
- Development of a pH-responsive system, utilising a pH-responsive polymer EUDRAGIT® FS 30 D.
- *In vitro* release kinetics of phage K or ciprofloxacin from the pH-responsive system at pH 8.0
- Stability of antimicrobial-loaded pH-responsive system at pH 6.5
- Microbiological analysis of the antimicrobial-loaded pH-responsive system against three clinically relevant *S. aureus* species (*S. aureus* H560, MRSA252, and MSSA101).

## **5.3. Methods**

### **5.3.1. Bacterial and Bacteriophage Methods**

All methods relating to growth conditions and enumeration of *S. aureus* isolates and propagation of phage K were followed as outlined in Chapter 2, Section 2.2.1.3 and 2.2.3.1 unless otherwise stated.

### **5.3.2. Evaluation of Biofilm pH**

Biofilms were prepared as outlined in Chapter 2, Section 2.2.2.2. The pH of the developing biofilm was measured every 2 h using a flat top surface pH electrode (VWR). After each pH measurement, the biofilm was stripped and enumerated as outlined in Chapter 2, Section 2.2.1.4

### **5.3.3. Development of a pH-responsive System**

Antibiotic-loaded PLA-PEG (a-PPEG) films were prepared as outlined in Chapter 4, Section 4.3.2.1. To create the dip-coat solution, EUDRAGIT® FS 30 D was added to acetone in a ratio of 1:5 and stirred until dissolved. For dip-coating, the PPEG polymers were fully submerged in the dip-coat solution for approximately 1 s before drying at room temperature for 5 min to allow for the evaporation of acetone. This process was repeated up to a maximum of 50 times to create the pH-responsive system. After dip-coating, the films were allowed to dry for 1 h at room temperature before subsequent use.

### **5.3.4. Bacteriophage Survival**

#### **5.3.4.1. pH**

To determine if pH had an effect on phage titre, TSB was adjusted with 1 M NaOH/HCl to achieve a pH range between 2.0 – 10.0 and filter sterilised with a 0.22 µm filter before use. Stock phage lysates ( $10^9$  PFU/mL) were diluted 10-fold into the pH-adjusted TSB and incubated for 1 h at room temperature. After incubation, viable phage concentration at each pH was determined as outlined in Chapter 2, Section 2.2.3.3.

#### **5.3.4.2. Organic Solvents**

The organic solvent used in this chapter was acetone ((CH<sub>3</sub>)<sub>2</sub>CO), and the protocol was followed as in Chapter 4, Section 4.3.3.2.

### **5.3.5. *In vitro* Release Profiles**

*In vitro* release studies for phage K and ciprofloxacin were performed as described in Chapter 4, Section 4.3.5. The only modification to the assay is the pH of the buffer solution; PBS was pH-adjusted to a pH of 8.0 prior to the initiation of this experiment. Additionally, the measurements were conducted over 1 h intervals, with the final measurement occurring after 24 h incubation at 25 °C. When % cumulative release profiles were created, 100% release referred to the amount of therapeutic released from the uncoated PPEG film developed in Chapter 4. All *in vitro* release studies were carried out using three independent films.

### **5.3.6. Stability of pH-responsive System**

The stability of the films was measured as outlined in Chapter 4, Section 4.3.6, with slight modifications; PBS was pH-adjusted to a pH of 6.5 prior to the initiation of this experiment and measurements were taken at 24 h intervals over 5 days.

### **5.3.7. Colony Biofilm Wound Model**

*S. aureus* colony biofilms were prepared as outlined in Chapter 2, Section 2.2.2.2. The pH-responsive films were placed on top of the bacteria prior to incubation at 32 °C for 24 h. After incubation, the biofilms were stripped and enumerated as previously outlined (Chapter 2, Section 2.2.1.4, and 2.2.3.3).



## 5.4. Results and Discussion

### 5.4.1. pH Change in *S. aureus* Biofilms

Dr Laura Wallace from the University of Bath, UK, investigated the usefulness of pH as a trigger, conducting experiments to determine the pH of developing *S. aureus* biofilms using the modified colony biofilm model (Figure 5.2). It was hypothesised that if the pH rose to values above pH 7 before the development of an established biofilm occurred, pH could be a suitable trigger for stimuli-responsive wound dressings.

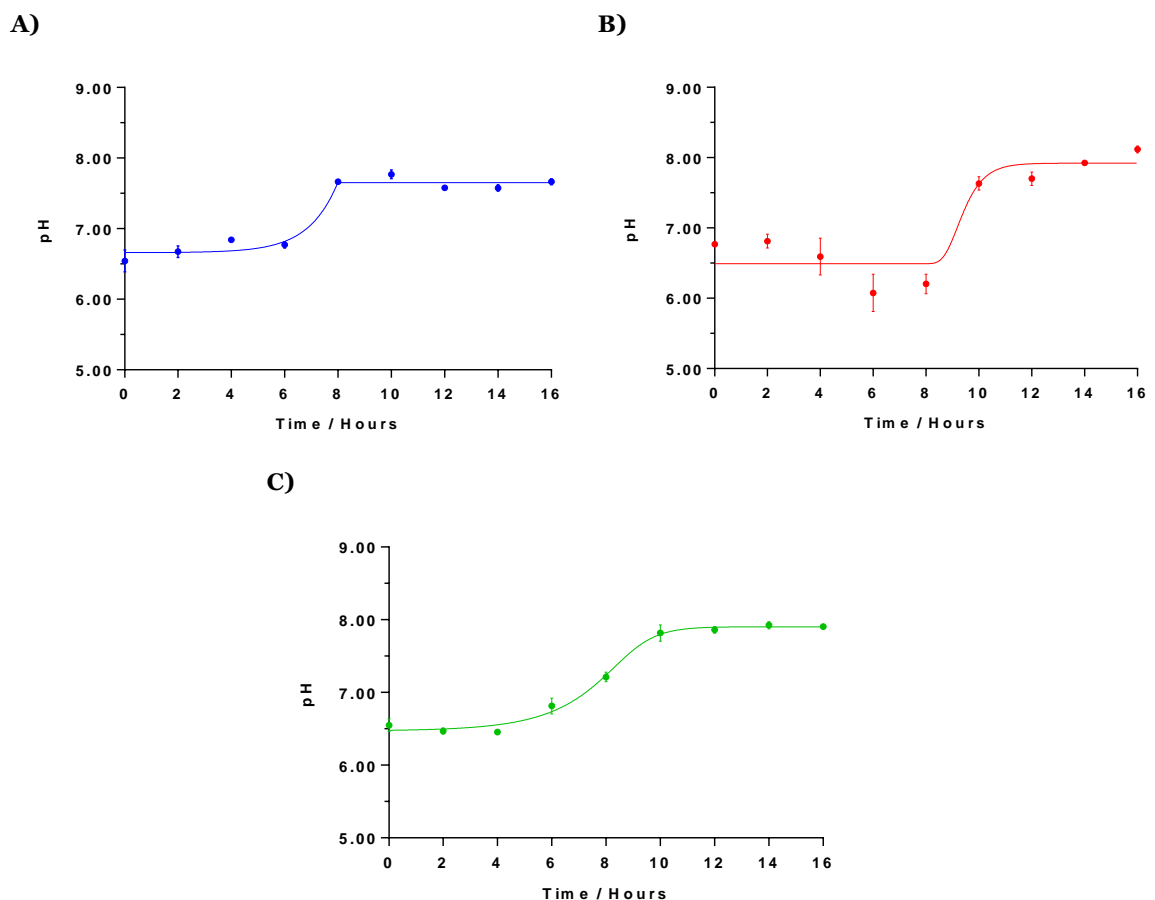


**Figure 5.2:** pH values associated with developing **A)** *S. aureus* H560, **B)** *S. aureus* MRSA252, and **C)** *S. aureus* MSSA101 biofilms. Results are shown as mean and SD, n = 3 biological replicates

The pH of *S. aureus* H560 rose above pH 7.0 after 6.8 h of biofilm development at 32 °C, corresponding to a concentration of approximately  $2.51 \times 10^4$  CFU/membrane (CFU data not shown). The pH change occurred before the exponential rise in bacterial concentration, with the final biofilm exhibiting a density of approximately  $10^{10}$  CFU/membrane and a pH of 7.66. As the pH rose before a significant increase in bacterial concentration, it can be hypothesised that the pH-responsive system could release its payload and target

metabolically active *S. aureus* H560 before the development of an established and mature biofilm.

For *S. aureus* MRSA252, the rise in pH above pH 7.0 occurred after 9.6 h of biofilm development at 32 °C, corresponding to a concentration of approximately  $3.16 \times 10^9$  CFU/membrane. Unlike *S. aureus* H560, this pH change occurred when the bacteria were approaching their stationary phase of their lifecycle, with a final bacterial concentration of approximately  $10^{10}$  CFU/membrane observed after 16 h incubation. As this pH change occurred later on in the biofilm development, further experiments were conducted to establish whether the pH-responsive system reported in this Chapter would be effective in targeting *S. aureus* MRSA252 infections; the efficacy of this system would depend on how fast the pH-responsive polymer EUDRAGIT® FS 30 D (Chapter 5, Section 5.4.2), would be able to dissolve and how quickly the reservoir PPEG film can release its therapeutic payload (see Chapter 4).

Finally, for *S. aureus* MSSA101, the pH of the biofilm rose above pH 7.0 after 7.1 h of biofilm development at 32 °C, corresponding to a concentration of approximately  $1.00 \times 10^6$  CFU/membrane. This increase in pH occurred when the bacteria were in their exponential growth phase; therefore, there may be adequate time for the pH-responsive system to release its therapeutic load before the development of an established, mature biofilm.

Although the time in which the pH increased past pH 7.0 varied, all three *S. aureus* had an alkaline biofilm pH after 16 h incubation. Therefore, pH could be used as a viable target for stimuli-responsive wound dressings that selectively release their antimicrobial payload in response to an active infection.

#### **5.4.2. EUDRAGIT®-coated Films**

In order to create a pH-responsive system, the PPEG film developed in Chapter 4 was dip-coated with a pH-responsive polymer. The pH-responsive polymer used in this study was EUDRAGIT® FS 30 D, manufactured by Evonik (Darmstadt, Germany); it is an anionic copolymer based on methyl acrylate, methyl methacrylate and methacrylic acid (Figure 5.3). EUDRAGIT® FS 30 D was chosen due to its dissolution pH value (pH 7.0) owing to the ratio of carboxyl to ester groups being 1:10.

The pH-responsive nature of EUDRAGIT® FS 30 D was due to the polymers pendent carboxyl groups. Upon increasing pH, the carboxyl groups are ionised, which results in a net overall charge of the molecule, causing the polymer to swell due to electrostatic repulsion. The solubility of the polymer further increases as the anionic centre of the

polymer is capable of forming dipole-dipole interactions with the water. The dissolution of this pH-responsive polymer allows the therapeutic within the PPEG film to be released in response to the elevated pH, subsequently eliminating *S. aureus* at the infection site.

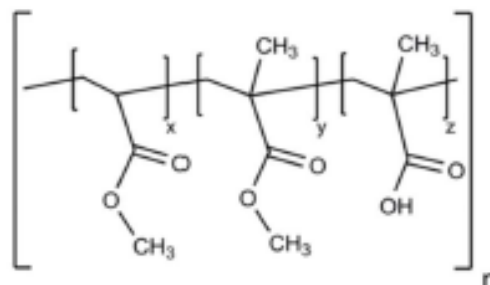


**Figure 5.3:** Chemical structure of EUDRAGIT® FS 30 D

### 5.4.3. Bacteriophage-loaded Films

#### 5.4.3.1. Bacteriophage Survival

As the antimicrobial-loaded PPEG film created in Chapter 4 was dip-coated in EUDRAGIT® FS 30 D and used for pH-sensing applications, it was imperative to determine phage K survival in the solvent system (acetone) used to create the pH-responsive polymer, and to ensure phage viability remains for pH values between pH 7.00 – 9.00.

Upon incubation with varying concentrations of acetone (% v/v) for 1 h, phage K concentration remained comparable to the control (phage K in PBS) up to acetone concentrations of 40%. Past this point, there was a significant decrease in phage viability compared to the control, resulting in log reductions of 0.45 (One-way ANOVA,  $p < 0.01$ ), 1.27 (One-way ANOVA,  $p < 0.0001$ ), and 4.05 (One-way ANOVA,  $p < 0.0001$ ) for acetone concentrations of 60, 80 and 90%, respectively (Figure 5.4A). These results suggest that phage K viability might be affected by the dip-coating process; therefore, this may result in a reduction in the phage K being successfully released from the film. However, the dip-coating process only requires minimal contact with acetone, and the solvent is fully evaporated before subsequent emersions in the solvent, which could minimise the negative effect of acetone on phage K viability. Owing to this, further experiments were conducted to evaluate phage K release from the pH-responsive system and the results were compared to that observed from the uncoated PPEG films (Chapter 5).

In literature, phage have been shown to be tolerant to a wide range of pH values,<sup>63,67</sup> so it is no surprise that phage K viability was stable in pH-adjusted TSB pH 6.0 – 8.0 (Figure 5.4B). While pH 4.0 and pH 10.0 resulted in a significant decrease in phage titre (log reductions of 0.78 and 0.79, respectively; One-way ANOVA,  $p < 0.001$  vs pH 7.0 control) these decreases in titre were not clinically significant and could, in part, be due to external factors such as human error within the methodology. At extreme pH values there was a clinical and significant decrease in phage K titre, with a log reduction of 6.36 observed for both pH 2.0 and pH 12.0 when compared to the control (pH 7.0). This decrease in phage K titre reached the limit of detection of this assay. However, as chronic wounds only rise to pH 8.0 – 9.0, phage K was deemed a suitable therapeutic as it was still viable within this pH range.

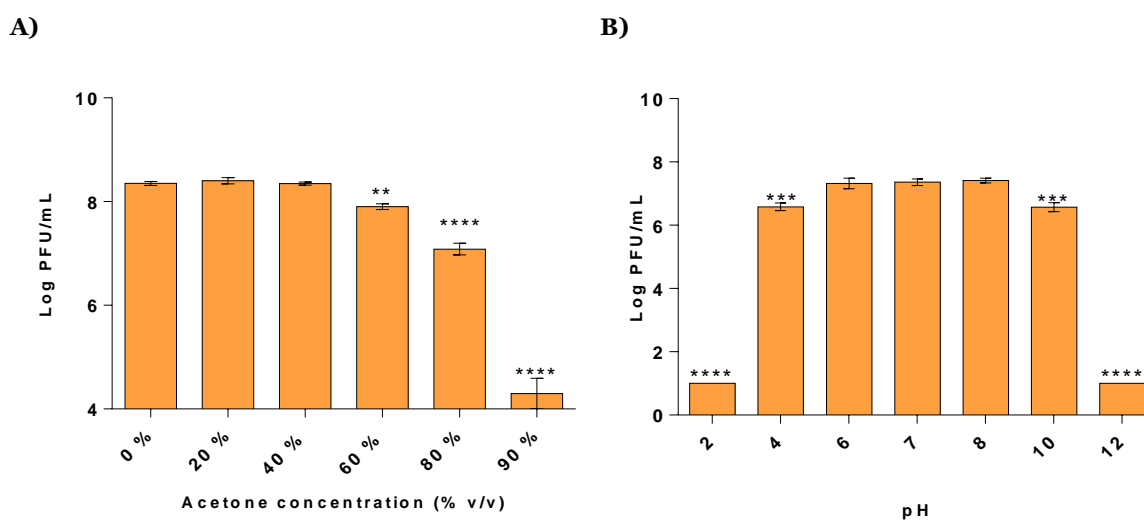


**Figure 5.4:** Phage K survival in the presence of **A)** increasing concentrations of acetone (in PBS), and **B)** increasing pH of TSB.  $n = 3$ , error bars indicate standard deviation. Statistical analysis conducted using a One-way ANOVA. \*  $p < 0.05$ , \*\*  $p < 0.01$ , \*\*\*  $p < 0.001$ , \*\*\*\*  $p < 0.0001$

### 5.4.3.2. *In vitro* release

The PPEG system developed in Chapter 4 was subjected to 50 dip-coat layers of EUDRAGIT® FS 30 D to successfully entrap both phage K and ciprofloxacin (see Section 5.4.4). Owing to this, *in vitro* release studies were carried out over a 24 h period to determine the release kinetics of phage K from the pH-responsive polymer in PBS at pH 8.0.

The resultant release profiles are shown in Figure 5.5. There was a slow release of phage K from the pH-responsive system into the PBS (pH 8.0) over the course of 24 h. After 1 h, 4.0 log PFU/mL of phage K were released from the system, rising to 5.73 log PFU/mL after 7 h incubation in PBS (pH 8.0). After 24 h, 7.62 log PFU/mL of phage K was released, corresponding to 91.89% release compared to phage released from the uncoated PPEG film.

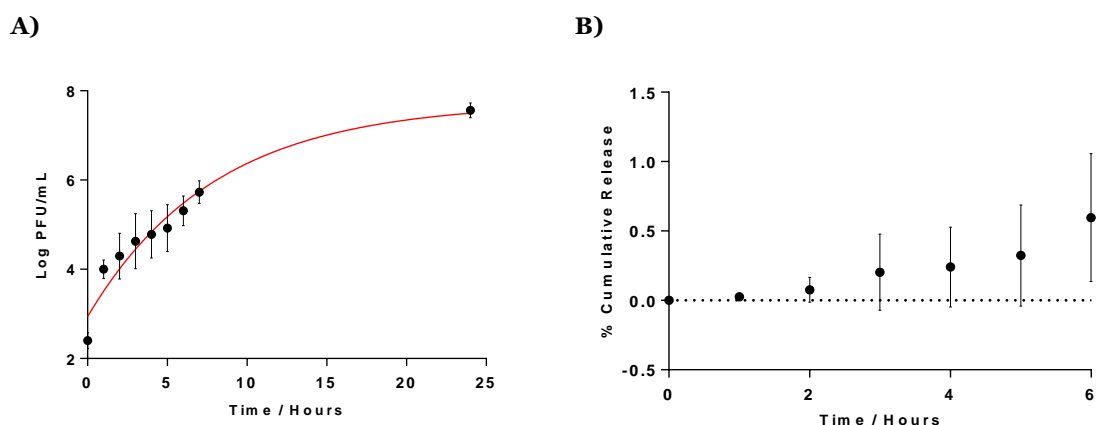


**Figure 5.5:** **A)** Log PFU/mL and **B)** % Cumulative release *in vitro* release profiles of phage K from the pH-responsive films in PBS (pH 7.4, 25 °C). n = 3, error bars indicate standard deviation. 100% cumulative release refers to the density of phage K released from the uncoated PPEG film

Next, mathematical models were used to evaluate the release kinetics of the pH-responsive system for phage K release. According to Table 5.1, the release profile with the best fit was Korsmeyer-Peppas. However, measurements for the *in vitro* release kinetics were only undertaken for the first 7 hours and as such, the experiment should be repeated to take more measurements over a longer time period to obtain a more accurate release profile, as the R<sup>2</sup> values obtained in Table 5.1 are very low.

The Korsmeyer-Peppas model is a semi-empirical model that is used to describe drug release from polymeric systems and is a useful model for the study of polymeric systems where the release mechanism is unknown or when there is more than one type of drug release involved. The equation used for the Korsmeyer-Peppas model is as follows:

$$\log \frac{M_{(i-l)}}{M_{\infty}} = \log K + n \log(t - l) \quad (12)$$

Where  $M_{\infty}$  is the amount of drug at the equilibrium state,  $M_i$  is the amount of drug released over time  $t$ ,  $K$  is the release velocity constant,  $n$  is the exponent of release in function of time  $t$  and  $l$  is the latency time.

To accurately determine  $n$ , it is recommended to use the portion of release curve until the point where  $M_i/M_{\infty} < 0.60$ . When  $n > 1$ , as it is for this system, it describes the Super Case II model of release, whereby during the sorption process there is concurrent breaking of the polymer chains (termed solvent crazing). Super Case II transport has been shown for planar

structures such as thin films and is observed when the solvent has a high affinity to the matrix. As a consequence, there is a rapid penetration of the solvent into the centre of the matrix.<sup>68</sup>

**Table 5.1:** Kinetic model and corresponding R<sup>2</sup> value for the release of ciprofloxacin from a pH-responsive system (PBS, pH 8.0)

Kinetic Model	R <sup>2</sup> value
Zero order	0.4908
First order	0.4896
Higuchi	0.3541
Korsmeyer-Peppas	0.6116
Hixson-Crowell	0.4911

### 5.4.3.3. Stability

To ensure that the pH-responsive system did not release phage K at pH values <7.0, phage K-loaded pH-responsive films were submerged in 2 mL of PBS (pH 6.5) for a maximum of 5 days at room temperature and assessed for the presence of phage release daily (Figure 5.6).

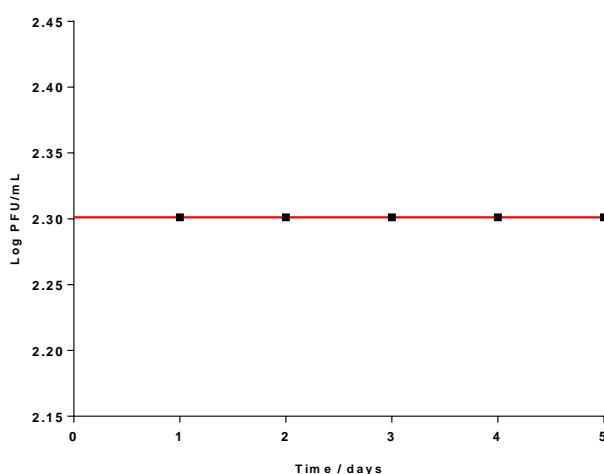


**Figure 5.6:** Log PFU/mL of phage K released from the pH-responsive system upon incubation in PBS, pH 6.5 for up to 5 days at 25 °C. n = 3 and error bars indicate standard deviation. The limit of detection of this assay was 2.33 Log PFU/mL

As shown in Figure 5.6, there was no detectable release of phage K from the polymer system over 5 days, with any release of phage K lower than the limit of detection of the assay. This result demonstrates the pH-responsiveness of the system, as phage K have been shown to be stable in the PPEG system for up to 5 days, with no loss in cell viability (Chapter 4). Additionally, this result demonstrates the utility of this system as a wound dressing, as often

they are left *in situ* for 5 – 7 days; hence, if the wound remains uninfected then the wound dressing would not release phage K into the surrounding environment.

#### **5.4.3.4. Colony Biofilm Wound Models**

As the *in vitro* release results suggested that phage K can be successfully released from the pH-responsive system at pH 8.0, the next step was to assess this system in treating developing *S. aureus* infections. Similarly to the biofilms tested in Chapter 4, a modified colony biofilm model was used where the film was placed onto developing *S. aureus* biofilms on polycarbonate membranes and incubated at 32 °C for 24 h (Figure 5.7).

For all three bacterial isolates tested, there was no significant difference in bacterial viability when the bacterial isolates were incubated with un-loaded pH-responsive films compared to the biofilm only control; therefore, any reduction in bacterial biomass could be attributed to the release of phage K from the pH-responsive film.

When phage K was encapsulated within the pH-responsive film, a significant log reduction of 1.96 was observed in *S. aureus* H560 biofilm density compared to the control (One-way ANOVA,  $p < 0.0001$ ). Likewise, a 1.14 log reduction was observed when the phage K-encapsulated pH-responsive films were incubated with *S. aureus* MSSA101 compared to the control (One-way ANOVA,  $p < 0.01$ ). However, when *S. aureus* MRSA252 was incubated with phage K-encapsulated pH-responsive films, a log reduction of 0.46 in biofilm density was observed compared to the control. While this result was significant (One-way ANOVA,  $p < 0.01$ ), the log reduction is not clinically useful as it could be due to external factors such as human error within the experimental methodology.

While the log reductions in bacterial density of *S. aureus* H560 and *S. aureus* MSSA101 corresponded to a 90 – 99% reduction in viable cells, it does not meet the recommended  $\geq 3$  log reduction outlined in prEN16756, and therefore this system cannot be considered antimicrobial against all three bacterial isolates tested.

One reason for this decrease in antimicrobial efficacy compared to the uncoated PPEG films (Chapter 4) could be due to the difference in the release profile of this pH-responsive system. Release of phage K from the pH-responsive system is not as fast compared to the PPEG film, consequently, it would take longer for the phage to reach sufficient concentrations required to infect and lyse the bacterial cells. This could be the reason why the worst results were observed for *S. aureus* MRSA252, even though this bacterial strain was the most susceptible towards the phage loaded-PPEG films evaluated in Chapter 4. By the time the pH change had occurred, *S. aureus* MRSA252 would have been towards the

end of its exponential growth, after which there would be a delay in phage K reaching the bacteria. As phage are less successful in targeting stationary-phase bacteria, this could explain why only a 0.46 log reduction in bacterial density was observed for this pH-responsive system. Likewise, it could explain why the phage K loaded pH-responsive films were more effective towards *S. aureus* H560, as the pH rise above pH 7.0 occurred earlier in the growth cycle, allowing more time for the phage K to be released from the system and target metabolically active cells.

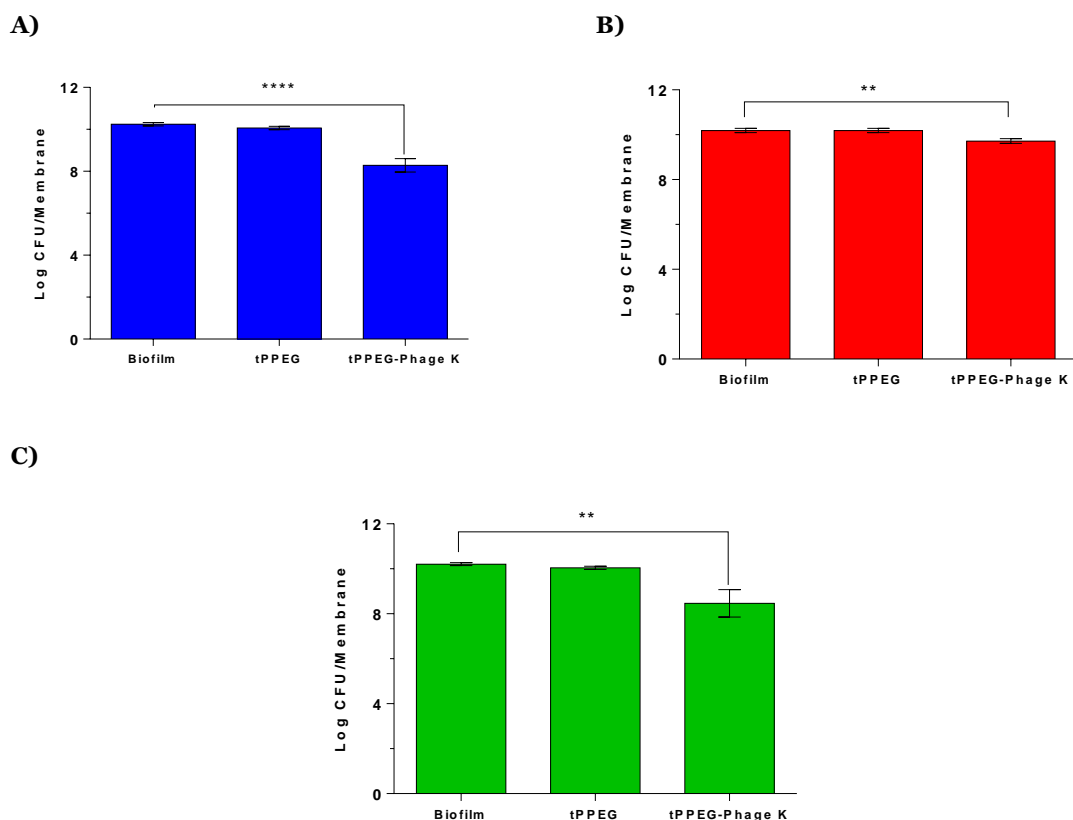


**Figure 5.7:** Log CFU/membrane counts of **A)** *S. aureus* H560, **B)** *S. aureus* MRSA252, and **C)** *S. aureus* MSSA101 biofilms upon incubation with pH-responsive systems (tPPEG) and phage K-loaded pH-responsive systems (tPPEG-phage K) 24 h at 32°C. n = 3, error bars indicate standard deviation. Statistical analysis conducted using a One-way ANOVA. \*p<0.05, \*\*p<0.01, \*\*\*p<0.001, \*\*\*\*p<0.0001

The corresponding phage counts are outlined in Figure 5.8. The phage K concentration was highest when the film was incubated with *S. aureus* H560, and lowest when incubated with *S. aureus* MRSA252. This is in line with the efficacy witnessed against these bacterial strains (Figure 5.7); hence, it could be hypothesised that the phage K-loaded pH-responsive film was more effective towards *S. aureus* H560 as it was able to multiply at the infection site, resulting in a reduction in bacterial cell density. However, only three bacterial strains have been used in this assay, so to further understand the relationship between pH, biofilm



formation, and effective phage release from the system – further repeats of these experiments must be undertaken.

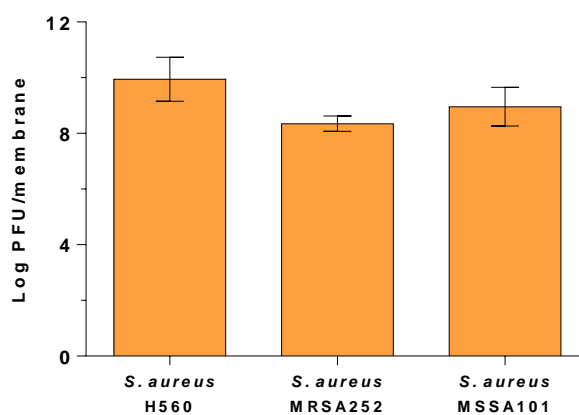


**Figure 5.8:** Log PFU/membrane counts of phage K released from the pH-responsive film after incubation with *S. aureus* H560, MRSA252, and MSSA101 biofilms for 24 h at 32°C. n = 3, error bars indicate standard deviation

## 5.4.4. Ciprofloxacin-loaded Films

### 5.4.4.1. Thickness of pH-responsive Layer

It was important to ensure that the pH-responsive EUDRAGIT® FS 30 D layer was of sufficient thickness to prevent any passive diffusion of ciprofloxacin through the system into the external environment. Owing to this, ciprofloxacin-loaded PPEG films were dip-coated 0 – 50 times in EUDRAGIT® FS 30 D before subsequent emersion in 2 mL PBS (pH 6.5) for 24 h at 25 °C. All ciprofloxacin concentrations were determined using UV-Vis and the appropriate calibration curves.

Upon increasing layers of EUDRAGIT® FS 30 D, there was a decrease in ciprofloxacin passively released from the pH-responsive films at pH 6.5, with a 92.43% reduction in release compared to the uncoated control for 20 layers, rising to 98.48% with 50 layers (Figure 5.9). As 50 layers resulted in a minimal non-specific release of ciprofloxacin, this was the thickness chosen for all experiments conducted.

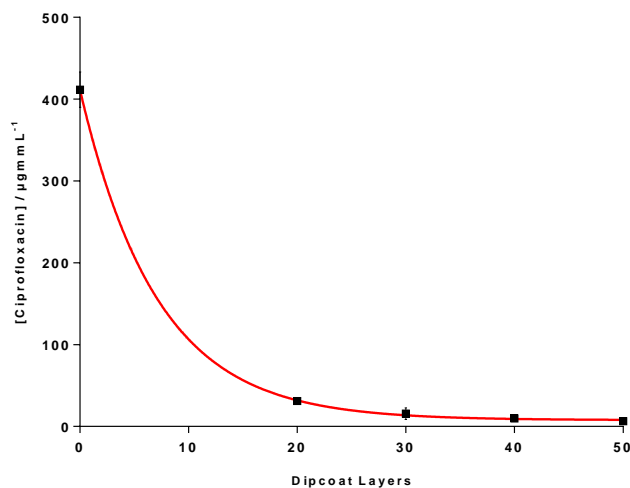


**Figure 5.9:** Concentration of ciprofloxacin released from pH-responsive systems with increasing EUDRAGIT® FS 30 D layers, incubated in 2 mL PBS (pH 6.5) for 24 h at 25 °C. n = 3, error bars indicate standard deviation

#### 5.4.4.2. *In vitro* Release

Next, the *in vitro* release kinetics was determined for ciprofloxacin release from pH-responsive films in pH (pH 8.0) at 25 °C. As shown in Figure 5.10, there was a gradual release of ciprofloxacin from the film, with 6.14% of ciprofloxacin released after 30 minutes, rising to 10.94% and 30.62% after 1 and 4 h, respectively. After 19 h, 42.02% of ciprofloxacin was released from the film, where 100% was defined as the concentration of ciprofloxacin released from the uncoated PPEG film ( $411.67 \pm 21.62 \mu\text{g/mL}$ ; Chapter 4).

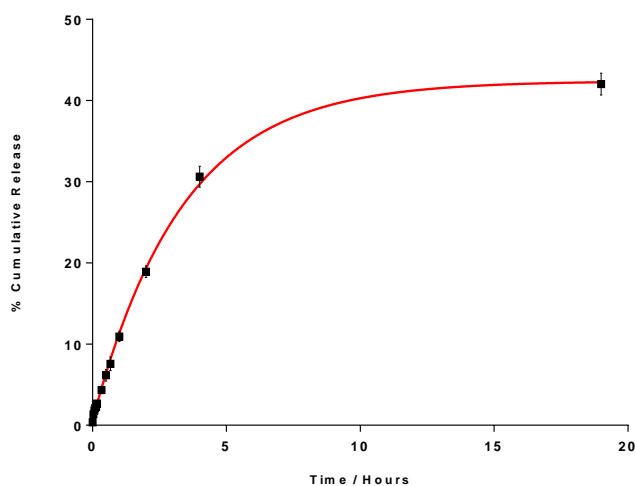


**Figure 5.10:** *In vitro* % cumulative release profile of ciprofloxacin from pH-responsive films in PBS (pH 8.0, 25 °C). n = 3, error bars indicate standard deviation. 100% cumulative release refers to the concentration of ciprofloxacin released from the uncoated PPEG film

Next, mathematical models were used to evaluate the release kinetics of the pH-responsive system for ciprofloxacin release. According to Table 5.2, the release profile with the best fit

was first-order kinetics, but it is interesting to note that for Korsmeyer-Peppas, the n value obtained was 0.577, which suggests non-fickian diffusion; therefore, there was an element of polymer swelling and erosion.

**Table 5.2:** Kinetic model and corresponding R<sup>2</sup> value for the release of ciprofloxacin from a pH-responsive system (PBS, pH 8.0)

<b>Kinetic Model</b>	<b>R<sup>2</sup> value</b>
Zero order	0.9857
First order	0.9950
Higuchi	0.9614
Korsmeyer-Peppas	0.9795
Hixson-Crowell	0.9857

In first order kinetics, the rate is directly proportional to the concentration of drug, i.e., the higher the concentration of drug, the faster the reaction, and can be expressed using the following equation:<sup>68</sup>

$$\frac{DC}{dt} = K_i C \quad (13)$$

Where K<sub>i</sub> is the first order rate constant, expressed as time<sup>-1</sup>.

The equation can be further derived to:

$$\log Q_1 = \log Q_0 + \frac{K_i t}{2.303} \quad (14)$$

Where Q<sub>1</sub> is the amount of active agent released on time *t*, Q<sub>0</sub> is the initial amount of drug dissolved, and K<sub>i</sub> is the first-order constant.

Equation 14 corresponds to linear kinetics, and the graph of log (% drug remaining) versus time would result in a straight line, with an angular coefficient of K<sub>i</sub>/2.303 and a linear coefficient equal to log Q<sub>0</sub>.<sup>68</sup>

#### **5.4.4.3. Stability**

Similarly to phage-loaded pH-responsive films, experiments were undertaken to determine the stability of the ciprofloxacin-loaded pH-responsive films at pH 6.5. These films were submerged in 2 mL of PBS (pH 8.0) for a maximum of 5 days at room temperature and the solution was assessed for the presence of ciprofloxacin daily. In this instance, 100%

cumulative release was the concentration of ciprofloxacin released from the un-coated PPEG film ( $411.67 \pm 21.62 \mu\text{g/mL}$ ; Chapter 4).

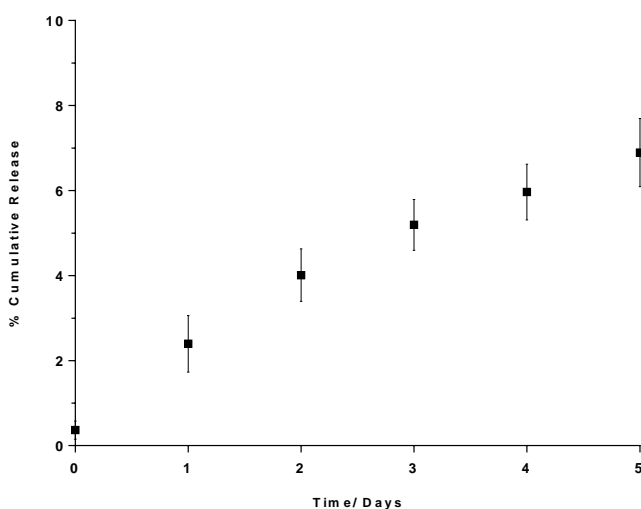


**Figure 5.11:** % Cumulative release of ciprofloxacin from the pH-responsive system upon incubation in PBS, pH 6.5 for up to 5 days at 25 °C. n = 3 and error bars indicate standard deviation. 100% cumulative release refers to the concentration of ciprofloxacin released from the uncoated PPEG film

The results show that there was minimal passive diffusion of ciprofloxacin at pH 6.50, with only 6.89% of ciprofloxacin released after 5 days incubation (corresponding to  $16.42 \mu\text{g/mL}$ ). Therefore, it can be concluded that the pH-responsive film only releases its therapeutic load in response to an increase in pH above pH 7.0. Further experiments could be conducted in the future to reduce the amount of passive diffusion from the film, but this may alter the film and subsequently reduce the efficacy of the film against *S. aureus* biofilms.

#### 5.4.4.4. Colony Biofilm Wound Models

The effectiveness of ciprofloxacin-loaded pH-responsive films were investigated against developing *S. aureus* biofilms (Figure 5.12).

As seen for phage-loaded pH-responsive films, there was no significant difference in bacterial viability when the bacterial isolates were incubated with un-loaded pH-responsive films compared to the biofilm only control for all bacterial isolates tested; therefore, any reduction in bacterial biomass could be attributed to the release of ciprofloxacin from the pH-responsive film. For *S. aureus* H560, there was a statistically significant log reduction in bacterial density compared to the biofilm control (log reduction of 3.13; One-way ANOVA,  $p < 0.0001$ ). This log reduction was similar to that observed for the uncoated PPEG

film (Chapter 4) and met the recommended  $\geq 3$  log reduction outlined in prEN 16756; therefore, this system can be considered antimicrobial against *S. aureus* H560.

For *S. aureus* MRSA252, there was a statistically significant log reduction in bacterial density observed upon incubation with the ciprofloxacin-loaded pH-responsive film (log reduction of 1.23; One-way ANOVA,  $p < 0.0001$ ). This result was similar to that observed for the uncoated PPEG film (Chapter 4). Similarly, there was a significant log reduction in *S. aureus* MSSA101 bacterial density upon incubation with ciprofloxacin-loaded pH-responsive system (log reduction 2.45; One-way ANOVA,  $p < 0.0001$ ); however this was one log lower than what was observed for the uncoated PPEG film (3.49, Chapter 4). These log reductions do not meet the criteria outlined in prEN 16756; therefore this system cannot be considered antimicrobial against *S. aureus* MRSA252 and MSSA101.

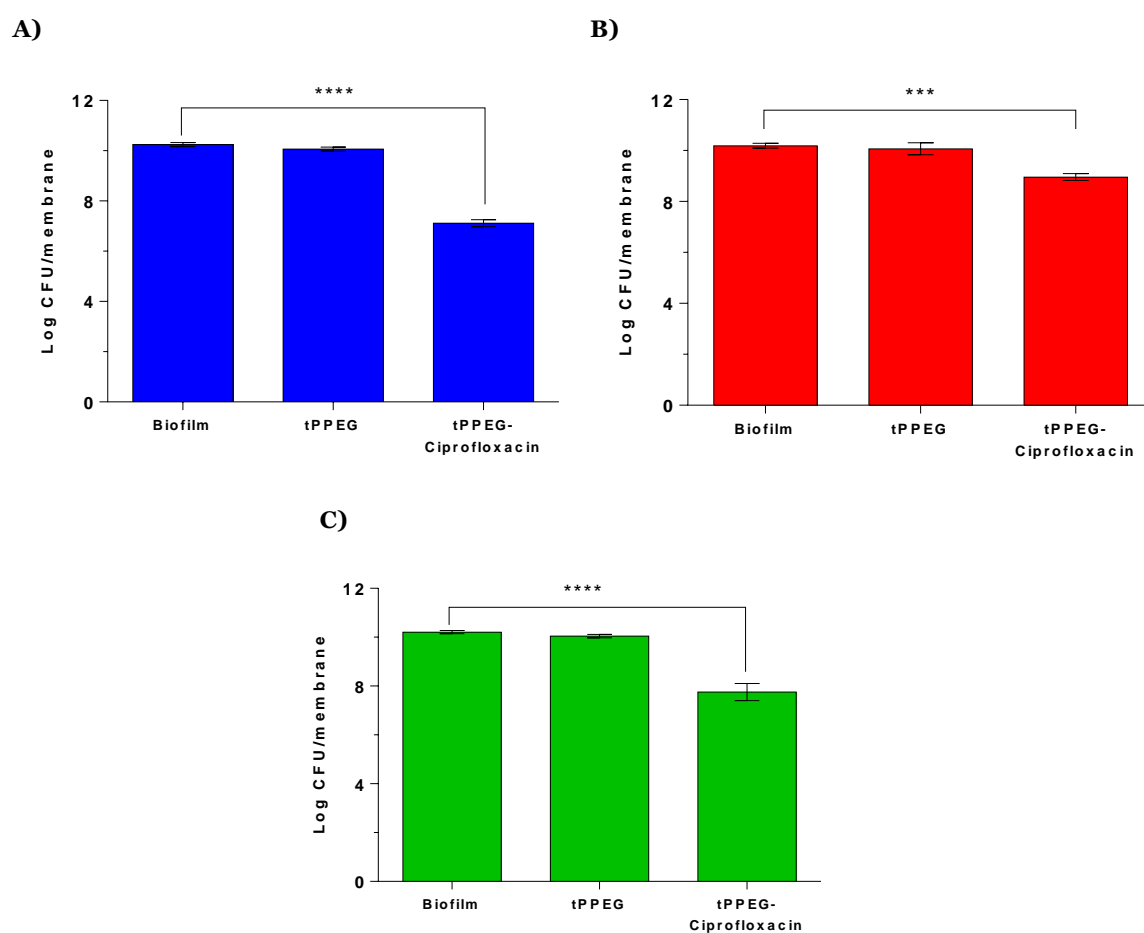


**Figure 5.12:** Log CFU/membrane counts of **A)** *S. aureus* H560, **B)** *S. aureus* MRSA252, and **C)** *S. aureus* MSSA101 biofilms upon incubation with pH-responsive systems (tPPEG) and ciprofloxacin-loaded pH-responsive systems (tPPEG-ciprofloxacin) for 24 h at 32°C. n = 3, error bars indicate standard deviation. Statistical analysis conducted using a One-way ANOVA. \* $p < 0.05$ , \*\* $p < 0.01$ , \*\*\* $p < 0.001$ , \*\*\*\* $p < 0.0001$

## 5.4.5. Combination-loaded Films

### 5.4.5.1. Stability

To ensure that the pH-responsive system did not release phage K and ciprofloxacin at pH values <7.0, the antimicrobial-loaded pH-responsive films were submerged in 2 mL of PBS (pH 6.5) for a maximum of 5 days at room temperature and the solution assessed for the presence of phage K and ciprofloxacin daily.

As shown in Figure 5.13, there was no detectable release of phage K from the polymer system over 4 days, with any release of phage K lower than the limit of detection of the assay. At day 5, there was an observable increase in phage K concentration within the solution; however, it only corresponded to an average increase of 0.3 log PFU/mL. As this release is minimal, the film was deemed sufficient for this proof-of-concept, pH-responsive design as the polymer became unstable towards the end of its therapeutic lifetime.

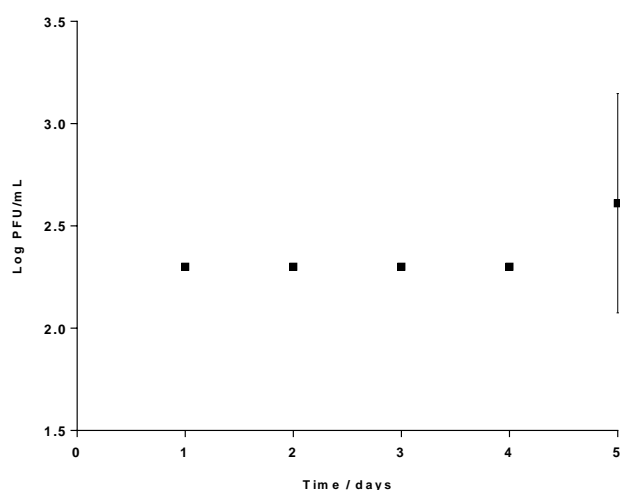


**Figure 5.13:** Log PFU/mL of phage K released from the pH-responsive system upon incubation in PBS, pH 6.5 for up to 5 days at 25 °C. n = 3 and error bars indicate standard deviation. The limit of detection of this assay was 2.33 Log PFU/mL

There was no difference in stability of ciprofloxacin within the pH-responsive systems when encapsulated with phage K compared to without (Figure 5.11 vs Figure 5.14). After 5 days incubation in PBS (pH 6.5) there was 7.76% release of ciprofloxacin from the system (corresponding to a mean ciprofloxacin concentration of 31.93 µg/mL).

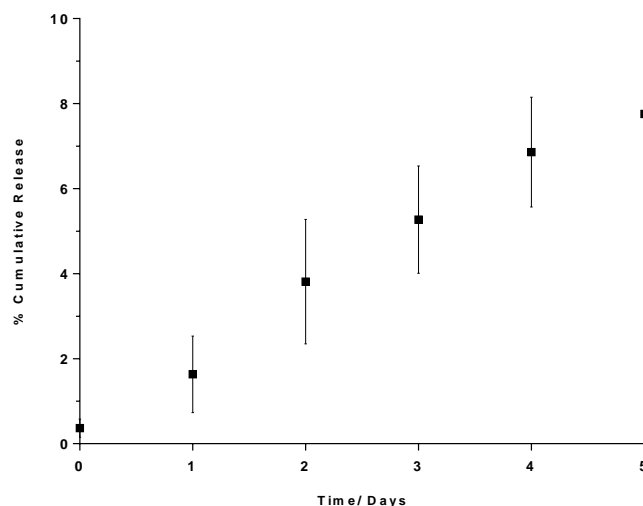


**Figure 5.14:** % Cumulative release of ciprofloxacin from the pH-responsive system upon incubation in PBS, pH 6.5 for up to 5 days at 25 °C. n = 3 and error bars indicate standard deviation. 100% cumulative release refers to the concentration of ciprofloxacin released from the uncoated PPEG film

#### 5.4.5.2. Colony Biofilm Wound Models

The efficacy of the phage K and ciprofloxacin-loaded pH-responsive films were evaluated against developing *S. aureus* biofilms (Figure 5.15).

As mentioned previously, there was no significant difference in bacterial viability when the bacterial isolates were incubated with un-loaded pH-responsive films compared to the biofilm only control for all bacterial isolates tested; therefore, any reduction in bacterial biomass could be attributed to the release of ciprofloxacin or phage from the pH-responsive film.

For *S. aureus* H560, there was a significant log reduction in bacterial biomass compared to the control (log reduction of 1.89; One-way ANOVA,  $p < 0.0001$ ); this was similar to what was observed for the uncoated PPEG films (log reduction of 1.19; Chapter 4). There was also a significant log reduction in *S. aureus* MSSA101 biofilm biomass upon incubation with the phage K and ciprofloxacin-loaded pH-responsive films (log reduction of 2.04; One-way ANOVA,  $p < 0.001$ ); this was less effective than the uncoated PPEG film (log reduction of 3.23; Chapter 4), probably due to the delay in treatment while waiting for the pH of the biofilm to rise to a pH above 7.0.

Finally, for *S. aureus* MRSA252 there was a log reduction of 0.89 in bacterial biomass compared to the control; however, this reduction was not statistically significant. As the uncoated PPEG film containing phage K and ciprofloxacin resulted in a 2.22 log reduction, the difference in bacterial density could be attributed to the delay in the release of the

therapeutic because of the slow release profile and the late-stage pH increase in *S. aureus* MRSA252 biofilms.

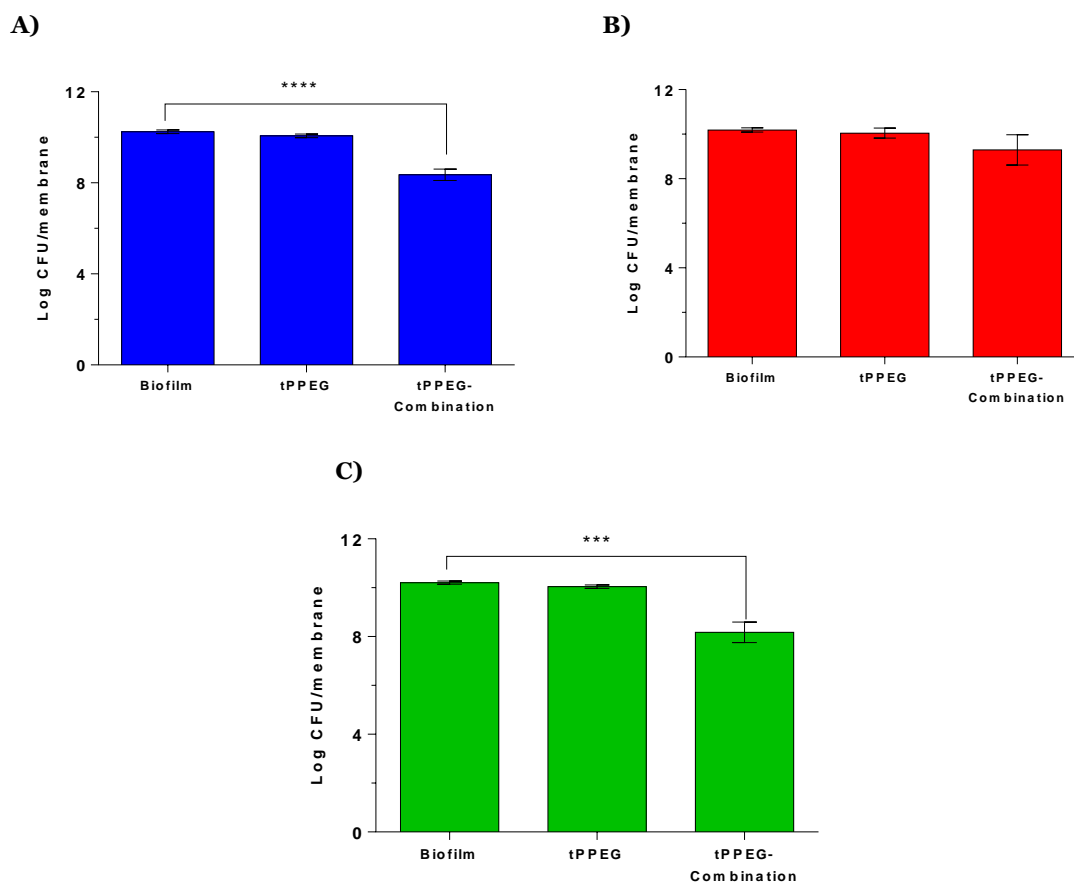


**Figure 5.15:** Log CFU/membrane counts of **A)** *S. aureus* H560, **B)** *S. aureus* MRSA252, and **C)** *S. aureus* MSA101 biofilms upon incubation with pH-responsive systems (tPPEG) and phage K and ciprofloxacin-loaded pH-responsive systems (tPPEG-combination) for 24 h at 32°C. n = 3, error bars indicate standard deviation. Statistical analysis conducted using a One-way ANOVA. \*p<0.05, \*\*p<0.01, \*\*\*p<0.001, \*\*\*\*p<0.0001

Furthermore, mixed-model analysis can be performed on the Log CFU/mL counts to determine the nature of the interaction between the antibiotic and phage within the combination therapy (synergistic, additive, or antagonistic), as described by Kumaran *et al.*<sup>69</sup> The equation used to determine this interaction is shown below (Equation 15):

$$COEF_{int} = \log_{10}(AB^R) - (\log_{10}(A^R) + \log_{10}(B^R)) \quad (15)$$

$COEF_{int}$  is the co-efficient of the interaction,  $AB^R$  is the reduction in bacterial counts followed by the combined treatment (AB),  $A^R$  is the reduction on bacterial counts due to treatment A and  $B^R$  is the reduction in bacterial counts due to treatment B.



An interaction was defined as being synergistic if the value  $> 0$ , additive if the value  $= 0$ , and antagonistic when the value  $< 0$ . The calculated co-efficients for this assay are shown in Table 5.3.

The calculated co-efficients highlight the results obtained in Figure 5.15, for all bacterial isolates tested the combination of phage K and ciprofloxacin resulted in an antagonistic interaction as all co-efficient values are negative. Further optimisation assays, i.e., altering the concentrations of phage K and ciprofloxacin could be conducted in the future to investigate whether it would be possible to achieve PAS within this pH-responsive system.

**Table 5.3:** Co-efficient of the interaction between phage K and ciprofloxacin from mixed-model analysis. An interaction was defined as being synergistic if the value  $> 0$ , additive if the value  $= 0$ , and antagonistic when the value  $< 0$

Bacterial strain	Co-efficient
<i>S. aureus</i> H560	-3.20
<i>S. aureus</i> MRSA252	-0.81
<i>S. aureus</i> MSSA101	-2.15

The corresponding phage concentrations are shown in Figure 5.16. There is a marked decrease in phage concentration compared to the phage K released in the monotherapy pH-responsive polymer (Figure 5.8), especially for *S. aureus* MRSA252 and MSSA101, which yielded phage concentration below the limit of detection of the assay.

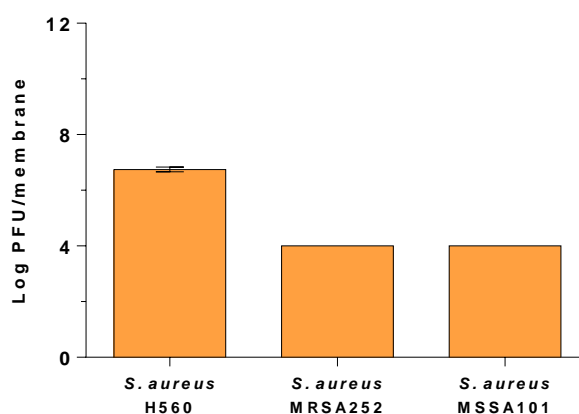


**Figure 5.16:** Log PFU/membrane counts of phage K released from the pH-responsive film after incubation with *S. aureus* H560, MRSA252, and MSSA101 biofilms for 24 h at 32°C. n = 3, error bars indicate standard deviation

This result could be due to the release profiles of phage K and ciprofloxacin being different, with ciprofloxacin releasing at a faster rate compared to phage K. As briefly mentioned in

Chapter 3 and Chapter 4, phage-antibiotic synergy has been shown to be dependent on the release of both antimicrobials, with greater PAS witnessed when phage is released prior to the conventional antimicrobial to allow time for effective phage replication. Therefore, the antagonistic effect observed in the combination therapy (Figure 5.15) could be due to the fact that ciprofloxacin was the first antimicrobial to reach the *S. aureus* infection, eliminating the bacterial cells before phage K has a chance to launch a successful attack. Therefore, further work would need to be conducted to investigate the optimal concentrations of phage K and ciprofloxacin loaded into the pH-responsive system in order for PAS to be witnessed.

## 5.4. Conclusions and Future Work

This proof-of-concept study demonstrated the utility of pH-responsive wound dressings for the treatment of developing *S. aureus* infections. This chapter found that pH could be used as a possible release trigger, as all three *S. aureus* isolates tested were shown to have an increase in pH upon biofilm formation. However, to ensure that it is possible to generalise this statement to all *S. aureus* isolates, further experiments should be conducted to measure the pH change in biofilm formation of multiple *S. aureus* strains.

The PLA-PEG (PPEG) film encapsulating phage K and/or ciprofloxacin were dip-coated with 50 layers of EUDRAGIT® FS 30 D to prevent the non-triggered passive release of the therapeutics from the pH-responsive system. This coating prevented the release of phage K, and resulted in minimal release of ciprofloxacin, for 5 days at pH 6.5 – a pH lower than the dissolution value of EUDRAGIT® FS 30 D.

When incubated at pH 8.0, the release profiles of phage K and ciprofloxacin were different, with phage K exhibiting Korsmeyer-Peppas release, while ciprofloxacin resulted in faster, first-order release. While both release models are diffusion-based, the difference in release profiles could be due to the relative size of the antimicrobials; phage K is much larger in comparison to ciprofloxacin, hence the release from the matrix is dependent on the polymer eroding and creating larger pores to allow for phage diffusion into the surrounding environment. Conversely, ciprofloxacin is smaller, so the polymer doesn't need to degrade to the same extent to allow for ciprofloxacin to be released from the matrix into the surrounding environment. However, the release profile obtained for phage K should be repeated to confirm this result, as the  $R^2$  values calculated from the mathematical modelling were low, lowering the confidence in this result.

Finally, these pH-responsive polymers were tested against three developing *S. aureus* biofilms. While the efficacy of the monotherapies encapsulated within the pH-responsive system were lower than those observed for the non-triggered PPEG system, the films still displayed a significant reduction in bacterial biomass.

In order to try and improve the efficacy of the pH-responsive film, a combination of phage K and ciprofloxacin was used at the same loading concentrations as the monotherapies. Unfortunately, the combination was not able to increase the efficacy of the system, in fact the combination displayed an antagonistic interaction. This was thought to be due, in part, to the slower release of phage K from the system compared to the ciprofloxacin, preventing the phage from being able to act effectively.

Finally, it would be useful to have a system that utilises the phage K – ciprofloxacin PAS observed in Chapter 3, to minimise the spread of antibiotic resistance. Owing to this, several studies could be conducted to improve the efficacy of the combination. Firstly, investigations should be carried out to determine the effect of different loading concentrations of ciprofloxacin and phage K. Additionally, it could be possible to create a modified wound dressing, whereby the individual therapies are contained within their own pH-responsive system, and then combined to create the wound dressing. The advantage of this approach is less Eudragit® FS 30 D coating on the phage pH-responsive polymer; as phage are larger molecules, a thinner coating would be needed for complete encapsulation. Owing to this, the release of phage K from the polymer would be quicker, increasing the efficacy of the combination of phage K and ciprofloxacin by potentially producing a synergistic effect, resulting in a greater reduction in *S. aureus* biofilm density.

Overall, these results show that pH can be used as a trigger for the selective release of antimicrobials from a pH-responsive system. Additionally, the antimicrobial-loaded pH-responsive systems were capable of reducing *S. aureus* biofilm density, both as a monotherapy and as a combination therapy. While further work must be carried out to optimise these films, this Chapter has demonstrated their utility as an antimicrobial wound dressing. Furthermore, this system can be optimised to contain different antimicrobials to treat a variety of different microbial infections, it is not limited to *S. aureus* infections or phage K and ciprofloxacin as antimicrobials.

## 5.5. References

1. LibreTexts C. The pH Scale [Internet]. [cited 2021 Jan 2]. Available from: [https://chem.libretexts.org/Bookshelves/Physical\\_and\\_Theoretical\\_Chemistry\\_Textbook\\_Maps/Supplemental\\_Modules\\_\(Physical\\_and\\_Theoretical\\_Chemistry\)/Acids\\_and\\_Bases/Acids\\_and\\_Bases\\_in\\_Aqueous\\_Solutions/The\\_pH\\_Scale](https://chem.libretexts.org/Bookshelves/Physical_and_Theoretical_Chemistry_Textbook_Maps/Supplemental_Modules_(Physical_and_Theoretical_Chemistry)/Acids_and_Bases/Acids_and_Bases_in_Aqueous_Solutions/The_pH_Scale)
2. Heuss E. Die reaktion des schweisses beim gesunden menschen. *Menschen Monast Prakt Dermatol*. 14th ed. 1892;14(341):400–501.
3. Du Plessis EM, Theron J, Joubert L, Lotter T, Watson TG. Characterization of a phosphatase secreted by *Staphylococcus aureus* strain 154, a new member of the bacterial class C family of nonspecific acid phosphatases. *Syst Appl Microbiol*. 2002;25(1):21–30.
4. du Plessis JL, Stefaniak AB, Wilhelm K-P. Measurement of skin surface pH. In: *pH of the Skin: Issues and Challenges*. Karger Publishers; 2018. p. 19–25.
5. Rippke F, Schreiner V, Schwanitz H-J. The acidic milieu of the horny layer. *Am J Clin Dermatol*. 2002;3(4):261–72.
6. Lambers H, Piessens S, Bloem A, Pronk H, Finkel P. Natural skin surface pH is on average below 5, which is beneficial for its resident flora. *Int J Cosmet Sci*. 2006;28(5):359–70.
7. Öhman H, Vahlquist A. The pH gradient over the stratum corneum differs in X-linked recessive and autosomal dominant ichthyosis: a clue to the molecular origin of the “acid skin mantle”? *J Invest Dermatol*. 1998;111(4):674–7.
8. Jones EM, Cochrane CA, Percival SL. The effect of pH on the extracellular matrix and biofilms. *Adv wound care*. 2015;4(7):431–9.
9. Williams S, Davids M, Reuther T, Kraus D, Kerscher M. Gender difference of in vivo skin surface pH in the axilla and the effect of a standardized washing procedure with tap water. *Skin Pharmacol Physiol*. 2005;18(5):247–52.
10. Dissemond J, Witthoff M, Brauns TC, Haberer D, Goos M. PH-Wert des milieus chronischer wunden. *Der Hautarzt*. 2003;54(10):959–65.
11. Wilhelm K-P, Cua AB, Maibach HI. Skin aging: effect on transepidermal water loss,

- stratum corneum hydration, skin surface pH, and casual sebum content. *Arch Dermatol.* 1991;127(12):1806–9.
12. Yosipovitch G, Maayan-Metzger A, Merlob P, Sirota L. Skin barrier properties in different body areas in neonates. *Pediatrics.* 2000;106(1):105–8.
  13. Grimes PE, Green BA, Wildnauer RH, Edison BL. The use of polyhydroxy acids (PHAs) in photoaged skin. *Cutis.* 2004;73(2 Suppl):3–13.
  14. Rawlings AV. Ethnic skin types: are there differences in skin structure and function? 1. *Int J Cosmet Sci.* 2006;28(2):79–93.
  15. Darlenski R, Fluhr JW. Influence of skin type, race, sex, and anatomic location on epidermal barrier function. *Clin Dermatol.* 2012;30(3):269–73.
  16. Hoeger PH, Enzmann CC. Skin physiology of the neonate and young infant: a prospective study of functional skin parameters during early infancy. *Pediatr Dermatol.* 2002;19(3):256–62.
  17. Fluhr JW, Elias PM. Stratum corneum pH: formation and function of the ‘acid mantle’. *Exog Dermatology.* 2002;1(4):163–75.
  18. Ali SM, Yosipovitch G. Skin pH: from basic science to basic skin care. *Acta Derm Venereol.* 2013;93(3):261–9.
  19. Chiller K, Selkin BA, Murakawa GJ. Skin microflora and bacterial infections of the skin. In: *Journal of Investigative Dermatology Symposium Proceedings.* Elsevier; 2001. p. 170–4.
  20. Korting HC, Lukacs A, Vogt N, Urban J, Ehret W, Ruckdeschel G. Influence of the pH-value on the growth of *Staphylococcus epidermidis*, *Staphylococcus aureus* and *Propionibacterium acnes* in continuous culture. *Zentralblatt für Hyg und Umweltmedizin= Int J Hyg Environ Med.* 1992;193(1):78.
  21. Gethin G. The significance of surface pH in chronic wounds. *Wounds uk.* 2007;3(3):52.
  22. Wallace LA, Gwynne L, Jenkins T. Challenges and opportunities of pH in chronic wounds. *Ther Deliv.* 2019;10(11):719–35.
  23. Roberts G, Chumley A, Mani R. The wound milieu in venous ulcers- further

observations: Abstract 502. *Wound Repair Regen.* 2006;14(1).

24. Leveen HH, Falk G, Borek B, Diaz C, Lynfield Y, Wynkoop BJ, et al. Chemical acidification of wounds. An adjuvant to healing and the unfavorable action of alkalinity and ammonia. *Ann Surg.* 1973;178(6):745.
25. Schneider LA, Korber A, Grabbe S, Dissemond J. Influence of pH on wound-healing: a new perspective for wound-therapy? *Arch Dermatol Res.* 2007;298(9):413–20.
26. Tsukada K. The pH changes of pressure ulcers related healing process of wound. *Wounds.* 1992;4:16–20.
27. Shukla VK, Shukla D, Tiwary SK, Agrawal S, Rastogi A. Evaluation of pH measurement as a method of wound assessment. *J Wound Care.* 2007;16(7):291–4.
28. Kaufman T, Eichenlaub EH, Angel MF, Levin M, Futrell JW. Topical acidification promotes healing of experimental deep partial thickness skin burns: a randomized double-blind preliminary study. *Burns.* 1985;12(2):84–90.
29. Korting HC, Braun-Falco O. The effect of detergents on skin pH and its consequences. *Clin Dermatol.* 1996;14(1):23–8.
30. Kurabayashi H, Tamura K, Machida I, Kubota K. Inhibiting bacteria and skin pH in hemiplegia: effects of washing hands with acidic mineral water. *Am J Phys Med Rehabil.* 2002;81(1):40–6.
31. Strohal R, Mittlböck M, Hämmerle G. The management of critically colonized and locally infected leg ulcers with an acid-oxidizing solution: a pilot study. *Adv Skin Wound Care.* 2018;31(4):163.
32. Agrawal KS, Sarda AV, Shrotriya R, Bachhav M, Puri V, Nataraj G. Acetic acid dressings: finding the Holy Grail for infected wound management. *Indian J Plast Surg Off Publ Assoc Plast Surg India.* 2017;50(3):273.
33. Bojar RA, Cunliffe WJ, Holland KT. Disruption of the transmembrane pH gradient—a possible mechanism for the antibacterial action of azelaic acid in *Propionibacterium acnes* and *Staphylococcus epidermidis*. *J Antimicrob Chemother.* 1994;34(3):321–30.
34. Seal LA, Robson MC. The influence of pH on chronic wound healing and the antimicrobial activity of chlorine. *Ostomy Wound Manag.* 2018;64:8–10.

35. Percival SL, Thomas J, Linton S, Okel T, Corum L, Slone W. The antimicrobial efficacy of silver on antibiotic-resistant bacteria isolated from burn wounds. *Int Wound J*. 2012;9(5):488–93.
36. Thomas JG, Slone W, Linton S, Okel T, Corum L, Percival SL. In vitro antimicrobial efficacy of a silver alginate dressing on burn wound isolates. *J Wound Care*. 2011;20(3):124–8.
37. James GA, Swogger E, Wolcott R, Pulcini E deLancey, Secor P, Sestrich J, et al. Biofilms in chronic wounds. *Wound Repair Regen*. 2008;16(1):37–44.
38. Malone M, Bjarnsholt T, McBain AJ, James GA, Stoodley P, Leaper D, et al. The prevalence of biofilms in chronic wounds: a systematic review and meta-analysis of published data. *J Wound Care*. 2017;26(1):20–5.
39. Khatoon Z, McTiernan CD, Suuronen EJ, Mah T-F, Alarcon EI. Bacterial biofilm formation on implantable devices and approaches to its treatment and prevention. *Heliyon*. 2018;4(12):e01067.
40. Liechty WB, Kryscio DR, Slaughter B V, Peppas NA. Polymers for drug delivery systems. *Annu Rev Chem Biomol Eng*. 2010;1:149–73.
41. Deng Z, Guo Y, Zhao X, Ma PX, Guo B. Multifunctional stimuli-responsive hydrogels with self-healing, high conductivity, and rapid recovery through host–guest interactions. *Chem Mater*. 2018;30(5):1729–42.
42. Raza A, Rasheed T, Nabeel F, Hayat U, Bilal M, Iqbal H. Endogenous and exogenous stimuli-responsive drug delivery systems for programmed site-specific release. *Molecules*. 2019;24(6):1117.
43. Qiu Y, Park K. Environment-sensitive hydrogels for drug delivery. *Adv Drug Deliv Rev*. 2001;53(3):321–39.
44. Heskins M, Guillet JE. Solution properties of poly (N-isopropylacrylamide). *J Macromol Sci*. 1968;2(8):1441–55.
45. Shibayama M, Tanaka T. Volume phase transition and related phenomena of polymer gels. In: *Responsive gels: volume transitions I*. Springer; 1993. p. 1–62.
46. Bae YH, Okano T, Kim SW. Temperature dependence of swelling of crosslinked poly (N, N'-alkyl substituted acrylamides) in water. *J Polym Sci Part B Polym Phys*.



1990;28(6):923–36.

47. Hathaway H, Alves DR, Bean J, Esteban PP, Ouadi K, Sutton JM, et al. Poly (N-isopropylacrylamide-co-allylamine)(PNIPAM-co-ALA) nanospheres for the thermally triggered release of Bacteriophage K. *Eur J Pharm Biopharm.* 2015;96:437–41.
48. Hathaway H, Ajuebor J, Stephens L, Coffey A, Potter U, Sutton JM, et al. Thermally triggered release of the bacteriophage endolysin CHAPK and the bacteriocin lysostaphin for the control of methicillin resistant *Staphylococcus aureus* (MRSA). *J Control Release.* 2017;245:108–15.
49. Shahriari M, Zahiri M, Abnous K, Taghdisi SM, Ramezani M, Alibolandi M. Enzyme responsive drug delivery systems in cancer treatment. *J Control Release.* 2019;308:172–89.
50. Li M, Zhao G, Su W-K, Shuai Q. Enzyme-Responsive Nanoparticles for Anti-tumor Drug Delivery. *Front Chem.* 2020;8.
51. Radhakrishnan K, Tripathy J, Gnanadhas DP, Chakravorty D, Raichur AM. Dual enzyme responsive and targeted nanocapsules for intracellular delivery of anticancer agents. *RSC Adv.* 2014;4(86):45961–8.
52. Bean JE, Alves DR, Laabei M, Esteban PP, Thet NT, Enright MC, et al. Triggered release of bacteriophage K from agarose/hyaluronan hydrogel matrixes by *Staphylococcus aureus* virulence factors. *Chem Mater.* 2014;26(24):7201–8.
53. Thet NT, Hong SH, Marshall S, Laabei M, Toby A, Jenkins A. Visible, colorimetric dissemination between pathogenic strains of *Staphylococcus aureus* and *Pseudomonas aeruginosa* using fluorescent dye containing lipid vesicles. *Biosens Bioelectron.* 2013;41:538–43.
54. Laabei M, Jamieson WD, Massey RC, Jenkins ATA. *Staphylococcus aureus* interaction with phospholipid vesicles—a new method to accurately determine accessory gene regulator (*agr*) activity. *PLoS One.* 2014;9(1):e87270.
55. Thet NT, Mercer-Chalmers J, Greenwood RJ, Young AER, Coy K, Booth S, et al. SPaCE Swab: Point-of-Care Sensor for Simple and Rapid Detection of Acute Wound Infection. *ACS sensors.* 2020;5(8):2652–7.
56. Ganta S, Devalapally H, Shahiwala A, Amiji M. A review of stimuli-responsive

- nanocarriers for drug and gene delivery. *J Control release*. 2008;126(3):187–204.
57. Vaupel P, Kallinowski F, Okunieff P. Blood flow, oxygen and nutrient supply, and metabolic microenvironment of human tumors: a review. *Cancer Res*. 1989;49(23):6449–65.
  58. Sharma S, Dua A, Malik A. Biocompatible stimuli responsive superabsorbent polymer for controlled release of GHK-Cu peptide for wound dressing application. *J Polym Res*. 2017;24(7):1–8.
  59. Cengiz N. Fabrication of Multifunctional Stimuli-Responsive Hydrogels Susceptible to both pH and Metal Cation for Visual Detections. *Macromol Chem Phys*. 2019;220(17):1900212.
  60. Lowman AM, Morishita M, Kajita M, Nagai T, Peppas NA. Oral delivery of insulin using pH-responsive complexation gels. *J Pharm Sci*. 1999;88(9):933–7.
  61. Torres-Lugo M, Peppas NA. Molecular design and in vitro studies of novel pH-sensitive hydrogels for the oral delivery of calcitonin. *Macromolecules*. 1999;32(20):6646–51.
  62. Kamei N, Morishita M, Chiba H, Kavimandan NJ, Peppas NA, Takayama K. Complexation hydrogels for intestinal delivery of interferon  $\beta$  and calcitonin. *J Control release*. 2009;134(2):98–102.
  63. Milo S, Hathaway H, Nzakizwanayo J, Alves DR, Esteban PP, Jones B V, et al. Prevention of encrustation and blockage of urinary catheters by *Proteus mirabilis* via pH-triggered release of bacteriophage. *J Mater Chem B*. 2017;5(27):5403–11.
  64. Milo S, Thet NT, Liu D, Nzakizwanayo J, Jones B V, Jenkins ATA. An in-situ infection detection sensor coating for urinary catheters. *Biosens Bioelectron*. 2016;81:166–72.
  65. Milo S, Acosta FB, Hathaway HJ, Wallace LA, Thet NT, Jenkins ATA. Development of an Infection-Responsive Fluorescent Sensor for the Early Detection of Urinary Catheter Blockage. *ACS sensors*. 2018;3(3):612–7.
  66. Rasool A, Ata S, Islam A. Stimuli responsive biopolymer (chitosan) based blend hydrogels for wound healing application. *Carbohydr Polym*. 2019;203:423–9.
  67. Nobrega FL, Costa AR, Santos JF, Siliakus MF, Van Lent JWM, Kengen SWM, et al. Genetically manipulated phages with improved pH resistance for oral administration

in veterinary medicine. *Sci Rep.* 2016;6:39235.

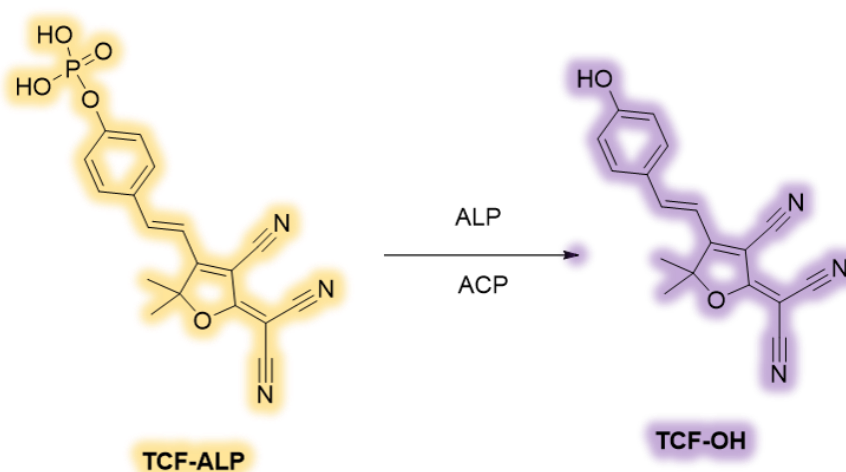
68. Bruschi ML. *Strategies to modify the drug release from pharmaceutical systems.* Woodhead Publishing; 2015.
69. Kumaran D, Taha M, Yi Q, Ramirez-Arcos S, Diallo J-S, Carli A, et al. Does treatment order matter? Investigating the ability of bacteriophage to augment antibiotic activity against *Staphylococcus aureus* biofilms. *Front Microbiol.* 2018;9:127.

# Chapter 6: TCF-based Fluorescent Probe for the Detection of Alkaline Phosphatase

## 6.1. Overview

The research presented in this chapter describes the synthesis of the novel fluorescent and colorimetric probe, **TCF-ALP** (Scheme 6.1). Experiments were conducted with **TCF-ALP** to determine its limit of detection, selectivity, and kinetic parameters towards alkaline phosphatase (ALP). As **TCF-ALP** was also found to be active towards acid phosphatase (ACP), further experiments were conducted to determine the selectivity of **TCF-ALP** towards both ACP and ALP at each enzyme's optimal pH (pH 5.0 and pH 9.2, respectively) and at neutral pH (pH 7.1).

The aim of this chapter was to build a foundation of knowledge so **TCF-ALP** could be further exploited for the detection of *S. aureus* species; discussed in greater detail in Chapter 7.



**Scheme 6.1:** A TCF-based fluorescent probe (**TCF-ALP**) for the detection of alkaline and acid phosphatase

## 6.2. Introduction

### 6.2.1. Fluorescence

#### 6.2.1.1. Basics of Fluorescence

Luminescence is the emission of light from electronically excited states of any substance and can be divided into two categories, fluorescence and phosphorescence.<sup>1</sup> The process of fluorescence and phosphorescence (absorption, excitation and emission) is best illustrated with a Jablonski diagram (Figure 6.1).

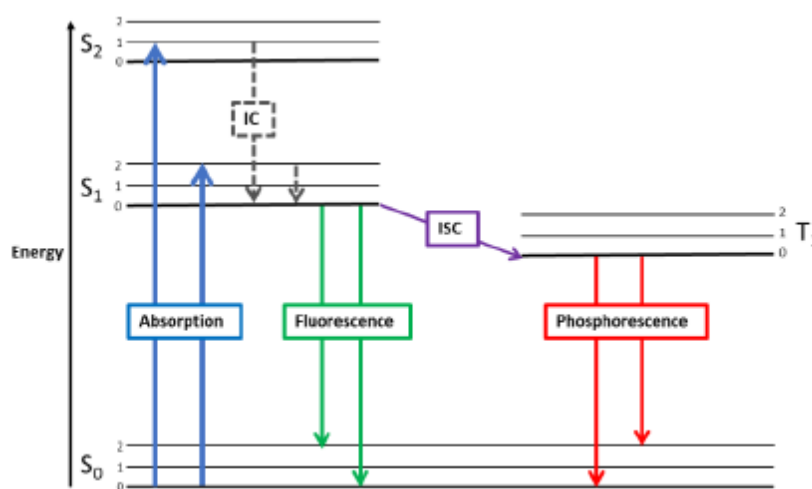


**Figure 6.1:** A Jablonski diagram showing  $S_0$ ,  $S_1$ , and  $S_2$  singlet energy levels and the  $T_1$  triplet level. Internal conversion and intersystem crossing, which lead to fluorescence and phosphorescence, respectively, are depicted. Figure reproduced from Gardner *et al* with permission<sup>2</sup>

The singlet ground, first, and second electronic states are depicted by  $S_0$ ,  $S_1$ , and  $S_2$ , respectively. At each of these energy levels, there are a number of vibrational energy levels, denoted by 0, 1, 2, etc. The transitions between states are often shown as vertical lines as transitions occur within a time-frame too short for significant displacement of nuclei (Franck-Condon principle).<sup>1</sup>

For both fluorescence and phosphorescence, the first step is absorption. Absorption of a photon occurs when an external light source emits light of a sufficient wavelength, and typically occurs in molecules with the lowest vibrational energy. This excites an electron to a higher vibrational level of either  $S_1$  or  $S_2$ , before rapid relaxation to the lowest vibrational level of  $S_1$  in a process called internal conversion (IC).<sup>1</sup> This occurs as the electron is in an unstable configuration and consequently adopts a more semi-stable configuration in a

slightly lower energy level via non-radiative processes such as vibrational relaxation or heat to the solvent.<sup>1</sup> Additionally, IC occurs faster than fluorescence lifetimes, therefore it is generally complete prior to emission.<sup>1</sup> This excited state is higher in energy than the ground state, resulting in a thermodynamic driving force towards the ground state.<sup>3</sup>

For fluorescence, the electron of the excited orbital is of the opposite spin to the electron in the ground state orbital (paired), therefore, the return to the ground state is spin-allowed and occurs rapidly by emission of a photon via fluorescence.<sup>1</sup>

On the other hand, phosphorescence occurs when the electron in the  $S_1$  state undergoes a spin conversion to the excited triplet state  $T_1$  in a process called intersystem crossing (ISC). This process is spin-forbidden as the electron now has the same spin orientation as the electron in the ground state. As a result of this, the rate of emission is slower, and generally shifted towards longer wavelengths, compared to fluorescence ( $10^{-3} - 10^0 \text{ s}^{-1}$ ). Molecules containing heavy atoms such as bromine and iodine are frequently phosphorescent.<sup>1</sup>

Fluorescence spectral data are generally presented as emission spectra. According to Kasha's rule, upon excitation of an electron into the higher energy levels, the excess energy is quickly dissipated, leaving the fluorophore in the lowest vibrational level of  $S_1$ . Because of this rapid relaxation, emission spectra are usually independent of excitation wavelength. Additionally, the symmetric nature of these spectra is a result of the same transitions being involved in both absorption and emission and the similarities of the vibrational energy levels of  $S_0$  and  $S_1$ . (Figure 6.2)<sup>1</sup>

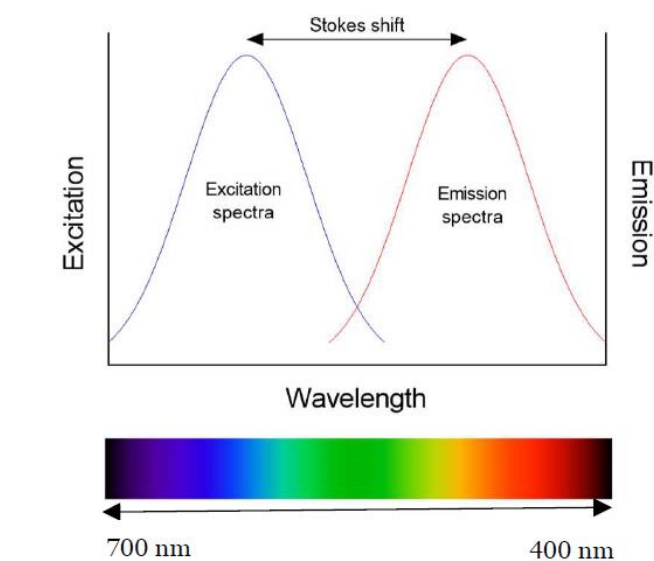


**Figure 6.2:** Diagram depicting the excitation and emission spectra of a fluorescent molecule, and the corresponding Stokes shift

Excitation occurs in a shorter time frame compared with structural relaxation; hence, the excited state is initially formed at the optimal structure for the ground state. However, as the excited state molecules subsequently undergo structural relaxation,<sup>3</sup> emission leads to the formation of the ground state that has the optimal structure of the excited state. These effects narrow the energetic separation of the ground and excited state, which leads to emission at longer wavelengths compared to absorption – termed the Stokes shift.<sup>3</sup>

### **6.2.1.2. Design of Fluorescent Probes**

Many substrates, particularly those with delocalised electronic structures, e.g., conjugated  $\pi$  systems, exhibit fluorescent properties.<sup>3</sup> Owing to this, fluorescence spectroscopy has become a useful tool for the detection of certain analytes via the creation of fluorescent probes.<sup>2</sup>

Fluorescent probes change their fluorescence emission in response to a trigger, such as a binding event, chemical reaction, or change in the immediate environment.<sup>4</sup> In the literature, triggers have included reactive oxygen and nitrogen species, metal ions, and enzymes – with both *in vitro* and *in vivo* studies performed.<sup>5–10</sup>

Fluorescent probes are often used in drug discovery and medical applications as they offer high selectivity and sensitivity,<sup>11,12</sup> are easy to use,<sup>3</sup> are non-invasive,<sup>13</sup> and capable of real-time monitoring<sup>11,12</sup> with minimal disruption to the sample.<sup>1,14</sup> Additionally, they are easy to synthesise and modify depending on the target or use of the probe.<sup>15</sup>

Fluorescent probes are generally comprised of three units, a receptor, linker and a reporter.<sup>2</sup> The receptor unit should be specific towards the target analyte by being designed in such a way to minimise off-target reactions and be non-toxic to avoid damage to the biological system under investigation. The receptor is connected to a reporter unit via a linker, designed to optimally position the two units and modulate solubility<sup>2</sup>. The reporter unit of the probe is the fluorophore; like the receptor unit, it should be non-toxic to avoid damaging the biological system. The choice of fluorophore is important; fluorophores that have absorption and emission wavelengths in or near the near-infrared (NIR) region are often advantageous as they are more biocompatible, have deeper tissue penetration, and have minimal interference from background auto-fluorescence of the sample.<sup>16–19</sup>

Several requirements need to be considered when designing fluorescent probes, including efficient excitation, limited auto-fluorescence, limited cellular photodamage, a high molar extinction coefficient and quantum yield (enabling the use of lower concentrations and

therefore reduced toxicity), and the presence of a highly-selective functional group that recognises the target.<sup>3,20</sup>

### 6.2.1.3. Fluorescence Mechanisms

There are four fluorescence mechanism commonly used in the design of fluorescent probes: Photoinduced Electron Transfer (PET), Forster Resonance Energy Transfer (FRET), Excited State Intramolecular Proton Transfer (ESIPT), and Internal Charge Transfer (ICT).

#### 6.2.1.3.1. Photoinduced Electron Transfer

Suppression of photoinduced electron transfer (PET) is one of the most commonly used methods for converting a non-fluorescent molecule into a fluorescent molecule.<sup>21</sup> PET involves excitation of an electron from the highest occupied molecular orbital (HOMO) of a fluorophore (acceptor) to its lowest unoccupied molecular orbital (LUMO). In the fluorescent probes 'off' state, an electron from the HOMO of the receptor (donor) moves to fill the HOMO of the fluorophore, resulting in fluorescence quenching and the electron in the LUMO of the fluorophore returning to the ground state via a non-radiative pathway (Figure 6.3).<sup>21,22</sup> For this to occur, the HOMO of the receptor must be slightly higher than the HOMO of the fluorophore.<sup>21,22</sup> This is called a-PET; d-PET can also occur where the receptor is excited, however, the same mechanisms happen, and the fluorescence is quenched.<sup>15,23</sup> Upon binding of the target, the redox potential of the receptor is raised so that the relevant HOMO becomes lower in energy compared to the HOMO of the fluorophore. Consequently, PET is no longer possible, and fluorescence occurs.<sup>3</sup>

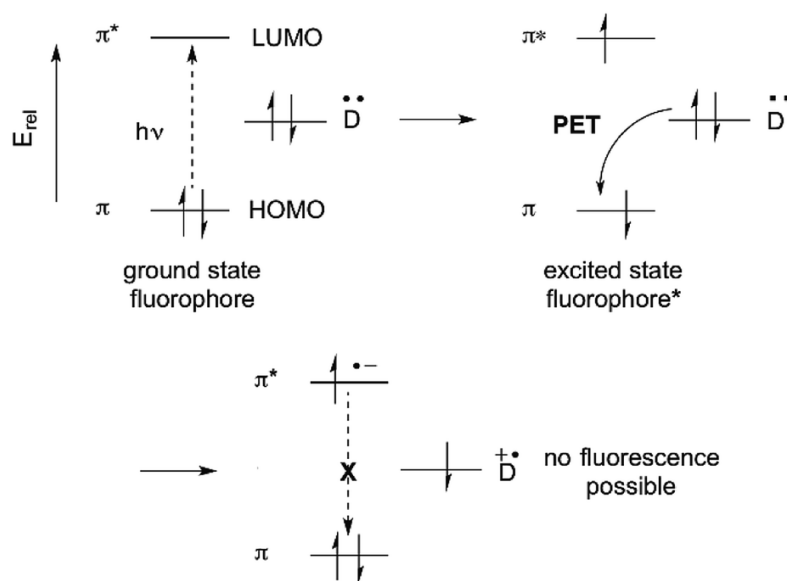


**Figure 6.3:** Photoinduced electron transfer (PET) quenching by a donor (D). Adapted from Fu *et al* with permission by The Royal Society of Chemistry<sup>21</sup>



### 6.2.1.3.2. Förster Resonance Energy Transfer

Förster resonance energy transfer (FRET) is a non-radiative energy transfer process that does not rely on the classic photon emission/absorption phenomenon.<sup>24</sup> Instead, a FRET molecule consists of a donor and acceptor fluorophore,<sup>3</sup> which transfer their energies via long-range dipole-dipole resonance interactions.<sup>2,20</sup>

If the FRET acceptor is not close enough to the donor fluorophore when the donor fluorophore is excited, the excited electron decays to the ground state via a non-radiative pathway.<sup>20</sup> However, if the distance between the donor and acceptor fluorophores is between 10 – 100 Å,<sup>20,21</sup> the energy transfers from the donor to the acceptor fluorophore with a lower energy excited state, via a non-radiative dipole-dipole coupling mechanism, provided that there is a matching acceptor excited state vibrational level available.<sup>3,21,25</sup> After excitation, the excited acceptor emits a photon and returns to the ground state (Figure 6.4). The efficiency of this energy transfer is inversely proportional to  $\times 10^6$  distance between the two FRET units.<sup>26–28</sup>

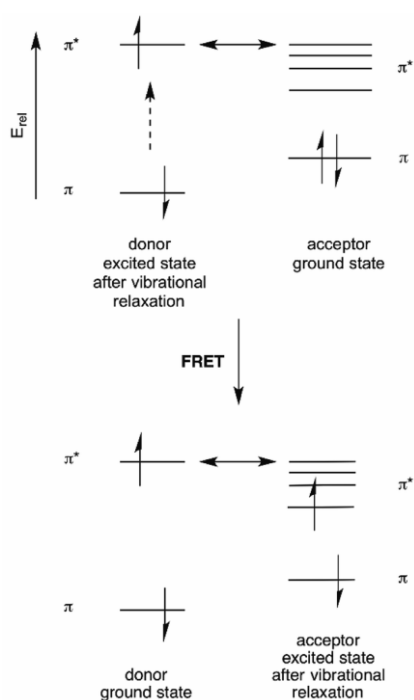


**Figure 6.4:** Energy diagram for FRET. The double-headed arrow denotes the energy-matching of the lowest energy vibrational state of the donor excited state with a high energy vibrational level of the acceptor excited state. Adapted from Fu *et al* with permission by The Royal Society of Chemistry<sup>21</sup>

To enhance FRET efficiency, there needs to be good overlap between the emission spectra of the donor and the absorption spectra of the acceptor, correct orientation of the transition

dipoles of the donor and acceptor fluorophore, and the donor fluorophore needs to have a high extinction coefficient and a high quantum yield.<sup>20,21</sup>

### 6.2.1.3.3. Excited-state Intramolecular Proton Transfer

Excited-state intramolecular proton transfer (ESIPT) is a four-level photochemical process involving a fluorophore that can tautomerize, often utilising switching between enol and keto forms; therefore, it must contain an intramolecular hydrogen bond between a hydrogen donor and acceptor (Figure 6.5). The ground state fluorophore typically exists in the enol form, but upon excitation, the electron density is redistributed, ensuing the greater acidity of the hydrogen bond donor group and basicity of the hydrogen acceptor group. As a result, a rapid enol to keto phototautomerization occurs, with the excited enol form ( $E^*$ ) converting to the excited keto form ( $K^*$ ), which is stabilised by the intermolecular hydrogen bond.<sup>29</sup> After radiative decay, a reverse proton transfer takes place to produce the original enol form.<sup>30</sup> However, exceptions do exist where the fluorescence observed for ESIPT molecules is a result of the enol form.<sup>31</sup>

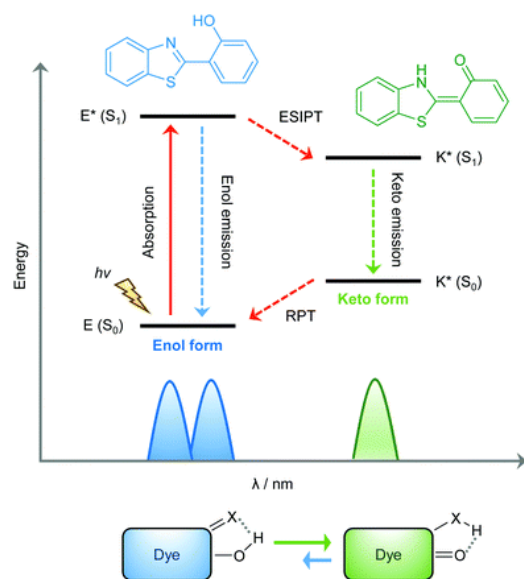


**Figure 6.5:** Schematic representation of the ESIPT process. Adapted from Sedgwick *et al* with permission by The Royal Society of Chemistry<sup>30</sup>

### 6.2.1.3.4. Internal Charge Transfer

Fluorescent probes utilising internal charge transfer (ICT) have both electron donating and electron accepting groups as ICT relies on the intramolecular movement of charge, often due to these “push-pull” groups.<sup>23</sup> Upon excitation, there is charge transfer from the electron donor to the electron acceptor, thereby changing the emission peak of the fluorescence spectra (Figure 6.6).<sup>31,32</sup> If the target analyte interacts with the electron

donating group, there is a blue-shift (increase in energy, decrease in wavelength) in the absorption spectrum and concurrent decrease of the extinction coefficient. Conversely, if the target analyte interacts with the electron accepting group, there is a red-shift (decrease in energy, increase in wavelength) and concurrent increase of the extinction coefficient.<sup>15</sup>

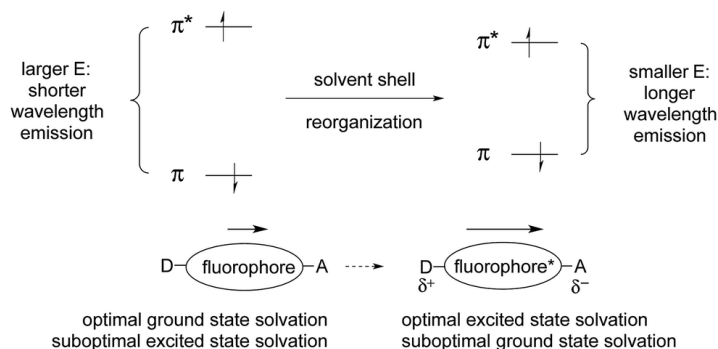


**Figure 6.6:** Energy diagram correlating ICT with solvation, in polar solvents. Adapted from Fu et al with permission by The Royal Society of Chemistry<sup>621</sup>

#### 6.2.1.3.4.1. TCF-based Fluorescent Probes

Dicyanomethylene-3-cyano-4, 5, 5-trimethyl-2, 5-dihydrofuran (**TCF**)-based probes are examples utilised in the literature that exploit the ICT mechanism of fluorescence. **TCF** has three conjugated, electron-withdrawing cyano groups,<sup>33,34</sup> and its derivative **TCF-OH** has a donor- $\pi$ -acceptor (D- $\pi$ -A) structure suitable for ICT.<sup>35-37</sup>

**TCF** has been used to construct colorimetric and long-wavelength probes, resulting in reduced interference from the auto-fluorescence of the samples.<sup>17,34,37-39</sup> **TCF** has also been used to develop non-linear optical materials,<sup>40,41</sup> and has been used in red fluorophore bioimaging<sup>42,43</sup> and pH sensing.<sup>44</sup> Recently, a variety of **TCF**-based probes have been used for biological imaging.<sup>33,34,36,37,45,46</sup>

## 6.2.2. Enzymes

Enzyme are proteinaceous biological catalysts (also called biocatalysts), capable of accelerating chemical reactions that facilitate many biological processes within living cells without being consumed or altered.<sup>46</sup> Enzymes are highly specific, both in the reactions they catalyse and the substrates that they target.<sup>47</sup> As enzymes are proteins, they can lose their catalytic activity upon exposure to high temperatures, extreme pH, and denaturing agents.<sup>48</sup> Additionally, some enzymes contain a non-protein component, known as a co-factor. These co-factors are typically metals, such as iron, manganese, cobalt, copper or zinc; however,

other organic molecules have been known to act as co-factors – in which case, it is called a co-enzyme.<sup>49</sup>

Enzymes work by lowering the activation energy required to reach the intermediate or transition state, therefore more molecules reach this transition state, increasing the rate of the reaction (Figure 6.7). Additionally, enzymes achieve this without modifying the net energy change or altering the equilibrium position of the reaction, which is thermodynamically determined.<sup>48,50</sup>

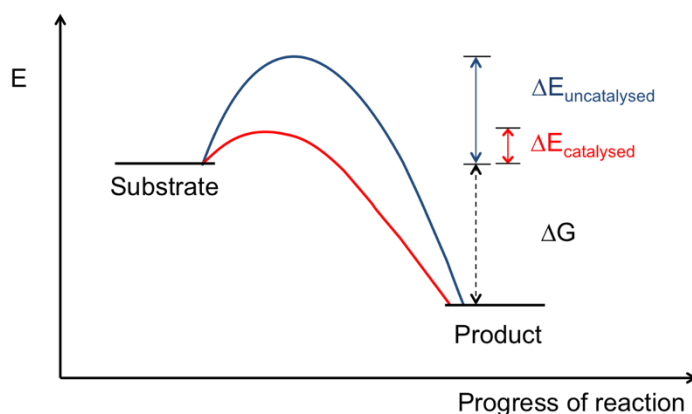


**Figure 6.7:** Energy diagram depicting a catalysed (red) and un-catalysed reaction (blue), with the reaction proceeding from left to right. In the presence of an enzyme the activation energy is lowered, resulting in an increase in rate

During the course of the reaction, the substrate binds non-covalently to the active site of the enzyme to form a transient enzyme-substrate [ES] complex. The substrate bound to the enzyme then undergoes structural changes, resulting in the formation of the product and the unchanged enzyme (Equation 1):<sup>50</sup>



Enzymes are highly specific due to their complex protein structure, with two main binding models proposed. The first model is the “lock and key” hypothesis, proposed by Fischer in 1894 (Figure 6.8A).<sup>48</sup> This model presumes that the catalytic site of the enzyme is rigid, and the substrate has the correct shape to fit into this site.<sup>48</sup> However, this model requires a high level of rigidity that is incompatible with current knowledge of enzymes’ molecular structures, such as changes to the enzyme structure in the presence of allosteric modulators.<sup>48,50</sup>

Another model termed the “induced fit” hypothesis has been proposed by Koshland, which is more accepted in the academic community (Figure 6.8B).<sup>50</sup> It hypothesises that the enzyme structure is flexible, not rigid. Upon contact with the correct substrate, conformational changes within the enzyme occur (i.e., the enzyme adapts its structure to the optimal conformation required to form the ES complex).<sup>50</sup>

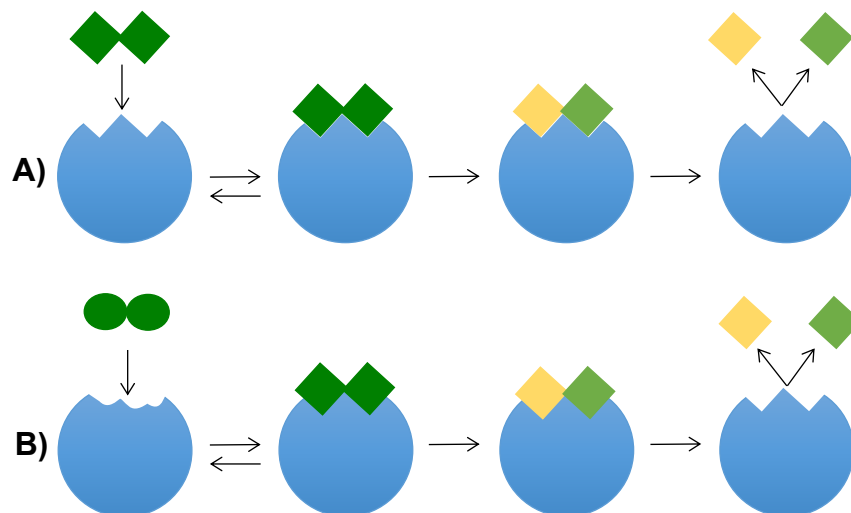


**Figure 6.8:** Schematic of enzyme-substrate binding: **A)** the lock-and-key model and **B)** the induced-fit model, where substrate binding distorts the conformations of both substrate and enzyme

### 6.2.2.1. Enzyme Kinetics

Enzyme kinetics is the study of various factors that determine the speed of enzyme-catalysed reactions.<sup>49</sup> The activity of an enzyme can be determined experimentally by measuring the initial velocity of the conversion of differing concentrations of substrate against a fixed concentration of enzyme.<sup>49</sup> In steady-state kinetics, this is the phase where the rate of formation of intermediates and the rate of decomposition remain the same, thus the concentrations of reactive intermediates remains the same.<sup>48</sup> During this reaction, substrate concentration is greater than enzyme concentration.<sup>48</sup> This substrate-activity relationship is well known, with Michaelis-Menten first describing this phenomenon. Put simply, at high concentrations of substrate, a maximum velocity of reaction is reached (first order<sup>48</sup>); however, upon increasing substrate concentration, a point is reached where all the enzymes' active sites are occupied, thus the enzyme becomes saturated.<sup>50</sup> If the substrate concentration continues to increase past this point, a steady-state is achieved, and the reaction rate does not increase any further – the reaction behaves as zero order.<sup>50</sup> Therefore, steady-state enzyme kinetics assumes that a catalytic reaction remains constant if the reaction is not exposed to continuous change.<sup>48</sup>

Michaelis and Menten were the first people to derive simple assumptions about enzymatic reactions from first principles.<sup>49</sup> The main concept of Michaelis-Menten kinetics is that the reaction takes place via the formation of the ES complex, which once formed can create the product ( $k_2$ ) or dissociate in the reverse direction without the formation of the product ( $k_{-1}$ ) (Equation 1).

The Michaelis-Menten derivation requires two important assumptions: firstly, it only considers the initial velocity of the reaction, where the product concentration will be negligible ( $[S] > [P]$ ). Therefore, it is possible to ignore the possibility of the product reverting back to the substrate. Secondly, it assumes that the concentration of the substrate exceeds the concentration of enzyme ( $[S] > [E]$ ).<sup>49</sup>

The derivation begins with an expression of the initial rate for the formation of the product. This is based upon the rate constant  $k_2$  and the concentration of the ES complex, as follows:<sup>49</sup>

$$v_0 = \frac{d[P]}{dt} = k_2[ES] \quad (2)$$

The concentration of ES is unknown; hence, it needs to be expressed in terms of known values. In a steady-state approximation it is possible to assume that  $[ES]$  remains constant, even though  $[S]$  and  $[P]$  concentrations can vary.<sup>49</sup> The rate of formation of ES and the rate of its breakdown must therefore balance, where:

$$\text{Rate of ES complex formation} = k_1[E][S] \quad (3)$$

and

$$\text{Rate of ES complex breakdown} = (k_{-1} + k_2)[ES] \quad (4)$$

Hence, at steady state:

$$k_1[E][S] = (k_{-1} + k_2)[ES] \quad (5)$$

Solving for  $[ES]$ :

$$[ES] = \frac{k_1[E][S]}{k_{-1} + k_2} \quad (6)$$

The Michaelis constant,  $K_m$ , can be defined as follows:

$$K_m = \frac{k_{-1} + k_2}{k_1} \quad (7)$$

Thus, equation (6) can thus be simplified to:

$$[ES] = \frac{[E][S]}{K_M} \quad (8)$$

Since  $[S] \gg [E]$ , the concentration of free substrate  $[S]$  is almost equal to the total concentration of substrate, and the concentration of uncombined enzyme  $[E]$  is equal to the total enzyme concentration  $[E]_T$  minus  $[ES]$ . Including these terms into Equation 8 and solving for ES gives:

$$[ES] = \frac{[E]_T[S]}{[S] + K_M} \quad (9)$$

We can then introduce this term into Equation 2

$$v_0 = k_2[E]_T \frac{[S]}{[S] + K_M} \quad (10)$$

The term  $k_2[E]_T$  represents  $V_{max}$ , the maximal velocity. Thus, the final equation is:

$$v_0 = \frac{V_{max}[S]}{[S] + K_M} \quad (11)$$

The Michaelis constant,  $K_m$ , is used to define the relationship between initial velocity and substrate concentration.<sup>49</sup>  $K_m$  corresponds to the substrate concentration at which the reaction rate reaches a value equal to half the maximum. The  $K_m$  value is characteristic for each enzyme and each of its substrates when determined under the same experimental conditions,<sup>50</sup> and is typically in the lower millimolar range.<sup>49</sup> The value is inversely related to the affinity of the enzyme for its substrate; higher affinity to a substrate is indicated by a lower  $K_m$  value.<sup>50</sup>

To reiterate,  $V_{\max}$  is the point of maximal velocity, where the enzyme is becoming close to saturation with the substrate. It is important to note that  $V_{\max}$  is a theoretical limit that cannot be achieved experimentally.<sup>49</sup>

### 6.2.2.2. Clinical Diagnostic Applications of Enzymes

Enzymes can be used for the detection and/or diagnosis of disease.<sup>51</sup> Abnormalities in the normal physiology within the human body may cause a disruption to the concentration of particular enzymes, which can be exploited for disease diagnosis.<sup>52</sup> Certain enzymes specific to diseased organs can be released into blood circulation; therefore, measuring these enzyme activities has been employed to aid clinical diagnosis of disease.<sup>51</sup> There are a wide range of diseases where enzymes are used as ‘markers’, including cancer, diabetes, autoimmune diseases, and liver and heart malfunctions.<sup>52</sup> For example, lactose dehydrogenase has two different isozymes in heart and skeletal muscle; any increase of this enzyme in the blood indicates tissue damage and the presence of the heart isozyme is indicative of a heart attack. Additionally, enzymes have been used as markers to determine the pathology of disease. For example, creatine kinase has been associated with myocardial infarction and muscle diseases, while alanine aminotransferase is known to be a liver-specific indicator of disease.<sup>53</sup> Commonly used enzymes for the diagnosis of various disease are outlined in Table 6.1.

**Table 6.1:** Enzymes commonly used in the clinical diagnosis of disease. Adapted from Sarup Singh *et al*<sup>51</sup>

Enzyme	Disorder/disease	Reference
Acid phosphatase	Malaria	54
Alkaline phosphatase	Chronic kidney disease	55
Amylase	Pancreatitis	56
Aspartate aminotransferase	Hepatic diseases	57
Creatine kinase	Myocardial damage	58
Lactate dehydrogenase	Necrosis	59
Leukocyte esterase	Urinary tract infection	60
Lipase	Skin disorders	61
Lysozyme	Rheumatoid arthritis	62

### 6.2.2.3. Alkaline Phosphatase

Alkaline phosphatase (ALP) was the earliest serum enzyme to be recognised to have clinical significance; in the 1920s it was discovered in high concentrations for bone and liver disease.<sup>53</sup> ALP is a ubiquitous enzyme found in the majority of human tissues<sup>63</sup> and catalyses the dephosphorylation process of various substrates, such as nucleic acids, proteins and small molecules.<sup>64</sup> It also plays an important role in signal transduction and regulation of



intracellular processes (cell growth, apoptosis and signal transduction pathways).<sup>65</sup> ALP is thus regarded a key biomarker in medical diagnosis.<sup>64,66</sup> Abnormal levels of ALP in serum are an indicator of several diseases including bone disease,<sup>67</sup> liver dysfunction,<sup>68</sup> breast and prostatic cancer,<sup>69,70</sup> and diabetes.<sup>71</sup> Therefore, there is an increasing need to develop a novel system for the rapid and selective detection of ALP activity for use in clinical diagnosis.

There have been numerous approaches to determining ALP levels, including colorimetric,<sup>72,73</sup> chemiluminescence,<sup>74</sup> electrochemical,<sup>75</sup> surface-enhanced Raman spectroscopy<sup>76</sup> and fluorescence.<sup>77,78</sup> While there have been many fluorophores developed for assaying ALP activity (organic dyes,<sup>79,80</sup> conjugated polymers,<sup>81</sup> inorganic semiconductor dots,<sup>82</sup> noble metal clusters<sup>83</sup>), many need high probe concentrations and have short wavelength emission, which limit their application in biological systems. Owing to this, focus has been placed on developing long wavelength/NIR probes, as they enable deeper tissue penetration and have reduced background interference from autofluorescence of living cells.<sup>84-86</sup>

### **6.2.3. Aims of Study**

The aim of this chapter was to design a novel fluorescent and colorimetric probe that could be used for the detection of ALP to aid in the diagnosis of clinically-relevant diseases. This Chapter aimed to:

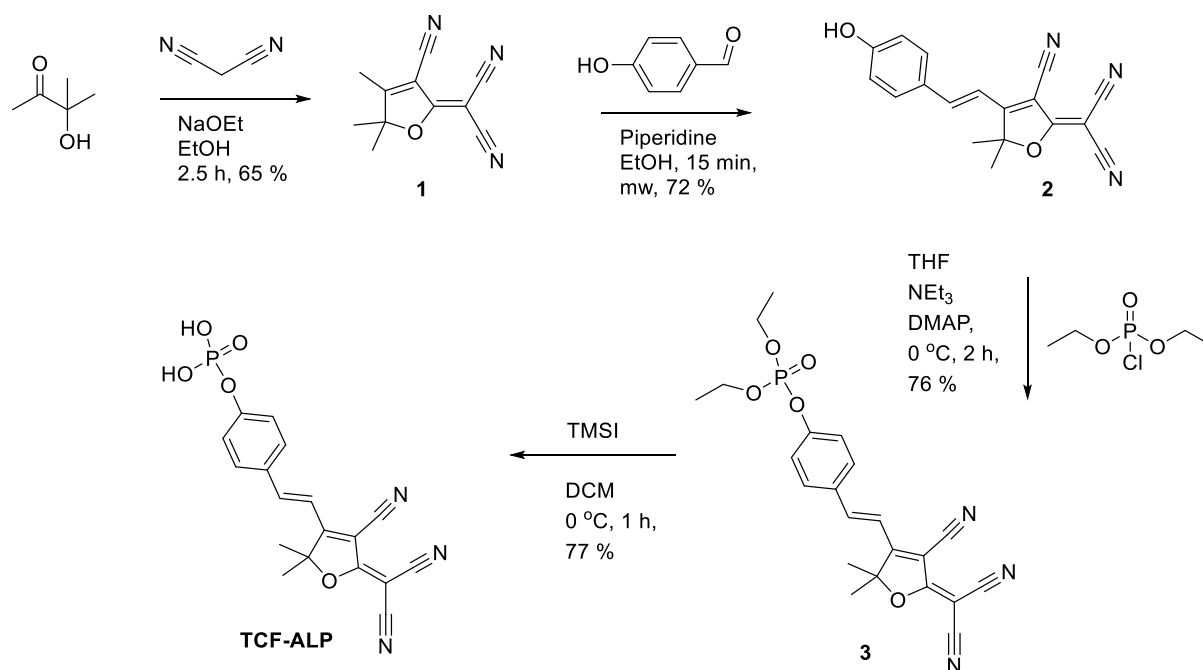
- Synthesise a novel fluorescent and colorimetric probe (termed **TCF-ALP**)
- Optimise the conditions of the assay required for efficient ALP detection
- Determine **TCF-ALP** sensitivity and selectivity
- Determine the rate of reaction and kinetic parameters for **TCF-ALP** (Michaelis-Menten kinetics)
- To explore the use of ALP in clinically-relevant cell lines

Additionally, the aim of this Chapter was to build a foundation of knowledge so **TCF-ALP** could be further exploited for the detection of *S. aureus* species; discussed in greater detail in Chapter 7.

## 6.3. Methods

### 6.3.1. Synthesis of TCF-ALP

For the corresponding NMR spectra, please see Figures S1 – S9 in the Appendix. Briefly, **TCF-ALP** was synthesised in four steps with an overall yield of 27% (Scheme 6.2).



Scheme 6.2: Synthetic route to TCF-ALP

#### 6.3.1.1. 2-(3-Cyano-4,5,5-trimethylfuran-2(5H)-ylidene) malonitrile (**1**)

NaOEt (0.391 g, 5.75 mmol) was added to a solution of 3-hydroxy-3-methyl-2-butanone (4 mL, 38 mmol) and malonitrile (4.9 g, 74 mmol) in EtOH (10 mL) and stirred for 1.5 h. The reaction mixture was refluxed for 1 h, then cooled to room temperature and the solid precipitate filtered to afford the title compound (**1**) as a pale grey solid (4.92 g, 24.70 mmol, 65%); M.p. 204 – 208 °C (decomp).

### 6.3.1.2. (E)-2-(3-Cyano-4-(4-hydroxystyryl)-5,5-dimethylfuran-2(5H)-ylidene)malononitrile (**2**)

Two drops of piperidine were added to a mixture of 4-hydroxybenzaldehyde (0.122 g, 1 mmol) and TCF (**1**) (0.228 g, 1.15 mmol) in EtOH (10 mL). The reaction mixture was heated in the microwave for 15 min at 100 °C and allowed to cool to room temperature. The solid precipitate was filtered off to afford the title compound (**2**) as a red solid (0.22 g, 0.72 mmol, 72%)

### 6.3.1.3. (E)-4-(2-(4-Cyano-5-(dicyanomethylene)-2,2-dimethyl-2,5-dihydrofuran-3-yl)vinyl)phenyl diethyl phosphate (**3**)

Intermediate 2 (0.20 g, 0.66 mmol) was dissolved in a solution containing THF (10 mL) and NEt<sub>3</sub> (0.3 mL). This was followed by the addition of DMAP (0.050 g). The resulting solution was cooled to 0 °C and diethylchlorophosphate (0.14 mL, 1 mmol) was added dropwise over the course of 15 min. The reaction mixture was monitored via TLC, and once the starting material was consumed (~ 2 hrs), EtOAc (50 mL) and H<sub>2</sub>O (50 mL) were added to the reaction mixture. The organic layer was washed with H<sub>2</sub>O (2 x 50 mL) and brine (50 mL). It was then dried (MgSO<sub>4</sub>) and concentrated *in vacuo* to afford the crude material. This crude material was purified via column chromatography over silica gel EtOAc:petroleum ether (30:70) to afford the title compound (**3**) as an orange solid (0.22 g, 0.50 mmol, 76%).

### 6.3.1.4. (E)-4-(2-(4-Cyano-5-(dicyanomethylene)-2,2-dimethyl-2,5-dihydrofuran-3-yl)vinyl)phenyl phosphate (TCF-ALP)

A solution of **3** (0.15 g, 0.34 mmol) in DCM (5 mL) was cooled to 0 °C before the dropwise addition of TMSI (0.1 mL, 0.68 mmol). The reaction mixture was stirred for 1 h before the solvent was removed *in vacuo* to afford the crude solid, which was purified via trituration (diethyl ether) to afford an orange solid (0.10 g, 0.26 mmol, 77 %).

## 6.3.2. Mass Spectrometry

High resolution mass spectrometry (HRMS) results were acquired on an externally calibrated Bruker Daltonics micrOTOF time-of-flight mass spectrometer coupled to an electrospray source (ESI-TOF). Calibration was achieved using sodium formate solution. Samples were introduced either by syringe pump or flow injection using an autosampler in an Agilent 1100 LC system. Bruker Daltonics software, DataAnalysis, was used to process the data. In this study, HRMS analysis was carried out on TCF-ALP before and after addition of ALP.

### 6.3.3. UV-Vis Spectroscopy of TCF-ALP

UV-Vis measurements were carried out on a SPECTROstar Omega (BMG Labtech). UV-Vis spectra of **TCF-ALP** were obtained before and after the addition of 1 U/mL of ALP. The measurements were conducted in triplicate, in 50 mM Tris-HCl (pH 9.2) at 25 °C.

### 6.3.4. Fluorescence of TCF-ALP Over Time

In brief, 180 µL of differing concentrations of ALP (0.0 – 0.8 U/mL) in 50 mM Tris-HCl, pH 9.2, were added to a black 96-well microtiter plate. The fluorescence intensity of these enzyme solutions were measured using a BMG Labtech CLARIOstar with excitation and emission wavelengths of 542 nm and 606 nm, respectively. After 3 min, 20 µL of 100 µM **TCF-ALP** in 50 mM Tris-HCl, pH 9.2 was added to the enzyme solutions and the fluorescence intensity was measured for 1 h at 1 min intervals at 25 °C. Blank (50 mM Tris-HCl, pH 9.2) and negative (10 µM **TCF-ALP** and 50 mM Tris-HCl, pH 9.2) controls were conducted in tandem. All measurements were performed in triplicate.

### 6.3.5. Limit of Detection (LOD)

To determine the limit of detection, **TCF-ALP** (10 µM) was added to various concentrations of ALP (0.0 – 0.2 U/mL) in 50 mM Tris-HCl, pH 9.2 and incubated for 15 min at 25 °C. After incubation, the solutions were transferred to a black 96-well plate and emission spectra were obtained. Blank and negative controls were conducted in tandem. All measurements were performed in triplicate.

After the spectra were obtained, the relative fluorescence intensity (RFI) at 606 nm was plotted versus concentration of enzyme, and the limit of detection (LOD) was calculated using the following formula (Equation 12):

$$LOD = 3\sigma / slope \quad (12)$$

### 6.3.6. Inhibition Assay

A stock solution of 4 mM of sodium orthovanadate (Na<sub>2</sub>VO<sub>3</sub>) was prepared in dH<sub>2</sub>O, and the pH adjusted to pH 10 with 1 M NaOH. The resultant yellow solution was then heated until the solution turned colourless. After cooling, the pH was checked, and the process repeated until the solution remained colourless after pH-adjustment. After, ALP (0.8 U/mL, 50 mM Tris HCl, pH 9.2) was pre-incubated for 30 minutes with varying inhibitor

concentrations (0 – 2000  $\mu\text{M}$ ) at room temperature before the addition of **TCF-ALP** (10  $\mu\text{M}$ ). The solution was incubated for 1 h at room temperature prior to fluorescence analysis to determine ALP activity.

### **6.3.7. Enzyme Kinetics Assay**

Increasing concentrations of **TCF-ALP** (0.0– 20.0  $\mu\text{M}$ ) were added to 0.2 U/mL ALP in 50 mM Tris-HCl, pH 9.2 and the subsequent enzymatic reaction was monitored through change of fluorescence intensity at 606 nm every 60 s for 30 min. The initial reaction velocities were obtained from the resultant kinetic curves and plotted against substrate concentration. The kinetic parameters ( $K_m$  and  $V_{max}$ ) were determined by using nonlinear fitting models provided by the software package GraphPad Prism 6.0. The kinetic constants were reported as the mean  $\pm$  standard deviation of triplicate experiments.

### **6.3.8. Selectivity of TCF-ALP**

To determine the selectivity of **TCF-ALP**, 40  $\mu\text{L}$  of 100  $\mu\text{M}$  **TCF-ALP** was added to 360  $\mu\text{L}$  of various biologically relevant enzymes (ALP, acid phosphatase [ACP], protease from *Streptomyces griseus*, porcine liver esterase, proteinase K) and non-specific binding proteins (bovine serum albumin and trypsin) at a concentration of 0.4 U/mL or equivalent (in 50 mM Tris HCl at pH 9.2, 7.1, or 5.0 dependent on experiment). The resultant solutions were incubated for 30 min at 25 ° C. After incubation, the solutions were transferred to a black 96-well plate and emission spectra were obtained. Blank and negative controls were conducted in tandem; all measurements were performed in triplicate.

### **6.3.9. Cell Culture**

HeLa cells (human epithelial adenocarcinoma) were purchased from the Korean Cell Line Bank (Seoul, Korea). Cells were cultured in Eagle's Minimum Essential Medium (MEM) supplemented with heat-inactivated 10% fetal bovine serum, 100 U/mL penicillin and 100 U/mL streptomycin. All cells were kept in 5%  $\text{CO}_2$  at 37 °C.

### **6.3.10. Confocal Microscopy Imaging**

Cells were seeded in 35-mm glass bottomed dishes at a density of  $3.0 \times 10^5$  cells per dish in culture media. After culturing for 24 h, cells were incubated with 10  $\mu\text{M}$  of the probe for 30 min and washed with DPBS. Fluorescence images were recorded by means of confocal laser scanning microscopy (FV1200, Olympus, Japan). To prevent intracellular ALP activity, a 30 min pretreatment with 5 mM levamisole or 0.5 mM  $\text{Na}_3\text{VO}_4$  (ALP inhibitors) was

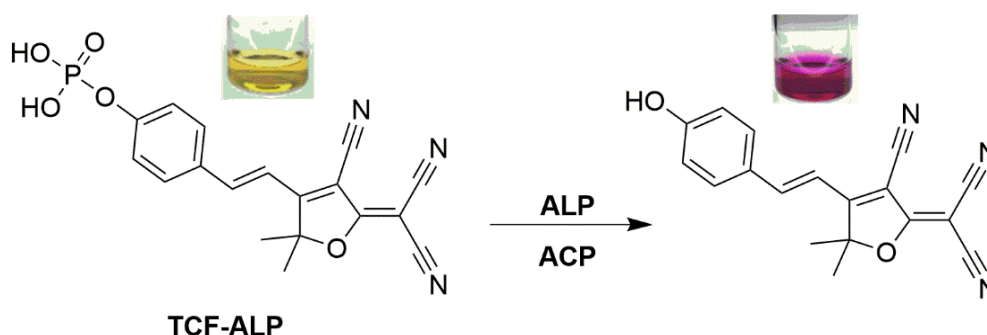
carried out. To acquire the fluorescence image, cells were excited with a 559 nm laser and a 575-675 nm emission filter was used.

### **6.3.11. Cytotoxicity Tests**

Cells were seeded in a 96-well plate with culture media. After culturing overnight, cells were incubated with various concentrations of sample for 24 h. To identify cell viability, reagents were removed and 0.5 mg/mL of MTT (Sigma) was added to the cells, which were then incubated for 4 h at 37 °C in a CO<sub>2</sub> incubator. The formazan produced was dissolved in 0.1 mL of dimethylsulfoxide (DMSO) and read at OD 650 nm with a Spectramax Microwell plate reader. Absorbance was determined and the mean cell viability was calculated as a percentage of the mean vehicle control. Results of are the average of 3 independent experiments.

## 6.4. Results and Discussion

As shown in Scheme 6.3, **TCF-ALP** was based on the conjugation of **TCF** to an electron-donating moiety, a phosphorylated phenol. This conjugation afforded an ICT D- $\pi$ -A system, whose fluorescence properties varied dramatically following ALP-mediated phosphate group cleavage.



**Scheme 6.3:** A TCF-based fluorescent probe (**TCF-ALP**) for the detection of alkaline phosphatase and/or acid phosphatase

### 6.4.1. pH Optima

Once **TCF-ALP** was synthesised, optimisation assays were performed to ensure the correct conditions were employed for successful colorimetric and fluorescent ALP detection by **TCF-ALP**. As **TCF** was originally used as a pH sensing fluorescent probe,<sup>44</sup> it was not unreasonable to assume that pH would have an effect on **TCF**-based fluorescence; hence, the effect of pH on the rate of ALP-mediated hydrolysis of **TCF-ALP** was evaluated (Figure 6.9).

Without ALP, **TCF-ALP** displayed a negligible increase in fluorescence intensity between pH 3.0 – 10.0. However, upon incubation with ALP, a sharp increase in fluorescence intensity was observed between pH 6.0 – 10.0, with a maximum intensity observed at pH 9.2. This was thought to be due to the combination of **TCF-OH** becoming deprotonated and ALP having an optimum pH of ~9.2. Consequently, all further *in vitro* experiments were conducted in 50 mM Tris-HCl buffer at pH 9.2.

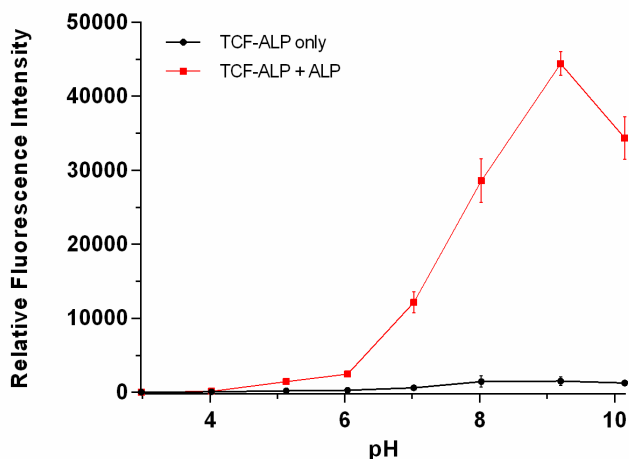


**Figure 6.9:** Relative fluorescence intensity of **TCF-ALP** (10  $\mu$ M) as determined with and without alkaline phosphatase (0.8 U/mL) in 50 mM Tris-HCl buffer at pH 3.0 – 10.0. Measurements taken 1 h after incubation at 25  $^{\circ}$ C.  $\lambda_{\text{ex}} = 542$  (bandwidth 15) nm/  $\lambda_{\text{em}} = 606$  nm. Error bars indicate standard deviation (n = 3)

### 6.4.2. Confirmation of ALP-mediated Hydrolysis

Confirmation of the ALP-mediated hydrolysis of **TCF-ALP** was further confirmed by NMR (Figure 6.10).  $^{31}\text{P}$  NMR studies found that upon incubation with ALP, there was a decrease in **TCF-ALP** concentration ( $\sim 2.4$  ppm) and an increase in product formation ( $\text{H}_3\text{PO}_4$ ;  $\sim 0.5$  ppm) over 1 h. These results confirm that ALP was able to cleave the phosphorylated phenol; hence, the fluorescence of **TCF-ALP** was due to ALP-mediated hydrolysis forming the fluorescent, deprotonated **TCF-OH**.

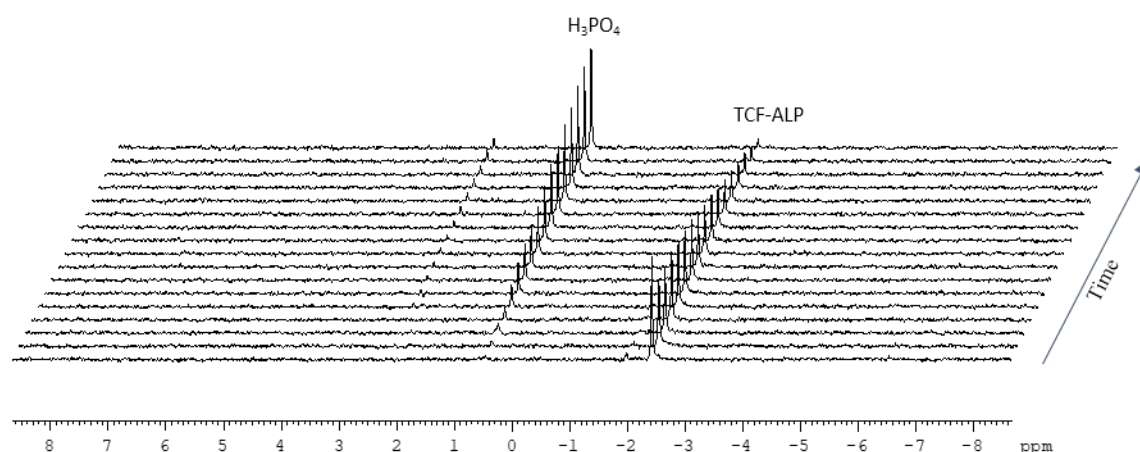


**Figure 6.10:**  $^{31}\text{P}$  NMR monitoring of **TCF-ALP** in the presence of ALP in 50 mM Tris-HCl buffer, pH 9.2. Scans were performed at 25  $^{\circ}$ C every 4 min for 1 h. The spectra show decreasing **TCF-ALP** concentration ( $\sim 2.4$  ppm) with increasing product formation ( $\text{H}_3\text{PO}_4$ ;  $\sim 0.5$  ppm) over time

The ALP-mediated hydrolysis of **TCF-ALP** was also confirmed via HRMS (Table 6.2). The results showed that upon incubation with ALP, the phosphate moiety of the **TCF-ALP**



probe was successfully cleaved, leaving behind the deprotonate, fluorescent **TCF-OH** moiety.

**Table 6.2:** HRMS (FTMS-NSI) of **TCF-ALP** before incubation with ALP (m/z calculated for C<sub>18</sub>H<sub>14</sub>N<sub>3</sub>O<sub>5</sub>P: requires 382.0598 for [M-H]<sup>-</sup>, found 382.0604), and after 1 h incubation with ALP (m/z calculated for C<sub>18</sub>H<sub>13</sub>N<sub>3</sub>O<sub>2</sub>: requires 302.1081 for [M-H]<sup>-</sup>, found 302.0941)

Time (min)	Compound Label	RT (min)	Observed mass (m/z)	Neutral observed mass (Da)	Theoretical mass (Da)	Mass error (ppm)	Isotope match scope (%)
0	C18 H14 N3 O5 P	0.80	382.0677	383.0677	383.0671	1.57	99.59
60	C18 H13 N3 O2	0.79	302.0941	303.1014	303.1008	2.15	99.25

Mass errors of between -5.00 and 5.00 ppm with isotope match scores above 60% are considered confirmation of molecular formulae.

### 6.4.3. UV-Vis Spectroscopy

Once it was confirmed that **TCF-ALP** could be successfully cleaved by ALP, UV-Vis titrations were performed. As shown in the UV-Vis spectra (Figure 6.11), **TCF-ALP** was found have an absorption maxima of ~430 nm. Upon incubation with 0.8 U/mL ALP, a bathochromic shift in the UV absorption maximum was observed (from 430 to 580 nm), which was accompanied by a colour change from yellow to purple.

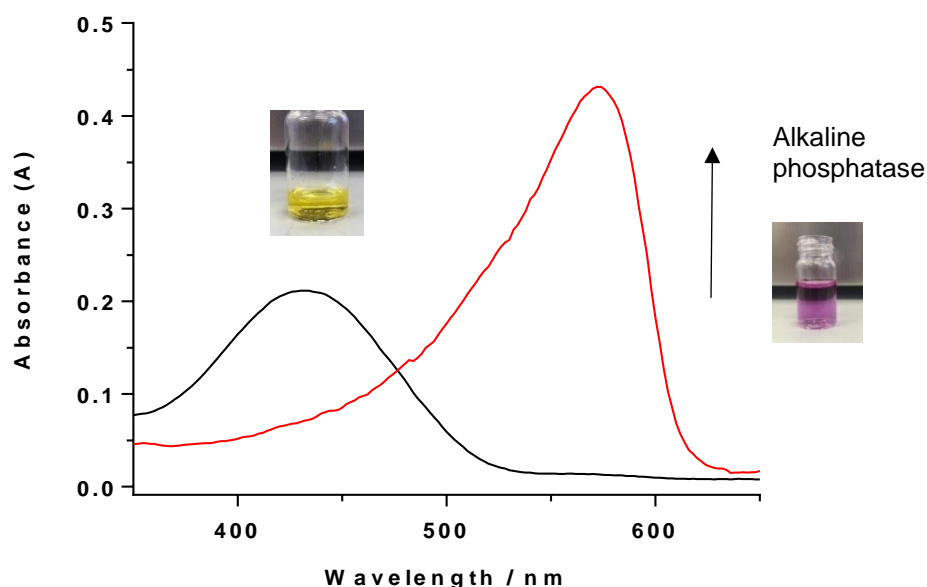


**Figure 6.11:** UV-Vis spectra of **TCF-ALP** (10 μM) with (red) and without (black) 0.8 U/ml of ALP in 50 mM Tris-HCl buffer pH 9.2

## 6.4.4. Fluorescence Assays

### 6.4.4.1. Time Drive

Next, fluorescence measurements were undertaken to determine the fluorescence response of **TCF-ALP** upon incubation with ALP. In brief, 10  $\mu\text{M}$  of **TCF-ALP** was incubated with varying concentrations (0.0 – 0.8 U/mL) of ALP and the fluorescence intensity measured every minute for 1 h (Figure 6.12). There was a concentration-dependent increase in RFI with increasing concentrations of ALP. Additionally, the RFI increased with longer incubation times, with the higher ALP concentrations (0.4 – 0.8 U/mL) plateauing at ~ 50000 after ~20, 40, and 60 minutes, respectively.

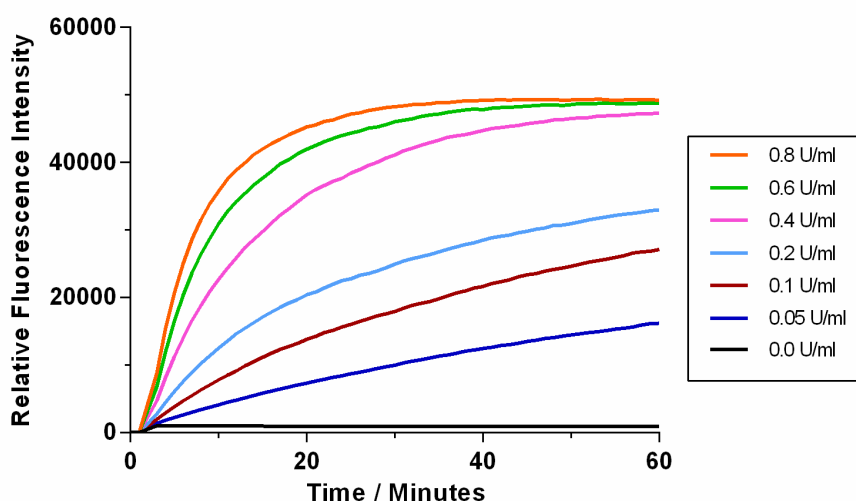


**Figure 6.12:** Time drive of **TCF-ALP** (10  $\mu\text{M}$ ) with the addition of ALP (0.0 – 0.8 U/mL) in 50 mM Tris HCl, pH 9.2 at 25 °C.  $\lambda_{\text{ex}} = 542$  (bandwidth 15) nm /  $\lambda_{\text{em}} = 606$  (bandwidth 20) nm.

### 6.4.4.2. Limit of Detection

As there was a concentration-dependent increase in RFI upon increasing ALP concentration, further studies were undertaken to determine the LOD of **TCF-ALP**. Various concentrations of ALP (0.0 – 0.2 U/mL) were incubated with 10  $\mu\text{M}$  of **TCF-ALP** for 15 minutes at 25 °C before fluorescence spectra were obtained (Figure 6.13). As expected, a linear relationship was observed between ALP concentration and RFI (Figure 6.14).

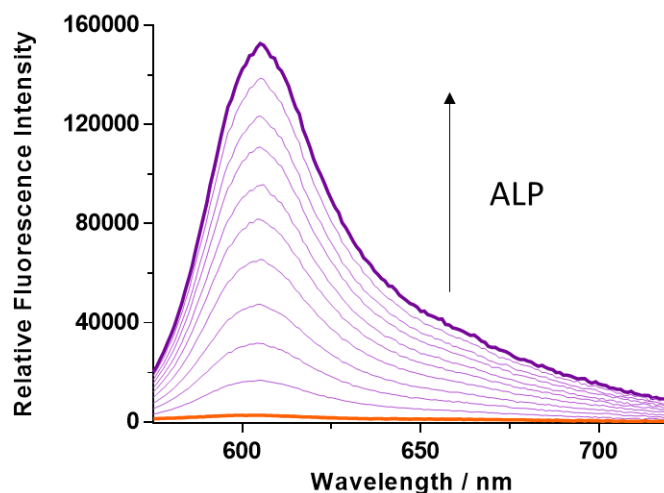


**Figure 6.13:** Fluorescence spectra of **TCF-ALP** (10  $\mu\text{M}$ ) produced via the addition of ALP (0 – 0.2 U/mL) in 50 mM Tris-HCl buffer, pH 9.2 at 25  $^{\circ}\text{C}$ .  $\lambda_{\text{ex}} = 542$  (bandwidth 15) nm. All measurements were made 15 min after the addition of ALP

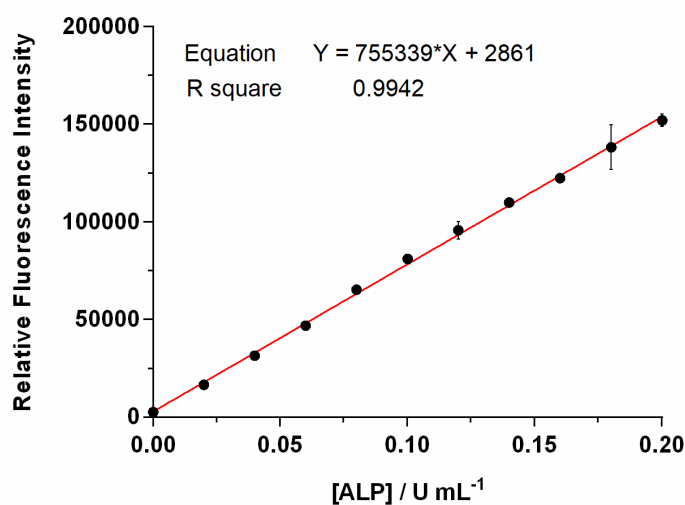


**Figure 6.14:** Relative fluorescence intensity seen for **TCF-ALP** (10  $\mu\text{M}$ ) upon the addition of ALP (0.0 – 0.2 U/mL) in 50 mM Tris-HCl buffer, pH 9.2 at 25  $^{\circ}\text{C}$ .  $\lambda_{\text{ex}} = 542$  (bandwidth 15) nm/  $\lambda_{\text{em}} = 606$  nm. Error bars indicate the standard deviation ( $n = 3$ ). The measurements were made 15 min after the addition of ALP

Using Equation 12, the LOD was calculated to be 0.12 mU/mL. This sensitivity seemed to be in accordance with other fluorescent-based methods found in the literature, even displaying increased sensitivity in comparison to other fluorescent probes (Table 6.3). As the majority of ALP probes in the literature have focused on detecting ALP as a biomarker for human disease, it was important to ensure that **TCF-ALP** could reliably detect ALP in serum. It is widely accepted that serum ALP levels in healthy adults lies between 39 – 117 U/mL;<sup>87,88</sup> thus, owing to the LOD of **TCF-ALP**, it can be suggested that **TCF-ALP** is

capable of detecting clinically relevant levels of ALP, and therefore could be used in clinical assays.

**Table 6.3:** Fluorescent probes and their corresponding limit of detection

Fluorescence Mechanism	Emission Wavelength (nm)	LOD (mU/mL)	Incubation time (min)	Reference
AIE	495	0.0077	60	89
Carbon dots	~ 445-465	0.90	15	90
Carbon dots	500	0.0003	20	91
ESIPT	400	1.3	40	78
FRET	494/548/624	0.06	8	92
FRET/AIE	570	0.2	10	93
ICP nanoparticles	738	3.00	20	94
Quenching	402	0.27	10	95
ICT	738	3.00	20	96
ICT	700	0.07	30	86
ICT	550/650	3.8	30	97
ICT	606	0.12	15	This Work

#### 6.4.5. Inhibition of TCF-ALP

To further confirm that the hydrolysis of **TCF-ALP** was due to ALP activity, inhibition studies were performed using sodium orthovanadate,  $\text{Na}_2\text{VO}_3$ , a common competitive inhibitor for ALP.<sup>98</sup> Competitive inhibitors work by increasing the value of the Michaelis-Menten constant without modifying the maximum velocity of the enzyme. Competitive inhibitors achieve this through three different mechanisms:<sup>50</sup>

- Competitive inhibitors can be structurally similar to the substrate and compete for the enzyme's active site
- Competitive inhibitors do not possess a similar structure to the substrate; however, they still compete for the enzyme's active site
- Competitive inhibitor and substrate bind to different sites on the enzyme, but the binding of one prevents the binding of the other, likely by inducing protein conformational changes

As  $\text{Na}_2\text{VO}_3$  can adopt a stable trigonal bipyramidal structure similar to that of phosphate, it inhibits by replacing ALP as a substrate, leading to the formation of unstable analogues of the enzyme-substrate complex.<sup>99</sup>

ALP (0.8 U/mL, 50 mM Tris HCl, pH 9.2) was pre-incubated for 30 min with varying inhibitor concentrations (0.0 – 2000.0  $\mu\text{M}$ ). After pre-incubation, **TCF-ALP** (10  $\mu\text{M}$ ) was added and the change in fluorescence was measured over 1 h (Figure 6.15).

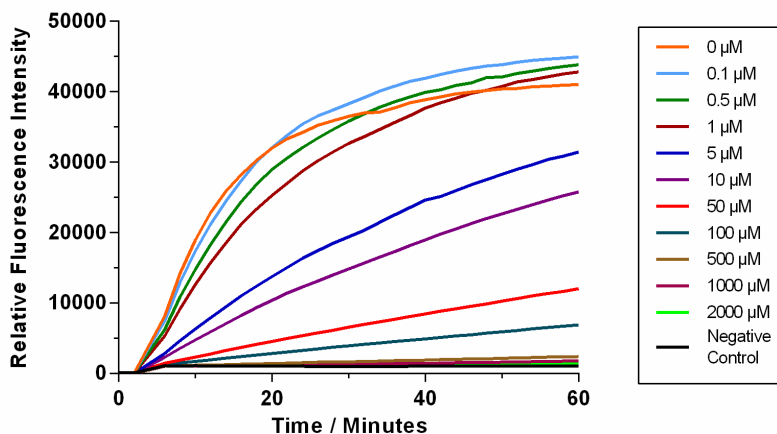


**Figure 6.15:** Fluorescence intensity of **TCF-ALP** (10  $\mu\text{M}$ ) in the presence of 0.8 U/mL of ALP pre-treated for 30 minutes with  $\text{Na}_3\text{VO}_4$  (0.0 – 2000  $\mu\text{M}$ ). Measurements were taken every minute for 1 h at 25 °C in 50 mM Tris HCl, pH 9.2.  $\lambda_{\text{ex}} = 542$  (bandwidth 15) nm/  $\lambda_{\text{em}} = 606$  (bandwidth 20) nm

As shown in Figure 6.15, there was a decrease in RFI with increasing inhibitor concentrations. At the 30 min time point, the RFI was plotted as a function of natural logarithm of inhibitor concentration (Figure 6.16) so the half maximal inhibitory concentration ( $\text{IC}_{50}$ ) could be determined. The  $\text{IC}_{50}$  measures the potency of a substance at inhibiting a specific biological or biochemical function. For this system, it was found to be 6.23  $\mu\text{M}$  ( $R^2 = 0.9932$ ), which was similar to values quoted in the literature.<sup>75,86</sup>

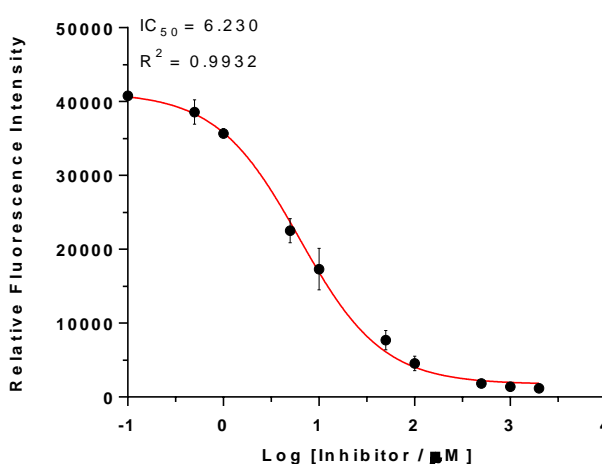


**Figure 6.16:** Inhibition study with **TCF-ALP** (10  $\mu\text{M}$ ) in the presence of different concentrations of  $\text{Na}_3\text{VO}_4$ . Fluorescence Intensity was recorded after 30 min incubation time with **TCF-ALP**. All reactions were performed with 0.8 U/ml ALP in 50 mM Tris-HCl pH 9.2 at 25 °C.  $\lambda_{\text{ex}} = 542$  (bandwidth 15) nm/  $\lambda_{\text{em}} = 606$ . Error bars indicate standard deviation ( $n = 3$ )

IC<sub>50</sub> can be converted to an absolute inhibition constant K<sub>i</sub> using the Cheng-Prusoff equation for competitive inhibitors. (Equation 13).

$$K_i = \frac{IC_{50}}{1 + \frac{[S]}{K_m}} \quad (13)$$

Where K<sub>i</sub> is the binding affinity of the inhibitor, IC<sub>50</sub> is the functional strength of the inhibitor, [S] is the fixed substrate concentration and K<sub>m</sub> is the concentration of substrate at which enzyme activity is at half maximal.

K<sub>i</sub> is often used as it is an absolute value, whereas IC<sub>50</sub> may vary between experiments depending on experimental conditions. K<sub>i</sub> values relate to the dissociation of the inhibitor-bound enzyme complex,<sup>100</sup> with smaller values denoting tighter binding affinity of the inhibitor. For this study K<sub>i</sub> was calculated to be 4.87 μM, which is similar to other values reported in the literature.<sup>101</sup>

#### 6.4.6. Selectivity of TCF-ALP

To determine the selectivity of **TCF-ALP**, it was incubated with ALP and the fluorescence intensity compared to **TCF-ALP** incubated with biologically relevant enzymes and non-specific binding proteins (at their optimal pH values), after 30 minute incubation at 25 °C. As shown in Figure 6.17, **TCF-ALP** displayed high selectivity towards ALP over other common enzymes or non-specific binding proteins (58-fold increase in fluorescence, pH 9.2). Interestingly, **TCF-ALP** produced a 20-fold increase in fluorescence intensity when treated with ACP at pH of 5.0.

As ACP displayed activity towards **TCF-ALP**, further experiments were undertaken to determine the selectivity of **TCF-ALP** at a neutral pH of 7.1. As shown in Figure 6.18, **TCF-ALP** proved capable of detecting ACP (25-fold fluorescence enhancement) and ALP (38-fold enhancement) at a physiological pH of 7.1. These results suggest that **TCF-ALP** can be used to detect both ALP and ACP at physiological pH, with a preference towards ALP. Further kinetic determination of this result will be discussed in Section 6.4.7.

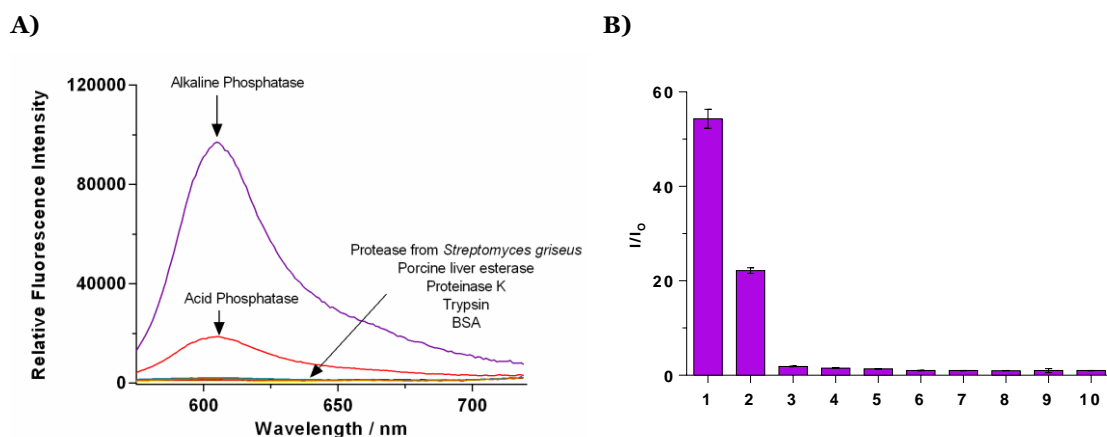


**Figure 6.17: A)** Fluorescence spectra and **B)** selectivity bar chart of TCF-ALP (10 μM) recorded in the presence of **1.** alkaline phosphatase (50 mM Tris-HCl, pH 9.2), **2.** acid phosphatase (50 mM Tris-HCl, pH 5.0), **3.** bovine serum albumin (0.1 mg/mL), **4.** protease from *Streptomyces griseus*, **5.** porcine liver esterase, **6.** proteinase K, **7.** trypsin (0.8 BAEE U/mL). **8-10.** negative controls at pH 5.0, 7.1 and 9.2, respectively. All enzymes were standardised to 0.8 U/mL in Tris-HCl buffer pH 7.1 unless otherwise stated.  $\lambda_{ex} = 542$  (bandwidth 15 nm)/  $\lambda_{em} = 606$  nm. The measurements were made 30 min after enzyme addition. Error bars indicate the standard deviation (n = 3)

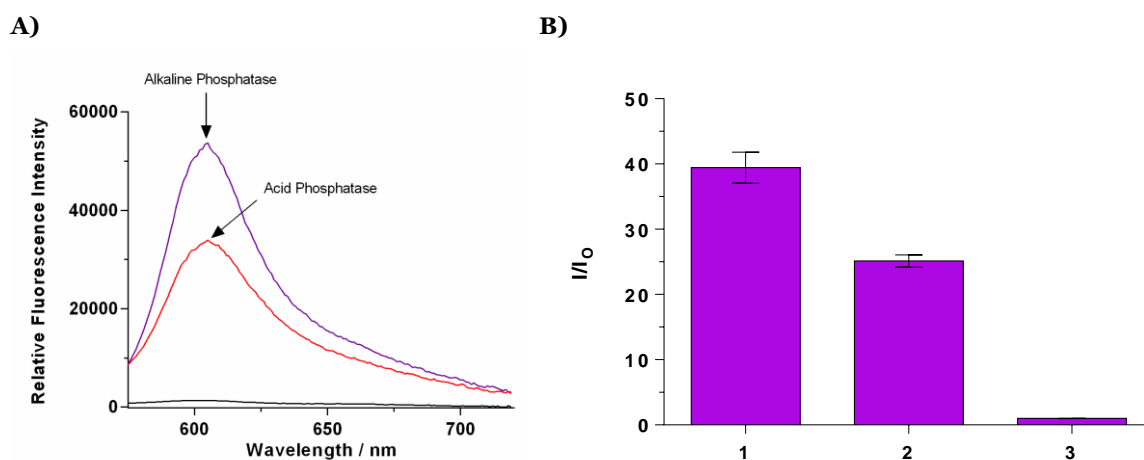


**Figure 6.18: A)** Fluorescence spectra and **B)** selectivity bar chart of TCF-ALP (10 μM) recorded in the presence of **1.** alkaline phosphatase, **2.** acid phosphatase, and **3.** negative control. All enzymes were standardised to 0.8 U/mL in Tris-HCl buffer pH 7.1 unless otherwise stated.  $\lambda_{ex} = 542$  (bandwidth 15 nm)/  $\lambda_{em} = 606$  nm. The measurements were made 30 min after enzyme addition. Error bars indicate the standard deviation (n = 3)

According to current standards, determination of ALP and ACP is undertaken at the phosphatase's optimum pH. For example, the Centers for Disease Control and Prevention (CDC) procedure for ALP determination is carried out in 2-amino-2-methyl-1-propanol (AMP) buffer at pH 10.3.<sup>102</sup> Likewise, ACP determination is carried out at pH 4.0 – 6.0.<sup>103</sup>

Following these observations, further studies were conducted to determine selectivity at pH 5.0 and 9.2 (Figures 6.19 – 6.20). Results showed that **TCF-ALP** acts selectively towards ACP at acidic pH, and ALP at alkaline pH. Therefore, **TCF-ALP** can be used to selectively detect ALP/ACP in clinical assays, or live cell systems (provided the buffer solution is optimal for the phosphatase under study).

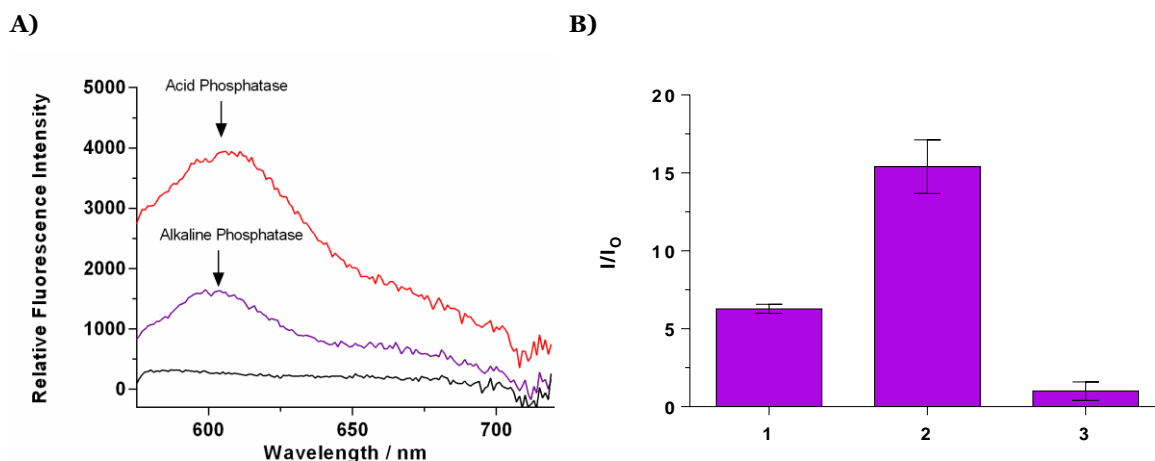


**Figure 6.19:** A) Fluorescence spectra and B) selectivity bar chart of **TCF-ALP** (10 μM) recorded in the presence of **1.** alkaline phosphatase, **2.** acid phosphatase, and **3.** negative control. All enzymes were standardised to 0.8 U/mL in Tris-HCl buffer pH 5.0.  $\lambda_{ex} = 542$  (bandwidth 15 nm)/  $\lambda_{em} = 606$  nm. The measurements were made 30 min after enzyme addition. Error bars indicate the standard deviation (n = 3)

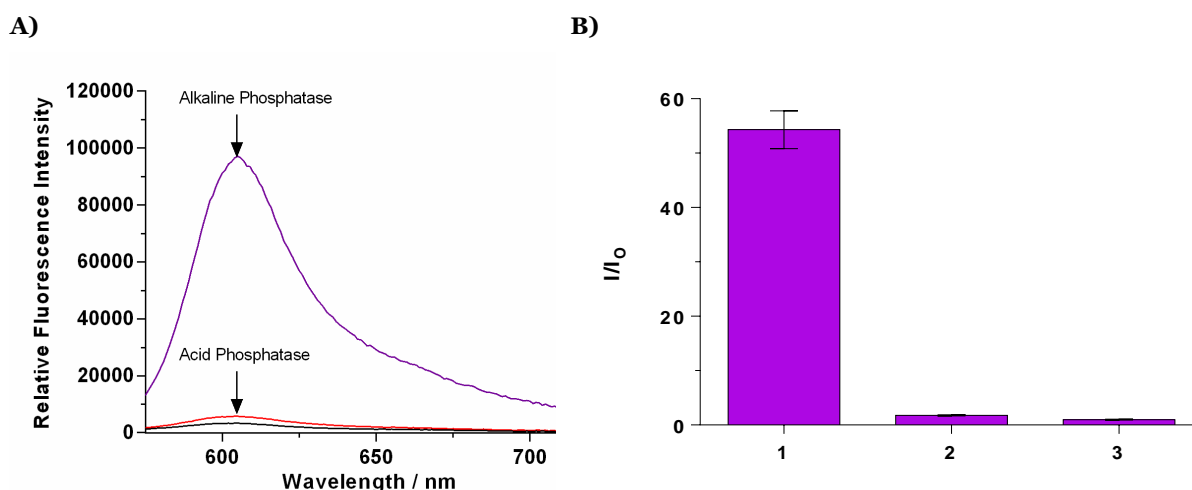


**Figure 6.20:** A) Fluorescence spectra and B) selectivity bar chart of **TCF-ALP** (10 μM) recorded in the presence of **1.** alkaline phosphatase, **2.** acid phosphatase, and **3.** negative control. All enzymes were standardised to 0.8 U/mL in Tris-HCl buffer pH 9.2.  $\lambda_{ex} = 542$  (bandwidth 15 nm)/  $\lambda_{em} = 606$  nm. The measurements were made 30 min after enzyme addition. Error bars indicate the standard deviation (n = 3)



### 6.4.7. Enzyme Kinetics

As **TCF-ALP** was selective towards ACP and ALP, further studies were needed to determine the kinetic parameters of **TCF-ALP** towards these enzymes. Firstly, kinetic parameters were obtained for ALP at pH 9.2, and to confirm **TCF-ALP** was more selective towards ALP versus ACP at neutral pH, kinetic parameters were obtained for both ALP and ACP at pH 7.1.

The kinetics of ALP towards **TCF-ALP** at pH 9.2 were determined via fluorescence spectroscopy. Various concentrations of **TCF-ALP** (0 – 20  $\mu\text{M}$ ) were incubated with 0.2 U/mL of ALP and the RFI was measured for 30 minutes. The initial velocity was calculated from the resultant data, and subsequently fitted to the Michaelis-Menten equation (Equation 11).

As shown in Figure 6.21, fluorescence increased with increasing **TCF-ALP** concentration upon incubation with 0.2 U/mL ALP in 50 mM Tris-HCl, pH 9.2. Once the initial velocities were determined and plotted, the  $V_{\text{max}}$  was calculated to be  $3029 \pm 157.3$  RFI/min and the  $K_m$   $35.81 \pm 2.63$   $\mu\text{M}$ . These results denote a strong binding between the substrate and enzyme, as  $K_m$  values for the majority of enzymes lie between  $10^{-1}$  and  $10^{-7}$  M.<sup>47</sup>

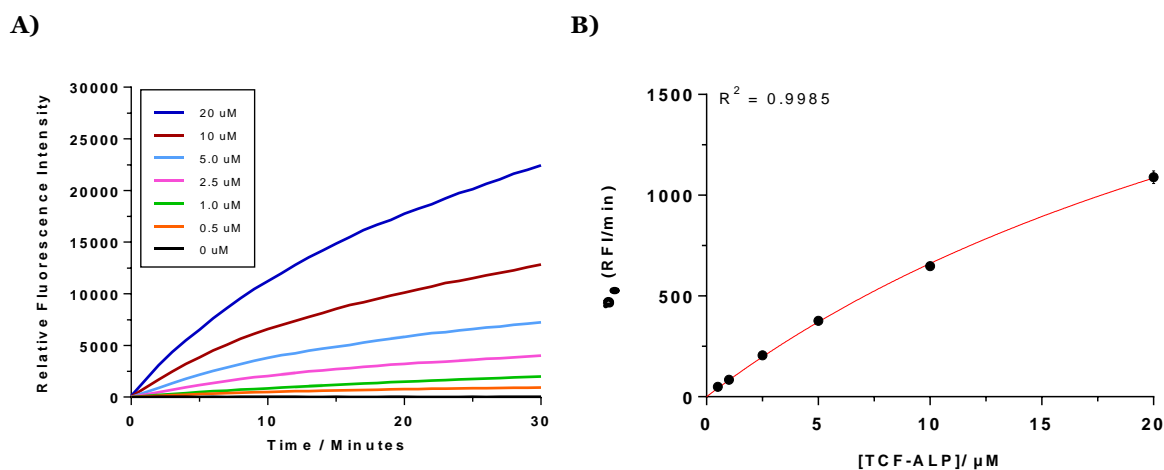


**Figure 6.21:** **A)** Time-dependent fluorescence intensity seen for increasing concentrations of **TCF-ALP** (0 – 20  $\mu\text{M}$ ) in the presence of 0.2 U/mL of ALP in 50 mM Tris-HCl buffer, pH 9.2. **B)** Plot of initial velocity ( $v_0$ ) against **TCF-ALP** concentration. Measurements taken at 25  $^\circ\text{C}$ ,  $\lambda_{\text{ex}} = 542$  (bandwidth 15 nm)/  $\lambda_{\text{em}} = 606$  (bandwidth 20) nm. Error bars indicate standard deviation ( $n = 3$ )

To confirm **TCF-ALP** was more selective towards ALP than ACP at neutral pH, kinetic experiments were conducted at pH 7.1, and the resultant  $K_m$  and  $V_{\text{max}}$  were compared (Figures 6.22 and 6.23). It was found that ALP has a smaller  $K_m$  value in comparison to ACP ( $0.38 \pm 0.042$   $\mu\text{M}$  and  $99.22 \pm 13.16$   $\mu\text{M}$ , respectively) and a lower  $V_{\text{max}}$  ( $208 \pm 3.81$   $\text{min}^{-1}$

and  $1962 \pm 223.6 \text{ min}^{-1}$ , respectively). Hence, ALP has higher affinity towards TCF-ALP compared to ACP, thus is more selective towards ALP at physiological pH.

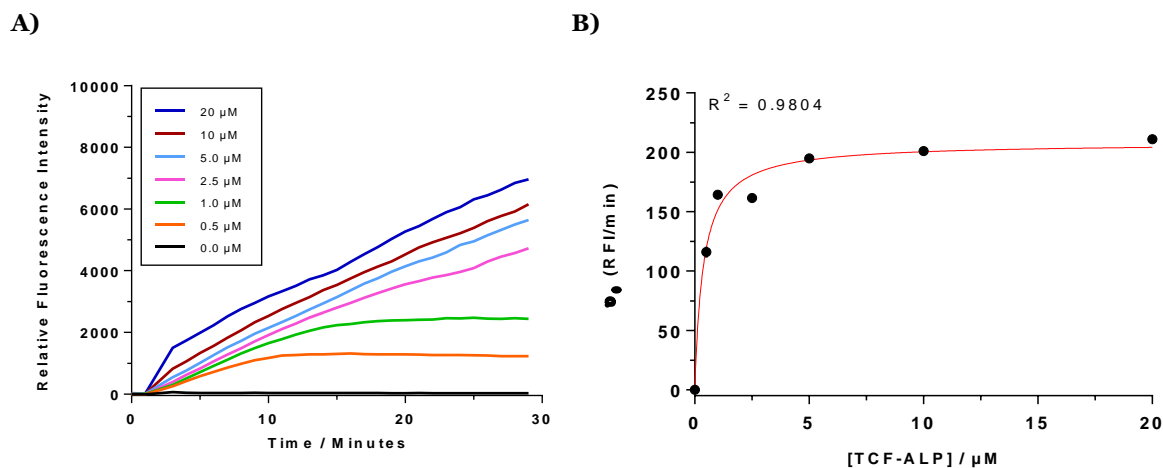


**Figure 6.22: A)** Time-dependent fluorescence intensity seen for increasing concentrations of TCF-ALP (0 – 20 μM) in the presence of 0.2 U/mL of ALP in 50 mM Tris-HCl buffer, pH 7.1. **B)** Plot of initial velocity ( $v_0$ ) against TCF-ALP concentration.  $K_m = 0.38 \pm 0.042 \mu\text{M}$ ,  $V_{\text{max}} = 208.00 \pm 3.81 \text{ min}^{-1}$ ,  $R^2 = 0.9804$ . Measurements taken at 25 °C,  $\lambda_{\text{ex}} = 542$  (bandwidth 15 nm)/  $\lambda_{\text{em}} = 606$  (bandwidth 20) nm. Error bars indicate standard deviation ( $n = 3$ )

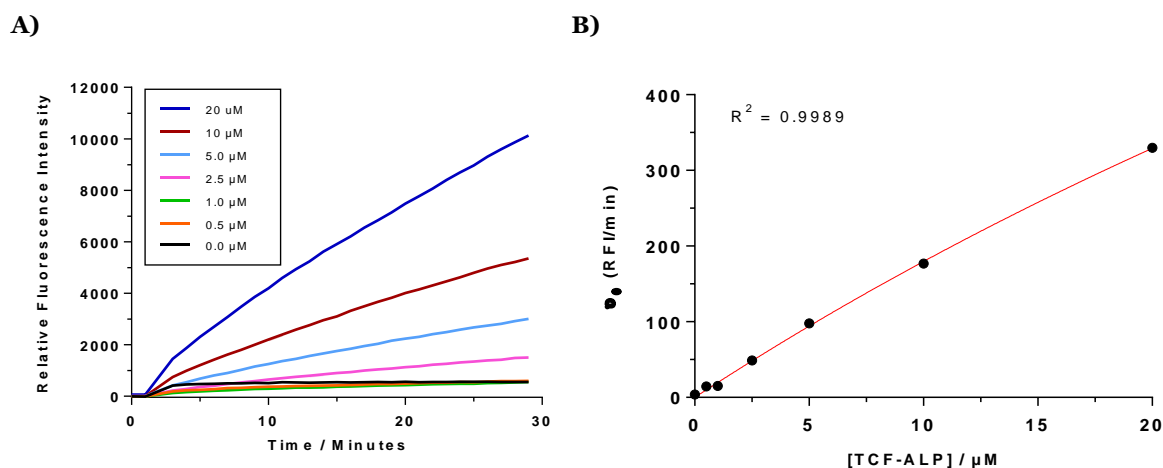


**Figure 6.23: A)** Time-dependent fluorescence intensity seen for increasing concentrations of TCF-ALP (0 – 20 μM) in the presence of 0.2 U/mL of ACP in 50 mM Tris-HCl buffer, pH 7.1. **B)** Plot of initial velocity ( $v_0$ ) against TCF-ALP concentration.  $K_m = 99.22 \pm 13.16 \mu\text{M}$ ,  $V_{\text{max}} = 1962 \pm 223.6 \text{ min}^{-1}$ ,  $R^2 = 0.9989$ . Measurements taken at 25 °C,  $\lambda_{\text{ex}} = 542$  (bandwidth 15 nm)/  $\lambda_{\text{em}} = 606$  (bandwidth 20) nm. Error bars indicate standard deviation ( $n = 3$ )

### 6.4.8. Cell-based Assays

While the principle aim of this probe was for it to be used as a diagnostic marker for bacterial infections (see Chapter 7), the detection of ALP also has a clinical utility in the diagnosis of other diseases. Owing to this, **TCF-ALP** was sent to Juyoung Yoon at Ewha Womans University, Seoul, South Korea to perform cell culture experiments. Firstly, the cytotoxicity of **TCF-ALP** was assessed using a 3-(4,5-dimethylthiazol-2-yl)-2,5-diphenyl-2H-tetrazolium bromide (MTT) assay (Figure 6.24). The MTT assay measures cellular metabolic activity; it is often used to determine the cell viability and proliferation of specific cells in response to incubation with a substrate (e.g., fluorescent probe), and therefore can be used to determine parameters such as cytotoxicity. The MTT assay is a colorimetric assay based on the reduction of a yellow tetrazolium salt to purple formazan crystals by metabolically active cells via oxidoreductase enzymes. The more intense the purple colour, the greater the number of viable, metabolically active cells.<sup>104</sup>

Figure 6.24 shows that negligible cell toxicity was observed for **TCF-ALP** concentrations between 0 – 5  $\mu\text{M}$ , and cell viability was only slightly reduced (cell viability: 91%) when incubated with 10  $\mu\text{M}$  **TCF-ALP** – indicating good biocompatibility.

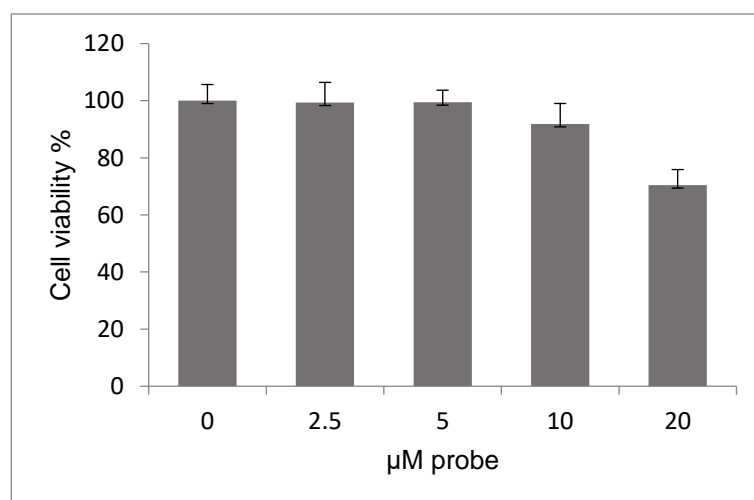


**Figure 6.24:** HeLa cells were incubated with increasing concentrations of **TCF-ALP** for 24 h. After incubation, cells were treated with MTT media and cultured for another 4 h. Absorbance of the untreated cells were determined as 100 % live.  $n = 3 \pm$  standard deviation

For cell imaging, 10  $\mu\text{M}$  of **TCF-ALP** was incubated with HeLa cells as they are known to overexpress ALP. As shown in Figure 6.25, **TCF-ALP** was cell permeable in HeLa cells, and provided a clear ‘turn on’ response. To determine whether this increase in fluorescence was due to ALP, cells were pre-treated with varying concentrations of  $\text{Na}_3\text{VO}_4$  and a minimal

'turn on' response was observed when cells were pre-incubated with 0.5 mM of  $\text{Na}_3\text{VO}_4$ , with further reduction in fluorescence intensity observed upon increasing inhibitor concentration. The decrease in **TCF-ALP** activity upon increasing inhibitor concentrations supports the hypothesis that any increase in **TCF-ALP** fluorescence levels seen for HeLa cells in the absence of  $\text{Na}_3\text{VO}_4$  was due to ALP activity. We thus conclude **TCF-ALP** is capable to selectively detect ALP activity in cellular imaging.

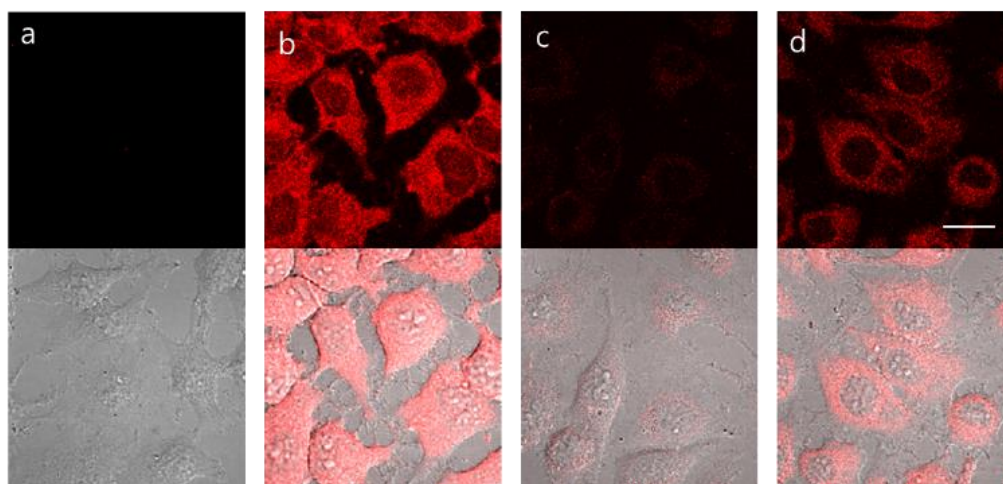


**Figure 6.25:** Images of HeLa cells incubated under the following conditions: (a) No treatment. (b) **TCF-ALP** (10  $\mu\text{M}$ , 30 min). (c) Pre-treated with  $\text{Na}_3\text{VO}_4$  (5 mM, 30 min), followed by the addition of **TCF-ALP** (10  $\mu\text{M}$ , 30 min). (d) Pretreated with  $\text{Na}_3\text{VO}_4$  (0.5 mM, 30 min) and **TCF-ALP** (10  $\mu\text{M}$ , 30 min). Cells were washed with DPBS before their fluorescence images were acquired using a confocal microscope. Top half: fluorescence images, bottom half: fluorescence images merged with its corresponding DIC image. Ex. 559 nm/ em. 575-675 nm. Scale bar : 20  $\mu\text{m}$ . DIC - differential interference contrast

Next, the focus shifted towards myogenic murine C2C12 cells; they are a subclone from a myoblast line established from normal adult C3H mouse leg muscle (Figure 6.26). Treatment of C2C12 cells with **TCF-ALP** resulted in a low fluorescence 'turn-on', indicating low ALP levels. Upon pre-treatment of C2C12 cells with bone morphogenic protein-2 (BMP-2) (300 ng/mL, 3 days) resulted in a significant increase in **TCF-ALP**-derived fluorescence intensity, indicative of high ALP levels. BMP-2 is capable of inducing osteoblast differentiation in a variety of cell types and regulates the expression of genes activated during osteoblast differentiation.<sup>17</sup> Additionally, BMP-2 has been shown to increase ALP mRNA expression and ALP activity,<sup>106,107</sup> which could explain why pre-treatment with BMP-2 resulted in increased levels of ALP activity and corresponding fluorescence intensity upon incubation with **TCF-ALP**.

Once again, pre-incubation with an ALP inhibitor (levamisole) led to a limited fluorescence response being observed in the cells treated with **TCF-ALP** (with or without BMP-2),

further providing support for the theory that **TCF-ALP** is capable of imaging endogenous ALP activity, including ALP activity induced by BMP-2.

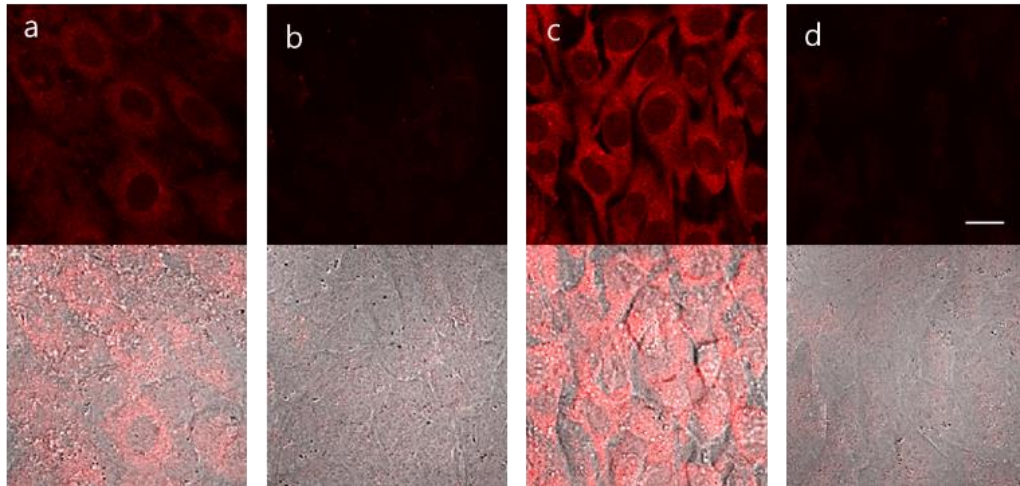


**Figure 6.26:** Images of C2C12 cells incubated under the following conditions: (a) **TCF-ALP** only (b) levamisole + **TCF-ALP**, (c) BMP-2 + **TCF-ALP** (d) BMP-2 + levamisole + **TCF-ALP**. Top : fluorescence images, bottom: merged with DIC image. Ex. 559 nm/ em. 575-675 nm. Scale bar : 20  $\mu$ m. DIC - differential interference contrast

## 6.5. Conclusions and Future Work

This chapter describes the novel synthesis of **TCF-ALP**, a fluorescent and colorimetric probe used to detect phosphatase activity. The hydrolysis of **TCF-ALP** by ALP was confirmed via  $^{31}\text{P}$  NMR and mass spectrometry.

Subsequent experiments found that **TCF-ALP** was capable of detecting ALP, with a LOD of 0.12 mU/mL; a concurrent colorimetric response from yellow to purple was also observed. Additionally, inhibition experiments using sodium orthovanadate further confirmed the dephosphorylation and subsequent activation of **TCF-ALP** with ALP, as there was a decrease in fluorescence intensity upon increasing inhibitor concentrations, with  $\text{IC}_{50}$  and  $\text{K}_i$  values similar to that reported in the literature.

**TCF-ALP** displayed high selectivity towards ALP compared to other biologically relevant enzymes and non-specific binding proteins at their optimal pH, with the exception of ACP. Owing to the increase in fluorescence intensity when **TCF-ALP** was incubated with ACP, further experiments were conducted to evaluate the selectivity of **TCF-ALP** towards ALP and ACP at pH 9.2, 7.1, and 5.0. It was found that **TCF-ALP** was more selective towards ALP at pH 9.2, while it was more selective towards ACP at pH 5.0. At physiological pH, the selectivity assay showed that **TCF-ALP** was more selective towards ALP vs ACP, and this was confirmed by calculating their corresponding  $\text{K}_m$  and  $\text{V}_{\text{max}}$  values.

Finally, **TCF-ALP** was investigated using human HeLa cells and murine C2C12 cells pre-treated with BMP-2 to increase ALP activity. The results showed that **TCF-ALP** was cell permeable and capable of detecting ALP activity within the cells at concentrations (10  $\mu\text{M}$ ) that were non-toxic. These results suggest that **TCF-ALP** could be used as a tool for measuring ALP and ACP activity levels in clinical assays or in live cell systems.

## 6.6. Appendix

### 6.6.1. Nuclear Magnetic Resonance (NMR) Spectra

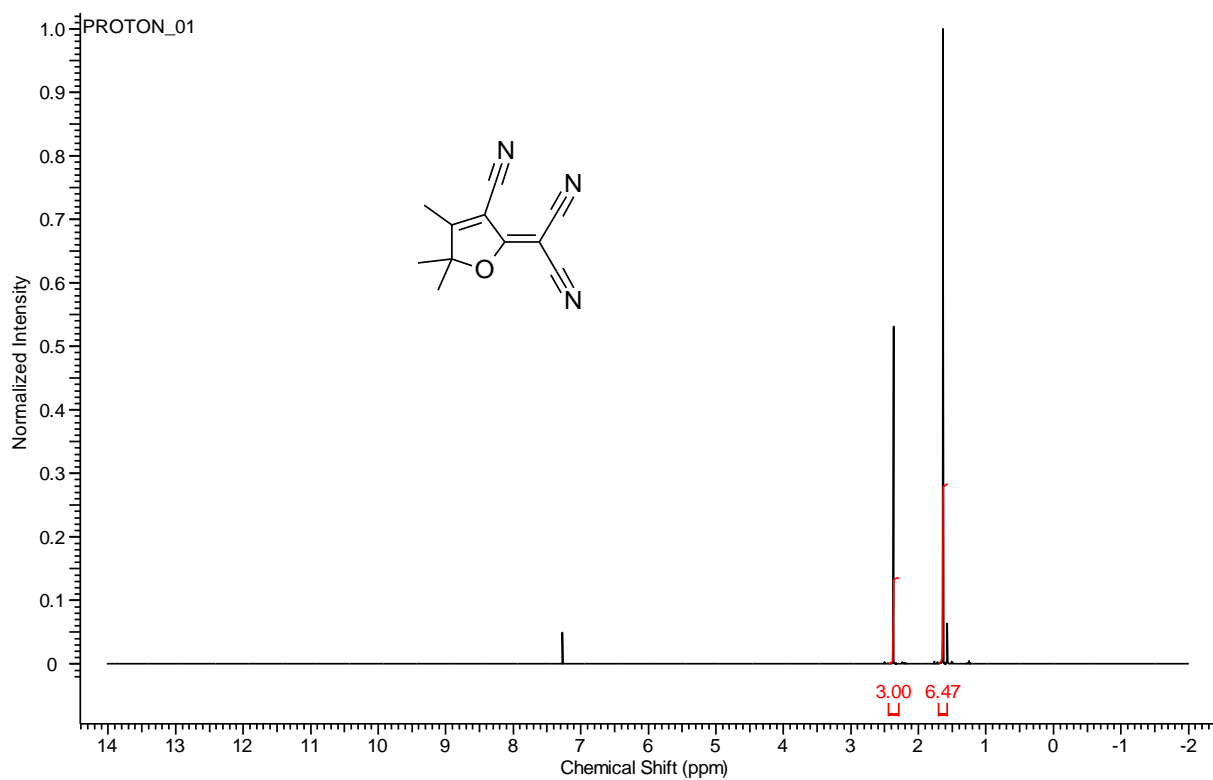


**Figure S1:** <sup>1</sup>H NMR of 2-(3-Cyano-4,5,5-trimethylfuran-2(5H)-ylidene)malononitrile (**1**) (500 MHz, CDCl<sub>3</sub>)

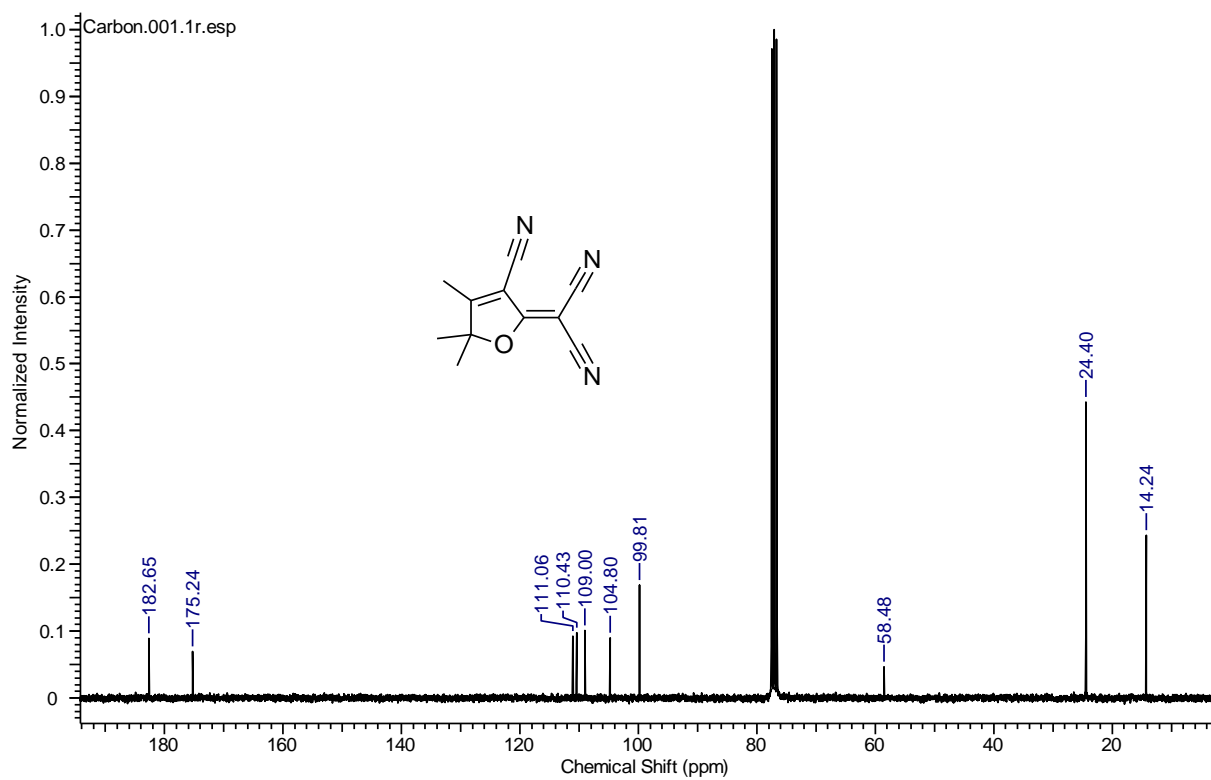


**Figure S2:**  $^{13}\text{C}$  NMR of 2-(3-Cyano-4,5,5-trimethylfuran-2(5H)-ylidene)malononitrile (**1**) (75.5 MHz,  $\text{CDCl}_3$ )



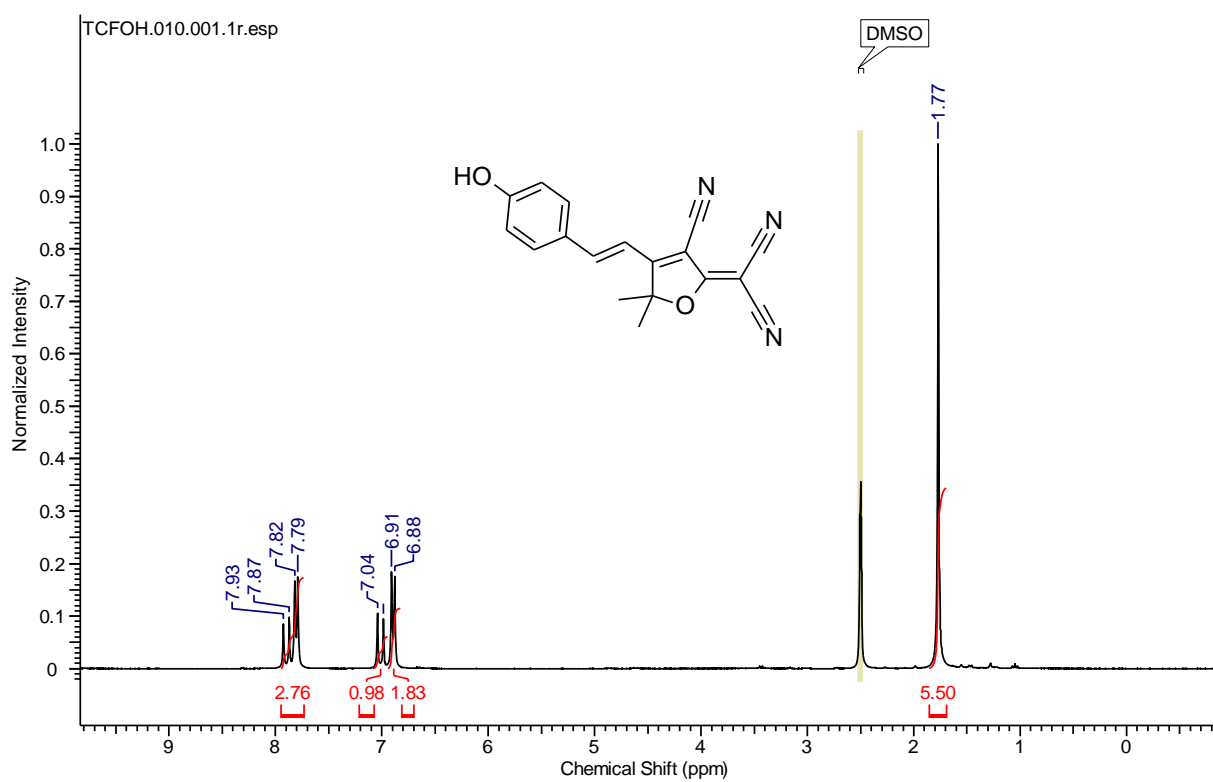


**Figure S3:**  $^1\text{H}$  NMR of (E)-2-(3-Cyano-4-(4-hydroxystyryl)-5,5-dimethylfuran-2(5H)-ylidene)malononitrile (**2**) (300 MHz,  $\text{CDCl}_3$ )

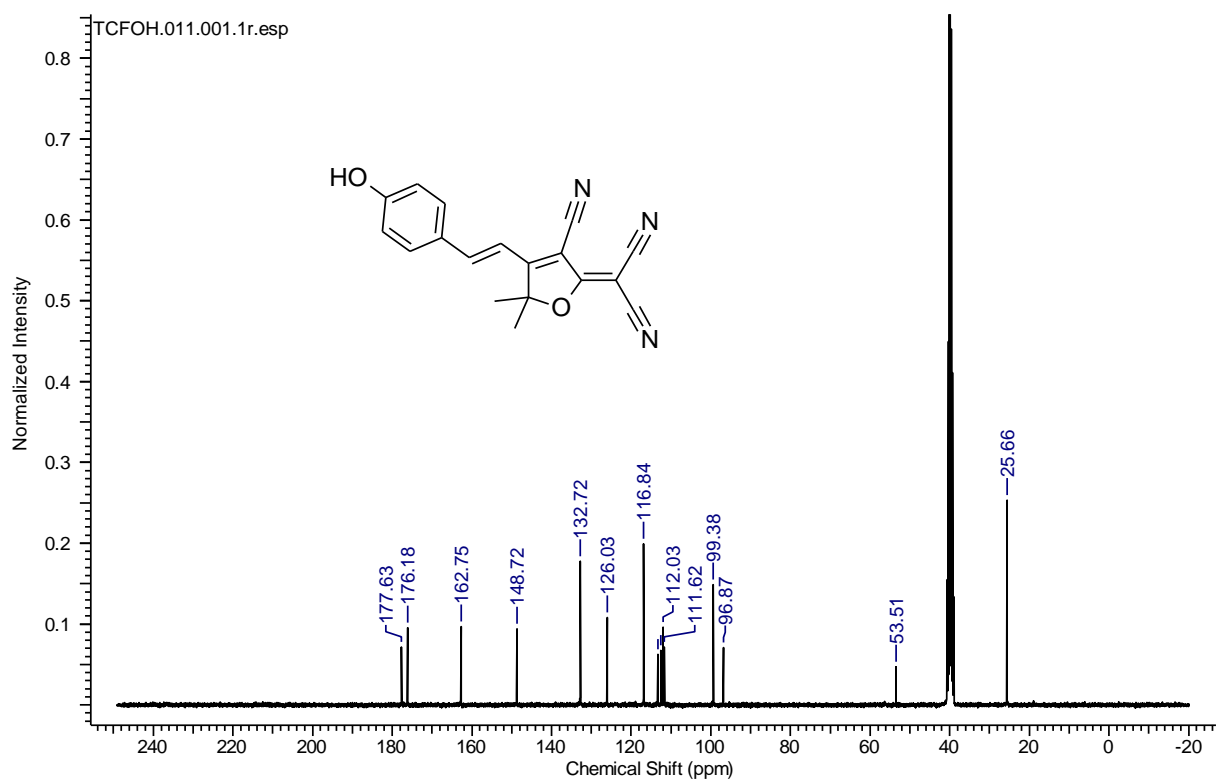


**Figure S4:**  $^{13}\text{C}$  NMR of (E)-2-(3-Cyano-4-(4-hydroxystyryl)-5,5-dimethylfuran-2(5H)-ylidene)malononitrile (**2**) (75.5 MHz,  $\text{CDCl}_3$ )

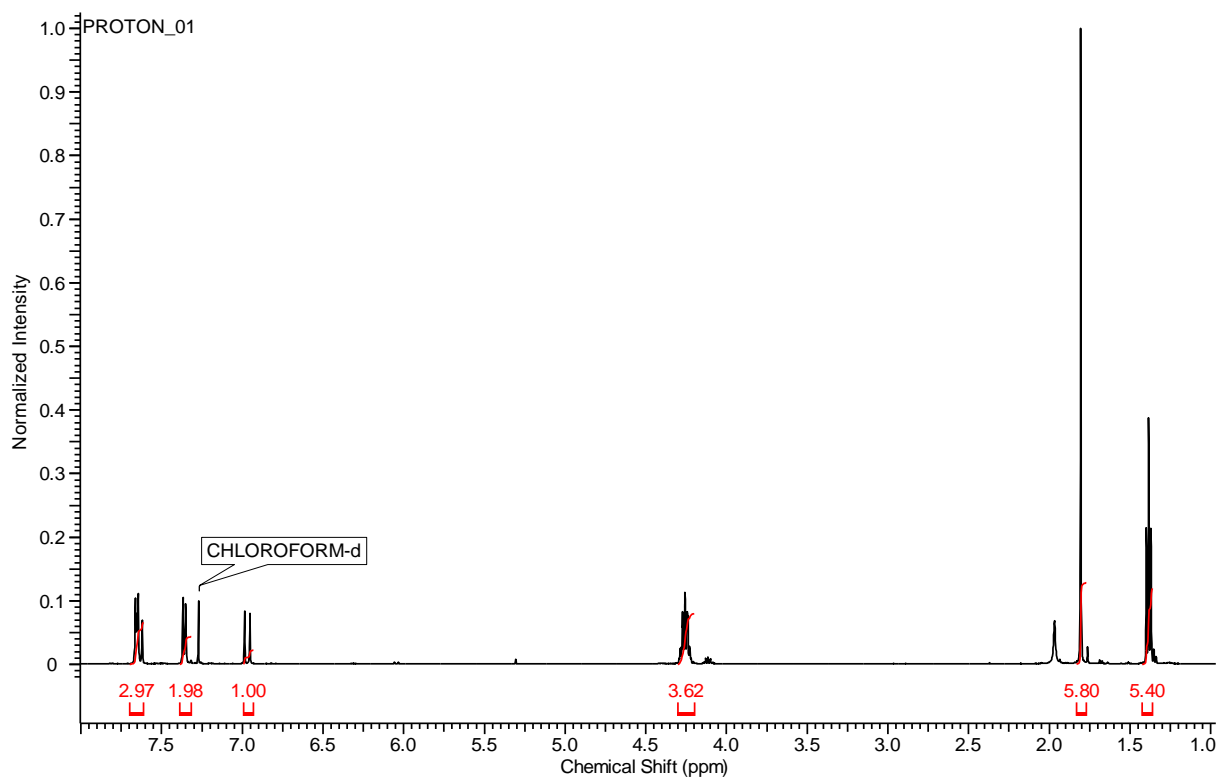
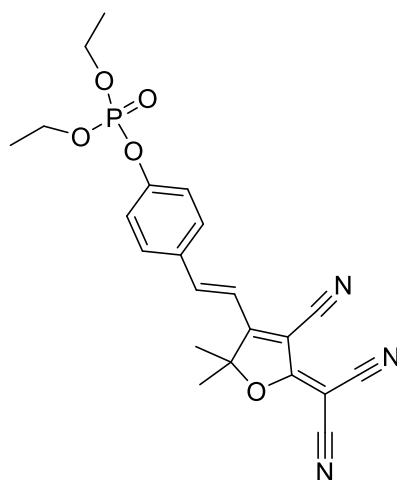


**Figure S5:**  $^1\text{H}$  NMR of (E)-4-(2-(4-Cyano-5-(dicyanomethylene)-2,2-dimethyl-2,5-dihydrofuran-3-yl)vinyl)phenyl diethyl phosphate (**3**) (500 MHz,  $\text{CDCl}_3$ )

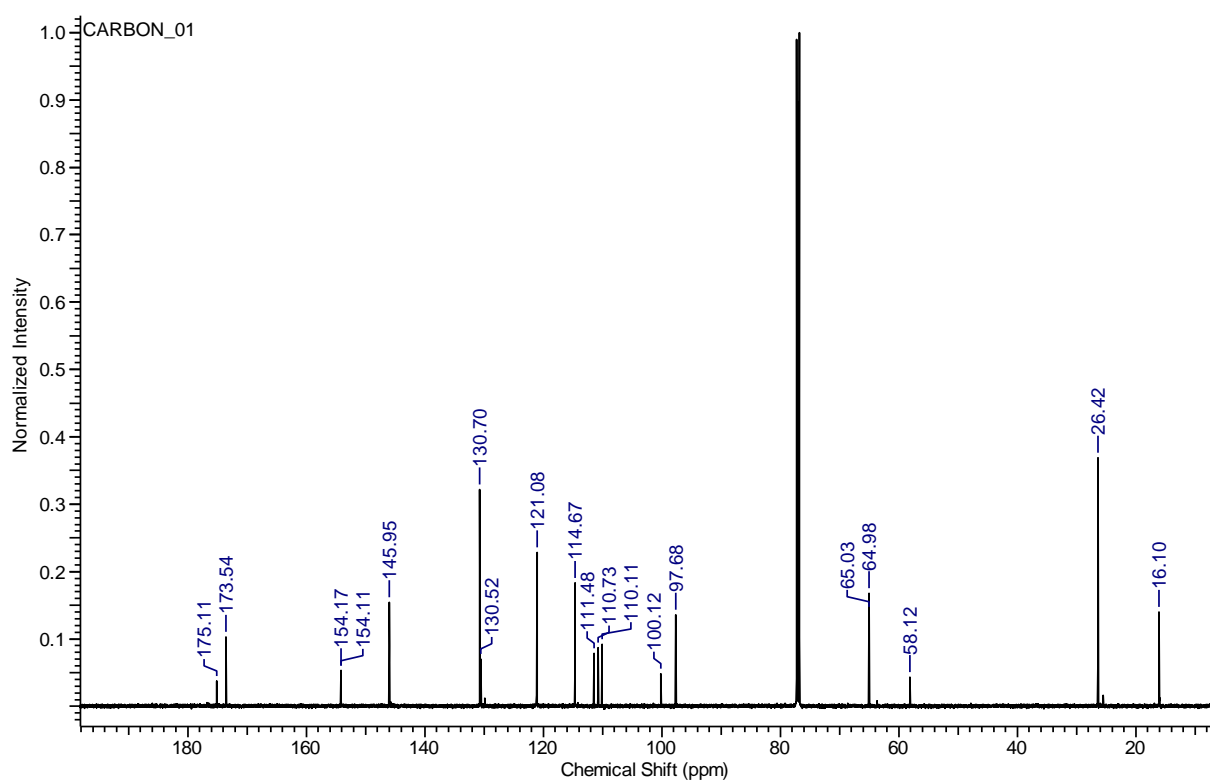
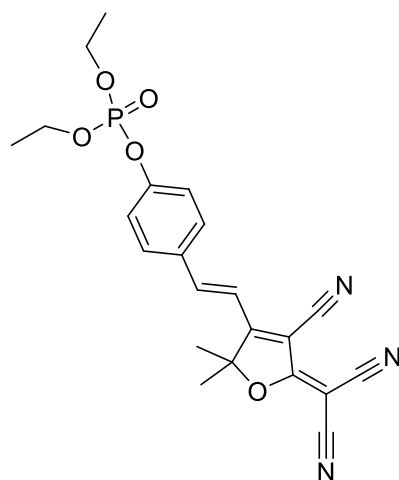


**Figure S6:**  $^{13}\text{C}$  NMR of (E)-4-(2-(4-Cyano-5-(dicyanomethylene)-2,2-dimethyl-2,5-dihydrofuran-3-yl)vinyl)phenyl diethyl phosphate (**3**) (125.7 MHz,  $\text{CDCl}_3$ )

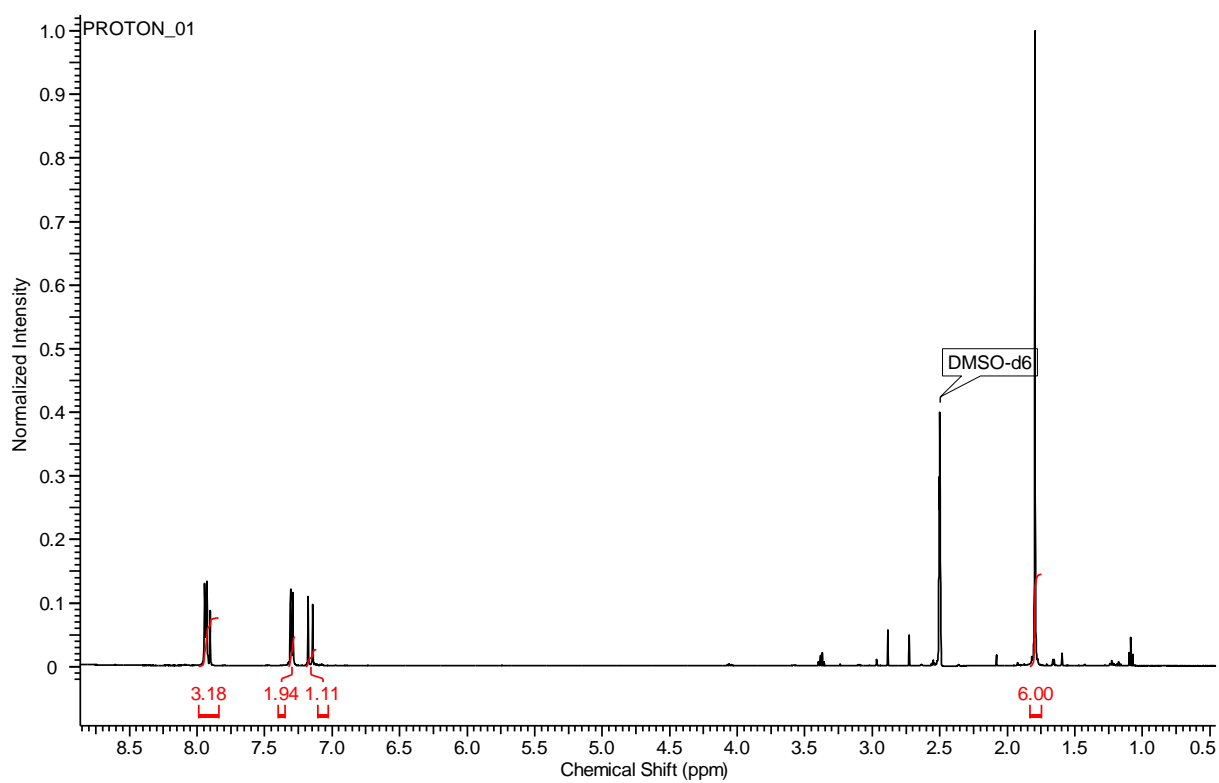
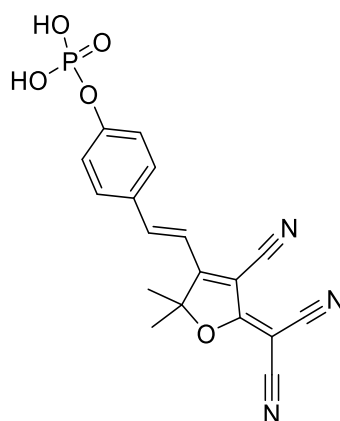


**Figure S7:**  $^1\text{H}$  NMR of (E)-4-(2-(4-Cyano-5-(dicyanomethylene)-2,2-dimethyl-2,5-dihydrofuran-3-yl)vinyl)phenyl phosphate (**TCF-ALP**) (500 MHz, DMSO-d6)

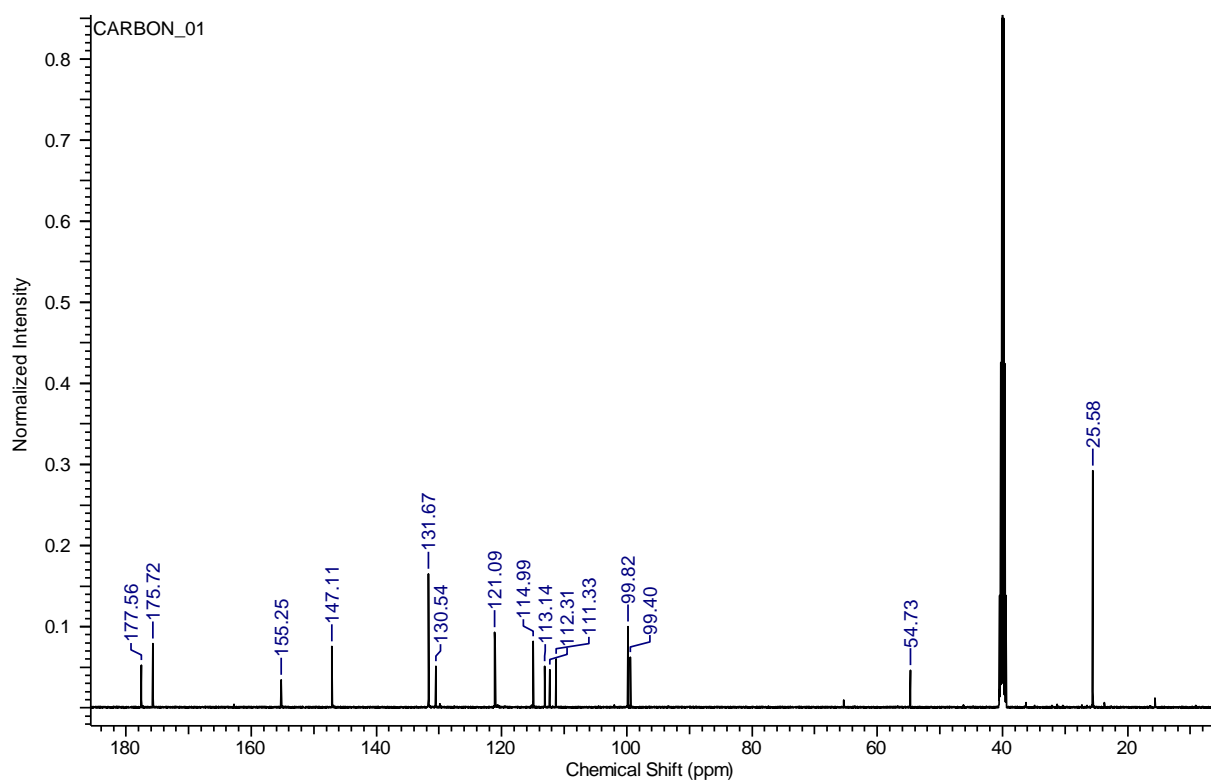
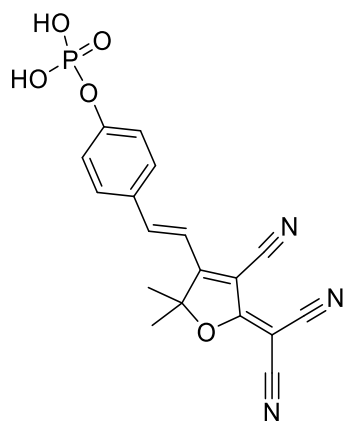


**Figure S8:**  $^{13}\text{C}$  NMR of (E)-4-(2-(4-Cyano-5-(dicyanomethylene)-2,2-dimethyl-2,5-dihydrofuran-3-yl)vinyl)phenyl phosphate (**TCF-ALP**) (125.7 MHz,  $\text{DMSO-}d_6$ )

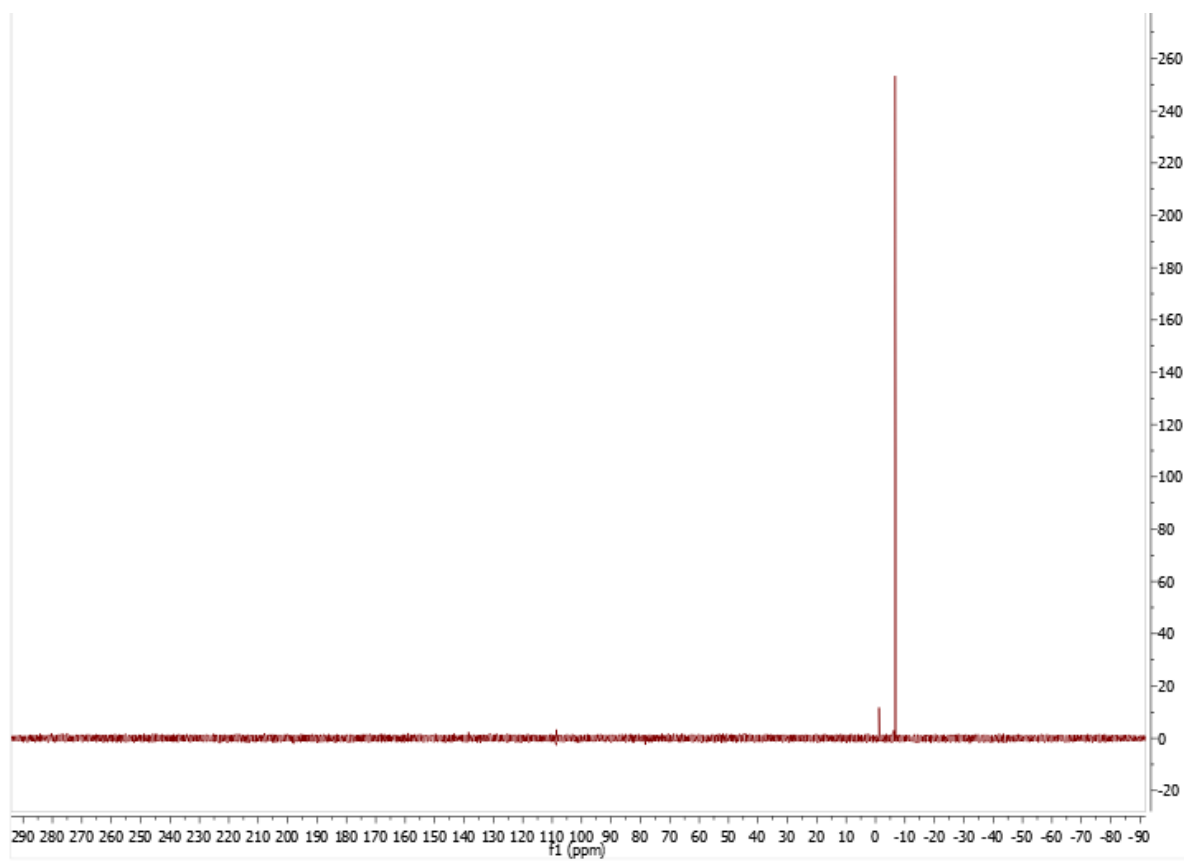
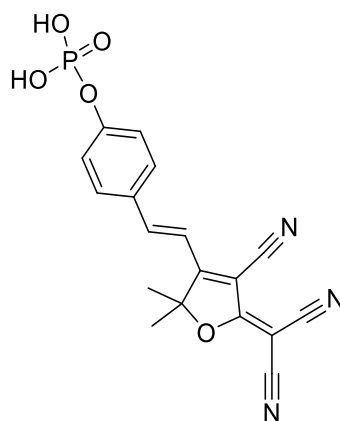


**Figure S9:**  $^{31}\text{P}$  NMR of (E)-4-(2-(4-Cyano-5-(dicyanomethylene)-2,2-dimethyl-2,5-dihydrofuran-3-yl)vinyl)phenyl phosphate (**TCF-ALP**) (202.4 MHz,  $\text{DMSO-}d_6$ )

## 6.7. References

1. Lakowicz JR. Principles of fluorescence spectroscopy. Springer science & business media; 2013.
2. Gardiner J. Fluorescence probes for the detection of biologically relevant species. University of Bath; 2019.
3. Suzuki Y, Yokoyama K. Development of functional fluorescent molecular probes for the detection of biological substances. *Biosensors*. 2015;5(2):337–63.
4. Wu D, Sedgwick AC, Gunnlaugsson T, Akkaya EU, Yoon J, James TD. Fluorescent chemosensors: the past, present and future. *Chem Soc Rev*. 2017;46(23):7105–23.
5. Chen X, Tian X, Shin I, Yoon J. Fluorescent and luminescent probes for detection of reactive oxygen and nitrogen species. *Chem Soc Rev*. 2011;40(9):4783–804.
6. Cheng D, Peng J, Lv Y, Su D, Liu D, Chen M, et al. De novo design of chemical stability near-infrared molecular probes for high-fidelity hepatotoxicity evaluation in vivo. *J Am Chem Soc*. 2019;141(15):6352–61.
7. Liu H-W, Chen L, Xu C, Li Z, Zhang H, Zhang X-B, et al. Recent progresses in small-molecule enzymatic fluorescent probes for cancer imaging. *Chem Soc Rev*. 2018;47(18):7140–80.
8. Niu L-Y, Chen Y-Z, Zheng H-R, Wu L-Z, Tung C-H, Yang Q-Z. Design strategies of fluorescent probes for selective detection among biothiols. *Chem Soc Rev*. 2015;44(17):6143–60.
9. Rodriguez-Cuenca S, Pellegrinelli V, Campbell M, Oresic M, Vidal-Puig A. Sphingolipids and glycerophospholipids—the “ying and yang” of lipotoxicity in metabolic diseases. *Prog Lipid Res*. 2017;66:14–29.
10. Zheng J, Yang R, Shi M, Wu C, Fang X, Li Y, et al. Rationally designed molecular beacons for bioanalytical and biomedical applications. *Chem Soc Rev*. 2015;44(10):3036–55.
11. Lichtman JW, Conchello J-A. Fluorescence microscopy. *Nat Methods*. 2005;2(12):910–9.
12. Ren T-B, Xu W, Zhang W, Zhang X-X, Wang Z-Y, Xiang Z, et al. A general method to



- increase stokes shift by introducing alternating vibronic structures. *J Am Chem Soc.* 2018;140(24):7716–22.
13. Terai T, Nagano T. Fluorescent probes for bioimaging applications. *Curr Opin Chem Biol.* 2008;12(5):515–21.
  14. Bruemmer KJ, Brewer TF, Chang CJ. Fluorescent probes for imaging formaldehyde in biological systems. *Curr Opin Chem Biol.* 2017;39:17–23.
  15. Valeur B, Berberan-Santos MN. A brief history of fluorescence and phosphorescence before the emergence of quantum theory. *J Chem Educ.* 2011;88(6):731–8.
  16. Yuan L, Lin W, Zheng K, He L, Huang W. Far-red to near infrared analyte-responsive fluorescent probes based on organic fluorophore platforms for fluorescence imaging. *Chem Soc Rev.* 2013;42(2):622–61.
  17. Guo Z, Park S, Yoon J, Shin I. Recent progress in the development of near-infrared fluorescent probes for bioimaging applications. *Chem Soc Rev.* 2014;43(1):16–29.
  18. Nolting D, Gore J, Pham W. Near-infrared dyes: probe development and applications in optical molecular imaging. *Curr Org Synth.* 2011;8(4):521–34.
  19. Escobedo JO, Rusin O, Lim S, Strongin RM. NIR dyes for bioimaging applications. *Curr Opin Chem Biol.* 2010;14(1):64–70.
  20. Carter KP, Young AM, Palmer AE. Fluorescent sensors for measuring metal ions in living systems. *Chem Rev.* 2014;114(8):4564–601.
  21. Fu Y, Finney NS. Small-molecule fluorescent probes and their design. *RSC Adv.* 2018;8(51):29051–61.
  22. De Silva AP, Moody TS, Wright GD. Fluorescent PET (Photoinduced Electron Transfer) sensors as potent analytical tools. *Analyst.* 2009;134(12):2385–93.
  23. Qin W, Xu C, Zhao Y, Yu C, Shen S, Li L, et al. Recent progress in small molecule fluorescent probes for nitroreductase. *Chinese Chem Lett.* 2018;29(10):1451–5.
  24. Taya P, Maiti B, Kumar V, De P, Satapathi S. Design of a novel FRET based fluorescent chemosensor and their application for highly sensitive detection of nitroaromatics. *Sensors Actuators B Chem.* 2018;255:2628–34.
  25. Turro NJ, Ramamurthy V, Ramamurthy V, Scaiano JC. Principles of molecular

photochemistry: an introduction. University science books; 2009.

26. Forster T. Delocalization excitation and excitation transfer. *Mod quantum Chem.* 1965;
27. Clegg RM. Fluorescence resonance energy transfer. *Fluoresc imaging Spectrosc Microsc.* 1996;137:179–251.
28. Lakowicz JR. *Principles of Fluorescence Spectroscopy*, vol. 410. Kluwer-Plenum, New York; 1999.
29. Zhao J, Ji S, Chen Y, Guo H, Yang P. Excited state intramolecular proton transfer (ESIPT): from principal photophysics to the development of new chromophores and applications in fluorescent molecular probes and luminescent materials. *Phys Chem Chem Phys.* 2012;14(25):8803–17.
30. Sedgwick AC, Wu L, Han H-H, Bull SD, He X-P, James TD, et al. Excited-state intramolecular proton-transfer (ESIPT) based fluorescence sensors and imaging agents. *Chem Soc Rev.* 2018;47(23):8842–80.
31. Iijima T, Momotake A, Shinohara Y, Sato T, Nishimura Y, Arai T. Excited-state intramolecular proton transfer of naphthalene-fused 2-(2'-hydroxyaryl) benzazole family. *J Phys Chem A.* 2010;114(4):1603–9.
32. Li G, Han K. The sensing mechanism studies of the fluorescent probes with electronically excited state calculations. *Wiley Interdiscip Rev Comput Mol Sci.* 2018;8(2):e1351.
33. Zhu B, Wang W, Liu L, Jiang H, Du B, Wei Q. A highly selective colorimetric and long-wavelength fluorescent probe for Hg<sup>2+</sup>. *Sensors Actuators B Chem.* 2014;191:605–11.
34. Zhu B, Kan H, Liu J, Liu H, Wei Q, Du B. A highly selective ratiometric visual and red-emitting fluorescent dual-channel probe for imaging fluoride anions in living cells. *Biosens Bioelectron.* 2014;52:298–303.
35. Teng X, Tian M, Zhang J, Tang L, Xin J. A tcf-based colorimetric and fluorescent probe for palladium detection in an aqueous solution. *Tetrahedron Lett.* 2018;59(29):2804–8.
36. Sedgwick AC, Gardiner JE, Kim G, Yevglevskis M, Lloyd MD, Jenkins ATA, et al.

- Long-wavelength TCF-based fluorescence probes for the detection and intracellular imaging of biological thiols. *Chem Commun.* 2018;54(38):4786–9.
37. Sedgwick AC, Han H-H, Gardiner JE, Bull SD, He X-P, James TD. Long-wavelength fluorescent boronate probes for the detection and intracellular imaging of peroxynitrite. *Chem Commun.* 2017;53(95):12822–5.
  38. Meng Y-L, Xin Z-H, Jia Y-J, Kang Y-F, Ge L-P, Zhang C-H, et al. A near-infrared fluorescent probe for direct and selective detection of cysteine over homocysteine and glutathione. *Spectrochim Acta Part A Mol Biomol Spectrosc.* 2018;202:301–4.
  39. Wang YJ, Shi Y, Wang Z, Zhu Z, Zhao X, Nie H, et al. A Red to Near-IR Fluorogen: Aggregation-Induced Emission, Large Stokes Shift, High Solid Efficiency and Application in Cell-Imaging. *Chem Eur J.* 2016;22(28):9784–91.
  40. Gopalan P, Katz HE, McGee DJ, Erben C, Zielinski T, Bousquet D, et al. Star-shaped azo-based dipolar chromophores: design, synthesis, matrix compatibility, and electro-optic activity. *J Am Chem Soc.* 2004;126(6):1741–7.
  41. Liao Y, Bhattacharjee S, Firestone KA, Eichinger BE, Paranjli R, Anderson CA, et al. Antiparallel-aligned neutral-ground-state and zwitterionic chromophores as a nonlinear optical material. *J Am Chem Soc.* 2006;128(21):6847–53.
  42. Lord SJ, Conley NR, Lee HD, Samuel R, Liu N, Twieg RJ, et al. A photoactivatable push– pull fluorophore for single-molecule imaging in live cells. *J Am Chem Soc.* 2008;130(29):9204–5.
  43. Bouffard J, Kim Y, Swager TM, Weissleder R, Hilderbrand SA. A highly selective fluorescent probe for thiol bioimaging. *Org Lett.* 2008;10(1):37–40.
  44. Jin Y, Tian Y, Zhang W, Jang S-H, Jen AK-Y, Meldrum DR. Tracking bacterial infection of macrophages using a novel red-emission pH sensor. *Anal Bioanal Chem.* 2010;398(3):1375–84.
  45. Gwynne L, Sedgwick AC, Gardiner JE, Williams GT, Kim G, Maillard J-Y, et al. Long wavelength TCF-based fluorescence probe for the detection of Alkaline Phosphatase in live cells. *Front Chem.* 2019;7:255.
  46. Wang X, Min J, Wang W, Wang Y, Yin G, Wang R. A novel porphyrin-based near-infrared fluorescent probe for hypochlorite detection and its application in vitro and in vivo. *Analyst.* 2018;143(11):2641–7.

47. Berg JM, Tymoczko JL, Stryer L. Biochemistry, 5th edn WH Freeman. New York[Google Sch. 2002;
48. Bhatia S, Kharb R, Kulkarni GT, Mazhar M, Sunder S. Introduction to enzymes and their applications.
49. Robinson PK. Enzymes: principles and biotechnological applications. Essays Biochem. 2015;59:1–41.
50. Blanco A, Blanco G. Chapter 8—Enzymes. Med Biochem Blanco, A, Blanco, G, Eds. 2017;153–75.
51. Singh RS, Singh T, Singh AK. Enzymes as Diagnostic Tools. In: Advances in Enzyme Technology. Elsevier; 2019. p. 225–71.
52. Vimal A, Kumar A. Transforming the healthcare system through therapeutic enzymes. In: Enzymes in Food Biotechnology. Elsevier; 2019. p. 603–25.
53. Raja MMM, Raja A, Imran MM, Santha AMI, Devasena K. Enzymes application in diagnostic prospects. Biotechnology. 2011;10(1):51–9.
54. Devi CS, Nadiger HA, Krishna TS, Naidu JN. Serum acid phosphatase level-is it a marker for diagnosis of malaria. Int J Res Med Sci. 2017;5(10):4400.
55. Freethi R, Raj AV, Ponniraivan K, Khan MR, Sundhararajan A. Study of serum levels of calcium, phosphorus and alkaline phosphatase in chronic kidney disease. Int J Med Res Heal Sci. 2016;5(3):49–56.
56. Esmaili HA, Mehramuz B, Maroufi P, Ghasemi A, Pournalak T. Diagnostic value of amylase and lipase in diagnosis of acute pancreatitis. Biomed Pharmacol J. 2017;10(1):389–94.
57. Fleisher LA. Anesthesia and Uncommon Diseases E-Book. Elsevier Health Sciences; 2012.
58. Dimarakis I, Joshi V, Hesford W, Asimakopoulos G. Minimized extracorporeal circulation: physiology and pathophysiology. In: Minimized Cardiopulmonary Bypass Techniques and Technologies. Elsevier; 2012. p. 35–44.
59. Chan FK-M, Moriwaki K, De Rosa MJ. Detection of necrosis by release of lactate dehydrogenase activity. In: Immune Homeostasis. Springer; 2013. p. 65–70.

60. Wilson ML, Gaido L. Laboratory diagnosis of urinary tract infections in adult patients. *Clin Infect Dis*. 2004;38(8):1150–8.
61. Higaki S, Morohashi M. Propionibacterium acnes lipase in seborrheic dermatitis and other skin diseases and Unsei-in. *Drugs Exp Clin Res*. 2003;29(4):157–9.
62. Torsteinsdóttir I, Håkansson L, Hällgren R, Gudbjörnsson B, Arvidson N-G, Venge P. Serum lysozyme: a potential marker of monocyte/macrophage activity in rheumatoid arthritis. *Rheumatology*. 1999;38(12):1249–54.
63. Millán JL. Alkaline phosphatases. *Purinergic Signal*. 2006;2(2):335.
64. Coleman JE. Structure and mechanism of alkaline phosphatase. *Annu Rev Biophys Biomol Struct*. 1992;21(1):441–83.
65. Julien SG, Dubé N, Hardy S, Tremblay ML. Inside the human cancer tyrosine phosphatome. *Nat Rev Cancer*. 2011;11(1):35–49.
66. Ooi K, Shiraki K, Morishita Y, Nobori T. High-molecular intestinal alkaline phosphatase in chronic liver diseases. *J Clin Lab Anal*. 2007;21(3):133–9.
67. Garnerio P, Delmas PD. Assessment of the serum levels of bone alkaline phosphatase with a new immunoradiometric assay in patients with metabolic bone disease. *J Clin Endocrinol Metab*. 1993;77(4):1046–53.
68. Rosen E, Sabel AL, Brinton JT, Catanach B, Gaudiani JL, Mehler PS. Liver dysfunction in patients with severe anorexia nervosa. *Int J Eat Disord*. 2016;49(2):151–8.
69. Ritzke C, Stieber P, Untch M, Nagel D, Eiermann W, Fateh-Moghadam A. Alkaline phosphatase isoenzymes in detection and follow up of breast cancer metastases. *Anticancer Res*. 1998;18(2B):1243–9.
70. Wymenga LFA, Boomsma JHB, Groenier K, Piers DA, Mensink HJA. Routine bone scans in patients with prostate cancer related to serum prostate-specific antigen and alkaline phosphatase. *BJU Int*. 2001;88(3):226–30.
71. Tibi L, Collier A, Patrick AW, Clarke BF, Smith AF. Plasma alkaline phosphatase isoenzymes in diabetes mellitus. *Clin Chim acta*. 1988;177(2):147–55.
72. Yang J, Zheng L, Wang Y, Li W, Zhang J, Gu J, et al. Guanine-rich DNA-based

- peroxidase mimetics for colorimetric assays of alkaline phosphatase. *Biosens Bioelectron.* 2016;77:549–56.
73. Hu Q, Zhou B, Dang P, Li L, Kong J, Zhang X. Facile colorimetric assay of alkaline phosphatase activity using Fe (II)-phenanthroline reporter. *Anal Chim Acta.* 2017;950:170–7.
74. Jiang H, Wang X. Alkaline phosphatase-responsive anodic electrochemiluminescence of CdSe nanoparticles. *Anal Chem.* 2012;84(16):6986–93.
75. Zhang L, Hou T, Li H, Li F. A highly sensitive homogeneous electrochemical assay for alkaline phosphatase activity based on single molecular beacon-initiated T7 exonuclease-mediated signal amplification. *Analyst.* 2015;140(12):4030–6.
76. Ruan C, Wang W, Gu B. Detection of alkaline phosphatase using surface-enhanced Raman spectroscopy. *Anal Chem.* 2006;78(10):3379–84.
77. Cao F-Y, Long Y, Wang S-B, Li B, Fan J-X, Zeng X, et al. Fluorescence light-up AIE probe for monitoring cellular alkaline phosphatase activity and detecting osteogenic differentiation. *J Mater Chem B.* 2016;4(26):4534–41.
78. Fan C, Luo S, Qi H. A ratiometric fluorescent probe for alkaline phosphatase via regulation of excited-state intramolecular proton transfer. *Luminescence.* 2016;31(2):423–7.
79. Zhang H, Xu C, Liu J, Li X, Guo L, Li X. An enzyme-activatable probe with a self-immolative linker for rapid and sensitive alkaline phosphatase detection and cell imaging through a cascade reaction. *Chem Commun.* 2015;51(32):7031–4.
80. Zhao L, Xie S, Song X, Wei J, Zhang Z, Li X. Ratiometric fluorescent response of electrospun fibrous strips for real-time sensing of alkaline phosphatase in serum. *Biosens Bioelectron.* 2017;91:217–24.
81. Li Y, Li Y, Wang X, Su X. A label-free conjugated polymer-based fluorescence assay for the determination of adenosine triphosphate and alkaline phosphatase. *New J Chem.* 2014;38(9):4574–9.
82. Qian Z, Chai L, Tang C, Huang Y, Chen J, Feng H. Carbon quantum dots-based recyclable real-time fluorescence assay for alkaline phosphatase with adenosine triphosphate as substrate. *Anal Chem.* 2015;87(5):2966–73.

83. Sun J, Yang F, Zhao D, Yang X. Highly sensitive real-time assay of inorganic pyrophosphatase activity based on the fluorescent gold nanoclusters. *Anal Chem.* 2014;86(15):7883–9.
84. Liu H-W, Hu X-X, Zhu L, Li K, Rong Q, Yuan L, et al. In vivo imaging of alkaline phosphatase in tumor-bearing mouse model by a promising near-infrared fluorescent probe. *Talanta.* 2017;175:421–6.
85. Zhang H, Xiao P, Wong YT, Shen W, Chhabra M, Peltier R, et al. Construction of an alkaline phosphatase-specific two-photon probe and its imaging application in living cells and tissues. *Biomaterials.* 2017;140:220–9.
86. Tan Y, Zhang L, Man KH, Peltier R, Chen G, Zhang H, et al. Reaction-based off–on near-infrared fluorescent probe for imaging alkaline phosphatase activity in living cells and mice. *ACS Appl Mater Interfaces.* 2017;9(8):6796–803.
87. Saif MW, Alexander D, Wicox CM. Serum alkaline phosphatase level as a prognostic tool in colorectal cancer: a study of 105 patients. *J Appl Res.* 2005;5(1):88.
88. Sahran Y, Sofian A, Saad A. Pre-treatment serum lactate dehydrogenase (LDH) and serum alkaline phosphatase (ALP) as prognostic factors in patients with osteosarcoma. *J Cancer Prev Curr Res.* 2018;9(2):58–63.
89. Zhang W, Yang H, Li N, Zhao N. A sensitive fluorescent probe for alkaline phosphatase and an activity assay based on the aggregation-induced emission effect. *RSC Adv.* 2018;8(27):14995–5000.
90. Tang C, Qian Z, Huang Y, Xu J, Ao H, Zhao M, et al. A fluorometric assay for alkaline phosphatase activity based on  $\beta$ -cyclodextrin-modified carbon quantum dots through host-guest recognition. *Biosens Bioelectron.* 2016;83:274–80.
91. Mao M, Tian T, He Y, Ge Y, Zhou J, Song G. Inner filter effect based fluorometric determination of the activity of alkaline phosphatase by using carbon dots codoped with boron and nitrogen. *Microchim Acta.* 2018;185(1):17.
92. Xu A-Z, Zhang L, Zeng H-H, Liang R-P, Qiu J-D. Fluorometric determination of the activity of alkaline phosphatase based on the competitive binding of gold nanoparticles and pyrophosphate to CePO<sub>4</sub>: Tb nanorods. *Microchim Acta.* 2018;185(6):288.
93. Han X, Han M, Ma L, Qu F, Kong R-M, Qu F. Self-assembled gold nanoclusters for

- fluorescence turn-on and colorimetric dual-readout detection of alkaline phosphatase activity via DCIP-mediated fluorescence resonance energy transfer. *Talanta*. 2019;194:55–62.
94. Ou-Yang J, Li C-Y, Li Y-F, Yang B, Li S-J. An infinite coordination polymer nanoparticles-based near-infrared fluorescent probe with high photostability for endogenous alkaline phosphatase in vivo. *Sensors Actuators B Chem*. 2018;255:3355–63.
  95. Mei Y, Hu Q, Zhou B, Zhang Y, He M, Xu T, et al. Fluorescence quenching based alkaline phosphatase activity detection. *Talanta*. 2018;176:52–8.
  96. Li S-J, Li C-Y, Li Y-F, Fei J, Wu P, Yang B, et al. Facile and sensitive near-infrared fluorescence probe for the detection of endogenous alkaline phosphatase activity in vivo. *Anal Chem*. 2017;89(12):6854–60.
  97. Lu Z, Wu J, Liu W, Zhang G, Wang P. A ratiometric fluorescent probe for quantification of alkaline phosphatase in living cells. *RSC Adv*. 2016;6(38):32046–51.
  98. BioLabs. Sodium orthovanadate [Internet]. [cited 2021 Jan 2]. Available from: [https://international.neb.com/products/p0758-sodium-orthovanadate-activated-vanadate#Product Information](https://international.neb.com/products/p0758-sodium-orthovanadate-activated-vanadate#Product%20Information)
  99. Benabe JE, Echegoyen LA, Pastrana B, Martinez-Maldonado M. Mechanism of inhibition of glycolysis by vanadate. *J Biol Chem*. 1987;262(20):9555–60.
  100. Burlingham BT, Widlanski TS. An intuitive look at the relationship of  $K_i$  and  $IC_{50}$ : a more general use for the Dixon plot. *J Chem Educ*. 2003;80(2):214.
  101. Ma F, Liu W, Liang L, Tang B, Zhang C-Y. Sensitive detection of alkaline phosphatase by dephosphorylation-initiated transcription reaction-mediated dual signal amplification. *Chem Commun*. 2018;54(19):2413–6.
  102. CDC. Alkaline Phosphatase (ALP) in Refrigerated Serum: NHANES 2011-2012.
  103. Myers JK, Widlanski TS. Mechanism-based inactivation of prostatic acid phosphatase. *Science* (80- ). 1993;262(5138):1451–3.
  104. Sigma Aldrich. MTT assay [Internet]. [cited 2021 Jan 2]. Available from: <https://www.sigmaaldrich.com/technical->



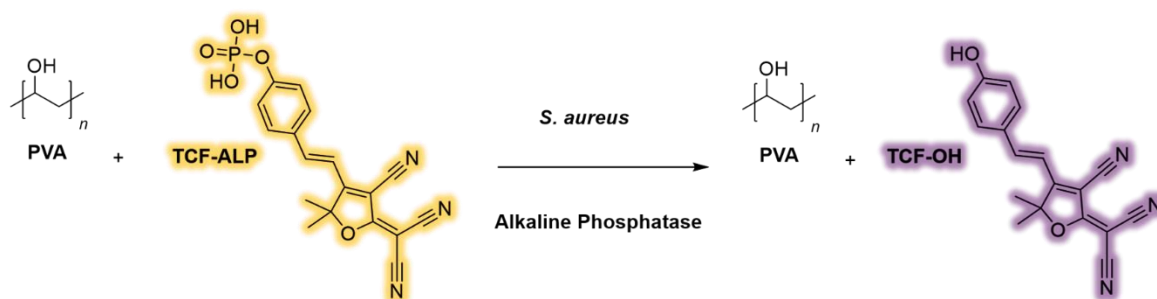
documents/protocols/biology/roche/cell-proliferation-kit-i-mtt.html

105. British Society for Immunology. HeLa Cells [Internet]. [cited 2021 Jan 2]. Available from: <https://www.immunology.org/hela-cells-1951>
106. Wang G, Zhang X, Yu B, Ren K. Gliotoxin potentiates osteoblast differentiation by inhibiting nuclear factor- $\kappa$ B signaling. *Mol Med Rep.* 2015;12(1):877–84.
107. Kim Y-J, Lee M-H, Wozney JM, Cho J-Y, Ryoo H-M. Bone morphogenetic protein-2-induced alkaline phosphatase expression is stimulated by *Dlx5* and repressed by *Msx2*. *J Biol Chem.* 2004;279(49):50773–80.

# Chapter 7: Using TCF-ALP for the Detection of *Staphylococcus aureus*

## 7.1. Overview of Chapter

The research presented in this chapter describes the initial proof-of-concept studies for the use of the novel fluorescent probe **TCF-ALP** in the detection of *S. aureus* alkaline phosphatase (Scheme 7.1). Herein, **TCF-ALP** underwent extensive microbiological examination to determine its ability to detect *S. aureus*. Experiments included selectivity and sensitivity assessments via planktonic suspension assays, biofilm studies, and *ex vivo* testing on porcine skin. Owing to promising results, **TCF-ALP** was immobilised within a poly (vinyl alcohol) (PVA) hydrogel and the resultant material was examined for its feasibility as a point-of-care (PoC) diagnostic device. The **TCF-ALP** hydrogel system underwent the aforementioned microbiological tests and was deemed successful if an increase in fluorescence intensity, and a corresponding colour change from yellow to purple, was witnessed.



**Scheme 7.1:** A TCF-based fluorescent probe (**TCF-ALP**) for the detection of *S. aureus* alkaline phosphatase

## 7.2. Introduction

### 7.2.1. Detecting Pathogenic Bacteria

Traditionally, the gold-standard method to detect pathogenic bacteria in a clinical setting is via the use of culture and counting methods.<sup>1</sup> Bacterial isolates are routinely grown on agar plates (non-differential, differential, selective, chromogenic, or a combination of all four) and incubated at a set temperature and time. If needed, observable colonies are then

subjected to further investigation (e.g. microscopy and biochemical tests) to identify the pathogenic bacteria present.<sup>2</sup> Despite the accuracy of these tests, they are time consuming, require highly skilled personnel, and are only applicable to pathogens that can be routinely grown in a laboratory environment.<sup>1,2</sup>

An improvement over conventional culture-based methods was seen with the introduction of molecular diagnostic methods that identify microbial pathogens using genomic makers. These methods include: Enzyme-linked Immunosorbent Assays (ELISA), hybridisation-based detection systems, Polymerase Chain Reaction (PCR) amplification methods, and DNA microarrays. While they are rapid and offer high sensitivity and selectivity, there are drawbacks, including high cost, complicated methodology, and requiring specialised equipment and personnel.<sup>3-6</sup>

Consequently, research has shifted towards the development of biosensors and organic-based fluorescent probes for the detection of pathogenic bacteria. Biosensors are composed of a biorecognition unit that recognises the bacterial target (such as a nucleic acid, antibody, enzyme, or whole cell) and a transducer that converts the recognition event into a measurable readout (e.g., optical, electrochemical, thermal, or mechanical).<sup>7</sup> As shown in the previous chapter, organic-based fluorescent probes can recognise pathogenic bacteria through the detection of compounds such as enzymes, which upon recognition of the target molecule result in the formation of a fluorescent compound. Both biosensors and organic-based fluorescent probes are advantageous as they can confirm the presence of a bacterial infection without the need for isolation or pre-incubation, reducing the time of the assay.<sup>8-10</sup> Additionally, they are easy to synthesise, relatively low-cost, have a high degree of selectivity and sensitivity, and most importantly, can be used as a point-of-care (PoC) device without the need of a specialist user.<sup>8-10</sup> For the purposes of this work, the focus will be on the use of fluorescent and colorimetric probes for the detection of pathogenic bacteria.

### **7.2.2. Use of Fluorescent and Colorimetric Probes for the Detection of Pathogenic Bacteria**

Dyer<sup>11</sup> and Bascomb<sup>12</sup> were some of the first researchers to develop fluorescent probes for the detection of bacterial enzymes. Certain bacteria possess enzymes that are unique to their species or overexpress certain enzymes during the course of an infection, and as such can be used as a target for bacterial detection.

The introduction to this chapter will discuss the development of novel colorimetric and fluorescent-based probes for the detection of bacterial enzymes. While all probes are

predominately used in liquid suspension, some have been utilised for the development of chromogenic or fluorescent media, or as PoC devices via the use of paper and/or nanoparticles.

### 7.2.2.1. Glycosidases

#### 7.2.2.1.1. $\beta$ -D-Glucuronidase

*E. coli* is an indicator of faecal contamination, and as such there is a pressing need to be able to identify it in food and water samples. One method is through the detection of  $\beta$ -D-Glucuronidase (GUD), a glycosidase that catalyses the hydrolysis of  $\beta$ -D-glucopyranosiduronic derivatives into their corresponding aglycons and D-glucuronic acid.<sup>13</sup> While the majority of *Enterobacteriaceae* do not possess GUD activity (excluding *Shigella*, *Salmonella*, and *Yersinia* spp.),<sup>13</sup> it is present in 94 – 96% of *E. coli* strains,<sup>14</sup> making it is an attractive target for fluorescent and colorimetric probes. However, it is important to note that some pathogenic *E. coli* strains such as *E. coli* O157:H7 do not possess GUD activity,<sup>15</sup> hence the detection of GUD is often performed in parallel with the detection of  $\beta$ -galactosidase ( $\beta$ -gal; Section 7.2.2.1.2.).

The most commonly used substrate for GUD detection is 4-methylumbelliferyl- $\beta$ -D-glucuronide (**MUG**; Figure 7.1), which upon hydrolysis by GUD yields the quantifiable 4-methylumbelliferone (**4-MU**) fluorogenic product.<sup>13</sup> The use of **MUG** for *E. coli* identification is advantageous over conventional culture-based methods as *E. coli* found in natural waters can lose its ability to be cultured, a condition known as viable but non-culturable (VBNC) bacteria. However, VBNC bacteria can still retain metabolic activity, and hence **MUG** can still be used to detect GUD<sup>16,17</sup> as shown by George *et al*, who found that the presence of low concentrations of VBNC bacteria within freshwater samples resulted in a higher enzymatic activity per culturable coliform in contaminated waters.<sup>18</sup> Additionally, **MUG** has been utilised in the development of hand-held fluorimeters for the rapid on-site identification of *E. coli* in drinking water.<sup>19,20</sup>

However, an inherent disadvantage of 4-MU is its relatively high pKa value of 7.8, which at physiological pH (pH 7.4) results in partial dissociation of 4-MU to the highly fluorescent anion. To improve upon this, Perry *et al* synthesised 6-chloro-4-methylumbelliferyl- $\beta$ -D-glucuronide (**CMUG**; Figure 7.1) and investigated its ability to detect GUD-producing *E. coli*.<sup>21</sup> Of the 38 *E. coli* strains investigated, 90% tested positive for GUD after 18 h incubation, and all strains exhibited a higher fluorescence with **CMUG** compared to **MUG**, owing to its lower pKa value.

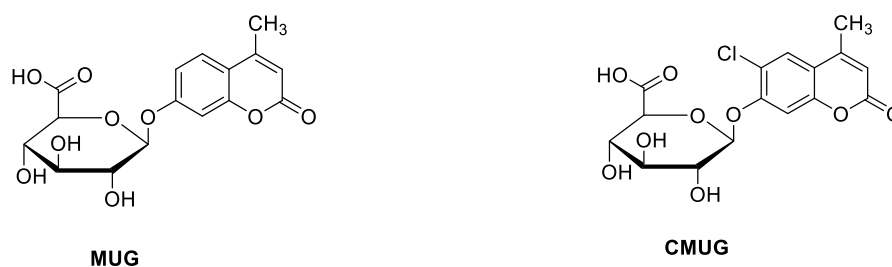
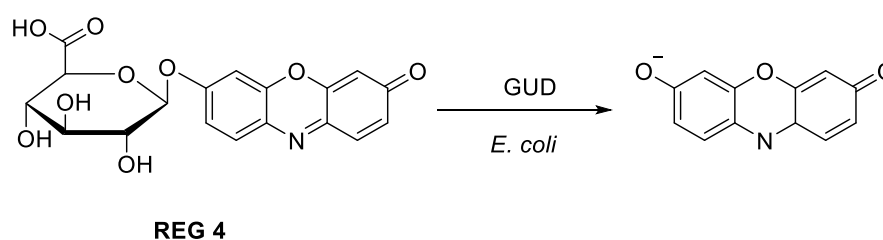


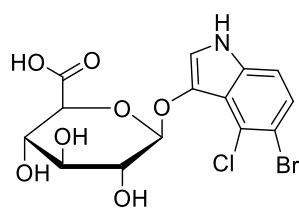
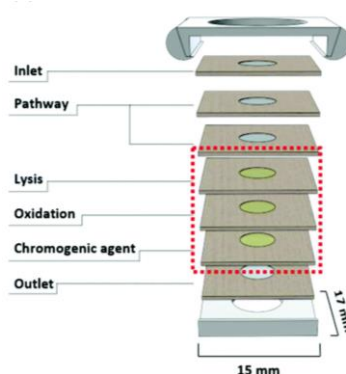
**Figure 7.1:** Chemical structure of 4-methylumbelliferyl- $\beta$ -D-glucuronide (**MUG**) and 6-chloro-4-methylumbelliferyl- $\beta$ -D-glucuronide (**CMUG**)

There are also a variety of colorimetric probes that have been utilised for the detection of *E. coli*. Magro *et al* developed resorfin- $\beta$ -D-glucuronide (**REG 4**; Scheme 7.2), which underwent a colour change from orange to deep pink upon hydrolysis by GUD.<sup>22</sup> **REG 4** was selective for *E. coli*, with the negative controls of *P. aeruginosa* and *K. pneumonia* not displaying a colour change. Like **CMUG**, the deprotonated form of **REG 4** predominates at physiological pH, therefore making it a favourable probe over the conventional **MUG**.



**Scheme 7.2:** Hydrolysis of resorfin- $\beta$ -glucuronide (**REG 4**) in the presence of GUD-producing *Escherichia coli*

A PoC paper-based device ( $\mu$ PAD) for the detection of *E. coli* has also been developed utilising 5-bromo-4-chloro- $\beta$ -D-glucuronic acid (**X- $\beta$ -gluc**; Figure 7.2).<sup>23</sup> When a sample contaminated with *E. coli* was placed on the device, the bacterial cells were lysed, releasing the intracellular GUD, which subsequently reacted with **X- $\beta$ -gluc**, turning the paper sheet blue. Experiments showed that without enrichment of the sample the LOD of this system was  $10^7$  CFU/mL, but with up to 12 h of enrichment in growth medium, the LOD was significantly reduced to  $10^1$  CFU/mL.

**A)****X-β-gluc****B)**

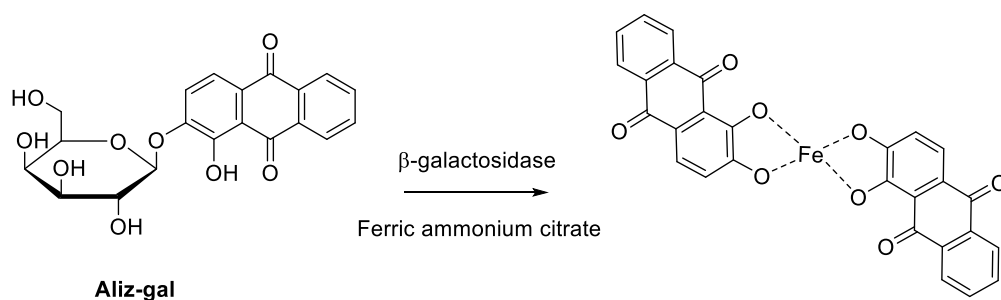
**Figure 7.2:** **A)** Chemical structure of 5-bromo-4-chloro-β-D-glucuronic acid (**X-β-gluc**) and **B)** Schematic of the paper-based device showing the layers of the point-of-care device for the detection of GUD from *Escherichia coli*. Adapted from Kim et al with permission by the Royal Society of Chemistry<sup>23</sup>

#### 7.2.2.1.2. β-D-Galactosidase

β-D-Galactosidase (β-GAL) catalyses the breakdown of lactose into galactose and glucose and is commonly used as a target for detection of the coliform group within *Enterobacteriaceae*.<sup>13</sup> Like GUD, β-GAL is predominately used to measure the hygienic quality of water and food samples.<sup>24</sup>

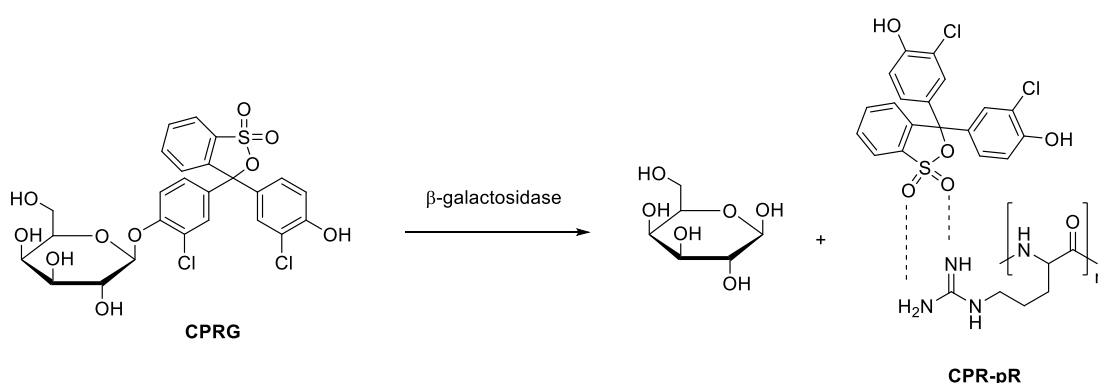
Fluorescent probes based on 4-MU are predominately used to detect β-GAL (e.g. **4-MU-GAL**). However, Chilvers *et al* synthesised other coumarin-based fluorescent probes and found that they were less inhibitory towards bacteria compared to **4-MU-GAL** and displayed enhanced fluorescence.<sup>25</sup> In particular ethyl-7-hydroxycoumarin-3-carboxylate-β-D-galactoside (**EHC-GAL**) showed promising results in the identification of coliform bacteria.

Further fluorescent probes have also been developed such as 2-arylbenzothiazone derivatives, which were able to identify coliform bacteria, especially *E. coli*, *Enterobacter cloacae*, and *Serratia marcescens*.<sup>26</sup> Additionally, novel colorimetric probes have been synthesised for the development of chromogenic agar. Alazarin-β-galactopyranoside (**Aliz-gal**; Scheme 7.3) can be hydrolysed by β-GAL, releasing alizarin, subsequently complexing with various metal ions to form brightly coloured chelates.<sup>27</sup> **Aliz-gal** was able to detect 100% (n=182) of strains that displayed β-GAL activity, producing localised, bright violet colonies when chelated with ferric ammonium.



**Scheme 7.3:** Hydrolysis of Alazarin-β-galactopyranoside (**Aliz-gal**) and subsequent complexation with iron (Fe)<sup>27</sup>

Another colorimetric probe that is frequently used to detect β-GAL is chlorophenol red β-galactopyranoside (**CPRG**), as it is faster and more sensitive than the colorimetric O-nitrophenyl-β-galactopyranoside (**ONPG**) and the fluorescent **4-MU-GAL**.<sup>28,29</sup> Further derivatives of **CPRG** have been developed, for instance, Sicard *et al* found that when **CPRG** was hydrolysed by β-gal, the sulphonated pyranine of chlorophenol red (**CPR**) can interact with poly-L-arginine (pR) forming a **CPR-pR** complex which is strongly fluorescent, creating an ‘off-on’ fluorescent probe for the detection of *E. coli* (Scheme 7.4).<sup>30</sup> While the complex was inhibitory towards actively growing bacteria (due to cell lysis by 1 wt% pR), it could be used for bacteria that had been previously cultured and/or isolated. When *E. coli* was incubated with **CPR-pR** complex for 30- or 60- min, with and without the addition of B-PER (a lysing agent), results showed a ~10-fold increase in fluorescence intensity in samples with lysed bacteria, due to the release of intracellular β-GAL. The activity of **CPR-pR** was typically 40-fold better than the other dyes used in this experiment (**ONPG**, **4-MU-GAL**, **CPRG**) for the detection of *E. coli*.



**Scheme 7.4:** Hydrolysis of chlorophenol red β-galactopyranoside (**CPRG**) and subsequent complexation with poly-L-arginine (pR) to form the fluorescent **CPR-pR** in the presence of β-galactosidase

POC μPADs have been developed that utilise **CPRG** for the detection of coliform bacteria.<sup>31</sup> Samples of *E. coli* were isolated and cultured in enrichment media for 4.5 h before subsequent lysing of the cells and placement onto the μPAD. The device was able to detect

pure cultures of *E. coli*, indicated by a colour change from yellow to red, with the overall assay time (including enrichment and detection) between 8 – 12 h. This device was improved upon by Jahanshahi-Anbuhi *et al*, who included a layer of paper containing a lysing agent (B-PER) in the stacked  $\mu$ PAD.<sup>32</sup> This device could detect coliform bacteria, detecting *E. coli* concentrations as low as  $10^5$  CFU/mL (with no previous enrichment). Kim *et al* utilised a different colorimetric substrate (5-bromo-6-chloro-3-indoxyl- $\beta$ -galactose (**Magenta- $\beta$ -gal**) for their  $\mu$ PAD and found that without enrichment it could detect  $10^7$  CFU/mL of *E. coli*, lowered to  $10^1$  CFU/mL with enrichment – indicated by a colour change from colourless to purple.<sup>23</sup>

### 7.2.2.1.3. $\beta$ -D-Glucosidase

$\beta$ -D-glucosidase ( $\beta$ -Glu) is present in numerous bacterial species and has been used in the differentiation of *Streptococci* spp.,<sup>33</sup> coagulase-negative *Staphylococci* (CoNS)<sup>34</sup> and the differentiation of *Salmonella* from other *Enterobacteria* spp.<sup>35</sup>

While 4-methylumbelliferyl- $\beta$ -D-glucosidase (**MU-GLU**) has been used for the identification of  $\beta$ -Glu,<sup>33</sup> Perry *et al* synthesised four other coumarin-based fluorescent probes (Figure 7.3) and evaluated their ability to detect  $\beta$ -Glu activity in *Enterococci* spp.<sup>21</sup> A total of 42 *Enterococci* strains were tested, including *Enterococcus faecalis* (*E. faecalis*) and *Enterococcus faecium* (*E. faecium*). *Streptococcus* spp. were used as a negative control. Results showed that all *Enterococci* spp. displayed  $\beta$ -Glu activity after 18 h incubation with the fluorescent probes, and that probes **2** – **4** displayed, on average, a higher fluorescence signal than the conventional **MU-GLU**.

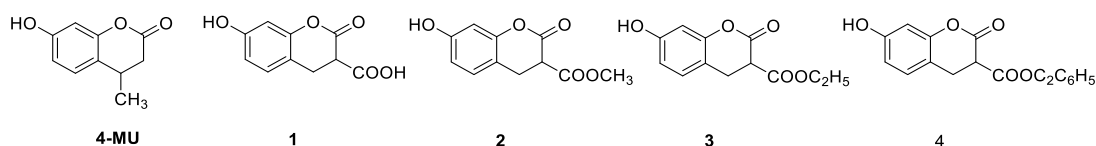


**Figure 7.3:** Chemical structure of **4-MU** and the corresponding coumarin derivatives **1-4**

In colorimetric assays, *p*-nitrophenyl- $\beta$ -glucopyranoside (**pNPG**) is frequently used for the identification of  $\beta$ -GLU bacteria.<sup>36</sup> **pNPG** entrapped within an agarose gel has been utilised for the detection of *E. faecium*,<sup>37</sup> whereby upon hydrolysis the liberated *p*-nitrophenol (**pNP**) becomes trapped within the agarose gel and a colour change from colourless to yellow can be observed by the naked eye. An initial inoculum of  $1.0 - 1.5 \times 10^4$  CFU/mL, and an incubation time of approximately 18 h was needed to observe a detectable colour change.

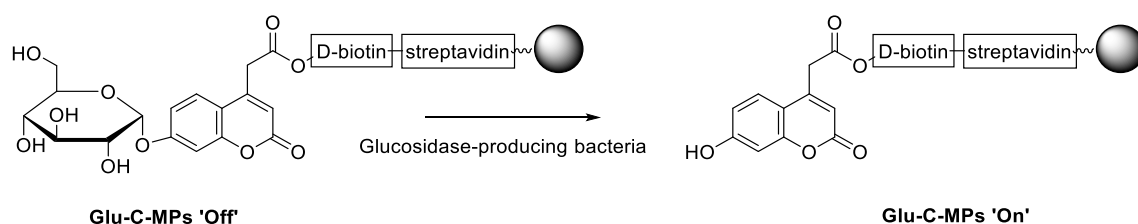


#### 7.2.2.1.4. $\alpha$ -Amylase and $\alpha$ -Glucosidase

$\alpha$ -amylase is frequently utilised in the detection of *Bacillus* spp. The standard method to detect  $\alpha$ -amylase is the colorimetric assay using dinitrosalicylic acid (DNS).<sup>38,39</sup> However, Xia *et al* developed a fluorescence *in situ* enzyme-staining approach using a boron dipyrromethene (BODIPY) fluorescein-labelled (FL) DQ™ starch.<sup>40</sup> Upon incubation with *Bacillus* spp.,  $\alpha$ -amylase hydrolysed the probe and fluorescence was observed. However, this assay was only suitable for *Bacillus* spp. in their vegetative state, as the endospores were not fluorescent.

Assays for  $\alpha$ -glucosidase ( $\alpha$ -Glu) have been used to differentiate *Bacillus anthracis* from *Bacillus mycoides* and *Bacillus thuringiensis*, and 4-methylumbelliferyl- $\alpha$ -D-glucoside (**MUGlu**)<sup>41</sup> has been used as a component within a selective and differential media for the identification of *Enterobacter sakazkii*.<sup>42</sup>

Giovannini *et al* described the synthesis of an 'off – on' fluorescent-based sensor where streptavidin-coated magnetic microparticles were functionalised with a biotinylated coumarin-derived probe with glucose as the recognition moiety (**Glu-C-MPs**; Scheme 7.5).<sup>43</sup> This probe was able to detect  $\alpha$ - and  $\beta$ -glucosidase at a concentration of 75 CFU/mL for *E. coli*, *K. pneumonia*, and *P. aeruginosa* after 1 h incubation, whereas 3 h was required for the detection of *Enterococcus* spp. and *S. aureus*.



**Scheme 7.5:** Streptavidin-coated magnetic microparticles functionalised with coumarin-based glucosidase probe

A PoC  $\mu$ PAD has also been developed for the colorimetric detection of *Cronobacter* spp. as  $\alpha$ -Glu activity can distinguish it from other *Enterobacteriaceae* bacteria.<sup>44</sup> Bacterial cultures were grown overnight, lysed and placed onto the paper-based device. The released  $\alpha$ -Glu subsequently hydrolysed 5-bromo-4-chloro-3-indolyl- $\alpha$ -D-glucopyranoside (**X $\alpha$ Glu**), producing a purple colour in the presence of oxygen. For *Cronobacter sakazakii*, the  $\mu$ PAD had a LOD of  $10^6$  CFU/cm<sup>2</sup>, but if combined with an enrichment process it was capable of detecting bacterial concentrations as low as 10 CFU/cm<sup>2</sup>.

### 7.2.2.2. Esterases and Lipases

Esterases and lipases are found in the majority of bacterial species<sup>13</sup> and numerous probes have been developed to detect esterase activity including fluorogenic probes based on coumarin, fluorescein, rhodamine and resorufin,<sup>45</sup> and colorimetric probes based on p-nitrophenol (**pNP**).<sup>46</sup> These fluorescent molecules are usually masked by acetate esters that often suffer from auto-hydrolysis, resulting in high levels of background noise and failure to detect low levels of esterase activity.

The detection of C<sub>8</sub> esterase is used in the identification of *Salmonella* spp.<sup>31</sup> Novel fluorescent probes based on 2-arylbenzothiazone have been developed to detect C<sub>8</sub> esterase within *Salmonella* spp.;<sup>26</sup> however, the most widely used fluorescent probe is 4-methylumbelliferyl caprylate (**MUCAP**).<sup>35</sup> In the presence of a C<sub>8</sub> esterase the substrate is cleaved, resulting in the formation of the fluorescent **4-MU**. This probe had a sensitivity of 95% and specificity of 91% when tested with 83 *Salmonella* strains and 349 non-*Salmonella* strains.<sup>47</sup> This was further supported by Olsson *et al*, who tested 750 *Salmonella* strains and 130 other *Enterobacteriaceae* species with **MUCAP**.<sup>48</sup> It was found that 99.7% of *Salmonella* strains tested positive with **MUCAP**, with one false-positive reported with *Hafnia alvei*, although the signal was weaker compared to the majority of *Salmonella* strains. *Pseudomonas* spp. and *Proteus* spp. are normally responsible for false-positive results,<sup>49</sup> *P. aeruginosa* and *Proteus mirabilis* were tested in this study; the former displayed a positive result with **MUCAP**, and the latter a negative result.<sup>48</sup>

Other fluorescent probes have been developed for the detection of bacterial esterases. One such example is by Tallman *et al* who developed two fluorescent probes derived from 7-hydroxy-9*H*-(1,3-dichloro-9,9-dimethylacridin-2-one) (DDAO), termed **DDAO-AME 1** and **DDAO-AME 2**, for the detection of *Mycobacterium tuberculosis* (Figure 7.4).<sup>45</sup> They were tested against lysates from *Mycobacterium* spp. that were both members and non-members of the *Mycobacterium tuberculosis* complex (MTBC). All species tested displayed esterase activity by hydrolysing the acetoxymethyl ether on both probes, resulting in a detectable fluorescent signal within 10 min.

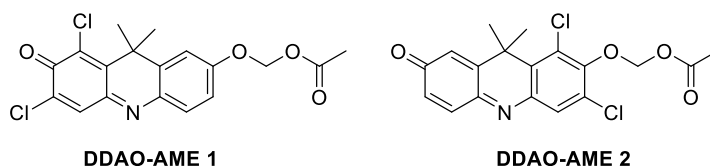


**Figure 7.4:** Chemical structures of 7-hydroxy-9*H*-(1,3-dichloro-9,9-dimethylacridin-2-one) (DDAO)-derived probes, **DDAO-AME 1** and **DDAO-AME 2**

### 7.2.2.3. Aminopeptidases

Aminopeptidases (AP) are enzymes that catalyse the cleavage of amino acid residues at the N-terminal position of peptides and proteins. A wide variety of amino acids have been used for the detection of different bacterial species<sup>50–52</sup> e.g. L-pyrrolidonyl peptidase has been used in the identification of *Salmonella* spp.,<sup>53</sup> *Enterococci* spp., and Group A *Streptococci*;<sup>54,55</sup> L- $\gamma$ -glutamic acid aminopeptidase is used to differentiate *Shigella* spp.; and finally, proline aminopeptidases have been used for the detection of *Neisseria meningitidis*<sup>56</sup> and bacterial vaginosis.<sup>57</sup> The majority of novel colorimetric and fluorescent probes synthesised have been utilised in the development of chromogenic and fluorogenic agar to improve current conventional microbiological culturing techniques, some of which will be discussed here.

One key area of interest is the differentiation of gram-positive and gram-negative bacteria, and this can be achieved via the detection of L-alanine APs, with only the latter possessing L-alanine AP activity. Colorimetric probes<sup>58</sup> such as L-alanyl-*p*-nitroanilide<sup>59</sup> have been utilised to detect gram-negative bacteria, but other probes based on the chromogenic moiety 9-(4'-aminophenyl)acridines have also been developed.<sup>52</sup> While these probes inhibited gram-positive bacteria, it needed to be protonated by acetic acid to produce various shades of red-coloured colonies for *E. coli*, *Klebsiella pneumonia*, *P. aeruginosa*, and *Burkholderia cepacia*.

Fluorescence-based methods have also been employed for the detection of L-alanine AP to identify gram-negative bacteria.<sup>60</sup> Cellier *et al* synthesised two substrates based on 2-(2-hydroxyphenyl)heterocycles (Figure 7.5; **5** and **6**), which upon hydrolysis by L-alanine AP fluoresce via the ES IPT mechanism.<sup>61</sup> The probes were inhibitory towards gram-positive bacteria and gave moderately to strongly blue fluorescent colonies; however, there was diffusion into the agar that could make identification of gram-negative bacteria difficult in clinical samples.

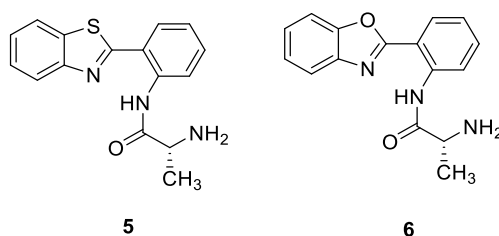
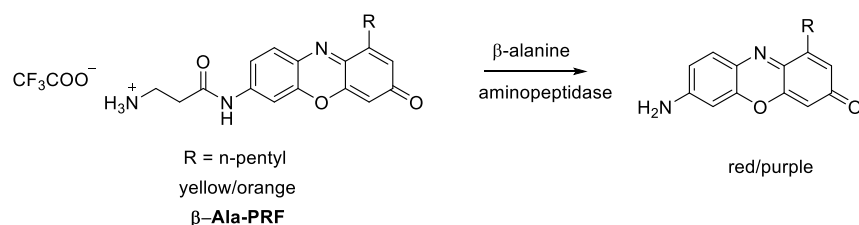


**Figure 7.5:** Chemical structures of 2-(2-(hydroxyphenyl)heterocycle)-derived probes, **5** and **6**

Other fluorescent probes have been developed, with derivatives of 2-arylbenzothiazone producing moderately fluorescent colonies of gram-negative bacteria, while being

inhibitory towards gram-positive bacteria and certain gram-negative bacteria such as *E. coli* and *Salmonella typhimurium*.<sup>26</sup> Additionally, Cellier *et al* synthesised L-alanyl derivatives of 2-aminoacridone that supported the growth of gram-negative bacteria (although growth of *E. coli* and *K. pneumoniae* was inhibited) and produced yellow fluorescent colonies, without any diffusion through the agar, increasing the clinical utility of this dye as a component in fluorogenic agar.<sup>60</sup>

Additionally,  $\beta$ -alanine ( $\beta$ -Ala) AP activity has been detected for *P. aeruginosa*, and has been used as a target for colorimetric and fluorescent-based probes.<sup>26,52,58,60,62,63</sup> Currently, a  $\beta$ -alanyl pentylresorufamine ( **$\beta$ -Ala-PRF**; Scheme 7.6) colorimetric probe is used commercially to detect *P. aeruginosa* (chromID *P. aeruginosa*, bioMérieux) that results in the formation of red/purple colonies.<sup>64,65</sup> When tested,  **$\beta$ -Ala-PRF** was capable of detecting 99% of *P. aeruginosa* strains, but also showed varying activity against *Burkholderia* spp., other *Pseudomonas* spp., *Ralstonia* spp., and *Moraxella* spp.<sup>64</sup>



**Scheme 7.6:**  $\beta$ -alanyl pentylresorufamine ( **$\beta$ -Ala-PRF**) hydrolysis in the presence of  $\beta$ -alanine producing bacteria

One disadvantage of this colorimetric probe was that it diffused into the agar, making the identification of *P. aeruginosa* colonies difficult. Owing to this, the authors developed a series of 7-amino-phenozacin-3-one (**7**) and 8-aminophenoxacin-3-one (**8**) colorimetric probes, which in the presence of  $\beta$ -Ala produced pale red/orange and pink/purple colonies, respectively (Figure 7.6).<sup>66</sup> All probes were able to detect *P. aeruginosa*, with **7** and **8** detecting 100% and 80% of *P. aeruginosa* strains, respectively (n = 30 strains). Although **8** was less sensitive, there was a lack of diffusion through the agar, making it a useful substrate for chromogenic agar, whereas **7**, and  **$\beta$ -Ala-PRF** could be used in solution-based assays, where localisation would not be required.

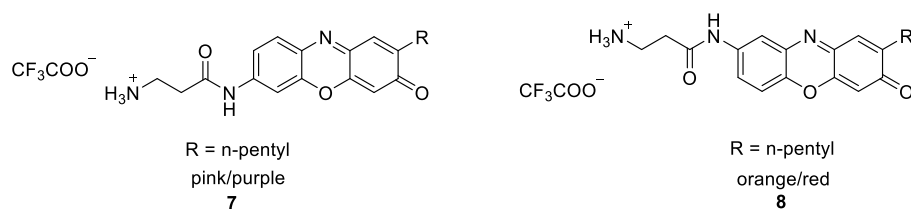
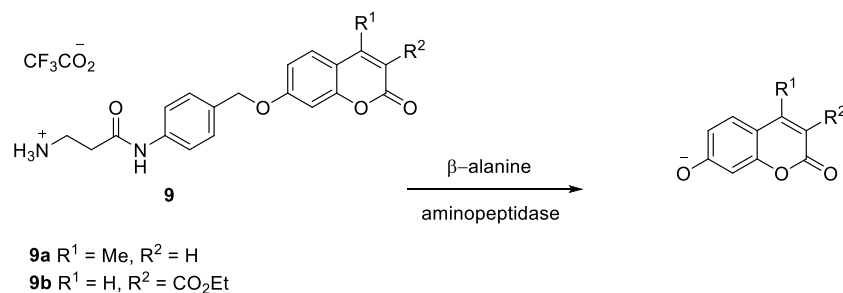


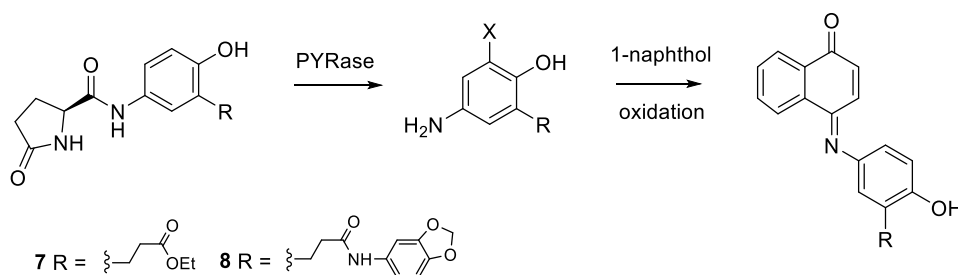
**Figure 7.6:** Structures of 7-amino-phenozacin-3-one (**7**) and 8-aminophenoxacin-3-one (**8**)

The authors followed on this work by producing fluorescent substrates to overcome the inherent disadvantages of chromogenic agar (i.e. time taken to produce a visible signal, interference from agar colour).<sup>67</sup> The fluorescent probes were derived from coumarin (Scheme 7.7) and upon hydrolysis by  $\beta$ -Ala a 1,6-elimination occurred and fluorescence was observed. **9a** was able to discriminate between  $\beta$ -Ala producers, with *P. aeruginosa* giving a positive result and *S. marcescens* giving a negative result. **9b** resulted in fluorescence for *P. aeruginosa*, *S. marcescens*, and *B. cepacia*.



**Scheme 7.7:** Coumarin-based fluorescent probes **9a** and **9b** for the detection of  $\beta$ -alanine

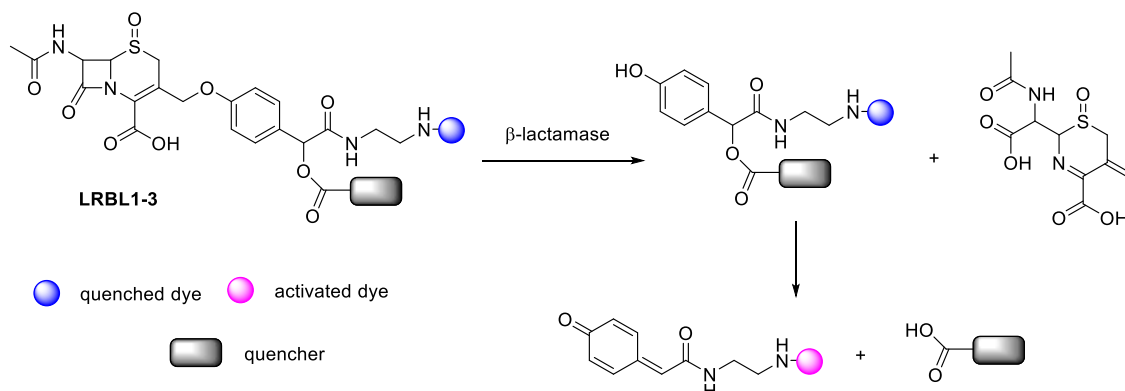
Pyroglutamyl AP (PYRase) can be used for the differentiation of *Enterobacteriaceae*,<sup>13,68</sup> and the detection of *Enterococci* and *Streptococcus pyogenes* from most other gram-positive cocci.<sup>69,70</sup> 4-aminophenol derivatives were synthesised (Scheme 7.8) and added to agar along with 1-naphthol and NaOH, before subsequent inoculation with  $10^8$  bacteria and incubation at 37 °C for 24 h.<sup>58</sup> Upon incubation with PYRase-producing bacteria, the colorimetric probe was hydrolysed, which in turn reacted with 1-naphthol, and following oxidation *in situ*, pink colonies were observed. A positive result was observed for *Enterococcus faecium*, *E. faecalis*, and *Bacillus subtilis*. Some *Enterobacteriaceae* also produced pink colonies, including *K. pneumoniae* and *Serratia marcescens*.



**Scheme 7.8:** 4-aminophenol derivatives **7** and **8** under incubation with PYRase-producing bacteria and 1-naphthol

#### 7.2.2.4. Antibiotic-resistance Enzymes

One emerging trend is the development of colorimetric and fluorescent probes for the detection of antibiotic-resistance enzymes in pathogenic bacteria; the focus has predominately been on the detection of  $\beta$ -lactamases.<sup>71–76</sup> Shao *et al* developed three fluorogenic probes (termed **LRBL 1 – 3**) encompassing a fluorophore and quencher (Scheme 7.9), which produced FRET-based fluorescence in the presence of  $\beta$ -lactamase producing *E. coli*.<sup>76</sup>



**Scheme 7.9:** FRET-based fluorescent probes **LRBL 1 – 3** hydrolysis in the presence of  $\beta$ -lactamase bacteria.

Recently, a fluorescent probe was designed to detect AmpC  $\beta$ -lactamase, a  $\beta$ -lactamase that primarily hydrolyses the third generation cephalosporins, ampicillin, and cefox.<sup>77,78</sup> The probe, termed **CDC-559** (Figure 7.7), was tested against two sensitive *S. aureus* strains, and two resistant bacterial strains (one *S. aureus*, one *Enterobacter cloacae* [*E. cloacae*]).<sup>77</sup> When **CDC-559** was incubated with the susceptible strains, no noticeable change in fluorescence was observed. A slight decrease in fluorescence intensity was detected when incubated with the resistant *S. aureus*, although it was not as strong as the rapid decrease in fluorescence intensity when incubated with *E. cloacae*. This was due to their differing mechanisms of resistance, with *S. aureus* expressing PBP2a proteins, whereas *Enterobacter cloacae* produces large amounts of AmpC  $\beta$ -lactamase.

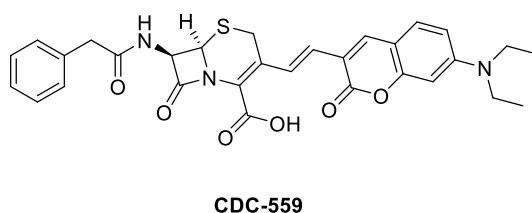


**Figure 7.7:** Chemical structure of **CDC-559**

Carbapenemase-sensitive fluorescent probes have also been synthesised Mao *et al* who developed **CB-1** (Figure 7.8) that employed an alkenyl-linked BODIPY dye as the active fluorophore.<sup>79</sup> **CB-1** was tested with a variety of carbapenemase-producing bacteria (CPO), and **CB-1** was able to distinguish between CPOs and other bacterial strains. Mao *et al* then synthesised a carbapenem-sensitive umbelliferone-based probe (**CPC-1**; Figure 7.8), which showed specificity to metallo- $\beta$ -lactamases over other serine- $\beta$ -lactamases.<sup>80</sup> **CPC-1** produced fluorescence when incubated with metallo- $\beta$ -lactamase producing *E. coli* and *K pneumoniae*. Recently, Kim and co-workers further developed this work by synthesising a probe they termed **1b**.<sup>81</sup> Probe **1b** had excellent selectivity towards CPO compared to non-CPO, displaying higher sensitivity than **CPC-1** (i.e., 97.1% versus 58.3% for the detection of carbapenemase-producing *Enterobacteriaceae*, respectively).

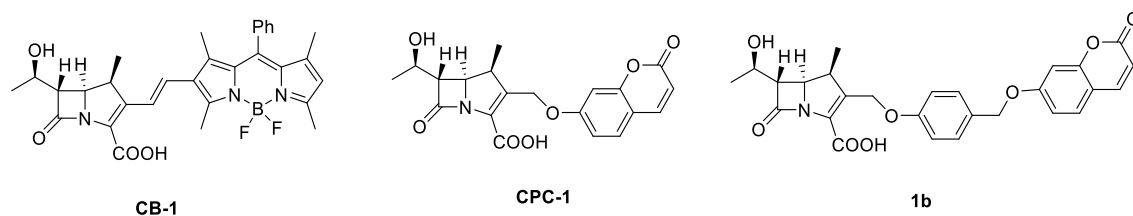


**Figure 7.8:** Chemical structure of **CB-1**, **CPC-1**, and **1b**

$\beta$ -lactamase detection has also been useful in the identification of *Mycobacteria* spp.<sup>82,83</sup> Kong and co-workers utilised a reporter-enzyme fluorescence test using a FRET-based, near-infrared fluorogenic substrate (**CNIR5**), which allowed for real-time detection of mycobacteria in mice.<sup>84</sup> Cheng *et al* synthesised the fluorescent probe **CDG-3**,<sup>85</sup> which became the fluorogenic probe used in the TB REaD™ assay for the detection of *Mycobacterium tuberculosis*; this assay was then used by Nabeta *et al* who investigated the accuracy of TB REaD™ compared to conventional culture-based methods;<sup>86</sup> while Cheng *et al* and Sule *et al* reported good sensitivity and selectivity of **CDG-3**,<sup>85,87</sup> this study reported a lower sensitivity and selectivity of 58.6% and 59.5%, respectively.<sup>86</sup>

### 7.2.3. Alkaline Phosphatase

While ALP has been used excessively for the detection of conditions such as cancer and diabetes, it has been under-explored for the detection of pathogenic bacteria. ALP is present in numerous bacterial species to help with the uptake of essential phosphate into the bacterial cell and is governed by the phosphate (Pho) regulatory system.

### 7.2.3.1. Pho Regulatory system

Phosphorous is one of the main elements present in microbial cells; it is important for several biological functions including energy metabolism, membrane integrity, regulation of protein activity, and maintenance of acid-based homeostasis.<sup>88,89</sup> Bacteria have evolved mechanisms to acquire and store the orthophosphate anion ( $\text{PO}_4^{3-}$ ), often known as inorganic phosphate (Pi),<sup>88</sup> through governance by the Pho regulon, first characterised in *E. coli*.<sup>90</sup> The Pho system activates enzymes capable of obtaining Pi from organic phosphates, Pi-specific transporters (including Pi-specific ATP-binding cassette transporter [PstSCAB]),<sup>91</sup> and enzymes involved in the storage of the nutrient.

The Pho regulon is controlled by a two-component regulatory system (TCS) that enables the bacteria to adapt to changing environmental phosphate levels.<sup>92</sup> This system has a variety of names dependent on the bacteria under investigation (PhoRB in *E. coli*,<sup>93</sup> PhoRP in *Bacillus subtilis*,<sup>94</sup> and PhoPR in *S. aureus*),<sup>95</sup> but is essentially composed of a histidine kinase that receives sensory input and a response regulator protein that controls output. Upon Pi limitation, the response regulator is phosphorylated by the sensor kinase and is able to activate or repress the transcription of genes.<sup>88</sup> Among the Pi scavengers, alkaline phosphatases, phospholipases, glycerophosphodiester phosphodiesterases, phytases, and 5'nucleotidases are the most common enzymes induced in response to Pi starvation in bacteria.<sup>90</sup>

### 7.2.3.2. Alkaline Phosphatase Expression

The majority of the knowledge of ALP stems from the study of an ALP obtained from *E. coli*.<sup>96</sup> ALPs are metalloenzymes, thought to contain  $\text{Zn}^{2+}$  or  $\text{Mg}^{2+}$ ;<sup>97</sup> they are usually homodimeric, however, monomeric<sup>97</sup> and oligomeric<sup>98</sup> forms have been described. In *E. coli*, synthesis of ALP is under the control of one structural (*phoA*) and two regulator (*phoR* and *phoX*) genes.<sup>99,100</sup> Upon Pi-limitation, ALP synthesis is up-regulated through the transcription of the *phoA* gene, which is mediated through the Pho regulon.<sup>96</sup> The main responsibility of ALP is to breakdown organic phosphate esters to release Pi,<sup>89,90</sup> although ALP can exhibit transphosphorylase<sup>101</sup> and pyrophosphorylase<sup>102</sup> activities.

ALP is present in numerous bacterial species, such as *E. coli*,<sup>96</sup> *P. aeruginosa*,<sup>103</sup> *S. aureus*,<sup>104</sup> and *B. subtilis*.<sup>105,106</sup> While the majority of ALP enzymes are repressed in the presence of Pi,<sup>100,104,107</sup> some studies have described the presence of constitutive ALP.<sup>108,109</sup> ALP is located in the periplasmic space between the cell wall and the cell membrane in *E. coli*<sup>110</sup> and generally thought to be located here in other gram-negative bacteria.<sup>111,112</sup> For gram-positive bacteria, such as *S. aureus*, ALP is usually associated with



the surface of the cell membrane.<sup>104,113</sup> Additionally, the expression of ALP has been shown to be heterogenous in bacterial biofilms in response to phosphate starvation.<sup>114</sup>

#### **7.2.3.2.1. *Staphylococcus aureus* Alkaline Phosphatase**

*S. aureus* ALP is located in the cell membrane.<sup>115</sup> In phosphate deficient media *phoB* (ALP) and *phoP* (encoding an ALP synthesis transcriptional regulatory protein) are upregulated. Prunty *et al* showed that the *phoB* operon is expressed at very low levels in parental *S. aureus* Newman; however, expression is upregulated ~9.16-fold in strain *dphoR*, indicating that the expression is under the positive control of PhoPR.<sup>89</sup> ALP activity was found to increase with size of inoculum and time of incubation.<sup>116</sup> Additionally, the amount of phosphatase produced by *S. aureus* has been correlated with coagulase production as a biochemical index of pathogenicity and implicated as a virulence factor for *S. aureus*.<sup>117,118</sup>

#### **7.2.3.3. Use of Alkaline Phosphatase Reported in the Literature**

One of the main uses of ALP reported in literature is to determine bacterial cell permeability.<sup>119</sup> As ALP is located in periplasmic space (gram-negative bacteria), or cell-membrane bound (gram-positive bacteria), there should be minimal ALP activity in the extracellular environment of healthy, structurally-intact, bacterial cells. When healthy bacteria are incubated with certain antimicrobials, the antimicrobial creates pores, or disrupts the structural integrity of the cell wall, resulting in the release of ALP into the extracellular environment. Therefore, an increase in extracellular ALP is related to the structural integrity of the cell wall of the bacteria under investigation.

Additionally, ALP has been used as a 'reporter enzyme' in immunoassays<sup>120</sup> and DNA-based probes.<sup>121</sup> ALP has also been used in aptamer/DNA based electrochemical studies,<sup>122</sup> and the *phoA* gene has been used in general 'fusion studies'<sup>123</sup> and polypeptide<sup>124</sup> fusion studies. However, there have been limited studies on the detection of ALP for the identification of bacteria.<sup>125,126</sup> Kang *et al* were able to synthesise a phosphorylated fluorescent probe (2-hydroxychalcone [HCAP]) and conjugate it to an adhesive cationic polymer (**HCAP-PVP**) to detect ALP in bacterial species.<sup>127</sup> Upon incubation with *E. coli* and *S. aureus*, the phosphate group was cleaved and the green/yellow emission ratiometrically changed to a deep-red emission; this system was able to detect 10<sup>3</sup> and 10<sup>5</sup> *S. aureus* and *E. coli*, respectively. Furthermore, Cellier *et al* synthesised a phosphatase probe based on 2-arylbenzothiazone for the detection of *Staphylococcus* spp., particularly *S. aureus*. However, fluorescence and blue colonies were witnessed for all gram-negative and gram-positive bacteria tested, suggesting that this assay was not specific for *S. aureus* detection.<sup>26</sup>

One commercial diagnostic product that utilises ALP for the detection of *S. aureus* is RapdiDEC® Staph (Biomérieux). The test provides a 2 h presumptive identification of *S. aureus*, *S. epidermidis*, and *Staphylococcus saprophyticus* on the basis of fluorogenic coagulase, ALP, and galactosidase tests, respectively.<sup>128</sup>

#### 7.2.4. Aims and Objectives

The aim of this study was to further develop knowledge of ALP for the detection of bacteria, specifically *S. aureus*. **TCF-ALP** was used as it had previously shown to be effective in detecting ALP using both enzyme suspensions and cell-based assays (HeLa and C2C12 cells). The objectives of this chapter are:

- To optimise **TCF-ALP** to detect ALP in bacterial cells
- To determine if **TCF-ALP** can detect ALP in planktonic, biofilm, and *ex vivo* porcine skin models
- To evaluate the selectivity of **TCF-ALP** against a library of clinically-relevant bacterial isolates
- To develop a hydrogel incorporating **TCF-ALP** for use as a diagnostic wound dressing in a clinical environment.

## **7.3. Methods**

### **7.3.1. Synthesis of TCF-ALP**

**TCF-ALP** was synthesised as outlined in Chapter 6. Stock solutions of **TCF-ALP** were stored in DMSO at 4 °C until required.

### **7.3.2. Preparation of TCF-ALP Based PVA Hydrogels**

A 10% w/v PVA solution was prepared by dissolving PVA in 50 mM Tris HCl (pH 9.2). After the resultant solution had cooled to room temperature, aliquots of 1 mL were transferred into a 12-well microtiter plate and 38.5 µL of **TCF-ALP** (2.6 mM in DMSO) was added to produce homogenous yellow solutions. These solutions were placed at -80 °C and underwent one freeze-thaw cycle to produce mechanically stable hydrogels, which were protected from light and stored at 4 °C prior to use.

### **7.3.3. Bacterial Growth Conditions**

Bacterial strains were stored at -80 °C in broth containing 15% (v/v) glycerol until required. Working stocks of *S. aureus* and *S. epidermidis* were prepared by streaking TSA, while *P. aeruginosa* and *E. coli* were plated onto Luria Bertani (LB) agar before incubation at 37 °C for 24 h. Plates were stored at 4 °C for up to a month for further use. Overnight cultures of bacterial strains were routinely propagated by transferring a single colony to 5 mL Müeller-Hinton broth and incubating at 32 °C for 18 h. Cultures were washed via centrifugation (4000 g, 10 min) before being re-suspended in 50 mM Tris-HCl (pH 9.2) to an optical density at 600 nm of ~ 1 (c. 5.0 x 10<sup>8</sup> CFU/mL).

### **7.3.4. Bacterial Enumeration**

Estimation of the total viable count of bacterial cultures were determined as outlined in Chapter 2, Section 2.2.1.4.

### **7.3.5. Effect of Broth on Alkaline Phosphatase Production**

Overnight cultures of *S. aureus* NCTC 10788 were grown in either Tryptic Soy Broth (TSB), Luria Bertani (LB) broth, or Mueller Hinton broth at 32 °C for 18 h. After incubation, bacterial cells were washed and re-suspended in 50 mM Tris-HCl (pH 9.2) to an optical density at 600 nm of ~ 1 (c. 5.0 x 10<sup>8</sup> CFU/mL). Prior to testing, bacterial cells underwent

centrifugation (4000 g, 10 min) and were re-suspended in an equal volume of 10  $\mu$ M **TCF-ALP** in 50 mM Tris-HCl (pH 9.2). Bacterial cultures were then protected from light and incubated at 32 °C for a further 24 h. Analysis of ALP production was performed after 1 and 24 h incubation with **TCF-ALP**. A 200  $\mu$ L aliquot was removed and centrifuged at 10 000 g for 3 min. The supernatant was subsequently placed into a black 96-well microtiter plate and the fluorescence was measured using a CLARIOstar fluorimeter (BMG LabTech, UK),  $\lambda_{\text{ex}} = 542 \text{ nm}$ ,  $\lambda_{\text{em}} = 606 \text{ nm}$ .

### **7.3.6. Detecting Alkaline Phosphatase in Planktonic Bacteria**

Optically-adjusted bacterial cultures (Chapter 2, Section 2.2.1.3) underwent centrifugation (4000 g, 10 min) and were re-suspended in an equal volume of 10  $\mu$ M **TCF-ALP** in 50 mM Tris-HCl (pH 9.2). For **TCF-ALP** hydrogel analysis, 2 mL of the bacterial culture in 50 mM Tris HCl (pH 9.2) was transferred to a 12-well microtiter plate containing a 100  $\mu$ M **TCF-ALP** based PVA hydrogel. These suspensions were subsequently protected from light and incubated at 32 °C for 24 h, unless stated otherwise. After incubation, 1 mL was removed from each suspension and centrifuged at 10 000 g for 3 min. The supernatant was subsequently placed into a black or clear 96-well microtiter plate for fluorescence and UV-Vis analysis, respectively. The fluorescence was measured using CLARIOstar fluorimeter (BMG LabTech, UK),  $\lambda_{\text{ex}} = 542 \text{ nm}$ ,  $\lambda_{\text{em}} = 606 \text{ nm}$ , and the UV-Vis by SPECTROstar Omega (BMG LabTech, UK). Appropriate controls were carried out in tandem and a minimum of three biological replicates per bacterial strain were used.

### **7.3.7. Detecting Alkaline Phosphatase in 96-well Plate Biofilm Models**

#### **7.3.7.1. Alkaline Phosphatase Activity of Biofilm**

Overnight cultures of *S. aureus* NCTC 10788 were sub-cultured into fresh Mueller Hinton broth to attain a concentration of  $10^6$  CFU/mL, before being placed into a 96-well microtiter plate and incubated at 32 °C for 18 h. After incubation, planktonic bacteria were discarded, and the remaining biofilm was washed three times with sterile dH<sub>2</sub>O. Plates were left to dry at room temperature for 20 min, before subsequent addition of 220  $\mu$ L of 10  $\mu$ M **TCF-ALP** in 50 mM Tris-HCl (pH 9.2) and further incubation at 32 °C for 24 h. Analysis of ALP production was performed as outlined in Section 7.3.6. The experiment was carried using

three biological replicates, and the assay performed in duplicate to ensure fluorescence readings at both 1 h and 24 h.

### **7.3.7.2. Inhibition of Alkaline Phosphatase Activity**

#### **7.3.7.2.1. Preparation of Sodium Orthovanadate**

A 50 mM stock of sodium orthovanadate was prepared in dH<sub>2</sub>O. Once dissolved, the pH was adjusted to 9.2 with 1 M NaOH and the resultant yellow solution (indicative of dimers) was boiled until colourless. Upon cooling, the pH was re-measured and adjusted if needed. This was repeated until the solution remained colourless.

#### **7.3.7.2.2. Minimum Inhibitory Concentration**

The Minimum Inhibitory Concentration of sodium orthovanadate was determined as outlined in Chapter 2, Section 2.2.1.5, with Mueller Hinton used as the broth.

#### **7.3.7.2.3. Minimum Biofilm Inhibitory Concentration**

The Minimum Biofilm Inhibitory Concentration of sodium orthovanadate was determined as outlined in Chapter 2, Section 2.2.2.1, with Mueller Hinton used as the broth.

#### **7.3.7.2.4. Inhibition of Alkaline Phosphatase Activity**

Biofilms of *S. aureus* NCTC 10788 were prepared as outlined in Chapter 2, Section 2.2.2.1. After 24 h incubation planktonic bacteria were discarded, and the remaining biofilm was washed three times with sterile dH<sub>2</sub>O and left to dry for 20 min at room temperature. Next, wells were pre-treated with various concentrations of sodium orthovanadate (0 – 3.75 mM; pH 9.2) for 30 min at room temperature, before addition of 10 µM **TCF-ALP** in 50 mM Tris-HCl (pH 9.2). Bacterial cultures were then protected from light and incubated at 32 °C for a further 24 h. Analysis of ALP production was performed as outlined in Section 7.3.6

### **7.3.8. Colony Biofilm Wound Model**

First, 19 mm polycarbonate membranes were UV sterilised for 10 min on Mueller Hinton agar, before being inoculated with 30 µL Artificial Wound Fluid (AWF; 50% fetal bovine serum in 50% peptone water [0.9% sodium chloride in 0.1% peptone]). Once dry, 50 µL of sub-cultured *S. aureus* NCTC 10788, *P. aeruginosa* PA01, or *E. coli* NSM56 (10<sup>6</sup> CFU/mL in 50 mM Tris HCl pH 9.2) was placed on the membrane and allowed to dry at room temperature. The inoculated polycarbonate membranes were then incubated for 24 h at 32 °C. Next, biofilms were removed from the agar plate, and placed into 2 mL of 10 µM **TCF-**

**ALP** in 50 mM Tris-HCl (pH 9.2), before being protected from light and incubated at 32 °C for 24 h. After, 1 mL of the suspension was removed and centrifuged at 10 000 g for 3 min. The supernatant was subsequently placed into a black 96-well microtiter plate for fluorescence analysis of ALP production. For **TCF-ALP** hydrogel analysis, biofilms were transferred to a 12-well microtiter plate containing bacteriological agar (to prevent the drying out of the biofilm). A 100 µM **TCF-ALP** based PVA hydrogel was subsequently placed on top of the biofilm. After being protected from light and incubated for 24 h at 32 °C, the hydrogels were removed from the biofilm and directly measured for fluorescence intensity using wavelengths as outlined previously.

To determine bacterial concentration, 24 h old biofilms were placed into 10 mL of PBS (pH 7.4) and stripped by sonication (44 KHz) for 15 min twice, with a 60 s interval of vortexing. Viable cells were quantified as outlined in Chapter 2, Section 2.2.1.4.

### **7.3.9. Ex vivo Porcine Skin Model**

#### **7.3.9.1. Sterilisation**

Porcine skin was washed with H<sub>2</sub>O before being cut into 2 x 2 cm squares, and subsequently underwent three 15-minute vortex cycles of washing in sterile dH<sub>2</sub>O. After, porcine skin was vortexed once for 15 min in 70 % ethanol, before a further two washes with sterile dH<sub>2</sub>O. Finally, the skin was UV-irradiated using a commercial UV source (Hamanatsu, Japan) equipped with a 254 nm UV lamp for 10 min before use.

#### **7.3.9.2. Alkaline Phosphatase Activity**

A 10 µL aliquot of *S. aureus* NCTC 10788 (10<sup>8</sup> CFU/mL in 50 mM Tris HCl pH 9.2) was added to the sterilised skin and left to dry for 20 min at room temperature. Next, 1 mL of 10 µM **TCF-ALP** in 50 mM Tris-HCl (pH 9.2) was added to the skin via use of a Franz Cell. Inoculated porcine skin was then protected from light and incubated at 32 °C for 24 h. After, the suspension was removed and centrifuged at 10 000 g for 3 min. The supernatant was subsequently placed into a black 96-well microtiter plate for fluorescence analysis of ALP production. For **TCF-ALP** hydrogel analysis, a 100 µM **TCF-ALP** based PVA hydrogel was subsequently placed on the top of the inoculated skin. After being protected from light and incubated for 24 h at 32 °C, the hydrogels were removed from the skin and directly measured for fluorescence intensity using wavelengths as mentioned previously.

## 7.4. Results and Discussion

### 7.4.1. UV-Vis of TCF-ALP

To determine whether the colorimetric change witnessed in Chapter 6 could be applied to whole-cell bacterial sensing, a stationary phase culture of *S. aureus* NCTC 10788 was harvested, washed, and resuspended in 1 mL of 10  $\mu$ M **TCF-ALP** in 50 mM Tris-HCl (pH 9.2). The concentration of **TCF-ALP** and pH of the buffer remained the same as the enzymatic assays undertaken in Chapter 6; however, the incubation time and temperature were different for optimal bacterial sensing and will be discussed further in this chapter.

After 24 h incubation at 32 °C, the bacterial suspensions were centrifuged, and the supernatant removed to obtain the UV-Vis spectra of **TCF-ALP** (Figure 7.9). A clear bathochromic shift of UV absorption occurred, which corresponded to a colour change from yellow to purple. This result is indicative of ALP production within *S. aureus* NCTC 10788, and further supports literature reports that ALP production is membrane-bound as the cells did not need to be lysed to detect ALP activity.<sup>115</sup>

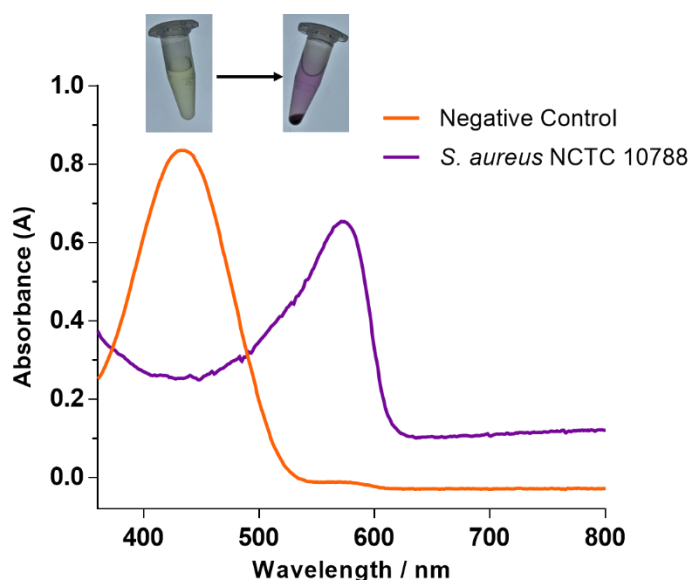


**Figure 7.9:** UV-Vis spectra of **TCF-ALP** (10  $\mu$ M) after 24 h incubation at 32 °C with *S. aureus* NCTC 10788 ( $10^{10}$  CFU/mL) in 50 mM Tris-HCl buffer pH 9.2

## 7.4.2. Optimisation of Assay

### 7.4.2.1. Role of Bacterial Growth Media on Alkaline Phosphatase Production

It is known that the addition of inorganic phosphate into culture media can result in reduced ALP activity in bacteria due to the repressive-nature of the enzyme.<sup>115</sup> To confirm this phenomenon, *S. aureus* NCTC 10788 was grown in three different broths, with different phosphate concentrations: Mueller Hinton, LB, and TSB. After incubation, bacterial cells were washed, resuspended in 10  $\mu\text{M}$  TCF-ALP (50 mM Tris-HCl, pH 9.2), and incubated for 1 or 24 h at 32 °C. After incubation, ALP activity was determined by measuring fluorescence intensity.

After 1 h incubation with TCF-ALP (Figure 7.10), a statistically significant increase in fluorescence intensity was observed for bacterial isolates propagated in Mueller Hinton broth compared to LB and TSB (One way ANOVA;  $p < 0.01$ ). After 24 h incubation (Figure 7.11), bacterial isolates grown in Mueller Hinton had a statistically significant increase in fluorescence (One way ANOVA;  $p < 0.0001$ ) compared to TSB, while there was no statistical difference between Mueller Hinton and LB.

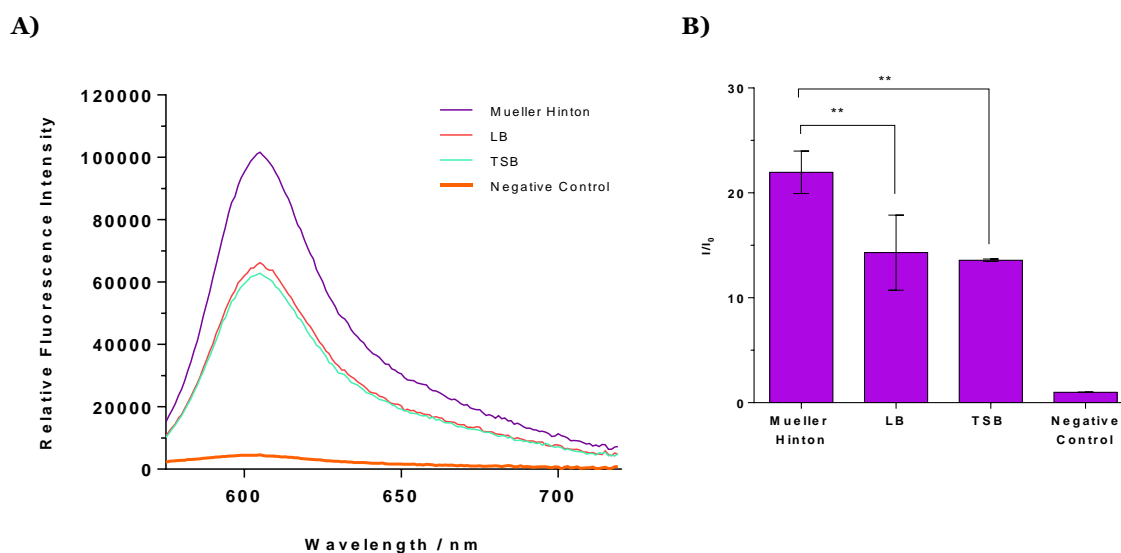


**Figure 7.10:** *Staphylococcus aureus* NCTC 10788 ( $10^8$  CFU/mL) was grown in: Mueller Hinton, LB or TSB before being inoculated for 1 h with TCF-ALP (10  $\mu\text{M}$ ) in 50 mM Tris-HCl buffer pH 9.2 at 32 °C. **A)** Fluorescence spectra and **B)** corresponding change in fluorescence ( $I/I_0$ ).  $\lambda_{\text{ex}} = 542$  (bandwidth 15) nm.  $\lambda_{\text{em}} = 606$  nm. Error bars indicate standard deviation ( $n = 3$ ). Statistical significance was assessed by performing a One-way ANOVA followed by Turkey post-hoc test.  $p$  values are indicated \*\*,  $p < 0.01$



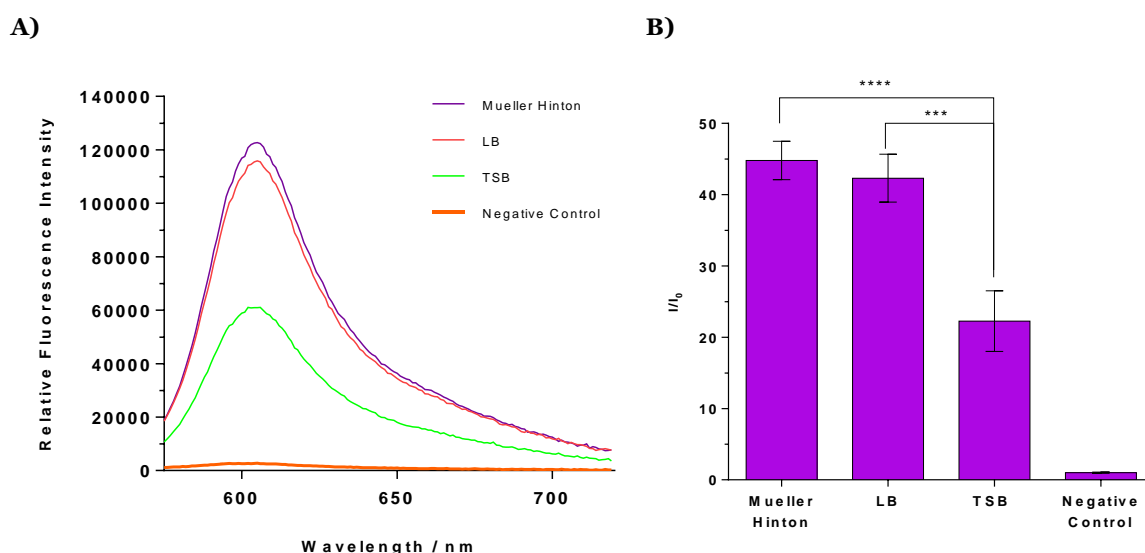


**Figure 7.11:** *Staphylococcus aureus* NCTC 10788 ( $10^8$  CFU/mL) was grown in either Mueller Hinton, LB or TSB before being inoculated for 24 h with TCF-ALP (10  $\mu$ M) in 50 mM Tris-HCl buffer pH 9.2 at 32 °C. **A)** Fluorescence spectra and **B)** corresponding change in fluorescence ( $I/I_0$ ).  $\lambda_{ex}$  = 542 (bandwidth 15) nm.  $\lambda_{em}$  = 606 nm. Error bars indicate standard deviation ( $n = 3$ ). Statistical significance was assessed by performing a One-way ANOVA followed by Turkey post-hoc test.  $p$  values are indicated \*\*\*,  $p < 0.001$ , \*\*\*\*,  $p < 0.0001$

As TSB contains 2.5 g/L of dipotassium hydrogen phosphate, it was expected that this broth would hinder ALP production during *S. aureus* growth. This correlates with the results obtained in Figures 7.10 and 7.11, as fluorescence intensity was significantly lower than the other media tested, suggesting lower amounts of ALP were produced.

The chemical compositions of Mueller Hinton and LB are different; hence, it is difficult to pinpoint what variable resulted in reduced phosphatase activity in LB compared to Mueller Hinton. However, it can be assumed that the differences in ALP production at 1 h is due to the differing amounts of trace phosphate levels in the growth medium. Unlike Mueller Hinton, LB contains yeast extract to supply vitamins, amino acids and trace elements, including phosphate.<sup>130</sup> This additional phosphate could have resulted in ALP being repressed in the early stages of growth, before being induced once the medium became phosphate-deficient.

Additionally, it has been shown by Sen *et al* that broth composition can have an effect on the morphology of bacterial cells,<sup>131</sup> while Ray *et al*<sup>132</sup> and Oogai *et al*<sup>133</sup> have suggested that the growth medium used for bacterial propagation has major effects on the expression of virulence and regulatory genes. Therefore, further study is needed to fully comprehend the relationship between growth media and the expression of ALP in *S. aureus*. Nevertheless, for the duration of this study Muller Hinton was utilised as the growth medium as it displayed the highest levels of ALP production.

### 7.4.2.2. Washing Steps

Next, experiments were undertaken to ensure that residual growth-medium did not affect ALP detection, hence washing steps were employed to remove the growth medium and any secreted ALP produced by *S. aureus*. Results show that washing the bacterial pellet had no statistical effect on the Log CFU/mL of *S. aureus* NCTC 10788, nor did it have any statistical effect on the fluorescence intensity when incubated with **TCF-ALP** (Figure 7.12). It was therefore concluded that upon harvesting, bacterial pellets would be washed once with 50 mM Tris HCl buffer (pH 9.2) before undergoing incubation with **TCF-ALP** to remove residual broth from the assay.

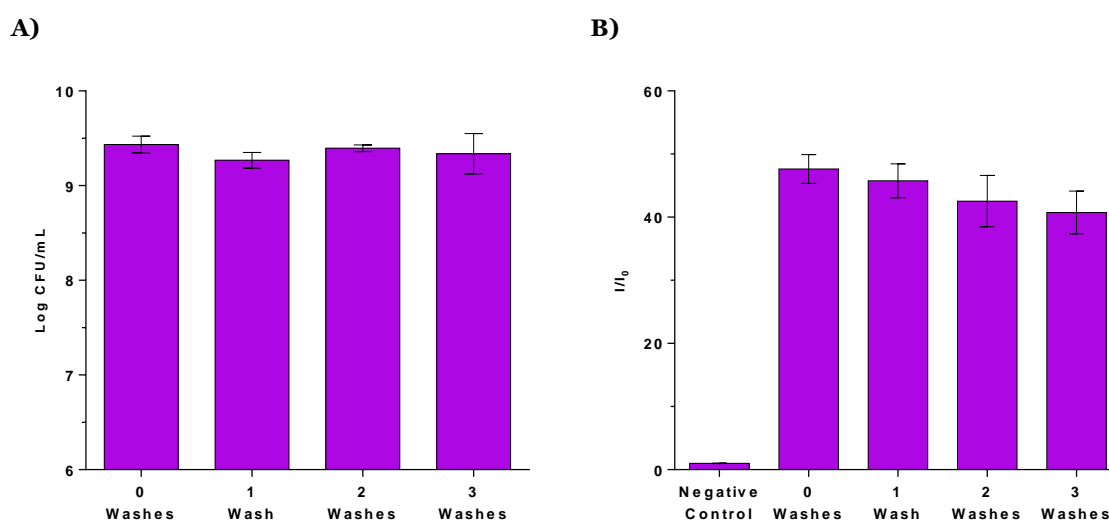


**Figure 7.12:** A) Log CFU/mL of *Staphylococcus aureus* NCTC 10788 after different amounts of wash cycles (0 – 3) and B) Change in fluorescence (I/I<sub>0</sub>) of **TCF-ALP** (10 μM) after 24 h incubation with washed suspensions of *Staphylococcus aureus* NCTC 10788 (10<sup>8</sup> CFU/mL) in 50 mM Tris-HCl buffer pH 9.2 at 32 °C. λ<sub>ex</sub> = 542 (bandwidth 15) nm. λ<sub>em</sub> = 606 nm. Statistical significance was assessed by performing a One-way ANOVA followed by Turkey post-hoc test

### 7.4.2.3. Incubation Temperatures

An investigation was undertaken to assess the role of temperature on ALP production. As previously mentioned, *S. aureus* grows at an optimum temperature of 37 °C, while the surface of the skin is cooler – with healthy skin having an average temperature of 32 °C. Therefore, to determine if there was any difference in ALP production at these two temperatures, *S. aureus* NCTC 10788 was incubated in Mueller Hinton broth at both temperatures prior to ALP determination.

Once the bacteria were grown, they were re-suspended in 50 mM Tris HCl buffer (pH 9.2) containing 10 μM of **TCF-ALP**. The bacteria and probe were then incubated at the following

temperatures: 25 °C, to assess the efficacy of **TCF-ALP** as a PoC test at the hospital bedside; 32 °C, to assess efficacy of **TCF-ALP** at wound-bed temperatures; and 37 °C, to assess the efficacy of **TCF-ALP** at the optimum temperature for *S. aureus* growth.

After 1 h incubation with 10 μM **TCF-ALP** (Figure 7.13A) there was no statistical difference between the ALP activity measured for bacteria grown at 32 °C compared to 37 °C for all **TCF-ALP** incubation temperatures measured. Although it seems that **TCF-ALP** incubation at 37 °C provides a faster detection of ALP for bacteria originally grown at 32 °C and 37 °C, the difference was not statistically significant. By 24 h (Figure 7.13B) all variables tested resulted in similar fluorescence intensities, and hence similar ALP activities. There was a statistical difference for bacteria grown at 37 °C and then subsequently incubated with **TCF-ALP** at 25 °C compared to 37 °C; however, the *p* value was 0.0499.

Overall, the results show that there is no difference in ALP production for *S. aureus* NCTC 10788 when grown at 32 °C compared to 37 °C. Likewise, **TCF-ALP** incubation temperatures did not have a substantial effect on ALP detection. Therefore, for the duration of this study, the bacterial cultures were incubated at 32 °C and once grown, incubated at 32 °C with **TCF-ALP** to mimic **TCF-ALP** being used as a wound dressing.

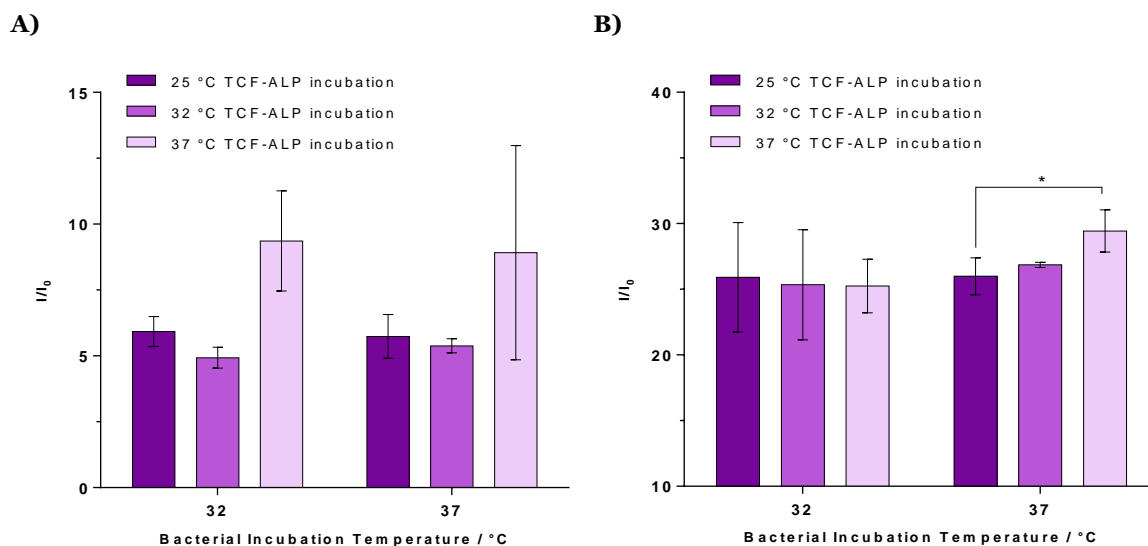


**Figure 7.13:** Change in fluorescence ( $I/I_0$ ) of **TCF-ALP** (10 μM) after **A)** 1 h and **B)** 24 h incubation with *Staphylococcus aureus* NCTC 10788 ( $10^8$  CFU/mL) in 50 mM Tris-HCl buffer pH 9.2. Bacterial cultures were grown at either 32 °C or 37 °C and incubated with **TCF-ALP** (10 μM) at 25°C, 32 °C or 37 °C.  $\lambda_{ex}$  = 542 (bandwidth 15) nm.  $\lambda_{em}$  = 606 nm. Statistical significance was assessed by performing a t-test with Welch's correction. *p* values are indicated \*, *p*<0.05

### 7.4.3. Time-dependant Alkaline Phosphatase Detection

A known concentration of *S. aureus* NCTC 10788 ( $10^8$  CFU/mL) was incubated with  $10\ \mu\text{M}$  of **TCF-ALP** (50 mM Tris-HCl, pH 9.2) and the fluorescence intensity measured over the course of 24 h (Figure 7.14). There was a noticeable increase in fluorescence intensity after 1 h incubation, rising linearly until a plateau after approximately 8 h. After this time, the fluorescence intensity remained constant for a further 16 h.

From this data it was concluded that fluorescence measurements using **TCF-ALP** were to be conducted at 1 h and 24 h. The time point of 1 h was chosen as it was the first time point capable of detecting ALP activity at this bacterial concentration and represented a ‘rapid’ detection of ALP activity and thus *S. aureus* NCTC 10788 infection. The longer incubation time of 24 h was chosen to allow for **TCF-ALP** to detect ALP activity in bacterial strains that have lower ALP expression, which could be missed at the 1 h timepoint.

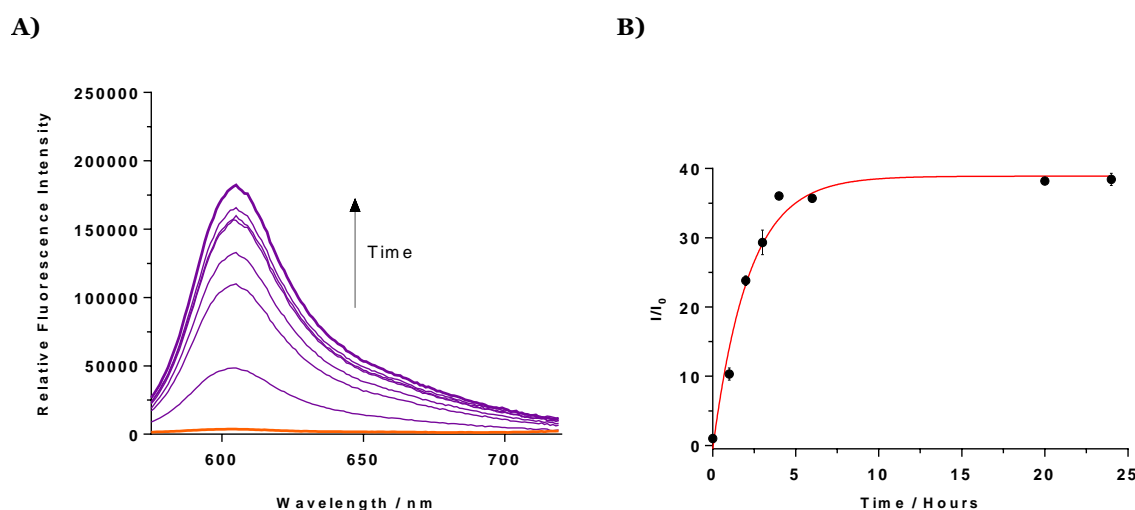


**Figure 7.14:** **A)** Fluorescence spectra of **TCF-ALP** ( $10\ \mu\text{M}$ ) recorded over the course of 24 h upon addition of *Staphylococcus aureus* NCTC 10788 ( $10^8$  CFU/mL) in 50 mM Tris-HCl buffer pH 9.2 at 32 °C. **B)** Corresponding change in fluorescence ( $I/I_0$ ) of **TCF-ALP** ( $10\ \mu\text{M}$ ) upon addition of *Staphylococcus aureus* NCTC 10788 ( $10^8$  CFU/mL) in 50 mM Tris-HCl buffer pH 9.2 at 32 °C.  $\lambda_{\text{ex}} = 542$  (bandwidth 15) nm /  $\lambda_{\text{em}} = 606$  nm. Error bars indicate standard deviation ( $n = 3$ )

### 7.4.4. Relationship Between Alkaline Phosphatase Production and Bacterial Concentration

To determine the concentration of *S. aureus* NCTC 10788 required to elicit a ‘turn on’ response of **TCF-ALP**, *S. aureus* NCTC 10788 was propagated, washed, and resuspended to achieve final bacterial densities of  $10^5 - 10^{10}$  CFU/mL in  $10\ \mu\text{M}$  of **TCF-ALP** (50 mM

Tris-HCl buffer, pH 9.2). The fluorescence intensity of each bacterial concentration was measured after 1 h and 24 h incubation at 32 °C. After, the intensities were normalised and plotted against a Log CFU/mL scale; the linear section of the graph was obtained, and the LOD was defined as the x-intercept.

After 1 h incubation, a linear, concentration-dependent increase in fluorescence intensity was seen for bacterial titres greater than  $10^7$  CFU/mL (Figure 7.15). Upon performing linear regression, it was found that the X-intercept was 7.50 (95 % Confidence Interval (CI) of 7.47 – 7.53), which corresponded to  $3.17 \times 10^7$  CFU/mL (95 % CI of  $2.95 - 3.40 \times 10^7$  CFU/mL).

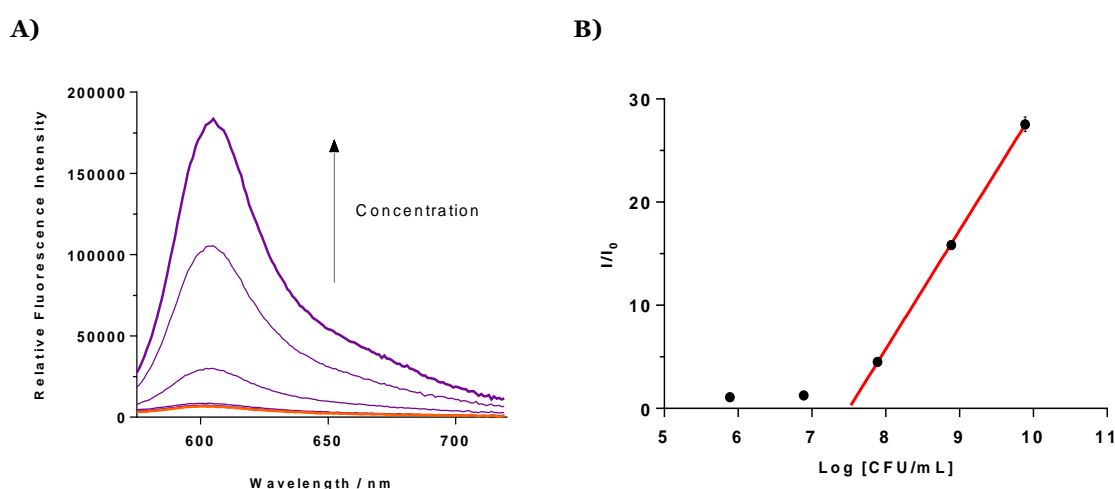


**Figure 7.15:** A) Fluorescence spectra of **TCF-ALP** (10 μM) after 1 h incubation with various concentrations of *Staphylococcus aureus* NCTC 10788 ( $10^5 - 10^{10}$  CFU/mL) in 50 mM Tris-HCl buffer pH 9.2 at 32 °C, and B) corresponding selectivity graph at 606 nm.  $\lambda_{ex} = 542$  (bandwidth 15) nm.  $\lambda_{em} = 606$  nm. (X-intercept 7.501 =  $3.17 \times 10^7$  CFU/mL;  $Y = 11.52X - 86.38$ ;  $R^2 0.9983$ )

After 24 h incubation with **TCF-ALP**, the LOD of *S. aureus* NCTC 10788 decreased (Figure 7.16), with the X-intercept becoming 6.57 (95 % CI of 6.32 – 6.76), which corresponded to  $3.70 \times 10^6$  CFU/mL (95 % CI of  $2.08 - 5.79 \times 10^6$  CFU/mL). However, at high bacterial concentrations ( $10^{10}$  CFU/mL) the fluorescence intensity decreased. One possible reason for this could be due to the assay methodology, whereby the bacterial suspension containing **TCF-ALP** was centrifuged and the supernatant removed for fluorescence measurements. Therefore, it is possible that at higher bacterial cell density there was a greater increase in uptake of **TCF-ALP** into the bacterial cells, and thus resulted in a lower fluorescence intensity in the supernatant.

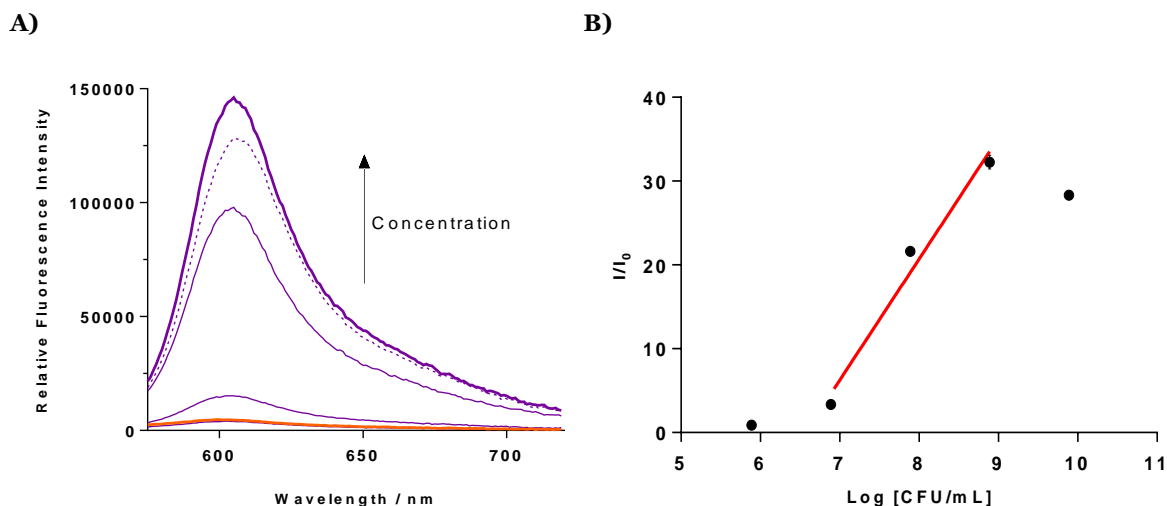


**Figure 7.16:** **A)** Fluorescence spectra of **TCF-ALP** (10  $\mu$ M) after 24 h incubation with various concentrations of *Staphylococcus aureus* NCTC 10788 ( $10^5 - 10^{10}$  CFU/mL) in 50 mM Tris-HCl buffer pH 9.2 at 32  $^{\circ}$ C, the dotted line represents  $10^{10}$  CFU/mL. **B)** corresponding selectivity graph at 606 nm.  $\lambda_{ex} = 542$  (bandwidth 15) nm.  $\lambda_{em} = 606$  nm. (X-intercept  $6.568 = 3.70 \times 10^6$  CFU/mL;  $Y = 14.45X - 94.88$ ;  $R^2 0.9759$ )

The LOD of **TCF-ALP** was compared to the LOD of other chemiluminescent, colorimetric, and fluorescent probes that detected bacteria *via* enzymes (Table 7.1). Most of the recent publications have focused on the detection of *E. coli* through the use of several enzymes ( $\beta$ -galactosidase and  $\beta$ -glucuronidase), and the detection of antibiotic-resistant bacteria through the use of  $\beta$ -lactamase and carbapenemase. As shown in Table 7.1, most of the fluorescent and colorimetric probes developed have a similar LOD between  $10^5 - 10^7$  CFU/mL. Some fluorescent probes that could detect concentrations as low as  $10^1$  CFU/mL were only able to do so after an 'enrichment', where the initial bacterial suspension ( $10^1$  CFU/mL) was added to broth and allowed to grow for a set period of time. Therefore, the concentration after the enrichment process is significantly higher than what is recorded as the LOD. This is evident with Kim *et al*, where without enrichment the LOD was  $10^7$  CFU/mL, and with a 7 h enrichment it was lowered to  $10^1$  CFU/mL.<sup>23</sup>

Additionally, some of these fluorescent and colorimetric probes detect enzymes that are intracellular, such as  $\beta$ -galactosidase and  $\beta$ -glucuronidase. Owing to this, the bacterial cells must be lysed prior to testing with the probe, resulting in a complicated system where the bacteria must be pre-treated for detection to occur, which can be costly and difficult to achieve as a PoC device.

**Table 7.1:** Table outlining Limits of Detection for fluorescent and colorimetric probes for the detection of bacterial enzymes

Bacteria	Enzyme	Detection Method	LOD (CFU/mL)	Time	Year	Ref.
<i>Salmonella</i>	C8-Esterase	Chemi-luminescence	10 cells	6 h	2019	134
<i>Listeria monocytetes</i>	PI-PLC	Chemi-luminescence	10 <sup>4</sup>	24 h	2019	134
<i>Pseudomonas aeruginosa</i>	Carbapenemase	Chemi-luminescence	10 <sup>7</sup>	20 min	2020	135
<i>Klebsiella pneumonia</i>	Carbapenemase	Chemi-luminescence	10 <sup>7</sup>	20 min	2020	135
<i>Escherichia coli</i>	β-lactamase	Chemi-luminescence	10 <sup>5</sup>	30 min	2020	136
<i>Escherichia coli</i>	β-lactamase	Fluorescence	10 <sup>7</sup>	30 min	2020	136
<i>Escherichia coli</i>	β-galactosidase	Colorimetric	10 <sup>5</sup> with cell lysis, 10 <sup>7</sup> without.	40 min	2017	32
<i>Escherichia coli</i>	β-galactosidase	Colorimetric hydrogel	10 <sup>2</sup>	60 min	2010	137
<i>Escherichia coli</i>	β-glucuronidase	Fluorescence*	10 <sup>2</sup>	30 min	2010	19
<i>Escherichia coli</i>	β-glucuronidase	Fluorescence	10 <sup>5</sup>	-	1999	138
<i>Escherichia coli</i>	Numerous	Colorimetric	10 <sup>1</sup> with 7 h enrichment, 10 <sup>7</sup> without	4 h for enrichment, 60 min without	2019	23

\*this work developed a novel hand-held fluorimeter to detect *Escherichia coli*.

- unknown

It has long been theorised that the healing of chronic wounds is directly related to the number of colonising bacteria – often termed the critical colonisation.<sup>139,140</sup> However, there remains much debate over this term, as the threshold concentration for the bacterial burden to progress from contamination to localised infection is ambiguous. An alternative school of thought is that the presence of an infection is dependent on the bacterial species present and not the bacterial bioburden within the wound. The most probable rationale is that the progression to infection is a result of several factors: what pathogenic bacteria are present at the wound site, the pathogen’s ability to cause disease (virulence), the concentration of these pathogens, and the host’s ability to mount an immune response.<sup>141</sup>

While there is a debate over the number of bacteria required to result in a localised infection, it is generally accepted that it lies between  $10^4$  to  $10^6$  CFU/mL, depending on the bacterial species and the location of the wound.<sup>142</sup> Work conducted by Robson *et al* found that the healing of pressure ulcers and surgical site infections could be predicted by quantifying the bacteria in biopsied tissue; this formed the basis of the  $10^5$  guideline, which is the theory that  $10^5$  viable bacterial cells per gram of tissue is necessary to cause wound infections.

Additionally, biofilms are present in approximately 60 to 90% of chronic wounds and contribute to the pathogenicity of the invading bacterial species.<sup>143–145</sup> Biofilms usually have higher bacterial cell density, with results in our laboratory showing bacterial concentrations as high as  $10^{11}$  CFU/membrane – significantly higher than the  $10^5$  standard needed to cause infection. However, one main issue with chronic wounds is that there is no gold-standard tests available to diagnose wound infections.<sup>144,146</sup> **TCF-ALP** could potentially be able to diagnose such infections, with a clear “turn-on” response witnessed at concentrations higher than  $10^6$  CFU/mL after 24 h incubation. As concentrations below this fluorescence response are not indicative of a localised infection, **TCF-ALP** might be able to accurately diagnose wounds that are clinically infected, helping health care professionals accurately diagnose and treat infected wounds.

#### 7.4.5. Selectivity of TCF-ALP

To ensure that **TCF-ALP** is selective towards *S. aureus* species, selectivity assays were performed using  $10^8$  CFU/mL of different bacterial isolates. Initially, six *S. aureus*, three *S. epidermidis*, three *P. aeruginosa*, and three *E. coli* strains were tested using **TCF-ALP** (50 mM Tris-HCl, pH 9.2). After 24 h incubation, all *S. aureus* and *S. epidermidis* strains were capable of eliciting a fluorescence response, while negligible fluorescence was observed for *E. coli* and *P. aeruginosa* strains. This negligible fluorescence response was not due to a decrease in bacterial concentration, with cell counts showing a minimal decrease in bacterial density after 24 h incubation with **TCF-ALP** (Appendix).

The results shown in Figure 7.17 were interesting, as all bacterial strains were shown to produce ALP;<sup>88,104</sup> however, gram-positive bacterial species produced a higher fluorescence response compared to gram-negative species. One hypothesis for this variance is that *Staphylococcal* spp. produce more ALP compared to their gram-negative counterparts and therefore displays a stronger response to **TCF-ALP**. Alternatively, the differences in fluorescence response could be due to the differences in cell wall structure and location of ALP within the bacterial cell. *S. aureus* and *S. epidermidis* are both gram-positive organisms with a thick peptidoglycan layer; ALP is normally membrane-bound, hence is



easily accessible. For gram-negative bacteria, **TCF-ALP** would have to pass through the outer membrane via passive diffusion or through the use of efflux pumps in order to be de-phosphorylated by the ALP within the periplasmic space.<sup>111</sup> Therefore, it could be possible that these transporter proteins are unable to recognise **TCF-ALP** and consequently the fluorescent probe is unable to enter the bacterial cell. However, further work is required to determine the reason behind this selectivity.

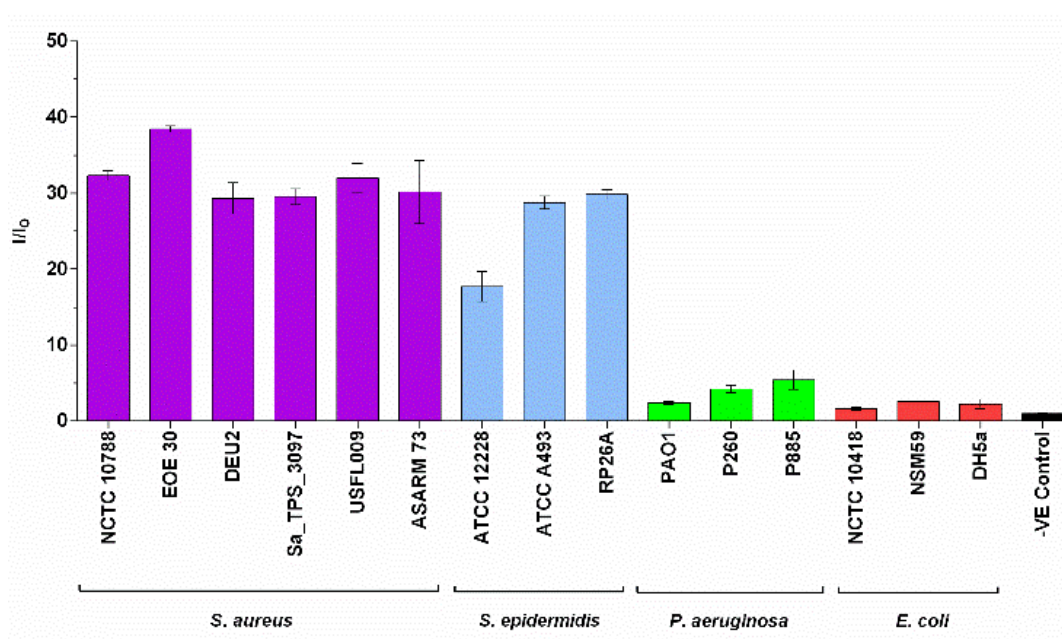


**Figure 7.17:** Selectivity bar chart of **TCF-ALP** (10  $\mu$ M) in 50 mM Tris-HCl buffer pH 9.2 after 24 h incubation with various bacterial strains ( $10^8$  CFU/mL) at 32 °C.  $\lambda_{ex}$  = 542 (bandwidth 15) nm.  $\lambda_{em}$  = 606 nm. Error bars indicate standard deviation (n = 3)

To ensure that **TCF-ALP** was selective to *S. aureus*, further experiments were conducted using a larger library of *S. aureus* isolates. In total, 42 *S. aureus* strains were tested, and the fluorescence intensity measured after 1 and 24 h incubation with **TCF-ALP**. For all *S. aureus* strains tested, there was an increase in fluorescence intensity after 1 h incubation with **TCF-ALP**, which further increased after 24 h incubation (Figures 7.18 and 7.19).

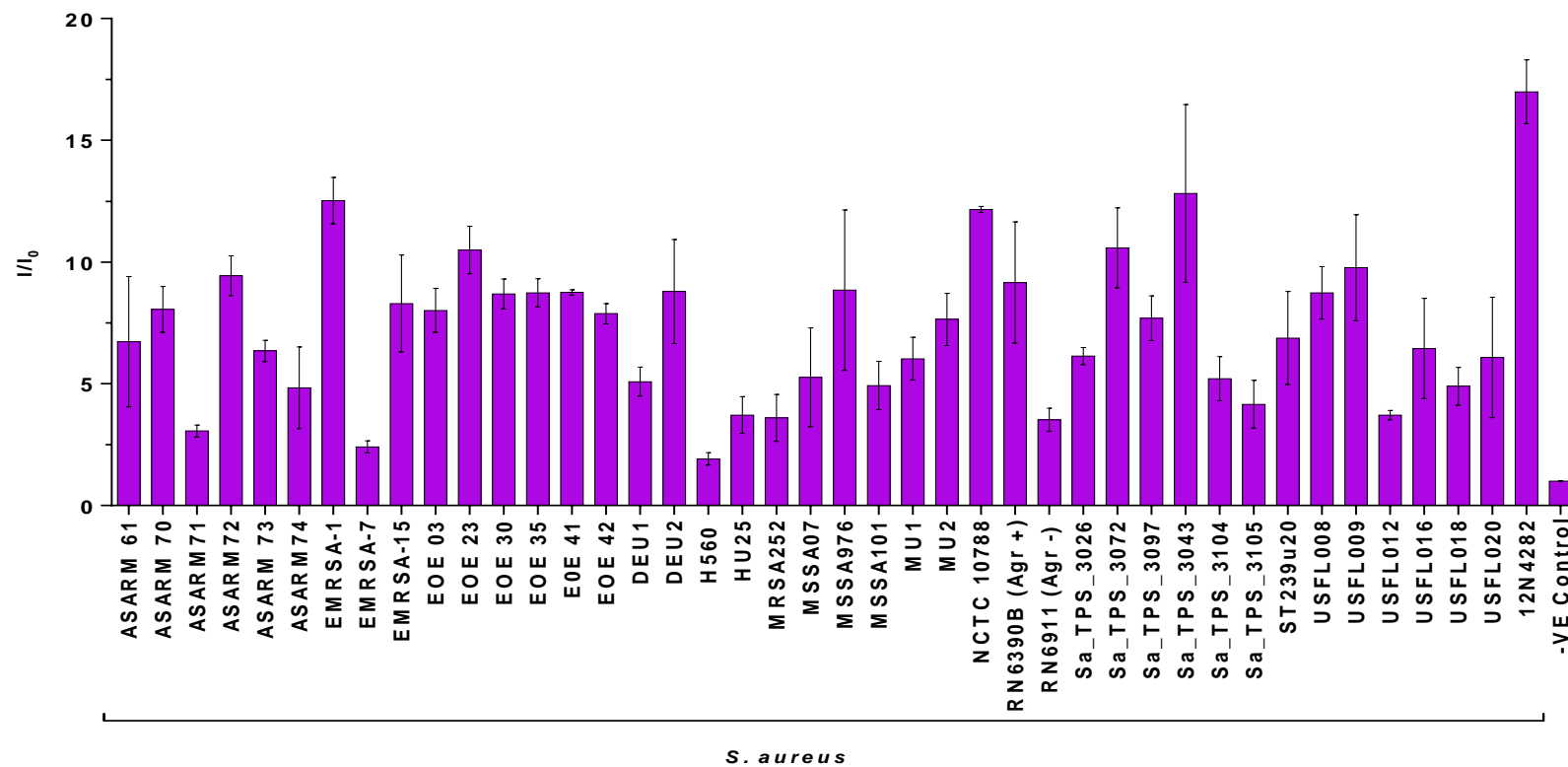


**Figure 7.18:** Selectivity bar chart of TCF-ALP (10  $\mu$ M) in 50 mM Tris-HCl buffer pH 9.2 after 1 h incubation with various bacterial strains ( $10^8$  CFU/mL) at 32 °C.  $\lambda_{\text{ex}} = 542$  (bandwidth 15) nm,  $\lambda_{\text{em}} = 606$  nm. Error bars indicate standard deviation (n = 3).

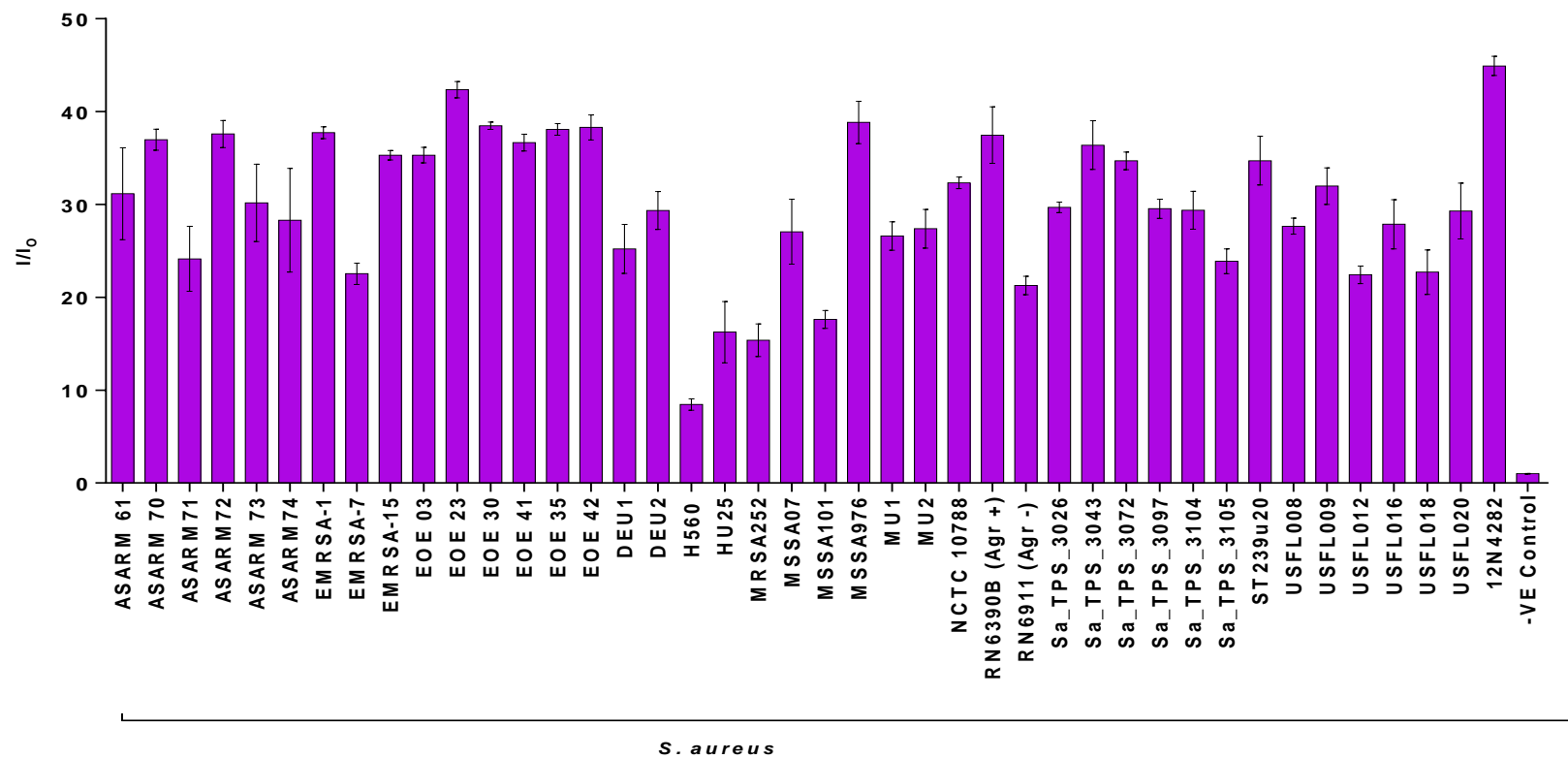


**Figure 7.19:** Selectivity bar chart of **TCF-ALP** (10  $\mu$ M) in 50 mM Tris-HCl buffer pH 9.2 after 24 h incubation with various bacterial strains ( $10^8$  CFU/mL) at 32 °C.  $\lambda_{\text{ex}} = 542$  (bandwidth 15) nm.  $\lambda_{\text{em}} = 606$  nm. Error bars indicate standard deviation (n = 3).

The results above show that **TCF-ALP** was capable of producing a fluorescence response in the presence of all 42 *S. aureus* strains tested. Interestingly, the majority of *S. aureus* strains were capable of producing at least a 20-fold increase in fluorescence intensity, regardless of the phenotype. This suggests that ALP is conserved within *S. aureus* and therefore could be used as a tool for *S. aureus* detection within an infected wound.

One interesting observation is the fact that *S. aureus* Agr- (RN6911) has a decreased fluorescence response compared to its counterpart, *S. aureus* Agr+ (RN6390B). In these studies, *S. aureus* Agr- is a derivative of *S. aureus* Agr+, where the accessory gene regulator (*agr*) system has been replaced with a tetracycline resistance gene. The *agr* system controls and regulates a variety of *S. aureus* virulence factors that contribute to *S. aureus* pathogenicity through coordinated expression of specific virulence genes. Often cell surface adhesins are synthesised and expressed before the secretion of toxins and enzymes.<sup>147</sup> Agr- mutants have been isolated in clinical and laboratory settings,<sup>148,149</sup> exhibiting increased fitness, especially under antibiotic stress,<sup>150</sup> which can therefore be linked to higher patient mortality.<sup>147</sup> While in a chronic infection *agr*- phenotype strains have increased persistence, *agr*+ phenotype strains seem to be important for bacterial virulence to create an established infection.<sup>151</sup>

In these studies, *S. aureus* Agr- and Agr+ both display a fluorescence “turn-on” in response upon incubation with **TCF-ALP**. Therefore, it can be suggested that ALP expression is not under the control of *agr*. However, ALP production could be *agr*-dependent as the ALP activity of *S. aureus* Agr- was observed to be lower than that of *S. aureus* Agr+. One hypothesis for this observation is that as the *agr* system is dependent on phosphorylation, it needs inorganic phosphate to operate successfully.<sup>151</sup> In order to aid this phosphorylation, ALP production may need to be increased in *S. aureus* Agr+, while the same level of ALP is not needed for *S. aureus* Agr- as the *agr* operon is not present. However, there are other mechanisms within *S. aureus* that rely on phosphorylation of a protein to function; therefore, further exploratory analysis is required to investigate the relationship between ALP and regulation systems within *S. aureus*.

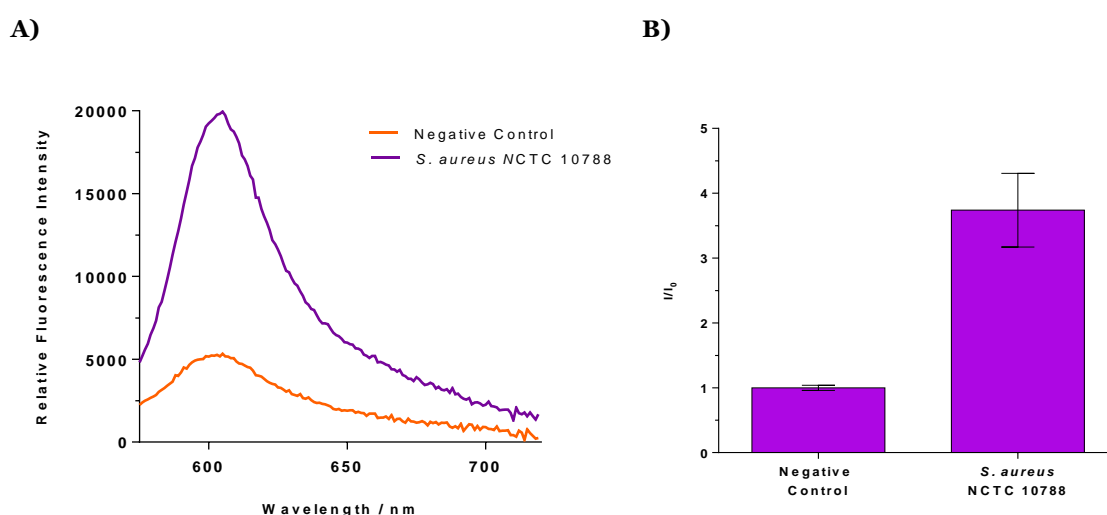
#### **7.4.6. Alkaline Phosphatase Production in Established Biofilms**

As previously mentioned, approximately 60% of chronic wounds contain a biofilm.<sup>145,152,153</sup> To determine the clinical utility of the probe, all work herein utilised 24 h old biofilms to investigate the efficacy of **TCF-ALP** in detecting ALP activity in bacterial biofilms.

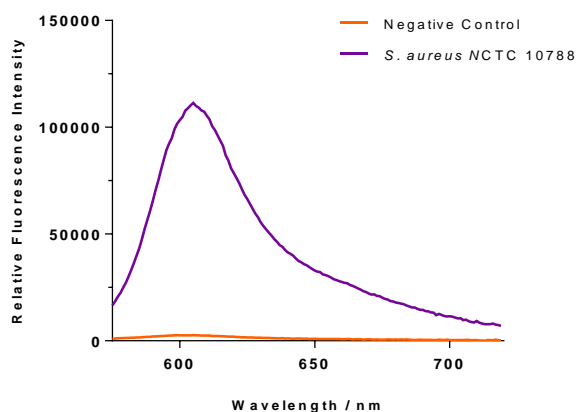
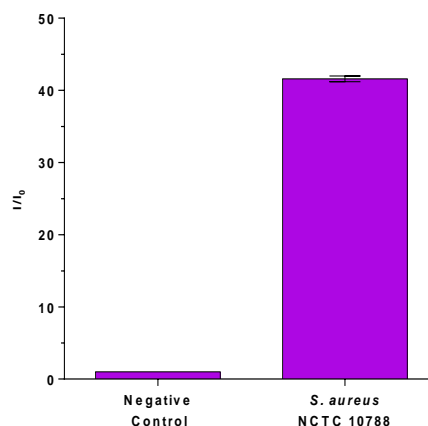
The role of ALP in *S. aureus* biofilm formation is currently unknown.<sup>154</sup> A variety of factors are known to influence biofilm formation, including pH, temperature and nutrient availability.<sup>155</sup> Interestingly, studies have found that phosphorous concentration is also important for successful biofilm formation,<sup>156</sup> with Li *et al* corroborating this theory by showing that ALP activity is elevated in *S. aureus* biofilms compared to their planktonic counterparts,<sup>157</sup> and Danikowski *et al* finding that the use of an ALP inhibitor greatly disrupted biofilm formation.<sup>154</sup> Furthermore, ALP has been shown to possess phosphodiesterase activity, which has been linked to hyper-formation of biofilms in *Serratia marcescens* and *S. aureus*.<sup>154,158</sup> Therefore, it can be hypothesised that ALP is required for *S. aureus* biofilm formation. While ALP could become a target for anti-biofilm therapeutics, it could also be used to target *S. aureus* in chronic wounds to help guide infection treatment for patients, leading to improved clinical outcomes.

#### 7.4.6.1. 96-well Microtiter Plate Biofilm Model

To investigate ALP activity within *S. aureus* biofilms, a standard static biofilm model was used employing a 96-well microtiter plate. Muller Hinton broth was used in line with planktonic assays, with the addition of glucose evaluated prior to the start of this assay (Appendix). Glucose supplementation was ineffective in enhancing bacterial biofilm formation, thus was not used in these experiments. Briefly, 24-h old biofilms were treated with **TCF-ALP** (10  $\mu$ M, 50 mM Tris-HCl, pH 9.2) for 1 h and 24 h before the solution was transferred to a fresh black 96-well microtiter plate and the fluorescence intensity recorded (Figures 7.20 and 7.21).



**Figure 7.20:** **A)** Fluorescence spectra of **TCF-ALP** (10  $\mu$ M) after 1 h incubation with a 96-well plate biofilm of *S. aureus* NCTC 10788 in 50 mM Tris-HCl buffer pH 9.2 at 32 °C, and **B)** corresponding selectivity bar chart.  $\lambda_{ex}$  = 542 (bandwidth 15) nm.  $\lambda_{em}$  = 606 nm. Error bars indicate standard deviation (n = 3)

**A)****B)**

**Figure 7.21: A)** Fluorescence spectra of **TCF-ALP** (10  $\mu$ M) after 24 h incubation with a 96-well plate biofilm of *S. aureus* NCTC 10788 in 50 mM Tris-HCl buffer pH 9.2 at 32  $^{\circ}$ C, and **B)** corresponding selectivity bar chart.  $\lambda_{ex} = 542$  (bandwidth 15) nm.  $\lambda_{em} = 606$  nm. Error bars indicate standard deviation (n = 3)

Figure 7.20 shows an increase in fluorescence intensity of **TCF-ALP** after 1 h incubation with *S. aureus* NCTC 10788, which increased further after 24 h incubation (Figure 7.21). This study proved that ALP is produced within a biofilm, which corresponds with literature reports suggesting that ALP is involved in *S. aureus* biofilm formation.<sup>154</sup>

To ensure that **TCF-ALP** was activated only in response to ALP, further experiments were conducted using a known ALP inhibitor – sodium orthovanadate. Briefly, 24 h biofilms of *S. aureus* NCTC 10788 were grown in 96-well microtiter plates before subsequent incubation with various sub-inhibitory concentrations of sodium orthovanadate (Appendix) for 30 min. After, **TCF-ALP** (10  $\mu$ M) was added (200  $\mu$ L) and incubated for a further 24 h at 32  $^{\circ}$ C, before the biofilms were assessed for fluorescence activity.

Figure 7.22 and 7.23 show that upon increasing concentrations of phosphate inhibitor there is a corresponding decrease in fluorescence intensity, suggesting that ALP production within *S. aureus* biofilms is reduced in the presence of a phosphatase inhibitor. The effect is more pronounced after 24 h incubation with **TCF-ALP**, although the trend is the same. In conclusion, fluorescence response observed in *S. aureus* biofilms incubated with **TCF-ALP** is due to phosphatase expression.

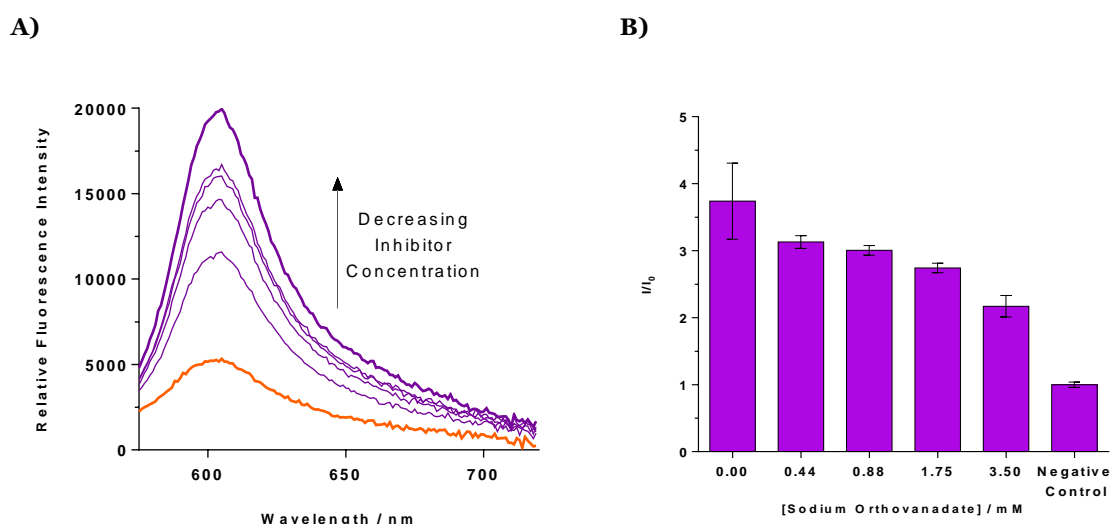


**Figure 7.22:** **A)** Fluorescence spectra of TCF-ALP (10 μM) in 50 mM Tris-HCl buffer pH 9.2 after 1 h at 32 °C incubation with *S. aureus* NCTC 10788 (10<sup>8</sup> CFU/mL) pre-incubated for 30 min with various concentrations of sodium orthovanadate (0.00-3.50 mM), and **B)** corresponding selectivity bar chart.  $\lambda_{ex}$  = 542 (bandwidth 15) nm.  $\lambda_{em}$  = 606 nm. Error bars indicate standard deviation (n = 3).

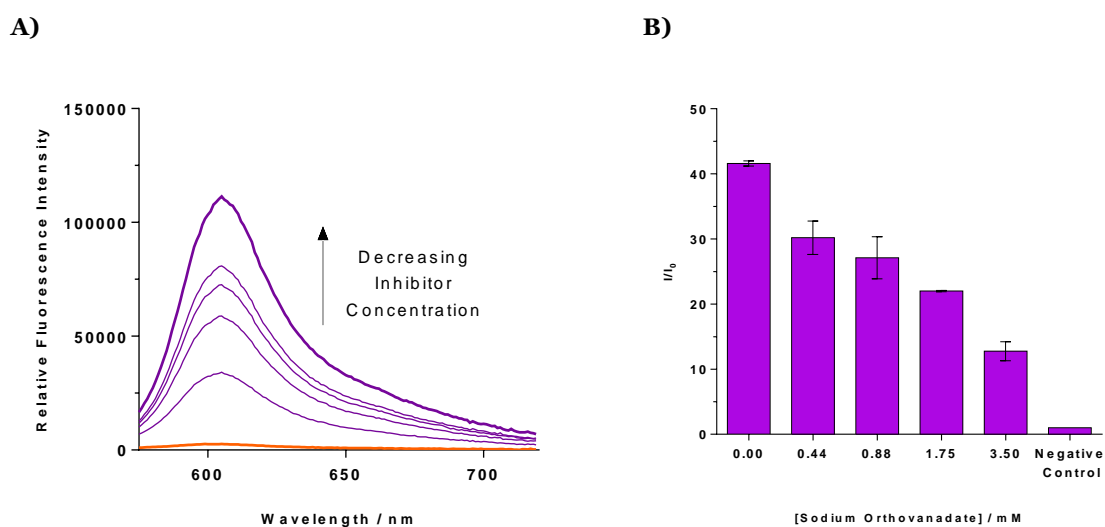


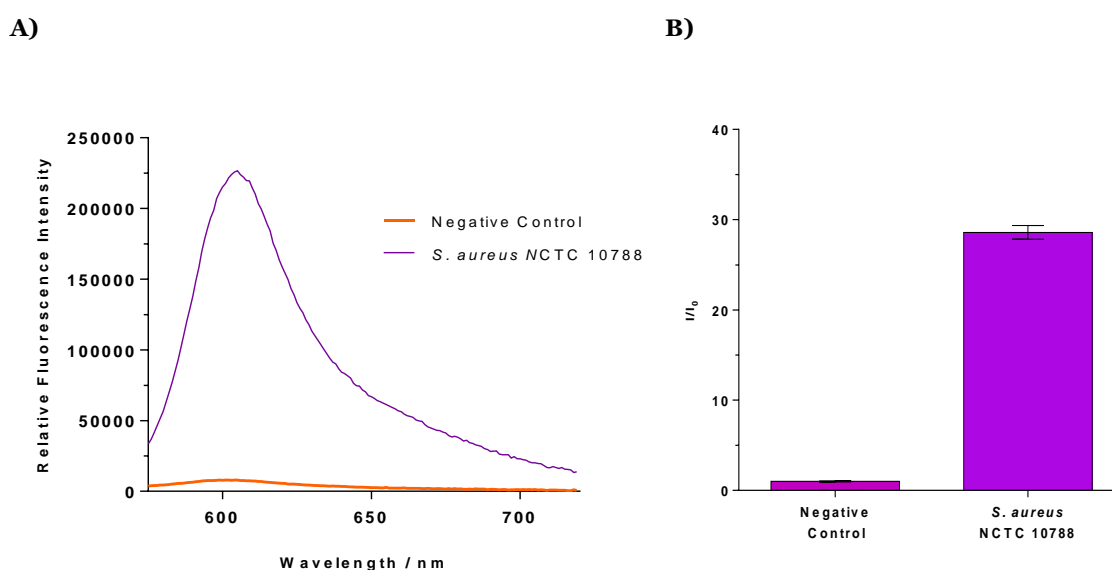
**Figure 7.23:** **A)** Fluorescence spectra of TCF-ALP (10 μM) in 50 mM Tris-HCl buffer pH 9.2 after 24 h at 32 °C incubation with *S. aureus* NCTC 10788 (10<sup>8</sup> CFU/mL) pre-incubated for 30 minutes with various concentrations of sodium orthovanadate (0.00-3.50 mM), and **B)** corresponding selectivity bar chart.  $\lambda_{ex}$  = 542 (bandwidth 15) nm.  $\lambda_{em}$  = 606 nm. Error bars indicate standard deviation (n = 3).

#### 7.4.6.2. Colony Biofilm Model

The colony biofilm model is a static biofilm model was used as it is more indicative of a wound environment than traditional static biofilm models using 96-well plates. Sub-cultured *S. aureus* NCTC 10788 (c. 10<sup>6</sup> CFU/mL) was added to 19 mm sterile membranes

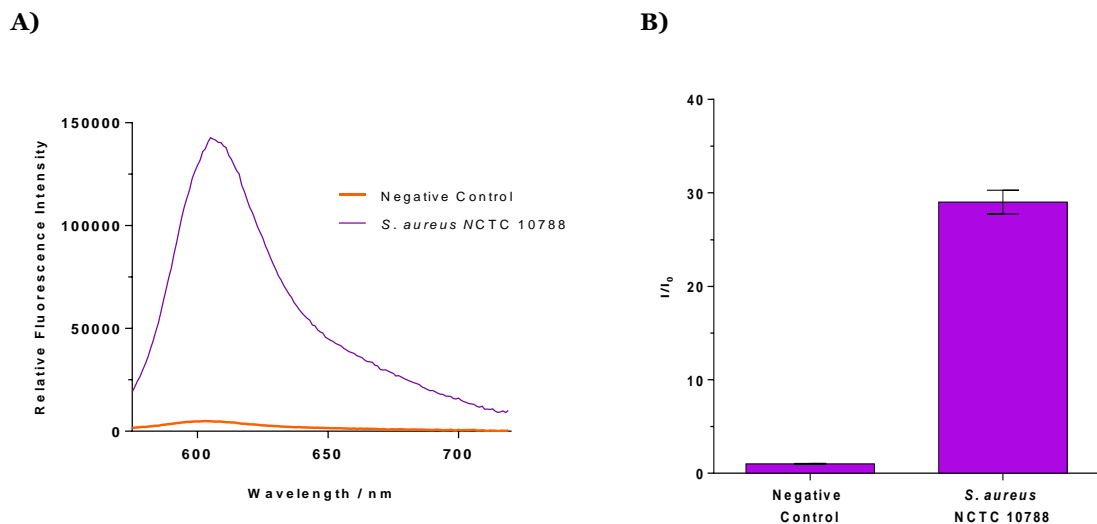
pre-treated with AWF and incubated at 32 °C for 24 h. After, the membranes were transferred to a 12 well microtiter plate containing bacteriological agar to ensure that the bacterial biofilm did not dry out throughout the remainder of the experiment, thus preventing premature cell death. Next, 1 mL of **TCF-ALP** (10  $\mu$ M, 50 mM Tris HCL, pH 9.2) was added to the surface of the biofilms and incubated for 1 h or 24 h at 32 °C before undergoing fluorescence measurements. It is important to note that incubation with **TCF-ALP** did not significantly decrease the viable count of *S. aureus* NCTC 10788 compared to the untreated controls (bacterial biofilms incubated with 50 mM Tris-HCl, pH 9.2; see Appendix).

Upon incubation of *S. aureus* NCTC 10788 with **TCF-ALP**, there was a sharp increase in fluorescence intensity (Figure 7.24) that remained for the duration of the study (Figure 7.25). The ratio of the RFI of the sample to the RFI of the negative control ( $I/I_0$ ) the values were similar (~30-fold increase), signifying that the probe was saturated with ALP before the 1 h measurement, indicating a high level of ALP activity within the biofilm compared to its planktonic counterpart.

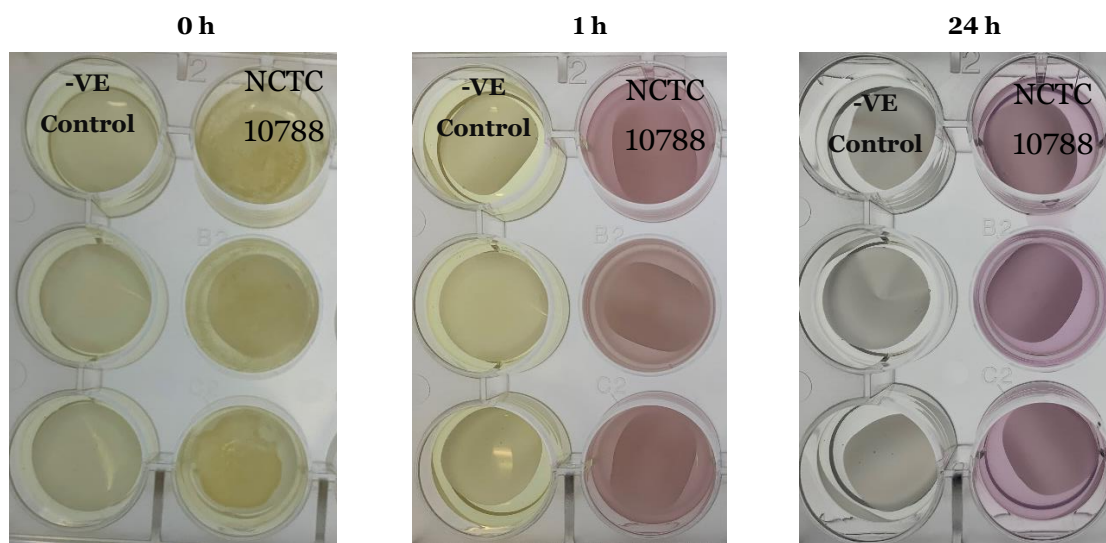


**Figure 7.24:** A) Fluorescence spectra of **TCF-ALP** (10  $\mu$ M) after 1 h incubation with biofilms of *S. aureus* NCTC 10788 (1011 CFU/membrane) in 50 mM Tris-HCl buffer pH 9.2 at 32 °C and B) corresponding selectivity bar chart.  $\lambda_{ex}$  = 542 (bandwidth 15) nm.  $\lambda_{em}$  = 606 nm. Error bars indicate standard deviation (n = 3)





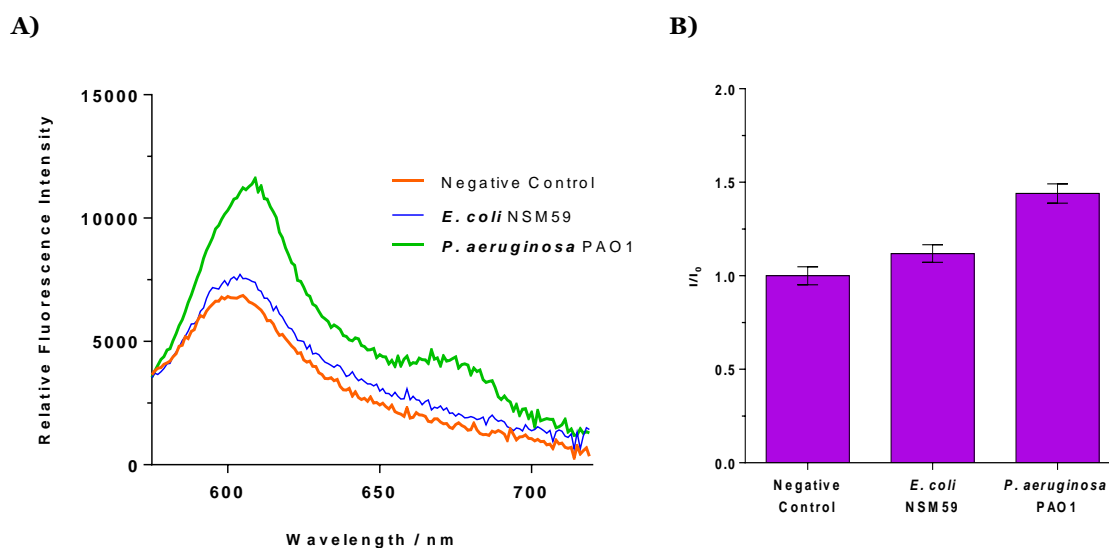
**Figure 7.25:** **A)** Fluorescence spectra of **TCF-ALP** (10 μM) after 24 h incubation with biofilms of *S. aureus* NCTC 10788 (10<sup>11</sup> CFU/membrane) in 50 mM Tris-HCl buffer pH 9.2 at 32 °C, and **B)** corresponding selectivity bar chart.  $\lambda_{ex} = 542$  (bandwidth 15) nm.  $\lambda_{em} = 606$  nm. Error bars indicate standard deviation (n = 3)



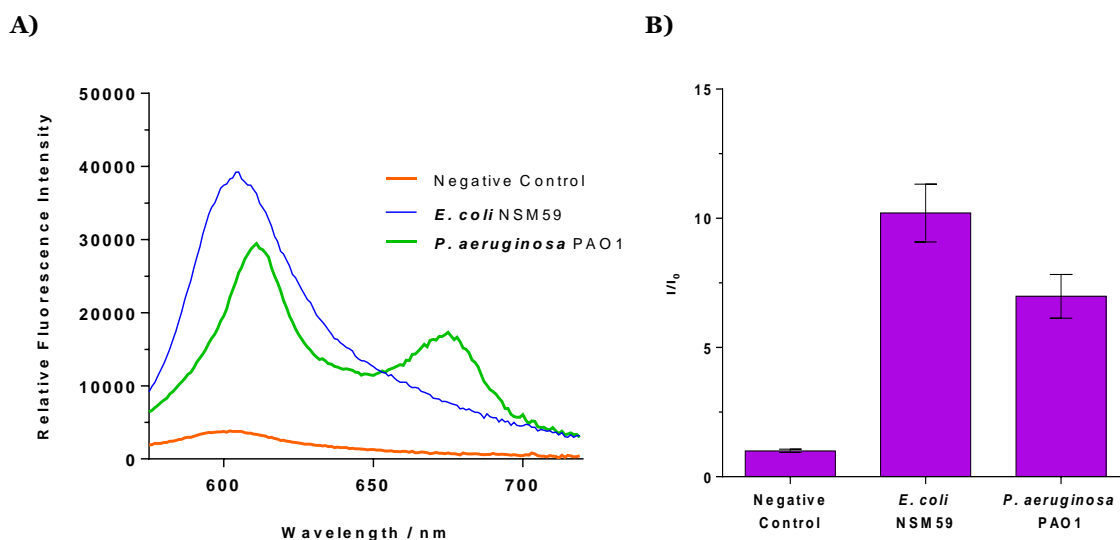
**Figure 7.26:** Images taken of negative controls (Membrane and Artificial Wound Fluid (AWF) only) and biofilms of *S. aureus* NCTC 10788 (10<sup>11</sup> CFU/membrane) after 0, 1, and 24 h incubation with 10 μM **TCF-ALP** in 50 mM Tris-HCl buffer pH 9.2 at 32 °C

Figure 7.26 shows the distinct colour change from yellow to purple of **TCF-ALP** after 1 h incubation with *S. aureus* NCTC 10788, which was maintained for up to 24 h post-incubation with *S. aureus* NCTC 10788.

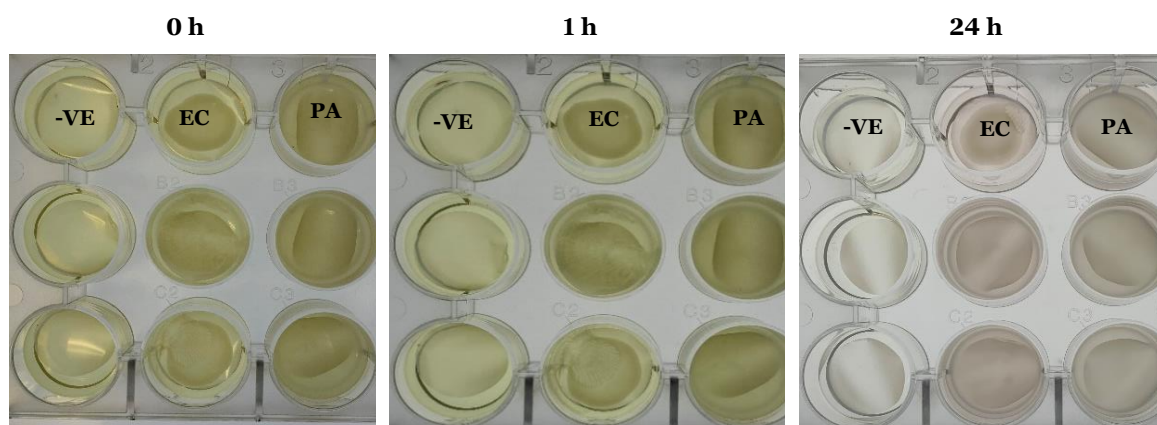
Biofilms exhibit an altered phenotype compared to planktonic bacteria,<sup>159</sup> thus experiments were conducted using biofilms of *E. coli* NSM59 and *P. aeruginosa* PAO1 to re-examine the selectivity of TCF-ALP (Figures 7.27, 7.28, and 7.29).



**Figure 7.27:** **A)** Fluorescence spectra of TCF-ALP (10 μM) after 1 h incubation with biofilms of *E. coli* NSM59 and *P. aeruginosa* PAO1 (10<sup>11</sup> CFU/membrane) in 50 mM Tris-HCl buffer, pH 9.2 at 32 °C and **B)** corresponding selectivity bar chart.  $\lambda_{\text{ex}} = 542$  (bandwidth 15) nm.  $\lambda_{\text{em}} = 606$  nm. Error bars indicate standard deviation (n = 3)



**Figure 7.28:** **A)** Fluorescence spectra of TCF-ALP (10 μM) after 24 h incubation with biofilms of *E. coli* NSM59 and *P. aeruginosa* PAO1 (10<sup>11</sup> CFU/membrane) in 50 mM Tris-HCl buffer pH 9.2 at 32 °C and **B)** corresponding selectivity bar chart.  $\lambda_{\text{ex}} = 542$  (bandwidth 15) nm.  $\lambda_{\text{em}} = 606$  nm. Error bars indicate standard deviation (n = 3)



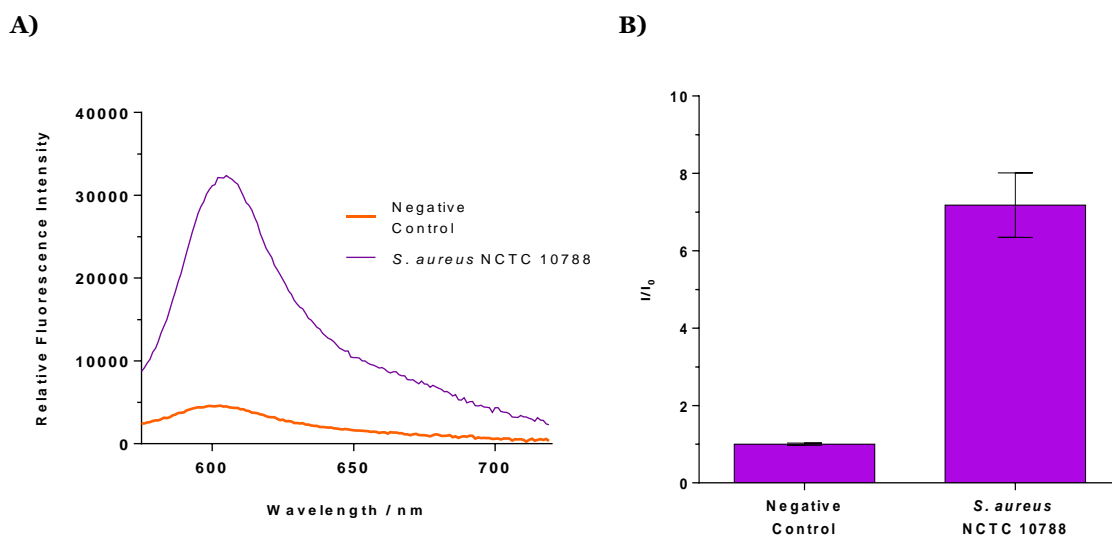
**Figure 7.29:** Images taken of negative controls (Membrane and Artificial Wound Fluid (AWF) only) and biofilms of *E. coli* NSM59 (EC) and *P. aeruginosa* PAO1 (PA) ( $10^{11}$  CFU/membrane) after 0, 1, and 24 h incubation with 10  $\mu$ M **TCF-ALP** in 50 mM Tris-HCl buffer, pH 9.2 at 32  $^{\circ}$ C

Figure 7.27 shows that after 1 h incubation with **TCF-ALP**, there was minimal turn-on response for both *E. coli* NSM59 and *P. aeruginosa* PAO1, with  $I/I_0$  values similar to the control. Additionally, there was no visible colour change, with the solutions of **TCF-ALP** remaining yellow (Figure 7.29). After 24 h (Figure 7.28), a  $\sim 10$ -fold and  $\sim 5$ -fold increase in fluorescence intensity was observed for *E. coli* NSM59 and *P. aeruginosa* PAO1, respectively. However, this was 3-fold lower than what was observed for *S. aureus* NCTC 10788 at the 24 h time-point, and it can be speculated that the fluorescence intensity of *S. aureus* NCTC 10788 would be higher if **TCF-ALP** was not saturated. This is supported by Figure 7.29, which shows a faint colour change from yellow to pink/purple for *E. coli* NSM59 and *P. aeruginosa* PAO1. Therefore, it can be concluded that while **TCF-ALP** is able to detect *E. coli* NSM59 and *P. aeruginosa* PAO1 biofilms, the fluorescence response is quicker, and more intense, for *S. aureus* NCTC 10788 – allowing the user to distinguish between the gram-positive *S. aureus* bacteria and the gram-negative bacteria with relative ease.

#### 7.4.7. *Ex vivo* Porcine Skin Assay

To test the viability of **TCF-ALP** in realistic situations, experiments were carried out using an *ex vivo* porcine skin model. A 10  $\mu$ L suspension of *S. aureus* NCTC 10788 ( $10^8$  CFU/mL) was inoculated onto porcine skin and allowed to dry at room temperature for 20 min. Next, 1 mL of 10  $\mu$ M of **TCF-ALP** was added to the skin via the use of a Franz cell, and subsequently incubated for 24 h at 32  $^{\circ}$ C.

The results in Figure 7.30 show that after 24 h incubation with **TCF-ALP**, *S. aureus*-inoculated pig skin had a marked increase in fluorescence intensity compared to the negative control. This was confirmed by Figure 7.31, where an observable colour change from yellow to purple was observed.



**Figure 7.30:** **A)** Fluorescence spectra of **TCF-ALP** (10  $\mu$ M) in 50 mM Tris-HCl buffer pH 9.2 after 24 h incubation with *S. aureus* NCTC 10788 inoculated porcine skin at 32  $^{\circ}$ C, and **B)** corresponding selectivity bar chart.  $\lambda_{ex}$  = 542 (bandwidth 15) nm.  $\lambda_{em}$  = 606 nm. Error bars indicate standard deviation (n = 3)

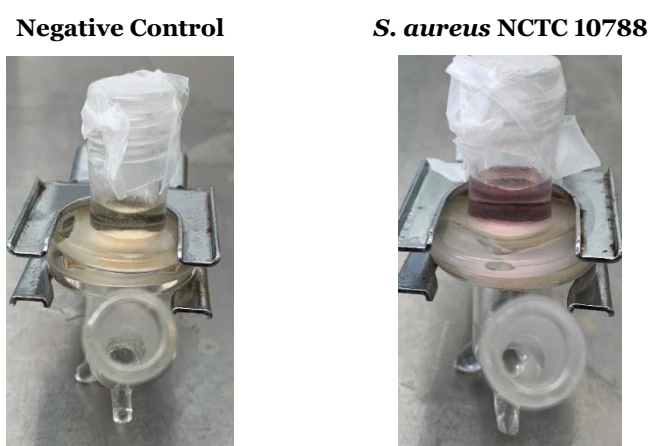


**Figure 7.31:** Images of negative control (no bacteria) and *S. aureus* NCTC 10788 on porcine skin after 24 h incubation at 32  $^{\circ}$ C with 10  $\mu$ M **TCF-ALP** in 50 mM Tris-HCl buffer pH 9.2

This study shows the potential of **TCF-ALP** as a diagnostic tool for the detection of *S. aureus* in an *ex vivo* setting. The lower fluorescence intensity observed in this model can be attributed to the fact that the concentration of bacteria inoculated onto the porcine skin

was lower than the preceding studies; the small inoculum volume (10 µL) of *S. aureus* NCTC 10788 used equates to a final concentration of 10<sup>6</sup> CFU/mL, compared to planktonic assays where 10<sup>8</sup> CFU/mL was used. Owing to the bacteria remaining on the porcine skin for the duration of the incubation with **TCF-ALP**, the bacterial isolates grew approximately 1 log during this time period, consistent with results obtained during the optimisation of this assay. Upon incubation with **TCF-ALP**, there was a slight reduction in cell count of *S. aureus* NCTC 10788, although this reduction was not statistically significant (t-test,  $p = 0.1728$ ), therefore it is possible to assume that **TCF-ALP** doesn't inhibit bacterial growth on porcine skin (see Appendix).

#### **7.4.8. TCF-ALP Based Hydrogels**

Hydrogels are three-dimensional macromolecular structures that are produced by chemical or physical crosslinking of natural or synthetic hydrophilic polymers. Hydrogels typically have a water content between 90 – 95% by mass,<sup>160</sup> have a range of physical forms,<sup>161</sup> and are biocompatible;<sup>162</sup> hence, are frequently used in a variety of clinical applications. Furthermore, it is possible to use hydrogels to encapsulate drugs for controlled-release system that can be controlled via the degree of crosslinking in the gel.<sup>161</sup>

Hydrogels have been utilised in wound care as they can protect the wound site from further damage and provide a moist environment, thereby preventing scar formation.<sup>160,163</sup> They are frequently used for the management of pressure ulcers,<sup>164</sup> diabetic foot ulcers<sup>165</sup> and burns.<sup>166</sup> Additionally, hydrogels can facilitate autolytic debridement by increasing the moisture content of necrotic tissue.<sup>167</sup> Hydrogels can also act as soothing and cooling agents for cutaneous wounds<sup>168,169</sup> and are thought to reduce the inflammatory process.<sup>169</sup> Other advantages of hydrogels include ease of removal, acceleration of the wound healing process, reduction of pain, and ease of development and handling.<sup>168</sup> However, hydrogels also have drawbacks which include being semi-permeable to gases and water vapour, acting as a poor barrier to bacterial infection, and in some instances having poor mechanical stability.<sup>168</sup>

Wichterle and Lim were the one of the first researchers to develop hydrogels using 2-hydroxyethyl methacrylate (HEMA), which has since been used in a variety of biomedical applications.<sup>170</sup> HEMA was further developed by Winter, who produced the first-generation of polymeric dressings.<sup>171</sup> Since then, a variety of hydrogels have been created for wound care, leading to several commercial hydrogels, including: TachoSil® and Apligraf®.<sup>167</sup>

In this study PVA was used to create a hydrogel matrix. PVA is a synthetic-water soluble, biocompatible polymer.<sup>172</sup> PVA is versatile, hence it has been used extensively in the

creation of wound dressings,<sup>168</sup> wound management,<sup>168</sup> drug delivery systems,<sup>173</sup> biosensors,<sup>174</sup> artificial organs,<sup>175</sup> and contact lenses.<sup>176</sup> PVA can be chemically crosslinked, with agents such as maleic acid, formaldehyde or glutaraldehyde,<sup>172</sup> or undergo physical crosslinking via freeze-thaw cycles. This study used the latter method to create biocompatible polymers which can be used in wound care. In the freeze-thawing process ice crystals are formed within the hydrogel; these ice crystals result in the polymer chains being packed together, forming polymer crystallites where hydrogen bonds are formed between the chains. These crystallites act as physical crosslinks, holding the amorphous chains together.<sup>177</sup>

Hydrogels have been shown to help with the disadvantages associated with colorimetric and fluorescent-based probes (i.e., non-specific interactions, auto-fluorescence, and low stability in reaction environments), which reduce the sensitivity, and therefore accuracy, of the probes.<sup>178</sup> Hydrogels also help minimize auto-fluorescence and provide an aqueous environment that is biologically-compatible, while preventing non-specific protein adsorption.<sup>178</sup> Additionally, hydrogels are porous, which allows enzymes and/or bacteria to penetrate the hydrogel to react with the probe. Hydrogel-based fluorescent detection systems have been shown to enhance sensitivity and reduce detection time.<sup>178</sup>

Gunda *et al* developed a hydrogel system which contained a colorimetric probe, growth medium, and a lysing agent to detect *E. coli* in contaminated water samples.<sup>137</sup> The system was capable of detecting 400 CFU/mL of *E. coli*, via a visual colour change, after 1 h. Also, Bhattacharya *et al*, developed a carbon-dot hydrogel hybrid for the detection of bacteria.<sup>179</sup> Secreted bacterial esterases and lipases fluidised the hydrogel, resulting in aggregation and fluorescence quenching of the carbon dots; this system was capable of detecting multiple bacterial species, including *Bacillus cereus*, *Bacillus subtilis*, *P. aeruginosa* and *S. aureus*. When *Bacillus cereus* was used as the model system, a LOD of 10<sup>5</sup> was observed.

As shown in previous sections of this chapter, **TCF-ALP** has proven to be capable of detecting *S. aureus* isolates. Therefore, the attention of this study turned towards creating a wound dressing capable of detecting *S. aureus* via the incorporation of **TCF-ALP** into a PVA-based hydrogel.

Bacterial colonisation is heterogenous within a wound; *S. aureus* is as an early-coloniser predominately located near the surface of the wound, and gram-negative bacteria (e.g., *P. aeruginosa*) are late-stage colonisers, located within the deep regions of the wound.<sup>180</sup> Owing to this, it was hypothesised that a diagnostic wound dressing would be able to

preferentially detect *S. aureus* and other gram-positive bacteria over gram-negative pathogenic bacteria present in a wound.

A diagnostic wound dressing is advantageous over current swab and biopsy methods as the current methods are not able to determine the aetiology of the wound infection; they do not give a representative indication of the pathogenic bacteria present within a wound owing to the small wound surface area sampled.<sup>142</sup> The PVA-based **TCF-ALP** diagnostic wound dressing would be in contact with the whole surface of the wound, and therefore would be capable of detecting localised *S. aureus* infection across the wound.

PVA was dissolved in PBS buffer (pH 7.4), and after incubation with *S. aureus* NCTC 10788 there was a colour change from yellow to green due to the protonation of the TCF moiety (Figure 7.32). This was a disadvantage as the colour change was less noticeable, and **TCF-ALP** in neutral and acidic environments displays reduced fluorescence intensity. Therefore, 10 % PVA was dissolved in Tris HCl (pH 9.2) keeping the hydrogel environment alkaline in nature, allowing for deprotonation of the TCF moiety of the probe.



**Figure 7.32:** 10% w/v PVA hydrogel loaded with 100  $\mu\text{M}$  of **TCF-ALP** in PBS, pH = 7.4 after 24 h incubation at 32  $^{\circ}\text{C}$  with porcine skin inoculated with and without *S. aureus* NCTC 10788.

For this research, 100  $\mu\text{M}$  **TCF-ALP** was used to ensure probe stability for the duration of the freeze-thaw cycle of hydrogel preparation and to provide an enhanced colour change from yellow to purple to identify the presence of a *S. aureus* infection. As this system is designed to be an easy PoC test for diagnosing an infection, without the use of specialised equipment, it is vital that the colour change of the hydrogel is noticeable to signal to the healthcare provider that the wound has an established infection and requires medical intervention. In brief, a stock solution of **TCF-ALP** in DMSO was prepared (2.6 mM), and 38.5  $\mu\text{L}$  transferred to 1 mL of 10% w/v PVA and mixed to produce a homogenous yellow PVA solution. While the hydrogel contained DMSO, it had a minimal effect on bacterial viability (see Appendix 7.6.6).

#### 7.4.8.1. Detecting Planktonic *Staphylococcus aureus*

Planktonic suspension assays were undertaken to assess the viability of the **TCF-ALP** hydrogel as a PoC for wound infections. *S. aureus* NCTC 10788 was grown in Mueller Hinton broth overnight, centrifuged and resuspended in 50 mM Tris HCl (pH 9.2) to attain a final concentration of  $10^8$  CFU/mL. Thawed **TCF-ALP** hydrogels were placed in 1 mL aliquots of bacterial suspensions before being incubated at 32 °C for 24 h. Figure 7.33 shows the colour of the **TCF-ALP** hydrogels at regular time points during the 24 h incubation with *S. aureus* NCTC 10788. The results show that upon incubation with bacteria, **TCF-ALP** undergoes a colour change from yellow to purple – visible to the naked eye at approximately 5 – 6 h; after 24 h the colour of the hydrogel is a deep purple.

It is also worth noting that some leaching of **TCF-ALP** occurred and was evident by the bacterial suspension also turning purple in colour. This could be attributed to only one freeze-thaw cycle being performed to crosslink the 10% w/v PVA solution, which would result in a more porous hydrogel than if it was subjected to multiple cycles. While 10% w/v PVA was chosen as it has previously been shown to have good structural integrity,<sup>181</sup> further experiments could be undertaken to determine the appropriate number of freeze-thaw cycles required to prevent leaching while retaining a high degree of porosity for the bacteria to penetrate the hydrogel and cleave the **TCF-ALP** probe. For the purposes of this proof-of-concept study, one freeze-thaw cycle was deemed to be sufficient as leeching was minimal and **TCF-ALP** was retained within the hydrogel, allowing visualisation of the colour change within the hydrogel.

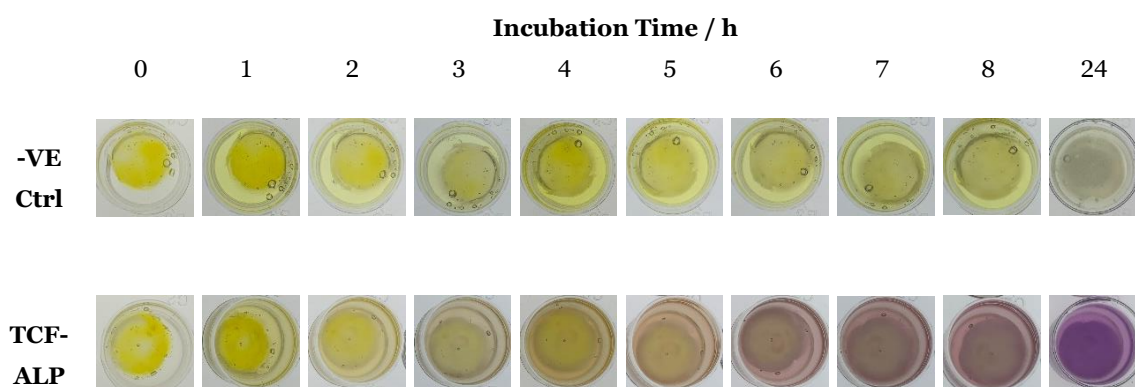


**Figure 7.33:** Images of 10% w/v PVA hydrogels loaded with 100  $\mu$ M **TCF-ALP** in 50 mM Tris-HCl buffer pH 9.2 at 0 – 8 h and 24 h incubation at 32 °C with *S. aureus* NCTC 10788 planktonic culture (c.  $10^8$  CFU/mL).

After 24 h incubation, the **TCF-ALP** hydrogels were removed from the planktonic suspension, rinsed with 50 mM Tris HCl (pH 9.2), and assessed for fluorescence intensity. As evident in Figure 7.34, upon incubation with *S. aureus* NCTC 10788, **TCF-ALP** displayed over a 30-fold increase in fluorescence intensity compared to the negative control.



This correlates to the colour change observed in Figure 7.33 and results obtained using the solution-based **TCF-ALP** outlined previously.

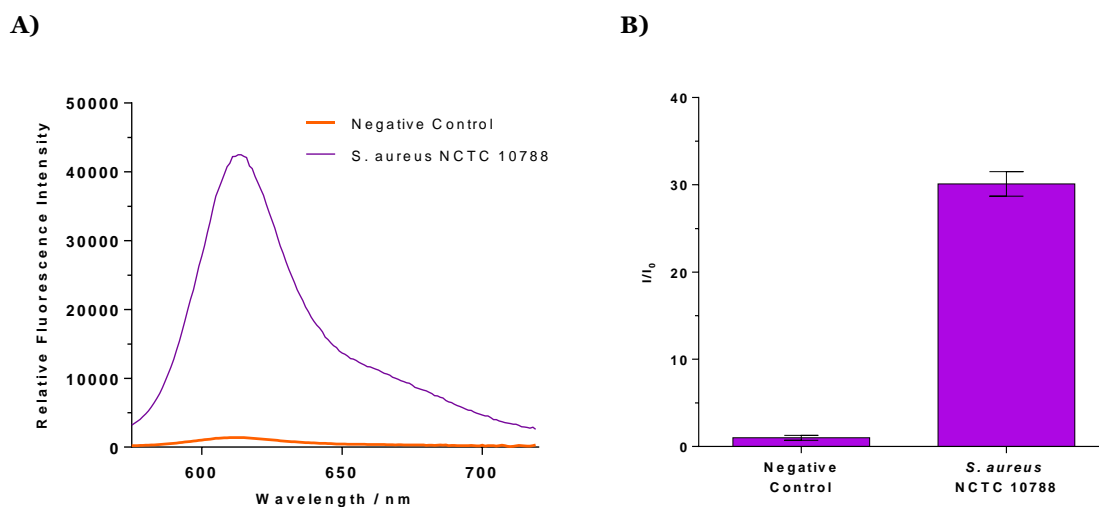


**Figure 7.34:** **A)** Fluorescence spectra of **TCF-ALP** (100 μM) in a 10% w/v PVA hydrogel after 24 h incubation at 32 °C with planktonic cultures of *S. aureus* NCTC 10788, and **B)** corresponding selectivity bar chart.  $\lambda_{\text{ex}} = 542$  (bandwidth 15) nm.  $\lambda_{\text{em}} = 606$  nm. Error bars indicate standard deviation (n = 3).

#### 7.4.8.2. Colony Biofilm Wound Model

Owing to the success of the planktonic suspension assays, next the utility of the **TCF-ALP** hydrogel to detect *S. aureus* biofilms was assessed. Bacterial biofilms were grown on 19 mm polycarbonate membranes supplemented with AWF. After 24 h incubation at 32 °C for 24 h the biofilms were transferred from Mueller Hinton agar to bacteriological agar within a 12-well microtiter plate. Bacteriological agar was used to prevent the bacterial biofilms from drying out.

**TCF-ALP** hydrogels were placed onto the biofilms and incubated at 32 °C for 24 h. At periodic intervals the biofilms were photographed to assess colour change (Figure 7.35). Colour change was evident within the hydrogel after 1 h incubation with *S. aureus* NCTC 10788 biofilms, probably due to the high cell concentration ( $10^{10}$  CFU/membrane).

Throughout the incubation period the negative control remained yellow in colour, while the **TCF-ALP** hydrogels incubated with *S. aureus* NCTC 10788 progressively turned purple, originating from the centre of the hydrogel. However, as this experiment was repeated in triplicate, while all hydrogels displayed a colour change at 1 h, the colour didn't always originate from the centre of the hydrogel. In fact, it seemed to be the section of the hydrogel which was in the closest contact with the bacteria. At 24 h the whole hydrogel was deep

purple in colour. Unfortunately, leaching occurred and the bacteriological agar underneath the biofilms turned purple in colour.

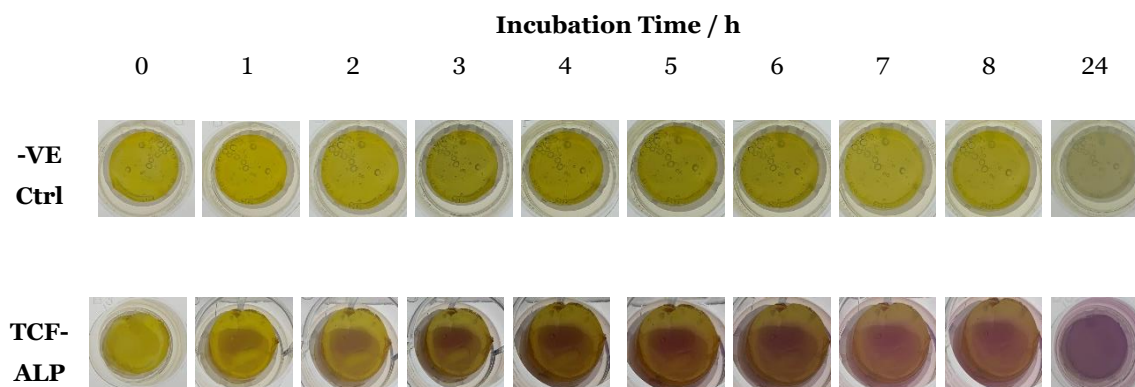


**Figure 7.35:** Images taken of 10% w/v PVA hydrogels loaded with 100  $\mu$ M **TCF-ALP** in 50 mM Tris-HCl buffer pH 9.2 at 0 – 8 h and 24 h incubation at 32 °C with *S. aureus* NCTC 10788 biofilms.

After 24 h incubation, hydrogels were removed from the biofilms and rinsed with 50 mM Tris HCl (pH 9.2) before being assessed for fluorescence. As expected, there was a noticeable increase in fluorescence for the **TCF-ALP** gels incubated with *S. aureus* NCTC 10788 compared to the negative control (Figure 7.36), suggesting that ALP activity within *S. aureus* biofilms could still be measured with **TCF-ALP** entrapped within a hydrogel matrix. This result is promising, as a simple and clear PoC prototype diagnostic hydrogel wound dressing was created, which clearly displays *S. aureus* infection via a visible colour change that is easy to detect by either the patient or healthcare provider without any specialised equipment. If necessary, the wound dressing could be removed with ease, and with minimal discomfort to the patient,<sup>168</sup> and fluorescence of the gel measured to semi-quantitatively determine the *S. aureus* bacterial bioburden within an infected wound.

Concurrently, bacterial biofilms were stripped and the viability of *S. aureus* NCTC 10788 was determined by using a standardised enumeration assay. The presence of a 10% w/v PVA hydrogel did not affect bacterial viability, nor did a 10% PVA hydrogel containing 100  $\mu$ M **TCF-ALP** (Appendix). Thus, it is possible to conclude that the **TCF-ALP** hydrogel would not cause bacterial cell death if used as a wound dressing and hence provide a semi-quantitative determination of bacterial density within the wound. Future studies would have to be conducted to test the viability on mammalian cells.

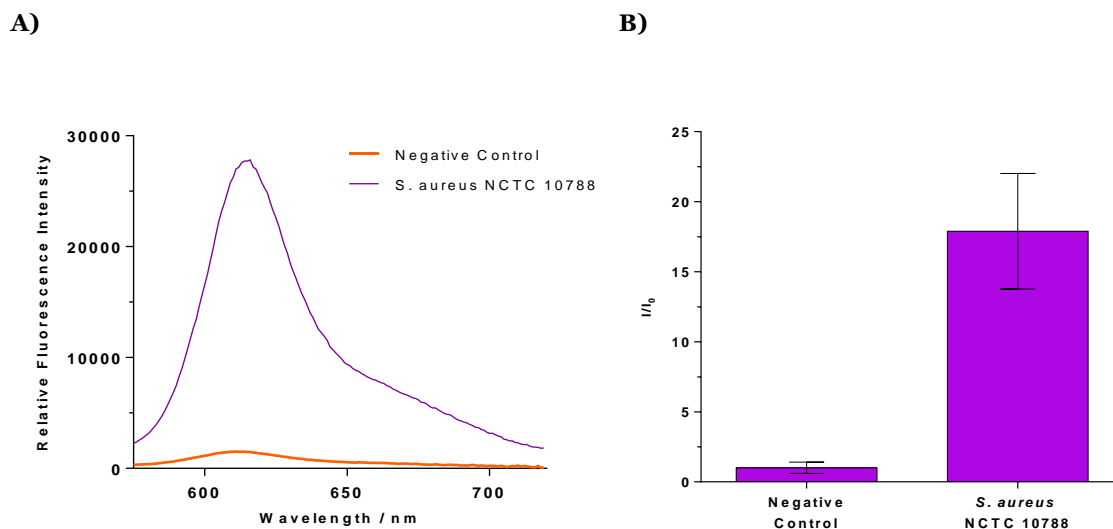
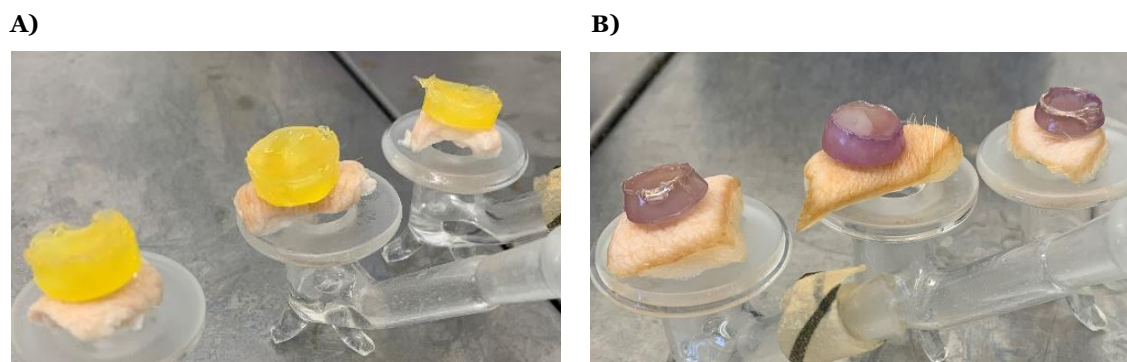


**Figure 7.36:** **A)** Fluorescence spectra of **TCF-ALP** (100  $\mu\text{M}$ ) in a 10% w/v PVA hydrogel after 24 h incubation at 32  $^{\circ}\text{C}$  with *S. aureus* NCTC 10788 biofilms, and **B)** corresponding selectivity bar chart.  $\lambda_{\text{ex}} = 542$  (bandwidth 15) nm.  $\lambda_{\text{em}} = 606$  nm. Error bars indicate standard deviation ( $n = 3$ ).

### 7.4.8.3. *Ex vivo* Porcine Skin Assay

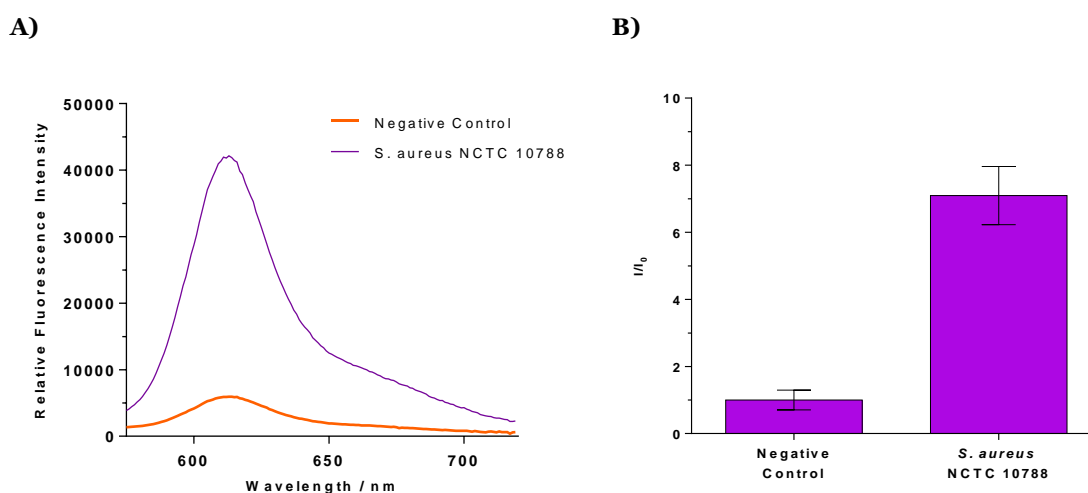
Finally, the ability of **TCF-ALP** hydrogels to determine ALP activity of *S. aureus* NCTC 10788 on porcine skin was investigated. A 10  $\mu\text{L}$  suspension of *S. aureus* NCTC 10788 ( $10^8$  CFU/mL) was inoculated onto porcine skin and allowed to dry at room temperature for 20 min. Once dry, **TCF-ALP** hydrogels were added to the surface of the skin and subsequently incubated for 24 h at 32  $^{\circ}\text{C}$ . The bottom half of a Franz cell was used, as it contained 1 mL sterile  $\text{dH}_2\text{O}$  to provide moisture, preventing the porcine skin from drying out.

Figure 7.37 shows that upon incubation with *S. aureus* NCTC 10788 **TCF-ALP** hydrogels underwent a colorimetric change from yellow to purple, indicative of ALP activity on the surface of the skin which was not detected on the negative control. Even though a smaller initial inoculum was used the colour change was clear, with a distinct deep purple colour observed after 24 h incubation. While the hydrogels did not lose their structural integrity, they did appear to dehydrate during the course of this experiment due to being exposed to the external environment.



**Figure 7.37:** Images taken of 10% w/v PVA hydrogels loaded with 100  $\mu\text{M}$  **TCF-ALP** in 50 mM Tris-HCl buffer pH 9.2 after 24 h incubation at 32  $^{\circ}\text{C}$  **A)** without and **B)** with *S. aureus* NCTC 10788 incubated on porcine skin.

After 24 h incubation, as described previously, hydrogels were washed with 50 mM Tris HCl (pH 9.2) and the fluorescence measured. As already observed, incubation with *S. aureus* NCTC 10788 resulted in an approximately 7.5-fold increase in fluorescence intensity of **TCF-ALP** compared to the negative control (Figure 7.38). Bacterial concentration on the porcine skin was also investigated, and there was no significant difference between the control (porcine skin without hydrogel) and porcine skin incubated with 10% w/v PVA with and without 100 $\mu\text{M}$  **TCF-ALP**, further demonstrating its utility as a diagnostic wound dressing.



**Figure 7.38:** **A)** Fluorescence spectra of **TCF-ALP** (100  $\mu\text{M}$ ) in a 10% w/v PVA hydrogel after 24 h incubation at 32  $^{\circ}\text{C}$  with *S. aureus* NCTC 10788 inoculated onto porcine skin, and **B)** corresponding selectivity bar chart.  $\lambda_{\text{ex}} = 542$  (bandwidth 15) nm.  $\lambda_{\text{em}} = 606$  nm. Error bars indicate standard deviation ( $n = 3$ ).

## 7.5. Conclusions and Future Work

To conclude, this chapter demonstrates that **TCF-ALP** could be utilised to detect *S. aureus* infections. This is of great clinical importance as new diagnostic methods are needed for the timely detection of infections within wounds. This chapter has shown that **TCF-ALP** is capable of being optimised to detect bacterial pathogens at clinically significant temperatures (37 °C for “classic” microbiology, 32 °C for wound infections, and 25 °C for a point-of-care device) without the need for extensive preparation.

Solutions of **TCF-ALP** were capable of detecting planktonic *S. aureus* NCTC 10788, with an excellent colorimetric and fluorescence response, corresponding to a limit of detection of  $3.7 \times 10^6$  CFU/mL after 24 h incubation. **TCF-ALP** was selective towards gram-positive bacteria, albeit in a limited sample size, compared to gram-negative *E. coli* and *P. aeruginosa*. **TCF-ALP** was also capable of rapidly detecting *S. aureus* NCTC 10788 biofilms (both 96-well plate and colony biofilm models), with a clear fluorescence “turn-on response” and colour change from yellow to purple within 1 h of incubation time. With these promising results in hand, *ex vivo* models were conducted showing the utility of **TCF-ALP** in detecting *S. aureus* NCTC 10788 in clinically-significant situations, therefore demonstrating the capability of **TCF-ALP** in diagnosing *S. aureus* wound infections. Expanding on this, **TCF-ALP** was encapsulated in PVA-based hydrogels as a proof of concept for “smart” wound dressing applications. The same experiments mentioned above were conducted for **TCF-ALP**-based hydrogels and similar results were found. **TCF-ALP**-based hydrogels were capable of detecting planktonic *S. aureus* NCTC 10788 after ~4 h and colony biofilm models of *S. aureus* NCTC 10788 after 1 h of incubation. *Ex vivo* models displayed a similar result, with a clear colour change of the hydrogel from yellow to purple observed after 24 h.

Future work would need to be conducted to further examine the selectivity of **TCF-ALP**, with future experiments focusing on different clinically significant bacteria such as *Bacillus*, *Klebsiella*, and other Enterobacteria spp. Additionally, focus should be shifted to determine the genetic mechanism behind ALP-production, and why **TCF-ALP** was able to detect gram-positive bacteria over gram-negative bacteria. Finally, **TCF-ALP**-based hydrogels would need to be optimised further to prevent leaching of **TCF-ALP** into the extracellular environment; studies would also have to be conducted to demonstrate the hydrogel has no effect on mammalian cells – as shown with solutions of **TCF-ALP** shown in the chapter prior.

## 7.6. Appendix

### 7.6.1. Cell Count for Selectivity Assay

Cell counts were performed for bacterial strains that were unable to elicit a fluorescence response upon incubation with **TCF-ALP**. Figure S1 shows that the bacterial concentration of all *E. coli* strains (NCTC 10418, NSM59, and DH5 $\alpha$ ) were unaffected after 24 h incubation with **TCF-ALP**. All *P. aeruginosa* strains (PAO1, P260, P885) had a statistically significant reduction in bacterial concentration; however, this correlated to a 1-log reduction, which should have a minimal effect on the efficacy of **TCF-ALP**. Therefore, bacterial concentration is not the primary explanation for *E. coli* and *P. aeruginosa* failing to produce a “turn-on” response of **TCF-ALP**.

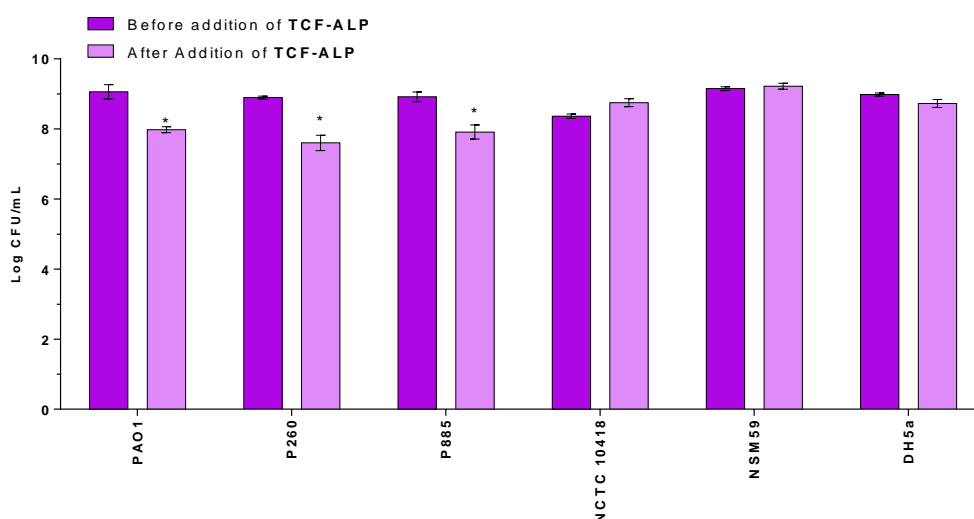


**Figure S1:** Log CFU/mL of *P. aeruginosa* (PAO1, P260, and P885) and *E. coli* (NCTC 10418, NSM59, and DH5 $\alpha$ ) before and after 24 h incubation with 10  $\mu$ M **TCF-ALP** in 50 mM Tris-HCl, pH 9.2 at 32°C. Error bars show standard deviation (n = 3). Statistical significance was assessed by performing a t-test. *p* values are indicated \*, *p* < 0.05.

## 7.6.2. Glucose Supplementation for 96-well Biofilm Models

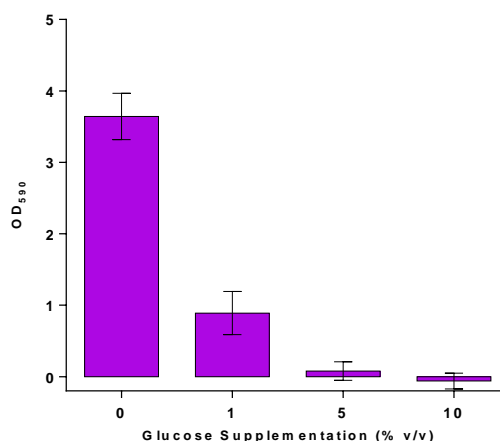
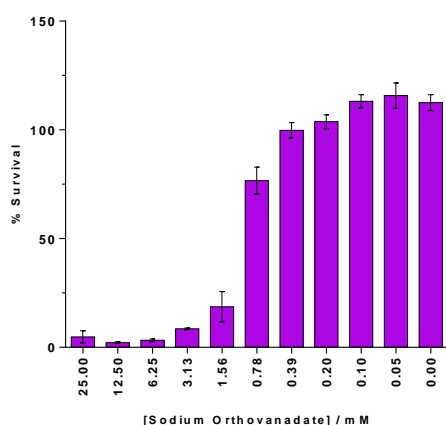


**Figure S2:** Evaluation of glucose supplementation on the formation of *Staphylococcus aureus* NCTC 10788 biofilms. Biofilm biomass was quantified using crystal violet biofilm staining by measuring the absorbance at 590 nm. Error bars show standard deviation (n = 3).

## 7.6.3. Sodium Orthovanadate MIC and MBIC

A)



B)

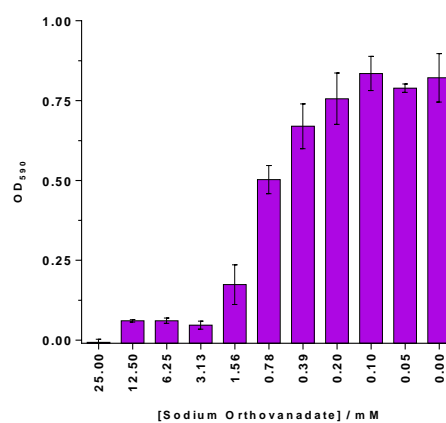


**Figure S3: A)** Minimum Inhibitory Concentration (MIC) of sodium orthovanadate for *Staphylococcus aureus* NCTC 10788. MIC was found to be 6.25 - 3.13 mM. **B)** Minimum Biofilm Inhibitory Concentration (MBIC) of sodium orthovanadate for *Staphylococcus aureus* NCTC 10788. Biofilm biomass was quantified using crystal violet staining by measuring the absorbance at 590 nm MBIC was found to be 3.13 – 1.56 mM. Error bars show standard deviation (n = 3).

## 7.6.4. Cell Count for Colony Biofilm Models

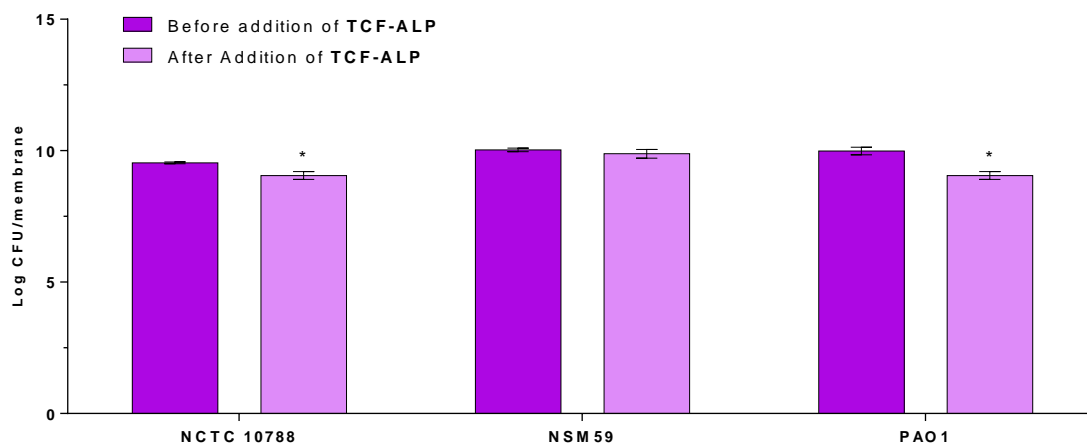


**Figure S4:** Log CFU/membrane of *S. aureus* NCTC 10788, *E. coli* NSM59, and *P. aeruginosa* PAO1 biofilms after 24 h incubation at 32°C with solutions of **TCF-ALP** (10 µM) in Tris-HCl, pH 9.2. Error bars show standard deviation (n = 3). Statistical significance was assessed by performing a t-test. *p* values are indicated \*, *p* < 0.05

## 7.6.5. Porcine Skin

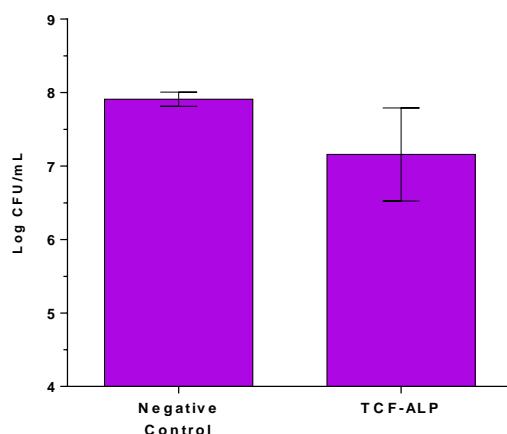


**Figure S5:** Log CFU/mL of *S. aureus* NCTC 10788 incubated on porcine skin for 24 h at 32°C with a solution of **TCF-ALP** in 50 mM Tris-HCl, pH 9.2 (10 µM; 1 mL). The negative control was undertaken using a solution of 50 mM Tris-HCl, pH 9.2 (1 mL). Error bars show standard deviation (n = 3).



## 7.6.6. Hydrogel Detection

### 7.6.6.1. Colony Biofilm Assays

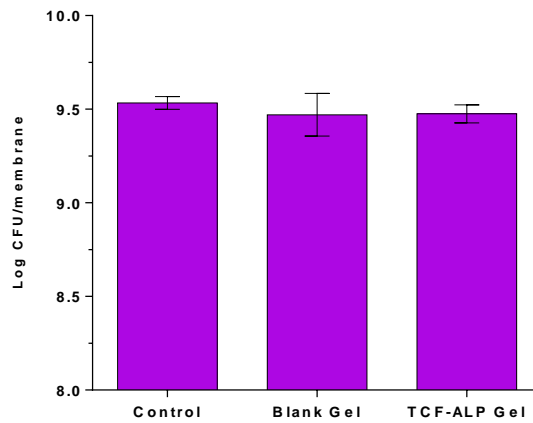


**Figure S6:** Log CFU/membrane of *S. aureus* NCTC 10788 colony biofilm model biofilms after 24 h incubation at 32°C with 10% w/v PVA hydrogels loaded with **TCF-ALP** (100 µM). Error bars show standard deviation (n = 3).

### 7.6.6.2. Porcine Skin

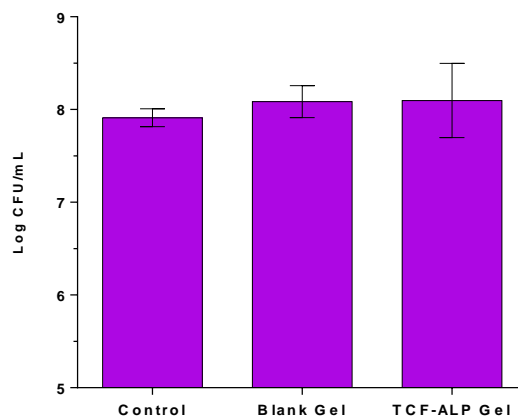


**Figure S7:** Log CFU/mL of *S. aureus* NCTC 10788 on porcine skin after 24 h incubation at 32°C with 10% w/v PVA hydrogels loaded with **TCF-ALP** (100 µM). Error bars show standard deviation (n = 3).

## 7.7. References

1. Habimana J de D, Ji J, Sun X. Minireview: trends in optical-based biosensors for point-of-care bacterial pathogen detection for food safety and clinical diagnostics. *Anal Lett.* 2018;51(18):2933–66.
2. Váradi L, Luo JL, Hibbs DE, Perry JD, Anderson RJ, Orenge S, et al. Methods for the detection and identification of pathogenic bacteria: past, present, and future. *Chem Soc Rev.* 2017;46(16):4818–32.
3. Zhang P, Liu H, Ma S, Men S, Li Q, Yang X, et al. A label-free ultrasensitive fluorescence detection of viable *Salmonella enteritidis* using enzyme-induced cascade two-stage toehold strand-displacement-driven assembly of G-quadruplex DNA. *Biosens Bioelectron.* 2016;80:538–42.
4. Liu X, Hu Y, Zheng S, Liu Y, He Z, Luo F. Surface plasmon resonance immunosensor for fast, highly sensitive, and in situ detection of the magnetic nanoparticles-enriched *Salmonella enteritidis*. *Sensors Actuators B Chem.* 2016;230:191–8.
5. Vaisocherová-Lísalová H, Víšová I, Ermini ML, Špringer T, Song XC, Mrázek J, et al. Low-fouling surface plasmon resonance biosensor for multi-step detection of foodborne bacterial pathogens in complex food samples. *Biosens Bioelectron.* 2016;80:84–90.
6. Deisingh AK, Thompson M. Biosensors for the detection of bacteria. *Can J Microbiol.* 2004;50(2):69–77.
7. Ahmed A, Rushworth J V, Hirst NA, Millner PA. Biosensors for whole-cell bacterial detection. *Clin Microbiol Rev.* 2014;27(3):631–46.
8. Shi X, Kadiyala U, VanEpps JS, Yau S-T. Culture-free bacterial detection and identification from blood with rapid, phenotypic, antibiotic susceptibility testing. *Sci Rep.* 2018;8(1):1–11.
9. Xu Q, Liang K, Liu R-Y, Deng L, Zhang M, Shen L, et al. Highly sensitive fluorescent detection of p53 protein based on DNA functionalized Fe<sub>3</sub>O<sub>4</sub> nanoparticles. *Talanta.* 2018;187:142–7.
10. Ganea GM, Kolic PE, El-Zahab B, Warner IM. Ratiometric coumarin– neutral red (CONER) nanoprobe for detection of hydroxyl radicals. *Anal Chem.*

2011;83(7):2576–81.

11. Dyer DL. Microbiological detection and identification system. Google Patents; 1970.
12. Bascomb S. 3 Enzyme Tests in Bacterial Identification. In: *Methods in microbiology*. Elsevier; 1988. p. 105–60.
13. Manafi M, Kneifel W, Bascomb S. Fluorogenic and chromogenic substrates used in bacterial diagnostics. *Microbiol Rev*. 1991;55(3):335–48.
14. Hartman PA. The MUG (glucuronidase) test for *Escherichia coli* in food and water. *Rapid Methods Autom Microbiol Immunol A Balows, RC Tilton, A Turano (eds) Brixia Acad Press Brescia, Italy*. 1989;290–308.
15. Frampton EW, Restaino L. Methods for *Escherichia coli* identification in food, water and clinical samples based on beta-glucuronidase detection. *J Appl Bacteriol*. 1993;74(3):223–33.
16. Fiksdal L, Tryland I. Application of rapid enzyme assay techniques for monitoring of microbial water quality. *Curr Opin Biotechnol*. 2008;19(3):289–94.
17. Servais P, Prats J, Passerat J, Garcia-Armisen T. Abundance of culturable versus viable *Escherichia coli* in freshwater. *Can J Microbiol*. 2009;55(7):905–9.
18. George I, Petit M, Servais P. Use of enzymatic methods for rapid enumeration of coliforms in freshwaters. *J Appl Microbiol*. 2000;88(3):404–13.
19. Wildeboer D, Amirat L, Price RG, Abuknesha RA. Rapid detection of *Escherichia coli* in water using a hand-held fluorescence detector. *Water Res*. 2010;44(8):2621–8.
20. Hesari N, Alum A, Elzein M, Abbaszadegan M. A biosensor platform for rapid detection of *E. coli* in drinking water. *Enzyme Microb Technol*. 2016;83:22–8.
21. Perry JD, James AL, Morris KA, Oliver M, Chilvers KF, Reed RH, et al. Evaluation of novel fluorogenic substrates for the detection of glycosidases in *Escherichia coli* and enterococci. *J Appl Microbiol*. 2006;101(5):977–85.
22. Magro G, Bain RES, Woodall CA, Matthews RL, Gundry SW, Davis AP. Synthesis and application of resorufin  $\beta$ -d-glucuronide, a low-cost chromogenic substrate for detecting *Escherichia coli* in drinking water. *Environ Sci Technol*. 2014;48(16):9624–31.

23. Kim HJ, Kwon C, Lee BS, Noh H. One-step sensing of foodborne pathogenic bacteria using a 3D paper-based device. *Analyst*. 2019;144(7):2248–55.
24. Tryland I, Braathen H, Wennberg AC, Eregno F, Beschorner A-L. Monitoring of  $\beta$ -D-Galactosidase activity as a surrogate parameter for rapid detection of sewage contamination in urban recreational water. *Water*. 2016;8(2):65.
25. Chilvers KF, Perry JD, James AL, Reed RH. Synthesis and evaluation of novel fluorogenic substrates for the detection of bacterial  $\beta$ -galactosidase. *J Appl Microbiol*. 2001;91(6):1118–30.
26. Cellier M, Fazackerley E, James AL, Orenca S, Perry JD, Turnbull G, et al. Synthesis of 2-arylbenzothiazole derivatives and their application in bacterial detection. *Bioorg Med Chem*. 2014;22(4):1250–61.
27. James AL, Perry JD, Chilvers K, Robson IS, Armstrong L, Orr KE. Alizarin- $\beta$ -d-galactoside: a new substrate for the detection of bacterial  $\beta$ -galactosidase. *Lett Appl Microbiol*. 2000;30(4):336–40.
28. Sambrook J, Russell DW. *Molecular Cloning: A Laboratory Manual*, vol 3, Cold Spring Harbour Laboratory Press. New York. 2001;
29. Eustice DC, Feldman PA, Colberg-Poley AM, Buckery RM, Neubauer RH. A sensitive method for the detection of beta-galactosidase in transfected mammalian cells. *Biotechniques*. 1991;11(6):739–40.
30. Sicard C, Shek N, White D, Bowers RJ, Brown RS, Brennan JD. A rapid and sensitive fluorimetric  $\beta$ -galactosidase assay for coliform detection using chlorophenol red- $\beta$ -d-galactopyranoside. *Anal Bioanal Chem*. 2014;406(22):5395–403.
31. Jokerst JC, Adkins JA, Bisha B, Mentele MM, Goodridge LD, Henry CS. Development of a paper-based analytical device for colorimetric detection of select foodborne pathogens. *Anal Chem*. 2012;84(6):2900–7.
32. Jahanshahi-Anbuhi S, Kannan B, Pennings K, Ali MM, Leung V, Giang K, et al. Automating multi-step paper-based assays using integrated layering of reagents. *Lab Chip*. 2017;17(5):943–50.
33. Ekin IH, Gurturk K, Ilhan Z, Arabaci C, Gulaydin O. Detection of enzyme activities and their relation to serotypes of bovine and human group B streptococci. *J Med Microbiol*. 2015;64(9):985–9.

34. White DG, Harmon RJ, Langlois BE. Fluorogenic assay for differentiating *Staphylococcus warneri* and *Staphylococcus hominis* strains of bovine origin. *J Clin Microbiol.* 1990;28(3):602.
35. Manafi M. New developments in chromogenic and fluorogenic culture media. *Int J Food Microbiol.* 2000;60(2–3):205–18.
36. Strahsburger E, de Lacey AML, Marotti I, DiGioia D, Biavati B, Dinelli G. In vivo assay to identify bacteria with  $\beta$ -glucosidase activity. *Electron J Biotechnol.* 2017;30:83–7.
37. Tait E, Stanforth SP, Reed S, Perry JD, Dean JR. Analysis of pathogenic bacteria using exogenous volatile organic compound metabolites and optical sensor detection. *RSC Adv.* 2015;5(20):15494–9.
38. Ravindar DJ, Elangovan N. Molecular identification of amylase producing *Bacillus subtilis* and detection of optimal conditions. *J Pharm Res.* 2013;6(4):426–30.
39. Salihu Y, Saidu AY, Rabiou GA, Umar AA, Zeynep A, Unzile G. Detection of Alpha-Amylase Activity from Soil Bacteria.
40. Xia Y, Kong Y, Nielsen PH. In situ detection of starch-hydrolyzing microorganisms in activated sludge. *FEMS Microbiol Ecol.* 2008;66(2):462–71.
41. Sadler DF, Ezzell JW, Keller KF, Doyle RJ. Glycosidase activities of *Bacillus anthracis*. *J Clin Microbiol.* 1984;19(5):594–8.
42. Oh S-W, Kang D-H. Fluorogenic selective and differential medium for isolation of *Enterobacter sakazakii*. *Appl Environ Microbiol.* 2004;70(9):5692–4.
43. Giovannini G, Gubala V, Hall AJ. ‘Off–on’ switchable fluorescent probe for prompt and cost-efficient detection of bacteria. *New J Chem.* 2019;43(33):13094–102.
44. Sun L, Jiang Y, Pan R, Li M, Wang R, Chen S, et al. A novel, simple and low-cost paper-based analytical device for colorimetric detection of *Cronobacter* spp. *Anal Chim Acta.* 2018;1036:80–8.
45. Tallman KR, Beatty KE. Far-red fluorogenic probes for esterase and lipase detection. *ChemBioChem.* 2015;16(1):70–5.
46. Huang B, Siqueira WL, Cvitkovitch DG, Finer Y. Esterase from a cariogenic

- bacterium hydrolyzes dental resins. *Acta Biomater.* 2018;71:330–8.
47. Aguirre PM, Cacho JB, Folgueira L, Lopez M, García J, Velasco AC. Rapid fluorescence method for screening *Salmonella* spp. from enteric differential agars. *J Clin Microbiol.* 1990;28(1):148–9.
  48. Olsson M, Syk A, Wollin R. Identification of *Salmonellae* with the 4-methylumbelliferyl caprylate fluorescence test. *J Clin Microbiol.* 1991;29(11):2631–2.
  49. Humbert F, Salvat G, Colin P, Lahellec C, Bennejean G. Rapid identification of *Salmonella* from poultry meat products by using ‘Mucap test’. *Int J Food Microbiol.* 1989;8(1):79–83.
  50. Sanz Y, Toldrá F, Vila R. Simple, sensitive assay for microbial aminopeptidase. *J Food Sci.* 1997;62(3):583–5.
  51. Peterson EH, Hsu EJ. Rapid detection of selected gram-negative bacteria by aminopeptidase profiles. *J Food Sci.* 1978;43(6):1853–6.
  52. James AL, Perry JD, Rigby A, Stanforth SP. Synthesis and evaluation of novel chromogenic aminopeptidase substrates for microorganism detection and identification. *Bioorg Med Chem Lett.* 2007;17(5):1418–21.
  53. Inoue K, Miki K, Tamura K, Sakazaki R. Evaluation of L-pyrrolidonyl peptidase paper strip test for differentiation of members of the family Enterobacteriaceae, particularly *Salmonella* spp. *J Clin Microbiol.* 1996;34(7):1811–2.
  54. Gordon DB, Degirolami PC, Bolivar S, Karafotias G, Eichelberger K. A comparison of the identification of group A streptococci and enterococci by two rapid pyrrolidonyl aminopeptidase methods. *Am J Clin Pathol.* 1988;90(2):210–2.
  55. Wellstood SA. Rapid, cost-effective identification of group A streptococci and enterococci by pyrrolidonyl-beta-naphthylamide hydrolysis. *J Clin Microbiol.* 1987;25(9):1805–6.
  56. Sperry JF, Cohenford MA, Campognone P, Lawton W, Chee DO. Increased detection of prolylaminopeptidase in *Neisseria meningitidis* by Identicult-*Neisseria*. *J Clin Microbiol.* 1986;24(1):145.
  57. Schoonmaker JN, Lunt BD, Lawellin DW, French JI, Hillier SL, McGregor JA. A new proline aminopeptidase assay for diagnosis of bacterial vaginosis. *Am J Obstet*

- Gynecol. 1991;165(3):737–42.
58. Cellier M, James AL, Orenga S, Perry JD, Rasul AK, Robinson SN, et al. Novel chromogenic aminopeptidase substrates for the detection and identification of clinically important microorganisms. *Bioorg Med Chem.* 2014;22(19):5249–69.
  59. Carlone GM, Valadez MJ, Pickett MJ. Methods for distinguishing gram-positive from gram-negative bacteria. *J Clin Microbiol.* 1982;16(6):1157–9.
  60. Cellier M, James AL, Orenga S, Perry JD, Turnbull G, Stanforth SP. The synthesis of l-alanyl and  $\beta$ -alanyl derivatives of 2-aminoacridone and their application in the detection of clinically-important microorganisms. *PLoS One.* 2016;11(7):e0158378.
  61. Cellier M, Fabrega OJ, Fazackerley E, James AL, Orenga S, Perry JD, et al. 2-Arylbenzothiazole, benzoxazole and benzimidazole derivatives as fluorogenic substrates for the detection of nitroreductase and aminopeptidase activity in clinically important bacteria. *Bioorg Med Chem.* 2011;19(9):2903–10.
  62. Thompson R, Stephenson D, Sykes HE, Perry JD, Stanforth SP, Dean JR. Detection of  $\beta$ -alanyl aminopeptidase as a biomarker for *Pseudomonas aeruginosa* in the sputum of patients with cystic fibrosis using exogenous volatile organic compound evolution. *RSC Adv.* 2020;10(18):10634–45.
  63. Váradi L, Wang M, Mamidi RR, Luo JL, Perry JD, Hibbs DE, et al. A latent green fluorescent styrylcoumarin probe for the selective growth and detection of Gram negative bacteria. *Bioorg Med Chem.* 2018;26(16):4745–50.
  64. Zaytsev A V, Anderson RJ, Bedernjak A, Groundwater PW, Huang Y, Perry JD, et al. Synthesis and testing of chromogenic phenoxazinone substrates for  $\beta$ -alanyl aminopeptidase. *Org Biomol Chem.* 2008;6(4):682–92.
  65. Laine L, Perry JD, Lee J, Oliver M, James AL, De La Foata C, et al. A novel chromogenic medium for isolation of *Pseudomonas aeruginosa* from the sputa of cystic fibrosis patients. *J Cyst Fibros.* 2009;8(2):143–9.
  66. Bedernjak AF, Zaytsev A V, Babolat M, Cellier M, James AL, Orenga S, et al. Synthesis and Evaluation of Novel 7-and 8-Aminophenoxazinones for the Detection of  $\beta$ -Alanine Aminopeptidase Activity and the Reliable Identification of *Pseudomonas aeruginosa* in Clinical Samples. *J Med Chem.* 2016;59(10):4476–87.
  67. Váradi L, Hibbs DE, Orenga S, Babolat M, Perry JD, Groundwater PW.  $\beta$ -Alanyl

- aminopeptidase-activated fluorogenic probes for the rapid identification of *Pseudomonas aeruginosa* in clinical samples. *RSC Adv.* 2016;6(64):58884–9.
68. Mulczyk M, Szewczuk A. Pyrrolidonyl peptidase in bacteria: A new colorimetric test for differentiation of enterobacteriaceae. *Microbiology.* 1970;61(1):9–13.
  69. Mitchell MJ, Conville PS, Gill VJ. Rapid identification of enterococci by pyrrolidonyl aminopeptidase activity (PYRase). *Diagn Microbiol Infect Dis.* 1987;6(4):283–6.
  70. Dealler SF, Campbell L, Kerr KG, McGoldrick J, Flannigan KA, Hawkey PM. Reliable five-minute test strip method for identification of *Streptococcus pyogenes*. *Eur J Clin Microbiol Infect Dis.* 1989;8(4):308–10.
  71. Li L, Li Z, Shi W, Li X, Ma H. Sensitive and selective near-infrared fluorescent off-on probe and its application to imaging different levels of  $\beta$ -lactamase in *Staphylococcus aureus*. *Anal Chem.* 2014;86(12):6115–20.
  72. Chen Y, Xianyu Y, Wu J, Zheng W, Rao J, Jiang X. Point-of-care detection of  $\beta$ -lactamase in milk with a universal fluorogenic probe. *Anal Chem.* 2016;88(11):5605–9.
  73. Rukavishnikov A, Gee KR, Johnson I, Corry S. Fluorogenic cephalosporin substrates for  $\beta$ -lactamase TEM-1. *Anal Biochem.* 2011;419(1):9–16.
  74. Mizukami S, Watanabe S, Hori Y, Kikuchi K. Covalent protein labeling based on noncatalytic  $\beta$ -lactamase and a designed FRET substrate. *J Am Chem Soc.* 2009;131(14):5016–7.
  75. Zhang J, Shen Y, May SL, Nelson DC, Li S. Ratiometric Fluorescence Detection of Pathogenic Bacteria Resistant to Broad-Spectrum  $\beta$ -Lactam Antibiotics. *Angew Chemie.* 2012;124(8):1901–4.
  76. Shao Q, Zheng Y, Dong X, Tang K, Yan X, Xing B. A Covalent Reporter of  $\beta$ -Lactamase Activity for Fluorescent Imaging and Rapid Screening of Antibiotic-Resistant Bacteria. *Chem Eur J.* 2013;19(33):10903–10.
  77. Yu P, Yang J-N, Yan J-W, Meng Z-Z, Hong WD, Roberts AP, et al. A novel fluorescent probe for the detection of AmpC beta-lactamase and the application in screening beta-lactamase inhibitors. *Spectrochim Acta Part A Mol Biomol Spectrosc.* 2020;118257.



78. Coudron PE, Moland ES, Thomson KS. Occurrence and detection of AmpC beta-lactamases among *Escherichia coli*, *Klebsiella pneumoniae*, and *Proteus mirabilis* isolates at a veterans medical center. *J Clin Microbiol.* 2000;38(5):1791–6.
79. Mao W, Xia L, Xie H. Detection of Carbapenemase-Producing Organisms with a Carbapenem-Based Fluorogenic Probe. *Angew Chemie.* 2017;129(16):4539–43.
80. Mao W, Wang Y, Qian X, Xia L, Xie H. A Carbapenem-Based Off–On Fluorescent Probe for Specific Detection of Metallo- $\beta$ -Lactamase Activities. *ChemBioChem.* 2019;20(4):511–5.
81. Kim J, Kim Y, Abdelazem AZ, Kim HJ, Choo H, Kim HS, et al. Development of carbapenem-based fluorogenic probes for the clinical screening of carbapenemase-producing bacteria. *Bioorg Chem.* 2020;94:103405.
82. Xie H, Mire J, Kong Y, Chang M, Hassounah HA, Thornton CN, et al. Rapid point-of-care detection of the tuberculosis pathogen using a BlaC-specific fluorogenic probe. *Nat Chem.* 2012;4(10):802–9.
83. Cheng Y, Xie J, Lee K-H, Gaur RL, Song A, Dai T, et al. Rapid and specific labeling of single live *Mycobacterium tuberculosis* with a dual-targeting fluorogenic probe. *Sci Transl Med.* 2018;10(454):eaar4470.
84. Kong Y, Yao H, Ren H, Subbian S, Cirillo SLG, Sacchettini JC, et al. Imaging tuberculosis with endogenous  $\beta$ -lactamase reporter enzyme fluorescence in live mice. *Proc Natl Acad Sci.* 2010;107(27):12239–44.
85. Cheng Y, Xie H, Sule P, Hassounah H, Graviss EA, Kong Y, et al. Fluorogenic Probes with Substitutions at the 2 and 7 Positions of Cephalosporin are Highly BlaC-Specific for Rapid *Mycobacterium tuberculosis* Detection. *Angew Chemie Int Ed.* 2014;53(35):9360–4.
86. Nabeta P, Seshadri P, Havumaki J, Mbhele S, Hendricks L, Perkins MD, et al. First clinical assessment of a prototype assay to detect the enzymatic activity of  $\beta$ -lactamase as a marker for pulmonary tuberculosis. *Diagn Microbiol Infect Dis.* 2020;115026.
87. Sule P, Tilwawala R, Mustapha T, Hassounah H, Noormohamed A, Kundu S, et al. Rapid tuberculosis diagnosis using reporter enzyme fluorescence. *J Clin Microbiol.* 2019;57(12).

88. Santos-Beneit F. The Pho regulon: a huge regulatory network in bacteria. *Front Microbiol.* 2015;6:402.
89. Prunty M. Investigation of the PhoPR two-component signal transduction system in *Bacillus subtilis*, *Staphylococcus aureus* and *Staphylococcus epidermidis*. Trinity College Dublin; 2017.
90. Wanner BL, Chang B-D. The *phoBR* operon in *Escherichia coli* K-12. *J Bacteriol.* 1987;169(12):5569–74.
91. Gardner SG, Johns KD, Tanner R, McCleary WR. The PhoU protein from *Escherichia coli* interacts with PhoR, PstB, and metals to form a phosphate-signaling complex at the membrane. *J Bacteriol.* 2014;196(9):1741–52.
92. Wanner BL. Phosphorus assimilation and control of the phosphate regulon. *Escherichia coli Salmonella Cell Mol Biol* 2nd ed ASM Press Washington, DC. 1996;41:1357–81.
93. Tommassen J, de Geus P, Lugtenberg B, Hackett J, Reeves P. Regulation of the *pho* regulon of *Escherichia coli* K-12: cloning of the regulatory genes *phoB* and *phoR* and identification of their gene products. *J Mol Biol.* 1982;157(2):265–74.
94. Hulett FM, Lee J, Shi L, Sun G, Chesnut R, Sharkova E, et al. Sequential action of two-component genetic switches regulates the PHO regulon in *Bacillus subtilis*. *J Bacteriol.* 1994;176(5):1348–58.
95. Kelliher JL, Radin JN, Kehl-Fie TE. PhoPR contributes to *Staphylococcus aureus* growth during phosphate starvation and pathogenesis in an environment-specific manner. *Infect Immun.* 2018;86(10).
96. Agrawal DK, Wanner BL. A *phoA* structural gene mutation that conditionally affects formation of the enzyme bacterial alkaline phosphatase. *J Bacteriol.* 1990;172(6):3180–90.
97. Zappa S, Rolland J-L, Flament D, Gueguen Y, Boudrant J, Dietrich J. Characterization of a highly thermostable alkaline phosphatase from the euryarchaeon *Pyrococcus abyssi*. *Appl Environ Microbiol.* 2001;67(10):4504–11.
98. Goldman S, Hecht K, Eisenberg H, Mevarech M. Extracellular Ca<sup>2+</sup> (+)-dependent inducible alkaline phosphatase from extremely halophilic archaeobacterium *Haloarcula marismortui*. *J Bacteriol.* 1990;172(12):7065–70.

99. Aono H, Otsuji N. Genetic mapping of regulator gene *phoS* for alkaline phosphatase in *Escherichia coli*. *J Bacteriol.* 1968;95(3):1182.
100. Echols H, Garen A, Garen S, Torriani A. Genetic control of repression of alkaline phosphatase in *E. coli*. *J Mol Biol.* 1961;3(4):425–38.
101. Wilson IB, Dayan J, Cyr K. Some properties of alkaline phosphatase from *Escherichia coli*. *J Biol Chem.* 1964;239:4182.
102. Hørder M. Enzyme catalyzed hydrolysis of inorganic pyrophosphate. *Enzyme.* 1975;19:165–91.
103. Cheng K-J, Ingram JM, Costerton JW. Alkaline phosphatase localization and spheroplast formation of *Pseudomonas aeruginosa*. *Can J Microbiol.* 1970;16(12):1319–24.
104. Shah DB, Blobel H. Repressible alkaline phosphatase of *Staphylococcus aureus*. *J Bacteriol.* 1967;94(3):780.
105. Anagnostopoulos C. Alkaline phosphatase formation in *B-subtilis*. In: federation proceedings. Federation Amer Soc Exp Biol; 1960. p. 48.
106. Glenn AR, Mandelstam J. Sporulation in *Bacillus subtilis* 168. Comparison of alkaline phosphatase from sporulating and vegetative cells. *Biochem J.* 1971;123(2):129–38.
107. Campbell LL, Hulett-Cowling FM. Purification and properties of an alkaline phosphatase of *Bacillus licheniformis*. *Biochemistry.* 1971;10(8):1364–71.
108. Kuo M-H, Blumenthal HJ. Absence of phosphatase repression by inorganic phosphate in some micro-organisms. *Nature.* 1961;190(4770):29–31.
109. Cheng K-J, Costerton JW. Localization of alkaline phosphatase in three gram-negative rumen bacteria. *J Bacteriol.* 1973;116(1):424–40.
110. Malamy M, Horecker BL. The localization of alkaline phosphatase in *E. coli* K12. *Biochem Biophys Res Commun.* 1961;5(2):104–8.
111. Cheng K-J, Ingram JM, Costerton JW. Release of alkaline phosphatase from cells of *Pseudomonas aeruginosa* by manipulation of cation concentration and of pH. *J Bacteriol.* 1970;104(2):748–53.
112. MacAlister TJ, Costerton JW, Thompson L, Thompson J, Ingram JM. Distribution of

- alkaline phosphatase within the periplasmic space of gram-negative bacteria. *J Bacteriol.* 1972;111(3):827–32.
113. Greenman J, Melville TH, Appleton J. The localization of phosphatase activity in two oral strains of *Streptococcus*. *Arch Oral Biol.* 1980;25(11–12):759–65.
  114. Huang C-T, Xu KD, McFeters GA, Stewart PS. Spatial patterns of alkaline phosphatase expression within bacterial colonies and biofilms in response to phosphate starvation. *Appl Environ Microbiol.* 1998;64(4):1526–31.
  115. Okabayashi K, Futai M, Mizuno D. Localization of acid and alkaline phosphatases in *Staphylococcus aureus*. *Jpn J Microbiol.* 1974;18(4):287–94.
  116. Gupta KG, Blobel H, Brückler J, Schaeg W. Release of some staphylococcal enzymes and toxins under the influence of size of inoculum and time of incubation. *Comp Immunol Microbiol Infect Dis.* 1981;4(1):107–9.
  117. Fodor M, Rozgonyi F, Csepke E. Correlation between phage-type, coagulase, hyaluronidase and phosphatase activity, and mercuric chloride resistance of *Staphylococcus aureus*. *Acta Microbiol Acad Sci Hung.* 1963;10:19–25.
  118. Kedzia W, Musielak M, Kedzia B, Koniar H, Pniewska E. Enzymatic activity of coagulase-positive *Staphylococcus aureus* strains isolated from patients and healthy carriers. *Pathol Microbiol (Basel).* 1966;29(3):307–23.
  119. Jin MY, Piao XC, Wu XH, Fan MZ, Li XF, Yin CR, et al. *Oplopanax elatus* adventitious root production through fed-batch culture and their anti-bacterial effects. *Plant Cell, Tissue Organ Cult.* 2020;140(2):447–57.
  120. Fan E, Peng J, He Y, Wu Y, Ouyang H, Xu Z, et al. Chemiluminescent analysis of *Staphylococcus aureus* utilizing phe11-protonectin against Gram-positive bacteria. *Sensors Actuators B Chem.* 2019;285:271–6.
  121. Liu M, Xiang H, Hua E, Wang L, Jing X, Cao X, et al. Ultrasensitive electrochemical biosensor for the detection of the *mecA* gene sequence in methicillin resistant strains of *Staphylococcus aureus* employing gold nanoparticles. *Anal Lett.* 2014;47(4):579–91.
  122. Luo C, Lei Y, Yan L, Yu T, Li Q, Zhang D, et al. A rapid and sensitive aptamer-based electrochemical biosensor for direct detection of *Escherichia coli* O111. *Electroanalysis.* 2012;24(5):1186–91.

123. Williams RJ, Ward JM, Henderson B, Wilson M, Nair SP. Rapid screening for putative exported proteins from *Staphylococcus aureus* using alkaline phosphatase as a reporter molecule. *Mol Biotechnol.* 2000;15(1):11–20.
124. Dartois V, Djavakhishvili T, Hoch JA. KapB is a lipoprotein required for KinB signal transduction and activation of the phosphorelay to sporulation in *Bacillus subtilis*. *Mol Microbiol.* 1997;26(5):1097–108.
125. Robby AI, Park SY. Recyclable metal nanoparticle-immobilized polymer dot on montmorillonite for alkaline phosphatase-based colorimetric sensor with photothermal ablation of Bacteria. *Anal Chim Acta.* 2019;1082:152–64.
126. Biswas S, McCullough BS, Ma ES, LaJoie D, Russell CW, Brown DG, et al. Dual Colorimetric and Fluorogenic Probes for Visualizing Tyrosine Phosphatase Activity and High Throughput Screening.
127. Kang EB, Mazrad ZAI, Robby AI, In I, Park SY. Alkaline phosphatase-responsive fluorescent polymer probe coated surface for colorimetric bacteria detection. *Eur Polym J.* 2018;105:217–25.
128. Janda WM, Ristow K, Novak D. Evaluation of RapiDEC Staph for identification of *Staphylococcus aureus*, *Staphylococcus epidermidis*, and *Staphylococcus saprophyticus*. *J Clin Microbiol.* 1994;32(9):2056–9.
129. Miles AA, Misra SS, Irwin JO. The estimation of the bactericidal power of the blood. *J Hyg (Lond).* 1938;38(6):732–49.
130. Wijesinghe G, Dilhari A, Gayani B, Kottegoda N, Samaranayake L, Weerasekera M. Influence of laboratory culture media on in vitro growth, adhesion, and biofilm formation of *Pseudomonas aeruginosa* and *Staphylococcus aureus*. *Med Princ Pract.* 2019;28(1):28–35.
131. Sen S, Sirobhusanam S, Johnson SR, Song Y, Tefft R, Gatto C, et al. Growth-environment dependent modulation of *Staphylococcus aureus* branched-chain to straight-chain fatty acid ratio and incorporation of unsaturated fatty acids. *PLoS One.* 2016;11(10):e0165300.
132. Ray B, Ballal A, Manna AC. Transcriptional variation of regulatory and virulence genes due to different media in *Staphylococcus aureus*. *Microb Pathog.* 2009;47(2):94–100.

133. Oogai Y, Matsuo M, Hashimoto M, Kato F, Sugai M, Komatsuzawa H. Expression of virulence factors by *Staphylococcus aureus* grown in serum. *Appl Environ Microbiol*. 2011;77(22):8097–105.
134. Roth-Konforti M, Green O, Hupfeld M, Fieseler L, Heinrich N, Ihssen J, et al. Ultrasensitive Detection of *Salmonella* and *Listeria monocytogenes* by Small-Molecule Chemiluminescence Probes. *Angew Chemie*. 2019;131(30):10469–75.
135. Das S, Ihssen J, Wick L, Spitz U, Shabat D. Chemiluminescent Carbapenem-Based Molecular Probe for Detection of Carbapenemase Activity in Live Bacteria. *Chem Eur J*. 2020;
136. Maity S, Wang X, Das S, He M, Riley LW, Murthy N. A cephalosporin–chemiluminescent conjugate increases beta-lactamase detection sensitivity by four orders of magnitude. *Chem Commun*. 2020;56(24):3516–9.
137. Gunda NSK, Chavali R, Mitra SK. A hydrogel based rapid test method for detection of *Escherichia coli* (*E. coli*) in contaminated water samples. *Analyst*. 2016;141(10):2920–9.
138. Langlet S, Beaupère F, Contant G, Scheftel JM. A new gel tube method for the direct detection, identification and susceptibility testing of bacteria in clinical samples. *FEMS Microbiol Lett*. 1999;170(1):229–35.
139. Powers JG, Higham C, Broussard K, Phillips TJ. Wound healing and treating wounds: Chronic wound care and management. *J Am Acad Dermatol*. 2016;74(4):607–25.
140. Trengove NJ, Stacey MC, McGeachie DF, Stingemore NF, Mata S. Qualitative bacteriology and leg ulcer healing. *J Wound Care*. 1996;5(6):277–80.
141. Landis SJ. Chronic wound infection and antimicrobial use. *Adv Skin Wound Care*. 2008;21(11):531–40.
142. Bowler PG. The bacterial growth guideline: reassessing its clinical relevance in wound healing. *Ostomy Wound Manage*. 2003;49(1):44.
143. Kucera J, Sojka M, Pavlik V, Szuszkiewicz K, Velebny V, Klein P. Multispecies biofilm in an artificial wound bed—A novel model for in vitro assessment of solid antimicrobial dressings. *J Microbiol Methods*. 2014;103:18–24.

144. Pomponio G, Tedesco S, Peghetti A, Bianchi T, Rowan S, Greco A, et al. Improving the quality of clinical research on chronic wound infection treatment: expert-based recommendations. *J Wound Care*. 2019;28(Sup1):S26–31.
145. James GA, Swogger E, Wolcott R, Pulcini E deLancey, Secor P, Sestrich J, et al. Biofilms in chronic wounds. *Wound Repair Regen*. 2008;16(1):37–44.
146. Percival SL, McCarty SM, Lipsky B. Biofilms and wounds: an overview of the evidence. *Adv wound care*. 2015;4(7):373–81.
147. Gor V, Takemura AJ, Nishitani M, Higashide M, Romero VM, Ohniwa RL, et al. Finding of Agr phase variants in *Staphylococcus aureus*. *MBio*. 2019;10(4):e00796-19.
148. Shopsin B, Drlica-Wagner A, Mathema B, Adhikari RP, Kreiswirth BN, Novick R. Prevalence of agr dysfunction among colonizing *Staphylococcus aureus* strains. *J Infect Dis*. 2008;198(8):1171–4.
149. Traber KE, Lee E, Benson S, Corrigan R, Cantera M, Shopsin B, et al. agr function in clinical *Staphylococcus aureus* isolates. *Microbiology*. 2008;154(Pt 8):2265.
150. Paulander W, Varming AN, Bæk KT, Haaber J, Frees D, Ingmer H. Antibiotic-mediated selection of quorum-sensing-negative *Staphylococcus aureus*. *MBio*. 2012;3(6).
151. Vuong C, Saenz HL, Götz F, Otto M. Impact of the agr quorum-sensing system on adherence to polystyrene in *Staphylococcus aureus*. *J Infect Dis*. 2000;182(6):1688–93.
152. Malone M, Bjarnsholt T, McBain AJ, James GA, Stoodley P, Leaper D, et al. The prevalence of biofilms in chronic wounds: a systematic review and meta-analysis of published data. *J Wound Care*. 2017;26(1):20–5.
153. Khatoon Z, McTiernan CD, Suuronen EJ, Mah T-F, Alarcon EI. Bacterial biofilm formation on implantable devices and approaches to its treatment and prevention. *Heliyon*. 2018;4(12):e01067.
154. Danikowski KM, Cheng T. Alkaline phosphatase activity of *Staphylococcus aureus* grown in biofilm and suspension cultures. *Curr Microbiol*. 2018;75(9):1226–30.
155. Sabater S, Guasch H, Romaní A, Muñoz I. The effect of biological factors on the

- efficiency of river biofilms in improving water quality. *Hydrobiologia*. 2002;469(1–3):149–56.
156. Venkateswara Prasad U, Vasu D, Yeswanth S, Swarupa V, Sunitha MM, Choudhary A, et al. Phosphorylation controls the functioning of *Staphylococcus aureus* isocitrate dehydrogenase—Favours biofilm formation. *J Enzyme Inhib Med Chem*. 2015;30(4):655–61.
157. Li S, Wang C, Qin H, Li Y, Zheng J, Peng C, et al. Influence of phosphorus availability on the community structure and physiology of cultured biofilms. *J Environ Sci*. 2016;42:19–31.
158. Kumar V, Roy S, Baruah K, Van Haver D, Impens F, Bossier P. Environmental conditions steer phenotypic switching in acute hepatopancreatic necrosis disease-causing *Vibrio parahaemolyticus*, affecting PirAVP/PirBVP toxins production. *Environ Microbiol*. 2020;22(10):4212–30.
159. Valen H, Scheie AA. Biofilms and their properties. *Eur J Oral Sci*. 2018;126:13–8.
160. Weller C, Team V. Interactive dressings and their role in moist wound management. In: *Advanced textiles for wound care*. Elsevier; 2019. p. 105–34.
161. Agarwal A, McAnulty JF, Schurr MJ, Murphy CJ, Abbott NL. Polymeric materials for chronic wound and burn dressings. In: *Advanced Wound Repair Therapies*. Elsevier; 2011. p. 186–208.
162. Caló E, Khutoryanskiy V V. Biomedical applications of hydrogels: A review of patents and commercial products. *Eur Polym J*. 2015;65:252–67.
163. Song S, Wang L, Li J, Fan C, Zhao J. Aptamer-based biosensors. *TrAC Trends Anal Chem*. 2008;27(2):108–17.
164. Khampieng T, Wongkittithavorn S, Chairwut S, Ekabutr P, Pavasant P, Supaphol P. Silver nanoparticles-based hydrogel: characterization of material parameters for pressure ulcer dressing applications. *J Drug Deliv Sci Technol*. 2018;44:91–100.
165. Zhao Y, Li Z, Song S, Yang K, Liu H, Yang Z, et al. Skin-inspired antibacterial conductive hydrogels for epidermal sensors and diabetic foot wound dressings. *Adv Funct Mater*. 2019;29(31):1901474.
166. Mohamad N, Loh EYX, Fauzi MB, Ng MH, Amin MCIM. In vivo evaluation of



- bacterial cellulose/acrylic acid wound dressing hydrogel containing keratinocytes and fibroblasts for burn wounds. *Drug Deliv Transl Res.* 2019;9(2):444–52.
167. Xue K, Wang X, Yong PW, Young DJ, Wu Y, Li Z, et al. Hydrogels as emerging materials for translational biomedicine. *Adv Ther.* 2019;2(1):1800088.
  168. Kamoun EA, Kenawy E-RS, Chen X. A review on polymeric hydrogel membranes for wound dressing applications: PVA-based hydrogel dressings. *J Adv Res.* 2017;8(3):217–33.
  169. Jandera V, Hudson DA, De Wet PM, Innes PM, Rode H. Cooling the burn wound: evaluation of different modalities. *Burns.* 2000;26(3):265–70.
  170. Gibas I, Janik H. Synthetic polymer hydrogels for biomedical applications. 2010;
  171. Winter GD. Formation of the scab and the rate of epithelization of superficial wounds in the skin of the young domestic pig. *Nature.* 1962;193(4812):293–4.
  172. Figueiredo KCS, Alves TLM, Borges CP. Poly (vinyl alcohol) films crosslinked by glutaraldehyde under mild conditions. *J Appl Polym Sci.* 2009;111(6):3074–80.
  173. Li JK, Wang N, Wu XS. Poly (vinyl alcohol) nanoparticles prepared by freezing–thawing process for protein/peptide drug delivery. *J Control Release.* 1998;56(1–3):117–26.
  174. Şehitoğullari A, Uslan AH. Preparation of a potentiometric immobilized urease electrode and urea determination in serum. *Talanta.* 2002;57(6):1039–44.
  175. Chen D, Leu J, Huang T. Transport and hydrolysis of urea in a reactor–separator combining an anion-exchange membrane and immobilized urease. *J Chem Technol Biotechnol Int Res Process Environ Clean Technol.* 1994;61(4):351–7.
  176. Driest PJ, Allijn IE, Dijkstra DJ, Stamatialis D, Grijpma DW. Poly (ethylene glycol)-based poly (urethane isocyanurate) hydrogels for contact lens applications. *Polym Int.* 2020;69(2):131–9.
  177. Oliveira RN, McGuinness GB, Ramos MET, Kajiyama CE, Thiré RMSM. Properties of PVA Hydrogel Wound-Care Dressings Containing UK Propolis. In: *Macromolecular Symposia.* Wiley Online Library; 2016. p. 122–7.
  178. Jung IY, Kim JS, Choi BR, Lee K, Lee H. Hydrogel based biosensors for in vitro

diagnostics of biochemicals, proteins, and genes. *Adv Healthc Mater.* 2017;6(12):1601475.

179. Bhattacharya S, Nandi S, Jelinek R. Carbon-dot–hydrogel for enzyme-mediated bacterial detection. *RSC Adv.* 2017;7(2):588–94.
180. Serra R, Grande R, Butrico L, Rossi A, Settimo UF, Caroleo B, et al. Chronic wound infections: the role of *Pseudomonas aeruginosa* and *Staphylococcus aureus*. *Expert Rev Anti Infect Ther.* 2015;13(5):605–13.
181. Milo S, Acosta FB, Hathaway HJ, Wallace LA, Thet NT, Jenkins ATA. Development of an Infection-Responsive Fluorescent Sensor for the Early Detection of Urinary Catheter Blockage. *ACS sensors.* 2018;3(3):612–7.

## Chapter 8: Overall Conclusions and Future Work

The overall aim of this thesis was to create and evaluate a novel stimuli responsive system that could be used as a “smart” wound dressing for the treatment of *S. aureus* within chronic wounds.

The first three results chapters of this thesis set out to design a therapeutic system utilising the antibacterial properties of bacteriophage. Herein, we found that bacteriophage K was able to act in a synergistic manner with four different antibiotics: ciprofloxacin, vancomycin, amikacin, and amoxicillin, resulting in increased bacterial cell reductions compared to their monotherapy counterparts. This synergistic interaction was also capable of preventing *S. aureus* biofilm formation, and in some cases, reducing the bacterial biomass of an established infection. However, these results also highlighted the fact that the efficacy of the phage-antibiotic concentrations are dependent upon the strain of the bacteria under investigation; hence, there could be issues with this therapy in a clinical setting where it is not known what strain of bacteria is causing an infection.

With those promising results in hand, focus turned to developing a system whereby the antimicrobials can be released in a burst-like manner upon recognition of bacterial pathogens. The reservoir film used in this study was a blend of PLA and PEG as it was shown to have good biocompatibility and excellent drug release properties. Both phage K and ciprofloxacin were successfully encapsulated within this film and were shown to be capable of reducing bacterial density in planktonic, biofilm, and *ex vivo* studies.

To create a stimuli-responsive system, the PLA-PEG film was coated with a pH-responsive polymer. Earlier work conducted by Dr Wallace (University of Bath, UK) had suggested that pH could be a suitable trigger for drug release as it correlated with the formation of a biofilm. The PLA-PEG film was successfully coated with EUDRAGIT® FS 30 D and the resultant system was shown to be pH sensitive, within minimal diffusion of the antimicrobials from the system and pH values less than 7.0. However, one drawback of this film was that it hindered antimicrobial release from the polymer system, resulting in lower log reductions of bacterial concentrations. However, with further optimisation assays investigating the effect of polymer thickness and antimicrobial concentrations, this system has great potential to be used in a clinical setting.

Concurrently, work was being undertaken to develop a novel colorimetric and fluorescent probe for the detection of *S. aureus*. Alkaline phosphatase was chosen as it had been previously used in literature for the detection of *S. aureus* species. We were successfully able to synthesise a probe, **TCF-ALP**, that was capable of detecting ALP, and to a lesser extent, ACP, which could be easily monitored via the colour change of yellow to purple. What is exciting is that we were able to use this probe to selectively detect *S. aureus* in planktonic, biofilm, and *ex vivo* studies. Further work needs to be undertaken to determine the specificity and selectivity of **TCF-ALP**, but this thesis has demonstrated its capabilities as a probe for the diagnosis of wound infections via incorporation into a PVA-based hydrogel.

Moving forward, it is my hope that the two systems could be combined to create a novel theranostic dressing. This could potentially be achieved by creating a 'checkerboard'-type wound dressing that is composed of both polymer systems. Therefore, upon *S. aureus* infection, the theranostic system would be able to detect *S. aureus* by multiple triggers (pH and ALP), releasing its therapeutic payload and alerting the patient, or health care provider, to the presence of an infection. I feel that this system has potential in the field of wound care, as it can be easily adapted to suit the clinical need.